Targeted Therapy for Chordoma

A thesis submitted to University College London (UCL) for the degree of Doctor of Philosophy

Dr Mette Jorgensen

2016

UCL Cancer Institute, London UK

Declaration

I, Mette Jorgensen, confirm that the work presented in this thesis is my own. Where information has been derived from other sources, I confirm that this has been indicated in the thesis.

The high-throughput compound screening described in chapter 3 was conducted in conjunction with Cancer Research Technologies (CRT), Dr S. Scheipl and Dr L. Cottone.

Abstract

Chordoma is a rare and slow growing but locally aggressive bone tumour with a poor prognosis and limited treatment options. Current treatment strategies include surgical resection and radiotherapy. There are no approved drugs for the treatment of chordoma. The aim of this thesis was to explore novel therapeutics approaches.

Work presented within the thesis includes:
A high throughput screen of more than 1100 compounds in three chordoma cell lines. This work identified 27 compounds selective for chordoma; 78% were EGFR/ErbB inhibitors. These data adds to existing evidence that EGFR inhibitors are potential therapeutic agents for treatment of chordoma.

A gene therapy approach, using an Adeno-associated viral (AAV) vector for the delivery of RNAi targeting brachyury in vitro and in a xenograft model generated as part of the project. Chordoma cells were found to be permissive to AAV. Treatment with the brachyury-silencing vector resulted in tumour cell growth arrest.

In addition, two biomarkers were assessed to establish the potential to monitor for disease and disease response to treatment in chordoma patients. Detection of a protein biomarker AKR1B10, which has shown promise in breast cancer, was assessed but was not detectable in plasma from chordoma patients. Circulating tumour DNA (ctDNA) has shown great promise in high grade and advanced cancer. The potential to detect ctDNA in plasma from patients with chordoma was assessed following genomic profiling for tumour specific mutations. Digital PCR was used for detection of tumour DNA from 4 chordoma patients. Low levels of ctDNA were detected in 3 patients, establishing proof of concept that with further optimisation this method can potentially be used for detection of disease recurrence and monitoring response to treatment.

This work signposts the way towards further research into novel techniques to improve patient outcome for chordoma.

Acknowledgements

I would like to thank my supervisor Professor Adrienne Flanagan for giving me the opportunity to undertake this project and for her guidance throughout. Her support, encouragement and advice over the past few years have been invaluable. I am grateful to all the members of Adrienne's group, past and present in the UCL Cancer Institute and the Royal National Orthopaedic Hospital. I have received nothing but kindness, support and help from all the people working around her. I would in particular like to thank Nischalan for taking RNAi back to basic, for his support and patience, Roberto for knowing everything about chordoma and Nadege for her continuous support.

I would also like to thank Professor Amit Nathwani for adopting me into his group, I am hugely indebted for the help and support I received from him and all the members of his group. Particularly Marc Davis who has taught me almost everything I learnt in the lab. His patience, support and friendship have truly been valued. I would like to thank Doyoung for supporting me through many hours of virus production, Marco and Cecilia for helping the mice and me, and to Jenny and Alison for knowing something about everything and sharing their knowledge. I would also like to thank Professor Jeremy Whelan for his time, support and for always being in my corner.

It has been a real privilege to work with and around so many truly amazing people at UCL Cancer Institute. This has been an incredible journey, not one I would like to repeat but that I am happy to have done and completed.

I would like to thank my friends and family who has been incredibly supportive and encouraging over the past few years.

My boys Freddie and Ollie know more about xenograft models and cancer cells than they ever wanted to, though I hope it will inspire them in the future, however at present they feel that the best thing about my research is the discovery of how much fun you can have with dry ice. Above all I want to thank Matthew for his unwavering love and support. He has carried me through many challenges and his clarity of thought continues to amaze me. He is my rock and the greatest person I know.

Table of Contents

List of Figures

List of tables

Abbreviations

AAV	Adeno-associated virus
5-FC	5-flourocytosine
5-FU	5-flourouracil
AAP	Assembly-activated protein
ADA	Adenosine deaminase deficiency
Ago2	Argonaute
AKR1B10	Aldo-keto reductase family 1, member 10
AKT	Alpha serine/threonine-protein kinase
ALK	Anaplastic lymphoma kinase
AMD	Age-related macular degeneration
APC	Antigen presenting cell
ARID1A	AT rich interactive domain 1A (SWI-like)
ATMP	Advanced therapy medicinal product
ATP	Adenosine triphosphate
BCL-2	B-cell lymphoma 2
BNCT	Benign notochordal cell tumour
bp	Base pair
BRAF	v-raf murine sarcoma viral oncogene homolog B1
BRC-ABL	Philadelphia chromosome
BSA	Bovine serum albumin
c-MET	Met proto-oncogene (hepatocyte growth factor receptor)
CAP	Capsid
CAR	Chimeric antigen receptor
CAS9	CRISPR-associated protein 9
CD	Cytosine deaminase
CDK	Cycline dependent kinase
CDKN2A	Cycline dependent kinase inhibitor A2 (p16)
CDKN2B	Cycline dependent kinase inhibitor B2 (p15)
cDNA	Complimentary DNA
CEA	Cancer embryonic antigen
CEP	Chromosome enumeration probe
cfDNA	Cell free DNA
CG	Caspase Glo
CK18	Cytokeratin 18

CK19	Cytokeratin 19
cKIT	v-kit Hardy-Zuckerman 5 feline sarcoma viral oncogene homolog
CLL	Chronic lymphoblastic leukaemia
CLX	Cell line xenograft
CMV	Cytomegalovirus
CNG	Copy number gain
CNS	Central nervous system
CO2	Carbon dioxide
COSMIC	Catalogue of somatic mutations in cancer
CpG	Cytosine and guanine separated by a phosphate
CRISP	Clustered regularly interspaced short palindromic repeats
CRT	Cancer research technologies
CT	Computed tomography
ctDNA	circulating tumour DNA
CTG	Cell titre glo
CTL	Cytotoxic T-lymphocyte
CTNNB1	Catenin (cadherin-associated protein), beta 1
DC	Dendritic cell
DGCR8	DiGeorge syndrome chromosomal region 8
DMEM	Dulbrecco's modified eagle's medium
DMSO	Dimethylsylfoxide
DNA	Deoxyribonucleic acid
dNTP	Deoxyribonucleotide triphosphated
dPCR	Digital PCR
DPE	Differential phenotypic effect
dsRNA	Double stranded RNA
E-Cadherin	Epithelial Calcium-dependent adhesion protein
EDTA	Ethylene tetra-acetic acid
EGF	Epidermal growth factor
EGFR	Epidermal growth factor receptor
ELISA	Enzyme-linked immunosorbent assay
EMA	Epithelial membrane antigen
EMA	European Medicines Agency
EMT	Epithelial mesenchymal transition
ERK	Extracellular signal-regulated kinase
FACS	Fluorescence activated cell sorting

FBS	Fetal bovine serum
FBXW7	Fbox and WD40 domain containing 7
FCS	Fetal calf serum
FDA	Food and Drug Agency
FGF	Fibroblast growth factor
FGFR	Fibroblast growth factor receptor
FISH	Fluorescence in situ hybridisation
FLT3	fms-related tyrosine kinase 3
GAPDH	Glyceraldehyde-3-phosphate dehydrogenase
GEM	Genetically engineered mouse
GFP	Green fluorescent protein
GM-CSF	Granulocyte-macrophage colony-stimulating factor
GSK	GlaxoSmithKleine
GSK PKIS1/2	GSK compound libraries 1&2
GSK-3	Glycogen synthase kinase 3
GVAX	GM-CSF vaccine
Gy	Grey (unit of absorbed radiation dose)
H&E	Haematoxylin and eosin
HCC	Hepatocellular carcinoma
HDAC	Histone deacetylase
HEK 293T	Human embryonic kidney cell line
HeLa	Cervical carcinoma cell line
HER2	Human epidermal growth factor receptor 2
HGF	Hepatocyte growth factor
HGFR	Hepatocyte growth factor receptor
HIV-1	Human Immune-deficiency virus-1
HPSG	Heparan sulphate proteoglycan
HRAS	Harvey rat sarcoma viral oncogene homolog
HSV	Herpes simplex virus
ICGC	International Cancer Genome Consortium
IGF1-R	Insulin-like growth factor 1 (receptor)
IgG	Immunoglobulin G
IL-2	Interleukin 2
IL2GR	Interleukin-2 receptor gamma
IMDM	Iscove's modified dulbrecco's medium
INI1	SWI/SNF related, actin dependent regulator of chromatin

iNOS	Inducible nitric oxide
ITR	Inverted terminal repeats
JAK2	Janus Kinase 2
JHC7	Chordoma cell line
kb	Kilo-bases
KD	Knockdown
kDa	Kilo-dalton
KIT	v-kit Hardy-Zuckerman 5 feline sarcoma viral oncogene homolog
KRAS	v-Ki-ras2 Kirsten rat sarcoma viral oncogene homolog
KSP	Kinesin spindle protein
LamR	Laminin receptor
LB	Luria-Bertani broth
LIM	Lim homeodomain transcription factor
LMO2	LIM domain only 2
LMP2	Proteasome subunit beta type 9
LNA	Locked nucleic acid
LNP	Lipid nanoparticles
LPL	Lipoprotein lipase (deficiency)
LTR	Long terminal repeat
M	Molar
m	Mille (10e-3)
MAPK	Mitogen activated kinase-like protein
MDM2	Mouse double minute 2 (E3 ubiquitin-protein ligase)
MEK	Mitogen activated extracellular signal-regulated kinase
MHC	Major histocompatibility complex
miRNA	MicroRNA
MMP	Metalloproteinase
MOI	Multiplicity of infection
MRI	Magnetic resonance imaging
mRNA	Messenger RNA
mTOR	Mammalian target of rapamycin
MUG Chor	Chordoma cell line
n	Nano
NAb	Neutralising antibodies
NAHDF	Normal adult human dermal fibroblasts
NCI	National Cancer Institute

NF-Kβ	Nuclear factor of kappa light polypeptide gene enhancer in B-cells
NGS	Next generation sequencing
NHS	National Health Service
NOS	Not otherwise specified
NP	Nano-particles
NRAS	Neuroblastoma RAS viral oncogene homolog
NS	Non-silencing
NSCLC	Non-small cell lung cancer
ORF	Open reading frame
OTC	Ornithine transcarbamylase (deficiency)
PACT	Protein kinase activating protein
PAP	Prostate acid phosphatase
PBS	Phosphate buffered saline
PBS-T	Phosphate buffered saline - tween
PCR	Polymerase chain reaction
PD	Progressive disease
PDGFR	Platelet derived growth factor receptor
PDX	Patient derived xenograft
PET	Positron emission tomography
PFS	Progression free survival
PI3K	Phosphatidylinositol-4,5-bisphosphate 3-kinase
PIK3CA	Phosphatidylinositol-4,5-bisphosphate 3-kinase, subunit alpha
PKN3	Protein kinase N3
PLK	Polo-like kinase
PR	Partial response
PSMB10	Proteasome subunit beta type 9
PTEN	Phosphate and tensin homolog
rAAV	Recombinant Adeno-associated virus
RECIST	Response Evaluation Criteria in Solid Tumours
REP	Replication
RGEN	RNA-guided engineered nuclease
RISC	RNA inducing silencing complex
RNA	Ribonucleic acid
RNAi	RNA interference
RPMI	Roswell Park Memorial institute medium

RPP30	Ribonuclease P protein
RRM2	Ribonucleoside-diphosphate reductase subunit M2
RT	Reverse transcriptase
RT qPCR	Real time quantitative polymerase chain reaction
scAAV	Self-complimentary AAV
SCID	Severe combined immune deficiency
SD	Stable disease
SD	Standard deviation
SDS	Sodium dodecyl sulphate
SERCA2	Sarco(endo)plasmice reticulum Ca2+ ATPase 2
SFDA	Chinese State Food and Drug Administration
shRNA	Short hairpin RNA
SIN	Self-inactivating
siRNA	Small interfering RNA
SMARCB1/INI1	Integrase interactor 1
SNALP	Stable nucleic acid lipid particles
SNP	Single-nucleotide polymorphism
SP	Single point
Src	Proto-oncogene tyrosine-protein kinase
SRPN	Staurosporine
ssRNA	Single stranded RNA
STAT3	Signal transducers and activators of transcription 3
STR	Short tandem repeat
T	T, brachyury homolog (mouse)
T-cell	Thymus derived lymphocyte
T-vec	Talimogene Laherparepvec
TALEN	Transcription activator-like effector nuclease
TBE	Tris/Borate/EDTA
TBS	Tris-buffered saline
Tcf12	Transcription factor 12
TCS	Tuberous sclerosis complex
TGFβ	Transforming growth factor beta
tk	Thymidine-kinase
TKI	Tyrosine kinase inhibitor
TLR	Toll-like receptor
TORC1	Transducer of Regulated CREB activity, now referred to as

	CREB-regulated transcription co-activator 1 (CRTC1)
TP53	Tumour protein p53
TRBP	Tat-RNA binding protein
TT	Targeted therapy
U-CH1	Chordoma cell line
U-CH2	Chordoma cell line
UCL	University College London
UT	Un-transduced
VEGFR	Vascular endothelial growth factor receptor
WRN	Werner syndrome ATP dependent helicase
WST-1	Water soluble tetrazolium salt
WT	Wild-type
ZFN	Zink finger nuclease
α	Alpha
β	Beta
μ	Micro (10e-6)

1 INTRODUCTION

1.1 Background

Chordomas are rare malignant bone tumours which almost exclusively affect the axial skeleton. They are slow growing, locally destructive tumours with a high local recurrence rate and the potential to metastasise. Chordomas are thought to arise from cellular remnants of the notochord. They are characterised by their expression of the transcription factor *T*, brachyury homolog (mouse) commonly referred to as brachyury.

1.1.1 Incidence and epidemiology

Chordoma represents between 1 and 6% of primary malignant bone tumours(1,2), 20% of primary spinal tumours(3,4) and 50% of malignant sacral tumours(5). The incidence of chordoma is reported as 0.08 per 100,000 translating to an estimated 300 new cases in the United States(6-9) and approximately 50 cases in the UK per year. However, reported cases of chordoma in the UK amount to an average of 22 new cases per year over the past 10 years(1) suggesting a lower incidence or under-reporting of these tumours in the UK. Chordomas can present at any age though they are extremely rare under the age of 25. The incidence increases with age and nearly 80% of diagnoses are made in patients over the age of 50 years, with a peak incidence between 50-60 years of age(6).

Most chordomas arise in the axial skeletal with a few chordomas reported arising in extra-axial locations. These extra-skeletal chordomas have been described in different anatomical sites, including soft tissue(10) in the lung(11,12), and in a wide variety of bones including the thumb, ankle, shoulder and chest wall with no predilection for specific bones or sites within the bone(10-15). The extra-skeletal chordomas resemble the axial chordoma in histology and brachyury expression(10,13-16).

The reported distribution of axial chordomas, along the base of the skull to the coccyx, varies in different studies. A recent review of all malignant bone sarcomas registered in England between 1979 and 2007 found approximately 45% of chordomas arose from the pelvis, 23% arose from the vertebral bodies and 26% from the bones of the skull(1), aligning with historical data(17). A much larger cohort of 490 patients in a recent review of the California Cancer Registry identified 49% of chordomas arising in the skull, with approximately 25% arising in the spine or pelvis(18). Other studies have described an almost equal anatomical distribution between the base of skull, the mobile spine and the sacrococcygeal region(4,6). The location of chordoma varies with age at diagnosis. In patients under the age of 20, 70% of tumours occur at the base of skull compared with 21% of patients over the age of 50. In patients over the age of 50,

80% of tumours occur in the lower vertebral bodies, sacrum and coccyx(1,6,18). Chordoma occurs more frequently in males (ratio 1.6:1), especially for pelvic chordoma with a 3:1 male to female ratio(19). Cranial tumours occur more frequently in females(18).

Median survival for patients with chordoma is 7.7 years. Younger patients (aged <40 years) survive longer compared to older patients (10-year relative survival 68% vs 43%), excluding the very young children who have a dismal prognosis(20). The 5-year, 10-year, and 20-year survival rate across all age groups have recently been reported as 72%, 48%, and 31% respectively(7).

1.1.2 History and origin of chordoma

Chordomas were first characterised microscopically in 1857 by Virchow(21), who described the distinguishing feature of the cells of a clivus tumour as “ecchondrosis physaliferous” (Greek for “bubble-bearing”), due to the foamy appearance of the cytoplasm which contains multiple vacuoles. In 1858 Müller described chordoma dorsalis as “ecchordosis physaliphora”, thereby being the first to consider it of notochordal origin(22). Ribbert supported this in 1894 when he produced proliferative lesions resembling chordoma by releasing tissue of notochordal origin from the nucleus pulposus(23).

Examination of human embryos and fetuses(24,25) and cell-fate tracking experiments in mice(26) have shown that notochordal cell nests correspond topographically with the anatomic distribution of chordoma(25). Rare benign intra-osseous notochordal tumours (BNCT) have been described(27) as a possible precursor for conventional chordoma. These benign tumours were identified in 20% of 100 vertebral autopsy specimens in patients ranging in age from 7 to 82, with a distribution of 11.5% of the clival region, 5% of cervical vertebrae, 2% of lumbar vertebrae, 12% of sacrococcygeal vertebrae and none in the thoracic vertebrae(28). This distribution is similar for the anatomical sites of chordoma previously described, supporting the concept that the persistent notochord is the precursor of chordoma. The low incidence of chordoma suggests that transformation into a malignant tumour is a rare occurrence(29,30). Conclusive evidence supporting notochordal remnant cells as the origin of chordoma was confirmed when molecular phenotyping identified brachyury as a specific marker for chordoma(31-33).

1.1.3 Etiology

The vast majority of chordoma arise sporadically. Very occasionally it occurs in a familial setting with inheritance compatible with an autosomal dominant trait. In some families the inherited disease is associated with duplication of brachyury(19,34,35) (detailed below). Patients with familial chordoma are younger at presentation than those presenting with sporadic disease and the majority of patients present with a clival tumour(19,36). There is also a recognised, though rare, association of chordoma with tuberous sclerosis complex (TSC) - an autosomal neuro-cutaneous syndrome, characterised by abnormal tissue growth in multiple organ systems. TSC is caused by inactivation or loss of *TSC1/TSC2* where loss of function results in phosphorylation of the mTOR pathway, leading to enhanced cell growth and proliferation(37-39). Chordomas associated with TSC have mainly been described in children, is found more frequently in the sacrum and has a better outcome(39). The PI3K/AKT/TSC1/TSC2/mTOR pathway is activated in approximately 65% of sporadic chordoma, suggesting involvement in the pathogenesis of chordoma(40).

1.1.4 Histology

Chordomas not otherwise classified (NOS) were previously categorised as classical (or conventional) chordomas. Specific subtypes haven been categorised as chondroid or dedifferentiated(3,41). Chordomas generally have a homogenous histological appearance composed of large cells with clear to eosinophilic cytoplasm separated into lobules by fibrous septa. The tumour cells have round nuclei and copious vacuolated 'bubbly' cytoplasm, referred to as "physaliphorous cells", that are characteristic of classical chordomas. Cells are arranged as small cords embedded in abundant extracellular myxoid matrix, or as more densely arranged epithelioid tumours. Nuclear atypia and mitotic figures are not commonly seen except for in tumours with spindled sarcomatoid appearance where nuclear atypia and pleomorphism may be prominent. Necrosis is frequently present and may be extensive(41). Chondroid chordoma refers to chordoma in which the matrix mimics hyaline cartilaginous tumours. This component can be focal or extensive. The chondroid histological subtype accounts for 5-15% of all chordomas and up to 33% of all cranial chordomas(3). The outcome for the chondroid subtype is similar to classical chordoma(42). Dedifferentiated chordoma accounts for less than 10% of chordomas, characterised by being biphasic, comprised of classical chordoma with sarcoma-like regions with undifferentiated spindle-cell tumours(43-45). The dedifferentiated variant tends to be more aggressive and is associated with loss of brachyury expression(46).

1.1.5 Clinical presentation

Chordomas are indolent and slow growing, therefore often diagnosed late, presenting with large locally invasive and destructive lesions. The clinical manifestations vary depending on location, though pain and neurologic symptoms from local compression are the main presenting symptoms. Skull-base chordomas often grow from the clivus, and present with cranial nerve palsies. Patients often complain of headache and visual disturbances with diplopia, due to raised intracranial pressure(2). The skull-based tumours may erode distally and obstruct nasal passages with the potential to cause breathing difficulties(17). Clinical manifestations of vertebral column-based chordoma are a result of pressure on nerve roots, with the earliest presenting symptoms being paraesthesia in an upper or lower limb(2,47). Sacrococcygeal chordoma often presents late, as symptoms are often non-specific with initial symptoms of mild perianal pain and numbness. Patients present with urinary symptoms and/or constipation and go on to develop paraesthesia due to nerve compression(2,47,48).

Chordomas are locally invasive and typically have not metastasised at presentation. Distant metastases occur late in the course of the disease in 30-40% of patients(49-52) with metastases to lymph nodes, lungs, bone, skin and brain(52-54). Patient survival is less affected by distant metastases than by local progression(55-58). Local recurrence has been described in up to 66% of cases(50,59-61) emphasising the difficulties in obtaining clear resection margins, due to the infiltrative nature of the tumour, and the anatomical location. The disease can have a very protracted course often with multiple recurrences(1,6).

1.1.5.1 Chordoma in children and young adults

Chordoma in children and young adults (under the age of 20) is very rare, representing less than 5% of all chordomas(7,62,63) with equal incidence between male and female(20).

Sphenooccipital lesions are most frequent in children and adolescents (~64%), whilst sacrococcygeal tumours (~9%) are less common(20,39,63). The majority of chordomas in childhood are classical (58%) or chondroid variants (23%) while the poorly differentiated subtype is found in 8% of cases(20). The poorly differentiated subtype occurs mostly in very young children, its behaviour is aggressive and associated with a higher rate of metastases(20,63-67). Recently, a subset of early childhood chordoma was found to have *SMARCB1/INI1* loss, which was found to be associated with poorly differentiated chordoma and poor prognosis(68-70). *SMARCB1*/*INI1* loss is a rare finding in adult chordoma(71). In a recent systematic review comprising an analysis of

560 patients diagnosed with intracranial chordoma including children and adults, the only predictor of survival was age. Patients under the age of 5 were found to have worse outcomes, with an overall survival of 14% compared to patients over the age of 5, with an overall survival of 66%(72). Hoch et al. reported their experience, treating base of skull chordoma in children and young adults, from a single treatment centre. 73 children under the age of 18 were included, all treated with partial or gross surgical excision and post-operative proton beam irradiation. The overall survival rate was 81% with no difference noted in survival between patients with classical versus chondroid chordoma. However, of a subset of patients under the age of 5 with poorly differentiated chordoma, 83% died (5 of 6 patients). The survivor had metastatic disease and a short follow up period(20). In children with classical chordoma the 5-year overall survival of 81% is comparable with current data for adult patients treated with surgery and proton irradiation or carbon ion irradiation(73,74).

1.2 Brachyury

Brachyury is a member of the T-box family of transcription factors, characterised by a conserved DNA-binding domain called the T-box(75). The human ortholog of brachyury has been mapped to the conserved linkage group on chromosome 6q27(76). T-box transcription factors are vital to the development of the vertebrate embryo, playing essential roles in the control of morphogenesis and cell fate decisions(77,78). In the developing embryo, brachyury is expressed within the notochord, which forms the central axial skeletal element of the developing embryo. Brachyury expression from the notochord is essential for mesoderm formation and differentiation, and is involved in the control of early embryonal development (gastrulation) (79,80). Loss of brachyury expression leads to failure of notochord formation with homozygous loss being associated with embryonic lethality(79). Heterozygosity of the gene has been shown to cause skeletal abnormalities. This was first described by Dr Zavadskaia in 1927, as a mutation affecting tail length and sacral vertebrae in mice(81). Molecularly characterisation of the brachyury gene was first described in 1990(79). Recently a homozygous missense mutation in brachyury was identified within a consanguineous family, suggesting a causal effect in the development of sacral agenesis(82). A different missense mutation in brachyury has previously been associated with vertebral malformations(83), and a single nucleotide polymorphism in intron 7 has been found to be associated with an increased risk of spina bifida(84).

1.2.1 Brachyury implication on pathogenesis of chordoma

Brachyury expression was identified as the diagnostic hallmark of chordoma in a gene expression microarray study of 96 mesenchymal tumours identifying a gene-specific signature for chordoma, compared to 18 different mesenchymal tumours(33). Further studies using a polyclonal antibody confirmed that brachyury was expressed in all 53 chordomas tested, as well as in the embryonic notochord, but not in 300 other neoplasms tested(31). Brachyury has since become the diagnostic marker for chordoma(46), though the level of expression has not been found to be a prognostic indicator(85). It remains to be determined whether or how brachyury-expressing notochord cells turn into the brachyury expressing cells found in chordoma, though little doubt remain of brachyury's involvement in the pathogenesis of chordoma(86). The basis of this statement is presented below.

1.2.2 Brachyury Amplification

Familial chordoma has been described in 8 families including 24 cases of chordoma(19,87). Germline duplication of brachyury was found in 7 affected individuals in 4 of the families representing a major susceptibility mechanism in some chordoma families(87,88). In a study of 98 chordoma samples, non-germline amplification of brachyury was identified in 7% of sporadic cases, while 52% of tumours showed copy number gain (CNG) of brachyury and within these tumours 39% were polysomic for chromosome 6(89).

1.2.3 Single-nucleotide variant confer risk of chordoma

Recently a common single-nucleotide polymorphism (SNP) was identified in brachyury (rs2305089) which was found to be significantly associated with the risk of sporadic chordoma(90). The non-synonymous SNP was found in more than 95% of patients with chordoma with approximately 75% of patients being homozygous. Patients with homozygous alteration had relative higher expression of brachyury and downstream targets compared to heterozygous patients. The association has been confirmed in familial chordoma identifying the SNP in all 24 cases within the 8 families. A second common variant, rs1056048 was identified as strongly associated with chordoma in familial cases(87). These findings further highlight the importance of brachyury in the pathogenesis of both familial and sporadic chordoma.

1.2.4 Silencing of brachyury leads to cell senescence in vitro

In vitro silencing of brachyury, using RNA interference delivered by lenti-viral vectors, has been shown to lead to cell senescence and apoptosis in two different chordoma

cell lines: UCH1 and JHC7, thereby supporting the involvement of brachyury in the pathogenesis of chordoma(89,91).

1.2.5 Brachyury and epithelial mesenchymal transition

Brachyury has recently been identified as a major driver of epithelial to mesenchymal transition (EMT) in cancer progression(92,93). In normal development EMT plays a crucial role in the formation and differentiation of multiple tissues and organs, and is essential for numerous developmental processes including mesodermal formation and neural tube formation(94). EMT is a process where epithelial cells lose their cell polarity and cell-to-cell adhesion and gain migratory and invasive properties by becoming multi-potent stromal cells with stem cell properties. The transition, involving loss of E-cadherin expression, is considered a crucial step in the progression of epithelial tumours, during which the cells undergo a phenotypic conversion into mesenchymal cells. This progression enables them to metastasise and prevents apoptosis and senescence, an important mechanism leading to chemo- and radiotherapy resistance(93,95,96). Brachyury expression has been identified in many carcinomas, including breast (primary and metastatic), lung, hepato-cell-carcinoma, colorectal and adenoid cystic carcinoma. Expression of brachyury has been correlated with metastatic disease and poor outcome(96-105). Silencing of brachyury using RNAi in carcinoma cell lines and xenografts reversed the epithelial-mesenchymal transition with down-regulation of mesenchymal markers, reducing the ability of cell invasion and migration(102,106-109).

1.2.6 EMT and chordoma

The role of brachyury-mediated EMT in chordoma pathophysiology is unclear and the EMT signalling pathway is not fully understood but involves down-regulation of epithelial proteins such as E-cadherin and cytokeratins and the induction of mesenchymal proteins including fibronectin, N-cadherin, vimentin and matrix metalloproteinases (MMPs)(94,110-112). MMP expression levels have been linked with outcome in patients with chordoma, with increased levels associated with worse outcome(113,114). Histologically chordomas have epithelial features such as cell cohesiveness, a cord like structure and lobulation(115). The tumour cells are immunoreactive for epithelial markers including cytokeratin 8, 18 and 19, and epithelial membrane antigen (EMA)(13,115,116). Membrane expression for E-cadherin has been reported in 14-18% of chordoma, describing weak and focal expression(115,117). One study found no E-cadherin expression in 11 chordomas but all were immunoreactive for N-cadherin(118). Following gene silencing of brachyury in the chordoma cell lines

JHC7, U-CH1 and U-CH2, an increase in E-cadherin, a reduction in N-cadherin, and the mesenchymal transcription factors *Snail* and *Slug* were seen(119). *Snail* and *Slug* belong to a superfamily of zinc finger transcriptional repressors that participates in EMT, with *Snail* acting as a repressor of E-cadherin(92,120,121). There are two main *Snail* genes in vertebrates, *Snail1* and *Snail2* (called SNAI1 and SNAI2 or *Slug*). Snail genes represent a convergence point in EMT induction. Numerous signalling pathways induce EMT and all have been shown to activate the expression of these genes(122). The regulation is complex but includes transforming growth factor beta (TGFβ) superfamily of cytokines, and fibroblast growth factor (FGF), signalling(122,123). *FGF* as well as *TGFβ* have been implicated in the pathogenesis of chordoma and the control of brachyury(124-127). Findings in a recent study supported brachyury's involvement in EMT in chordoma, demonstrated interactions between brachyury and FGF/FGFR signalling via the MAPK pathway. FGF-activated FGFR/MEK/ERK/brachyury pathway was found to actively control cell growth, survival and EMT in chordoma(91,119).

1.3 Somatic mutations in chordoma

To date, no single recurrent somatic driver mutation has been identified in chordoma. A study of somatic point mutations in common cancer genes (*TP53, PTEN, BRAF*, *CTNNB1, FLT3, JAK2, APC, KIT, KRAS, NOTCH1* and *PIK3CA*) in 21 chordomas found no recurrent mutations(128). Choy et al. performed mutational analysis, genotyping 45 chordoma samples using focused genetic analysis, screening hotspot mutations in 111 oncogenes and selected tumour suppressor genes. Six mutations were identified in *ALK, CTNNB1, NRAS, PIK3CA, PTEN*, *CDKN2A* and *SMARCB1*. The mutations in *CDKN2A* and *PTEN* occurred in areas of chromosomal loss(129) Direct sequencing of mutational hotspots in the MAPK signalling pathway, including *EGFR, KRAS, NRAS, HRAS, BRAF* and *FGFR1-4,* have not identified any recurrent mutations in over 100 cases(119,130). Recently, exome or whole genome sequencing of 32 chordomas has not found a single unifying recurrent mutation (personal communication Professor A. Flanagan). Most chordomas have a bland genomic landscape harbouring only a few mutations although some cases have been described with chromothripsis(131,132). Chromothripsis, a recently reported cancer-initiating event, describing a phenomenon whereby tens to hundreds of genomic rearrangements occur in a one-off cellular crisis(133). This has been found in 2-3% of all cancers but in up to 25% of bone tumours and in 20% of chordomas. This was observed in a chordoma cell line where chromothripsis was reported to have

simultaneously affected the cancer-associated genes *CDKN2A*, Werner syndrome ATP dependent helicase (*WRN*) and Fbox and WD40 domain containing 7 (*FBXW7*)(133).

Other molecular profiling studies have shown chordomas are characterised by non-random genomic copy number alterations, with copy number losses being more frequent than copy number gains. The most common cytogenetic abnormality is monosomy 1 and gain of chromosome 7(125,126,128,134,135). Genomic homozygous and heterozygous loss of the tumour suppressors such as cyclin-dependent kinase inhibitor 2A (*CDKN2A), CDKN2B* (9p21) and *PTEN* has been reported to occur in up to 80% of chordomas(125,128).

1.4 Therapeutic options

1.4.1 Surgery and radiotherapy

The treatment option for chordoma is primarily surgical with complete resection being crucial for long-term event-free survival(56,136). The long-term survival after local relapse is low, and local control is rarely achieved(57,60,137-139). *En bloc* resection should be performed where possible with the aim of maximum tumour resection combined with preservation of neurological function and quality of life(140-142). Adjuvant radiotherapy is recommended following complete macroscopic resection and, for unresectable tumours, radiotherapy is given following biopsy. Chordomas are radiotherapy resistant requiring a high dose of at least 70-74Gy(143-145), which can be challenging to deliver due to toxicity to the surrounding tissue. Proton therapy has improved outcome for patients(143,144,146-148), achieving superior local control if radiotherapy is given as adjuvant therapy with surgery(74,146). Newer radiation therapies with carbon ion has shown promising results(73,149-151).

1.4.2 Chemotherapy

Chordoma has been shown to be chemo-resistant and at present there are no approved drug treatments for advanced chordoma(56). The experience with chemotherapy largely derives from case-reports(152-155). In a phase II trial utilising 9-nitroocamptothecin (9-NC), a topoisomerase I inhibitor to treat 15 patients with chordomas, one (7%) objective response was observed. The 6-month progression-free survival was 33%(156). The study was halted due to toxicity and inconsistent clinical activity(157). Patients with chordoma treated with chemotherapy have generally had a clinically aggressive tumour with metastatic or progressive disease(58,158,159).

Chemotherapy has shown initial response in dedifferentiated chordoma(160) but disease control has not been maintained.

1.4.3 Targetable tyrosine kinase receptors in chordoma

The first tyrosine kinase inhibitor used for treatment of chordoma was Imatinib, a kinase inhibitor developed to treat chronic lymphoblastic leukaemia (CLL) by blocking the BCR-Abl enzyme(161). Imatinib is a small molecule inhibitor of several tyrosine kinases including platelet-derived growth factor receptor *(PDGFR)* and *cKIT*(162). Subsequent work has shown that *PDGFR* is expressed in virtually all chordomas(163-165) and *cKIT* is expressed in 33-77% of chordomas(164,166). This provided the basis for further studies using Imatinib in patients with chordoma(167-169). The results of a multicentre, non-randomised, phase II study of Imatinib in patients with advanced chordoma showed an objective response in one (2%) of 50 patients assessed according to the Response Evaluation Criteria in Solid Tumours (RECIST)(170), whereas a minor response was seen in 20% of patients. Functional imaging using PET showed a 39% response rate which correlated with reported clinical symptomatic relief(171). Stabilisation of disease was achieved in 70% of patients with mean progression-free-survival (PFS) of 9.9 months in a patient group with active progressive disease, supporting activity of Imatinib in advanced stage chordoma(171,172).

The use of EGFR inhibitors for treatment in chordoma was reported in 2006 in a patient with progressive disease treated with the EGFR inhibitor Gefitinib, and a monoclonal antibody (Cetuximab) targeting *EGFR*. A degree of disease regression was observed, suggesting anti-tumour effect(173). Further pre-clinical studies and several case reports have reported activity of EGFR inhibitors including Gefitinib, Cetuximab, and Erlotinib in patients with chordoma(173-178). However, a recent phase II study testing efficacy of Lapatinib (EGFR and HER2 dual inhibitor) reported minimal activity(179). *EGFR* has been reported to be expressed in 24-100% of chordomas(165,166,180,181), with *EGFR* polysomy and gene amplification reported in 17-52% of tumours(164,180,182-184). No mutations have been detected in *EGFR* in chordoma(40,164).

Imatinib and EGFR inhibitors are amongst the most commonly tested drugs in chordoma patients totalling approximately 120 patients identified in the literature (Table 1.2). Imatinib efficacy in chordoma was only investigated in a preclinical setting in 2013, following nearly 9 years of clinical use. Imatinib was included in a large

compound high throughput drug screen and found to exert only a moderate inhibitory effect(185). EGFR inhibitors (Erlotinib and Gefitinib) were found to exert a modest growth inhibitor activity on the U-CH1 and U-CH2 cell lines, whilst Erlotinib demonstrated a significant inhibitory effect in a primary cell culture C24(185). This observation correlated with data testing Erlotinib and Gefitinib in a newly established patient derived xenograft model(178).

Expression of other potentially targetable tyrosine kinase receptors include the proto-oncogene Mesenchymal Epithelial Transition factor (*MET)* or (*c-MET)* also known as the hepatocyte growth factor receptor (*HGFR*) found in 60-100% of chordomas(181,186). The level of *c-MET* expression was found to be a prognostic factor in recurrent lesions, with low levels being associated with a worse outcome in spinal (vertebra) and skull-based chordoma(187). *HGF/c-MET* interacts with both the *PI3K/AKT/mTOR* and *RAS/RAF/MEK/MAPK* pathways(188), which are often dysregulated in cancer(189-191), and have been found to be dysregulated in chordoma(40,119,192). Active phosphorylated forms of the transduction molecules *ERK* and *AKT* were expressed in 86% and 76-92% respectively of chordomas(40,165). Mammalian target of rapamycin (*mTOR*) expression has been reported in 24-56% of chordomas(40,166). Rapamycin, an mTOR inhibitor has been tested in preclinical studies and treatment response has been reported in one patient describing reduced tumour growth rate and clinical improvement(193). A phase II study of imatinib plus everolimus (mTOR inhibitor) is in progress(56).

Vascular endothelial growth factor receptor 2 (*VEGFR2*) and inducible nitric oxide (iNOS) are involved in the angiogenesis and recurrence of chordoma, and have been associated with poorer outcome in spinal(194) and in sacral chordoma(195). However, the expression of *VEGFR2* in chordoma has not been observed in all studies(194) indicating that further work is required to clarify the expression pattern of this receptor in chordoma. The combination of Bevacizumab (VEGFR2 inhibitor) and Erlotinib or Cetuximab (EGFR inhibitor) was reported in three patients with chordoma, leading to symptom relief and stable disease(176,196). None of the genes coding for the proteins aberrantly expressed in chordoma have been found to have activating mutations(40,163-165,180).

Table 1.1 Preclinical drug screening in chordoma cell lines and xenografts

Year	Drug	Target	Cell lines	Effect	Reference
2014	FGFR inhibitor (VEGFR) (PD173074), MEK inhibitor (MAPK/ERK kinase)(PD 0325901 and PD 184352)	FGF2, MEK, ERK	JHC7, UCH1, UCH2	Decreased brachyury expression, induced apoptosis, and inhibited cell growth and EMT	(119)
2014	Lapatinib	EGFR/Her2/Neu	Xenograft (PDX)	Minimal effect	(177)
2013	SAHA (Vorinostat; Suberoylanilide hydroxyamic acid), LBH-589 (Panobinostat), PXD101 (Belinostat)	HDAC	UCH1, MUG	Apoptosis & cell cycle arrest	(198)
2014	Erlotinib and Gefitinib	EGFR	UCH1 and patient-derived xenograft	Reduced proliferation in cell line, reduced tumour growth in xenograft	(178)
2013	NCGC Pharmaceutical collection (NPC)		UCH1, UCH2, CCL4 control (+3 primary chordoma cell cultures	Inhibition of cell growth, Apoptosis (UCH1)	(185)
2012	Methotrexate, Doxorubicin, Cisplatin, Paclitaxel		CH22 (new chordoma cell line)	Chemo-resistance	(199)
2011	Doxorubicin, Vincristine, Etoposide, Cisplatin, Fludarabine, Methotrexate, Nilotinib and Imatinib. Trans-retinoic acid (ATRA)		UCH1	High doses used for effect. The addition of ATRA improved cell kill. Imatinib no effect. Doxorubicin killed all cells at 10uM	(200)
2011	Tyrphostin (AG1478)	EGFR	UCH1	Inhibition of proliferation	(180)
2010	CDDO-Me (synergistic effect with Cisplatin and Doxorubicin)	STAT3, Src	UCH1, CH8 (GB60)	Inhibition of proliferation and apoptosis	(201)
2010	Doxorubicin, Cisplatin, Methotrexate, Zalypsis, Paclitaxel, Yondelis		UCH1, CH8, (GB60)	MTT assay, reduced proliferation	(202)
2009	SD-1029 (+Cisplatin or Doxorubicin)	STAT3 inhibition (JAK2 inhibition)	UCH1, CH8 (GB60)	MTT assay, reduced proliferation	(88)
2009	PI-103 (+/- Cisplatin or Doxorubicin)	PI3K/mTOR inhibition	UCH1	Reduced proliferation and induction of apoptosis	(192)
2009	Rapamycin	mTOR	UCH1	Reduced proliferation	(203)

Some of the cell lines described as generated from chordomas has not been fully characterised, and have not become part of the ATCC repository. Indeed the GB60 cell line has been shown not to represent chordoma(197). U-CH1, U-CH2, MUG and JHC7 are all well characterised (www.chordomafoundation)

Table 1.2 Overview of targeted therapy used in the treatment of chordoma

Year	Drug	Target	Number of patients treated	Effect	Adjuvant therapy	Additional details	Reference
2014	Bevacizumab & Erlotinib	VEGF-A & EGFR	3	Stable disease	Surgery & radiotherapy	All three patients had progressive disease and all achieved long term stable disease (2-4 years follow up).	(176)
2013	Rapamycin	mTOR (mTORC1)	1	Reduced growth rate, clinical improvement	Surgery & radiotherapy	Patient-derived sample used: Rapamycin tested in cell line generated from patient tumour sample. Cell line used to generate xenograft, treated with Rapamycin (reduced growth/histological changes). The patient responded with reduced tumour growth rate. Tumour genome showed PTEN loss & KRAS mutation.	(193)
2013	Imatinib & metronomic cyclophos-phamide	PDGFR, c-Kit	7	Symptomatic relief, stable disease.	Surgery & radiotherapy .	All had progressive disease prior to treatment, all achieved SD with 42% PFS at 12 months. 2 of 7 patients previously treated with Imatinib as single therapy.	(204)
2013	Lapatinib (phase II)	EGFR/ ErbB2	18	PR 6 patients (33%), SD 7 patients (38.9%). Clinical benefit reported by 22% of patients.	Surgery & radiotherapy	Phase II study;18 patients with metastatic or locally advanced EGFR-positive chordoma treated with lapatinib. 16 of the 18 patients had prior therapy with imatinib	(179)
2012	Imatinib (phase II)	PGDFR	50	1 PR (RECIST) 13/26 (Choi), 35 SD, 14 PD, 9 SD. 64% reported clinical benefit.	Surgery & radiotherapy	Phase II study involving 50 patients with locally advanced or metastatic chordoma expressing PDGFR, 1 PR (by RESIST), 35 SD. 64% reported clinical response. Minor dimensional response was detected in <20% of patients. Median PFS 9 months.	(171)
2011	Imatinib	PDGFR	1	PD	Surgery	Sacral tumour with lung and brain metastases. Progression of metastases on Imatinib.	(205)
2011	Erlotinib (Imatinib)	EGFR	1	Regression of thoracic lesion (12months). Symptomatic relief.	Surgery	Pelvic tumour, lung metastases, disease progression on Imatinib. Relapse tumour biopsy with > 90% of tumour cells showing strong staining for EGFR.	(206)
2010	Imatinib	PDGFR	16	Pain relief (54%), 5- and 10 year survival 76% and 59%)	3/22 patients received adjuvant radiotherapy	Progressive disease, local and/or metastatic disease.	(207)

2009	Imatinib	PDGFR, KIT	3	1x SD, 2xPD Single agent not found to have efficacy	Not recorded	Target driven study of imatinib in paediatric solid tumours. The patient with initial SD subsequently had progressive disease and died.	(208)
2009	Erlotinib	EGFR	1	Partial responds (11months)	Sacral, relapse LN involvement	Progressive disease, refractory to radiotherapy and imatinib.	(209)
2009	Sunitinib	VEGFR, PDGFR, KIT, FLT3	9	44% SD (RECIST)	Surgery & radiotherapy	Qualitative decrease in tumour density was observed	(174)
2009	Cetuximab & Gefitinib	EGFR	1	PR with clinical improvement	Cervical lesion, local relapse	Symptoms of cord compression relieved by treatment. Reduction of tumour size.	(175)
2009	Imatinib & Sirolimus	PDGFR-β, mTOR	10	1 PR (RECIST) 7 PR (Choi) 1PD, 89% clinical improvement	6/10 previously received adjuvant radiotherapy	Patients progressing on Imatinib (+/- cisplatin). 50% (5 patients continuing treatment for regressive disease) 50% came off treatment as disease progression on treatment	(169)
2007	Imatinib & Cisplatin	PDGFR-β	6	PET response and clinical improvement, 4 patients had SD on CT/MRI	Surgery & radiotherapy Progression on Imatinib	Addition of low dose cisplatin (25mg/m2/week) showed synergistic effect and restored response to Imatinib.	(168)
2006	Cetuximab & Gefitinib	EGFR	1	PR; regression of all lesions (9 months)	Surgery	Sacral, local relapse with LN and pulmonary disease	(173)
2005	Imatinib	PDGFR, c-KIT, BCR-ABL	18	11% dimensional response, 61% radiological signs of tissue response	Surgery	Follow-on reporting of patients from 2004 paper (ASCO meeting)	(167)
2004	Imatinib	PDGFR, c-KIT, BCR-ABL	6	Symptomatic relief	Surgery	Anti-tumour effect, all patients +ve for PDGFRb. 2005 update of data now a total of 18 patients with continued effect.	(210)
PR: partial response, SD: stable disease, PD: progressive disease							

1.5 Novel therapies

With the lack of treatment options and minimal effect of current therapies for the treatment of chordoma, alternative approaches are needed. One such approach could be gene therapy, which is currently undergoing a renaissance in the field of cancer treatment. A gene therapy approach is reported as part of this thesis (Chapter 3) involving preclinical studies utilising an Adeno-Associated viral vector delivering RNA interference (RNAi) targeting brachyury.

1.5.1 Gene therapy

Gene therapy was conceptualised in the 1970s and refers to the transfer of genetic material, using a vector, with the intention of altering gene expression to prevent, halt or reverse a pathological process(211). The European Medicines Agency (EMA) defines a gene therapy medicinal product as a biological medicinal product with the following characteristics: (A) it contains an active substance which contains a recombinant nucleic acid administered to human beings with a view to regulating, repairing, replacing, adding or deleting a genetic sequence; (B) its therapeutic, prophylactic or diagnostic effect relates directly to the recombinant nucleic acid sequence it contains, or to the product of genetic expression of this sequence(212).

1.5.2 History of gene therapy

Frederick Griffith, a British bacteriologist researching the epidemiology and pathology of bacterial pneumonia, published a report in 1928 describing transformation of one pneumococcal type to another *in vivo*. By observing that mice infected with a living bacteria of the non-virulent R form of Type I pneumococcus, and co-infected with heat-inactivated bacteria of the virulent S form of Type II pneumococcus, developed pneumonia and died, he developed the idea that a virulence factor or information determining virulence could be transferred from one bacteria to another. The transformation of bacteria was subsequently observed *in vitro* by Dawson and Sia in 1931(213,214) and in 1944 the transforming substance was identified to be deoxyribonucleic acid (DNA)(215).

Key research in the development of gene therapy was performed by Joshua Lederberg, a geneticist and microbiologist, who received the Nobel Prize in 1958 for his work on bacterial genetics. He introduced the term “transduction” following the discovery of bacteriophages, and uncovered their ability to transfer DNA from one bacterium to another. This discovery was significant as it explained how bacteria of

different species could gain resistance to the same antibiotic very quickly. The understanding that phages transfer genetic material brought about their development as gene transfer tools and further extended research to eukaryotic viruses(216,217). Initial proof-of-concept studies demonstrating that viruses were capable of mediating gene transfer(218) led to the first human gene therapy trial for arginase deficiency in 1973(219,220). This first attempt at human gene transfer with therapeutic intent involved a wild-type virus with no added recombinant DNA. The aim was to transfer a functional arginase gene from the virus itself. The attempts were unsuccessful, and later it was discovered that the Shope Papilloma virus used did not encode for arginase(221).

While the emergence of recombinant DNA technology(222-224) brought about the development of functional gene-expressing units, major challenges remain. In particular the most efficient and safe way to deliver these therapeutic agents to patients still requires optimisation. Many mammalian viruses have been explored as gene delivery vectors, with adenoviral and retroviral vectors amongst the most commonly used gene transfer vectors in clinical trials (Figure 1.4). The first trial using a therapeutic gene involved two children suffering from adenosine deaminase deficiency (ADA-SCID)(225). The study did not demonstrate therapeutic benefit, yet generated great enthusiasm for the potential of gene therapy. In 1999 a major setback occurred when a young man died following a high dose of adenovirus in a trial for ornithine transcarbamylase (OTC) deficiency(226).

The first successful cure using gene therapy came in 2000. Autologous bone marrow cells were transduced with Moloney retrovirus expressing the cytokine receptor interleukin-2 receptor gamma (IL2RG) and transplanted into patients, resulting in the development of a functional immune system in children with X-linked severe combined immune deficiency (SCID)(227). The success was tempered by the fact that 5 of the 20 patients treated developed leukaemia due to the clonal expansion of T-lymphocytes derived from the modified haematopoietic stem cells. This transformation was driven by aberrant expression of the LIM domain only 2 (*LMO2*) proto-oncogene as a result of transcriptional read-through from the viral promoter of the integrated retroviral cassette(228,229). The safety of Moloney retroviruses remains a cause for concern although clinical efficacy and safety has been reported following the development of a self-inactivating retrovirus(230). Further safety measures have included the use of lentiviral vectors, which has substantially increased in recent years. Whilst lentivirus also integrates into the host cell genome, the frequency of integration at promoter sites

is substantially lower than that seen with retrovirus(231). Consequently the risk of insertional mutagenesis is lowered and, to date, no patients have developed malignancy(211,232). Despite such improvements, further assessment of these vectors is required, if they are to be used widely in the clinic(233,234).

Another class of viral vectors are those that remain predominantly episomal and at the forefront of these is the Adeno-Associated Virus (AAV). Recent years have seen a dramatic success using AAV vectors for the treatment of monogenic disorders with specific protein deficiencies such as haemophilia B(235), Lebers congenital amaurosis(236), Parkinson disease(237) and α-1 anti-trypsin deficiency(238). Two gene therapy therapeutics utilising AAV vectors have been licensed for use. The first gene therapy product to be licensed in Europe was Glybera, utilising an AAV vector for delivery of the human lipoprotein lipase (LPL) gene by intramuscular injection in patients with lipoprotein lipase deficiency (LPLD)(239-244). The US Food and Drug Agency (FDA) has not yet approved Glybera. The FDA has not yet approved a gene therapy product but in 2014 the gene therapy product MYDICAR was granted designation by the FDA. MYDICAR utilises an AAV vector for delivery of a copy of *SERCA2a* gene, linked with systolic dysfunction, into the patient's cardiac muscle in order to restore the SERCA2a enzyme in patients with heart failure(245,246).

While replacement gene therapy is the basis for the majority of gene therapy clinical trials for inherited disorders, these represent less than 8% of all gene therapy clinical trials conducted(247). Since 1989 more than 1800 gene therapy clinical trials have been conducted. More than 60% of these trials have been against cancer and have accounted for more than 80% of patients entered into gene therapy clinical trial(248,249) (Figure 1.1). The majority are phase I and phase II trials (Figure 1.2).

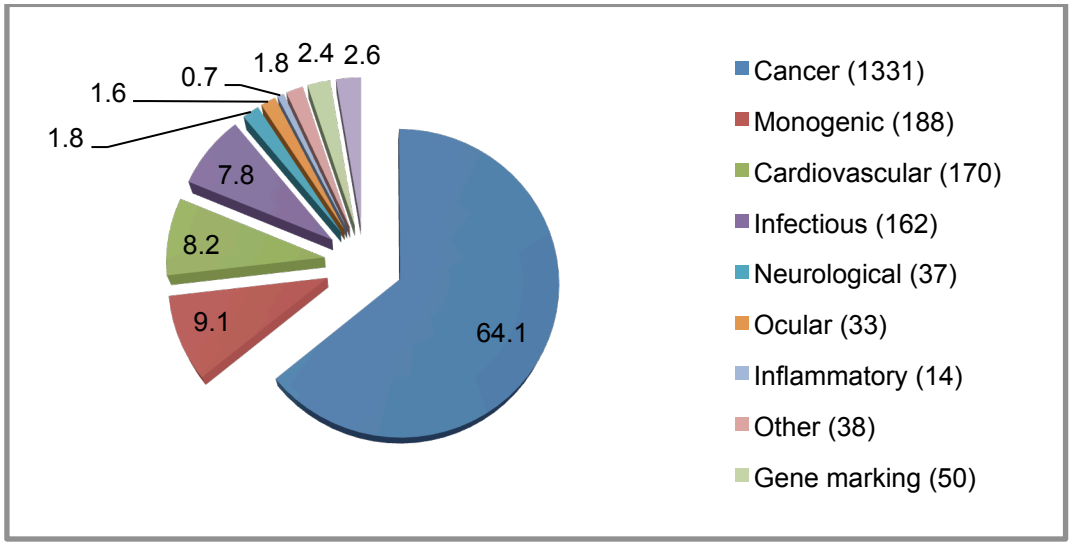

Figure 1.1 Review of indications for the use of gene therapy
Indications addressed by gene therapy in clinical trials. Initial studies were on monogenetic diseases, but cancer soon became the major interest. Source: The Journal of Gene Medicine, Wiley and Sons. Accessed February 2015.

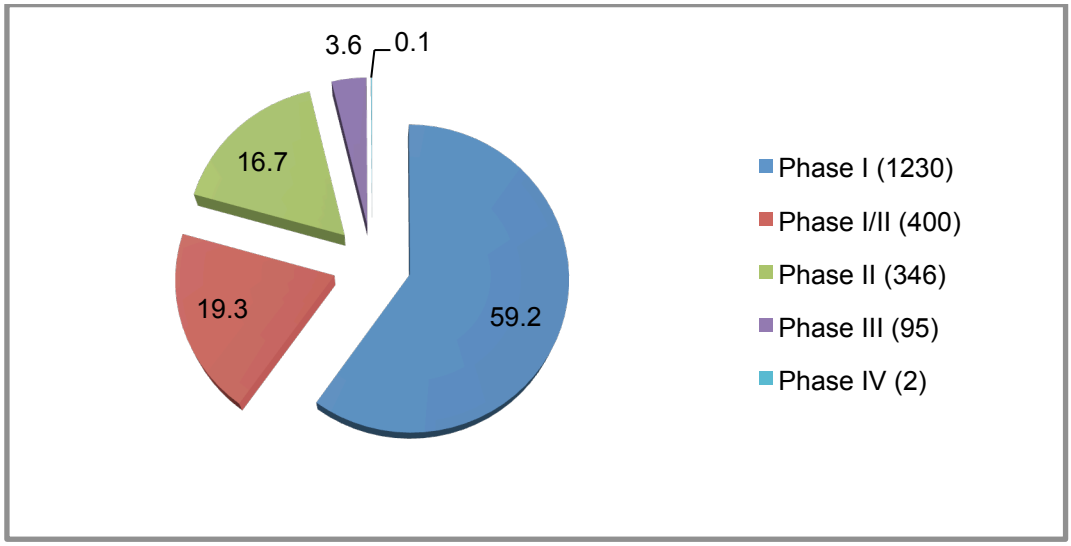

Figure 1.2 Review of the current trial phases for gene therapy
Source: The Journal of Gene Medicine, Wiley and son. Accessed February 2015.

1.5.3 Gene therapy's potential applications for cancer therapy

Numerous potential therapeutic targets involved in the regulation of pathogenic processes of tumours are amenable to gene transfer. These include genes involved in angiogenesis, tumour growth, invasion, metastasis, and immune response against tumours(250,251). Inter-tumour heterogeneity and treatment resistance has led to a range of strategies for targeting cancer using gene therapy, including: (a) inserting a wild-type tumour suppressor gene to compensate for its loss/deregulation; (b) enhancing tumour sensitivity to conventional drug/radiation therapy using an oncolytic virus carrying a suicide gene, and inducing apoptosis; (c) enhancing immunogenicity of the tumour to stimulate immune cell recognition; (d) blocking expression of an oncogene by using an antisense (RNAi) approach(252).

1.5.3.1 Regulation of tumour suppressor gene (a)

Tumour suppressors act as "cellular guardians" by inhibiting cell growth pathways and/or by inducing cellular apoptosis, consequently preventing cancer formation. One of the most important tumour suppressors is *TP53*, which functions as a sensor of DNA damage and other cellular and metabolic stresses including hypoxia(253). In response to stress, *TP53* induces cell cycle arrest and subsequent DNA repair, senescence or apoptosis, depending on the level of cellular compromise(254,255). Many types of cancer show a high incidence of *TP53* mutations and disturbance of the *TP53* signalling pathway is believed to be required for the development of most cancers(256-258). Evidence suggests that restoration or activation of *TP53* function will have significant therapeutic benefit(257). Strategies targeting *TP53* have been developed including gene therapy to restore *TP53* function, inhibition of *TP53*-*MDM2* interaction, as well as *TP53*-based vaccines(257,259,260). Some of these TP53-targeted therapies have entered clinical trials(253). *TP53* gene therapy using an adenoviral vector Ad-p53 (Gendicine) was approved in China in 2003 without data from a standard phase III clinical trial(261,262). Subsequent publications have reported a good safety profile and efficacy in combination with radiotherapy in hepatocellular carcinoma(263) and advanced nasopharyngeal carcinoma(264). This is in contrast to a study in ovarian cancer which did not reveal any therapeutic benefit(265). Nearly 2500 patients have received treatment in China(266). Two years after the approval of Gendicine the Chinese State Food & Drug Administration (SFDA) granted approval of another gene therapy product, Oncorine. The gene therapy products have not been approved in the US or Europe as efficacy has not yet been established(260). *TP53* vaccine-based studies have also entered early phase clinical trials. Phase I/II clinical trials of a TP53 synthetic vaccine for the treatment of metastatic colorectal cancer(267) and small lung

cell cancer(268) found it to be well tolerated and generating a specific anti-TP53 immune response. MDM2 small molecule inhibitors of the MDM2-TP53 protein-protein interaction are currently being evaluated in human clinical trials for cancer treatment(260,269).

1.5.3.2 Oncolytic virus (b)

Gene therapy strategies involving oncolytic virus therapy were first introduced in the 1950s but the field has been slow to develop(270,271). Oncolytic viruses selectively replicate in tumour cells with the burden of viral progeny eventually resulting in lysis of the malignant cell. In addition to mediating direct destruction of the host cell, it also results in the release of tumour-derived antigens, providing relevant antigenic targets for T-cell activation(272) and stimulation of a system-wide anti-tumour immune response(273). Oncolytic Herpes Simplex Virus (HSV) vectors expressing immune stimulatory genes such as granulocyte-macrophage colony-stimulating factor (GM-CSF) or suicide genes such as thymidine-kinase (tk) or cytosine deaminase (CD), have been developed to maximise tumour destruction(274). So-called 'suicide genes' are enzymes that mediate the conversion of a pro-drug into a cytotoxic product. In addition to inducing apoptosis of the malignant cell, it can increase the cells susceptibility to chemotherapy and radiotherapy(249,275-278). Viral thymidine kinase (HSV-tk) mediates the conversion of the inert pro-drug Ganciclovir into Ganciclovir monophosphate, which is then rapidly converted into the toxic purine analogue Ganciclovir triphosphate. Incorporation of this molecule inhibits DNA synthesis, resulting in the apoptosis of the malignant cell(279,280). In a similar manner, the suicide gene CD converts the relatively non-toxic 5-fluorocytosine (5-FC) molecule into 5-fluorouracil (5FU), a known anti-cancer drug(276,281,282). In a phase II study for prostate cancer, the utility of an oncolytic adenovirus with two cytotoxic gene systems CD/5-FC and HSV-1 tk/ganciclovir demonstrated clinical benefit when combined with radiotherapy(283). The first oncolytic virus approved for a phase III clinical trial was an oncolytic HSV vector encoding human GM-CSF for treatment of metastatic melanoma. The data demonstrated durable tumour response with reduction in size in approximately two-thirds of the tumours injected. The therapeutic product, Talimogene Laherparepvec (T-vec) is being considered for approval by the FDA(284-286).

1.5.3.3 Immunotherapy (cancer vaccines) (c)

Different types of immunotherapy strategies have been applied for cancer treatment. Some of these approaches currently in trial include the development of vaccination using tumour cells or antigen presenting cells (APCs), engineered to express immune-

stimulatory GM-CSF to elicit an immune response against the cancer cells(248,287,288). Tumour-associated antigens can be recognised by the immune system, however these antigens often evoke only weak immune responses, as they are usually 'self' antigens(289). To prevent autoimmunity, immune cells capable of targeting such antigens with high affinity have been purged or suppressed through central and peripheral tolerance mechanisms(287,289). In addition many cancers have developed a range of immune evading mechanisms to avoid eradication(290). To overcome the immune-suppression and to develop a successful vaccine, the vaccine must induce a cytotoxic T-lymphocyte (CTL) response rather than rely on an innate antibody response(291). Various approaches for generating cancer vaccines have been developed over the past 20 years with more than 175 reported clinical trials, with less than 10% of recipients of cancer vaccines demonstrating clinical response(248,289,292,293).

Of specific interest for the treatment of chordoma is a phase I/II clinical trial conducted under the National Cancer Institute (NCI) (NCT01519817) using a yeast-brachyury vaccine (GI-6301) in patients with advanced solid tumours including chordoma(294). Brachyury, like other transcription factors, is localised to the nucleus; however, brachyury peptides have been found to be expressed on the surface of some carcinomas in the context of major histocompatibility complex (MHC) class I molecules(103). Preclinical studies have demonstrated that brachyury-specific T-cells can lyse human chordoma cells expressing brachyury in an MHC restricted fashion(294). In this vaccine-study the yeast *Saccharomyces cerevisiae* has been genetically modified to express the full-length brachyury gene to stimulate an antigen specific T-cell response. The vaccine was tested in xenografts (carcinoma murine models) where the vaccine elicited a CD4+ and CD8+ T-cell response capable of reducing tumour burden. In view of involvement of brachyury in EMT, toxicity was assessed through monitoring wound healing and embryonic development. No toxicity was observed(295,296). Early clinical data has been encouraging, suggesting that patients with chordoma can elicit a brachyury specific T-cell immune response(297). Disease assessment has shown evidence of clinical benefit with stable disease or partial response. The early phase trial demonstrated safety and immunogenicity of the vaccine and has lead to a phase II clinical trial enrolling patients for a randomised trial receiving radiotherapy with or without the GI-6031(298). It will be of interest to discover if this approach improves local control.

The first FDA-approved immunotherapy product was the therapeutic vaccine Sipuleucel-T, for treatment of metastatic prostate cancer, approved in 2010, and subsequently by the EMA under Advanced Therapy Medicinal Product (ATMP) or gene therapy in 2013. This therapeutic vaccine involves the harvesting of individual patients' white blood cells, primarily APCs (dendritic cells), by leukapheresis. Harvested cells are incubated with a fusion protein consisting of antigen prostatic acid phosphatase (PAP), which is present in 95% of prostate cells and GM-CSF to enhance immune response. Cells are reinfused into the same patient to stimulate a T-cell response against PAP-GM-CSF and consequently against cancerous prostatic cells. The overall survival was prolonged for men with metastatic prostate cancer, though disease-free interval was not increased(299-303). The product is considered too expensive for the NHS and has not been introduced in the UK. A recent phase I trial for patients with metastatic prostate cancer has shown tolerability and early data suggest response when combining Sipuleucel-T with Ipilimumab(301,304).

Additional T cell-based immunotherapy such as chimeric antigen receptors (CARs) and engineered tumour specific T-cells (CAR-T cells) developed to confer specificity to tumour-associated antigens is a rapidly developing field(305). Application has mainly been in haematologic malignancies(306), although preclinical studies and early phase clinical trials exploring the potential application in targeting solid tumour antigens with CAR-T cells are on-going(307).

1.5.3.4 RNA interference (d)

RNA interference (RNAi) is a naturally occurring endogenous, evolutionary conserved and sequence-specific post-transcriptional mechanism of gene silencing. The technique exploits mechanisms that repress protein expression by degradation of mRNA thereby effectively resulting in silencing gene expression. In primitive organisms, RNAi is involved in several processes such as cell growth, tissue differentiation, hetero-chromatin formation and cell proliferation(308). RNAi also protects the genome from viruses by suppressing active replication of the virus-like transposable element, likely to be fossilised remnants, present in the human genome(309-312), and regulates gene expression during development(313-315). Dysfunction in the RNAi pathway is linked to cardiovascular diseases(316), neurological disorders(317), and cancer(318,319).

The discovery of RNAi followed observations that the introduction of the chalcone synthase gene into petunias to increase the intensity of their purple colour

paradoxically resulted in areas of hypopigmentation(320,321). Further work by Fire and colleagues in *C. elegans*, demonstrated that introducing long double-stranded RNA (dsRNA) led to targeted degradation of homologous RNA(322,323). Subsequently, RNAi was found to be a highly conserved mechanism in eukaryotic cells(324) and interest in the technology increased when observed that RNAi provided a tool for studying gene function in mammalian cells(325-328).

The spectrum of gene therapy applications has further increased with the use of small nucleic acids(247,329). The ability of small interfering RNA (siRNA) to silence target genes with high efficiency and specificity has stimulated efforts to develop these molecules as therapeutic agents. This approach is of interest for cancer therapy where many key therapeutic targets remain beyond current treatment options(330,331). Transcription factors are known to be non-targetable and brachyury is such a target. Silencing of brachyury in two different chordoma cell lines using short hairpin RNA (shRNA) delivered by lentiviral vectors, resulted in cell death and cell senescence, emphasising brachyury's role in the pathogenesis of chordoma. This work provided the rationale for developing a gene therapy approach for the treatment of chordoma(89,91).

1.5.4 The mechanism of RNAi

RNAi is the process of sequence-specific post-transcriptional gene silencing triggered by double-stranded RNA(327,332). The actions of RNAi can be mediated either through the chemically synthesised siRNA or the shRNA transcribed from a DNA expression vector(333,334).

When double-stranded RNA (dsRNA) composed of a passenger (sense) strand and a guide (antisense) strand is imported into the cytoplasm, it is cleaved into short fragments by the ATP-dependent ribonuclease (RNase III) enzyme Dicer(335,336). Dicer cleaves the long dsRNA, molecules into short double stranded fragments of ~22 nucleotides of mature microRNA (miRNA) or siRNAs(337). With the assistance of Dicer, miRNA is loaded onto the intracellular Argonaute protein containing RNA interfering silencing complex (RISC). One strand of the siRNA, the sense strand, is degraded(338). RISC loaded with the anti-sense strand attaches with the complimentary base pairs in a messenger RNA molecule inducing cleavage, degradation, and sequestration. Endonucleolytic cleavage of the target mRNA is mediated by Argonaute, the catalytic component of the RISC complex, leading to post-transcriptional gene silencing(327,328,339).

Unlike siRNA, vector-driven-expression of shRNA needs to be transcribed in the nucleus. ShRNA can be transcribed from the RNA polymerase III or modified polymerase II promoter, following a plasmid transfection or delivery through infection (transduction) using virally produced vectors, some of which facilitate DNA integration and long term stable expression, compared to the short-term silencing achieved by siRNA(340-342).

Transcribed shRNA consists of two complementary 19–22 base pairs (bp) RNA sequences linked by a short loop of 4–11 unpaired nucleotides (nt) similar to the hairpin found in naturally occurring pre-miRNA(343). This structure is processed in the nucleus by a microprocessor complex containing the RNase III enzyme Drosha, and the double-stranded RNA-binding domain protein DGCR8(344,345). The processed primary transcript is the pre-shRNA molecule, which is transported to the cytoplasm by Exportin 5(345,346). In the cytoplasm the pre-shRNA is loaded onto the complex containing the RNase III enzyme Dicer and the double-stranded Tat-RNA binding protein (TRBP) or the RNA-dependent protein kinase activating protein (PACT) where the transcript is processed, removing the loop, to form a double-stranded siRNA(341,343,347,348). The Dicer containing complex coordinates loading onto the Argonaute (Ago2) protein containing the RISC. The Ago2 protein contains the endonuclease activity necessary to cleave and release the passenger strand of the double stranded stem(338,349,350). Ago2 protein complex loaded with guide-strand siRNA seeks out complimentary target sites in mRNAs where endonucleolytically active Ago2 cleaves mRNA to initiate mRNA degradation and post-transcriptional gene silencing(332,341).

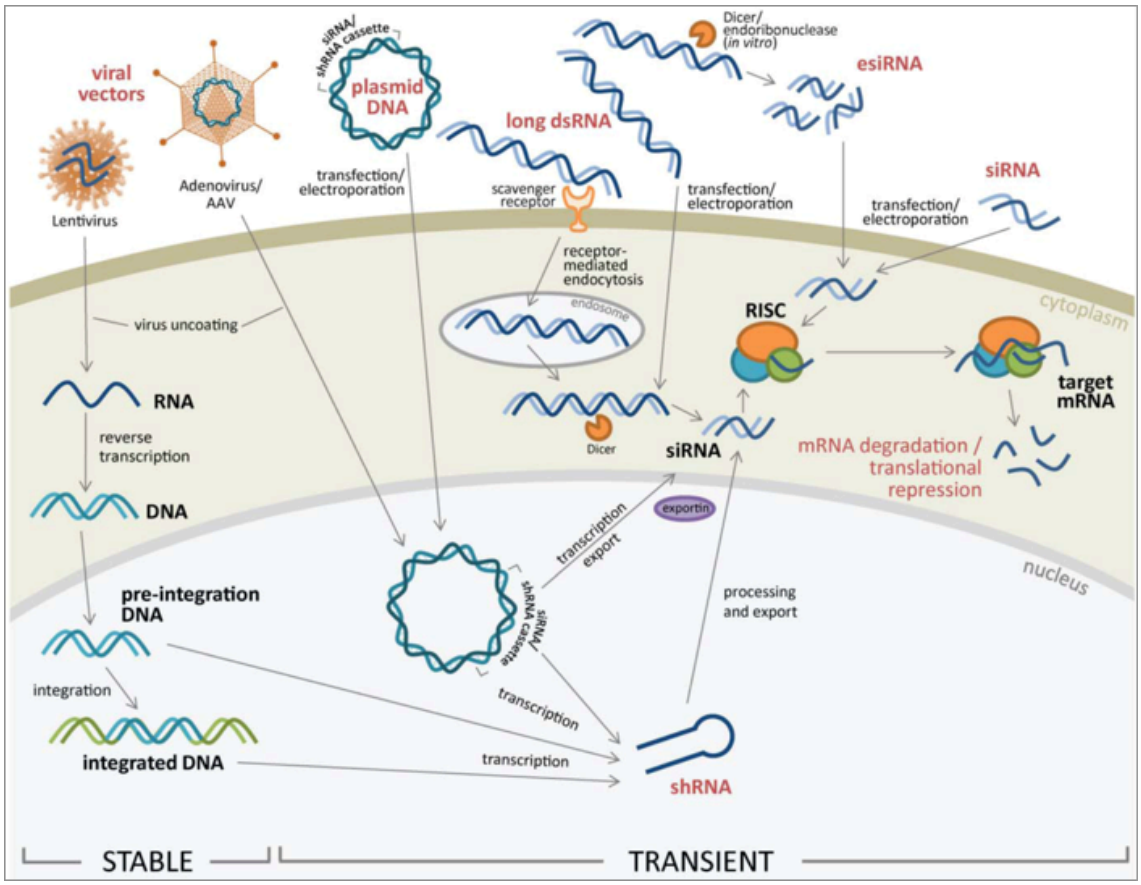

Figure 1.3 Vectors and RNAi construct processing in target cells
Naked RNAi constructs can be introduced to target cells in forms of siRNA or long dsRNA using a variety of transfection protocols such as lipid-based transfection reagents or electroporation, or active uptake by target cells through receptor-mediated endocytosis. Once inside the cytoplasm, RNAi constructs can be further processed by host endonucleases or directly loaded into RISC to facilitate gene expression knock down. Alternatively, RNAi can be introduced using viral vectors, such as lentiviral-, adenoviral- or AAV vectors carrying siRNA or shRNA expression cassettes. Once transcribed, shRNA can be processed and exported to cell cytoplasm for silencing gene expression. Figure used with permission from Professor Tripp(351).

Alternative methods for gene silencing include gene-editing technologies using programmable nucleases include zinc-finger nucleases (ZFNs), transcription activator-like effector nucleases (TALENs), and RNA-guided engineered nucleases (RGENs) from the type II clustered regularly interspaced short palindromic repeats (CRISPR) CRISPR-associated protein 9 (Cas9) system. These methods are now widely used for genome editing in higher eukaryotic cells and whole organisms(352,353) and have revolutionised almost every discipline in biological research, medicine and biotechnology. Each of these nucleases have their advantages and disadvantages, including specificity with off-target mutations at sites similar in sequence to on-target sites, limiting their utility in many applications including gene or cell therapy(354-356). These methods have not been utilised for the work presented in my thesis.

1.5.4.1 Clinical application of RNAi

The first clinical data on RNAi-based therapy was reported in 2005 from a phase I trial using siRNA targeting Vascular Endothelial Growth Factor Receptor 1 (*VEGFR-1*), a receptor in the pathway mediating blood vessel growth, for the treatment of age-related macular degeneration (AMD)(357). The single intravitreal siRNA dosing was well tolerated and resulted in stabilisation or improvement of visual acuity(358). The number of RNAi-based pre-clinical and clinical trials have grown over the last few years and have included studies focussed on viral infections, respiratory disorders, haemophilia, cardiovascular diseases, metabolic diseases and cancer(330,359).

1.5.5 RNAi in cancer therapy

The ability of RNAi to silence target genes has stimulated efforts to develop molecules for use as therapeutic agents. Cancer cell survival, unlike normal cellular survival, is dependent on a limited subset of signalling interactions through mutated or dysregulated genes(256,360).

SiRNA and shRNA have been used in high throughput screens for studying gene function in mammalian cancer cell lines(361-368). A number of preclinical studies targeting genes critical for tumour cell growth, metastasis, angiogenesis and chemotherapy resistance have identified key regulators in diverse biological pathways(290,359,369-372). Potentially, all identifiable genes can be targeted for gene silencing(341,373) however, careful selection of the target gene is critical to minimise/circumvent any effects upon healthy tissue. Consequently, for selective treatment of tumour cells, RNAi must be selected to target genes specifically involved in the growth and survival of the malignant cell. Targeting a driver of the disease may have the added benefit of reducing the ability of the tumour cells to acquire resistance. An additional strategy to minimise the impact of gene silencing in healthy tissues is to achieve targeted delivery and selective expression of shRNA to the tumour cells(211,374,375).

The first proof-of-concept study in man utilising systemic siRNA, delivered by targeted nano-particles, was undertaken on patients with metastatic melanoma. The predicted cleavage product of Ribonucleotide reductase M2 (RRM2) mRNA was detected from one patient who received the highest dose of nanoparticles. Therapy was well tolerated and no dose-limiting toxicities were observed. The effect on tumour reduction and clinical phenotypes were not reported(376). A small number of early phase clinical trials using siRNA in cancer have been reported. One: ALN-VSP trial, used lipid

nanoparticles (LNP)-formulated siRNA dual targeting *VEGF* and Kinesin spindle protein (*KSP*), formulated for intravenous administration to patients with solid tumours. A total of 41 patients were included: 3 patients showed a partial response or stable disease maintained after 19 months of treatment, and one patient with metastatic endometrial cancer demonstrated a complete response according to the RECIST criteria. Treatment consisting of twice weekly infusions was generally well tolerated. Toxicity included dose-dependent pro-inflammatory cytokine induction(377). Another early phase trial targeting polo-like kinase 1 (*PLK-1)*, a protein involved in tumour cell proliferation, confirmed tolerability and in some cases tumour response(378). In a study for patients with Glioblastoma multiforme (GBM) 46 patients received treatment delivered as naked RNAi, administered as double stranded RNA, targeting tenascin-C mRNA (ATN-RNA). The molecule of ATN-RNA was injected into the postoperative area resulting in improvement in progression free and overall survival, supporting site-specific delivery of therapy to achieve higher effective concentration in the tumour bypassing the blood-brain barrier while limiting the potential system exposure to drug degradation(379-381). These early phase trials have highlighted the feasibility of delivering siRNAs into tumours, demonstrating a good safety profile and an on-target effect(377,382). Current early phase cancer trials using RNAi are summarised in Table 1.3

Table 1.3 RNAi-based therapeutics in clinical cancer trials

RNAi therapeutics in clinical trials for cancer						
DISEASE	**TRIAL**	**TARGET**	**CARRIERS**	**TRIAL STATUS AND REMARKS**	**CLINICAL TRIAL ID**	**REF**
Solid tumours	CALAA-01	RRM2	Cyclodextrin NP	Phase I; terminated; details pending. First study using NP to target solid tumours	NCT00689065	(376)
Solid tumours	ALN-VSP2	VEGF/KSP	LNP		NCT01158079	(377)
Neuroendocrine tumours Adrenocortical carcinoma	TKM-PLK1	PLK1	LNP	Phase I/II; recruiting	NCT01262235	(378)
Pancreatic cancer	SIG12D LODER	KRAS-G12D mutant	LODER polymer	Phase II; not yet recruiting. First to target undruggable mutation in cancer	NCT01676259	(383)
Advanced, recurrent or metastatic solid malignancies	EPHARNA	EphA2	LNP	Phase I; start March 2015	NCT01591356	(384)
Metastatic melanoma	iPsiRNA	LMP2, LMP7, MECI1	Ex-vivo transfection	Phase I; completed	NCT 00672542	(385)
Advanced, recurrent or metastatic solid malignancies	Atu027	PKN3	LNP	Phase I; completed. First siRNA trial aimed at inhibiting metastasis	NCT00938574	(386)
Chronic lymphocytic leukaemia	SPC2296	BCL-2	LNA	Phase I/II	Not registered	(387)
Advanced, recurrent or metastatic solid malignancies	FANG	Furin	Autologous tumour cell vaccine	Phase II	NCT01309230	(388)

LNP (lipid nano-particles), LODER polymer, NP (nano-particles) LNA (locked nucleic acid); BCL-2, B-cell CLL/lymphoma; LMP2, also known as proteasome subunit beta type 9 (PSMB9); LMP7, also known as proteasome subunit beta type 8 (PSMB8); MECL1, also known as proteasome subunit beta type 10 (PSMB10); PKN3, protein kinase N3; PLK1, polo-like kinase 1; RRM2, ribonucleoside-diphosphate reductase subunit M2; VEGF, vascular endothelial growth factor, FANG vaccine (GM-CSF, bi-shRNAi targeting Furin convertase with then down regulation of TGF). Table adapted from Sherry Y. Wu 2014 and Beverley Davidson 2011(330,359)

1.5.6 Factors influencing activity of RNAi-based therapies

1.5.6.1 siRNA

There are many challenges to overcome in the process of moving RNAi-based therapies from the laboratory to the clinic. The major barrier facing siRNA therapeutics is the delivery to the desired cell type, tissue, or organ. siRNAs do not readily pass through the cell membrane due to their size and negative charge(359). Post-injection, the siRNA complex must navigate the circulatory system of the body avoiding kidney filtration, uptake by phagocytes, aggregation with serum proteins and enzymatic degradation by endogenous nucleases(389). Effective delivery also includes avoidance of host defence mechanisms(390). siRNA can induce non-specific activation of the immune system through the toll-like receptor (TLR) 7/8 pathway(391-393). TLR protect the host from pathogens by detecting infectious non-self agents including double-stranded RNA. Activation of TLR results in production of interferon and inflammatory cytokines, thereby inducing an innate immune response(391,393,394). Identification of immune stimulatory motifs have allowed chemical modifications of siRNAs thereby inducing minimal immune response(391,395).

1.5.6.2 shRNA

An additional limitation of siRNA mediated RNAi is that target repression is transient. Although this may be sufficient in some situations, stable integration of shRNA expression vectors overcomes this limitation(396). Considerable research into the delivery of shRNA and the factors that govern efficacy of shRNA have resulted in the development of variations in shRNA design and promoter sequences(364,397,398). Appropriate choice of promoter for shRNA transcription is vital for effective vector delivered RNAi(399). An additional benefit using shRNA is the ability to control expression by the use of inducible promoters, thereby increasing the control over gene knockdown studies(400,401). Viral vectors contain potential immune-stimulators, including CpG DNA in the plasmid from bacterial DNA or the viral genome. The viral protein from viral particles, transferred into targeted cells or tissues, may induce not only T cell-mediated immune responses to transduced cells, but also humoral immune responses by generating antibodies to viral proteins and transgene products. These immune responses against vectors, transgene products and transduced cells can lead to transient expression of the therapeutic genes and re-administration inhibition of the recombinant vectors(231,402-404).

1.5.6.3 Toxicity of RNAi

Specificity of RNAi and careful selection of targets also needs to be considered for development of a therapy for cancer. RNAi techniques were initially believed to be highly specific, however several studies have shown that RNAi can cause silencing of other genes in addition to the gene intended(405,406). 'Off target' activity can complicate interpretation of phenotypic effects in gene-silencing experiments and can potentially lead to unexpected toxicity(407). Much effort has been put into the design of shRNAs to increase specificity and reduce off-target effects(408-411). Another factor to consider regarding safety and specificity of RNAi is the level of shRNA expression. Dose dependent liver toxicity and fatality was observed in mice transduced with AAV/shRNA(412). Cytotoxicity was thought to be due to saturation of the endogenous miRNA pathways as a result of high levels of exogenous siRNA and shRNA(412-414). More recently, the cellular toxicity of shRNAs in the nervous systems of animals injected with AAV vectors has been described - in particular, high-level expression of shRNAs in the dorsal root ganglia of rats(415) and in mouse striatum(416). Numerous factors influencing activity have been identified, including the loop sequence, thermodynamic properties of the hairpin, secondary structure, and the surrounding sequences(396). By altering the design of the shRNA structure toxicity can be reduced without compromising targeted gene silencing(414,417,418).

1.6 Vectors for gene therapy

The success of RNAi therapeutics relies heavily on the ability to deliver the RNAi in an efficient and safe manner to the intended target cells. Delivery systems can be categorised into physical methods, conjugation methods (transfection), natural carrier (viruses and bacteria) and non-viral carrier methods(419-421). Non-viral delivery vectors can be classified as organic systems such as lipid complexes and conjugated polymers, and inorganic systems such as magnetic nanoparticles and gold nanoparticles(422,423).

1.6.1 Nano-particles

Nano-medicine is an emerging multi-disciplinary field exploring avenues for cancer detection and therapy, with more than 30 nano-carries currently approved for clinical use(424). Nanocarrier-based approaches include a carrier, a targeting moiety that is bound to the carrier via specific conjugation chemistry, and a therapeutic effector such as chemotherapy compound or RNAi. Carriers may be composed of lipids, polymeric nanoparticles, or inorganic nanoparticles. Targeting moieties conjugated to the carrier include either include high affinity ligands, antibodies or nucleic acids(424).

Nanoparticles have been investigated extensively for siRNA delivery(389,425). Current delivery approaches of siRNAs include the use of stable nucleic acid lipid particles (SNALP), applied as liposomes, or LNP. The LNPs are uniform lipid bilayers or solid cores which can entrap various cytotoxic drugs: hydrophilic drugs will be trapped in the aqueous region while a lipophilic drug will be captured in the lipid leaflets(424). The combination of LNPs and siRNAs have been applied successfully in studies for gene-silencing in tumors and viral infections(369,376,426-428) and utilised in early phase clinical trials(330,377,429,430) (Table 1.3) These studies indicate nanoparticles are well tolerated when administered systemically by intra-venous, or intra-peritoneal injection or by intranasal route, and have demonstrated effective uptake into tumour cells(376,424).

1.6.2 Viral vectors for gene therapy

Viruses have evolved over millions of years to infect human cells efficiently, resulting in the transfer of their genetic material into the host cell as part of their replication process. These systems have been exploited in the development of viral-mediated gene therapy, replacing the pathogenic sequences from the viral genome with a DNA sequence of therapeutic interest. Currently several classes of viral vector are under investigation in the development of gene therapy for clinical use, including retroviruses and lentiviruses (both members of the Retroviridae family), adenoviruses, AAV and HSV (Figure 1.4). The choice of vector depends largely on the application. Desirable properties such as high titre production, efficient delivery, transgene expression, cell specificity and toxicity vary between viral vectors. A comparison of vectors can be found in Table 1.4.

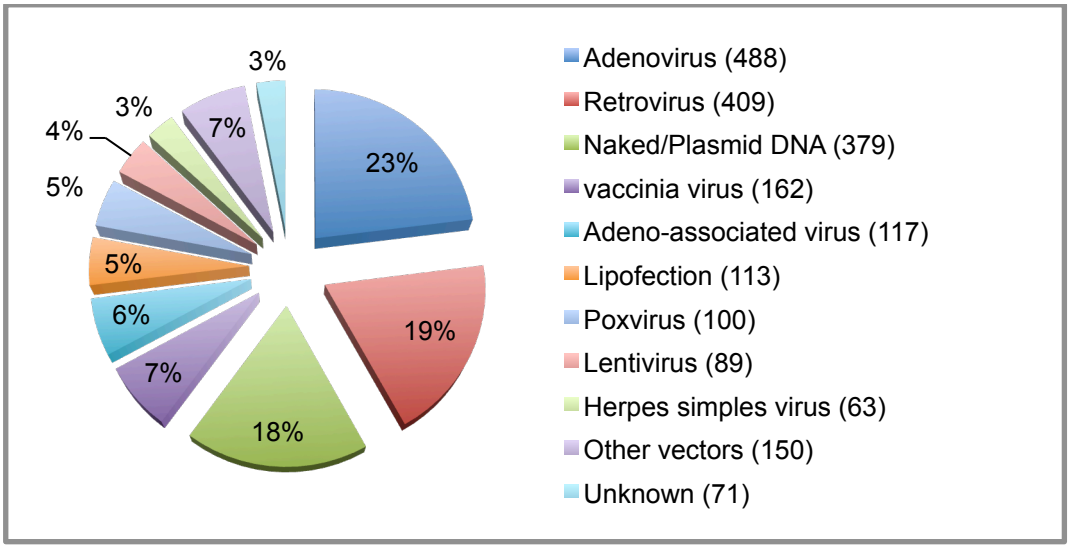

Figure 1.4 Vectors used for gene therapy
Overview of different gene transfer vectors used in clinical trials. Source: The Journal of Gene Medicine, Wiley and Sons (http://www.abedia.com/wiley/index.html). 13 of 89 trials utilised *in vivo* therapy. Database accessed April 2015.

Table 1.4 Properties of commonly used viral vectors

Vector	Genetic material	Transgene capacity	Tropism	Vector genome forms	Length of transgene expression	Main limitations	Main advantages	Use in clinical trials to date
Retrovirus	RNA	~9Kb	Broad Dividing cells only	Integrated	Long term	Only transduces dividing cells; Integration may induce oncogenesis	Persistent gene transfer in dividing cells	20.3% (362)
Lentivirus	RNA	~10Kb	Broad	Integrated	Long term	Integration might induce oncogenesis	Persistent gene transfer in most tissue	3.3% (67)
Herpes virus (HSV-1)	dsDNA	>30Kb	Broad, strong for neurons	Episomal	Transient	Inflammatory; transient gene expression in cells other than neurons	Large packaging capacity; strong tropism for neurons	3.1% (62)
Adenovirus	dsDNA	~30Kb	Broad	Episomal	Short term (weeks)	Capsid mediates a potent inflammatory response	Extremely efficient transduction of most tissue	23.5% (476)
AAV	ssDNA	<5Kb	Broad	>90% episomal <10% integrated	Medium to long term (years)	Small packaging capacity	Non-inflammatory; non-pathogenic	5.2% (105)

Adapted from Bouard et al. and Thomas et al. 2003. (431,432) and www.abedia.com.Wiley/vectors
AAV, Adeno-associated virus; dsDNA, double stranded DNA; ssDNA single stranded DNA

1.6.2.1 Integrating and non-integrating vectors

The main aim of gene therapy for genetic disease is to provide long-term therapeutic levels of gene transfer, to ameliorate or cure the clinical phenotype of the disease. The approach taken to achieve persistent expression of the therapeutic gene is often dependent upon the target cell. In cells that undergo regular division, integrating vectors, such as retrovirus or lentivirus, are necessary. Integration of the therapeutic gene into the host cell genome ensures it is copied during each mitotic event, providing stable, persistent expression of the therapeutic gene within the target cell population. In long-lived post-mitotic cells such as skeletal muscle(238), cardiac muscle(423,433), central nervous system(434) and liver cells(435), cell proliferation/turnover is minimal and the use of an integrating vector is less important. Consequently, non-integrating vectors such as AAV are commonly used to transduce such tissues as they ensure sufficient levels of gene expression whilst precluding the safety concerns associated with insertional mutagenesis(436). Lentiviral vectors have most frequently been used for gene transfer *ex vivo* in haematopoietic stem cells. In contrast AAV has, in the majority of trials, been used for *in vivo* transduction of post-mitotic cells(211). AAV has however also been used for the treatment of solid tumours in early phase clinical trials, underpinning the choice for using this vector for delivery of RNAi in chordoma, as reported in this thesis.

1.6.3 Adeno-associated viral vector

Vectors based on AAV are currently showing exceptional promise for gene therapy in the clinic(235,243,437). These vectors present an attractive gene therapy tool due to lack of pathogenicity and toxicity associated with wild type virus. More than 70% of adults are sero-positive for antibodies for one or more AAV serotypes(438), yet infection has not been associated with any symptoms or disease(439). AAV vectors are able to infect dividing and non-dividing cells of various tissue origins, thereby allowing efficient targeting of post-mitotic tissues while eliciting a low host immune response(439-441). The use of Recombinant AAV (rAAV) vectors in clinical trials started in the mid-1990s and present a proven safety profile with over 300 subjects enrolled in studies without any serious adverse events(437,441,442).

1.6.3.1 Adeno-associated virus biology

AAV was discovered in 1965 as a contaminant of adenovirus preparation(443). AAV is a non-enveloped virus with an icosahedral capsid of approximately 22nm which surrounds a single stranded DNA (ssDNA) genome of 4.7kb(444). Belonging to the

Parvoviridae family, AAV is classed as a *Dependovirus* as it requires a helper virus, such as adenovirus or herpes virus(445), to complete its replicative cycle(446,447). In the absence of a helper virus AAV establishes a latent infection within the cells, either by site-specific integration into the host genome(448-450) or by persisting in episomal form(451).

The AAV genome consists of a 145 nucleotide-long inverted terminal repeats (ITRs) that, due to the multipalindromic nature of its terminal 125 bases, can fold on itself and form a characteristic T-shaped hairpin structure(452) (Figure 1.5) The virus does not encode a polymerase but relies on host cell polymerase for DNA replication(453). The ITRs flank the two viral genes *rep* (replication) and *cap* (capsid). The *rep* gene encodes four regulatory proteins required for replication: Rep 78, Rep 68, Rep 52, and Rep 40. The two larger proteins (Rep 78 and Rep 68) are required for AAV DNA replication(454,455). The two smaller Rep proteins (Rep52 and Rep40) are required for packaging DNA into capsids(456). The *cap* gene encodes three structural proteins: VP1 (68kDa), VP2 (72kDa) and VP3 (62kDa), which interact together to form a capsid of an icosahedral structure(457). The capsid proteins VP1, VP2, VP3 are present in a 1:1:10 molar ratio. VP3, the most abundant subunit in the virion, is used for receptor recognition at the surface of cells, defining the tropism of AAV(458). The three proteins VP1, VP2, and VP3 share a common C-terminal region, but have different N-termini resulting from alternative start codon usage. As a result the entire sequence of VP3 is present in VP2, which in turn is entirely contained within VP1. Differences in the protein structures lead to differences in topology which defines the different serotypes(444,459), and are instrumental for virus infectivity, cellular tropism and genome packaging(460,461). Recently, a non-structural viral protein encoded by an alternative open reading frame (ORF) within the cap gene was identified and termed assembly-activating protein (AAP) for its role in capsid formation(462-464). There are three viral promoters within the viral genome: promoter 5 (p5), promoter 19 (p19), and promoter 40 (p40). The *rep* gene is transcribed from p5 and p19, whereas the *cap* gene is prescribed from p40(465) (Figure 1.5).

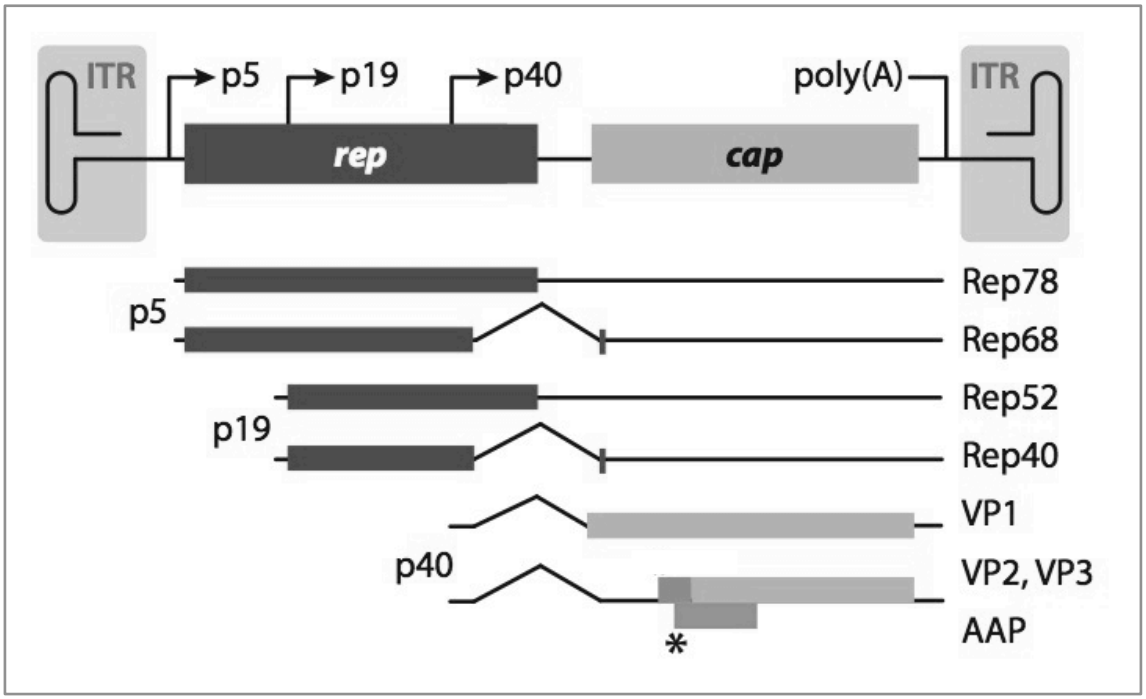

Figure 1.5 AAV genetic map
The ~5-kb AAV genome contains the rep and cap genes. Asterisk* indicates a weak CTG start codon for AAP. Also shown are the 145-base (not to scale) T-shaped AAV inverted terminal repeats (ITRs). Adapted from Jude Samulski et al. 2014(439).

1.6.3.2 Recombinant AAV vectors

The rAAV vectors are generated by replacing the AAV genome with the gene of interest, leaving no viral coding sequences except the viral ITRs. The ITRs contain all the *cis*-acting elements required for genome rescue, replication and packaging(466,467). All other viral sequences required for viral production are supplied in *trans*(468). The recombinant single stranded AAV relies on *de novo* synthesis of the complementary DNA strand, or base pairing of complementary strands. This is possible as AAV packages the plus or minus DNA strand with equal efficiency(469,470). The ITRs serve as primers for cellular DNA polymerase to synthesise the complementary strand after uncoating in the host cell(471). The requirement for complementary-strand synthesis, or recruitment for self annealing, is considered to be a limiting factor in the efficiency of rAAV vectors(472).

1.6.3.3 Self-complementary AAV vector

To avoid the rate-limiting step of second strand synthesis self-complementary vectors have been developed. Self-complementary AAV (scAAV) vectors allow the vector to package two complementary ssDNA strands, with the ability to fold to generate dsDNA thus circumventing the need for second strand synthesis(471). A deletion in the terminal resolution site of one of the ITRs allows replication to continue through the ITR

into the displaced strand generating the dsDNA template. The self-complementary form can promote faster onset and higher levels of transgene expression, however packaging capacity is reduced by half(471,473-475).

1.6.3.4 AAV serotypes and tissue tropism

Most of the rAAV characterisation studies have been performed using vectors of capsid serotype 2. A key finding in the development of rAAV as a gene therapy vector was the identification that vector genome containing ITRs of one serotype could be "cross-packaged" or pseudo-serotyped into the capsid of another serotype(476). Currently there are approximately twelve human serotypes of AAV and more than 100 variant capsid sequences. The identification of novel capsids and the ability to pseudo-serotype has dramatically expanded the potential of rAAV as a gene transfer vector. Each serotype has a distinct tissue tropism and receptor binding specificity (Table 1.5). Different serotypes exhibit variation in their immunologic profile(459,477-479). Specific gene delivery to the desired target cell type is key to gene therapy success. Targeted delivery has the potential to prevent adverse effects that may arise from off-targeting, allow reduction in therapeutic dose, and increase gene transfer efficiency(459,480-483). *In vitro* studies have demonstrated different cancer cell lines to be permissive to different serotypes of AAV(484) and evaluation of tissue tropism and bio-distribution of AAV serotypes have been characterised in pre-clinical animal models, unraveling vectors' suitability for specific clinical applications(482) (Table 1.6).

Table 1.5 Receptors for common AAV serotypes

Capsid Serotype	Primary receptor	Co-receptor	References
1	Sialic acid	-	(486)
2	Heparan sulphate Proteoglycan (HSPG)	Fibroblast growth factor receptor (FGFR), Hepatocyte growth factor receptor (HGFR), Laminin receptor (LamR), αVβ5 and αVβ1 integrin	(476,487,488)
3	HSPG	HGFR, LamR	(476,488)
4	Sialic acid	-	(486,489)
5	Sialic acid	Platelet derived growth factor receptor	(490,491)
6	Sialic acid/HSPG	EGFR	(476,492)
7	-	-	
8	-	LamR	(488)
9	Galactose	LamR	(488,493)
Rh10	-	-	

Table 1.6 AAV serotype and tissue tropism

AAV1	Skeletal muscle, CNS, pancreas
AAV2	Skeletal muscle, CNS, liver, kidney
AAV3	Skeletal muscle
AAV4	CNS, retina
AAV5	Skeletal muscle, CNS, eye,
AAV6	Skeletal muscle, heart, lung, liver
AAV7	Skeletal muscle, CNS, retina
AAV8	Skeletal muscle, liver, heart, pancreas
AAV9	Skeletal muscle, liver, heart, CNS, lung, kidney
AAV10	Heart, lung, liver, kidney, uterus
AAV11	Skeletal muscle, liver, kidney, heart
AAV12	Muscle, saliva glands

Adapted from Wu et al. (459), Asokan et al. (485) and Luo et al. (251).

1.6.3.5 Cellular processing of AAV vector

Transduction by AAV is a multistep process beginning with the virus binding to the cell surface, followed by viral uptake, intracellular trafficking, nuclear localisation, uncoating and second strand DNA synthesis. Most knowledge about this process is based on AAV2 transduction. After binding to its receptor, heparan sulfate proteoglycan(487) AAV2 is rapidly endocytosed via clathrin-coated pits(494). More than 60% of bound virus is internalised within the first 10 minutes of incubation at 37^0C. Following release into the cytosol, AAV accumulates in the peri-nuclear region and slowly penetrates through the nuclear membrane. The events and processes that regulate the trafficking of AAV particles into the nucleus are still not fully understood(457). Once in the nucleus the uncoated ssDNA from rAAV must become transcriptionally active by conversion to dsDNA. This occurs, as previously mentioned, by either second strand synthesis or annealing of complementary strands. Transgene expression can be detected within 3-4 hours post transduction(494).

Genomic studies of rAAV *in vivo* have shown that rAAV DNA molecules in non-dividing cells in the muscle, liver, heart, brain and lung are converted to circular constructs and persist predominantly as extra-chromosomal episomes, containing multiple copies of the transgene cassette, usually in a head-to-tail configuration(495-501). Stable transgene expression mediated by rAAV vectors without integration can persist for months and up to several years *in vivo*(235,502-506). However in dividing cells, AAV DNA is lost through cell division, as episomal DNA is not replicated along with the host cell DNA(451,507,508). It has been shown that one or two cell divisions can result in the loss of 90-95% of rAAV genomes(495).

1.6.3.6 AAV Immunogenicity

Immunogenicity of rAAV is very low, yet, in mice, it elicits a mild, innate immune response due to activation of Toll-like receptor 9 (TLR9), when rAAV infects APC(509). Activation of the TLR9 pathway induces the production of pro-inflammatory cytokines by activating the NF-κB pathway and inducing type I interferon response. This generates a CTL response, which activates B-cell lymphocyte, thereby stimulating production of neutralising antibodies (NAb)(510). In humans the immune response appears to be restricted to the generation of NAb as no clearly defined cytotoxic response has been identified(235,511-514). The generated immune response can be directed against the AAV vector component, the transgene product, or both, by pre-existing and/or recall responses to the wild-type virus from which the vector is

engineered(436). This response can dramatically interfere with therapeutic efficacy. Humoral immunity to wild-type AAV represents one of the most effective barriers to successful systemic gene delivery with AAV vectors. In the first clinical trial for haemophilia B, using an AAV2 vector delivered systemically, NAb titers were measured in recipients but were not used to exclude subjects from the trial, as it was unclear what level of titers would affect transduction. The study showed that relatively low NAb titers completely neutralised the vector(515). In a subsequent clinical trial for haemophilia B, utilising an AAV8 vector with a liver specific promoter, a transient elevation of capsid specific CTL was observed and was associated with liver toxicity. A short course of glucocorticoid therapy resolved the immune response without loss of transgene expression(235).

Animal models have predicted many aspects of the human immune response to transgene products, but have largely failed to predict responses to AAV capsids(516-520). The immune responses against AAV vectors can shorten or even prevent transgene expression, which is a major concern for the treatment of disease in which life-long gene expression is required(436,521-523). Switching serotype to one less prevalent in the human population, or inducing immunosuppression, are utilised to overcome these problems(235,404,515,524). However, a high degree of conservation in the amino acid sequence among AAV capsids(525) causes anti-AAV antibodies to have cross-reactivity over a wide range of serotypes(526-529). Strategies to map neutralising antibody epitopes on the serotypes are currently being explored for pre-clinical and clinical trials(479,529,530).

AAV2 is a common virus in the human population and most people have detectable antibodies against one or more AAV serotypes(438,531,532). Characterisation of the IgG subclass response to AAV, and the prevalence of both IgG and NAb to AAV serotypes 1, 2, 5, 6, 8, and 9 in the human population, revealed that the highest sero-prevalence neutralising factors were observed for AAV2 (59%) and AAV1 (50.5%). The lowest were observed for AAV8 (19%) and AAV5 (3.2%)(480). AAV4 and AAV5 are the most divergent, carrying one of the least conserved capsid sequences(533).

1.6.3.7 AAV integration and genotoxicity

Wild-type AAV has the ability to integrate stably into the host cell genome at a specific site on the human chromosome 19q13.3(449,450,534). Site-specific integration is mediated by AAV Rep proteins, which are absent from recombinant AAV vectors. Integration of rAAV DNA into the host genome occurs at a low but measurable rate

(0.1-1% of transduction events). The integration has not been found to be chromosome- or site-specific, though it has been shown that rAAV proviral genome preferentially integrates within or near transcriptionally active genes and double-stranded breaks(535-540). Latent AAV infection is common in the human population and yet AAV has never been associated with any human malignancy(532).

The safety of AAV as a vector has been challenged by a single study documenting the development of hepatocellular carcinoma (HCC) after AAV gene delivery in mice. This study was undertaken in a mouse (C3H/HeJ) liver model, prone to hepatocyte tumour formation, and HCC developed following exposure to a self-complementary AAV vector. This was not reproduced in the severe combined immune-deficient (SCID) mice(541). In a recent study in neonates (mice) a dose-dependent increase in HCC was observed, and this appeared to be independent of murine genotype or viral transgene. Factors that seem to influence HCC incidence were vector dose, promoter selection and timing of gene transfer. In addition AAV integration into the site of RNA Imprinted and Accumulated in Nucleus *(Rian)* locus was associated with an increased incidence of HCC(542). Tumour development has also been reported in a knockout mouse model, following liver transduction with single-stranded rAAV expressing β-glucuronidase. Correlation between integration of rAAV and the development of tumours was not observed(543,544). Two studies, one where expression of the *LacZ* transgene was associated with an increased incidence of tumour development(545), and another where overexpression of *Tcf12,* produced glioblastoma-like proliferation at the site of injection in rat brains(546), suggest that overexpression of a gene may lead to tumour formation even if the rAAV vector genome does not integrate. Most studies have not shown an increased incidence of liver tumours following exposure to AAV(547,548). The importance of this small number of studies is still uncertain, as the tumour formation has only been observed in small rodents. However, the risk of inducing tumours in man can not be excluded and each gene cassette may have to be monitored separately for potential oncogenic effects(439,542).

1.6.3.8 AAV in clinical trials for cancer gene therapy

AAV vectors have been successfully used to deliver and transfer a variety of therapeutic genes to cancer cells, including suicide genes, anti-angiogenic genes and immune-related genes, inhibiting tumour growth and metastasis(251). Preclinical use of AAV in xenograft cancer models has shown promising effect, in particular using AAV based immune gene therapy(549-558). There are currently 16 phase I-III clinical trials open, utilising an AAV vector for cancer therapy (Table 1.7). Preliminary data from

early phase clinical trials has shown tolerability and no severe adverse reaction. One trial involved AAV-based immunotherapy, with rAAV transduced dendritic cells (DCs), for expression of cancer embryonic antigen (CEA) to elicit CTL in patients with advanced stage IV gastric cancer(559). Other examples include the GVAX cancer vaccine-study with autologous or allogeneic tumour cells engineered by AAV (*ex vivo*) mediated gene transfer to secrete GM-CSF. The GVAX vaccine initiates a potent CTL response, thereby generating a pool of T-cells capable of recognising the tumour. The vaccine has been used for targeting various malignant solid tumours such as pancreas, prostate, melanoma and non-small lung cell carcinoma(560-565) www.wiley.co.uk/genetherapy/clinical.

Table 1.7 Gene therapy trials in cancer therapy utilising AAV vector

Trial ID	AAV vectors used in Cancer Gene therapy
CH-0025	Gene therapy for patients with malignant melanoma. AAV/GM-CSF (IT)
CN-0020	Adoptive T cell treatment of CTL generated from autologous dendritic cells transfected with rAAV virus containing tumour antigen gene
CN-0028	Phase I Study of Antigen-specific CTL Induced by Dendritic Cells Infected by rAAV with CEA Gene in Stage IV Gastric Cancer
ES-0021	A phase I, multi centre, open label, dose escalation study of intra-tumoural injection of VCN 01 oncolytic adenovirus in combination with intravenous gemcitabine in advanced pancreatic cancer
JP-0014	Phase I/II clinical trial of gene therapy for hormone refractory metastatic prostate cancer. IT injection of AAV/HSV-tk
NL-0012	GVAX immunotherapy in combination with Ipilimumab (MDX-010) in Hormone Refractory Prostate Cancer
NL-0013	Phase III studies in advanced metastatic prostate cancer patients using immunotherapy with an allogeneic prostate tumour cell vaccine, stably transduced with the human GM-CSF gene by non-pathogenic, replication defective, recombinant adeno-associated viral vector.
NL-0014	A Phase III Randomized, Open-Label Study of CG1940/CG8711 Versus Docetaxel and Prednisone in Patients with Metastatic Hormone-Refractory Prostate Cancer who are Chemotherapy-naïve (GM-CSF)
NL-0015	A Phase III Randomized, Open-Label Study of Docetaxel in Combination with CG1940/CG8711 versus Docetaxel and Prednisone in Taxane-Naive Patients with Metastatic Hormone-Refractory Prostate Cancer with Pain (GM-CSF)
NL-016	A Phase 1 Dose Escalation Trial of MDX-010 in Combination with CG1940 and CG8711 in Patients with Metastatic Hormone-Refractory Prostate Cancer (GM-CSF)
NL-0021	Adjuvant IL-12 immunotherapy prior to radical prostatectomy in patients with prostate cancer
UK-0133	A Phase III Randomized, Open-Label Study of Docetaxel in Combination with CG1940 and CG8711 versus Docetaxel and Prednisone in Taxane-Naive Patients with Metastatic Hormone-Refractory Prostate Cancer EudraCT: 2005-003275-20 (GM-CSF)
UK-0134	A Phase III Randomized, Open-Label Study of CG1940 and CG8711 Versus Docetaxel and Prednisone in Patients with Metastatic Hormone-Refractory Prostate Cancer who are Chemotherapy-Naive.EudraCT: 2005-002738-36
US-0675	Development of Effective Immunotherapy for Prostate Cancer Patients: Phase I/II Study of Human GM-CSF Gene Transduced Irradiated Prostate Allogeneic Cancer Cell Vaccines (Allogeneic Prostate GVAX) in Advanced Prostate Cancer Patients lympho-depleted by Chemotherapy and Infused with Autologous Peripheral Blood Mononuclear Cells
US-0834	Administration of LMP1- and LMP2-Specific CTL to Patients with EBV-Positive Nasopharyngeal Carcinoma
US-1165	A Neoadjuvant Immunologic Study of Androgen Deprivation Therapy Combined with a GM-CSF Secreting Allogeneic Prostate Cancer Vaccine and Low-dose Cyclophosphamide in Men with High-risk Localised Prostate Cancer Undergoing Radical Prostatectomy

CG1940 and CG8711 represent two prostate cancer cell lines (GVAX). IT: Intratumoral. LPM1 and LPM2: Latent membrane proteins encoded by EBV involved in pathogenesis for EBV(566-568). EudraCT: European Medicines Agency Clinical trials Database. Table adapted from data from www.wiley.co.uk/genetherapy/clinical (Accessed October 2015).

1.7 Pre-clinical models

Drug discovery and development for anti-cancer compounds is an inexact and inefficient process, as a large proportion of drugs entering preclinical testing fail to achieve FDA approval since a majority of phase III trials fail to meet their primary endpoint(569,570). The lack of preclinical models that closely recapitulate the heterogeneity of human tumours, with predictive value for therapeutic evaluation, represents one of the main reasons for the failure of successful development of new agents in oncology(571). This has been true for chordoma, as well as other cancers. However, through sheer determination by researchers and patients, an increasing number of cell lines for preclinical studies are being generated.

1.7.1 Human cancer cell lines

Since 1952 when the first human cell line HeLa was established(572,573) there has been an increase in the use of human cell lines as models for human diseases, particularly in cancer. Human cancer cell lines are widely used in *in vitro* models for studying cancer and its biology, including regulation of cell proliferation and gene expression(574,575). They have also proven a valuable tool for identifying biomarkers and genetic variants(576). Genome sciences, combined with bioinformatics, have allowed dissection of the genetic basis of diseases and from this identified the most suitable points of attack for future medicines(574,577). An example of this is the discovery of the somatic missense mutation (V600E) in the *BRAF* gene in multiple cancer cell lines(578). This discovery subsequently led to the development of Vemurafenib (PLX4032), a potent inhibitor of mutated *BRAF*(579,580) with antitumor effect against melanoma cell lines harbouring the BRAF V600E mutation, but not against cell lines with wild-type *BRAF*. The introduction of Vemurafenib has led to prolonged event-free and overall survival for patients with metastatic malignant melanoma(581). Cancer cell lines play a pivotal role in the early stages of drug discovery(582), facilitating screening of hundreds of potential drugs before translating into *in vivo* models and clinical trials(583). High-throughput screening of cancer cell lines for drug-sensitivity patterns provides a strategy to identify appropriate cancer subtypes and biomarkers that may guide the early-phase clinical trials of novel compounds(574). However the use of tumour-derived cell lines grown in two-dimensional culture has its limitations. Experimental models are needed that resemble the tumour microenvironment to increase our understanding of drug sensitivity(566,568). For this purpose various 3D culture models have been developed to simulate the growth environment taking into account the spatial organisation of the cells mimicking the native tissue(566,584,585).

1.7.2 Mouse models

Numerous mouse models have been developed to study human cancer; the pattern of invasion, metastasis and malignant transformation, as well as the response to anti-cancer therapy(586). The predictive value of tumour models relies on how closely they recapitulate the underlying genetic aberrations, tumour growth and metastatic potential as well as the surrounding neoplastic stromal and immune microenvironment(256,587).

The most widely used model is the human tumour-derived xenograft. Tumour can be generated following intravenous injection, or by subcutaneous, intra-peritoneal and orthotopic inoculation, using immune-deficient mice such as the athymic nude mouse or the SCID mouse(588,589). The lack of a functional immune system in mice appears to play an important role in the success of xenograft formation. However such models are compromised by this lack of immunity as it prevents the interactions between the tumour and the endogenous immune system. This is a particular limitation for the use of xenograft models in assessing efficacy of immunotherapies(568,590).

Tumours generated *in vivo* using cell lines established *in vitro* often lack the distinct histological features characteristic of tumours seen in patients, but instead appear more homogeneous due to the clonal selection of cells grown in culture(568,591). Patient-derived xenograft (PDX) models, where patient tumour is transplanted into immunodeficient mice, often retain the principal histologic and genetic characteristics of patients' tumours. They are biologically stable, in terms of global gene-expression patterns, mutational status, metastatic potential and drug responsiveness, across passages(589,592). The intratumoral heterogeneity, including genetic and non-genetic mechanisms, refers to biological differences amongst malignant cells originated within the same tumour. Through accumulated genetic changes several cellular subclones with significant biological differences can be identified(593). Different cancer cell clones display distinct behaviour and may contribute to the phenotypic variability of tumour cells(594). Clonal diversities have been found to correlate between the patient and the PDX(590,594-596). These models have been shown to be predictive of clinical outcomes and are being used for preclinical drug evaluation, biomarker identification, biologic studies, and personalised medicine strategies(597-600). The xenografts generated from patient-derived tumours may however not fully represent the inter-tumour heterogeneity as the tumours which are able to engraft and generate a xenograft have been shown to be biased towards the more aggressive tumours(590).

The genetically engineered mouse (GEM) model represents another method for studying human cancer and plays an increasingly important role in the development of novel therapeutics targeted at specific oncogenes and signalling pathways(601,602). In these mice the genetic profile has been changed by mutation of cancer genes in order to observe tumour development and response to therapy related to specific mutations(586). One of the benefits of using this model is the opportunity to observe the influence of the tumour microenvironment as immunocompetent mice can be used(603). Some of the weaknesses with the GEM model is that the tumour is a mouse tumour rather than a human tumour and that there is a limited number of target or mutated genes, which is not usually reflective of the complex heterogeneity of particularly adult human tumour cells(586,604,605). In contrast, transformation in many paediatric cancers is initiated by comparably few "driver" mutations that occur during a short window of programmed differentiation(602,606,607), providing an opportunity to develop GEM models to enhance the understanding of tumour development and improve therapy for some childhood cancers(601).

1.7.3 Chordoma preclinical models

The first chordoma cell line, U-CH1, was established in 2001(134) from a locally recurrent sacral chordoma. This was the only chordoma cell line until 2010 since when ~6 more cell lines have been established and characterised, which are available through the Chordoma Foundation and/or the American Type Culture Collection (ATCC). The first chordoma xenograft was generated following subcutaneous injection of U-CH1 cells in the NOD/SCID/interleukin 2 receptor [IL2r]γ null (NSG) mouse after 10 weeks. No xenografts were generated in CD1 mice(89). UCH2 and JHC7 cell lines have since been used to generate a xenograft in NSG mice. The xenograft histology resembled chordoma in all cases(89,91,608). In 2012 the first successful PDX in an athymic nude mouse was reported, derived from a recurrent clival chordoma. Genomic analysis confirmed that the xenograft was more than 99% genetically identical to the primary tumour(609). This PDX was treated with the EGFR inhibitor Erlotinib(178) which reduced tumour growth and phosphorylation of *EGFR,* demonstrating an on-target effect(178). A second study reported successful engraftment by 4 of 8 sacral chordomas in CD-1nu/nu mice. One PDX expressed *EGFR* and was treated with the EGFR inhibitor, Lapatinib. No reduction in tumour growth was observed, though MRI imaging showed a change in contrast enhancement and biochemical analysis demonstrated switching off of *EGFR, AKT* and *MEK* 1/2(610). Of note is a phase II study testing Lapatinib in advanced chordoma that showed only a slight effect(179).

This decrease in growth rate often viewed as positive in mouse xenograft may not register in standard clinical testing. RECIST criteria for evaluating efficacy in human clinical trials require >50% tumour reduction in two planes to be considered a response(170). Different methods for assessing tumour response to target therapies are being investigated as changes may be non-dimensional requiring functional imaging to assess tumour response(611-613). A consensus is being compiled for how to best validate response of chordoma to therapy, as overall survival is not an ideal endpoint due to slow disease progression, and to date no reliable tumour biomarker has been identified for chordoma. Consequently other measures such as clinical benefit, shrinkage or arrested disease progression may be used as surrogate markers for disease response (http://www.chordomafoundation.org/latest-updates/clinical-trials-roundtable-clarifies-path-get-drugs-approved-chordoma).

1.8 Biomarkers and response assessment

With cancer treatment moving towards personalised targeted therapy, it is becoming increasingly important to have biomarkers tracking tumour dynamics in real time for monitoring treatment response and early detection of disease progression or recurrence. Sampling of tumour tissue has its limitations due to the invasiveness of the procedure, and the tissue represents a single snapshot in time of the molecular profile of the tumour. Many cancers continue to be treated according to histology, immunohistochemistry and tissue origin of the primary tumour and, to a lesser extent, according to molecular markers. The importance of interpatient tumour genetic heterogeneity and intratumour genetic heterogeneity is recognised(614,615), and poses a challenge to personalised cancer treatment, as a single biopsy or surgical excision of the primary tumour is unlikely to capture the complete genomic landscape of a patient's cancer(616).

1.8.1 Cell-free DNA

A new generation of biomarkers has become available with the discovery of genetic alterations in solid tumours and the detection of cancer specific cell-free DNA (cfDNA) in the blood of cancer patients(617,618).

The most successful application for the utility of evaluating cfDNA has been the investigating of fetal DNA in the circulation of expectant mothers(619,620). Detection of fetal DNA by a maternal blood test for trisomy 13, 18 and 21 has become standard care(621,622).

Fragmented cfDNA deriving from tumours, also known as circulating tumour DNA (ctDNA), is shed into the bloodstream by cells undergoing apoptosis or necrosis(623). Necrotic and apoptotic cells are usually phagocytosed by macrophages or other scavenger cells(624). The proportion of ctDNA detectable in blood is influenced by clearance, degradation and other physiological filtering events of the blood and lymphatic circulation. Nucleic acid is cleared from the blood by the liver and kidney(s) and has a half-life in the circulation ranging from 15 minutes to several hours(625). Healthy patients have cfDNA concentration between 0 and 100ng/mL, cancer patients by comparison, have increased levels of cfDNA(625-632), with levels reported up to 1200ng/mL(632,633). The quantity of ctDNA can vary between 0.01% to more than 90% of the overall circulating DNA(618). The proportion of ctDNA has been found to be related to tumour burden and prognosis(634-636).

1.8.1.1 Detection of ctDNA

Discriminating ctDNA from normal cfDNA has been challenging due to issues with sensitivity and specificity. However, with increasing ability to detect single base-pair mutations present only in the genome of the cancer cells, specificity of ctDNA as a biomarker has been confirmed(623). Early efforts at detecting ctDNA focused on the application of allele-specific real-time quantitative polymerase chain reaction (RT qPCR) assays(623). The assays, which utilised TaqMan technology, were limited in their applicability to patients with high tumour burden due to their analytical sensitivity and specificity. Within the past decade, several methods have been developed allowing for ultrasensitive detection of ctDNA. These methods fall into two categories; next generation sequencing (NGS)(637-639), and digital PCR (dPCR)(634,635,640). These methods have detection thresholds between 0.001 and 0.1% for mutant alleles(641,642), which is 1000 times lower than RT qPCR. dPCR is a refinement of conventional PCR methods that can be used to directly quantify and clonally amplify nucleic acids including DNA, cDNA and RNA. The key difference between dPCR and traditional RT PCR lies in the method of measuring nucleic acids amounts. PCR carries out one reaction per single sample whereas dPCR also carries out a single reaction within a sample, but the sample is separated into a large number of partitions(640). Raindance® digital droplet technology generates up to 10 million picolitre-sized droplets whereas the BioRad platform partitions into approximately 20,000 droplets. Each droplet encapsulates a single nucleotide, enabling quantification of the number of droplets containing specific target DNA and comparing that to the number of droplets with background wild-type DNA. This separation allows a more reliable and sensitive measurement of nucleic acid amounts. Limitations of dPCR include the ability to

interrogate only one or a few genomic positions simultaneously and assays require optimisation for each mutation of interest, complicating clinical implementation. NGS-based methods for ctDNA detection can detect multiple somatic alterations simultaneously(643), but optimisation has been required to improve detection of ctDNA as this often represents a small fraction (<1.0%) of total cfDNA(617,618).

The different processes for detection of ctDNA have been applied for detection of tumour specific mutation, identified by sequencing of the primary tumour DNA. An alternative approach has been to scan regions of DNA extracted from plasma or serum for mutations of interest in a blinded manner when the tumour tissue has not been assessed(634,637,639). This method has been used for detecting the presence of specific but commonly observed mutations of known oncogenes, such as *KRAS, PIK3CA* and *EGFR* in hot spot locations(644-647).

In addition to ctDNA, circulating tumour cells (CTC) can be non-invasively assessed as a source of tumour DNA in the circulation(634,648). While ctDNA is composed of small fragments (70-200 base pairs) of nucleic acid(632) CTCs represent intact, often viable, tumour cells that can be isolated from blood by cell surface molecules, distinguishing them from normal blood cells. The basis of the validated CTC detection test has been based on the expression of epithelial markers(649). Limited sensitivity has been an issue using CTCs and recent reports suggest the difficulties may be due to incomplete characterisation of the CTCs as some of these cells have been found to undergo EMT and express mesenchymal markers(650). Few studies have compared the amounts of ctDNA and CTC and conclusions are mixed(634,648). Recent studies suggest ctDNA levels are higher than CTC levels(634,635,641), supporting ctDNA as the preferred biomarker to prognosticate survival, monitor for response to specific therapeutics and for detection of recurrence and progression in the metastatic phase(651,652).

1.8.1.2 Monitoring or molecular resistance

Acquired mutations leading to drug resistance can be detected using ctDNA(637,639,653,654). This has been shown by detection of a well characterised secondary resistant mutation (T790M) appearing during treatment, leading to resistance to the EGFR inhibitor Gefitinib in patients with colorectal cancer(655,656). Secondary resistance to *EGFR* inhibition has also been associated with the emergence of *KRAS* mutations or *MET* amplification. Detection of *KRAS* variants in ctDNA in patients receiving therapy with EGFR-inhibitors have identified relapse months before clinical and radiologic changes(655,657,658). Similarly, ctDNA has also been used for

detection of *HER2* amplification in patients with metastatic breast cancer which were not detected at primary diagnoses but present at time of recurrence, thereby changing the options for therapy(659).

CtDNA has prognostic significance and reflects the dynamics changes in the mutation profile that occur during therapy as well as the heterogeneity that emerges as a result of the therapeutic selection pressure(634,635,651), supporting the use of ctDNA as a 'liquid biopsy' to guide therapy(660).

1.9 Aims

This thesis covers the identification of targeted therapy for chordoma, the evaluation of potential biomarkers in plasma and the generation of new disease models.

Chordoma is a rare malignant tumour of bone. It is slow growing and often presents with a large tumour which impacts on the likelihood of successful treatment. Current standard therapy is en-bloc surgical resection followed by radiation therapy. No drugs have been approved for the treatment of chordoma and indeed no phase III trial has ever been conducted for this disease. Chordoma is resistant to chemotherapy leaving an unmet need for the treatment of residual and recurrent disease.

The transcription factor brachyury has been identified to play a role in the pathogenesis of chordoma, and silencing of brachyury *in vitro* results in apoptosis and cell senescence in chordoma cell lines. The hypothesis was that by using a viral vector for delivery of RNA interference to silence brachyury *in vivo*, at time of tumour resection for recurrent disease, this could possibly further reduce tumour burden and improve event free survival?

The AAV vector was chosen for delivery due to its safety profile and tolerability demonstrated in clinical trials. Local treatment was considered the most appropriate application to ensure adequate tumour dosing and the knowledge that local recurrence represents the biggest challenge in the treatment of chordoma.

To aim was to establish the suitability of the AAV vector and to identify a serotype for efficient transduction of chordoma cells. It was not known if silencing of brachyury *in vivo* could be maintained and if this would lead to tumour regression. A xenograft model was to be generated and intra-tumoural injection was to be performed to establish response. This would be assessed by xenograft tumour size and metabolic response as a measure of cell viability in the tumour.

To achieve cure of most cancers multimodality therapy and combination of compounds is required. Limited pre-clinical data is available for the treatment of chordoma. A high throughput compound screen of more than 1100 compounds was to be undertaken in three chordoma cell lines. The aim was that by performing a phenotypic screen and investigation the mechanism of death to potentially identify effective compounds for the treatment of chordoma. By testing multiple kinase inhibitors would it be possible to

identify important pathways involved in the pathogenesis of chordoma? Adding informed guidance on therapy and help identify compounds with synergistic effect suitable for screening in combination to improve therapeutic efficacy? By screening the compounds in multiple chordoma cell lines, would this demonstrate a homogeneous response to treatment? Or if heterogeneous response was observed would this add insight into inter-tumour heterogeneity and aid patient selection for guidance of future clinical trials?

Biomarkers play and important role in the assessment of response to therapy. Currently no tumour marker is available for chordoma. The protein marker, AKR1B10 is expressed on all chordoma tumour samples. The relevance of this protein in the pathogenesis of chordoma is still to be established. AKR1B10 levels in plasma have been shown to have prognostic implications in breast cancer patients. The aim was therefore to test if levels could be assessed in plasma from chordoma patients and if so to consider the potential of AKR1B10 as a tumour marker to assess response to therapy in patients with chordoma. More recently ctDNA has been shown to be a sensitive marker for persistent or recurrent disease in solid tumours, as well as a method for assessing response to therapy. Detection of ctDNA has been established in high-grade tumours where as in most CNS tumours and low grade tumours the evidence remains sparse. The aim was to establish if ctDNA can be detected in the plasma of chordoma patients and if proof of concept were established would this represent a potential marker for detection of recurrence in patients enabling early diagnosis of relapse.

Lack of disease models in chordoma has impact on the opportunities for scientific discoveries. To enable the work presented in this thesis two xenograft models were generated. A patient derived xenograft model to establish the persistence of morphology and assess genetic stability across multiple passages. This model was to be shared within the chordoma scientific community for compound screening. The 2nd xenograft was generated from the U-CH1 chordoma cell line. The U-CH1 cell line has previously been used to generate a xenograft. The aim was to generate a modified U-CH1 cell line expressing luciferase and to utilise this for the xenograft model to establish, if luciferase expression could be serially quantified and used as a method for assessing tumour response to gene therapy.

2 MATERIAL AND METHODS

2.1 Cell lines

2.1.1 Authentication of cell lines with DNA fingerprinting

DDC Medical, a division of DNA Diagnostics Center (DDC)(London, UK) was used for cell line authentication. DDC Medical's DNA STR analysis examines 17 highly polymorphic genetic markers, generating a DNA profile, which uniquely identifies the cell line. DNA was extracted from the three chordoma cell lines and sent for STR testing, confirming authenticity of the cell lines. Results are compared to the DSZM STR profile database, which include 2455 cell lines from ATCC, SMZX, JCRB and RilKEN databases. STR data represent allelic size and determinations performed by capillary electrophoresis of PCR products using primers mapping to a number of genetic loci

2.1.2 Chordoma cell lines

U-CH1 chordoma cell line

Provided by Dr David Alcorta, Duke University, Durham, NC, USA through the Chordoma Foundation. This cell line was established, from 56-year old male patient with a recurrent sacral chordoma. The cells morphology demonstrated physalipherous features. Brachyury expression approximately has been assessed as 10x of U-CH2 with no amplification of brachyury. Multiple chromosomal abnormalities including biallelic loss of 9q21 (*CDKN2A* and *CDKN2B* loci)(134).

U-CH2 chordoma cell line

Generated and provided by Silke Bruderlein, University of Ulm, Germany through the Chordoma Foundation. This cell line was established from a 72-year old female with recurrent sacral chordoma. The cell morphology is physalipherous, brachyury expression is positive (weaker than other cell lines). Chromosomal abnormalities are multiple, and including amplification of T/brachyury and biallelic loss at 9p21 (*CDKN2A* and *CDKN2B* loci)(197).

MUG-Chor chordoma cell line

Generated and provided by Dr Beate Rinner, University of Graz, Austria through the Chordoma Foundation. This cell line was established, from a 57-year old female patient with primary sacral chordoma. The cell morphology is physalipherous, brachyury expression is positive (10x that of U-CH1). Chromosomal abnormalities are multiple, including gain at 6q27 (T/brachyury), loss at 9p21 (*CDKN2A* and *CDKN2B* loci), loss at 10p (*PTEN*) and 10q (*PDCD4* loci)(661).

2.1.3 Other cell lines

HEK 293T cells

HEK 293T cells were purchased from ATCC (LGC Standards, Middlesex UK). This cell line is a human embryonic kidney adenoviral 5-transformed cell line(662,663). HEK 293T cell line was cultured in Dulbecco's Modified Eagle Medium (DMEM) (GIBCO® Invitrogen) with 10% Fetal bovine serum (FBS) (GIBCO®, Invitrogen) and Penicillin G 100U/mL and streptomycin 100µg/mL (Invitrogen).

Three breast cancer cell lines: MDA_MB_231, MDA_MB_435 and MCF7, three glioblastoma cell lines: U87, A172, U 251, two liver carcinoma cell lines: Sk.Hep.1 and HUH1 (kindly provided from Amit Nathwani's lab UCL Cancer institute) were used for control of experiments. These cell lines were all cultured in DMEM with 10% FBS and Penicillin G 100U/mL and streptomycin 100µg/mL.

2.1.4 Passaging of adherent cell lines

All cell lines were incubated at 37°C with 5% CO_2. Tissue culture flasks and plates were from TPP (TPP, Trasadingen Switzerland) unless otherwise stated.

U-CH1, U-CH2 and Mug-Chor cell lines were cultured as a monolayer in Iscove's Modified Dulbecco's medium (IMDM) (GIBCO® Invitrogen, Paisley, UK) and RPMI-1640 (GIBCO® Invitrogen) in a 4:1 ration of IMDM:RPMI medium (GIBCO®, Invitrogen) supplemented with 10% FBS (Reserved: South American FBS, catalogue number 10270106, Lot # 41A1241K, and previously Lot # 41F6034K) (Life technologies, UK) and 5 mL penicillin-streptomycin. Cells were grown in T175 (175cm^2) tissue culture flasks (Thermo scientific, Loughborough, UK) in incubators at 37°C with 5% CO_2 atmosphere. Cells were passaged when 75-80% confluent. Medium was removed, cells were washed using Dulbecco's phosphate buffered saline (PBS) (Sigma), and then incubated in trypsin/EDTA (Invitrogen) (5mL) for 5 minutes at 37°C and detached by tapping the flask. The trypsin/EDTA reaction was quenched using serum. The cell suspension was centrifuged at 400x *g* for 5 minutes. The supernatant was discarded, the cell pellet disrupted and resuspended in fresh medium before transferring to new flasks. U-CH1 cell line was maintained in collagen-coated flasks (Collagen solution Type 1 from rat tail product #C3867 Sigma Aldrich).

2.1.4.1 Cell count calculations

Cells were counted using a Neubauer Haemocytometer (Weber Scientific International Ltd. Middlesex, UK). Tryphan blue solution (Sigma Aldrich) was added to the cell suspension to identify dead cells.

2.1.4.2 Thawing of cells

Frozen vials of cells were removed from liquid nitrogen and thawed in warm water at 37°C. The cell suspension was transferred to a 50mL falcon tube containing 20mL of cold complete medium. The suspension was centrifuged at 50 × g at 4°C for 3 minutes. The supernatant was gently aspirated without disturbing the pellet. The cell pellet was resuspended in 10mL IMDM:RPMI with FBS and an aliquot set aside to determine cell number and viability using tryphan blue. After re-suspension cells were transferred to a new flask containing complete medium at a final volume of 5mL/25 cm^2, 10mL/75 cm^2, 20mL/150 cm^2 flask or 10mL/10 cm^2 dish.

2.1.4.3 Freezing cell lines in liquid nitrogen

Cell cultures were harvested as described in Section 1.1.3. After centrifugation they were resuspended in freezing medium (DMEM plus 20% (v/v) FBS and 10% (v/v) DMSO) for a cell density of 1-5×10^6/mL. The cell suspension was quickly aliquoted into cryo-vials (Corning), rested on ice briefly before storing overnight at -80°C prior to long-term storage in liquid nitrogen.

2.2 Generation of new cell lines

2.2.1 Puromycin Dose-Response

To select for transduced cell to generate a uniform cell population, a dose-titration was performed, to establish the correct dose of Puromycin required to cause 100% cell death within 48 hours. The cell lines were plated at 50% confluency in 6 well plates. The following day the medium was replaced with medium containing a range of concentrations (0, 1, 2, 3, 4, 5, 6, 7, 8, 9, 10µg/mL) of Puromycin: this was done in duplicate. Cells were monitored daily by microscopy, and the minimum amount of Puromycin required to kill 100% of non-transfected cells was determined at 3-7 days. For U-CH1 the dose required was 5µg/mL, and for HEK 293T the dose required to kill 100% of the cells was 2µg/mL.

2.2.2 U-CH1 luciferase cell line

The U-CH1 cell line was modified using a plasmid supplied by Addgene (Cambridge, MA, USA) (plasmid 17477): Lenti_CMV_Luciferase_Puromycin(664) to express luciferase.

From the bacterial stab, provided by Addgene, colonies were generated on an agar plate (ampicillin 100µg/mL) from which individual colonies were picked and grown overnight in 3mL Luria Broth (LB). Following plasmid purification the colonies were checked by restriction digest. 1mL of fresh LB were used in 300mL LB for large scale DNA preparation. Lentivirus was produced using 293T cells for packaging, and the supernatant was collected at two time points as described in the section on lentivirus production (section 2.6.1). The titre was determined using Lentivirus qPCR Titre kit from Gentaur catalogue # LV900 (Gentaur Ltd, London UK) viral titre as determined by qPCR was $5x10^{10}$ viral particles per mL. U-CH1 cells were transduced twice within 24 hours using a Multiplicity of infection (MOI) of 10. The cells underwent Puromycin (5µg/mL) (Sigma-Aldrich, Ayrshire, UK) selection 72 hours after the initial transduction.

Following Puromycin selection the cells were checked for luciferase expression. Cells were washed with PBS, and passive lysis buffer (Promega, WI, USA) was added to the plate to lyse the cells. A cell scraper was used to detach the cells, and the cells and solution was transferred to a micro-centrifuge tube. Debris was pelleted by centrifugation and the supernatant was transferred to a separate tube. Cell lysate was mixed with D-luciferin (Melford, Chelsworth, Ipswich, Suffolk, UK). Adding D-luciferin produces bioluminescence when oxidized by firefly luciferase there by confirming luciferase expression in the cell line. The luminescence was measured by a luminometer (Turner Biosystems Model TD 20/20; Promega).

2.2.3 293T_Brachyury-expressing cell line

Brachyury is expressed mainly in chordoma cell lines and these cells have proven notoriously difficult to transfect (personal experience) and evident by a small number of recent publications(119,665,666). Expression has also been documented in a colon cancer cell line SW480, however the expression in this cell line varies at different levels of cell confluency, making it a sub-optimal model for gene-silencing experiment. We therefore generated a HEK 293T cell line stably expressing brachyury for testing of gene-silencing constructs. This was achieved by generating cDNA from U-CH1 cell lines following RNA extraction (QIAzol) (section 2.72). Primers were designed for PCR amplification of the brachyury gene. Restriction enzyme sites (RE) were added to the 5'

of the primers for subsequent cloning, using restriction digest for insertion of the brachyury transcript into a vector.

Table 2.1 Primers for Brachyury transcript amplification

Brachyury forward	5'CAATTCCATGGATTATGAGCTCCCCTGGCACCGA 3'
Brachyury reverse	5' CGATCCTCGAGTCACATGGAAGGTGGCGACAC 3'

Primers for Brachyury transcript amplification for cloning into a vector for expression. Restriction enzyme sites: Forward: NcoI (5'CCATGG 3') / Reverse: XhoI 5' CTCGAG 3'

The PCR product was separated on an agarose gel, and the correct size band was visualised. The band was excised and isolated by gel-extraction (QIAGEN, GmBH, Hilden, Germany) as per manufactures recommendation. The PCR product was then digested with Nco1/Xho1 to create appropriate overhang for cloning into the receiving vector. This was followed by PCR clean-up to remove the enzymes as per manufactures recommendation (QIAGEN).

The PCR product was cloned into the entry vector: PENTR4_flag in which it was sequenced and subsequently gated into the lentiviral destination vector (pLenti_PGK_Puromycin) using the Gateway LR Clonase Enzyme Mix (Invitrogen) as described in section 2.5.3.2

Lentivirus was generated as described 2.6.1 and Lentivirus qPCR Titre kit previously described (section 2.6.2) was used to establish the titre. HEK 293T cells were transduced with an MOI of 10. The transduction was repeated within 24 hours and after further 48 hours cells Puromycin collection was commenced. The expression of brachyury was checked by RT qPCR.

2.3 Methods for Patient derived xenograft

The use of patient material was approved by the Cambridgeshire Research Ethics committee (REC reference 10/H1107/36).

Animal work was performed under the authority of UK Home Office Project and Personal License regulations (PPL 70/7511 & PIL 70/24801) and was compliant with University College London ethical re-view committee guidelines. Mice were obtained from Charles River Laboratories (Charles River UK, Kent, UK), and were housed in a pathogen-free room controlled for temperature and humidity. NOD/SCID/interleukin 2 receptor [IL2r]γ-null mice and Balb/C nude mice (athymic) were used.

For generating the patient derived xenograft, a freshly obtained tumour sample was transferred from the operating theatre to the laboratory, the sample was diced under sterile conditions into 2mm square fragments and placed directly into transport medium containing antibiotics (Penicillin and Streptomycin) and an antifungal agent (Amphotericin, GIBCO Invitrogen) and held at room temperature over night. The following morning, the tumour sample was mixed in a 1:1 ratio with growth factor–reduced Matrigel (BD Biosciences CA), and injected subcutaneously into both flanks of two 5-6-week-old female NOD/SCID/interleukin 2 receptor [IL2r]γ null mice. During the engraftment phase, tumours are allowed to establish and grow and then harvested upon reaching a size of 1-1.5cm^3 (P1). The tumour was subsequently expanded into 2-3 BalbC/nude mice (P2). Over a period of 14 months the tumours were passaged every 8-10 weeks into nude mice, though one additional passage went through NOD/SCID mice as the BalbC/nude mice growing the tumour became unwell and in the interest of time we used the mice available. Once the tumours had reached a volume of 1-1.5 cm^3 the mouse was sacrificed according the guidelines, and the tumour removed. The tumour was dissected as described into smaller sections; one small piece was sent for histology to monitor for histological resemblance to the primary tumour (10% formalin), at least one piece was frozen in freezing medium (for re-implantation at a later date, see below) or snap-frozen for histology review or DNA extraction. The remaining tumour was divided into small pieces for re-implantation into the flank of new mice by inoculation following a small incision. Over a period of 14 months the tumours were passaged every 8-10 weeks into nude mice, though one additional passage went through NOD/SCID mice. The treatment cohort (P6) was transferred to John Hopkins University, Baltimore, USA for further expansion and drug testing.

The mice were anaesthetised using isofluorane for inhalation, and placed on a heating mat to maintain a temperature of 37°C. The small incision was glued using surgical glue, in the nude mice, but for the NOD/SCID mice the incision was stitched as these mice have hair. They also have a much more inquisitive and aggressive behaviour, and the glue was found not to be sufficient for maintaining the wound.

2.3.1 Freezing xenograft tissue:

Multiple cuts were made in, but not through, the tissue using two scalpels to obtain the equivalent of tenderised meat, and the tissue was then placed in freezing medium:

Freezing Media for re-engraftment
50mL FBS
15mL DMSO
85mL of appropriate cell culture media according to tumour type/cell line
Total volume = 150mL

2.4 Luciferase expression chordoma xenograft

The U-CH1_luciferase cell line was engineered as described in section 2.2.2. The cells were intermittently put under Puromycin selection to maintain 100% pure population of cells. The U-CH1 luciferase expression cell line was subsequently expanded and stored in liquid nitrogen.

For injection into the mice, the cells were expanded, collected (disrupted by trypsin) and counted as previously described. The cells were pelleted, re-suspended in medium and pelleted again before they were mixed with matrigel on ice (BD Matrigel™ Basement Membrane, Scientific laboratory supplies, UK).

Matrigel solidifies at room temperature and therefore has to be kept on ice right to the point of injection. The matrigel was put in aliquots of 150µL and stored at -20°C. The night before the injection, the aliquots were thawed on ice in the fridge, and then kept on ice when mixing with the cells. The syringes and needles were also kept cool in an icebox. For injection a total of 200µL containing the cells and the matrigel was aspirated into 1mL syringes with a 26-gauge needle. The mice were manually immobilised in a prone position and the animals were injected subcutaneously in the flank and monitored periodically for tumour formation. $1x10^7$ cells were injected/xenograft. Assessment of the tumours were performed weekly by measurement of size using an external caliper(667).

2.4.1 Treatment of the xenograft

The mice were subsequently injected intraperitoneal with D-luciferin substrate, and intratumoral injection was done using the AAV vector (or PBS). The latter procedure was done under general anaesthetic in order to achieve accurate injection. 50µL (vg $1x10^{12}$) was injected in total using 3 different sites within each tumour.

2.4.2 In vivo imaging

The animals were image using the IVIS spectrum in vivo imaging system for non-invasive longitudinal monitoring of bioluminescence. The machine was set up with anaesthetic equipment to be used while obtaining the images and the measurement, as well as a temperature control to keep the animals comfortable.

Luciferase expression was detected using D-Luciferin (Melford Laboratories, Cat # L1350), which was injected intraperitoneal (IP) at a dose of 200µg/mouse, as substrate, using the IVIS Imaging System 100 Series (Perkin Elmer). The images were analysed using the Living Image software 3.1, by grouping the images from different time points the relative light units (photons) can be directly compared. Following intraperitoneal injection of D-luciferin, the luciferase enzyme catalyse the substrate into oxyluciferin, requiring the presence of oxygen, and cofactors such as adenosine triphosphate (ATP) and mg^2 ions(668). The resulting light photons generated by this reaction are captured non-invasively with a charge-coupled device (CCD) camera mounted within the BLI system(669).

Bioluminescence imaging (BLI) was used to quantitatively assess tumour growth by correlating this to the intensity of luciferase expression. After injection of the D-luciferin the signal increases gradually, reaching a peak 10-20 minutes after injection. The signal intensity at the peak, is often used as a quantitative indicator of the luciferase activity and, consequently, of the tumour burden(670). A single predetermined time point for imaging after D-luciferin injection was used based on preliminary experiments, a method which has been shown to similarly represent tumour burden(671-673). The protocol was to image the mice 3 minutes after D-luciferin injection, with 45 seconds exposure time, delay in imaging meant saturation and inability to analyse the data.

Baseline luciferase expression in the tumour was determined using bioluminescent imaging to establishing level of expression on “day 0” (week 1). Assessment of the tumours was performed weekly by bioluminescence *in vivo* imaging measuring luciferase activity following inter-peritoneal injection of D-luciferin.

2.4.3 Viral genome distribution in xenograft

On termination of the experiment, 21 days after intra-tumoural administration of $1x10^{11}$PCR-vg/mouse, the tumour from each mouse was harvested. A small biopsy from the tumour was used for DNA extraction to assess copy number of the virus per cell by qPCR.

2.4.4 Antibody staining of paraffin sections for immunohistochemistry

Antibody staining of paraffin sections for brachyury was performed on the xenograft tumours. Brachyury (H-210); sc20109 antibody (Santa Cruz Biotechnology Inc. Santa

Cruz, CA, USA) is a rabbit polyclonal antibody against amino acids 226-435 of brachyury of human origin. Immunohistochemistry was carried out as follows:
After fixation of xenograft tumours in 10% neutral buffered formalin (Sigma) tissue was prepared, paraffin-embedded, and cut into 3µm thick sections. These sections were dewaxed through two changes of xylene and rehydrated through a series of graded ethanols (100% (v/v) to 50% (v/v)). Antigen retrieval was carried out by heating the sections, using a pressure cooker for two minutes in an antigen-unmasking solution (Vector Laboratories, Peterborough, UK). The iVIEW DAB Detection Kit and NexES immunohistochemistry system (Ventana Medical Systems Inc. Tucson, AR, USA) was used according to the manufacturer's instructions. Briefly, the endogenous peroxidase activity was inhibited and the sections incubated with the primary brachyury antibody (diluted 1:50) for 30 minutes. After washing the secondary antibody, a biotinylated Ig rabbit antibody (Ventana Medical Systems Inc.) was applied to facilitate visualization of the primary antibody, and a streptavidin-horseradish peroxidase conjugate (Ventana Medical Systems Inc.) was applied. Diaminobenzidine (DAB)(Sigma) substrate solution was used for visualising positive staining. The slides were counterstained with haematoxylin, dehydrated and mounted with a glass cover slip.

2.4 Fluorescent *in situ* hybridisation (FISH) analysis

FISH was performed on TMAs using probes from the bacterial artificial chromosomes (BACs) from the RP-BACs library (BAC/PAC resources centre, Oakland, CA, USA). The details of the BACs used are shown below. Chromosome enumeration probes (CEP) were used as references and obtained from alpha satellite DNA for chromosomes 6 and 7 (Resources for Molecular Cytogenetics, Bari, Italy) labeled in green with Vysis reagents. Details of chromosome enumeration markers are listed below.
TMA sections were cut at 4µm thickness, de-paraffinised in xylene and rehydrated in ethanol. Sections were pre-treated using the Paraffin Pretreatment Reagent Kit II (Vysis). Briefly, the slides were placed in the pre-treatment solution at 80°C for 50 -70 minutes, and in pepsin solution 0.05% at 37°C 20 to 25 minutes. The probes were applied to the slides and co-denatured for 5 min at 73°C and hybridised for at least 16 hours at 37°C in a Thermo-Brite hybridizer (Iris, Westwood, MA, USA). The slides were washed in formamide-free solutions: 2XSCC/0.3% Igepal CA-630 (Sigma-Aldrich Company Ltd, Gillingham, Dorset, UK) at room temperature for 5 min, at 73°C for 2 minutes and at room temperature for 1 minute, and then counter-stained with 4',6'-diamidino-2-phenylindole (DAPI) and analysed under a fluorescent microscope (Olympus, Watford, Hertfordshire, UK) using AnalySIS software (Olympus). The

chromosome localisation of all BAC clones was confirmed on normal metaphase spread slides (Vysis). Fifty non-overlapping nuclei that contained unequivocal signals were counted for each case. For the probes used, amplification was defined by a ratio of more than 2 for the gene-specific probe compared to the chromosome-specific reference probe. FISH analysis for *EGFR* comprises two groups; FISH positive (*EGFR* genomic gain) and FISH negative (no or low *EGFR* genomic gain) according to the Colardo criteria developed or non small cell lung carcinoma, The former included high level polysomy (≥ 4 copies/cell in ≥ 40% of cells) and amplification (defined by the presence of tight gene clusters, or ratio *EGFR* gene signals/CEP7 signals ≥ 2, or ≥ 15 copies of the gene per cell in ≥ 10% of analysed cells). The latter included two subgroups; low level polysomy (> 2 copies/cell in ≤ 40% of cells or 3 copies/cell in ≥ 40% of cells) and diosomy (≤ 2 copies in > 90% of the cells)

Details of BACs used to generate FISH probes				
BAC reference	**Gene covered**	**Chromosome location**	**Type of aberration**	**Labeling colour**
RP11-235F13	Brachyury	6q27	Amplification	Orange
RP11-381G5	EGFR	7p11.2	Amplification	Orange
Details of probes used as chromosome enumeration markers				
	Location		Labeling colour	
Chromosome 6 alpha satellite DNA (CEP6)	Chromosome 6		Green	
Chromosome 7 alpha satellite DNA (CEP7)	Chromosome 7		Green	

2.5 Molecular biology techniques

2.5.1 Generation of Adeno-associated viral vector for RNAi delivery

The previous work within the lab had been undertaken using the GIPZ construct (GIPZ Lentivirus shRNA from Thermo Scientific Open Biosystems, Chesterville, AI, USA) Clone ID: V2LHS_153725. Within the GIPZ construct the shRNA are expressed as human microRNA-30 (miR-30) primary transcripts. This design adds a Drosha processing site to the hairpin construct and has been shown to greatly increase gene silencing efficiency(674). The hairpin stem consists of 22 nucleotides (nt) of dsRNA

and a 19 nucleotides loop from human miR-30. The addition of the miR-30 loop and a miR-30 flanking sequence (125 nucleotides) on either side of the hairpin, results in greater than 10-fold increase in Drosha and Dicer processing, of the expressed hairpins when compared with conventional shRNA designs(364). Increased Drosha and Dicer processing translates into greater shRNA production and greater potency for expressed hairpins. http://www.thermoscientificbio.com/uploadedFiles/Resources/GIPZ%20Lentiviral%20shRNA%20Technical%20Manual.pdf

Cloning of the shRNA with the miR-30 flanking sequences was undertaken, using PCR amplification, amplifying the sequence of interest having designed the primers to add restriction sites to the sequence, for cloning into the viral vector plasmid. A scAAV vector with a CMV promoter and green fluorescent protein (GFP) expression cassette was used. Generating a AAV_CMV_shRNA_GFP plasmid. Methods detailed below.
Subsequently a different donor vector was used to test a different expression cassette for generating an AAV vector. This vector was a pLKO.1 vector containing a U6 promoter expressing the shRNA and a PGK promoter for expression of Puromycin. The cloning strategy and methods used were similar for the different constructs used.

2.5.1.1 Plasmids

Self-complimentary AAV: pAAV sc_CMV_GFP (Amit Nathwani, UCL Cancer Institute)
Gateway cloning entry vector: PENTR4_flag; Invitrogen (Addgene 17423)
Lentiviral vector: pLenti PGK_Puro_DEST (Addgene 19068/pRRL vector)
Lentiviral vector: pLenti_CMV_Luciferase_Puromycin (Addgene 17477)
GIPZ Lentivirus shRNA from Thermo Scientific Open Biosystems, Chesterville, AI, USA) Clone ID: V2LHS_153725.

Table 2.2 GIPZ brachyury targeting clone

Clone ID Target region	Mature sense	Mature anti-sense
V2LHS_153725 Exon 4/exon 5	GAGGAGATCACAGCTCTTAA	TAAGAGCTGTGATCTCCTC

Gene silencing construct: pLKO.1 Lentivirus shRNA from Thermo Scientific Open Biosystems (RNAi consortium). Clone ID: TRCN0000005481-TRCN000005484. The pLKO.1 vectors hairpin stem consists of 21 nucleotides of dsRNA and a 6 nucleotides loop and short flanking sequence of 4-5 nucleotides.

Table 2.3 pLKO.1 Brachyury targeting clone

Clone ID Target region	Mature sense	Mature anti-sense
TRCN0000005481 Exon 4	CGAATCCACATAGTGAGAGTT	AACTCTCACTATGTGGATTCG
TRCN0000005482 Exon 8	GCATGTTTATCCATGCTGCAA	TTGCAGCATGGATAAACATGC
TRCN0000005483 Exon 4	GCATAAGTATGAGCCTCGAAT	ATTCGAGGCTCATACTTATGC
TRCN0000005484 Exon 4/exon 5	CGAGGAGATCACAGCTCTTAA	TTAAGAGCTGTGATCTCCTCG
Non-targeting SHC002	CAACAAGATGAAGAGCACCAA	TTGGTGCTCTTCATCTTGTTG

The different short hairpins targeting brachyury were purchased from Open Biosystems Thermo scientific as glycerol stocks. Each clone was streaked using a sterile loop transferring the frozen bacteria from the top of the glycerol stock to an agar plate, and grown overnight in an incubator at 37°C. Colonies were picked the following day and grown in 3mL of Luria Broth (LB) overnight: The following day, plasmid DNA was prepared as described in section 2.7.1. Clones were tested with restriction digest using the enzymes BamH1/Nde1 as per recommendation by Open Biosystems protocol.

2.5.2 Cloning of vectors

2.5.2.1 PCR amplification

Primers were designed manually and checked using clone manager. Restriction sites for cloning were added, and the primers were checked for primer dimers (NCBI BLAST web tools for alignment of two sequences). DNA sequences were generated using DYAD Peltier Thermal cycler (BioRad Laboratories Ltd, Hemel Hempstead, UK). Phusion® High-Fidelity DNA Polymerase (New England Biolabs UK Ltd. Hitchin, UK) were used for the amplification according to manufactures recommendations. A temperature gradient was used to find the optimal annealing temperature for each template-primer pair combination.

Table 2.4 Phusion PCR reaction

Component	20 µL reaction	50uL reaction	Final concentration
Nuclease-free water	To 20 µL	To 50 µL	
5X Phusion HF or GC Buffer	4 µL	10 µL	1X
10mM dNTPs	0.4 µL	1 µL	200 µM
10µM Forward primer	1 µL	2.5 µL	0.5 µM
10µM Reverse primer	1 µL	2.5 µL	0.5 µM
Template DNA	variable	variable	< 250 ng
DMSO (optional)	(0.6 µL)	(1.5µL)	3%
Phusion DNA polymerase	0.2 µL	0.5 µL	1.0 units/50 µL PCR

DNA template: Genomic DNA (50-250ng), cDNA or plasmid (1pg-10ng)

Table 2.5 Thermo cycling conditions for PCR

Step	Temperature	Time
Initial denaturation	98°C	30 seconds
25-35 cycles	98°C 45-72°C 72°C	5 seconds 30 seconds 15 seconds
Final extension	72°C	10 minutes
Hold	4-10°C	

2.5.2.2 Restriction enzyme digest

The production of adeno-associated viral (AAV) vectors relied on DNA digestion with restriction enzymes. Restriction sites were also used to accurately verify plasmid inserts. Digestion was performed in the presence of buffers designed to optimise enzyme efficiency. All restriction enzymes and buffers were supplied by New England Biolabs UK Ltd (Hitchin, UK). In brief the vector backbone was digested by the restriction enzymes added to the insert using specific primers, the linearised plasmid was then visualised on an agarose gel and the DNA was extracted from the gel. The linearised plasmid was de-phosphorylated using calf intestinal alkaline phosphatase (CIP) to prevent the exposed ends to re-ligate. A PCR clean up reaction was undertaken prior to ligation with the insert amplified by PCR, details below.

2.5.2.3 Material and reagents for cloning

Table 2.6 Restriction digest reagents

Restriction enzymes	New England Biolabs (NEB)
10X Enzyme buffer	NEB
100X Bovine Serum Albumin (BSA)	NEB
Ultrapure water	HyClone Laboratories, Utah, USA
DNA template	
Eppendorf Mastercycler Gradient PCR machine	Eppendorf
DNA loading buffer	NEB

2.5.2.4 Protocol for restriction digest reaction

Table 2.7 Restriction digest reaction

Plasmid DNA (0.2-5µg)	x µL
10X NEB Buffer	2 µL
100X NEB BSA solution	1 µL
Enzyme 1U	1 µL
Distilled water to final volume	x µL
Total volume	20 µL

Digests were carried out at 37°C for 1-3 hours, or as specified for optimal enzyme activity. Double digests were performed when required and buffer were compatible. When double digests with incompatible enzymes, a sequential digest was set up. The initial digest with the first enzyme was set up as a 20µL reaction. The second enzyme (1.2µL) and buffer (3µL) were added after completion of the first incubation. When performing these sequential digests, the enzyme requiring the buffer containing a lower salt concentration was used in the first reaction. For very dilute DNA samples, 50µL reaction volumes were used with the volume of individual components adjusted accordingly. Following incubation DNA loading buffer was added (3-5µL) to the reaction and run on an agarose gel.

2.5.2.5 Isolation of DNA fragments using agarose gel electrophoresis

Separation of DNA fragments was achieved using agarose gel electrophoresis. The constant mass to charge ratio of DNA molecules means that separation is determined by fragment size. Migration rates are therefore influenced by the pore size of the gel, which is determined by the agarose concentration (Table 2.8). Consequently, careful selection of the percentage of agarose used ensured optimal resolution of the fragments of interest.

Table 2.8 Agarose concentrations for separation of different size DNA fragments

Agarose (%w/v)	Range of separation (Kb)
0.5	0.7 - 25
0.8	0.5 - 15
1.0	0.25 -12
1.2	0.15 - 6
1.5	0.08 - 4

Agarose concentrations required for achieving separation of specific DNA fragments. Adapted from Sambrook J. & Russell DW (675).

Buffers and solutions;

10x TBE = 108g Tris-base, 55g boric acid, 9.3g EDTA in 1L deionised water

6x DNA Loading Buffer = Distilled water, 40% (w/v) sucrose, 0.25% (w/v) bromophenol blue, 0.25% (w/v) xylene cyanol.

Protocol

The protocol given below is for the production of a 1% 100mL agarose gel. The weight of agarose used and the volume of TBE into which it was dissolved differed depending upon the size and percentage of the gel required.

- One gram of agarose was mixed with 100mL 1x TBE and heated in a microwave oven (with regular agitation) until completely dissolved.
- After cooling 0.30μg/mL ethidium bromide was added and the mixture swirled vigorously to ensure even distribution.
- The gel was poured into a pre-cast mould, a comb inserted and the mixture was left to set at room temperature.
- Prior to loading, samples were mixed 5:1 with 6x DNA loading buffer. In addition to the samples, a 1kb DNA ladder was loaded to allow the size of migrating DNA fragments to be estimated.
- Once loaded, the gel was run at 5-8 V/cm until sufficient migration (as visualised by the loading dye) had occurred.
- The DNA was visualised with UV light at 254nm using a UV trans-illuminator. Images were taken using a TV zoom lens and thermal monochrome printer or the Universal Hood II Chemidoc system.

In instances when the DNA was required for further manipulation, the level of UV exposure was minimised to reduce the risk of mutagenesis.

2.5.2.6 Retrieval of DNA from agarose gels

Retrieval of DNA fragments from agarose gels enabled insertion into new vectors. Isolation of DNA from the agarose gel relies on the ability of the DNA to bind the silica membrane of a purification column in the presence of chaotropic salt. The DNA was subsequently eluted following the replenishment of the hydration shell upon the addition of water. Purification of the DNA from the agarose gel was achieved using the protocol for the QIAquick Gel Extraction Kit (QIAGEN, Crawley, UK) according to manufacture's recommendation.

2.5.2.7 Alkaline phosphatase treatment of digested plasmid DNA termini

Alkaline phosphatase enzyme was used to remove 5' phosphate groups from vector backbone DNA in order to prevent self-ligation. When digested DNA fragments had compatible or blunt ends, DNA was treated with calf intestinal alkaline phosphatase (CIP) (New England Biolabs, Ipswich, MA, USA) to dephosphorylate the ends prior to ligation. De-phosphorylation reactions were performed in restriction enzyme buffers immediately after digestion. 5U of CIP was added to the digestion reaction as well as 5μL 10X NEB Buffer 3, and incubated at 37°C for 1 hour. This step was always followed by PCR clean up to remove remaining reagent before proceeding with ligation (QIAGEN PCR clean up kit).

2.5.2.8 Fragment insertion using DNA ligation

The plasmid preparation for cloning included a restriction digest with the enzymes generated on the insert with the use of specific primers. DNA was quantified using a NanoDrop ND-1000 spectrophotometer (NanoDrop Technologies, Inc. Wilmington, DE, USA. Insertion of DNA fragments into a plasmid was performed using T4 DNA ligase (New England Biolabs) according to the manufacturer's instructions. Briefly, ligations were undertaken with 1:2 and 1:5 ratio of DNA concentration (vector:insert). A control was added using vector only (1:0). Reactions were incubated overnight at 16°C. The following day One Shot® Stbl3 or DH5α chemically competent Escherichia coli (E. Coli) cells (Invitrogen) were transformed using sterile technique with 10μl ligation mix by heat shock.

2.5.3 Additional cloning methods used:

2.5.3.1 TOPO® TA cloning

Once amplified, insertion of PCR fragments into the vector of choice was achieved using a four-step process. Firstly, the fragments required 'A-tailing' in order to facilitate

their introduction into a subcloning (TOPO) vector (step two). Bacterial colonies containing the fragment of interest was identified by restriction digest and sequencing (step three), the fragment was cloned into the vector of choice (step four).

Step One; A-tailing

The subcloning vector TOPO vector (Invitrogen) was used. For cloning the PCR product into the TOPO vector, a-tailing of the PCR product was performed according to manufacture's recommendation, briefly described below. TA cloning is a method of cloning PCR products that utilizes stabilisation of the single-base extension (adenosine) adding a 3' adenosine overhang produced by Taq polymerase to the complementary T (thymidine) of the T-vector (TOPO) where the insertion site is defined by the presence of single 3' thymidine overhangs. PCR products can be used directly without modification.

Following PCR clean of the PCR amplified DNA 2µL 100mM dATP (Invitrogen), 0.2 µL Taqman Polymerase (NEB), 5µL Buffer (NEB) and water was added to the completed PCR reaction mixture to a total volume of 50 µL. The reaction was incubated at 72°C for 30 minutes. An aliquot was subcloned into the TOPO vector (see below).

Step two; Sub-cloning into the TOPO vector

The following reaction mixture was produced:
3µL A-tailed PCR reaction; 1µL salt solution; 1µL water; 1µL TOPO vector
The mixture was incubated for 15 minutes at room temperature.

Step three; Screening for successful transformants

Blue/white screening was used to select bacterial clones transformed with the TOPO vector containing the desired insert. This technique harnesses the natural ability of the β-galactosidase enzyme to hydrolyse the β(1-4) glycosidic bond found in lactose. In the lactose analogue, X-gal, a galactose sugar is bound via a β(1-4) glycosidic bond to a chromophore. Hydrolysis of this glycosidic linkage by β-galactosidase releases the chromophore, which forms a blue product upon oxidation. Consequently, as the TOPO vector contains the coding region for the β-galactosidase enzyme, those bacteria transformed with this vector turn blue when supplied with X-gal. This process is optimised by also providing the *E.coli* with the allolactose analogue isopropyl-β-D-thiogalactopyranoside (IPTG). The IPTG binds to and releases an inhibitor bound to the β-galactosidase promoter, thereby maximising the transcription of this enzyme.

However, as the site of DNA fragment insertion in the TOPO vector is situated within the β-galactosidase coding region, ligation of a DNA fragment into this site disrupts β-galactosidase expression, thereby ensuring that the *E.coli* remain white.

Protocol

The reaction mixture was transformed into DH5α *E.coli* as previously described (Section 2.5.3.3). One notable exception is that prior to drying, plates were spread with β-galactosides (Invitrogen) to enable blue/white screening.

Following overnight incubation at 37°C, white colonies were picked and grown in liquid culture overnight in the presence of antibiotics.

Step four: Transfer of the DNA fragment into the vector of choice

The colonies generated overnight, were pelleted and plasmid DNA isolated. The DNA was subjected to an appropriate restriction digest to verify fragment insertion. The DNA from the miniprep was used for sequencing if the yield (concentration of DNA) was satisfactory, otherwise the colony was expanded and DNA was isolated by maxiprep. Sequencing within TOPO was done using standard primers as directed by the protocol. Subsequently those DNA preparations containing the correct fragment were ligated into the pre-digested backbone of the vector of interest as previously described (section 2.5.2.8)

The determine quickly and precisely DNA sequences was achieved using a technique based on the chain termination method originally described by Sanger *et al.,* (593,662) and utilised Big Dye Terminator chemistry. In this, the dideoxynucleotides (ddNTP) responsible for chain termination are fluorescently labelled (a different fluorophore for each base), thereby enabling their incorporation into DNA fragments to be easily distinguished. Sequencing of the DNA was achieved using capillary zone electrophoresis and was performed by the scientific support services at UCL Cancer Institute, using an Applied Biosystems 3730 DNA Analyser. Sequencing was analysed using Sequencing Scanner v1.0 and NCBI BLAST web tool for alignment of sequences. Subsequently those DNA preparations containing the correct fragment were ligated into the pre-digested backbone of the vector of interest as previously described (section 2.5.2.8)

2.5.3.2 Gateway cloning

The Gateway cloning system exploits the site-specific recombination system utilised by bacteriophage lambda to shuttle sequences between plasmids bearing flanking

compatible recombination attachment (*att*) sites(248,676). Once the sequence for expression has been captured within an entry clone, this DNA fragment can be recombined into a variety of destination vectors resulting in expression clones geared to specific applications. The recombination reactions are driven by two enzyme blends known by their commercial names: BP Clonase and LR Clonase(677,678).

Gateway® Technology was performed with a PENTR4_Flag (entry clone) and the Destination vector: pLenti_PGK_Puromycin (Addgene 19068)(664). The cloning reaction was performed according to the protocol from Invitrogen for the LR Clonase™ reaction. http://tools.lifetechnologies.com/content/sfs/manuals/pentr_man.pdf

LR Recombination reaction was performed. The reaction between an attL-containing entry clone and an attR-containing destination vector generate an expression clone with the gene of interest.
The following components were added to a 1.5 mL microcentrifuge tube at room temperature:

- Entry clone (supercoiled, 100-300 ng) 1-10µL
- Destination vector (supercoiled, 150 ng/µL) 2µL
- 5X LR Clonase™ reaction buffer 4µL
- 16µL TE Buffer, pH 8.0 (10mM Tris-HCl, pH 8.0, 1mM EDTA)
- Vortex LR Clonase™ enzyme-mix briefly. Add 4µL to the components above and mix well by vortexing briefly twice.

The reaction was incubated at 25°C for 1 hour.

- 2µL of 2µg/µL Proteinase K solution were added and incubated at 37°C for 10 minutes.

Competent *E. coli* were transformed and selected for the appropriate antibiotic-resistant expression clones (note the vector changes from kanamycin resistance to ampicillin resistance). Transformation described below.

Note: For propagation of the pENTR™ vector, Library Efficiency® DB3.1™ Competent Cells (Catalogue no. 11782-018) from Invitrogen for transformation are required. The DB3.1™ E. coli strain is resistant to CcdB effects and can support the propagation of plasmids containing the ccdB gene.

2.5.3.3 Transformation of One Shot® Stbl3 or DH5α

Replenishment of plasmid stocks and selection of newly produced vectors was achieved by introducing the plasmid into chemically competent *Escherichia coli* (*E.coli*). In general, the DH5α *E.coli* strain was used, however for amplification of lentiviral plasmids the DNA was introduced into the One Shot® Stbl3 strain of *E.coli* to reduce risk of inducing mutations. All steps followed common microbiological practice, using a Bunsen burner to provide the sterile vacuum.

Protocol

1. One vial of *E.coli* was thawed on ice prior to being incubated for 30 minutes on ice with 1μg plasmid DNA.
2. Bacteria were heat-shocked at 42°C for 90 seconds and subsequently incubated on ice for 5 minutes.
3. Following addition of 300μL SOC media, samples were shaken at 220rpm for one hour at 37°C. During this, agar plates containing the required antibiotic were dried in an oven at 37°C.
4. The *E.coli* were subsequently centrifuged at 4000*g* for 5 minutes and 150μL of supernatant removed.
5. Once resuspended in the remaining 150μL SOC media, bacteria were spread onto the pre-dried plate and incubated either at 37°C overnight, or at room temperature for 72 hours.
6. The antibiotic used for selection was dependent upon the plasmid being amplified.

2.5.3.4 Luria broth and Agar plates

Luria broth (LB-medium) (1L):

1. Dissolve 10g tryptone, 5g yeast extract, and 10g NaCl in 950mL deionised water.
2. Adjust the pH of the medium to 7.0 using 1N NaOH and bring volume up to 1 liter.
3. Autoclave on liquid cycle for 20 minutes at 15 psi. Allow solution to cool to 55°C, and add antibiotic if needed (100μg/mL of Ampicillin or 50μg/mL Kanamycin).
4. Store at room temperature or +4°C.

LB agar-plates:

1. Prepare LB medium as above, but add 15 g/L agar before autoclaving.
2. After autoclaving cool to approx. 40°C, add antibiotic (if needed), and pour into petri dishes.
3. Let solidify, then invert and store at 4°C in the dark.

2.5.3.5 Colony Analysis

Single bacterial colonies were selected using a sterile 200µL pipette tip and submerged in 3mL Luria Broth (LB) media containing 100µg/mL Ampicillin. The tubes were shaken at 220rpm for 16 hours at 37°C. The following day 2mL of the medium was centrifuged at 400x*g* for 10 minutes to pellet the bacteria. The supernatant was discarded and the pellet used for plasmid isolation. Retrieval of plasmid DNA was achieved using QIAquick Plasmid MiniPrep Kit (Qiagen GmBH, Hilden, Germany) according to the manufacturer's guidelines. Colonies were subsequently analysed using restriction digest with suitable enzymes generating differential sized bands to be visualised using gel-electrophoresis and UV exposure.

2.5.4 Large scale plasmid DNA preparation

Maxipreps were used for the production of concentrated DNA preparations. 300mL of LB was transferred to a 2L conical flask and inoculated with 1mL of fresh culture and incubated overnight at 37°C with agitation (220 rpm). Plasmid DNA was extracted using Macherey-Nagel NucleoBond Xtra Maxi kit (Macherey-Nagel (GmbH, Hilden, Germany) in accordance with manufactures recommendations. The DNA concentration following extraction was quantified using Nanodrop spectrophotometry (Thermo Scientific, Wilmington, DE, USA).

2.5.5 Cloning of the AVV knockdown construct

2.5.5.1 Generation of rAAV vector (GIPZ_ V2LHS_153725 construct)

A self-complimentary AAV (scAAV) plasmid was used to generate our vector, for expressing the shRNA sequence from the GIPZ_ V2LHS_153725 construct. The shRNA sequence was generated by PCR amplification, with restriction sites added with designing them into the primer sequence. The PCR product of the hairpin was initially cloned into the TOPO vector. The sequence was checked within the TOPO vector, using standard primers as per manufacture's recommendations, and the sequence was aligned manually using BLAST web based aligning tool to confirm the amplified sequence. The insert (shRNA) was subsequently cloned into the scAAV plasmid using restriction digest as described in section 2.5.2.2 and cloned using T4 DNA ligase. Two different knock down constructs were generated to establish if the miR30 scaffolding, and flanking sequence were needed for efficient processing of the shRNA. Control constructs were also generated consisting of an empty vector (scAAV_CMV_GFP) and a non-silencing (scrambled shRNA) with and without the miR30 regulatory region. The shRNA was inserted between the CMV promoter and the GFP (green fluorescent

protein) the generated expression cassette is illustrated below. Two control vectors were generated; one containing a non-silencing shRNA, and one empty vector containing only the CMV promoter and the gene sequence for GFP. All constructs were checked by restriction digests and sequenced to confirm insertion of the shRNA.

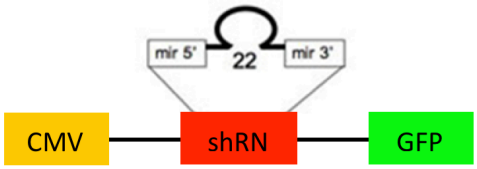

Figure 2.1 Expression cassette for rAAV CMV shRNA GFP

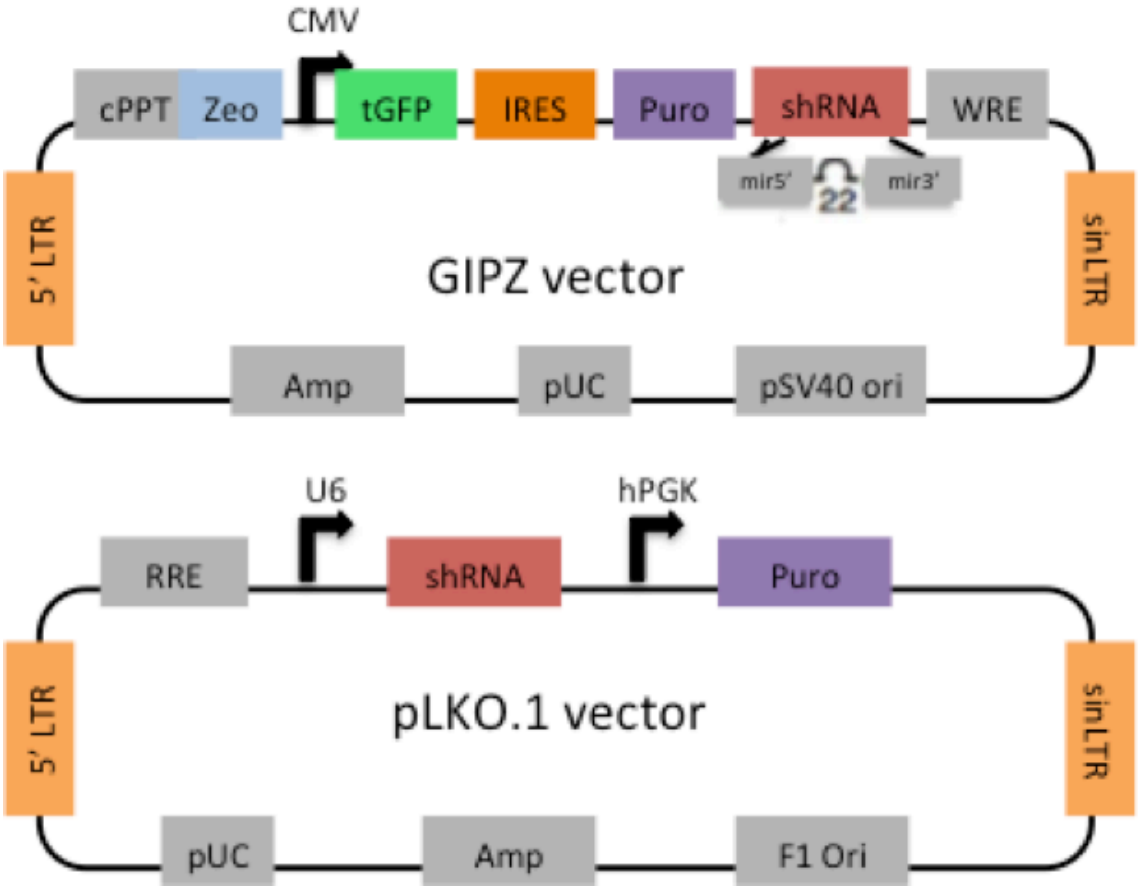

Figure 2.1 Examples of mammalian shRNA Lentiviral vectors
Two of the most commonly used mammalian shRNA expression vectors: the pGIPZ and the pLKO.1 construct. Available with a genome-wide shRNA collections and individual clones from Sigma (pKL0.1-puro) and Open Biosystems (pGIPZ). pGIPZ carries shRNAs with mir30 flanking sequences, whereas pLKO.1-puro carries simple snapback hairpins. A key difference is that pGIPZ uses a RNA polymerase II promoter (CMV) for shRNA expression, offering the potential for inducible and tissue-specific expression. The pLKO.1 uses a RNA polymerase III promoter (U6 promoter), less subject to cell-type-specific variation in its expression(343). Adapted from Chang et al. Cold Spring Harbor protocol(679).

2.5.5.2 Generation of rAAV vector (pLKO.1)

Primers were designed to amplify the hairpin with the whole expression cassette including the U6 promoter as well as the Puromycin-resistance selection cassette as illustrated below including the sequence amplified annotated with primers and genes.

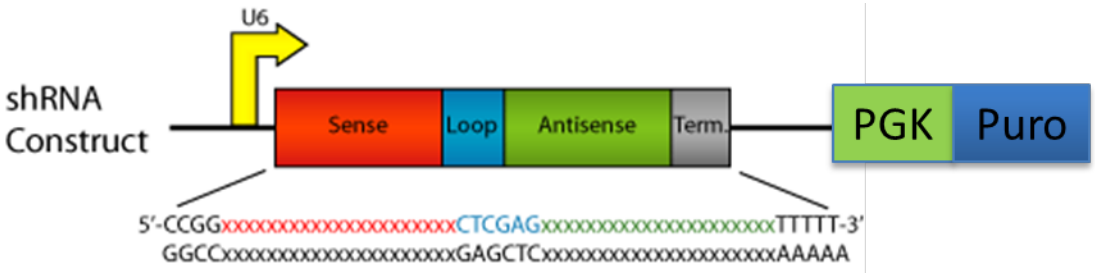

Table 2.9 Primers for pLKO.1 expression cassette

Forward primer	5' ctaGCGGCCGCaatCCTTCACCGAGGGCCTATTTC 3'
Reverse primer	5' ctaCTGCAGcgtTGGCTAAGATCTACAGCTGCC 3'

RE sites added: forward RE: Not1 5' GCGGCCGC 3' Reverse RE: Pst1 5' CTGCAG 3' (All primers purchased from Invitrogen, Paisley, UK).

PCR amplification of the expression cassette from the pLKO.1 vector was performed, using Phusion® High-Fidelity DNA Polymerase. The PCR product was identified on an agarose gel detected by fluorescence of intercalated ethidium bromide under UV illumination. The PCR product was cut from the gel and cleaned up using Qiagen gel extraction kit. The PCR product was subsequently A-tailed and cloned into TOPO TA. The constructs were verified by sequencing using primers: M13 reverse and M13-20 according to protocol. Following restriction digest the correct bands where visualized on the agarose gel and DNA was extracted from the gel. Generation of the rAAV vector constructs, were made using self-complimentary recombinant AAV plasmids. The expression cassette contained a CMV promoter and luciferase which was removed by restriction digest using Not1 and Pst1 restriction enzymes in a double digest. These restriction enzymes were also used to digest the expression cassette (insert) (U6_shRNA_PGK_Puromycin) from the TOPO vector. The scAAV backbone was dephosphorylated using Calf Intestine phosphorylation (CIP) before the insert was ligated into the vector using T4 DNA ligase. The AAV vector (pAAV_U6_shRNA_PGK_puro) was digested to confirm insert. Not1/Pst1 enzymes confirmed the presence of the insert, and DraIII/Xmn1 enzymes cut within the insert and the backbone respectively (right). Not1/Pst1 digest, expected bands: 1834 & 3166. Control: pAAV_CMV_Luciferase (bands: 2400 and 3169 bp). DraIII/Xmn1 digest expected bands of 1292 & 3708 bp. pAAV_CMV_Luciferase, contains only the Xmn1 site linearised by double digest.

Transformation of competent cells was undertaken and confirmation of ligation was demonstrated by the presence of colonies. The colonies were picked and grown in LB overnight. Restriction digest was performed on the mini-preps, the size of the insert was confirmed and an additional digest was done using restriction enzymes cutting within the insert as well as the backbone for further confirmation of successful ligation. The ITRs were checked using restriction enzymes Ahd1 or Bgl1 prior to producing large-scale plasmid DNA.

2.5.6 AAV5 production and transduction

2.5.6.1 Transient transfection

Transient transfection using PEI and HEK 293T cells for rAAV production:
PEI (polyethyleneimine, Polysciences cat. 24765 Polysciences Inc, Northampton, UK) of which 1g was dissolved in 900mL of water and the pH adjusted with sodium hydroxide to pH 7.2 and made up to 1L with water. This was filter sterilised and aliquoted for short-term storage at 4°C, and -20°C for long-term storage.

HEK 293T cells ($1.5x10^7$ cells/150mm plates, Greiner Bio-One GmbH) were seeded the day before transfection.

Table 2.10 Assays for AAV production (40 plates)

	Mix 1	Mix 2
DMEM (Serum free)	54mL	64mL
PEI	3mL	-
HGTI		1.8mg
Capsid		0.6mg
Transgene		0.6mg

In preparation for virus production from 40 plates, 6mL of PEI was added to 54mL of serum-free medium. In a separate tube, three plasmids were added (1.8mg HGTI, 0.6mg capsid, 0.6mg transgene) to 64mL of serum free medium. The mixture containing plasmid was filtered through a sterile filter (0.2µm) into the PEI mixture, and incubated at room temperature for 15 minutes before adding 3mL/plate. The following day the medium was changed to serum-free medium (SFM) and the cells were incubated for another 48 hours(680). The virus was harvested by collecting supernatant and cells using a cell scraper and then centrifuged at 500*g* for 10 minutes, the supernatant was stored at 4°C until purification was done. The pellet was resuspended in PBS, and following another centrifugation resuspended in 10mL TD buffer (100mM NaCl, 2mM MgCl2, 10mM Tris.HCl pH8). The lysate was stored at -

80°C. For the virus to be released from the cells, the cell lysate was freeze/thawed 5 times using liquid nitrogen and a water bath at 37°C. The cells were vortexed between each freeze/thaw cycle.

2.5.7 Purification of AAV5 with AVB Sepharose column

The cell lysate was thawed at 37°C and the supernatant, was placed in the water bath before adding $MgCl_2$ (1M) and benzonase (Sigma Aldrich)(50units/mL or 2units/10µL) and incubated for 30 minutes at 37°C. The solutions were then centrifuged at 3000*g* for 30 minutes at 4°C, the supernatant was gently removed from both cell lysate and supernatant, and filtered through a 0.2µm sterile filter before mixing prior to purification. The AVB Sepharose column (GE Healthcare UK Ltd, Buckinghamshire, UK) was set up according to protocol. Collecting tubes were prepared by adding 30µl Tris pH 8.8 to each tube to neutralise the glycine elution buffer. The sample was run through the AVB Sepharose column and eluted into the collecting tubes. Tubes from the second peak on the 260 and 280 graphs, were collected and pooled together, the waste from the run through was collected and run through the AVB Sepharose column a second time to collect as much virus as possible. Slide-A-Lyzer™ dialysis cassette (Life technologies), which facilitates effective dialysis, was briefly immersed in PBS, before injecting the virus into the cassette. The virus was then dialysed in 2 litres of PBS at 4°C stirring for 12-16 hours. The dialysed virus was sterilised by filtration through a 0.2µm filter and stored at 4°C.

2.5.7.1 Alkaline gel electrophoresis titration

For quantifying viral DNA viruses were run on denaturing alkaline gels and the band intensity was quantified by comparison against a standard DNA ladder I (Bioline, London, UK). Gels were made by dissolving 1g of agarose in 98mL water heated in a microwave, when cooled below 50°C 2mL of alkaline buffer (2.5M NaOH (50g), 50mL 0.5M EDTA (pH8.0) made up to 500mL of deionised water) was added. The gels were then cast and cooled further.

Alkaline sample loading buffer made from 200µL glycerol, 80µL 50X alkaline running buffer, 60µL 20% Ficoll (GE Healthcare UK Ltd, Buckinghamshire, UK), and xylene cyanol (enough to colour- dip pipette tip in powder)(Sigma) made up to 1mL of water 8.5µL of loading buffer was added to 25µL of sample (virus). Samples were mixed and placed on ice. The samples were then loaded onto the gel and run at 20V overnight in a cold room (4°C).

The next day the gel was washed for one hour in 300mL 1M Tris pH 8.0 with agitation. Gels were then transferred to 100mL of 4X Gelred (Cambridge Bioscience, Cambridge, UK) solution (prepared in 0.1M NaCl) and left for 2 hours in darkness with agitation. After rinsing twice with tap water the gel was imaged for quantification of viral DNA using Genesnap (Syngene) software. Output raw volume and background values for the intensity of each band were exported into an excel file. To calculate viral titre, background was subtracted from raw volume to obtain net volume values and a standard curve was generated by plotting ng of DNA in the Hyperladder against corresponding net volumes. The equation from the chart was used to calculate ng of DNA in each sample. To derive at a DNA concentration in ng/mL values were multiplied by 40. Viral titre was then calculated determining the number of AAV genomes in the given amount of DNA (based on the length of the viral genome in question).

2.5.7.2 Quantification of AAV titre by qPCR

The titre was determined against a standard curve generated from the plasmid used for virus production. The plasmid was linearised by a single cutter restriction enzyme and nano-dropped in order to calculate copy number. Serial dilutions (1:10) were made to generate the standard curve ($1x10^9$-$1x10^3$). Each virus was quantified in three dilutions (1:100, 1:1000 and 1:10000).

Table 2.11 Primers for RT qPCR viral titration

Forward GFP	GACGGCAACATCCTGGGGCACAAG
Reverse GFP	CGGCGGCGGTCACGAACTC
Forward U6	ACGATACAAGGCTGTTAGAGAGA
Reverse U6	AAAACTGCAAACTACCCAAGAAA
Forward U6_2	ATCCTTCACCGAGGGCCTAT
Reverse U6_2	TCTCTCTAACAGCCTTGTATCGT

All primers were purchase from Invitrogen, Paisley, UK.

Table 2.12 Assay for SYBR green RT qPCR viral titration

SYBR green master mix	12.5µL	
Forward primer (2.5 µM)	1µL	
Reverse primer (2.5 µM)	1µL	
Water	0.5µL	
Total (master mix)		15µL
Sample or standard		10µL

Samples and standards were run in triplicate. Water was used as a negative control.

Cycle conditions used: 95°C for 5 minutes, 95°C for 10 seconds and 60°C for 30 seconds. A melting curve was inserted in order to review the reaction and the accuracy

of the primers. Viral particles per mL was calculated as average of the diluted samples (1:100, 1:1000 and 1:10000) multiplying by dilution factor and 100 to obtain titre/mL.

2.5.7.3 AAV5 transduction of U-CH1

Cells were washed with PBS prior to transduction and serum-free medium was used for transduction. A Multiplicity of Infection (MOI) of $1x10^5$ (multiplicity of infection) was used after optimisation confirmed that increasing the MOI did not improve transduction efficiency. Virus was added to serum-free medium and applied drop-wise to the cells. The plate was gently shaken at regular intervals over the following 6-7 hours at which point the medium was topped up with serum containing medium. Calculation for determining the amount of virus to be added: ((number of cells x MOI) / titre) x1000 = µL virus.

2.5.7.4 WST-1 proliferation assay

Water Soluble Tetrazolium Salt (WST1) assay (Roche), a cell proliferation reagent is a colourimetric assay designed to measure the relative proliferation rates of cells in culture. The assay principle is based on the conversion of the tetrazolium salt WST-1 into a coloured dye by mitochondrial dehydrogenase enzymes. The soluble salt is released into the media. Within a given time period, the reaction produces a colour change, which is directly proportional to the amount of mitochondrial dehydrogenase in a given culture. As a result, the assay actually measures the net metabolic activity of cells which is reflective of cell number i.e. the more cells, the more dehydrogenase available to reduce the reagent. By the same reasoning, cell viability can be measured.

Cells were seeded $5x10^4$ in 96 well plates, 3 plates were seeded for end-point assays for 3 different time points (24 hours, 48 hours and 72 hours) the assay was read at time 30 minutes only on day 1 (24 hours) to have a starting point for the readout. The end point readout was then done at 4 hours for time point 24, 48 and 72 hours. Each condition was seeded in triplicates and the average was used for generating the data.
Puromycin selection was commenced 48 hours after transduction and maintained for 72 hours. The end point readout was then done at 4 hours for time point 24, 48 and 72 hours. Each condition was seeded in triplicates. The average was used for generating the data.

2.6 Lentivirus production and transduction

2.6.1 Transient transfection

Transient transfection using PEI and HEK 293T cells for lentiviral production:

PEI (polyethyleneimine, Polysciences cat. 24765) of which 1g was dissolved in 900mL of water and the pH adjusted with sodium hydroxide to pH 7.2 and made up to 1L with water. This was filter sterilised and aliquoted for short-term storage at 4°C and -20°C for long-term storage. Third-generation VSV-G pseudo-typed high titres lenti viruses were generated by transient co-transfection of 293T cells with a three-plasmid combination.

Plasmid:	DNA (2 plates)
KGP3R	4.6µg
RTR2	2.4µg
VSVG	5µg
Transgene	48µg

HEK 293T cells ($1x10^7$) were seeded into 15cm plates (Greiner Bio-One, GmbH) the day before transfection in 15mL of DMEM medium. For a small preparation of Lentivirus, 2 plates were used.

Preparation for 2 plates included: 3mL of serum-free medium mixed with 120µL of PEI. In a separate falcon DNA (as above) was added to 3mL of serum-free medium. The mix with DNA was then filtered (0.2µm sterile filter) into the serum-free medium containing PEI, mixed well and incubated at room temperature for 20 minutes. Following incubation 3mL were added drop-wise to each plate. After 12-16 hours the medium was replaced by fresh medium, as the PEI is toxic to the cells. Supernatant was harvested at 36 and 48 hours post transfection. The supernatant from the 1st harvest was spun at 1500rpm for 10 minutes, filtered and stored on ice at 4°C until after the 2nd harvest when the supernatant was mixed and ultra-centrifuged at 25000 rpm for 90 minutes at 4°C (Beckman ultra-centrifuge, Beckman Coulter Life Sciences, High Wycombe, UK). The supernatant was discarded and the virus (pellet) was resuspended in 200µL of serum-free medium, kept on ice for the pellet to dissolve for an hour, and then put in 20µL aliquots before storing at -80°C.

2.6.2 Titration of lentivirus

The viral titre was determined using a “Lentivirus qPCR Titre kit” from Gentaur Ltd London, UK. (Cat. Number LV900). This one step lentiviral vector titration employs a quick RNA extraction step, which is followed by a qRT-PCR assay. The viral RNA was extracted using a virus lysis buffer. The viral RNA was then mixed with reagent containing primers and Reverse Transcriptase (RT). The qPCR-RT program used: 42°C for 20 minutes, 95°C for 10 minutes, 95°C for 15 seconds and 60°C for 1 minute the last two steps are repeated x40. Standards were provided with the kit.

2.6.3 Lentivirus transduction of U-CH1

U-CH1 cells ($5x10^5$ cells/dish) were seeded in a 10 cm tissue culture dish the day before transduction. Cells were transduced with MOI of 10. Viral titres attained were: Lenti_pLKO.1_5484 ($7.5x10^9$ viral particles/mL), Lenti_pLKO.1_NS ($1.76x10^9$ viral particles/mL), Lenti_GIPZ_V2LHS_15327 ($1.01x10^9$ viral particles per mL). Virus was thawed and then kept on ice. The required amount of virus was added to 100µL of serum-free medium before being put onto the cells in their medium (without antibiotics). Polybrene was not used on the U-CH1 cell line, as this was found to be toxic to the cells.

72 hours following transduction Puromycin (5µg/mL) was added for selection, un-transduced U-CH cells were used as a control for the Puromycin selection. After 96 hours of Puromycin selection, when all un-transduced control cells had been killed by the Puromycin, the transduced cells were harvested for RNA extraction (QIAzol), cDNA was generated (GoScript Promega) for quantification of RNA expression by qRT-PCR as described in methods. U-CH1 cells were also transduced with a lentiviral vector expressing luciferase and Puromycin in order to generate a U-CH1 cell line, which stably express luciferase.

2.6.4 Lentiviral transduction

Polybrene (hexadimethrine bromide, Sigma-Aldrich, St. Louis, MO, USA) was used at 8µL/mL for transduction of HEK 293T cells. This was added to serum-free medium and virus mix prior to infection of the cells. Transduction was performed as described for U-CH1 except cells were grown in 6 well plates.

For assessment of toxicity of the silencing construct in multiple control cell lines $5x10^5$ cells were seeded in 6-well-plates and transduced the following day with the lentiviral vector pLKO.1_5484 targeting brachyury and the pLKO.1_non-silencing vector using an MOI of 10. Puromycin selection was commenced 48 hours post-transduction and maintained for 72 hours.

2.6.5 Transfection of U-CH1 cell line

Transfection of UCH-1 cells has been optimised using different transfection reagents, as well as testing transfection by nucleofector technology (Lonza Cologne GmbH). XtremeGene HP (Roche, Diagnostics Ltd. Burgess Hill, West Sussex, UL) was the reagent, which gave the best result in the U-CH1 cell line. Transfection was performed using 1µg DNA to 3µL of XtremeGene HP. DNA was diluted in 100µL of serum-free

medium and XtremeGene HP was added directly in to the serum-free medium with the DNA mix and incubated for 15 minutes. Following incubation the mix was added drop-wise to the cells in their normal medium without antibiotics. The transfected cells were then left in the incubator for 24-72 hours depending on the experiment and the time required to generate the results. For GFP expression cells were harvested at 24 and 48 hours. For the shRNA knockdown experiment cells were left for 72 hours at which point Puromycin selection was initiated. Transfections were done in duplicate or triplicate.

2.6.6 Transfection of HEK 293T cells

Fugene transfection reagent (Roche diagnostics Ltd) was used for transfection of HEK 293T cells, and HEK 293T_brachuyry-expressing cells. Transfection was performed using 1µg DNA to 3µL of Fugene. DNA was diluted in 96µL of serum-free medium. Fugene was added directly in to the serum-free medium/DNA mix and incubated for 15 minutes. Following incubation the mix was added drop-wise to the cells in their normal medium (no antibiotics). The cells were then monitored for 24-72 hours depending on the experimental end-point.

2.6.7 GFP quantification

Efficiency transduction and transfection was assessed by quantification of GFP

2.6.7.1 CYAN flow cytometry analysis

Cells were prepared by trypsinising and pellets were resuspended in PBS with 1% Bovine Serum Albumin (BSA) and filtered through a cell strainer. Samples were analysed using a CyAn ADP flow cytometry analyser and Summit v4.3 Software (DakoCytomation, Redwood City, CA. USA).

2.6.7.2 IncuCyte, kinetic imaging system

The IncuCyte (Essen BioScience, Inc. Michigan USA) is an imaging system that allows long-term, live-cell imaging. It can be utilised for documenting cellular proliferation, behaviour, and morphology. This was used to monitor GFP expression in U-CH1 cells transduced with AAV5 vector-expressing GFP. Cells were placed in the Incucyte imaging system in a 6 well plate and were monitored using a computer software program (Incucyte Zoom, Essen BioScience) downloaded to the desktop. The setting options allow monitoring and imaging of the cells at various time-intervals.

2.7 Molecular biology: Nucleic acid

2.7.1 DNA extraction

Cells were trypsinised, pelleted and resuspended in 200µl PBS. Genomic DNA was extracted using proteinase K (Qiagen, GmBH, Hilden, Germany) according to the manufacturer's protocol for "DNA purification from Blood or Body fluids". Briefly, 200µL of Buffer AL was added and sample was pulse-vortexed and subsequently incubated at 56^0C for 10 min. After brief centrifugation 200µL of 100% ethanol was added and samples were applied to separate QIAamp spin columns. Washing steps with buffers AW1 and AW2 were performed and DNA was eluted in 50-100µL of buffer AE. DNA was stored at -20^0C

2.7.2 RNA extraction

Total RNA was extracted from cell lines using miRNeasy Mini Kit (Qiagen). Cells grown in 175T flasks were trypsinised and collected as a cell pellet prior to lysis. Cells grown in wells were lysed directly in the plate. Medium was aspirated and cells were washed with PBS. Cells were lysed adding QIAzol lysis reagent (QIAGEN). RNA was extracted according to protocol "Purification of Total RNA from Animal cells". Briefly, 140µL of chloroform (Sigma-Aldrich) was added for phase separation and following centrifugation the aqueous phase was carefully removed and mixed with 1.5 times the volume of 100% ethanol (VWR International Ltd, Lutterworth, UK). Samples were centrifuged in RNeasy mini spin columns (Qiagen). On-column DNase digestion was performed and multiple washing steps were performed using RWT and RPE buffer. RNA was eluted in 30-50µL of RNase-free water and frozen at -80^0C.

2.7.3 cDNA synthesis

Reverse transcription of RNA to cDNA was performed according to the manufacture's instruction using GoScript™ Reverse Transcription system; First-strand cDNA synthesis (Promega, Madison, WI, USA) utilising equivalent amount (up to 5µg) of RNA.

2.8 RT qPCR

Brachyury expression at RNA level was assessed using RT qPCR. Total RNA was isolated from cells using the QIAzol Lysis Reagent (QIAGEN) with miRNeasy Mini Kit according to the manufacturer's protocol. Total RNA was reverse transcribed using GoScript reverse Transcription system (Promega). Quantitative PCR was performed using Taqman Universal Master Mix II no UNG (Applied Biosystems, Invitrogen).

100ng cDNA were amplified as follows: 95°C for 10 minutes, 95°C for 15 seconds, 60°C for 30 seconds, 60°C for 30 seconds. Steps 2 through 4 were repeated for 40 cycles. Each reaction was performed in triplicate. Results were normalised to those for PGK. The comparative threshold cycle (Ct) method with the calculation of 2-[delta][delta]Ct was used to assess the relative level of expression of brachyury.

Table 2.13 Primers for Taqman assays and SYBR green assays

Primer Brachyury TQM probe (FAM)	5' CTCACCAACAAGCTCAACGGAGGG 3'
Endogenous PGK TQM probe (VIC)	5' CCTTGGAGAGCCCACAGCGACCCT 3'
Brachyury (3BF) forward primer	5' CCCGTCTCCTTCAGCAAAGTC 3'
Brachyury (4BR) reverse primer	5' TGGATTCGAGGCTCATACTTATGC 3'
PGK forward primer	5' GAAGAAGGAGCTGAACTACTTTGC 3'
PGK reverse primer	5' TGATGAGCTGGATCTTGTCTG C 3'

GAPDH (cDNA) forward primer	5' GGAGTCAACGGATTTGGTCGTA 3'
GAPDH (cDNA) reverse primer	5' GGCAACAATATCCACTTTACCAGAGT
GAPDH (gDNA) forward primer	5' GAGGTAGAGGGGTGATGTGGGGAG
GAPDH (gDNA) reverse primer	5' GTGGCAGTGATGGCATGGACTGTGG
TENM3 forward primer (exon 24/25)	5' GTGTCTCGGGTCTTTGCTGA 3'
TENM3 reverse primer (exon 24/25)	5' GATGTACTGCCGCTGGCTAT 3'

2.9 Compound screen

2.9.1 Control cell line

Normal adult human dermal fibroblasts: NAHDF

Order from LGC (ATCC UK distribution)

Queens Road, Teddington, Middlesex, TW11 0LY UK

Dermal fibroblast, human adult product: PCS-301-012

Fibroblast basal medium: PCS-201-030

Fibroblast growth kit, low serum: PCS-201-041

2.9.2 Materials

Table 2.14 Materials for compound screen

Reagent/Consumable	Supplier	Catalogue number
Cell Lines	Flanagan lab	
Media	Flanagan lab	
Staurosporine	Sigma	S4400
White Walled 96 Clear Bottom TC Plates, Lid, Sterile (Corning)	Sigma	CLS3610
CellTiter-Glo Assay (100mL)	Promega	G7572
Caspase-Glo 3/7 Assay (100mL)	Promega	G8092
384LDV ECHO Compatible Plates	Labcyte	LP-0200
384PP Plates	Matrix Technologies	4314-11
ECHO 550	LabCyte	
Multidrop Combi (MDC)	Thermofisher	
Multidrop Standard Cassette	Thermofisher	
Pherastar	BMG Labtech	
Biomek FX	Beckman	

2.9.3 Quality control criteria

Quality control criteria in this study included the effect on cell viability and morphology: using the multi-drop combi (MDC) for seeding cells, viability and signal stability of WST1 assay determining timing of read out of the end-point assay, and the optimum number of cells to seed for each cell line was established, and the time-point for the cells reaching 90% confluency. In addition the tolerance for DMSO (dimethyl sulfoxide) was established to assess the effect as the assays needed to be configured according to the cell lines sensitivity to the concentrations of the solvent, as this was used for the initial dilution of the compounds.

2.9.4 Assay performance and optimisation

The signal window for each assay plate was defined by the controls (cells + 0.25% DMSO) and blanks (cells + 30μM Staurosporine) for which there were eight replicates of each. Robust Z factors were calculated using robust controls and robust blanks to measure signal window range and variance. The acceptance threshold of >0.4 was implemented due to inherent variability of the signal window for each cell line. All assay plates for each cell line came back with Z Factors >0.4. The Z-factor is defined in term of four parameters: the means and standard deviations of both the positive and negative control. In high-throughput screens, a large number of single measurements of unknown samples are compared to positive and negative control samples. The Z-factor is an attempt to quantify the suitability of a particular assay for use in a full-scale,

high-throughput screen. Zhang and colleagues developed a method to quantify the quality of an assay(681).

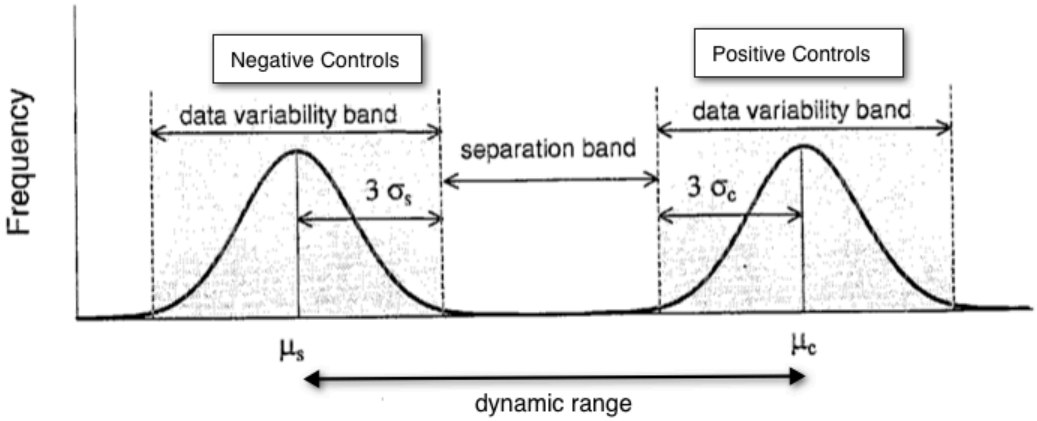

Z-factor is defined as the result of the following calculations.

1. Compute the threshold value for negative controls as the mean signal of the negative controls plus three times their standard deviation.
2. Compute the threshold value for positive controls as the mean signal of the positive controls minus three times their standard deviation.
3. Compute the difference between the two thresholds and call it the 'separation band' of the assay, S. If the threshold computed in step 1 is less than the one computed in step 2, then this difference is positive. Otherwise, this difference will have a negative value.
4. Compute the absolute value of the difference between the two means and call it the 'dynamic range' of the assay, R.
5. Compute the Z as S/R

To interpret the Z-factor, use these guidelines (direct from Zhang's paper).

A Z-factor of 1

An assay can never have a Z-factor of 1.0. This value is approached when you have a huge dynamic range with tiny standard deviations.

Z-factors can never be greater than 1.0.

A Z-factor between 0.5 and 1.0 is an excellent assay.

A Z-factor between 0 and 0.5 is marginal.

A Z-factor less than 0 means that the signal from the positive and negative controls could overlap, making the assay not very useful or screening purposes.

2.9.4.1 Effect of multi-drop combi on cell viability

The effect on cell viability, following cell seeding by Multi-Drop Combi (MDC) (Thermo Fisher Scientific) used for equal automated distribution of cells, was done by assessment of morphology and use of the viability assays: WST-1 and Cell Titre glow (CTG). Viability was compared with previous data on manual (pipette) seeding of cells.

2.9.4.2 Evaluation of WST-1 assay

WST previously discussed in section 2.5.7.4. WST-1, cell viability and proliferation assay was used to determine cell survival. The WST-1 assay signal stability was assessed as part of the optimisation and quality control. Cells were seeded using the MDC and treated the following day with Staurosporine in a 10 point IC_{50} format (10 doses across the plate), to establish the robustness of the assay format and reproducibility with automation (n=2). A 96-well absorbance assay was set up using three Chordoma cell lines, MUG Chor, U-CH1 and U-CH2. Assay technology used was the WST-1 cell viability kit from Roche. Method used was as stated by the manufacturer. The WST-1 assay was measured at regular interval to monitor if the signal was stable to determine the optimal time point for reading the assay. Importantly this had to be done before the point of saturation was reached.

WST-1 cell proliferation reagent is a colourimetric assay designed to measure the relative proliferation rates of cells in culture. The assay principle is based on the conversion of the tetrazolium salt WST-1 into a coloured dye by mitochondrial dehydrogenase enzymes. The soluble salt is released into the media. Within a given time period, the reaction produces a colour change, which is directly proportional to the amount of mitochondrial dehydrogenase in a given culture. As a result, the assay actually measures the net metabolic activity of cells. Theoretically, this is reflective of cell number – the more cells, the more dehydrogenase available to reduce the reagent. By the same reasoning, cell viability can be measured.

2.9.4.3 Optimisation of cell density

Cell proliferation and optimum numbers of cells for seeding were assessed in the planning process. Cells were seeded manually in densities of $6x10^3$, $5x10^3$, $3x10^3$ and $2x10^3$ cells per well in 90µL medium, in a 96 well plate. The confluency was assessed by light microscopy aiming for cells to be at 90% confluency at 120 hours.

2.9.4.4 Cell tolerance of DMSO

Cells were seeded by MDC. DMSO was tested in a dilutional format in a 96 well plated. WST-1 assay was used to assess the effect on proliferation.

2.9.5 Overview of compound screening

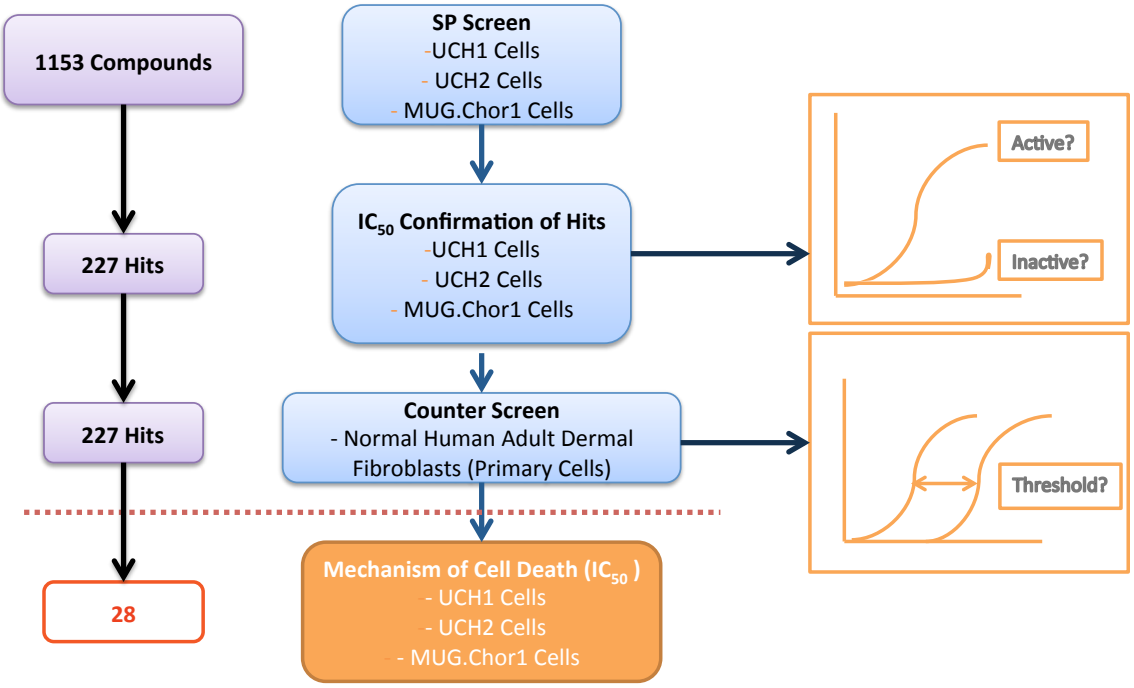

2.9.5.1 Single point screening

The compound screen was done using two kinase libraries, which were, screened 'blind' (PKIS1 and PKIS2) provided by GlaxoSmithKline (GSK). The screen was performed against pharmacologically active libraries held at CRT, namely the Calbiochem and Anti-Cancer libraries. The initial screening consisted of a high through-put screen (HTS), performing a single-point screen of approximately 1100 compounds using a cell viability endpoint assay. The compounds were tested in three well-characterised chordoma cell lines as models of disease. The compounds were screened at a concentration of 1μM based on experience gained from the collaboration with CRT and information provided by GSK regarding the potency of individual compounds *in vitro* for cell-based assays(682). The experiments in the screen were done in duplicate and in replicates using an automated screening format. Compounds causing a decrease in viability of more than 2 standard deviations (CI 95%) compared to the DMSO-controls (negative control) were regarded as hits. Staurosporine (SSP, 1μM, Calbiochem, Nottingham, Nottinghamshire) at 1μM concentration was used as positive control. Common and selective hits of each cell line was taken forward for IC_{50} profiling.

Compounds were screened in parallel in the single point screen with all compounds run in separate experiments (n=3). For each run of a total of 30 plates/run with10 plates/cell line, with a total of ~5 x T150 flasks for each cell line per was needed per run.

Protocol:

Day 1: $5x10^3$ cells/ well of U-CH1 and MUG Chor, and $2.5x10^3$ cells/well for U-CH2 cells were seeded by multi-drop combi (MDC) into 96 well plates 90µL/well.

Day 2: The compounds were aliquoted in 382 well mother plates at either 10 or 12mM concentration. Pre-dispensed daughter plates were generated with 100x the final concentration (1µM for single-point screening) in 2.5% DMSO. The plates were prepared by ECHO 550 and frozen in 384-format. Daughter plates were thawed for one hour at room temperature and sterile PBS was added to all wells at the required volume to dilute compounds to 10x the final concentration. 10µL of compound was then transferred from daughter cell to assay plate using the Biomek FX automated drug dispenser (96 head) (Beckman Coulter). DMSO (0.1%) was used as a negative control, and Staurosporine was used as a positive control. The compound-treated cells were incubated for 96 hours at 37ºC.

Day 6: WST1 assay was used to determine cell survival after 96 hours (the time point had been established in our optimisation experiments, aiming for a >90% confluence of control). 10µL of WST1 assay was dispensed using the Multi Drop Combi. The assay was incubated for 3 hours at 37ºC. Absorbance was read using a read-out at 440nm (maximum absorbance-spectrum of the dye) using a PHERAstar FS plate reader (BMG Labtech). Media controls containing the same amount of WST1 served as blanks. The raw data files were imported into the software programme: ActivityBase Visualisation by Vortex (Dotmatics) and analysed. CRT automated equipment was used.

Frequent calibration of equipment was undertaken to ensure minimal variation in the low-volume liquid dispensing. In addition the signal window for each assay plate was defined by the controls (cells + 0.25% DMSO) and blanks (cells + 30µM Staurosporine) for which there were eight replicates of each. Robust Z' Comparison of data was done between different runs to ensure comparability between experiments.

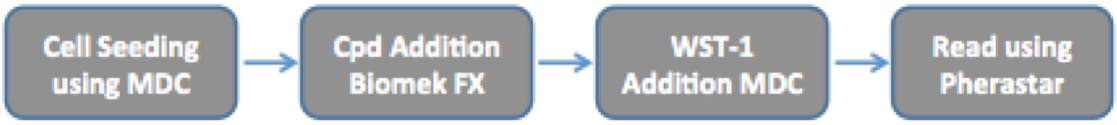

Automation pipeline for compound screening; MDC = multidrop combi, Cpd = compounds.

2.9.5.2 IC_{50} point compound screen

Confirmation of hits identified by the single-point screen was done using the IC_{50} format, with compound screening done in a 10-point dose response format with a top concentration of 20-30µM for all compounds, and a final DMSO concentration of 0.25% n=2. The % inhibition documented from the single-point screen was compared with the nearest equivalent dose (750nM) from the IC_{50} screen.

Day 1*:* Decontamination of the MDC cassette was performed with 50mL of 70% IMS, followed by 50mL of sterile PBS and then priming the cassette with 50mL of complete media. Cells were seeded (90µL/well) at defined cell density ($5x10^3$ cells/well U-CH1 and MUG Chor, $2.5x10^3$ cells/well UCH-2) into 96 well plates in columns 1-11. Cells were added to wells 12A-D (Staurosporine control) and medium only (background) to 12E-H manually. MDC speed setting: Medium. Two plates were seeded for each time point, per cell line. The MDC cassette was decontaminated MDC between cell lines as aforementioned, and cells were incubated o/n at 37ºC, 5% CO_2, 80% humidity. When the seeding was completed, the MDC cassette was decontaminate with 50mL 70% IMS.
Day 2: Compound treatment of plates (10-point IC_{50} format) was prepared 24 hours in advance at a 100x final assay concentration from 12mM/10mM compound stocks using the ECHO 550 (ECHO dispenses required dilution of compound, but 10x the final assay concentration was achieved when PBS was added on day 2). The 'mother' plates were in a 384 well format with compounds from which 'daughter' plates were generated by serial dilution at 1:3 from a top concentration of 300µM (100x) (for a final top concentration of 20-30µM). Staurosporine was the reference compound at one concentration and located in all wells of columns 23 and 24 at 300µM. DMSO was used as the control and was located in all wells of columns 21 and 22. Once prepared, 100x daughter plates was sealed (DMSO resistant foil seal) and frozen at minus 20ºC for 24 hours. Daughter plates were removed from the freezer and allowed to defrost at room temperature (RT) for 1.5 hour. Sterile PBS was equilibrated to RT. The MDC

cassette was decontaminated as described, but only primed with sterile PBS. The required volume of sterile PBS was added to all wells to bring the plates to the 10x concentration. Plates were sealed and left at RT for 15 minutes. The Biomek FX was decontaminated using Azowipes. The program was set up according to programme '96x4_Transfer_from_384_Version 16'. Assay plates were placed in the required spaces according to the programme. Sterile p20 96 well tips were placed in tip loader in between cell lines/mother plates. Lids were removed from assay plates. It was then indicated in the programme to transfer 10µL (diluted 10µL into 90µL to final concentration 1x) from relevant wells in daughter plate to assay plate. The programme stamped out each assay plate in duplicate. Eight plates per cell line were compound treated with the same compounds (e.g. from red locations in Figure 8) transferred to 8 x 96 well plates). The assay plates were placed back in the incubator at 37ºC, 5% CO_2, 80% humidity until assay end point. The MDC was decontaminated with 50mL 70% IMS.

Day 6: WST-1 reagent was defrosted at RT. The MDC was decontaminated with 50mL 70% IMS followed by 50mL PBS. The MDC cassette was then primed with WST-1 reagent. 10µL of WST-1 reagent was added to all wells of each assay plate and incubated at 37ºC, 5% CO_2, 80% humidity between 2 to 3 hours before reading on Pherastar FS using 'Chordoma Abs 96' protocol. The MDC was decontaminated as before with 50mL 70% IMS.

2.9.6 Summary of analysis

EC_{50} values were used as a measure of potency for the effect of a compound exerted on molecular targets. Values were determined from graphical plots of percentage inhibition *vs.* log [µM]. IC_{50} and EC_{50} can both be used as a measure of potency, however for using IC_{50}, a classic sigmoidal graphical profile would be expected spanning between 0 to 100% inhibition. EC_{50} is defined as the *effective* concentration, which elicits a half-maximal response (e.g. half way between the baseline and maximum response). In order to compare a compound that demonstrated heterogeneity, EC_{50} is the preferred measure of potency. In regard to this project, EC_{50} was used due to the nature of the data (baseline/maximum response was different between cell lines and did not always span 0 to 100% inhibition).

Raw data was converted to % inhibition and was plotted against [Log]. % Inhibition = 100*(1-(Sample – Mean Blank)/(Mean Positive – Mean Blank)). Potency was calculated by method of EC_{50} (due to the biased of Max/Min % Inhibition of the graphical profiles). Max % Inhibition was used as a tool to characterise compound

activity in conjunction with the EC_{50} (concentration of the compound which elicited 50% growth inhibition of the maximal response). EC_{50} values [µM] were converted to pEC_{50} values (-Log) to allow for easy comparison. pEC_{50} scale equals the inverse of molarity (pEC_{50} of 6 = 1µM or 9=1nM).

Compounds with a Max Inhibition (Maximal Response) of less than 40% were classed as inactive and were reported as 30µM (or >30µM). Compounds, which were potentially biphasic, were given an artificial potency of 100µM (pEC_{50} = 4) as EC_{50} cannot be calculated accurately on these types of curves.

Hit Confirmation Rate (HCR) characterises ability of a compound to reproduce activity over several experiments.

Hit confirmation rate (%) = (Number of confirmed compounds/Total Hits)*100

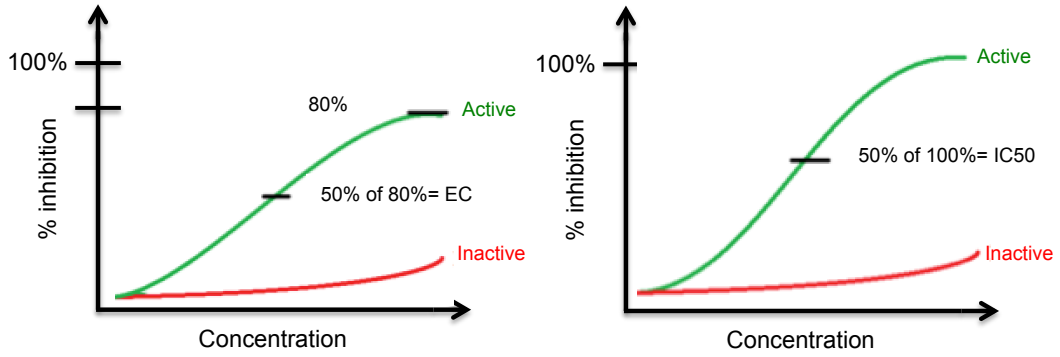

Figure 2.2 Illustration of IC50 in EC50 confirmation of hits
EC_{50} indicates 50% *efficacy* in a dose-response-profile, IC_{50} indicates 50% *inhibition* in dose-response-profiling, the latter being most informative in a setting where the sigmoidal graphical profiles span between 0 to 100% inhibition. EC50 values are more informative for comparison between heterogeneous profiles.

2.9.7 Hit selection criteria and calculations of EC50

Three runs of experiments were performed in four replicates for each cell line (U-CH1, U-CH2, MUG-Chor). Raw data were converted to percentage inhibition and Z-scores were calculated. The signal window for each assay plate was defined by the controls (cells + 0.25% DMSO) and blanks (cells + 30µM Staurosporine) for which there were eight replicates of each. Robust Z Factors were calculated using controls and blanks to measure signal window range and variance. Common hits across all cell lines as well as cell line specific selective hits above a threshold of 2 standard deviations (CI 95%) were selected unless otherwise stated. The half-maximal inhibitory concentration

(EC_{50}) was generated by testing a range of 10 concentrations from 1nM to 30μM in an automated format (IC_{50}). WST1 was used as an endpoint assay.

Within each run (n number) a standard compound, Staurosporine, was also tested in a 10-point dose response format at random alongside the test compounds. The pEC50 of each dose response was tracked to ensure reproducibility between each run. A potency acceptance range for each cell line measured reproducibility: Geomean ± 0.3 (equivalent to a 4-fold acceptance range of the mean pEC50 value).

2.9.8 Mechanism of cell death assay

The inhibition of cell growth may be brought about by a combination of mechanisms including apoptosis, alterations in cell cycle progression, cell senescence, autophagy, and increased toxicity leading to cell necrosis. Markers for apoptosis and cell viability were assessed.

Two 96-well luminescent assays were used to determine induction of apoptosis and cell viability, Caspase-Glo 3/7 (CG)(Promega) and CellTiter-Glo (CTG) (Promega) respectively. Each assay was performed on separate plates (at each time point) as both were lytic based. Method used was as stated by the manufacturer. Time points tested were 6, 24, 48 and 72 hours.

Caspase-Glo 3/7 assay provides a proluminescent caspase-3/7 DEVD-aminoluciferin substrate and a proprietary thermostable luciferase in a reagent optimized for caspase-3/7 activity, luciferase activity and cell lysis. Adding the single Caspase-Glo 3/7 Reagent in an "add-mix-measure" format results in cell lysis, followed by caspase cleavage of the substrate. This liberates free aminoluciferin, which is consumed by the luciferase, generating a "glow-type" luminescent signal. The signal is proportional to caspase-3/7 activity.

The CellTiter-Glo Luminescent Cell Viability Assay is a homogeneous method to determine the number of viable cells in culture based on quantification of the ATP present, which signals the presence of metabolically active cells. The homogeneous "add-mix-measure" format results in cell lysis and generation of a luminescent signal proportional to the amount of ATP present. The amount of ATP is directly proportional to the number of cells present in culture.

Compounds were tested using a non-randomised plate layout in a 96-well plate format (8 compounds per plate in a 10-point dose response). Profiling was conducted at a top concentration of 20-30μM with a 1:3 serial dilution for each test compound in two independent experiments. Data analysis was carried out using XLFit (IDBS). Raw data files were placed into a dose response template and for cell viability (CellTiter-Glo), percentage inhibition was calculated for each well from the raw data using positive (Staurosporine treated cells) and negative (DMSO treated cells) controls on each assay plate. For caspase-3/7 induction, percentage induction was calculated for each well from the raw data using the negative controls (i.e. percentage increase of compound treated cells *vs.* DMSO). All raw data was corrected for background (media only) in the first instance.

Time Points 6, 24, 48 and 72 Hours:

CTG and CG reagent were defrosted at RT, and reconstituted according to manufacturer's protocol. Two plates per cell line were equilibrated in the dark at RT for 30 minutes. One plate was used for the CG assay and the other CTG assay (decontaminate MDC with 50mL 70% IMS followed by 50mL PBS).
The MDC cassette was primed with CG reagent and 50μL of CG reagent were added to all wells of the assay plate. The plates were shaken gently at RT (protected from light with a cover plate) for 30 minutes and read on Pherastar FS using 'Chordoma CG 96' protocol (decontaminate MDC with 50mL 70% IMS, followed by 50mL PBS). Next the MDC cassette was primed with CTG reagent and 50μL CTG reagent were added to all wells of the assay plate. The plates were gently shaken at RT (protected from light with a cover plate) for 20 minutes and read on Pherastar FS.

2.9.9 Data Analysis

QC metrics were assessed for each assay plate, for each cell line, for both assays (Z Factor, percentage Coefficient Variation (CV) of controls/reference compound at one concentration). The curves were analysed for each time point. Caspase Glo calculated data was either the fold induction of caspase-3/7 or percentage induction of caspase-3/7 (treatment well increase in signal relative to DMSO control corrected for background). CTG calculated data as percentage inhibition (treatment well within the plate, decrease in signal relative to DMSO control, corrected for background).

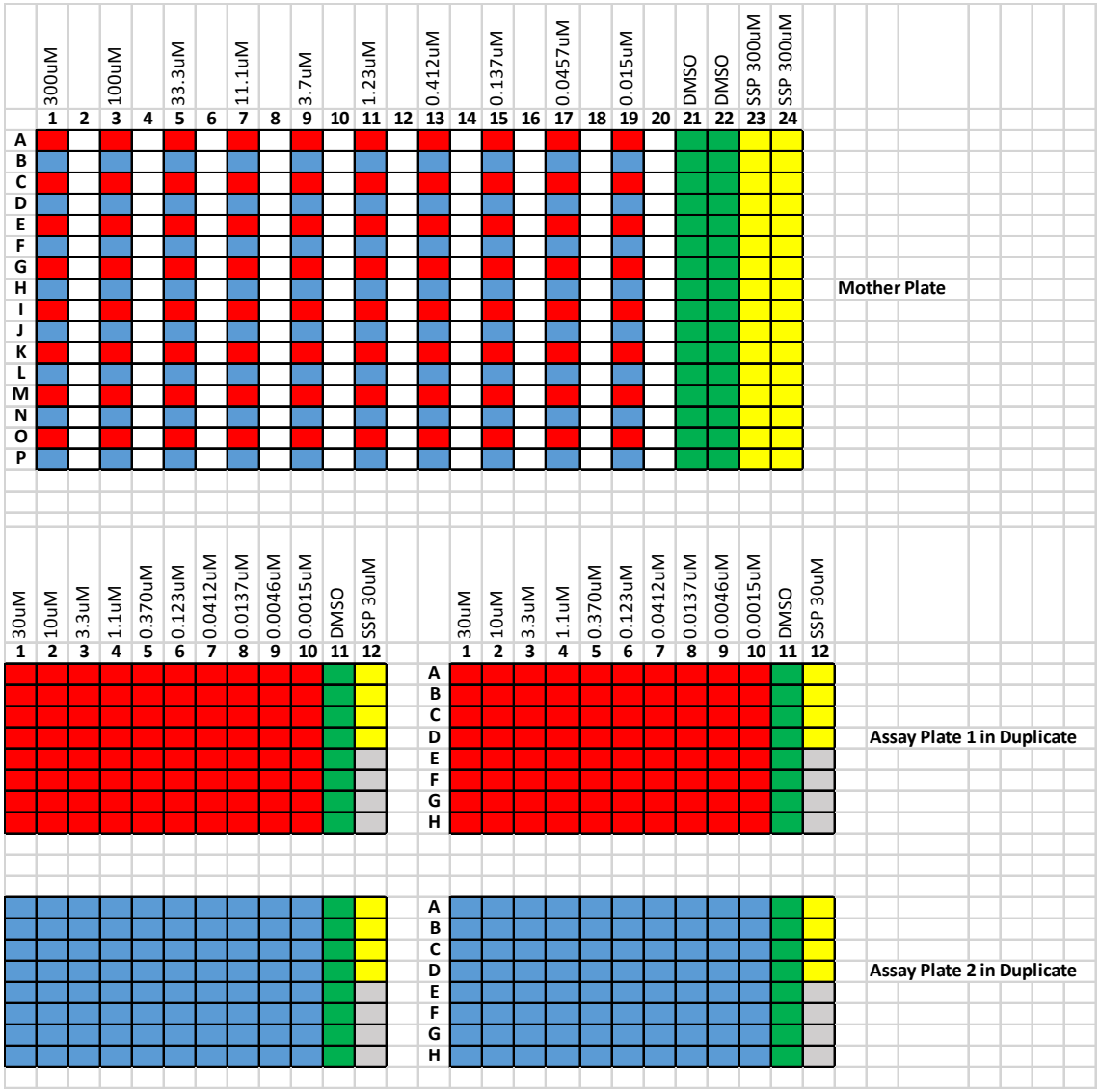

Figure 2.3 Mother Plate and Assay Plate Layout
(Grey indicates media only in 12E-H).

2.9.10 Western Blot

Reagents:

RIPA Buffer **Ingredients**	**Stock used**	**Total volume (10mL)**
20mM TRIS, pH 7.4	1M pH 7.4	200µL
150mM NaCl	5M	300µL
3mM EDTA	500mM pH 8	20µL
1mM EGTA	250mM pH 8	40µL
50mM NaF	1M	500µL
60.5% Sodium Deoxycholate (Sigma-S6750)	100%	50µL
0.1% SDS	20%	50µL
1% Nonidet P-40 Igepal® CA630-I3021 (Sigma)	100%	100µL
Fill up to 10mL with dH_2O 8.790mL. Keep it at 4^oC		

Add fresh before use:

Protease inhibitor cocktail (Complete, Roche, 04693116001), 25X stock (dissolving one tablet in 2mL water)

Phosphatase inhibitor Cocktail 2 (Sigma, P5726), use 1:100

Running Buffer 10X (1000mL)

30g TRIZMA BASE

144g Glycine

0.5% SDS

Transfer Buffer 10X (1000mL)

30g TRIZMA BASE

Glycine 144g

Transfer Buffer 1X (1000mL)

200mL Transfer Buffer 10X

20% Methanol

Blocking Buffer

PBS-T (Phosphate Buffered Saline with Tween® 20)

10X Concentration is 80mM Na_2HPO_4, 1.5M NaCl, 20mM KH_2PO_4, 30mM KCl, 0.5% Tween® 20, pH 7.4).

or TBS-T (Tris Buffered Saline with Tween®20)

For 1L TBS: 24g Tris-HCl (formula weight: 157.6g) 5.6g Tris base (formula weight: 121.1g) 88g NaCl (formula weight: 58.4g).

Dissolve in 900mL distilled water.

For 1L TBS-T: 100mL of TBS 10x, 900mL distilled water, 1mL Tween® 20

Bovine Serum Albumin (BSA) / Non-fat dried milk (Milk) 5% (5g)

5X Laemmli Buffer (50mL)

10% w/v SDS (5g)

50% w/v glycerol (25mL)

0,125% w/v bromophenol blue (5mL)

250mM Tris pH 6.8 (12.5mL of a 1M stock Tris pH 6.8)

2mM 2-mercaptoethanol (7.5mL)

20X TBS (2000mL)

30mL HCl 37% Anolar Normapur 20252.290 (under hood)

48g Trisma Base (Sigma, T1503) (MW 121.14)

152g NaCl S7653 Sigma Aldrich (MW 58.44)

Initially add 700mL H2O and solubilise the powder. pH adjusted to 7.4 using NaOH 1M. Add H_2O to total 2000mL.

TBS-T (1000mL)

20X TBS 50mL

0.1% Tween20 (1mL)

PBS-T (1000mL)

1X PBS 1000ml

0.1% Tween20 (1mL)

Protocol:

Lyse the samples:

1. RIPA Buffer was added (with freshly added Protease Inhibitor and Phosphatase Inhibitor) to the cell pellet and kept on ice for 15 minutes. The cell solution was then centrifuged for 15 minutes at 5000*g*, and the lysate was transferred to new clear Eppendorf and stored at -20^{o}C or protein concentration was determined by Pierce™ Bicinchoninic Acid Solution assay (BCA).
2. Protein concentration quantification was performed using Pierce™ BCA Protein Assay Kit (#23225, Thermo Scientific) according to manufacture's instructions.
3. The appropriate volume of RIPA-lysate was used to achieve 30µg of protein extract.
    a. A volume of 5X Laemmli loading buffer was added to all samples. The sample was boiled (in loading buffer) at 100^{o}C for 3–5 minutes.
4. Samples were loaded for electrophoresis on precast gels Criterion TGX Stain Free Gel and run at 150 volts until the bromophenol blue reached the bottom of the gel.
5. To transfer proteins, gels were placed on top of three pieces of 1mm filter paper soaked in transfer buffer. A piece of Whatman™ Protran nitrocellulose membrane standard pore size 45um (#10087970, GE Healthcare Life Sciences) soaked in transfer buffer was then placed on top of the gel followed by another 3 pieces of wet filter paper. To remove air bubbles a 5mL plastic pipette was rolled over the top of the gel stack. The stack was then placed in a transfer cassette on top of two sponges soaked in transfer buffer. Remaining space in the cassette was filled with more soaked sponges before clamping the cassette into an electrophoresis tank. Inside the tank, the cassette was filled

with transfer buffer and the outer chamber was filled with tap water to cool the transfer system. The transfer was then run at 70 volts for 2.5 hours at room temperature or at 30 volts overnight in a cold room (4^{o}C).

6. Efficiency of the transfer was checked by briefly incubating the nitrocellulose with Ponceau S Solution (P7170-1L, Sigma).
7. After transfer membranes were blocked with blocking buffer for 1 hour at room temperature with gentle agitation on a platform shaker.
8. Membranes were then washed with TBS-T 4 times over a period of 30 minutes at room temperature.
9. The filter was then incubated with primary antibody (see table 2.15) at 4^{o}C overnight with gentle agitation on a platform shaker.
10. The blocking solution was discarded and the filter was washed 3 times (10 minutes each time) with TBS-T.
11. Following this the filter was immediately incubated with the secondary antibody.
    a. IRDye 800CW Goat anti-Rabbit IgG (Thermo Scientific, #35571), 1:5000 in 5% milk in PBS-T.
    b. IRDye 680CW Goat anti-Mouse IgG (Thermo Scientific, #35518), 1:5000 in 5% milk in PBS-T.
12. The filter was incubated 1 hour at room temperature with gentle agitation.
13. The secondary antibody was discarded and washed with TBS-T 3 times for 10 minutes each time followed by one wash with PBS.
14. Protein bands were visualised using Li-Cor Odyssey scanner (Li-COR Biosciences, Ltd UK).

Table 2.15 Antibodies for Western blot analysis

Protein	KDa	Brand	Cat. Number	Species	Clonality	Washes	Dilution	Buffer	Store
EGFR	180	Cell Signalling	2232	Rabbit		TBS-T	1:500	5% BSA	4°C fridge
pEGFR-Y1068	180	Cell Signalling	2234	Rabbit		TBS-T	1:500	5% BSA	4°C fridge
AKR1B10	36/40	AbNova	H00057016-M01	Mouse	(M01), clone 1A6	PBS-T	1:1000	5% Milk	-20°C
PTEN	54	Millipore	04-035	Mouse	IgG, clone 6H2.1	TBS-T	1:1000	5% BSA	-20°C
B-actin	42	Sigma	A5441	Mouse	Monoclonal	PBS-T	1:5000	5% Milk	4°C fridge
Brachyury	47	Santa Cruz Biotechnology	sc-20109	Rabbit	Polyclonal	PBS-T	1:15000	5% BSA	4°C fridge

2.10 Circulation tumour DNA

Table 2.16 Kits for isolation of DNA and ctDNA

QIAamp DNA Mini kit (cat # 51304)	Qiagen
Qiagen FFPE Tissue Kit (cat #56404)	Qiagen
QIAamp Circulating Nucleic Acid kit (cat# 55114)	Qiagen

2.10.1 Patient samples

Consent was obtained for all samples, and collection of patient data under compliance with the Royal National Orthopaedic Hospital and University College London Hospital Biobank UK consent, approved by the Cambridgeshire Research Ethics committee (REC reference 10/H1107/36). Tumours were either frozen at a minimum of -80°C, or formalin-fixed paraffin-embedded (FFPE) according to histopathologic procedures. Tumours were dissected under a dissecting microscope to ensure a neoplastic cellularity of >60%. DNA was purified from the macro-dissected frozen tumours using QIAamp DNA Mini kit (Qiagen cat # 51304) and from macro-dissected FFPE tumours with a Qiagen FFPE Tissue Kit (Qiagen cat #56404) according to manufactures instruction. Exome and whole genome sequencing was done at the Sanger Institute Wellcome Trust as part of the International Cancer Genome Consortium (ICGC) project for bone tumours. Whole blood for isolation of white blood cells for DNA extraction (QiaAMP DNA mini kit) was used as normal tissue (constitutional DNA) for comparison and identification of somatic mutations.

Plasma was generated according to standard of procedures, from peripheral blood collected from patients into EDTA tubes, which was kept on ice until processed (max 2 hours). The tubes underwent centrifugation at 1200*g* for 10 minutes at 4°C and then 1mL of supernatant was transferred in aliquots to 1.5mL ml tubes and centrifuged at 14,000*g* for 10 minutes at 4°C to pellet any remaining cellular debris(683,684). The supernatant was transferred to fresh 1.5mL tubes and stored at −80°C.

Total genomic DNA was purified using QIAamp Circulating Nucleic Acid kit (Qiagen cat# 55114) according to manufacture's recommendation. 4mL of plasma was available from each patient. The plasma samples were in aliquots of 1mL each, DNA was extracted from each individual aliquot, but prior to DNA extraction samples were spiked with frog DNA (XENT) approximately 20,000 molecules in each sample in order to assess the extraction efficiency, and consistency of DNA extraction, as described in reference(685).

Patients were selected according to availability of plasma and mutations for which it was deemed possible to design Taqman probes.

2.10.2 Primer design

Primers were designed using BeaconDesigner software. Primer3 software was used and primers were checked using NCBI BLAST engine for nucleotide BLAST and Primer BLAST to align primers against the genome to confirm specificity and to check for primer dimer effect with complement sequences between the primers. The programs could not generate a Taqman assay for the GENE X deletion as the sequence was extremely AT rich. It was also not possible to design a SYBR assay on the BeaconDesigner as an appropriate sequence was not found. Attempts were made to manually design primers based on putting the deletion/normal sequence at the 3-prime-end and adding bases until a sensible melting temperature (TM) was reached. A common reverse primer was generated. 20 random bases were added to the mutant specific primer (in green).

GENE X mutation and primer design:

c.8894_8898delGTTAT
chr1:23589[redacted] AATAAC>A
range=chr1:2358[redacted]-2358[redacted] strand=+

WT
GACCATAG[redacted]TGTTGAGTCAAGAAGCCACTATTACCTTCTGATTTCT
GTCTATCCCTAAGGAGATACTTATTTGGAATAGTTAAATAACATCTCTGTAAACGTCTCCTC
TCTCGATTTGGCCCTTCT[redacted]GAGGTTGGATAGTAGATGGGGTCAT
ACCATACTGCTCTG

MT
GACCATAGTTCTCTGC[redacted]CAAGAAGCCACTATTACCTTCTGATTTCT
GTCTATCCCTAAGGAGATACTTATTTGGAATAGTTAAATCTCTGTAAACGTCTCCTCTCTCG
ATTTGGCCCTTCTGTTGG[redacted]GTTGGATAGTAGATGGGGTCATACCAT
ACTGCTCTG

WT Forward (with 20bp random sequence tag – green)
GGAGATACTTATTTGGAATAGTTAAATAAC

MT Forward
TCGGACCCCCTTGTCTATCCGGAGATACTTATTTGGAATAGTTAAATCTC

Common Reverse
CTACTATCCAACCTCATGGCAG

Primers for RT qPCR amplification was tested using tumour DNA to select the best primers prior to ordering the Taqman probes, and to confirm the presence of the mutation in the tumours (patients). Primers used in bold font.

Table 2.17 Primers for amplification of mutation and wild type

TARGET	FORWARD PRIMER	TARGET	REVERSE PRIMER
PIK3CA1_1F	GCTCAAAGCAATTTCTACA	PIK3CA1_1R	ACCTGTGACTCCATAGAA
PIK3CA1_2F	ACAGCTCAAAGCAATTTC	PIK3CA1_2R	ACCTGTGACTCCATAGAA
PIK3CA1_3F	**GCTCAAAGCAATTTCTACA**	**PIK3CA1_3R**	**CTGAGATCAGCCAAATTC**
PIK3CA2_1F	TAGCCTTAGATAAAACTGAG	PIK3CA2_1R	CCTGCTGAGAGTTATTAAC
PIK3CA2_2F	**CTAGCCTTAGATAAAACTGAG**	**PIK3CA2_2R**	**GCATGCTGTTTAATTGTG**
PIK3CA2_3F	TAGCCTTAGATAAAACTGAG	PIK3CA2_3R	TGAGCTTTCATTTTCTCAG
SETD_1F	**CAGACTGTTGGTTTGAATC**	**SETD_1R**	**CAGAGTGATGGTGTAGTAC**
SETD_2F	GACTGTTGGTTTGAATCC	SETD_2R	CAGAGTGATGGTGTAGTA
SETD_3F	ATCCCAAACACTATAATTCTG	SETD_3R	GAGTGATGGTGTAGTACA
GENE X1_1F	TGTTGAGTCAAGAAGCCACT	GENE X1_1R	AGCAGTATGGTATGACCCCA
GENE X1_2F	**ACAGGTAAGAGAGTGGTGGT**	**GENE X1_2R**	**CGAGAGAGGAGACGTTTACAG**
GENE X1_3F	AGTGGTGGTTTGACAACATCT	GENE X1_3R	CAGAAGGGCCAAATCGAGAG
GENE X2_1F	ATGGCAGCATATGACTTA	GENE X2_1R	GAGACGGAAGACTGTTAA
GENE X2_2F	**GCAGCATATGACTTAAAGG**	**GENE X2_2R**	**GAGACGGAAGACTGTTAA**
GENE X2_3F	GCAGCATATGACTTAAAGG	GENE X2_3R	GCCAATGACTCAGAAGATA

2.10.2.1 Optimisation of primers

The primers were used for RT qPCR amplification of DNA extracted from the tumours to identify the optimum primer sequence pair. The ability to amplify the correct sequence flanking/capturing the gene was assessed using a SYBR green assay to quantify the relative expression of the target gene comparing it to the endogenous control GAPDH. Three sets of primers were tested for each mutation. The RT qPCR products were run on an electrophoresis gel to visualise the amplified band confirming the right size band.

To confirm the probe's ability to detect the mutation sequence, DNA extracted from the tumour was amplified and digital PCR was used to quantify the mutation and wild type sequence. For the GENE X insertional frame-shift mutation, the PCR amplification product was sequenced confirming the primers amplified the intended region, as the assay had been developed manually. During the optimisation the DNA was tested under two different conditions with non-denatured DNA and following denaturing of DNA (95°C for 60 seconds), in order to see if denatured DNA would increase detection rate.

2.10.3 Digital PCR

Droplet digital PCR is a powerful tool to get quantitative measurement using Taqman primers and probes or similar hydrolysis/dual-labeled/FRET (fluorescence resonance energy transfer) probes. It gives absolute quantification of target DNA in the sample, unlike RT qPCR, which gives a relative quantification. PCR is performed within each

individual droplet, if the droplet contains the target sequence a fluorescent reporter dye will give off a fluorescent signal. If the target sequence is not present no PCR will take place and no fluorescent signal will be emitted. By scoring each droplet for fluorescent signal digital PCR obtains absolute quantification with high level of precision and single molecule sensitivity. The samples are amplified to endpoint in a conventional thermal cycler, if the droplets contain the targeted sequence they are read as positive while the droplets without the target sequence are read as negative. The assay can be multiplexed so that the target template probe is labeled with FAM and the wild-type template is labeled with VIC resulting in different colour fluorescent for the readout. The fraction of positive droplets determines the concentration of target template in the sample. The readout of the endpoint assay in the work in this thesis was done using BioRad QX200 droplet reader, digital technology automated system, where each droplet is individually passed through a two-colour fluorescent detector for the readout, determining which droplet contain the target template and which ones do not. The data using this method is recorded via QuantaSoft software, which allows the data to be visualised and analysed for quantification.

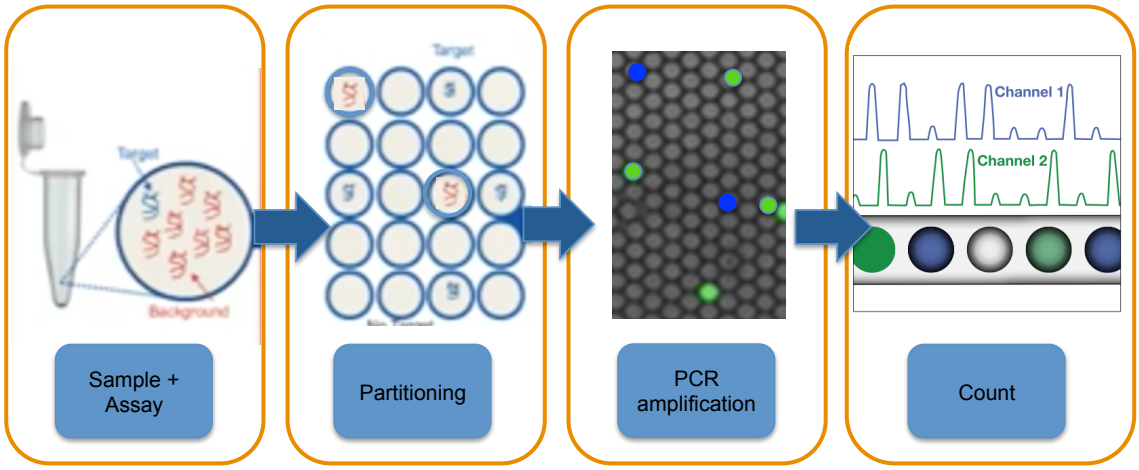

Figure 2.4 Digital PCR
The sample is prepared as a PCR assay and partitioned into droplets containing one nucleic acid containing the target template, the wild-type or no template sequence. Each droplet with an amplified sequence exhibits fluorescent, which is read for each droplet by two different channels

2.10.4 Mutation detection in ctDNA

Circulating tumour DNA was extracted from plasma and mutations were quantified by droplet digital PCR (dPCR) using Bio-Rad's QX200 Droplet Digital PCR system.

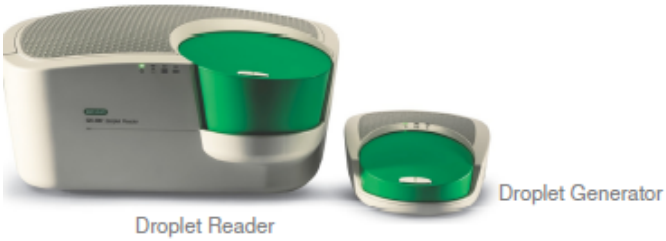

Figure 2.5 Illustration of Droplet digital PCR
Adapted from BioRad information guide for dPCR

2.10.4.1 Droplet generation

Before droplet generation, dPCR reaction was prepared in a similar manner as real-time PCR reactions using TaqMan hydrolysis probes labelled with FAM and HEX (or VIC) reporter fluorophores, or an intercalating dye such as EvaGreen. All reagents for the dPCR were from Bio-Rad and included dPCR supermix for probes and QX200 dPCR EvaGreen supermix and oil to partition DNA. Samples were placed into the QX200 droplet generator, using specially developed reagents and microfluidics to partition each sample into 20,000 nanoliter-sizes droplets.

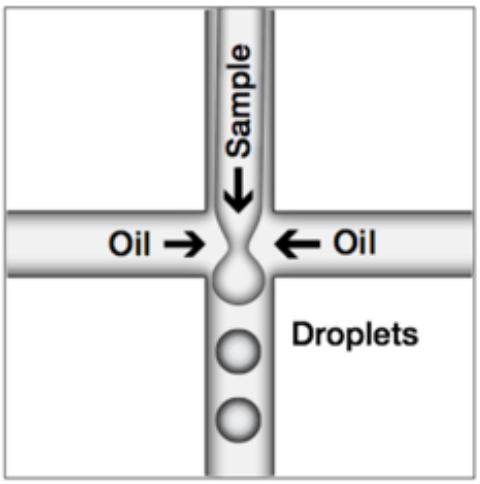

Droplet generation produced uniform droplets, enabling precise target quantification

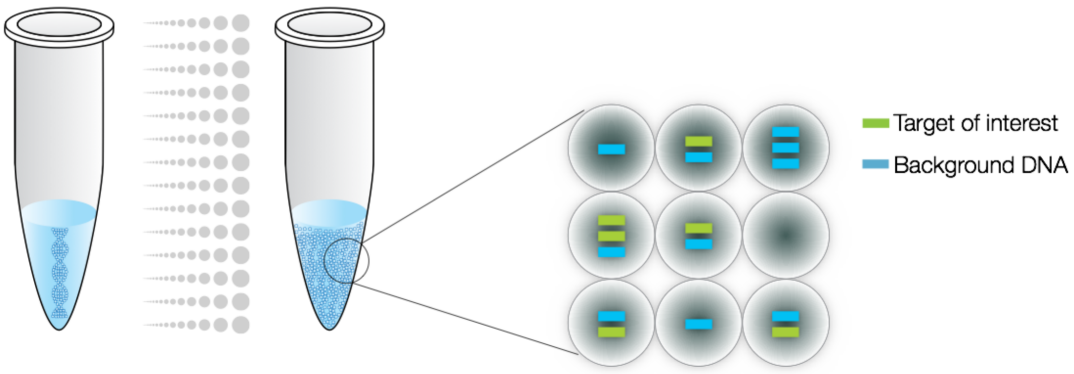

Figure 2.6 Droplet generation

Adapted from BioRad manuel:
http://www.bio-rad.com/webroot/web/pdf/lsr/literature/Bulletin_6407.pdf

2.10.4.2 PCR amplification

Droplets were transferred to a 96 well plate for PCR in a thermal cycler, as previously described.

2.10.4.3 Droplet reading

Following PCR amplification of the nucleic acid target in the droplets, the plate containing the droplets was placed in the QX200 droplet reader, which analyses each droplet individually using a two-colour detection system (set to FAM and HEX).

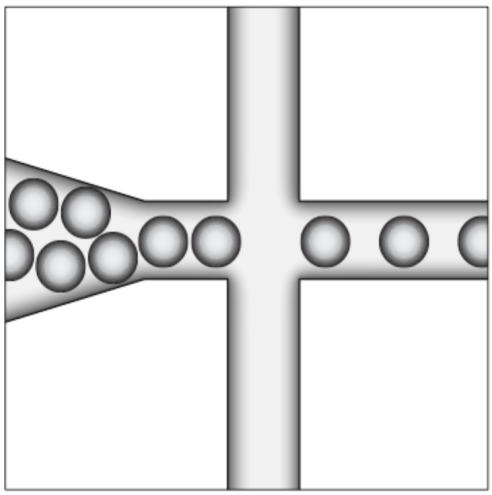

Droplets are being spaced out individually for fluorescence reading by the droplet reader.

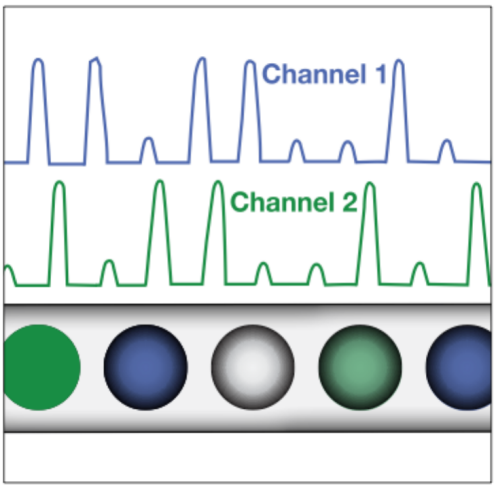

Positive droplets, which contains at least one copy of the target DNA molecule exhibit increased fluorescence compared to negative droplets. Fluorescence readings are measured for each droplet in two channels. Adapted from BioRad's protocol.

The partitioning of the sample, allows one to estimate the number of target (mutant) molecules by assuming that the molecule population follows the Poisson distribution. The Poisson distribution takes into account the fraction of positive droplets to determine the concentration of target template in the sample. In conventional real time

quantitative PCR the number of PCR amplification cycles is proportional to the starting copy number. Digital PCR is not dependent on the number of amplification cycles to determine the initial sample amount, eliminating the reliance on uncertain exponential data to quantify target nucleic acids providing an absolute quantification.

2.10.4.4 dPCR analysis

Droplet Digital PCR data can be viewed in d 2-D plot, data from a duplex experiment in which two targets are PCR amplified such as a wild type (WT) and a mutant (MT). Channel 1 fluorescence (FAM) is plotted against channel 2 fluorescence (HEX) for each droplet, example below:

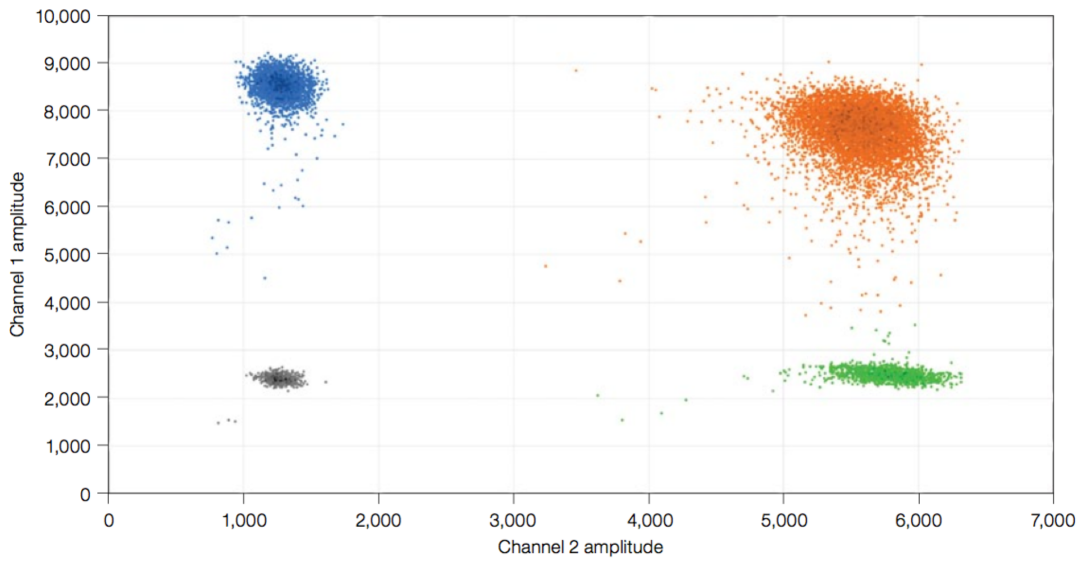

Example of 2-D plot of droplet fluorescence: Colour coding as our results, droplet clusters: blue was mutant sequence (FAM) detected, green was WT (HEX) sequence and orange droplets are double-positive droplets, containing both a WT and a MT (FAM and HEX) (not necessarily 1:1). Grey was DNA not containing the amplified sequences or empty droplets.

QuantaSoft™ software measures the number of positive and negative droplets for each fluorophores in each sample. The software then fits the fraction of positive droplets into a Poisson algorithm to determine the starting concentration of the target DNA molecule in units of copies/µL input.

In a typical digital PCR experiment, the sample is randomly distributed into discrete partitions such that some contain no nucleic acid template and others contain one or more template copies. The partitions are PCR amplified to end point and then read using a droplet reader to determine the fraction of positive partitions, from which the

concentration is estimated by modelling as a Poisson distribution. The positive and negative droplets are used to calculate the concentration of the target and reference DNA sequences.

Estimating target concentration by dPCR, as dPCR is an end-point measurement that enables one to quantify nucleic acids without the use of standard curves and independent of reaction efficiency. The ability to distinguish between the positive and the negative droplet clusters means an ability to achieve an absolute quantification without the need for endogenous controls http://www.bio-rad.com/webroot/web/pdf/lsr/literature/Bulletin_6407.pdf

A control for the PCR reaction was included using an endogenous gene (RNase P gene)(labelled: RPP30 in our experiments) recommended by Life technologies for human TaqMan copy number reference assays. This functioned as a control for the DNA and PCR run, and not as an endogenous control (TaqMan Copy number reference Assay, Life technologies cat. # 4403328).

2.10.4.5 Optimisation of DNA

To optimise amplification of the tumour DNA various steps were tested as advised by BioRad protocol.

a. Restriction digest was performed as previously described. Following confirmation the restrictions enzymes did not digest within the target sequence. This was tested as DNA extracted from FFPE can contain physical cross-links due to fixing with formalin, obstructing the partitioning and amplification of DNA. Restriction digestion can improve assay performance by improving template accessibility.
b. Dilution of the tumour DNA (1:10) was tested as PCR inhibitors can remain after the DNA extraction and dilution can sometimes overcome the inhibition.
c. Heat denaturation was done to separate the DNA strands to test if this would increase the detection of our target gene (DNA was heated to 92°C for 30 seconds).
d. PCR optimisation using thermal gradient to establish the optimal annealing temperature was tested.

2.10.4.6 EvaGreen assay

EvaGreen dsDNA binding dye enables double-stranded DNA detection with the convenience of only needing one primer to amplify and detect products. The idea being that the fluorescence amplitude of each droplet with EvaGreen varies with amplicon

length. Longer amplicons bind more EvaGreen dye molecules and are therefore brighter enabling quantification. This was the approach taken for the GENE X 1 mutation.

2.10.4.7 Statistical analysis of dPCR output

DNA molecules and PCR reagents are partitioned into droplets. Some droplets contain one or more copies of the target DNA molecule, and some do not contain any copies of the target. Droplets are subjected to PCR amplification and the targeted PCR product, with an associated fluorescence signal, is generated in droplets that initially contained the target DNA. The concentration of the target in the original sample is determined from the fraction of droplets that have a fluorescence signal. In dPCR, target molecules are distributed randomly into droplets. This assumption is at the heart of all digital PCR approaches. Random partitioning means a given target molecule is equally likely to end up in any of the 20,000 droplets. Random partitioning also means target molecules move independently of each other and do not interact with each other.

The droplet generator partitions samples into approximately 20,000 droplets of identical volume (about 1nL). Some droplets are lost in transfer steps and others are eliminated by the stringent metrics applied by QuantaSoft software as the droplets pass through the droplet reader resulting ultimately in data from 12,000–16,000 droplets being used in subsequent concentration calculations. Reading only a subset of the total droplets has no impact on the concentration measurement, because the concentration is calculated based on the fraction of droplets carrying the wild type (WT). Below is an example of outcome of droplet dPCR in two modes of analysis.

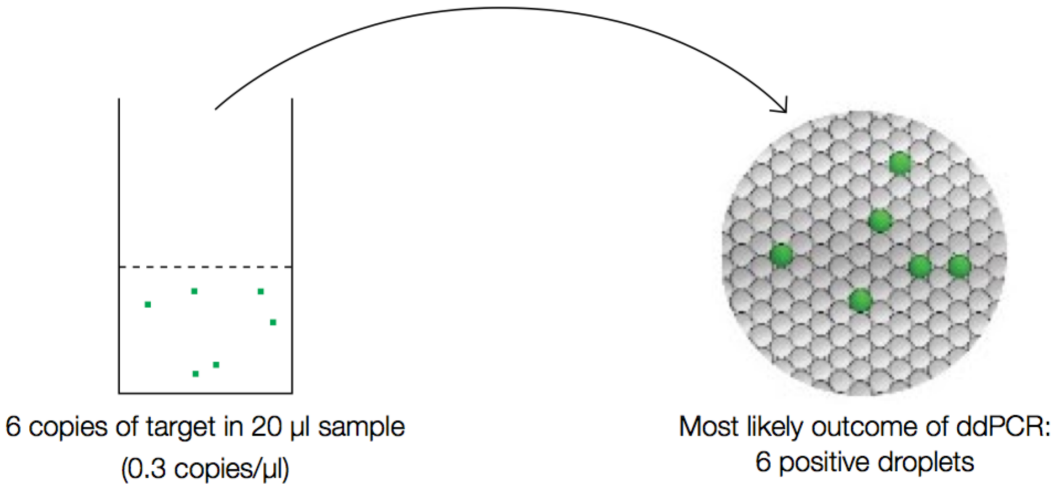

Controls used: (negative)

No template control (NTC)

Pooled plasma

Human genomic DNA (Bioline, Cat.# BIO-35025)

2.10.4.8 Example of set up for experiment

Test of chordoma assays on tumour tissue

Date 18/07/2014

Samples		**Sample ID**
Human genomic DNA		H
(1) 3814	Chordoma sample with PIK3CA c.1633G>A mutation	C1
(2) 7187	Chordoma sample with PIK3CA c.3129G>T mutation	C2
(4) 7168	Chordoma sample with c.6756delC mutation	C3
PPC3_1	DNA extracted from pooled plasma with spike (Rosenfeld) 17/07/14	P1
PPC3_2	DNA extracted from pooled plasma (Rosenfeld) 17/07/14	P2
NTC		NTC

PCR reaction mix setup (no-template room)

	Final
Volume DNA template (µL)	2
Remaining volume (µL)	18
Total volume (µL)	20

Prepare ddPCR reaction mixes (without template):
Thaw all components to room temperature.
Vortexing and briefly centrifuge supermix to avoid concentration gradient.

All chordoma assays 5

Reagent	[Original]	[Final]	Unit	1 rxn + excess (µL)	Total rxns (µL)
Supermix for probes	2	1	x	15	75
Forward primer	10	0.9	µM	2.7	13.5
Reverse primer	10	0.9	µM	2.7	13.5
Mutant probe	10	0.25	µM	0.75	3.75
Wild-type probe	10	0.25	µM	0.75	3.75
Water	-	-	-	5.1	25.5
			Total (µL)	27	135

IDH1-R132C 6

Reagent	[Original]	[Final]	Unit	1 rxn + excess (µL)	Total rxns (µL)
Supermix for probes	2	1	x	15	90
Forward primer	10	0.9	µM	2.7	16.2
Reverse primer	10	0.9	µM	2.7	16.2
Mutant probe	10	0.25	µM	0.75	4.5
Wild-type probe	10	0.25	µM	0.75	4.5
Water	-	-	-	5.1	30.6
			Total (µL)	27	162

RPP30 6

Reagent	[Original]	[Final]	Unit	1 rxn + excess (µL)	Total rxns (µL)
Supermix for probes	2	1	x	15	90
20x oligo mix	20	1	x	1.5	9
Water	-	-	-	10.5	63
			Total (µL)	27	162

XENT 5

Reagent	[Original]	[Final]	Unit	1 rxn + excess (µL)	Total rxns (µL)
Supermix for probes	2	1	x	15	75
20x oligo mix	20	1	x	1.5	7.5
Water	-	-	-	10.5	52.5
			Total (µL)	27	135

Aliquot 25.2 µL reaction mix into each well/tube of strip.

Sample addition

Limitations

Restriction digestion required for human gDNA concentrations ab	3.3	ng/µL
Reaction concentration must be below:	5000	copies/µL
And contain more than:	10	copies/rea

Estimated number of positive droplets

		Total			
Sample (ng/µL)	Reaction (ng/µL)	Reaction (copies/µL)	Copies/ reaction	CPD	Est. +ve droplets*
20	2	6.06E+02	1.21E+04	0.606	45%

Diluting control DNA

Template: Human genomic DNA (Bioline; Cat# BIO-35025; Lot# HG-314103)
Diluent: Nuclease-free water (Ambion; Cat# AM9937, Lot# 1402201, 18/06/14)

[Stock]	[Final]	Vol DNA (µL)	Vol diluent (µL)	Total vol (µL)	Req'd vol (µL)
200	20	5	45.0	50.0	25.2

Add 2.8 µL template into each well/tube of strip.

Setting up ddPCR

Follow instructions for:
QX200 Droplet Generator **Oil for Probes:** Cat# 1863030; BioRad
PX1 PCR Plate Sealer **Thermal cycler:**
QX200 Droplet Reader and QuantaSoft Software

RPP30: RNase P TaqMan control (control for PCR) (RPP gene)
XENT: frog spike for quantification of DNA extraction efficiency.
NTC: No template control

Experimental plan for setting up dPCR testing primers and Taqman probes on tumour DNA (example representing all similar experiment):

96-well plate setup

	1	2	3	4	5	6	7	8	9	10	11	12
A					H	C2	P1	P2				
B					H	NTC	P1	NTC				
C					C1	H	P2	H				
D					C1	H	P2	P1				
E					NTC	C3	NTC	P1				
F					H	C3	H	P2				
G					H	NTC	P1	P2				
H					C2	H	P1	NTC				

KEY (templates):

H	Human genomic DNA
C1	Chordoma PIK3CA1
C2	Chordoma PIK3CA2
C3	Chordoma SETD
P1	PPC3_1
P2	PPC3_2
NTC	NTC

KEY (assays):

	PIK3CA1_3
	PIK3CA2_2
	SETD_1
	RPP30
	XENT
	IDH1-R132C

a Add 2.8 µL of template to each well/tube.
b Transfer reactions to the droplet generator cartridge, and then transfer droplets to 96-well plate according to the above layout.

Cycling conditions

Cycling step	Temp (°C)	Time	# Cycles
Enzyme activation	95	10 min	1
Denaturation	94	30 sec	40
Annealing/extension	60	1 min	
Enzyme deactivation	98	10 min	1
Hold (optional)	4	Infinite	1

Temperature gradient to establish the best temperature for optimization of primers, Experiment layout (example representing all similar experiments):

96-well plate setup

	1	2	3	4	5	6	7	8	9	10	11	12	Temp (°C)
A	C1	C2	NTC										65.0
B	C1	C2	NTC										64.5
C	C1	C2	NTC										63.3
D	C1d	C2d	NTC										61.4
E	C1d	C2d	NTC		C2	C2	H	NTC	C2	C2	H	NTC	59.0
F	C1	C2	NTC										57.0
G	C1	C2	NTC										55.7
H	C1	C2	NTC										55.0

KEY (templates):

H	Human genomic DNA
C1	Chordoma PIK3CA1
C1d	C1, digested HindIII
C2	Chordoma PIK3CA2 & SETD2
C2d	C2, digested HindIII
NTC	Nuclease-free water

KEY (assays):

	PIK3CA1_3
	PIK3CA2_2
	SETD2_1 (wild-type only)
	SETD2_1 (mutant only)

a Add 2.8 µL of template to each well/tube.
b Transfer reactions to the droplet generator cartridge, and then transfer droplets to 96-well plate according to the above layout.

Cycling conditions

Cycling step	Temp (°C)	Time	# Cycles
Enzyme activation	95	10 min	1
Denaturation	94	30 sec	40
Annealing/extension	grad	1 min	
Enzyme deactivation	98	10 min	1
Hold (optional)	4	Infinite	1

2.10.5 Ion torrent

Tumour DNA was used for detecting the PIK3CA p.E545K mutation, and the PIK3CA p.M1043I mutation from two chordoma patients. Ion Torrent is a method of DNA sequencing, based on the detection of hydrogen ions that are release during the polymerisation of DNA when a template DNA strand in a microwell is flooded with a single species of deoxyribonucleotide triphosphate (dNTP). If the introduced dNTP is complementary to the leading template nucleotide, it is incorporated into the growing

complementary strand. The hydrogen release triggers an ion sensor indicating that a reaction has occurred.

Selected regions from a multi-gene panel (*Life Technologies Colon & Lung Panel V2*) was amplified using a highly multiplex Polymerase Chain Reaction approach. These were labeled using DNA barcodes unique to each specimen and then collectively sequenced on a Life Technologies PGM instrument using Ion PGMTM Sequencing 200 Kit v2 chemistry and a 318v2 chip. Data was analysed using Torrent suite v4.0.2 and VariantCaller v4.0 (r76860). An in-house developed script was then used to group Variant Caller output into the reported categories and construct variant descriptors according to Human Genome Variation Society recommended nomenclature (http://www.hgvs.org/) and COSMIC reference number.

2.11 AKR1B10 ELISA assay

2.11.1 Samples

Samples included: standard provided with the ELISA kit, patient plasma generated as described in the section for ctDNA, however for this experiment plasma was used without further processing. MUG Chor cell line lysate (positive control) was generated from $1x10^7$ MUG Chor cells. A cell pellet was washed with PBS and stored at -80°C over-night. The cells were freeze-thawed twice and then centrifuged at 4°C for 5 minutes at 5000*g*. The supernatant was removed and used immediately or stored in aliquots at -80°C for later use.

2.11.2 Materials

Reagents	Quantity
Assay plate (12x8 coated microwells)	1 (96 wells)
Standard (Freeze dried)	2
Biotin-antibody (100x concentrate)	1 x 120µL
HRP-avidin (100x concentrate)	1 x 120µL
Biotin-antibody Diluent	1 x 15mL
HRP-avidin Diluent	1 x 15mL
Sample diluent	1 x 50mL
Wash buffer (25x concentrate)	1 x 20mL
TMB Substrate	1 x 10mL
Stop solution	1 x 10mL
Adhesive strip (for 96 wells)	4

- Microplate reader for measuring absorbance at 450nm
- Incubator at 37°C
- Squirt bottle or automated microplate washer

- Absorbent paper for blotting the microtitre plate
- Distilled water

2.11.2.1 Preparation of standard

The standard (purified recombinant AKR1B10 protein) vial was centrifuged at 5000*g* for 30 seconds it was then reconstituted with 1.0mL of Sample Diluent producing a stock solution of 40ng/mL. 250µL of Sample Diluent was pipetted into each tube (S0-S6). The stock solution was used to produce a 2-fold dilution series (below). Each tube was mixed thoroughly before the next transfer. The undiluted Standard served as the high standard (40ng/mL). Sample Diluent served as the zero standard (0ng/mL).

2.11.3 ELISA

Human Aldo-keto reductase family 1 member B10 (AKR1B10) ELISA kit was purchased from CUSABIO® China, catalog number CSB-EL001540HU for the quantitative determination of human aldo-keto reductase family 1 member B10 (AKR1B10) concentrations in serum, plasma, tissue homogenates. The assay employs the quantitative sandwich enzyme immunoassay technique. Antibody specific for AKR1B10 was pre-coated onto a micro-plate. Standards and samples were pipetted into the wells and the immobilised antibody binds any AKR1B10 present. After removing any unbound substances, a biotin-conjugated antibody specific for AKR1B10 was added to the wells. After washing, avidin conjugated Horseradish Peroxidase (HRP) was added to the wells. Following a wash to remove any unbound avidin-enzyme reagent, a substrate solution was added to the wells and colour developed in proportion to the amount of AKR1B10 bound in the initial step. The colour development is stopped and the intensity of the colour is measured. The assay was performed according to the manufacture's instruction. The detection range was 0.625ng/mL - 40ng/mL.

Protocol

All reagents and samples were brought to room temperature before use. The samples were centrifuged after thawing before being used for the assay.

1. The number of wells to be used was determined and remaining wells were stored in the pouch (ziplocked), and stored at 4°C.
2. 100µL of standard or sample was added per well, covered with the adhesive strip provided, and incubated for 2 hours at 37°C.
3. After 2 hours the liquid of each well was removed (not washed).

4. 100µL of Biotin-antibody (1x) was added to each well, covered with a new adhesive strip, and incubated for 1 hour at 37°C.
5. Each well was aspirated and washed. This was repeated two times for a total of three washes. Washes was done by filling each well with Wash Buffer (200µL) using a squirt bottle or a multi-channel pipette, and left to stand for 2 minutes, complete removal of liquid at each step was essential for good performance. After the last wash, any remaining wash Buffer was removed by aspiration or decanting. The plate was then inverted and blotted against clean paper towels.
6. 100µL of HRP-avidin (1x) was added to each well, covered with a new adhesive strip, and incubated for 1 hour at 37°C.
7. The aspiration/wash process was repeated five times as in step 5.
8. 90µL of TMB Substrate was added to each well and incubated for 15-30 minutes at 37°C. Protected from light.
9. 50µL of Stop Solution was added to each well, gently tapping the plate to ensure thorough mixing.
10. The optical density of each well was determined within 5 minutes, using a micro-plate reader set to 450nm. Wavelength correction was set to 540nm to subtract readings at 540nm from the readings at 450nm. This subtraction corrects for optical imperfections in the plate.
11. Data was analysed using PRISM 6, GraphPad Software Inc. software.

2.11.4 Statistical analysis

The statistical analysis of data in the thesis was performed using GraphPad Prism 6 Software Inc. Where data was available for further analysis it was analysed using the Student's T-test (unpaired). The Student's T-test assumes unproven normal distribution. Significance was interpreted as $p < 0.05$. Quantification of gene expression was done by the comparative threshold cycle (Ct) method with the calculation of 2-[delta][delta]Ct.

3 GENE THERAPY USING AN ADENO-ASSOCIATED VIRAL VECTOR FOR DELIVERY OF RNAI TARGETING BRACHYURY IN CHORDOMA

3.1 Introduction

Despite advances in our understanding of the processes involved in the development and progression of cancer, treatment options for many patients are limited and prognoses still remain poor. The current treatment strategies for chordoma have been reviewed previously. The lack of treatment options for unresectable, and in particular recurrent disease, highlights the need for alternative approaches for treatment of this rare tumour.

Cancer is an acquired genetic disorder, with increasing evidence that there are extensive genetic variations not only between different cancers but also within each tumour(593). Gene and cell therapy promises the potential to deliver bespoke and effective treatment to the genetic structure of each tumour(248). Gene therapy consists of three basic steps: (1) construction of a gene-carrying vector, (2) transferring genes into cancer cells (3) expressing gene product to kill cancer cells.

3.1.1 Brachyury implication in the pathogenesis of chordoma:

Evidence, reviewed previously, suggests brachyury is involved in the pathogenesis of chordoma. In support of this is the fact that brachyury is highly expressed in the vast majority of chordomas(13,31,46). Germline tandem duplication of brachyury has been documented in familial cases, and brachyury gene amplification has been identified in a proportion of sporadic chordoma(36,87,89). 97% of patients with chordoma harbour at least one allele of the common non-synomous SNP (rs2305089) in the brachyury gene(87,90). In addition RNAi silencing of brachyury in chordoma cell lines induces growth arrest and apoptosis(89,91).

3.1.2 Gene therapy targeting Brachyury

Brachyury is important for gastrulation and mesodermal formation and is a major driver of EMT leading to tumour progression. It is expressed in several tumour types but not in normal adult tissue, with the exception of the testes. Expression in epithelial cancers has been associated with drug resistance and poor prognosis. The pathogenesis of resistance to therapy in chordoma is not understood, and may be similar to that associated with the gene expression involved in EMT. The wider implications of the involvement of brachyury in cancer, supports the rationale for development of therapies targeting this transcription factor.

Transcription factors are traditionally considered non-targetable for classical small molecules and therapeutic antibodies, due to their intracellular localisation and limited

surface protein expression. Recent evidence from preliminary data and early phase clinical trials targeting transcription factors such as *myc, SALL4* and *TP53* have shown promising results using RNAi or small molecules targeting the interaction between the transcription factor and the effector gene(269,330,686,687).

3.1.3 Viral vector for gene therapy in chordoma

The experience preceding the work presented here includes silencing of brachyury in two different chordoma cell lines(89,91) using lentiviral constructs, confirming the potential for using RNAi targeting brachyury. These lentiviral constructs were not considered suitable for *in vivo* experiments, and were not of the standard currently used in human trials(683). This study describes the use of an AAV vector for delivery of the specific shRNA, which demonstrated high efficiency in silencing of brachyury *in vitro,* to establish therapeutic effect of the application *in vivo.* An AAV vector was chosen for this project for the delivery of RNAi due to the favourable biology with lack of pathogenicity, low host immune response, and long-term gene expression(251). Its safety profile has been proven in clinical trails(231).

AAV serotype 5 was chosen for transduction of the chordoma cell line U-CH1, based on its ability to transduce primary cell lines efficiently *in vitro*(476). In addition AAV5 uses sialic acid for cell surface binding(491) with PDGFR identified as a co-receptor for transduction *in vitro* and *in vivo*(490). PDGFR is expressed by the majority of chordomas(165) and AAV5 was therefore considered a suitable serotype to test as a vector for transducing chordoma cells.

3.1.4 RNA interference

The possibility of artificially interfering with endogenous gene expression through the RNAi pathway has emerged as one of the most exciting areas for the development of disease-modifying treatments in several therapeutic areas including cancer(429,688). RNAi has previously been reviewed.

3.2 Aim

Can AAV vectors be engineered to deliver RNAi targeting brachyury and will brachyury silencing *in vivo* result in growth arrest and/or tumour regression?

3.3 Objectives

- To establish that the U-CH1 chordoma cell line is permissive to AAV5.
- To generate a vector for delivery of shRNA targeting brachyury, and to test efficacy and specificity *in vitro*.
- To assess response to recombinant AAV5 viral vector targeting brachyury in a chordoma xenograft model.

3.4 Results

3.4.1 The U-CH1 chordoma cell line is permissive to AAV5

3.4.1.1 Transduction and transgene expression

The cell line was transduced with the AAV5 vector containing the shRNA from the vector pGIPZ_V2LHS_153725, targeting brachyury. The efficiency of this shRNA in a lentiviral vector has previously been described(89,91). Successful transduction was assessed by transgene expression of GFP, using phase contrast fluorescence microscopy and fluorescence activated cell sorting (FACS) (Figure 3.1 & 3.2).

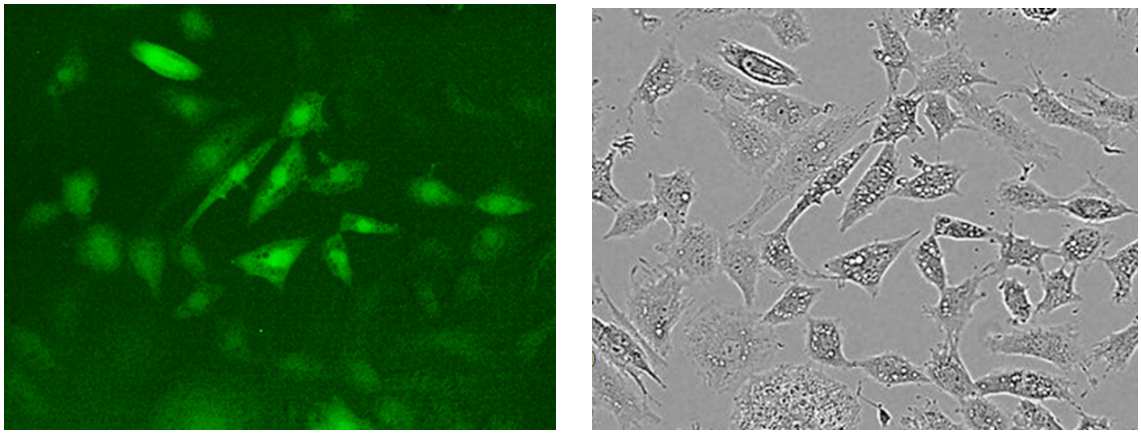

Figure 3.1 GFP expression in U-CH1 cells following transduction with AAV5
Phase contrast white light and fluorescent light microscopy of U-CH1 cells transduced with scAAV5_CMV_shRNA_GFP. The same cells are seen under different light sources.

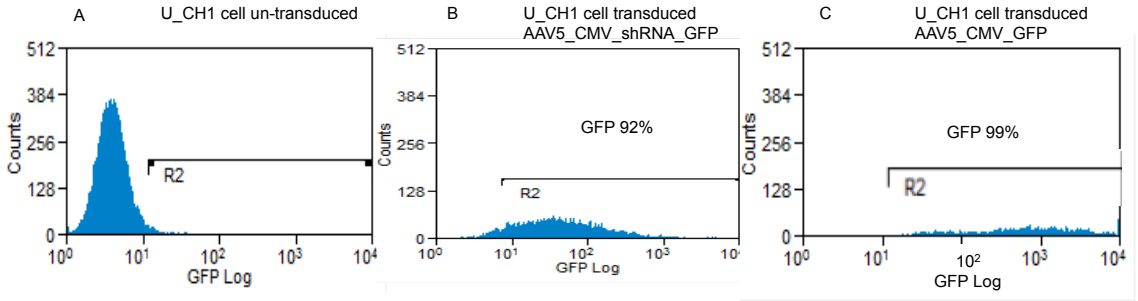

Figure 3.2 GFP expression by flow cytometry in AAV transduced U-CH1 cells
GFP expression assessed by FACS, 5 days following transduction of the U-CH1 cell line, using AAV5 viral vector. Cells were transduced with an MOI of $1x10^5$. (A) un-transduced U-CH1 cells used as negative control, gate set at 2%. (B) U-CH1 cells transduced by AAV5_CMV_shRNA_GFP showed 92% GFP expression. (C) U-CH1 cells transduced by AAV5_CMV_GFP showed 99.9% transduction.

Continuous monitoring using the Incucyte image analyser was utilised to monitor GFP expression as well as assessment of morphologic changes and cell proliferation. GFP expression was observed from 24-48 hours following transduction with the AAV5 vector. As the vector did not contain an antibiotic expression cassette no antibiotic selection could be undertaken. FACS sorting for GFP positive cells was attempted but was poorly tolerated by the cell line. Silencing of brachyury was expected to lead to growth arrest of the chordoma cell line, however the cells continued to proliferate and relative gene-expression assessed by RT qPCR confirmed comparable gene expression between the silencing and the non-silencing construct (Figure 3.3).

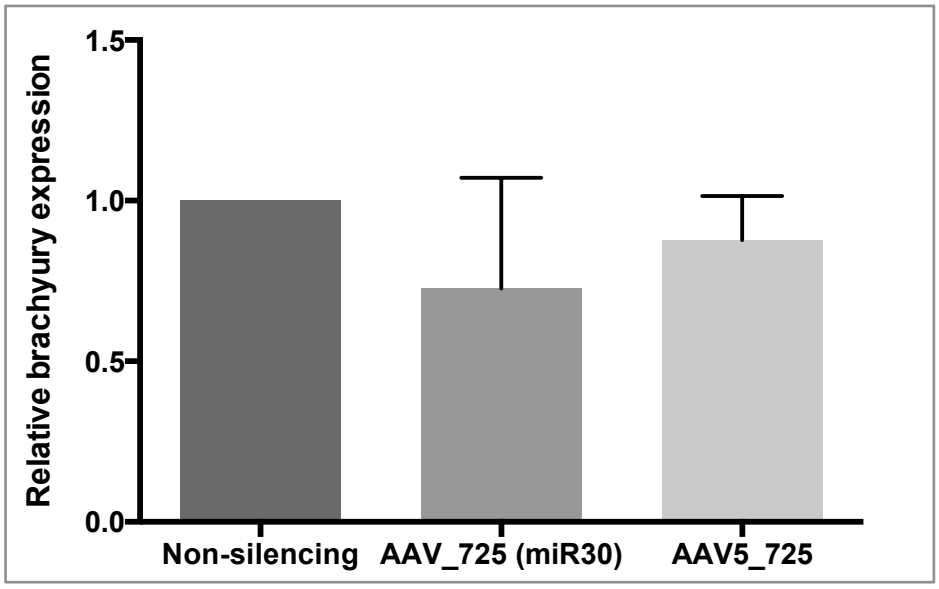

Figure 3.3 U-CH1 cell line transduced with AAV5_CMV_shRNA_GFP
Brachyury expression quantified by RT qPCR in the U-CH1 cell line generated. Expression of brachyury compared cells transduced with a non-silencing construct. Brachyury expression was corrected to the endogenous PGK expression as a reference gene. The experiment has been repeated n=3 and performed in triplicate. Error bars represent standard deviation. The comparative threshold cycle (Ct) method with the calculation of 2-[delta][delta]Ct was used to assess the relative level of expression of brachyury.

Neither the cell morphology nor proliferation of the cells was altered by the transduction with the gene-silencing construct. The transduced U-CH1 cells were maintained in culture and monitored in the incucyte. Unexpectedly the transduced cells maintained intense level of GFP expression despite continued proliferating (Figure 3.4).

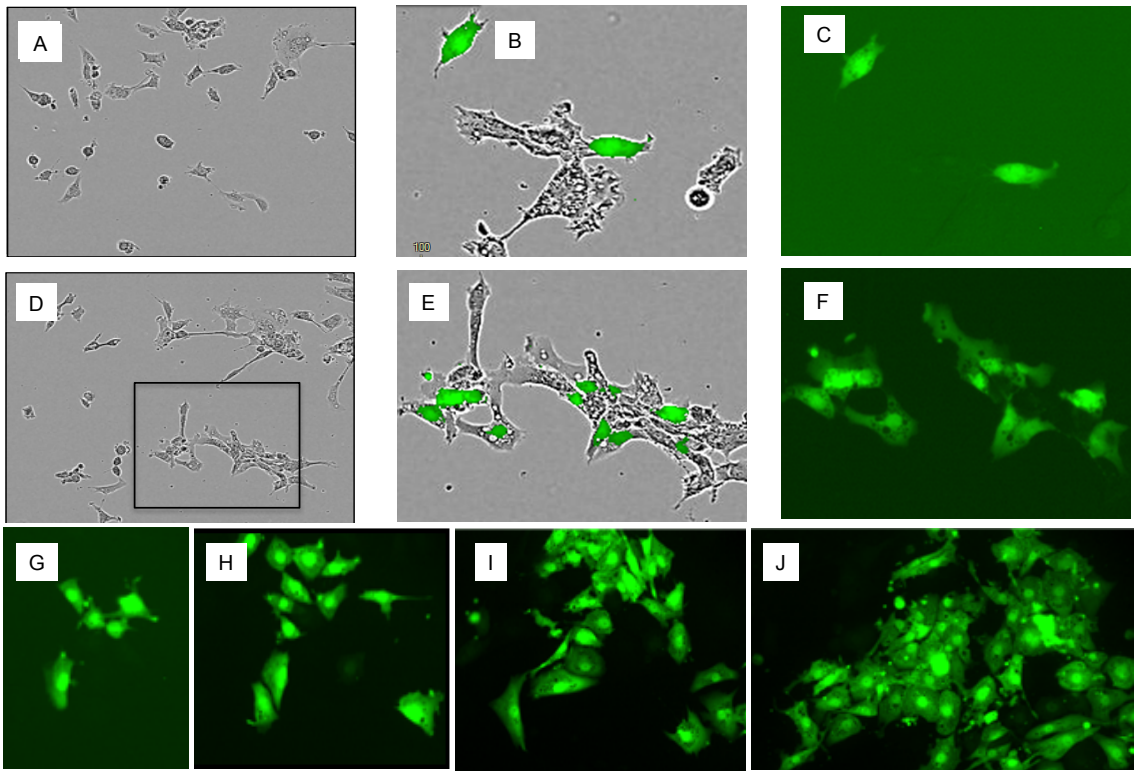

Figure 3.4 GFP expression maintained following transduction in U-CH1
AAV5 transduced U-CH1 cell line demonstrating clonal proliferation and continued GFP expression. Images from the incucyte with fluorescent and phase contrast microscopy. (A) demonstrating confluency following cell passaging 4 weeks after transduction of U-CH1 cell line with AAV_shRNA_GFP vector, phase contrast image. (B & C) demonstrating persistent GFP expression at 4 weeks post transduction ((C phase + fluorescent contrast)((D) fluorescent only). (D) Confluency 4 days after passaging. The boxed area in (D) is super-imposed in (E & F) demonstrating increased number of GFP expressing cells (the same field as image (B)) (E) fluorescent + phase contrast image. (F) Fluorescent microscopy. (G-J) demonstrating the proliferation of cells, left to right: day 1, 3, 7 & day 17 are from the same window/field. Experiment repeated twice.

Using flow cytometric analysis, 36% of the chordoma cells were found to have continued GFP expression five months post-transduction (Figure 3.5).

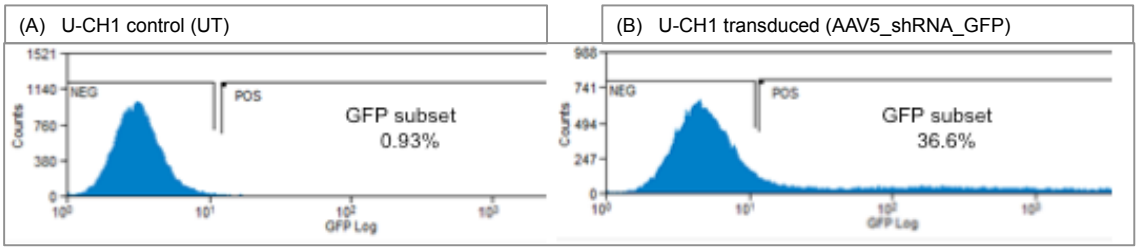

Figure 3.5 GFP expression in U-CH1 cells 5 months after transduction
The cells were maintained in the incucyte for 5 months and passaged when confluent. GFP expression was measured by FACS, Un-transduced U-CH1 cell used for setting the gate. GFP expression after 5 months was 36.6% Initial transduction efficiency/GFP expression using the AAV5_shRNA-GFP vector (MOI 10^5) showed 60-92% GFP expression 72 hours post transduction without Puromycin selection (data not shown).

3.4.2 AAV5 with new shRNA expression cassette silences brachyury

As a consequence of the lack of gene silencing, a different approach was pursued for the design of the knockdown construct.

The pLKO.1 vector, which had been used for silencing of brachyury in the JHC7 chordoma cell line causing cell senescence(91) had several advantages, over the GIPZ vector as a donor for the shRNA targeting brachyury. Whilst identical targeting sequences were available, the expression cassette within the pLKO.1 vector was smaller. In addition the expression cassette within the pLKO.1 vector contains a U6 promoter driving expression of the shRNA and a PGK promoter for expression of Puromycin, adding the option of antibiotic selection for transduced cells.

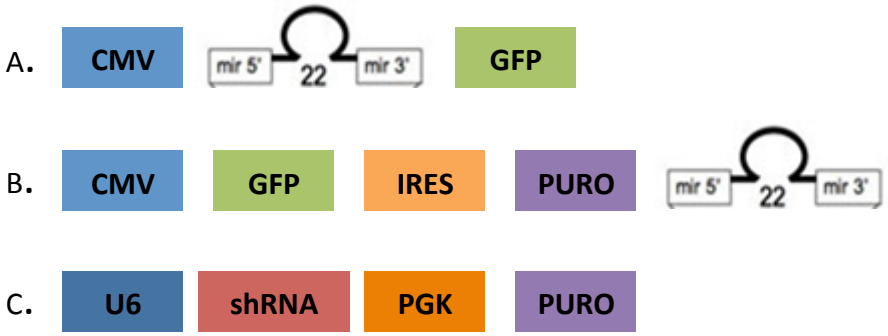

Figure 3.6 Expression cassettes for different shRNA constructs
(A) Expression cassette in the AAV vector containing a CMV promoter and GFP flanking the shRNA (extracted/cloned from the GIPZ vector). (B) Expression cassette in the GIPZ vector (total 3000bp) with the shRNA downstream from Puromycin (3'UTR). (C) Expression cassette in the pLKO.1 vector. The entire expression cassette is under 1800bp and could therefore be accommodated within the scAAV vector.

The design of the pLKO.1 vector allowed cloning of the whole expression cassette into the AAV vector. The use of the polymerase III (pol III) U6 promoter has been described and validated *in vitro*(343,689,690), and *in vivo* for expression in mice(691,692).

3.4.2.1 Transfection of the U-CH1 cell line

The U-CH1 cell line is known to be difficult to transfect, illustrated by the lack of publication on transfection of chordoma cell lines. Attempts were made to optimise the transfection using various transfection reagents. Results were unsatisfactory, achieving transfection efficiencies of less than 20% (data not shown). Following the initial experiments, though not in a timely manner, transfection of the U-CH1 cell line using X-tremeGENE HP DNA transfection reagent was established with transfection efficiencies up to 50% (Figure 3.14). The production of AAV is labour intensive, and therefore attempts were made to identify a brachyury expressing cell line, to test the

efficiency of gene silencing of the different cloning constructs, by transfection, to avoid generating virus for each individual construct required for transduction of the chordoma cell line.

3.4.2.2 Alternative brachyury expressing cell line

Brachyury expression has been described in the colon cancer cell line SW480(97), and used for knockdown experiments(96,104), however differential expression at different cell confluency has been reported which could make interpretation of reduced expression, due to gene silencing, difficult. The expression of brachyury was found to be very low in the SW480 cell line compared to expression in the U-CH1 cell line. No difference in expression was detected between 50% and 80% cell confluency (Figure 3.7). Due to low, and on-going concern of variable expression, the SW480 cell line was not used as a model for quantifying gene silencing efficiency.

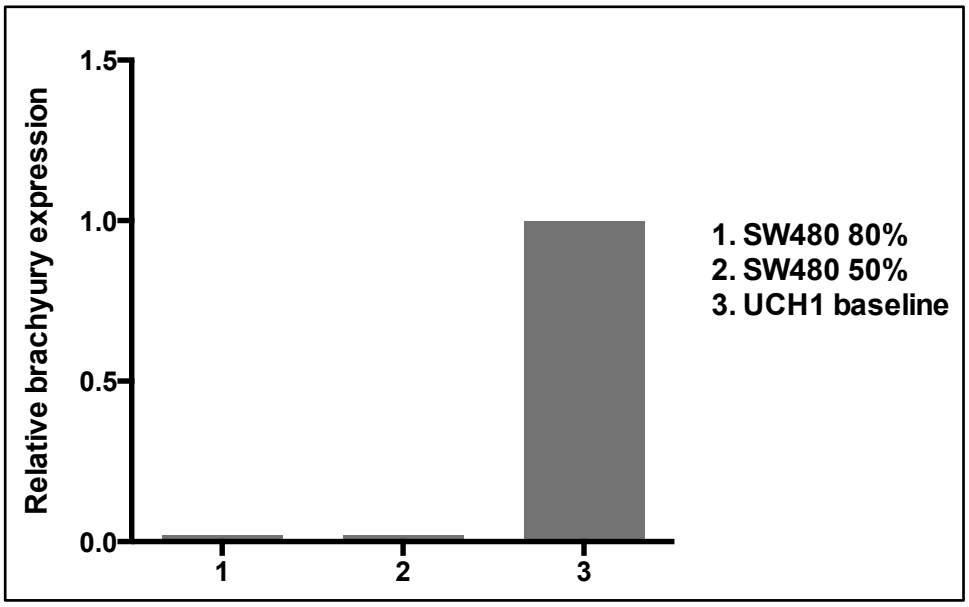

Figure 3.7 Brachyury expression in colon cancer cell line SW480
Relative expression of brachyury by RT qPCR in the SW480 colon cancer cell line, compared to expression in U-CH1 chordoma cell line (baseline), brachyury expression was corrected to the PGK expression as a reference gene. The comparative threshold cycle (Ct) method with the calculation of 2-[delta][delta]Ct was used to assess the relative level of expression of brachyury. Experiments run in triplicate, n=1.

For the purpose of testing the different cloning constructs, a HEK 293T cell line was generated which stably expresses brachyury. Brachyury expression was confirmed in the 293T_brachyury cell line by RT qPCR (Figure 3.8). This cell line was used to select the most efficient shRNA from a gene family set of 4 different shRNA sequences targeting brachyury. The HEK 293T cell line is generically resistant to Neomycin, as this was part of the expression cassette, together with the SV40 Large T-antigen added when initially developing the HEK 293T cell line(663). Neomycin and Puromycin

represented the only antibiotic selection marker available in the pLKO.1 vector leaving no possibility for selection in the 293T_brachyury cell line, which had been generated with a Puromycin selection cassette.

3.4.2.3 Brachyury can be silenced in the 293T_brachyury cell line.

To establish the ability to silence brachyury in the 293T_brachyury cell line, with brachyury expression driven by a viral promoter, the generated cell line was transfected using the lentiviral vector GIPZ_V2LHS_153725 targeting brachyury. This vector has previously been shown to silence brachyury in the U-CH1 cell line, with more than 90% reduction in expression(89). Transfection resulted in more than 70% reduction in gene expression 24 hours post-transfection (Figure 3.8).

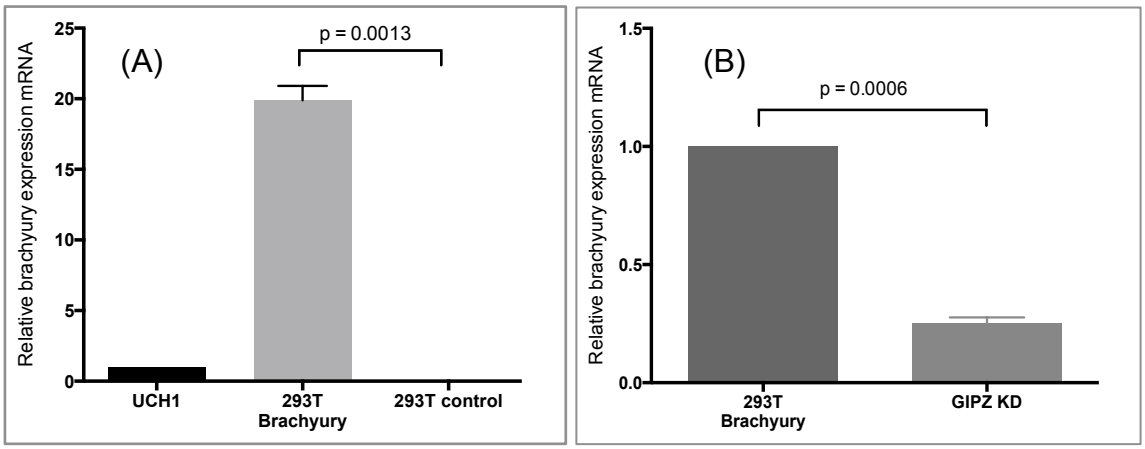

Figure 3.8 Brachyury expression in 293T brachyury expressing cells line
(A) Brachyury expression was quantified by RT qPCR in the 293T_brachyury cell line generated by lentiviral transduction to stably express brachyury. Expression in 293T_brachyury cells was compared to in the U-CH1 cell line and a non-transduced HEK 293T cells. (B) Silencing of brachyury in the 293T_brachyury cell line transfected using the lentiviral construct GIPZ_V2LHS_153725, targeting brachyury. Brachyury expression was corrected to endogenous PGK expression as a reference gene, un-transfected 293T_brachyury cells were used as control. The experiment was run in triplicate repeated twice.

3.4.2.4 Variation of efficacy between shRNA clones targeting brachyury

The pLKO.1_TRCN000005484 expression cassette was selected as the most efficient brachyury silencing construct to be cloned into the AAV construct (Figure 3.9). This shRNA had an identical targeting sequence to the shRNA from the GIPZ_V2LHS_153725 and this construct could therefore be used for comparison of efficiency of gene silencing. The shRNA target sequence was complimentary to the junction between the 3' end of exon 4 and the 5' end of exon 5 (Figure 3.10).

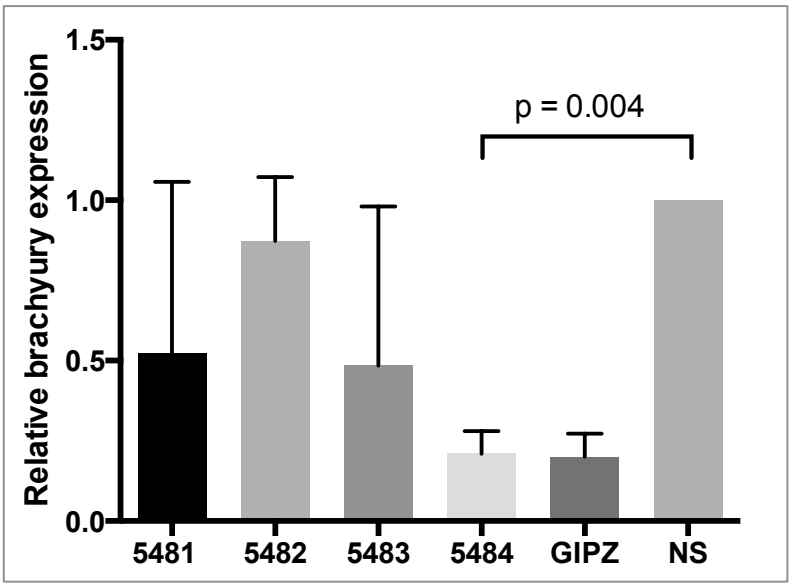

Figure 3.9 Efficiency in gene silencing by different clones of pLKO.1_shRNA
Results of RT qPCR for brachyury knockdown in the generated 293_brachyury cell line. Four different pLKO.1_shRNAs (pLKO.1_TRCN000005481-TRCN000005484)(5481-5484) targeting brachyury were tested by transfection. Brachyury expression was corrected to the endogenous PGK expression as a reference gene. GIPZ_V2LHS_153725 (GIPZ) used as positive control. Relative expression was assessed comparing expression after transfection with a non-silencing construct (NS). The figure represents results from three different experiments, each performed in triplicate. Error bars represent standard deviation. Significant difference in expression following knockdown with vector 5484 (and GIPZ) compared to non-silencing. Non-paired t-test.

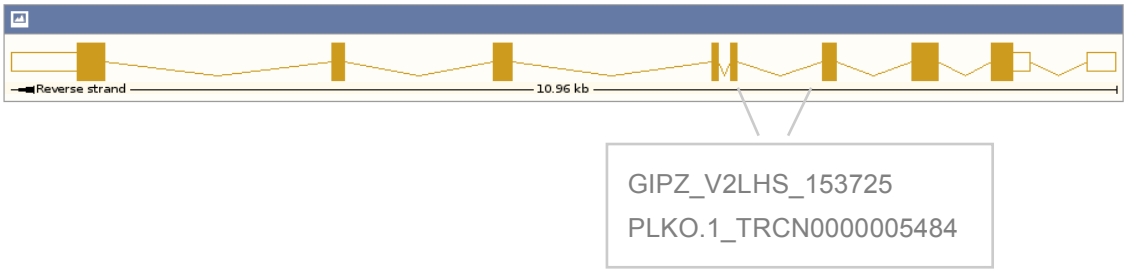

Figure 3.10 Brachyury gene mapping the target region for the shRNA constructs
The brachyury gene (transcript 1) depicted with its 9 exons (boxes) and the lines represents introns. The shRNA targeted region overlaps between exon 4 and exon 5. The GIPZ and the pLKO.1 construct have identical targeting sequence set within different scaffolds (flanking regions) and expressed off different promoters. Adapted from ENSEMBL genome browser.

3.4.2.5 Brachyury expression significantly reduced by pLKO.1 vector

In preparation for cloning the RNAi expression cassette into the AAV plasmid, efficiency of the pLKO.1_TRCN000005484 for silencing brachyury in the chordoma cell line U-CH1 was tested. The GIPZ_V2LHS_153725 construct was used as a positive control of gene silencing (Figure 3.11).

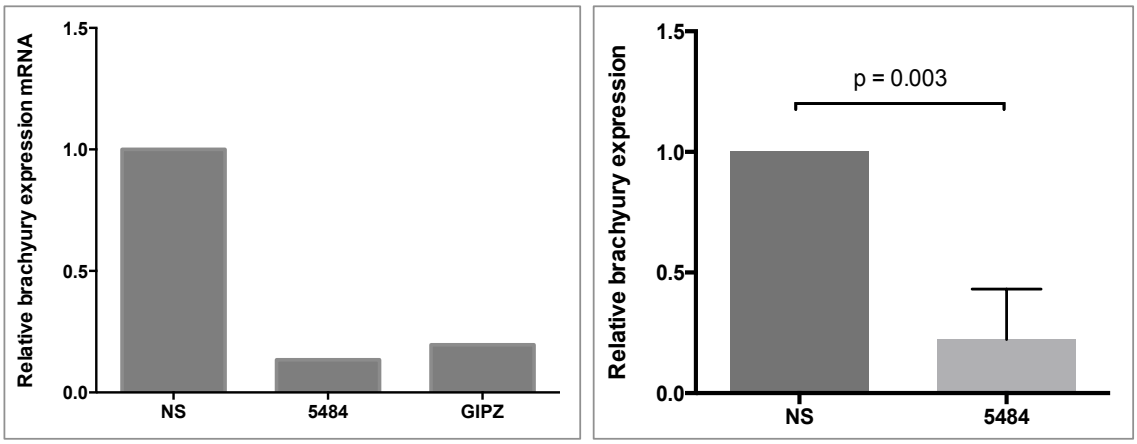

Figure 3.11 Silencing of brachyury in U-CH1 cell line (lentiviral transduction)
Relative expression by RT qPCR for brachyury knockdown in the U-CH1 cell line, knockdown was performed using pLKO.1_TRCN00008484 (pLKO.1_5484) and GIPZ_V2LHS153725 (GIPZ) (positive control) and a pLKO.1_non-silencing shRNA (NS)(negative control). Brachyury expression was corrected to the endogenous PGK expression as a reference gene and normalised to the non-silencing (NS) vector ($2^{-\Delta\Delta CT}$). The figure on the right represents results from 3 different experiments, each performed in triplicate. Error bars represent standard deviation. Non-paired t-test.

3.4.2.6 Brachyury silencing leads to morphologic changes in the U-CH1 cells

Knockdown of brachyury is known to alter the classic phenotype of chordoma cells including the physaliferous features and lead to stellate-appearing cells with spindling, flattening and extensive branching, as well as a significant decrease in average cell diameter size and near complete loss of cytoplasmic vacuoles(89,91,119). These morphological changes of the U-CH1 cell line were reproduced following transduction with the GIPZ_V2LHS153725 construct. The morphological changes in the U-CH1 cells transduced with the pLKO.1_TRCN00005484 were much more pronounced by comparison and were followed by cell death within 10 days of transduction (Figure 3.12). No morphologic changes were observed using a pLKO.1_non-silencing construct, used as a control for toxicity.

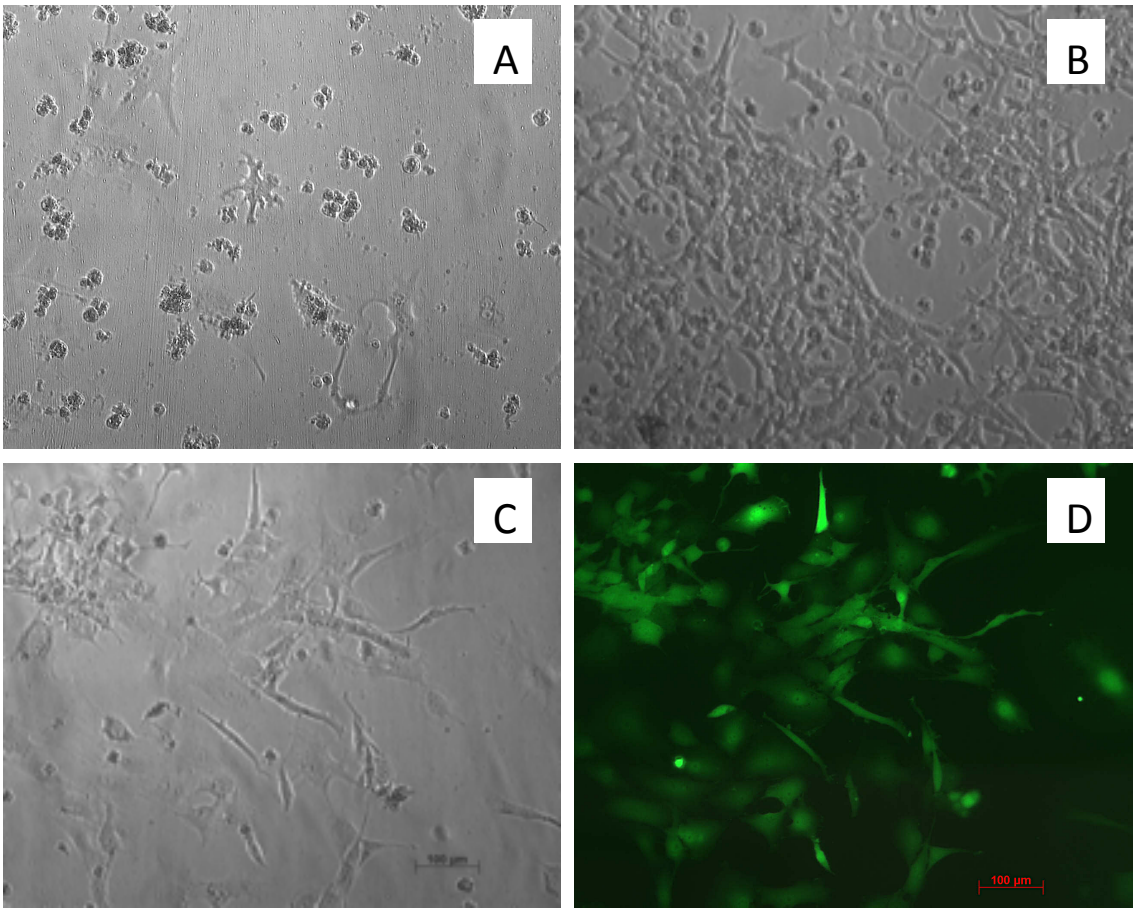

Figure 3.12 Morphological changes of U-CH1 cells after silencing of brachyury
U-CH1 cell line transduced with lentiviral vector and selected with Puromycin. Images acquired 8 days after transduction. Phase contrast photomicrographs of (A) U-CH1 cell line transduced with the pLKO.1_TCRN00005484 (B) U-CH1 cell line transduced with the pLKO.1 non-silencing (C) Phase contrast photomicrograph of U-CH1 cell transduced with the GIPZ_ V2LHS153725. (D) Fluorescent light photomicrograph demonstrating U-CH1 cell line expressing GFP transduced with GIPZ_ V2LHS_53725 (100% GFP expression), this image is a replicate of C. The pLKO.1 vector does not have a GFP expression cassette.

FACS analysis of the U-CH1 cells transduced with GIPZ_V2LHS153725 confirmed 100% GFP expression following selection with Puromycin of transduced cells (Figure 3.13).

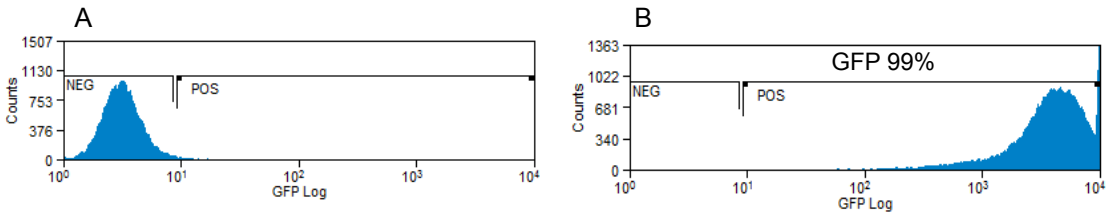

Figure 3.13 Transduction and Puromycin selection efficiency by GFP expression
Flow cytometry was used to assess the GFP expression in U-CH1 cell line, transduced with the GIPZ_V2LHS153725 construct (B), for assessing efficiency of transduction and subsequent Puromycin selection, validating the effect of gene silencing avoiding bias from un-transduced cells. Un-transduced U-CH1 cells used as control (A), gate set at <2%. 100% GFP positive cells correlated with 80% gene silencing shown in figure 3.11.

3.4.2.7 AAV vector with expression cassette for shRNA TCRN00005484

The construct pAAV_U6_shRNA(5484)_Puromycin also referred to as pAVV_5484 and the control pAAV_U6_shRNA(Non-silencing)_Puromycin, referred to as pAAV_NS were tested by transfection of the U-CH1 cell line. Transfection protocols were optimised for the U-CH1 cell line as previously discussed.

3.4.2.7.1 Transfection of U-CH1 cells

Transfection efficiencies of up to 50% were achieved in the U-CH1 cell line as assessed by GFP expression (Figure 3.14).

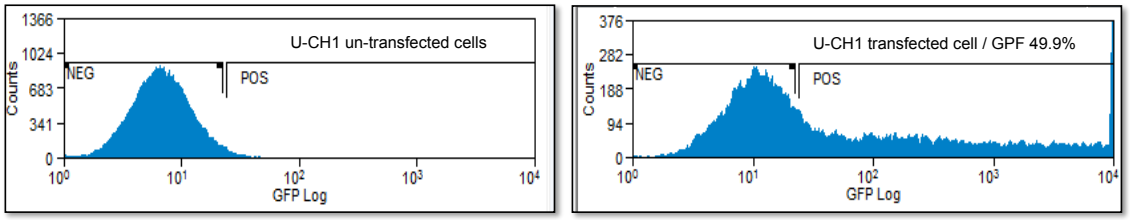

Figure 3.14 Transfection efficiency of AAV into U-CH1 cells
FACS results measuring GFP expression after transfection of the U-CH1 cell line using X-tremeGENE HP®. Un-transfected cells (Left). U-CH1 cells transfected with pAAV_CMV_GFP showing 50% of cells are transfected with GFP expressing plasmid (Right). Transfection with a larger plasmid (lentivirus) resulted in 20% transfection (data not shown).

The newly generated AAV constructs were transfected into U-CH1 cell line and efficiency of gene silencing assessed by relative gene expression. Brachyury expression was reduced by more than 90% following transfection and Puromycin selection (Figure 3.15).

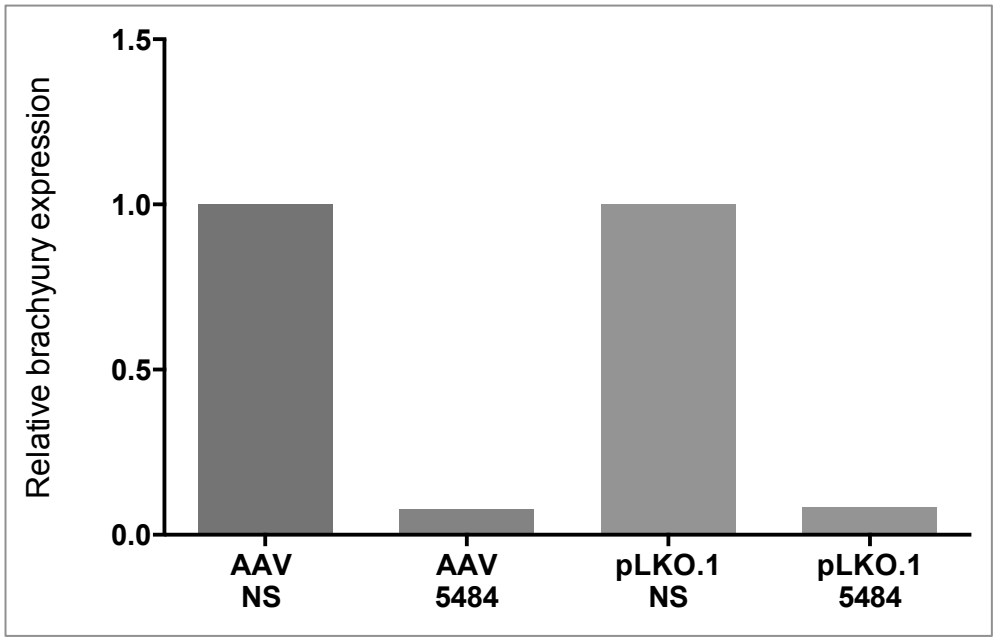

Figure 3.15 Silencing of brachyury in U-CH1 cells following transfection
The efficiency of the new pAAV_5484 knockdown construct compared to the non-silencing (NS) control was validated by transfection of the U-CH1 cell line. The pLKO.1_5484 lentiviral knockdown construct was used as a control for gene silencing. Puromycin selection was commenced 72 hours after transfection, overcoming the difference in transfection efficiency due to discrepancy of plasmid size. Brachyury expression was assessed by RT qPCR, brachyury expression was corrected to the endogenous PGK expression as a reference gene. Both knockdown constructs showed more than 90% silencing of brachyury compared to expression in cells transduced with the non-silencing construct. The comparative threshold cycle (Ct) method with the calculation of 2-[delta][delta]Ct was used to assess the relative level of expression of brachyury.

With confirmation that shRNA targeting brachyury was functional in the AAV vector the production of AAV5 was initiated.

3.4.2.8 AAV5 delivered shRNA silence brachyury in U-CH1

U-CH1 cells were transduced with AAV5 containing the expression cassette from the pLKO.1 vector for knockdown of brachyury. Three different conditions were tested to help understand toxicity and cell death. One condition was designed to assess the transduction efficiency and gene silencing without Puromycin selection, one to assess expression after Puromycin selection and one with the cells maintained in culture 7 days without Puromycin selection, due to concern that gene expression might be lost with cell division, and therefore render the cells sensitive to Puromycin. Gene silencing

was comparable between the conditions with reduction in expression between 70-80% (Figure 3.16).

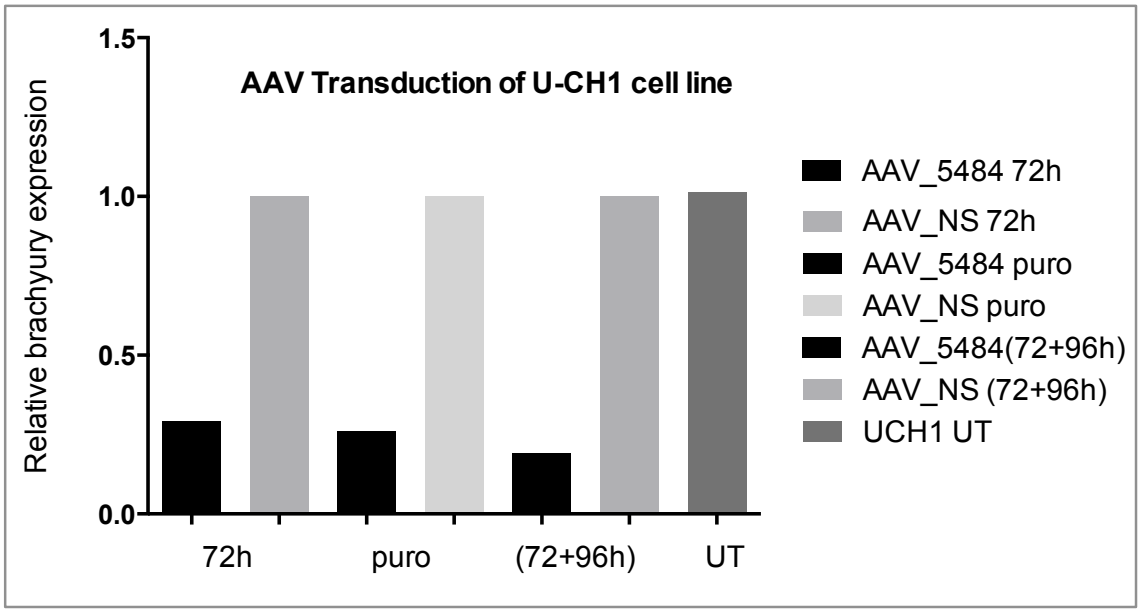

Figure 3.16 Brachyury expression in U-CH1 cells following AAV5 transduction
Results form RT qPCR (in triplicate) assessing relative brachyury expression compared to endogenous control (PGK). The knockdown was determined comparing to a non-silencing vector under the same conditions. (1) AAV_5484 & (2) AAV_non-silencing (NS) transduced cells were harvested for mRNA extraction at 72 hours post transduction. (3) AAV_5484 & (4) AAV_NS. Exposed to Puromycin selection 72 hours post transduction for 96 hours. (5) AAV_5484 & (6) AAV_NS (72+96h) where no Puromycin selection was undertaken, RNA was extracted day 7 (time scale as transduced cells under Puromycin selection. (7) UT=non-transduced U-CH1 cells. MOI 10^5. Experiment run in duplicate, n=1. The comparative threshold cycle (Ct) method with the calculation of 2-[delta][delta]Ct was used to assess the relative level of expression of brachyury.

Silencing of Brachyury was reflected in the cell confluency assessed by phase contrast microscopy of the cells (Figure 3.17).

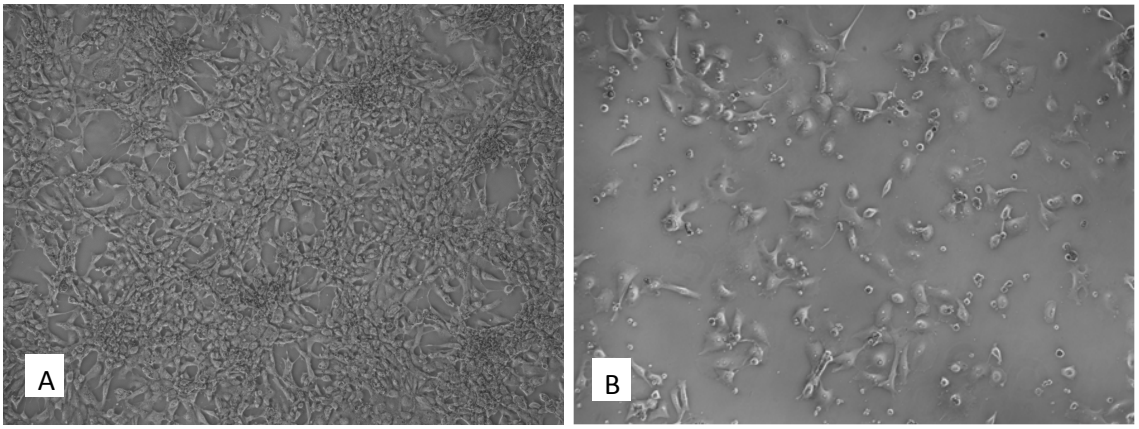

Figure 3.17 Confluency of U-CH1 cells after AAV5 delivered brachyury silencing
Phase contrast microscopy, U-CH1 cells 7 days following transduction with AAV5 knockdown construct and non-silencing vector. (A) U-CH1 cells transduced with non-silencing viral vector. (B) U-CH1 cells transduced with knockdown construct after 96 hours of Puromycin selection.

Morphological changes were observed in the U-CH1 cells transduced with the AAV5 knockdown construct. These changes were similar to those observed after transfection with the AAV plasmid containing the knockdown expression cassette, as well as in the knockdown experiment using the pLKO.1 lentiviral vector (Figure 3.12). The morphological changes were irreversible leading to cell death (Figure 3.18).

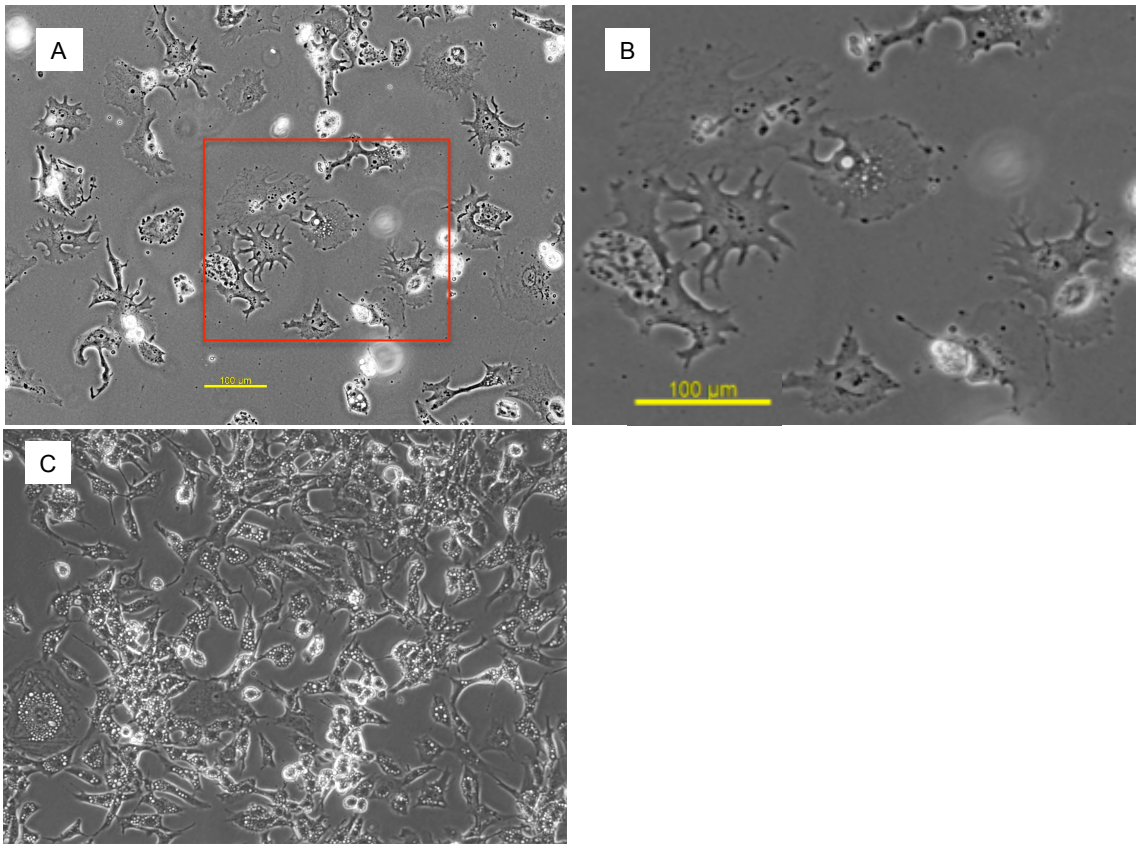

Figure 3.18 Morphologic changes in U-CH1 cells transduced with AAV vector
AAV vector transduction; phase contrast microscopy of U-CH1 cell line demonstrating morphologic changes typically seen following transduction (and transfection) using the shRNA (TRCN000005484) targeting brachyury. The cells become flattened, with changes to the cytoskeleton resulting in stellate appearance, and loss of the characteristic physaliferous features. The changes were irreversible and the cells died about day 10 post-transduction. (B) Technical replicate of the image highlighted in image (A). (C) U-CH1 cells transduced with non-silencing construct.

3.4.3 Toxicity of shRNA reproducible across various control cell lines

The observed morphological changes observed after AAV5 transduction with the brachyury silencing construct, was not replicated in the cells transduced with the non-silencing construct. Before proceeding with the viral vector, targeting brachyury in the xenograft, the construct was tested in a range of cell lines not known to express brachyury to assess toxicity (Table 3.1). Having established comparable efficiency of gene silencing between the AAV and lentiviral vectors, the lentiviral vector

pLKO.1_TRCN00005484 was used for toxicity testing. Phase contrast images were taken for assessment of morphologic changes.

Table 3.1 Cell lines for toxicity screening

U-CH1 used as a control	Chordoma
U251	Glioblastoma
U87	Glioblastoma
A172	Glioblastoma
MDA MB 231	Breast cancer (metastatic adenocarcinoma)
MCF7	Breast cancer (metastatic adenocarcinoma)
HUH7	Hepato-carcinoma
HEK 293T	Human embryonic kidney

The morphological changes with flattening of the cells and stellate changes to the cytoskeleton as well as the general toxicity of the pLKO.1 TRCN000005484 observed in the U-CH1 cell lines was reproduced to various degrees in all the cell lines transduced with this lentiviral vector targeting brachyury (Figure 3.19 & 3.20). The changes were irreversible and the majority of cells died around day 7 post-transduction.

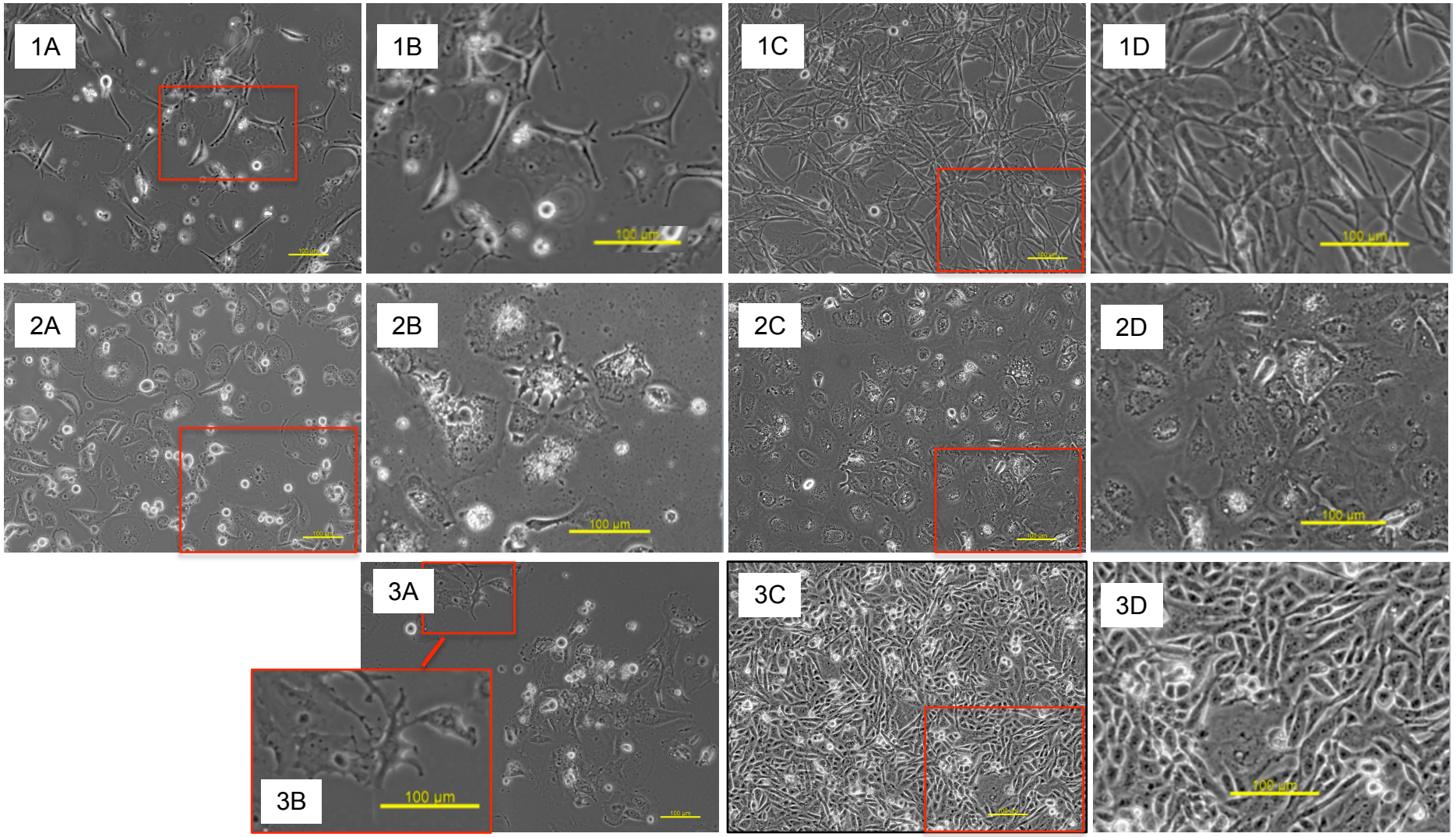

Figure 3.19 Morphology changes in U87, HUH7 and U251 cell lines
Phase contrast microscopy: Row 1: U87, row 2: HUH7, row 3: U251 cell line. A & B cell line transduced with brachyury silencing construct pLKO.1 TRCN000005484 vector, B is representing the area boxed in A demonstrating morphologic changes. C & D cell lines transduced with control vector (non-silencing) demonstrating morphologic changes. D represents boxed area in C.

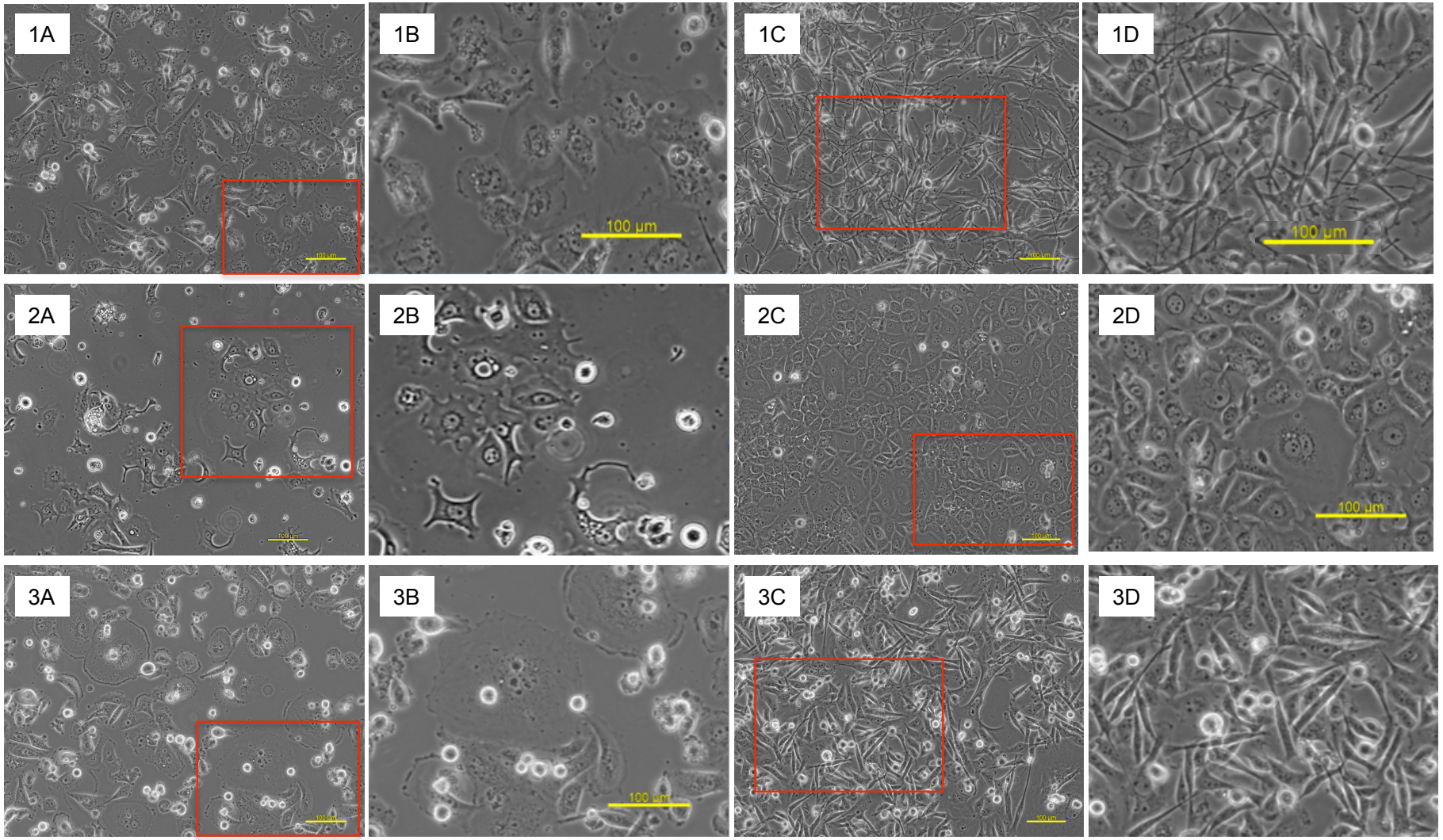

Figure 3.20 Morphology A172, MCF7 and MDA MB 231 cell lines
Phase contrast microscopy: row 1: A172, row 2: MCF7, row 3: MDA MB 231 cell line. A & B cell lines transduced with brachyury silencing construct pLKO.1 TRCN00005484 vector, B is representing the boxed in area in A demonstrating morphologic changes. C & D cell lines transduced with control vector (non-silencing). D represents boxed area in C.

The HEK 293T cell line did not tolerate transduction with the TRCN000005484 construct and the cells died during Puromycin selection. The non-silencing construct was tolerated without any obvious toxicity.

Due to the toxicity of the shRNA TRCN000005484 targeting brachyury across all cell lines, each cell line was tested for brachyury expression and potential off-targets for the shRNA sequence was revisited. Only the U-CH1 cell line was found to express brachyury.

3.4.4 Sequence homology supports potential off-target effect

The sequence for pLKO.1 TRCN000005484 identical to the sequence for GIPZ V2LHS_153725 was entered into NCBI BLAST (Basic local alignment search tool) for review of potential off-targets sequences. The sequence was aligned against the human genome plus transcript database (Table 3.2). This had previously been done but the potential off-targets were considered minimal, as this hairpin in the GIPZ construct had previously been used without any documented toxicity in both Hela and HEK 293T cell lines (Thesis by Asem Shalaby supervised by Professor A. Flanagan).

Table 3.2 Potential off-targets for shRNA pLKO.1 TRCN000005484

NCBI BLAST sequence: CGAGGAGATCACAGCTCTTAA	GENE	Query cover	E-Value
Brachyury	T	100%	0.006
Teneurin transmembrane protein 3	TENM3	76%	5.7
TTC28 antisense RNA1 (non-coding)	TTC28-AS1	71%	22
Dystonin	DST	71%	22
Zinc finger protein 829	ZNF829	66%	88
Homo sapiens chromosome 11 ORF 35	C11orf35	66%	88
Integral membrane protein 2C	ITM2C	66%	88

BLAST search as of April 2014. Query cover indicates the percentage of the query sequence covered by alignment to the database sequence. Brachyury has the lowest (best) E-value of 0.006 indicating a true alignment i.e. qualification of true alignments when coverage crosses intron/exon boundaries (ref. blast.ncbi.nlm.nih.gov). TENM3 has an E-value of 5.7 whilst the other genes have much higher values indication less likely alignment.

3.4.5 Brachyury-targeting shRNA demonstrates off-target silencing of *TENM3*

The sequence for the shRNA targeting brachyury aligned against the *TENM3* cDNA sequence with 16 of 21 nucleotides targeting within exon 5 of the *TENM3* genome. Expression of *TENM3* was assessed to validate this potential off-target effect as an

explanation for the toxicity observed, not only in the chordoma cell lines but also in the additional cell lines, none of which expressed brachyury (data not shown). The efficiency of gene silencing of *TENM3* following transduction using the vector targeting brachyury was also reviewed demonstrating knockdown and thereby a potential causal effect of the toxicity observed (Figure 3.21).

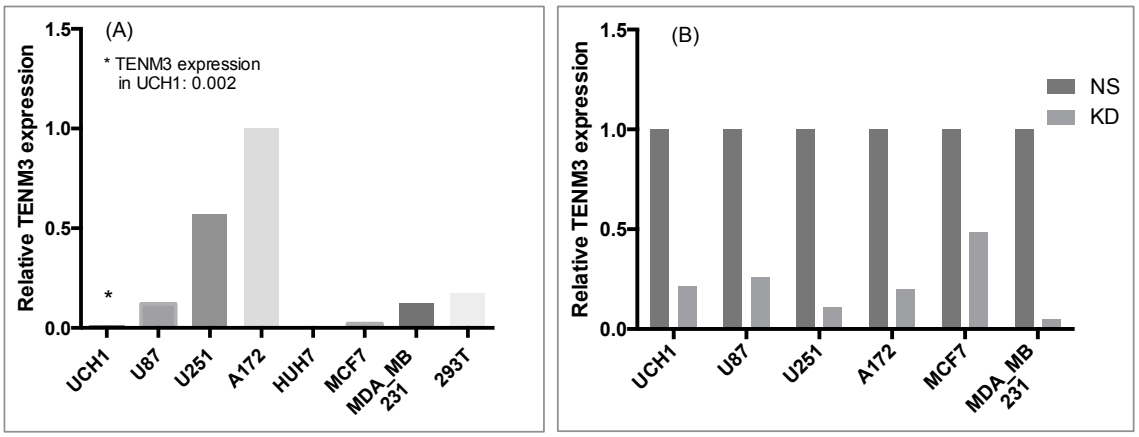

Figure 3.21 *TENM3* expression and off-target gene silencing in multiple cell lines
(A) Results of RT qPCR of relative expression of *TENM3* in U-CH1, U87, U251, A172, HUH7, MCF7, MDA_MB 231 and HEK 293T cell lines; A172 cell line had the highest level of *TENM3* expression. *TENM3* expression of the other cell lines has been shown relative to the expression in the A172 cell line. (B) Relative *TENM3* expression following transduction with the pLKO.1 TCRN000005484 (KD) vector compared to expression following transduction with the non-silencing construct (NS). Not all cell lines were included in the assessment of off-target effect. Expression of *TENM3* was relative to endogenous *GAPDH* expression, each cell line compared to itself, no comparison of gene silencing was done between different cell lines.

3.4.6 Selection of alternative shRNA for silencing of brachyury.

The gene-silencing construct pLKO.1_TCRN00005484 was discarded due to toxicity demonstrated in all cell lines tested. Previous data on efficiency of gene silencing of brachyury using different clones were reviewed to identify a different but equally efficient knockdown construct. All shRNA sequences were reviewed for possible off-target effects by alignment of the sequence against the human genome using NCBI BLAST. Brachyury clones TRCN000005480-5483 were tested (Table 3.3). The potential interaction of genes affected was also reviewed in STRING protein network database (data not shown).

Table 3.3 Off-targets aligning with brachyury targeting shRNA sequence

TRCN clone	Gene	Gene	Sequence alignment
TRCN000005480	Brachyury	T	100%
	Presenilin 1	PSEN1	76%
	Nuclear receptor co-activator 5	NCOA5	71%
	Family with sequence similarity 21 member A	FAM21A	66%
	Family with sequence similarity 21 member B	FAM21B	66%
	Family with sequence similarity 21 member C	FAM21C	66%
	CUB domain containing protein 2	CDCP2	66%
	CUB and sushi multiple domains 1	CSMD1	66%
TRCN000005481	**Brachyury**	**T**	**100%**
	Norrie disease (pseudoglioma)	NDP	66%
	Transmembrane protein 106C	TMEM106C	66%
	Zink finger matrin type 1	ZMAT	61%
TRCN000005482	**Brachyury**	**T**	**100%**
	GABA B protein receptor	GABRB	66%
	Zinc finger CCCH-type, antiviral 1-like	ZC3HAV1L	66%
	Sprouty hologo 3 (Drosophila)	SPRY3	66%
TRCN000005483	**Brachyury**	**T**	**100%**
	Methyltransferase like 25	METTL25	80%
	ATPase Na+/K+ transporting, alpha 1 polypeptide	ATP1A1	66%
	Cramped-like (Drosophila)	CRAMP1L	61%
	Guanylate cyclase alpha 3	GUCY1A3	61%
	Inositos 1.4.5-triphosphate receptor, type 1	ITPR1	61%
	Vitamin D receptor	VDR	61%

The TRCN clones as identifier for the different hairpins targeting brachyury. The target genes identified, according to NCBI BLAST alignment of the sequence against the Human genome. The column to the left shows the % of the maximum sequential alignment such as 16 nucleotides out of total of 21 nucleotides (76%). TRCN000005481 was found to have the most favourable off-target profile.

3.4.7 The TRCN000005481 vector demonstrates no off-target toxicity

Based on the results from previous gene silencing and the alignment for off-target effect, experiments proceeded with the pLKO.1_TRCN00005481 vector for silencing of brachyury in the U-CH1 chordoma cell line.

3.4.7.1 No morphological changes observed in control cell lines

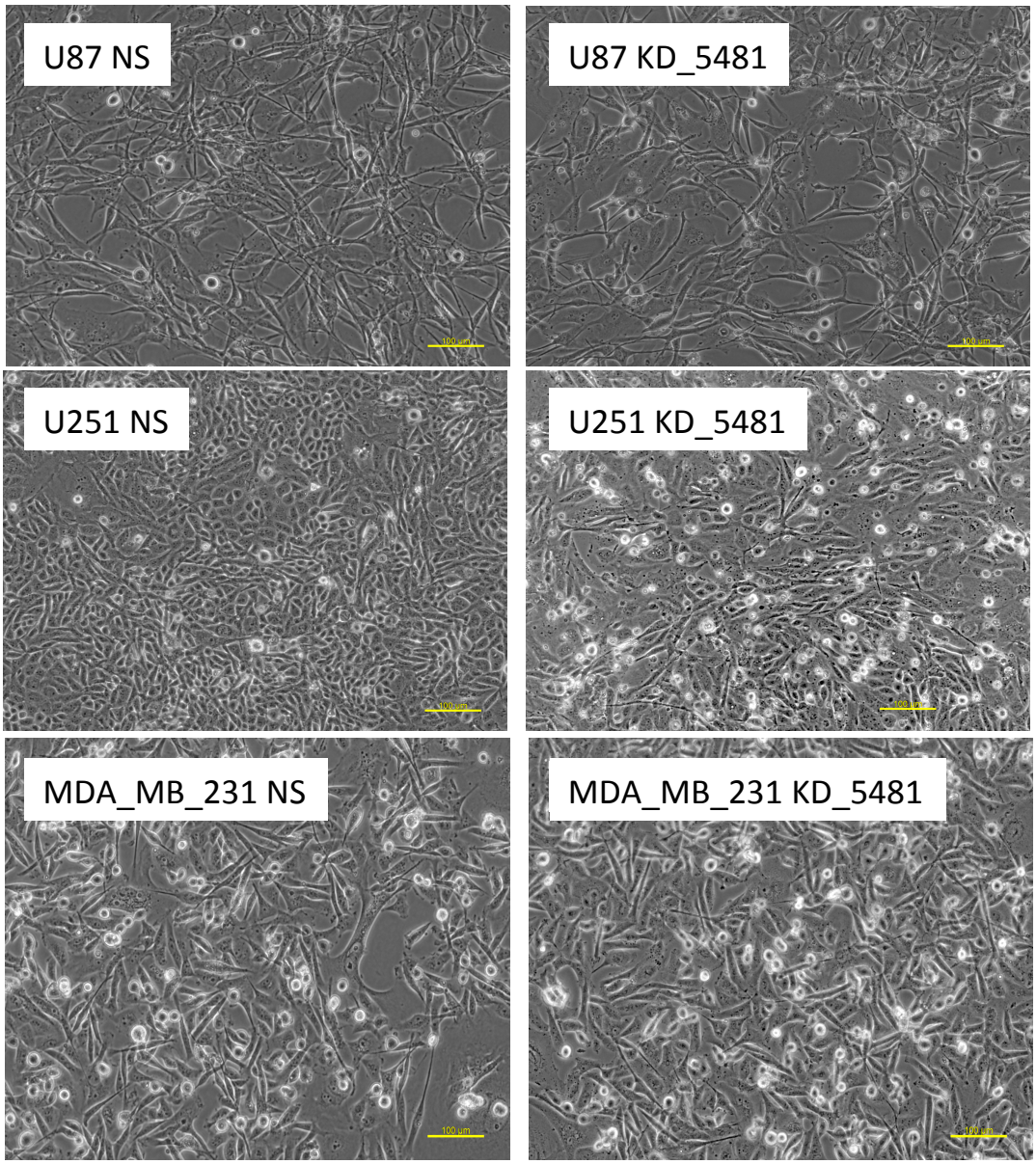

Figure 3.22 Control cell lines transduced with pLKO.1 TRCN00005481 vector
Phase contrast microscopy; the cell lines transduced with the pLKO.1_5481 (KD) vector targeting brachyury (right), for assessment of toxicity associated with potential off-target effect. Morphology compared to cell transduced with the non-silencing construct (left). MCF7, HEK 293T and HUH7 showed no morphological difference between the KD and the NS construct (images not included).

3.4.7.2 Proliferation not affected by new brachyury targeting shRNA

In addition to review of morphology, a WST-1 assay was used for further assessment of toxicity to determine whether proliferation was affected in cells transduced with the pLKO.1_TRCN00005481 construct. The pLKO.1_TCRN00005484 was used as a positive control in addition to the non-silencing vector. The proliferation assay showed no increase in cell death after transduction using the pLKO.1_ TRCN00005481 vector in contrast to the effect observed using the pLKO.1_ TRCN00005484 vector.

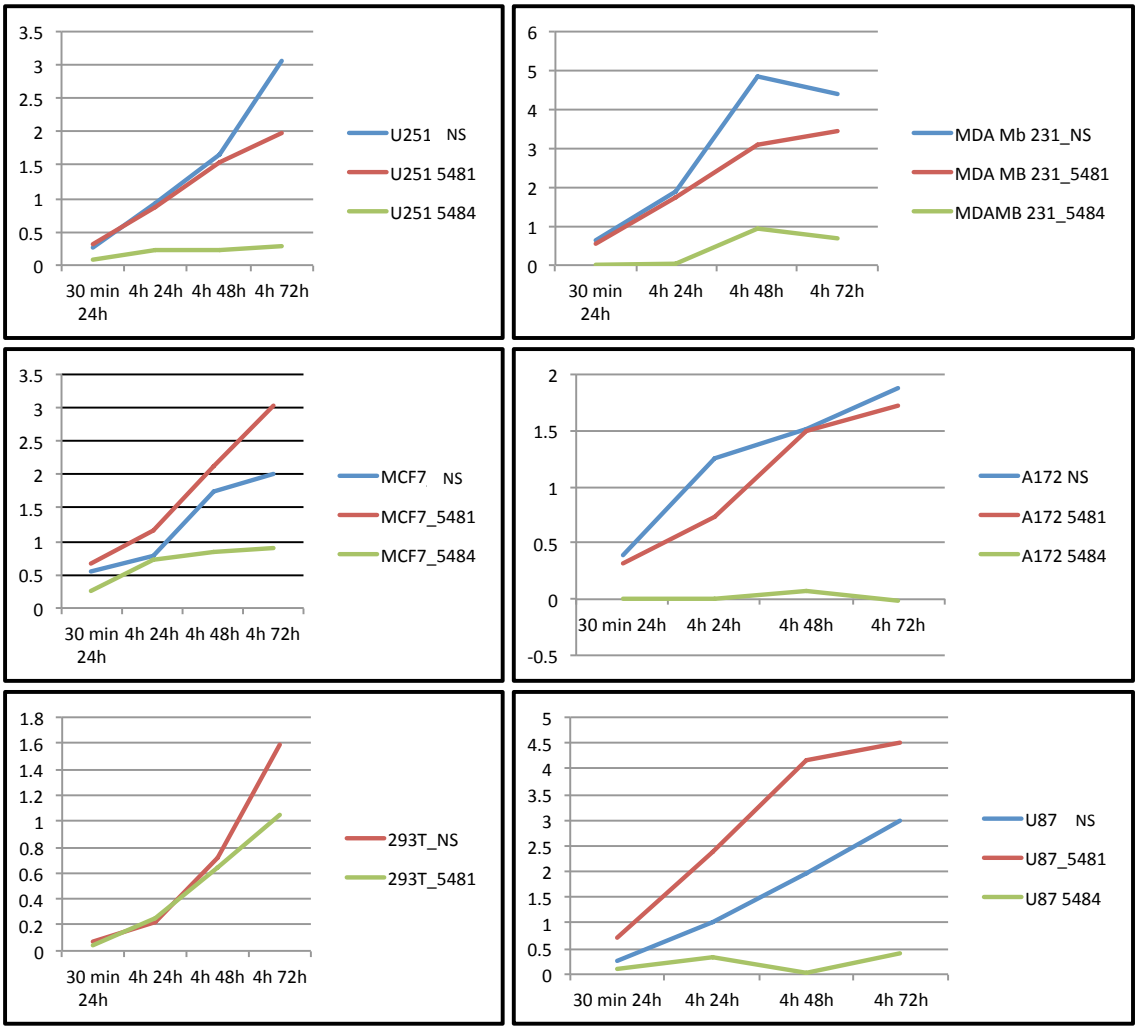

Figure 3.23 Cell viability following transduction with brachyury targeting shRNA
WST-1 assay used for assessment of proliferation. The different cell lines were transduced with the 3 different lentiviral constructs pLKO.1_5481, pLKO.1_5484 and pLKO.1_NS for assessment of toxicity of the selected hairpin (5481) replacing the hairpin (5484) following evidence of off-target effect. 3 plates were seeded for end-point assays for 3 different time points (24 hours, 48 hours and 72 hours) the assay was read at time 30 minutes only on day 1 (24 hours) to have a starting point for the readout. The end-point readout was then done at 4 hours for time point. Each condition was seeded in triplicates.

3.4.8 pLKO.1_TRCN00005481 silence brachyury in U-CH1

Following confirmation of the tolerability of the new construct suggesting no toxic off-target effect, significant gene silencing of brachyury in the U-CH1 chordoma cell line

was confirmed (Figure 3.24) and the vector was tested in two additional chordoma cell lines: U-CH2 and MUG Chor.

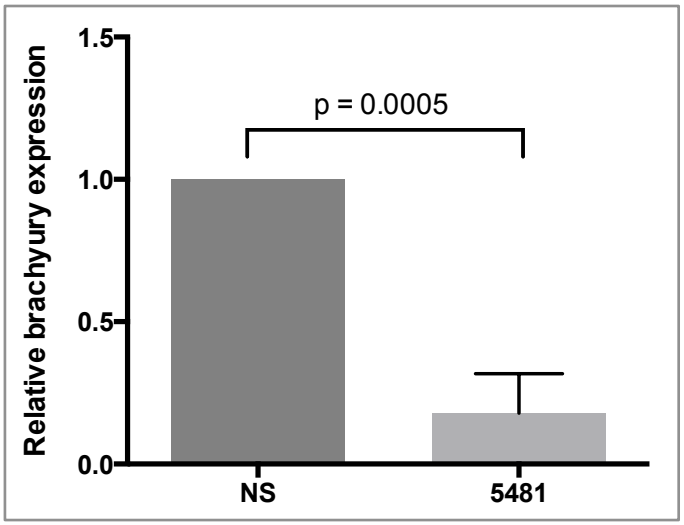

Figure 3.24 Brachyury knockdown with pLKO.1 TRCN000005481
Result of RT qPCR for brachyury knockdown in U-CH1 cell line using Lentiviral pLKO.1 TRCN00005481 and a non-silencing (NS) construct as control in U-CH1 cell line. Puromycin selection was done. Brachyury expression corrected to the endogenous PGK expression as a reference gene and normalised to the non-silencing vector, expression was reduced by 85%. The figure represents results from three different experiments, each performed in triplicate. Error bar represent standard deviation. No error bar for NS as set at 1 for comparison of expression.

The expression of brachyury was compared across 3 chordoma cell lines by RT qPCR for gene expression and by western blot for protein expression.

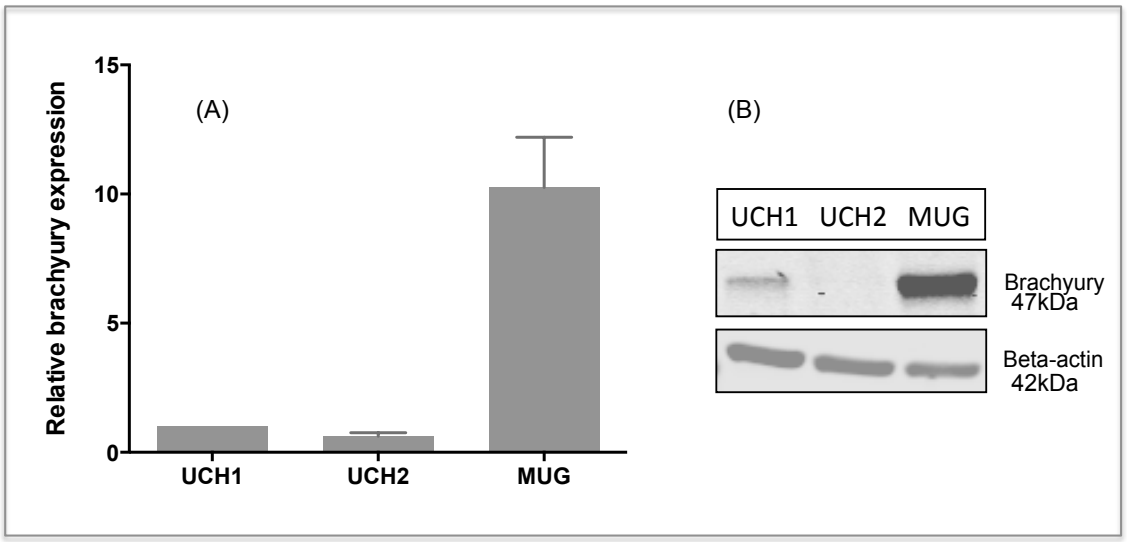

Figure 3.25 Brachyury expression in U-CH1, U-CH2 and MUG Chor cell lines
RT qPCR gene expression quantified from mRNA (A) and Western blot (WB) quantifying protein (B) comparing brachyury expression across 3 different chordoma cell lines. U-CH1 cell line is the first and most well established cell line and has been set as the reference for comparing relative expression in the two additional chordoma cell lines, brachyury expression quantified in relation to endogenous PGK and GAPDH expression (different experiments done for comparison). The experiment was done n=3 in with each experiment run in triplicate. Error bars indicate standard deviation. Beta-actin was used as endogenous control for the WB.

Gene silencing of brachyury was achieved in all 3 chordoma cell lines (Figure 3.26). It has previously been reported that the U-CH2 cell line has lower brachyury expression than the U-CH1 cell line(197), which was reproduced on the data presented here (Figure 3.24). However as demonstrated below brachyury expression declined in the U-CH2 cell line with increasing passages in culture (Figure 3.27), which became evident with the lack reproducibility of gene silencing. Cell line authentication with DNA profiling by short tandem repeats (STR) of various passages of U-CH2 excluded cross contamination and confirmed authenticity of the cell line (data not shown).

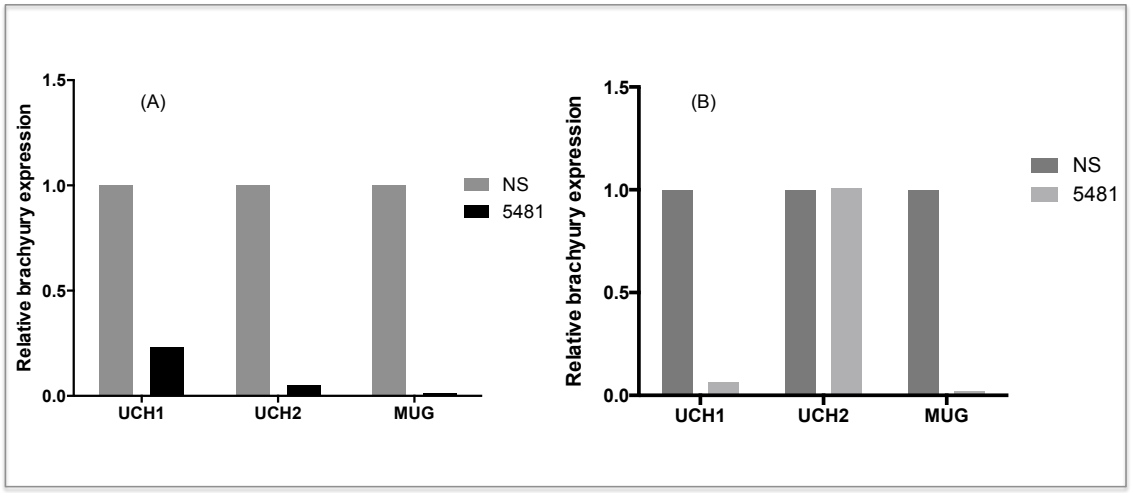

Figure 3.26 Brachyury silencing in three chordoma cell lines
RT qPCR results for relative brachyury expression in U-CH1, U-CH2 and MUG Chor cell lines following transduction with pLKO.1_5481 lentiviral vector targeting brachyury. Puromycin selection was performed. Brachyury expression was corrected to endogenous PGK expression, as reference gene, and normalised to the pLKO.1_non-silencing construct. The two graphs demonstrate two different experiments done 5 months apart. (A) U-CH2 cell passage 22, (B) U-CH2 cell passage 38. Brachyury expression in U-CH2 appeared not be silenced on the repeat experiment. The lack of knockdown was due to loss of brachyury expression in cell culture over time. U-CH1 and MUG Chor cell lines demonstrated consistent knockdown.

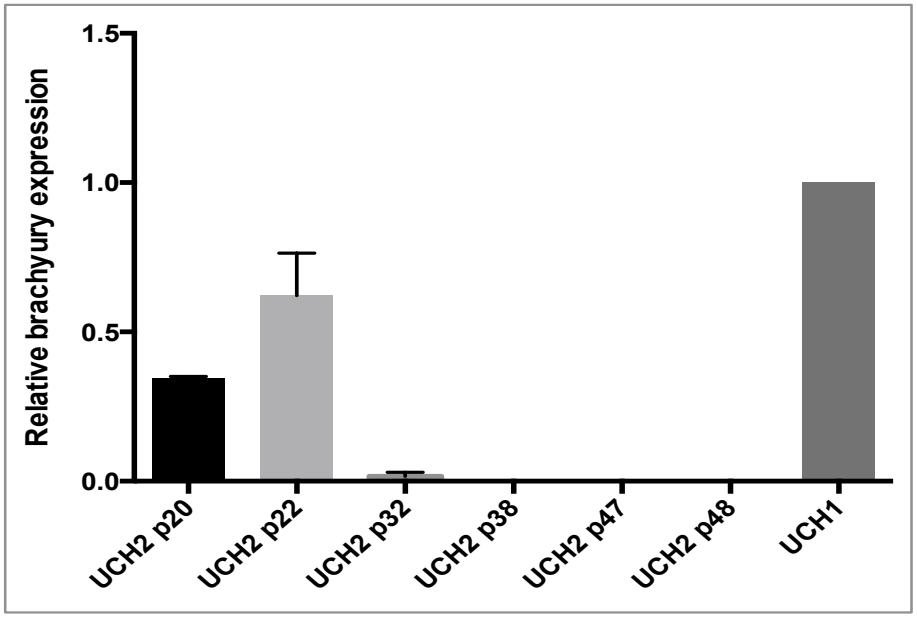

Figure 3.27 Brachyury expression in U-CH2 is lost in cell culture
Brachyury expression quantified by RT qPCR, brachyury expression corrected to both endogenous PGK and GAPDH in two separate experiments, each experiment was run in triplicate. Brachyury expression was normalised to U-CH1 as a standard for brachyury expression as the cycle threshold (ct) remained stable for U-CH1 in culture. U-CH1 and MUG Chor cell lines maintained brachyury expression (consistent ct) (data not shown).

The U-CH2 cell line was not included in further gene silencing experiment. Previous work within our lab found that gene silencing of brachyury in the U-CH2 cell line did not influence proliferation (PhD thesis by Dr Nischalan Pillay under Professor A. Flanagan's supervision), which correlated with observations after knockdown was achieved (data not shown).

Brachyury expression was quantified by Western blot following transduction with AAV and Lentiviral vector carrying the shRNA TRCN000005481 expression cassette for assessment of gene silencing at protein level (Figure 3.28).

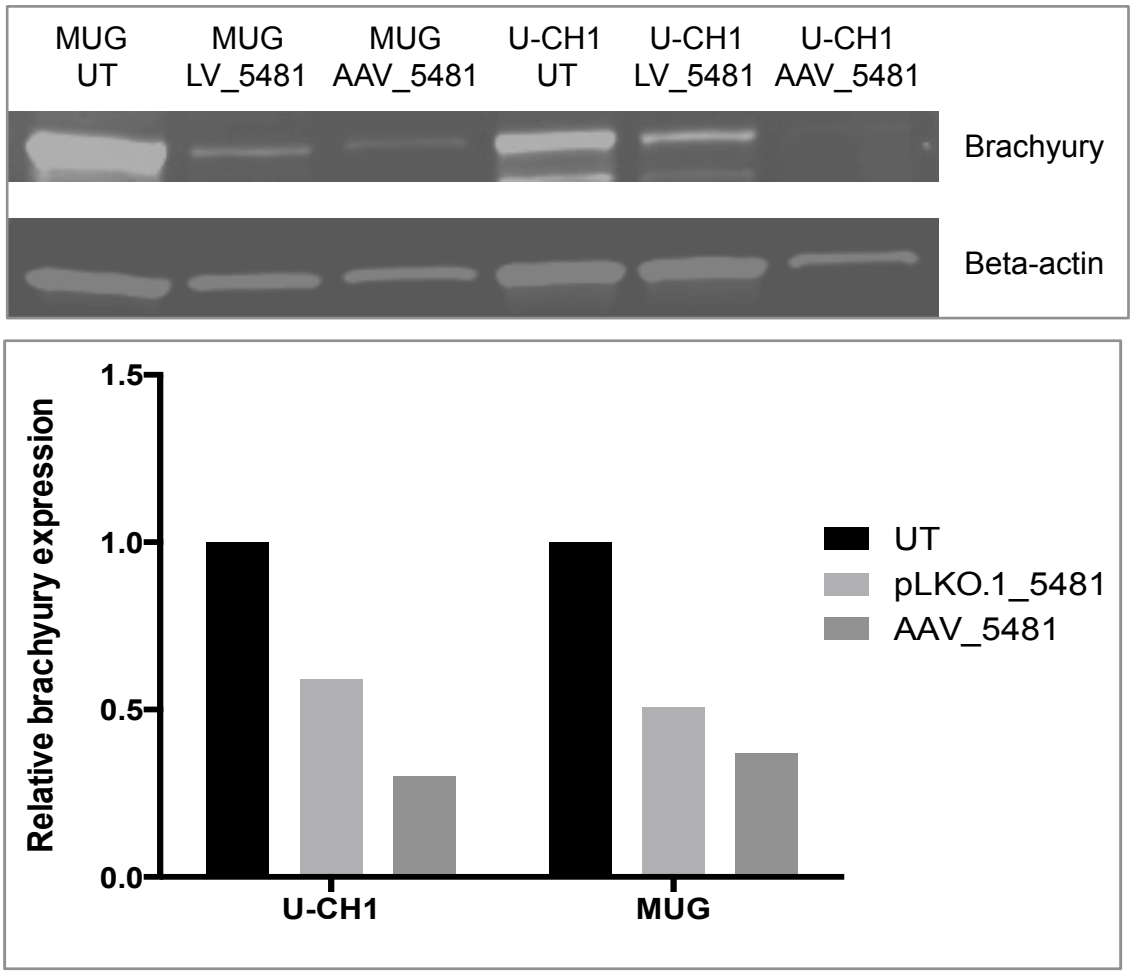

Figure 3.28 Brachyury protein expression following gene silencing
Brachyury protein expression in U-CH1 and MUG Chor cell lines transduced with viral vector targeting brachyury. Top image represents the Western blot images, and the image below represents densitometric measurement of relative brachyury expression corrected for beta-actin as a loading control. Expression in un-transduced (UT) cells shown for comparison. The cell lines were transduced with a Lentiviral vector (LV) or an AAV vector, both carrying the shRNA TRCN000005481 (5481) targeting brachyury. Puromycin selection was undertaken. Brachyury expression also assessed at RNA level by RT qPCR for the same experiment (Figure 3.29).

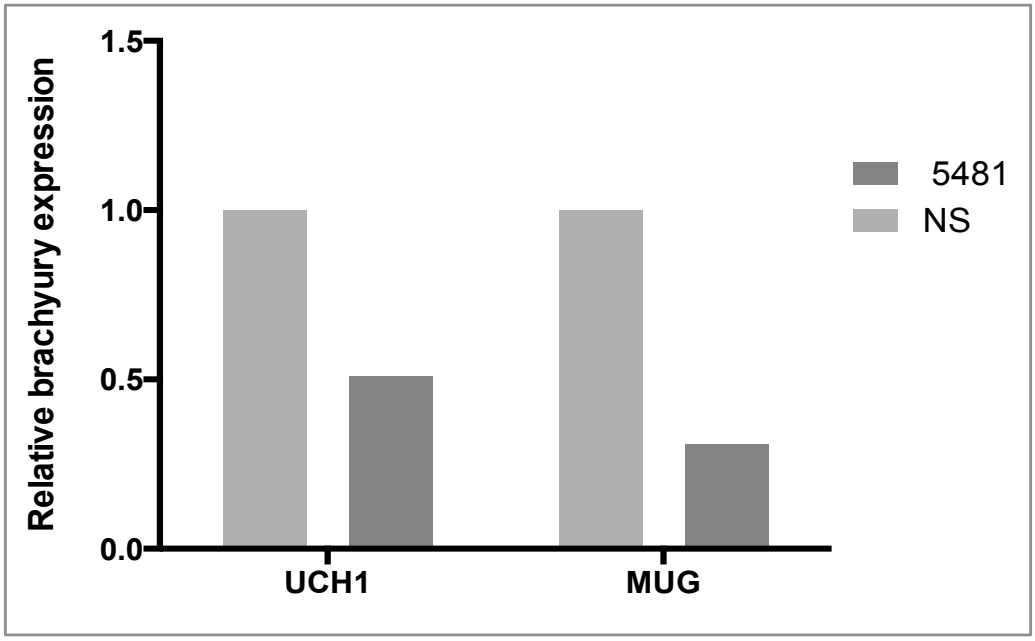

Figure 3.29 Brachyury gene silencing in U-CH1 and MUG (mRNA)
The above data is from a duplicate experiment run at the same time as the experiment for quantification of protein by WB (Figure 3.29) Brachyury expression was quantified by RT qPCR, brachyury expression was corrected to PGK, and each experiment was run in triplicate. Brachyury expression was normalised to cells transduced with non-silencing construct. Due to lack of availability of AAV vector, only the data for lentiviral vector was available.

3.4.8.1 Silencing of brachyury alters morphology in U-CH1 and MUG cell lines

Following gene silencing of brachyury in U-CH1 and MUG Chor cell lines, the cells demonstrated morphologic changes described in U-CH1 and JHC7 chordoma cell lines(89,91).

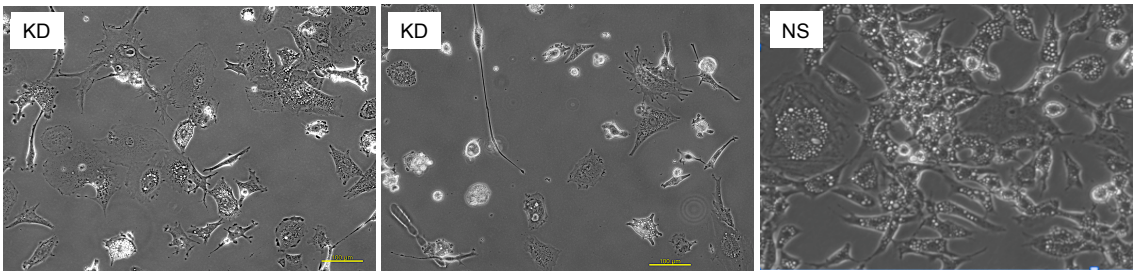

Figure 3.30 Morphologic changes in U-CH1 following silencing of brachyury
Phase contrast microscopy image of U-CH1 cells transduced with pLKO.1_5481 targeting brachyury. MOI 10. Puromycin selection commenced 72 hours after transduction, and was maintained for 96 hours or longer. The left and centre image demonstrate morphologic changes following knockdown of brachyury. The cells are flattened, with loss of the characteristic physalipherous features, and exhibit a more differentiated phenotype with stellate-appearing, or long slim cells.

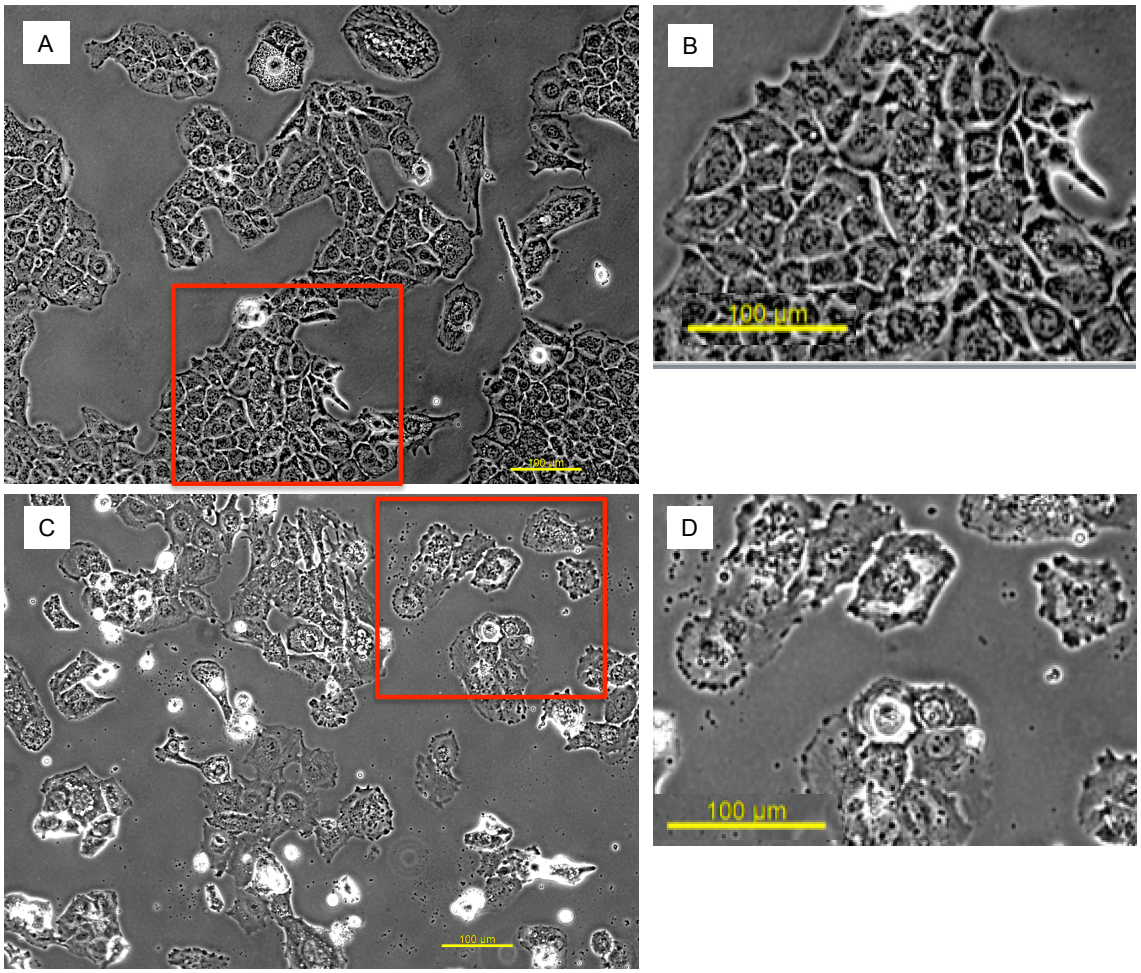

Figure 3.31 Morphologic changes in MUG Chor following silencing of brachyury
Phase contrast microscopy, image of MUG Chor cells transduced with pLKO.1_5481 targeting brachyury. Puromycin selection performed. The MUG chor cell line has a different growth pattern in cell culture than U-CH1, the cells grow closely together and are more uniform in their appearance, some cells have maintained the characteristic physaliferous features(91,231,661). The cell lines here are representative of the cells used in our lab, they are of high passage (p80+). Authenticity was confirmed by STR testing, younger passages had much prolonged doubling time. (A): represent un-transduced MUG Chor cells, the highlighted area has been magnified in (B). (C): represent MUG Chor cells transduced with pLKO.1_5481 with highlighted area magnified in (D). The cells changed morphology following transduction, the cells flattened, lost their structure and changed growth pattern, most cells died following brachyury knockdown.

Having established that the TRCN000005481 demonstrated no toxicity in non-brachyury expressing cell lines and shown that silencing of brachyury in two different chordoma cell lines leads to growth arrest and cell death, large scale production of AAV5 viral vector for delivery of this brachyury targeting shRNA was undertaken.

3.4.9 Xenograft for testing AAV5 gene therapy

As described in Chapter 5, a xenograft model was developed using the U-CH1 cell line modified to stably express luciferase. Following engraftment the tumours demonstrated typical chordoma morphology and immunohistochemistry. Tumours developed in 5 out of 6 mice over 9 weeks following subcutaneous injection. In three mice the tumour demonstrated accelerated growth and reached sufficient size for injection of viral vector. Two mice received the knockdown construct. One mouse was injected with an AAV5 viral vector containing a GFP expression cassette (Kindly supplied by Doyoung Lee in Professor Amit Nathwani's lab, UCL). The AAV5 vector production with the non-silencing construct did not generate sufficient titre for *in vivo* use. The tumour, in the two mice not initially included in the study, continued to grow and both were used as negative controls with injection of Phosphate Buffered Saline (PBS) day 14.

Table 3.4 Table of Treatment given to xenografts

Mouse Identifier	Viral vector received
Mouse 1	AAV5 KD construct
Mouse 2	AAV5 GFP
Mouse 3	*No tumour developed*
Mouse 4	PBS
Mouse 5	PBS
Mouse 6	AAV5 KD construct

3.4.9.1 Reduced tumour growth following AAV5 brachyury targeting treatment

The two mice receiving the AAV5_brachyury silencing vector showed reduced tumour growth compared to those treated with either AAV5_GFP or PBS injection (Figure 3.32).

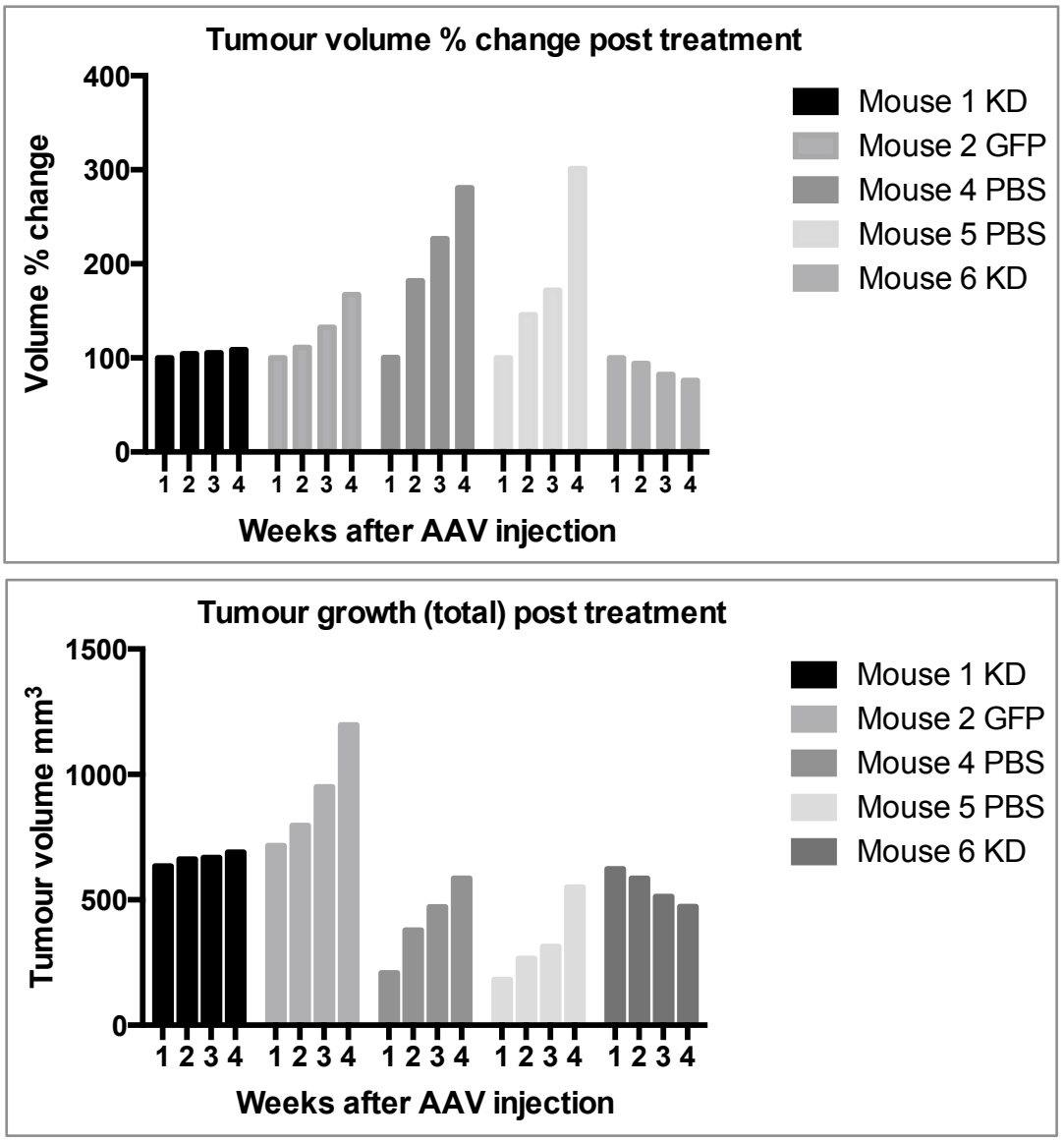

Figure 3.32 Tumour volume following intra-tumoural injection of AAV5 vector
Tumour volume depicted as percentage change (top), or total change (bottom) of volume from start of treatment. Mouse 1 & 6 received AAV5_shRNA targeting brachyury, mouse 2 received AAV5_GFP vector, and mouse 4 & 5 received PBS (injected week 3). Numbers on X-axis represents the weeks with week 1 being the time of intra-tumoral injection. The experiment was terminated week 4.

3.4.9.2 Expression of luciferase reduced with AAV5 brachyury targeting vector

Luciferase expression was measured in photons. Both mice treated with the knockdown construct showed reduction of luciferase expression. Mouse 6 (KD) demonstrated a marked reduction (day 7) but then a subsequent increase of expression. Expression remained stable in the mouse injected with AAV5 GFP as well as the two mice injected with PBS.

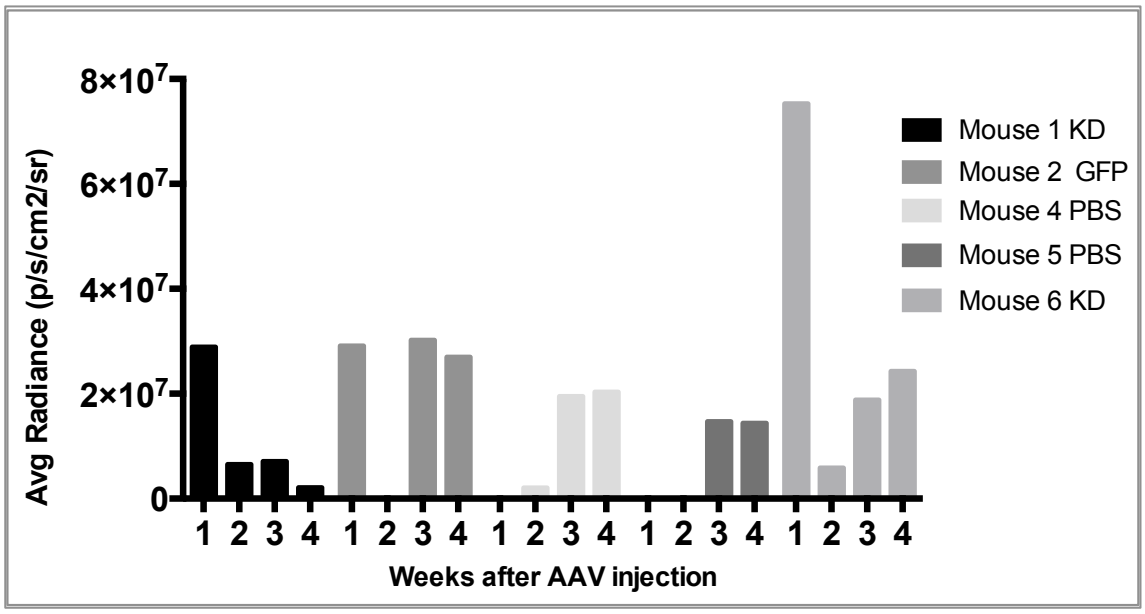

Figure 3.33 Luciferase expression following intra-tumoural injection of AAV5 vector
Average radiance of luciferase was measured in photons as photons/second/cm^2/steradian (p/s/cm^2/sr). Radiance of luciferase was measured at different time points. The bars are grouped for each mouse (labelled according to treatment), each time point (1-4) indicates weeks of treatment with week 1 being the time point of AAV intra-tumour injection. Week 1 is the time-point for AAV injection of the 3 mice receiving knockdown (KD) or GFP vector (control). Note data from "mouse 2 GFP" week 2 is missing due to failed injection of D-luciferin. Mouse 4 & 5 were injected with PBS week 3 as their tumours were too small for injection week 1 & 2, mouse 4 had the luciferase expression assessed week 2 and subsequent weeks, expression for mouse 5 was only measured week 3 & 4.

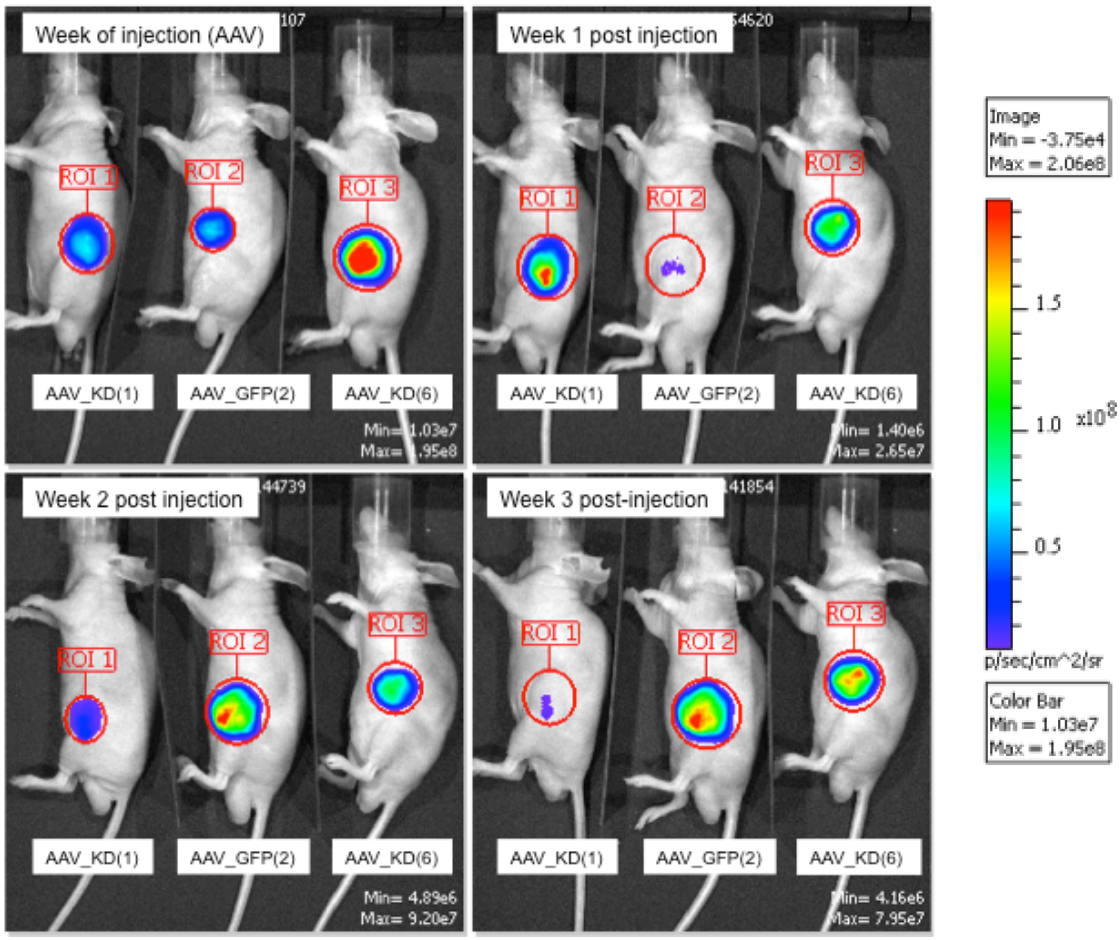

Figure 3.34 Live images of luciferase expression in xenograft tumours over time
Images were generated using Living Image Software 3.2 (IVIS Imaging Systems). The images were acquired over 21 days with the 1st image generated prior to AAV intra-tumoral injection. The subsequent images were acquired weekly up till week 4. The images show luciferase expression following injection of D-luciferin substrate by intra-peritoneal injection. The images were analysed as a group enabling comparison of photon expression. The labelling Region of interest (ROI): ROI 1-3 was used for measurement of average radiance of luciferase by photons (p/s/cm2/sr), ROI 1: mouse 1, ROI 2: mouse 2, ROI 3: mouse 6. Mouse 4 & 5 image below. The crude data can be found in the appendix.

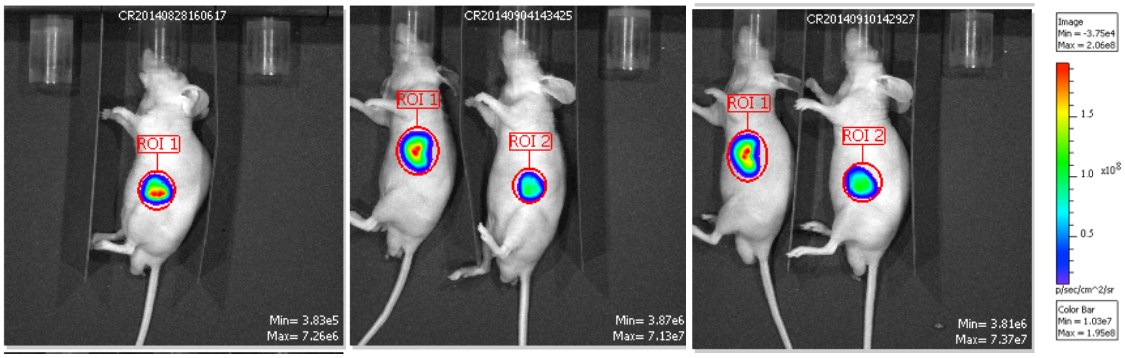

Figure 3.35 Live images of luciferase expression in xenograft tumours (controls)
Details as above (Figure 39), mice used for control (mouse 4 (ROI 1) & 5 (ROI 2)) on the left mouse 4 week 2, centre image and image in the right represents mouse 4 & 5 week 3 (time of PBS injection) and week 4. The analysis was grouped with the treatment group enabling comparison of photon expression at different time points.

The mice treated with AAV5 brachyury-silencing construct showed stable or reduced growth and reduced luciferase expression. Mouse 2 (GFP) showed increased tumour size but stable luciferase expression. Mouse 4 & 5 treated with PBS had increased tumour size, the luciferase expression was stable but the data set for the luciferase expression in those two mice was incomplete.

3.4.9.3 AAV5 vector was widely distributed throughout the mouse

To demonstrate the presence of AAV5 vector in xenografts injected with silencing vector detection of viral genome was assessed by qPCR (Figure 3.36). Vector bio-distribution showed that viral DNA from the AAV5 brachyury targeting vector was detectable in all tissue samples obtained from the necropsied animal. The liver had retained the highest copy number correlating with known serotype tropism for AAV5(693).

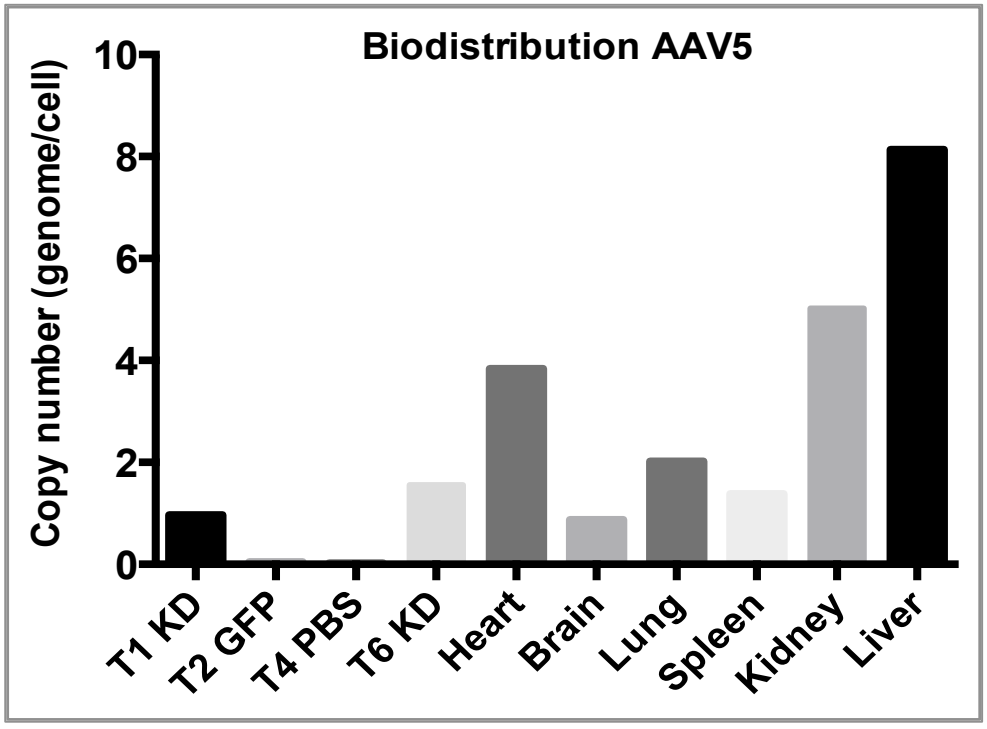

Figure 3.36 Vector genome in xenograft tumour and mouse organs
The level of vector genomes present in the tumours (T) in mouse number: 1, 2, 4 & 6 and in biopsies from different organs harvested from mouse 1 was determined by qPCR. Primers detecting the U6 promoter region of the expression cassette, only present in the knockdown vector was used. The qPCR was normalised to mouse genomic GAPDH. T2 and T4 served as negative control.

3.4.9.4 Xenograft retains chordoma histology and brachyury expression

The tumours generated in the xenograft, resembled the histology of chordoma (Figure 3.37). No changes in morphology or immunoreactivity were observed between the

tumours treated with different vectors. All tumours retained immunoreactivity for brachyury. None of the tumour samples demonstrated necrosis. Immunoreactivity for Ki67 showed scattered Ki67 positive cells with low proliferation rate in all samples (data not shown).

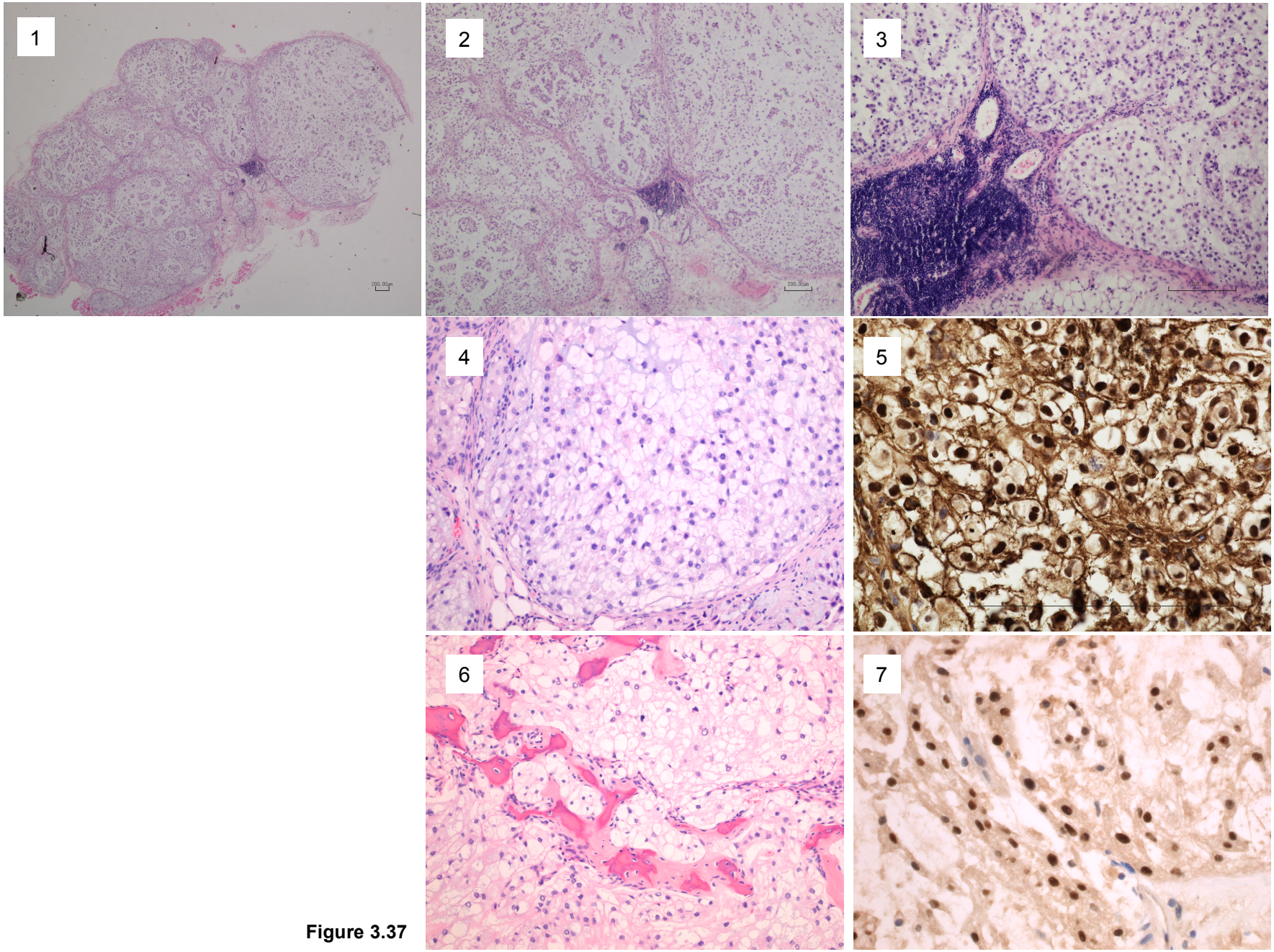

Figure 3.37

Figure 3.37 Morphology of chordoma xenograft and human chordoma sample
Xenograft (1-5) (1) Low power magnification x4, Haematoxylin and eosin stain (H&E) demonstrating 'classic' lobulated appearance; (2) Higher power magnification, x10, morphology in concordance with a 'classic' chordoma showing a myxoid matrix and embedded cords and tumor cells with eosinophilic cytoplasm as well as vacuolated tumor cells, known as physaliphorous cells. Central area is showing accumulation of lymphocytes. (3) Higher power magnification of lymphocytes from image 2; (4) higher power magnification, x20, xenograft displaying morphology with typical chordoma physaliphorous cells embedded in abundant eosinophilic extracellular matrix; (5) xenograft stained for brachyury, brachyury is expressed in the nucleus however in the xenograft there is a cross-reaction with the mouse antibody causing staining of the membrane. **Human chordoma** (6 & 7) (6) H&E stain showing classical appearance at high magnification (x10) and (7) brachyury stain demonstration nuclear reactivity. IHC was kindly done by the members of the histopathology lab at the Royal National Orthopaedic Hospital, under supervision of Professor A. Flanagan.

Lymphocyte infiltration was identified by microscopy in every tumour sample and did not correlate with the treatment, though less infiltration was observed in the two xenografts treated with PBS. The subtype of the lymphocytes was not determined as they did not demonstrate immunoreactivity to human antibodies for CD20 or CD79a (T-cell marker), or CD3 (B-cell marker).

3.5 Discussion

In the work presented here I have shown that the U-CH1 cell line is permissive to infection with AAV5. It was also observed that the U-CH1 cell line maintained GFP expression through cell proliferation, possibly by clonal proliferation due to AAV chromosomal integration or episomal replication, though the latter is unlikely due to lack of replicative genes within the recombinant vector(466,467). Integration of rAAV has been reported to occur in less than 1% of transduction events(535), however a preponderance for integration in this slow growing cell line (doubling time 1 week)(134) cannot be excluded.

In this study two separate examples demonstrated the difficulties of predicting the efficacy and specificity of the gene silencing construct, when shRNA from within one vector is transferred to another vector. The initial construct transferring the shRNA from the GIPZ_V2LHS vector, attempting to recapitulate the gene silencing described by Presneau et al.(89), demonstrated no evidence of brachyury silencing in the AAV vector. The detection of GFP expression suggests that this is not due to loss of viral vector but more likely due to insufficient shRNA expression. When cloning the constructs, transferring the hairpin from the GIPZ_V2LHS vector into the AAV vector, two constructs were generated, one with the miR30 sequence and one without. Both approaches have been validated in the literature(397,689,693). By including the miR30 flanking sequence, which has been reported to trigger the RNAi processing pathway(364), and maintaining the scaffolding for the shRNA(397), the processing of the hairpin was assumed to remain the same, retaining the specificity for the targeting sequence. Shifting the target sequence by just one or two bases has however been reported to change the silencing efficiency(405). It was not possible to establish if lack of expression or lack of specificity explains the lack of silencing of brachyury. It also cannot be excluded that the lack of gene silencing was due to compensatory brachyury gene expression from non-transduced cells, as the construct did not contain an antibiotic expression cassette for selection of the transduced cells. This however seems less likely as the initial transduction efficiency with AAV was excellent as evident by GFP expression.

The subsequent AAV delivery system was generated using the shRNA from the pLKO.1 system, a system used for silencing brachyury in the JHC7 cell line(91). The shRNA sequence was identical to the hairpin used by Presneau et al.(89). Using this construct both within the lentiviral and the AAV vector, knockdown of brachyury was

observed to cause severe irreversible morphologic changes and cell death in the U-CH1 cell line. The U6 promoter expressing the shRNA is more efficient than the previously tested CMV promoter(694) which would be expected to lead to more efficient knockdown. The increased toxicity was considered to be due to a higher level of expression of the hairpin, though the gene-silencing of brachyury was no more efficient compared to published data(89,91). The toxicity was unlikely to be caused by the viruses or the expression cassette, excluding the targeting sequence, as the morphologic changes were not observed using the non-silencing shRNA vector functioning as control for the expression cassette, the endogenous RNAi processing pathway and the virus. The dramatic effect on cell survival was reproduced in 7 non-brachyury expressing cell lines suggesting toxicity was due to sequence specific, off-target effects.

When the potential targets and off-targets of the hairpin were re-assessed, the sequence was found to be specific for brachyury targeting 100% (21/21 nucleotides). An additional mRNA was targeted with 76% (16/21) sequence alignment within the gene *TENM3*. The rules for achieving shRNA specificity are not fully defined, and off-target effect remains a concern(393). Some reports suggest that a single nucleotide mismatch in the middle of an shRNA can abolish its activity(695,696). In contrast, others have reported that shRNA can silence non-target genes containing as few as 14–15 consecutive complementary nucleotides(697) or less(405,698). The off-target effects have been described to be more prominent when there is a match between the seed region of shRNA (positions 2–7) and sequences aligning to the 3′UTR of the gene(374). The brachyury targeting shRNA (pLKO.1TCRN00005484) targets *TENM3* from the nucleotide in position 4 but does not target within the 3'UTR. The recommendation for shRNA design is to allow for at least 2 nucleotide mismatches between shRNA and closely related non-target genes(407). Numerous factors influencing activity have been identified, including; the loop sequence, thermodynamic properties of the hairpin, and the surrounding sequences(398). This may explain why no toxicity was reported using the identical shRNA targeting sequence in the GIPZ_V2LHS vector. It has been recognised that varying levels of off-target silencing can occur with different silencing platforms because the concentration of shRNA vary(359). Dosing is a function of the copy number and how efficiently the hairpin is expressed and processed(699). Assessment to quantify the cellular copy number of shRNA expressed following transduction was attempted but failed for TRCN00005484 shRNA. Expression level of the shRNA TRCN00005481 did not seem to correlate with gene silencing (data not included). Notably, AAV infect cells at multiple copies per cell,

which can be problematic with shRNA as dosing may be amplified. Higher expression is not always beneficial(359). In this study the toxicity was observed across all vectors including AAV and lentiviral vector as well as with naked plasmids. Supporting that toxicity was most likely due to a combination of higher expression of the shRNA achieved using the U6 promoter and/or the off-target alignment with *TENM3.*

TENM3 belongs to the teneurin family of proteins that are highly conserved among species with significant homology between the four different family members(700). Teneurins are a type II transmembrane protein with a large extracellular domain containing an epidermal growth factor-like repeat domain, which was initially described in the Drosophilia as *ODZ*(701). *TENM3* is expressed in the notochord in zebra fish and mice(702). The gene was not found to be highly expressed in chordoma(33) and expression in the U-CH1 cell line was found to be very low in the work presented here. Interestingly *TENM3* was observed to be differentially expressed when brachyury was silenced in the U-CH1 cell line using a different GIPZ vector (GIPZ_V2LHS_153729) targeting within the 3'UTR of brachyury. This hairpin sequence did not align with *TENM3* suggesting the regulation of brachyury and *TENM3* may be linked(127). Teneurin function involves maintenance of basal membrane integrity and mediation of haemophilic intercellular adhesions(703,704). A recent study of teneurin signalling in neuromuscular synapse in Drosophila showed that alterations in teneurin expression affected microtubule organisation and severely disrupted the cytoskeleton(705). These functions support the consistent morphologic changes seen in the different cell lines exposed to the off-target effect following transduction with the shRNA_5484 construct reducing the *TENM3* expression due to its off target effect.

A different shRNA was subsequently used where the sequence had limited off-target effects as determined by BLAST alignment with the human genome and which showed no toxicity or reduction in proliferation of non-chordoma cell lines. The lentiviral vector (pLKO.1 TRCN000005481) as well as the AAV5 vector generated with the expression cassette induced significant gene silencing of brachyury in the U-CH1 and MUG Chor chordoma cell lines, inducing changes in morphology, growth arrest and cell death.

A xenograft model was used to determine if our AAV vector targeting brachyury has therapeutic potential *in vivo*. Two mice were treated with the recombinant viral vector and in these mice the growth of the tumour stablised or reduced in size with diminished luciferase expression. Following intratumoural injection the AAV vector was detectable not only within the tumours but in all organs tested, indicating "off-target" tissue effects.

This is not likely to be of therapeutic concern as brachyury is not expressed in normal tissue, other than in testis. However, lack of tissue specificity may lead to insufficient dosing of target tissues(706). During post mortem evaluation brachyury immunoreactivity was retained in all tumour samples regardless of therapy received. In the two mice that received the brachyury-targeting vector it remains to be established if the lack of gene silencing was due to loss of the vector during cell division or the outgrowth of non-transduced cells. At the end of four weeks the average viral copy number per cell suggested that the ratio of tumour cell transduction was one to one. A marker was however not included in the construct to visualise distribution of the vector within the chordoma xenograft tumour specimen(707). It has not been established what level of shRNA expression is needed to maintain brachyury gene silencing. As chordomas have slow growth kinetics the tumour cells were expected to experience lengthy RNAi effects with knockdown of brachyury leading to cell senescence or cell death. It is conceivable that the transduced tumour cells found a way to escape the gene silencing, a phenomenon accepted by scientists working with RNAi but rarely reported. In a study by Gu et al.(708) lentiviral delivered shRNA silencing was found only to be durable for 2-3 weeks after which time an increase in expression was observed. The transduced cells initially demonstrated evidence of apoptosis and cell senescence *in vitro* and inhibition of tumour growth *in vivo*(709), however the effect was not maintained. Lentiviral-mediated silencing is thought to be permanent as the vector integrates into the host cell genome(664). Integration of the vector was confirmed by demonstrating persistent GFP expression. This demonstrated that the plasmid was still able to express the transgene and that overgrowth of non-transduced cells did not account for the loss of gene silencing. Others have reported similar difficulties with lack of durable RNAi in cancer cell lines(710-712). Escape from a single shRNA silencing complex has also been demonstrated in HIV-1 with the virus regaining the ability to multiply(713). The viral escape was circumvented by adding multiple shRNAs to the vector, targeting different sites within the genome(397,713,714). The use of bi-functional shRNA has also been used in pre-clinical studies in cancer cell lines, showing enhanced potency and durability of gene silencing(715,716). Having used a non-integrating viral vector for the study reported here there is less certainty regarding the possible causes for the lack of gene silencing. The possibility that cells have escaped gene silencing in this study is supported by the observation of reduction or stabilisation of tumour growth and reduction in luciferase expression early after transduction.

Loss of transgene expression might also explain the lack of a prolonged effect on tumour growth. Viral vectors and RNAi transgenes have been found to have immune stimulation potential(308,391,402). Though murine studies have not been helpful in predicting immune response to viral vectors(436,717), neutralising antibodies against the transgene are well documented in murine studies(235,435,718). The immune responses against vectors and transgene products can lead to silencing or loss of expression with only transient expression of the therapeutic genes(402,404,436). In the study presented here lymphocyte infiltration was identified by microscopy in every tumour sample and did not correlate with the treatment. The subtype of the lymphocytes was not determined, however the athymic Balb/c nude mouse is grossly deficient in peripheral T cells(719) and the lymphocyte population is mostly composed of B-lymphocytes(719-721), suggesting that B cells would most likely be present. Parameters for assessing immune stimulation, by detection of neutralising antibodies to the transgene or viral vector were not undertaken in this study and it was therefore not possible to assess the role this mechanism might play in the time dependent tumour effect.

While the small scale of this experiment presented lacks statistical power, there remains an indication that brachyury silencing can reduce tumour growth. These preliminary results warrant further investigation as a novel anti-tumour approach for chordoma. Indeed, the three established chordoma cell lines used in this work were all found to be permissive to AAV5, indicating its ability to target chordoma in a clinical setting. The potential ability to escape RNAi will need to be addressed through optimisation of the construct to express multiple shRNA targeting sequences. An additional solution might be to optimize the vector to include an immune modulator such as interferon, IL-2, GM-CSF or a suicide gene to the construct. This will stimulate a targeted inflammatory response to transduced cells, guiding the immune system to eradicate the tumour. It may also prove beneficial to combine gene therapy targeting brachyury with cytotoxic- or targeted therapies as silencing of brachyury may render the tumour cells sensitive to other therapies. This approach is currently being tested in a phase II trial using the brachyury vaccine in combination with radiotherapy (NCT02383498)(298).

Gene therapy for chordoma as defined by this experiment may not offer a definitive cure but delay of recurrence, offering relief and reduced morbidity for patients. A challenge facing clinical development is defining a meaningful end-point, in particular where the patient population is small, the natural history of the disease progression is

slow and biomarkers to monitor therapeutic efficacy have not yet been identified or validated. Treatment options are likely to be multi-faceted and require novel drug therapies and novel biomarkers such as ctDNA. This will be adressed in subsequent chapters.

4 HIGH-THROUGHPUT DRUG SCREEN

4.1 Background

The lack of effective treatment for chordoma has previously been discussed. Standard treatment includes surgery followed by proton beam radiotherapy. Chordoma has proven to be largely resistant to conventional ionising radiation and chemotherapy(56,722,723).

In the past decade advances have been made in the treatment of many cancers. The recognition that somatic genetic alterations in tumours correlate with clinical response to specific tyrosine kinase inhibitors (TKI) and that molecular profiling can identify 'driver' mutations allowing for genotype-directed therapy rather than empiric therapy has lead the concept of personalised medicine(162,579,724-728). One of the most successful examples of cancer-targeted therapy is inhibition of EGFR mutations which occurs in up to 30% of patients with NSCLC(729). The majority of patients with activating EGFR mutations have demonstrated good response to therapy with EGFR inhibitors(730). However, the vast majority of patients who initially responded to therapy developed resistance within 1-2 years(729,731,732). Mechanisms of acquired resistance include emergence of secondary mutations and altered gene expression within the targeted or alternative pathways(729,733,734). Many of the mechanisms of resistance are still unknown(729,735,736).

With the exception of brachyury amplification in a proportion of chordomas, no unifying recurrent genetic alteration has been identified and, in particular, no targetable mutation(125,128,129,135). Analysis of tyrosine kinases in chordoma has detected activated *PDGFR, EGFR* and *TGFα*(164). Studies of the downstream pathways have described activation of the PI3K/AKT and RAS/MAPK pathways(40,164), but no mutation or amplification has been identified within these gene pathways(40,130,180).

In view of the unmet need for effective treatment for chordoma and the lack of targetable genetic alterations, a high-throughput compound screen was undertaken. Performing a phenotypic screen has the potential to identify drug-sensitivity patterns, to help understand some of the mechanisms of this disease and potentially provide a strategy to identify biomarkers to guide the early-phase clinical trials of novel compounds.

4.2 High-throughput drug screening in chordoma (Declaration)

This project was undertaken in collaboration with Cancer Research Technologies UK (CRT) who gave technical assistance and advice on the project and provided a

screening report forming the basis for this chapter. CRT is in part funded by Cancer Research UK and has vast experience with high-throughput drug screening. The compound screening was done jointly with Michelle Barnard (CRT) and members of Professor A. Flanagan's lab: Lucia Cottone PhD, Susanne Scheipl (MD), and I. Susanne Scheipl screened the GSK PKIS1 library manually before the collaboration with CRT was established. CRT analysed the data, and compounds were selected for inclusion into the subsequent screening. The compound screen involved collaboration with GlaxoSmithKline (GSK) (GlaxoSmithKline, NC, USA) who supplied two different compound libraries containing small kinase inhibitors at various stages of their compound development(737). GSK remained involved throughout the project giving advice, and received the data following completion of the screening process. In addition to the GSK compounds, CRT made a set of 160 kinase inhibitors available, which were included in the screen; these compounds were from Calbiochem (Merck KGaA, Darmstadt, Germany). The majority of these compounds are currently being tested in early phase clinical trials. In addition, a selection of cytotoxic anti-cancer drugs were included, as a few small studies have suggested a synergistic effect of cytotoxic drugs and kinase inhibitors(88,200-202) (Table 1.1). Two epigenetic libraries (SCG) were also included in the screen - this was part of Lucia Cottone's project. The data features in the figures for the analysis and are included in the numbers, but will not be commented upon.

4.3 Aim

The aim was to identity compounds with therapeutic effect in chordoma. Identifying therapeutic targets relevant for chordoma, by performing a phenotypic high throughput compound screen in three chordoma cell lines, might help understand the mechanisms of this disease. Target identification will guide patient selection and identify compounds for clinical trials in the development of treatment for chordoma. For this purpose a phenotypic high-throughput screen was undertaken, testing approximately 1200 compounds, to identify small molecules which elicit a kill or arrest effect in three chordoma cell lines.

4.4 Objectives

1. To optimise cell lines to confirm authenticity by genetic fingerprinting using short tandem repeats (STR).
2. To study the effect on cell proliferation in a single point screen (1μM) in three well established chordoma cell lines (U-CH1, U-CH2, MUG Chor).
3. To confirm the hits from the single point screen in a dose-response format (IC_{50})
4. To identify selective hits by including a counter screen using a control cell line (human dermal fibroblasts).
5. To validate the mechanism of cell death by assessment of induction of apoptosis.
6. To select the lead compounds and benchmark them against approved drugs targeting the same targets.

4.5 Results

4.5.1 Chordoma cell lines

Specific information on the origin of the cell lines used for this study can be found in Materials and Methods.

4.5.1.1 Authentication of chordoma cell lines

STR analysis examining 17 highly polymorphic genetic markers generated a DNA profile uniquely identifying the cell lines. The markers were aligned against the data held at the American Type Culture Collection (ATCC), which confirmed authenticity of the chordoma cell lines used for the compound screen.

EV	Cell No.	Cell name	Locus names								
			D5S818	D13S317	D7S820	D16S539	VWA	TH01	AM	TPOX	CSF1PO
	Query (Your Cell)		*11,12*	*11,13*	*9,12*	*12,13*	*17,17*	*7,7*	*x,y*	*8,11*	*10,11*
1.22(44/36)	748	U-CH1	11,12	11,13	9,12	12,13	17,17	7,7	X,Y	8,11	10,11
1.11(40/36)	670	UPCI-SCC-090	11,12	11,11	9,10	12,13	17,17	7,7	X,Y	8,8	11,12
1.06(38/36)	706	OE-33	11,11	14,14	9,10	12,12	17,17	7,7	X,X	8,11	10,11
1.06(38/36)	CRL-5844	NCI-H838 [H838]	11,11	8,8	9,9	9,12	17,17	7,7	X,X	8,11	10,10
1.00(36/36)	460	CAL-148	12,12	13,14	9,10	12,12	17,19	7,7	X,X	8,11	10,11

EV	Cell No.	Cell name	Locus names								
			D5S818	D13S317	D7S820	D16S539	VWA	TH01	AM	TPOX	CSF1PO
	Query (Your Cell)		*10,11*	*11,11*	*8,12*	*12,12*	*17,17*	*9.3,9.3*	*x,x*	*8,8*	*11,12*
1.67(60/36)	749	U-CH2	10,11	11,11	8,12	12,12	17,17	9.3,9.3	X,X	8,8	11,12
1.44(52/36)	CRL-10302	SW756	11,12	11,11	10,12	12,13	17,17	9.3,9.3	X,X	8,8	11,12
1.39(50/36)	HTB-27	MDA-MB-361	10,11	11,11	9,12	11,12	17,17	9.3,9.3	X,X	8,11	12,12
1.33(48/36)	503	HCC-1599	12,12	11,11	10,11	12,13	17,17	9.3,9.3	X,X	8,8	12,12
1.33(48/36)	CRL-2331	HCC1599	12,12	11,11	10,11	12,13	17,17	9.3,9.3	X,X	8,8	12,12

EV	Cell No.	Cell name	Locus names								
			D5S818	D13S317	D7S820	D16S539	VWA	TH01	AM	TPOX	CSF1PO
	Query (Your Cell)		*11,12*	*11,11*	*8,11*	*11,14*	*15,15*	*9.3,9.3*	*x,x*	*8,8*	*11,11*
1.67(60/36)	755	MUG-CHOR-1	11,12	11,11	8,11	11,14	15,15	9.3,9.3	X,X	8,8	11,11
1.33(48/36)	HTB-78	SW 626 [SW-626, SW626]	12,12	11,11	10,12	11,11	17,18	9.3,9.3	X,X	8,8	11,11
1.24(42/34)	CRL-2980	SqCC/Y		11,11	8,11	11,13	15,16	7,9.3	X,X	8,8	9,11
1.22(44/36)	667	UPCI-SCC-072	14,14	11,11	11,12	11,12	15,15	6,6	X,X	8,8	11,11
1.22(44/36)	CCL-90	Cri du Chat	10,11	11,11	8,11	11,12	15,16	9.3,9.3	X,X	8,8	10,12

Figure 4.1 STR analysis of 3 chordoma cell lines
U-CH1 passage18 (top), U-CH2 passage 26 (middle), MUG Chor-1 passage 93 (bottom). STR data represent allele size. The query cell line is highlighted in green, below are the cell lines to which the chordoma cell lines align in order of best match.

4.5.1.2 Cell lines tested negative for mycoplasma

The cell lines used for the drug screen were tested for mycoplasma by culturing on broth and agar(738). All the cell lines tested negative for mycoplasma (data not shown).

4.5.1.3 The cell lines harbour no common cancer gene mutations

To support interpretation of the data from the compound screen the three chordoma cell lines were checked for mutations in common cancer-signalling pathways (hotspots). These included: *EGFR, KRAS, NRAS BRAF, PIK3CA, AKT1, TP53, PTEN, MAP2K1, ALK, CTNNB1, MET (HGFR), FGFR1/2/3/4, NOTCH1, JAK2, KIT and PDGFR*. No mutations were identified.

4.5.2 Results of single point screening

4.5.2.1 High-throughput screen set up and quality control

The initial step of the high-throughput screen included optimisation. Cell density experiments were undertaken to establish the number of cells that were to be seeded on day 1 so as to reach 90% confluency on day 5. The optimal time point for assay readout was determined as 5 days from seeding, and following 4 days of compound treatment. This was established during the initial compound runs by evaluation of morphology and cell death (data not shown). The timing for the colorimetric assay read-out was determined based on the stability of the WST-1 assay, identifying the time point before reaching saturation of the assay The Staurosporine (SSP) concentration was chosen on the basis of achieving 100% cell death (positive control) on day 5, and the DMSO concentration which exerted no effect (negative control) was determined by undertaking a dilution experiments. Antibiotics were tested for interference with the data (no interference was noted). Results of the optimisation are outlined in Table 4.1 below.

Table 4.1 Outcome of optimisation

Assay parameter	MUG Chor	U-CH2	U-CH1
Endpoint read time	2 hours	3 hours	3 hours
Cell density	5000 cells/well	2500 cells//well	5000 cells/well
SSP blank concentration	30μM	30μM	30μM
DMSO (%)	0.25	0.25	0.25
+/- Pen/Strep	+Pen/Strep	+Pen/Strep	+Pen/Strep

Table 4.2 Overview of compound libraries

Compound library	Number of compounds
GSK PKIS2	522
GSK PKIS1	364
SGC	20
Epigenetic	43
Calbiochem	160
Anti-cancer	43
Total number of compounds	1152

4.5.2.2 Good reproducibility of high-throughput screen data

The single point screen was conducted at a single concentration of 1μM for each compound. Good reproducibility of data was observed in all cell lines across three independent experiments (Figure 4.2).

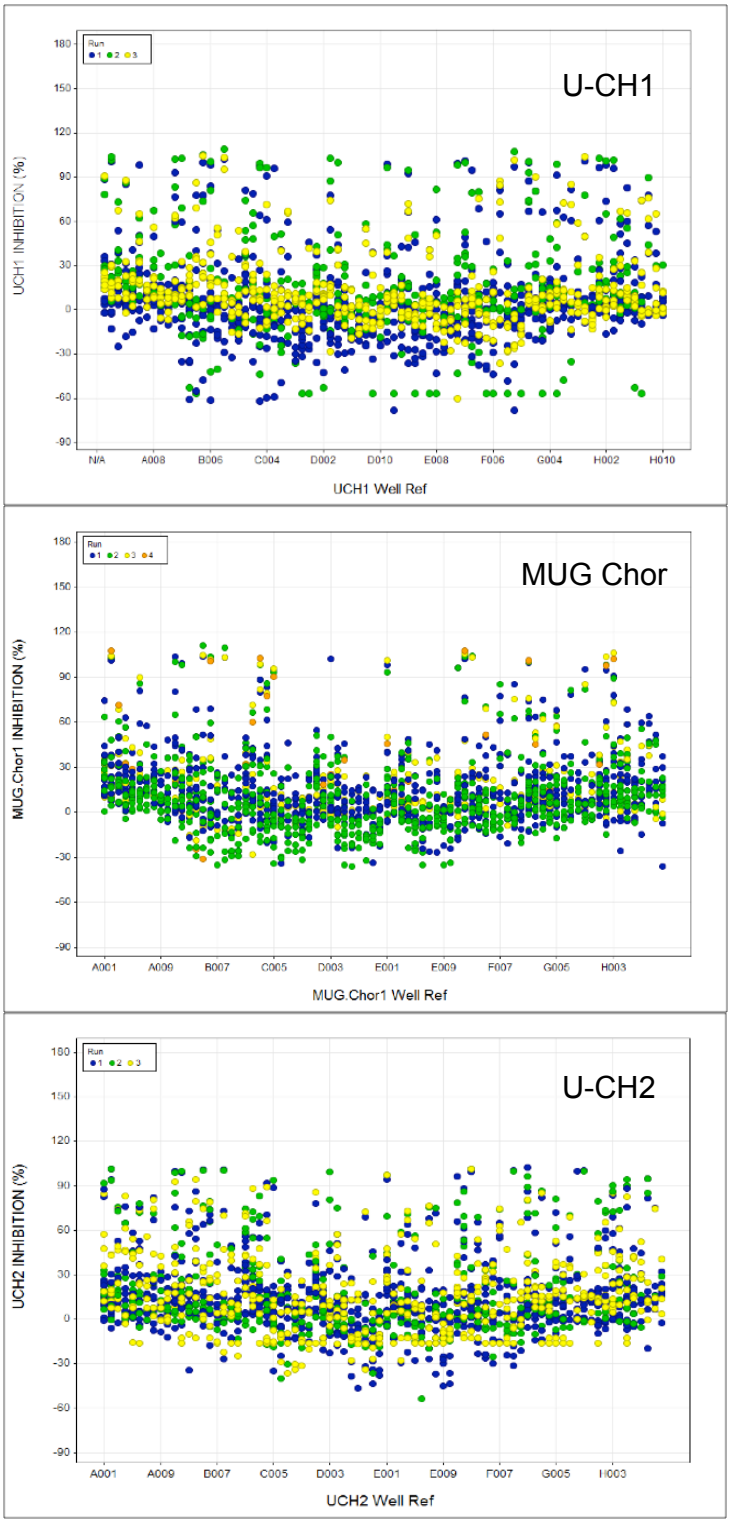

Figure 4.2 Distribution of percentage inhibition for each independent experiment
The raw data for each independent experiment was converted to percentage inhibition relative to the negative controls (cells + 0.25% DMSO) and positive controls (cells + 30μM Staurosporine) on each plate. The data from each experiment (n=3) were overlaid to assess variance within the data. Different colours identify individual experiments. Distribution of percentage inhibition vs. well reference for each experiment. Data representative of Calbiochem, Epigenetics, SGC, and GSK PKIS2 libraries. GSK PKIS1 was screened separately and was not included, but demonstrated equally good reproducibility between separate experiments (data not shown).

4.5.3 Hit selection

Due to the variability of activity between cell lines and/or only moderate percentage inhibition of proliferation, compounds causing a decrease in viability of more than 2x standard deviations (SD) (CI 95%) or, for some libraries, 1.5x SD compared to the controls were regarded as hits.

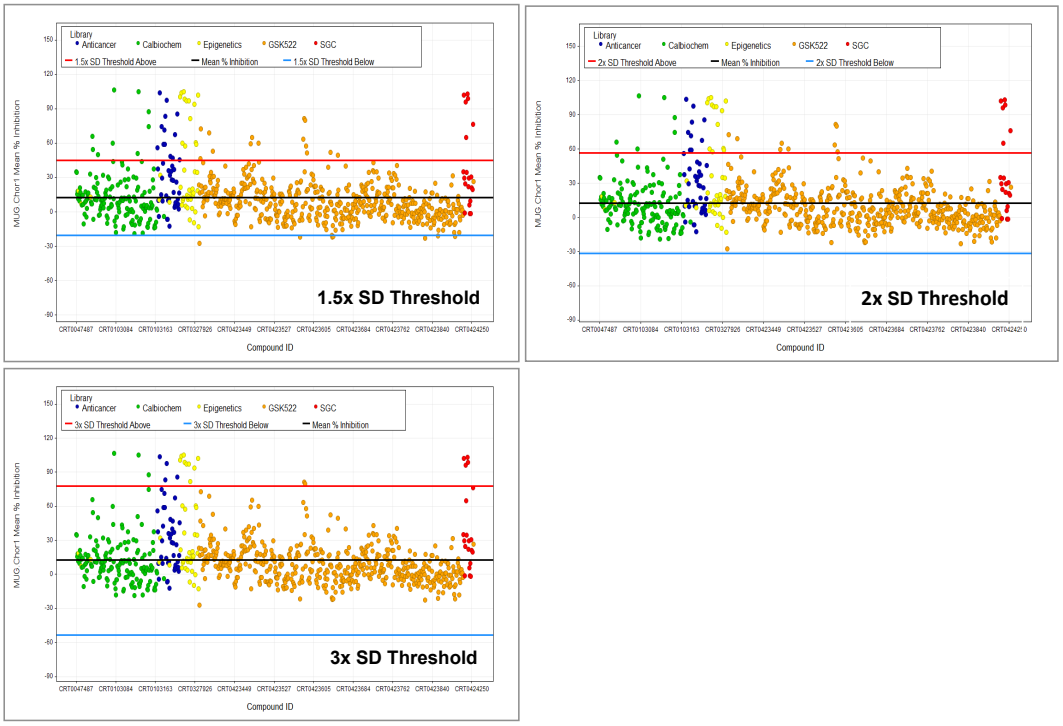

Figure 4.3 Depiction of 3x, 2x and 1.5x standard deviation for hit selection
SD of the data was used to determine mean percentage inhibition, and 1.5, 2 and 3 fold SD thresholds were calculated for each cell line. The difference in the number of hit selection between 1,5x, 2x and 3x SD is demonstrated. The red line is the SD above the threshold, the black line is the mean percentage inhibition, and the blue line is the SD below the threshold. The different coloured dots represent libraries with each dot representing a different compound. Green: Calbiochem, Blue: anti-cancer library. Orange: GSK PKIS2. Yellow & red: epigenetic libraries. These data are for the MUG Chor cell line. The data for U-CH2 and U-CH1 are similar (not shown). By lowering the SD it is possible to increase the yield and thereby ensuring inclusion of potential effective compounds.

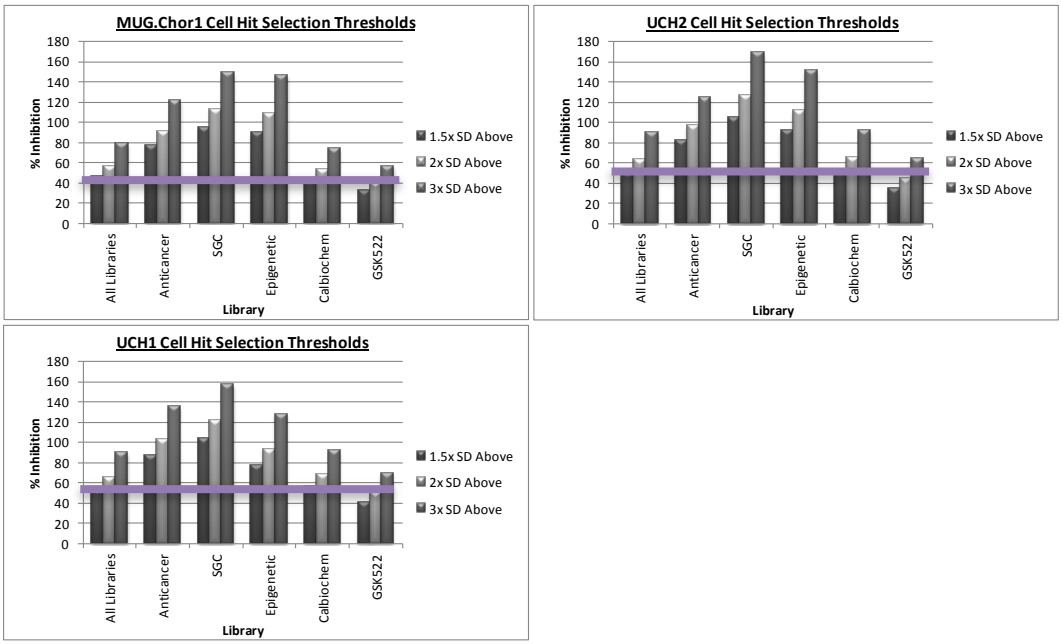

Figure 4.4 Compound hits according to 3x, 2x and 1.5x standard deviations
Illustration of data in figure 3 demonstrating the number of hits according to different standard deviations of percentage inhibition in the three cell lines. Data ranges for each library vary with high SD for some libraries (Anti-cancer, SGC, Epigenetic) leading to biased thresholds. This resulted in few or no hits from the GSK PIKS2 library. The mean SD for the GSK PKIS2 (GSK 552) library was re-calculated separately selecting hits according to 1.5x SD based on data for this library only and not across all libraries, in the interest of including potentially effective drugs. The purple line indicates mean percentage inhibition.

The 2x SD above the threshold identified compounds which gave >46% inhibition in MUG Chor, >50% inhibition in U-CH1 and >53% inhibition in U-CH2. This yielded a total of 113 hits above the relative percentage inhibition thresholds across all cell lines. A 2x SD below the threshold was used for each cell line thereby identifying 23 potential activators of cell growth/interferers (< -20% inhibition in MUG Chor/U-CH2 and < -29% in U-CH1).

The re-calculated thresholds using 1.5x SD based on mean percentage inhibition for each of the cell lines for the GSK PKIS2 library identified an additional 34 inhibitory hits above the relative thresholds (>33% inhibition in MUG Chor, >35% inhibition in U-CH1, and >41% inhibition in U-CH2). 20 potential activators of cell growth/interferers were identified below the relative thresholds (< -15% inhibition in MUG Chor, < -24% inhibition in U-CH1 and < -1% inhibition in U-CH2) inclusive of all cell lines. A total of 147 compounds above the defined thresholds and 43 potential activators/interferers below the thresholds (Calbiochem, GSK PKIS2, and Anti-Cancer Libraries) were identified for further profiling.

The GSK PKIS1 library, which had been screened manually was analysed by CRT for compound commonality vs. selectivity. 37 additional compounds were identified as inhibitory hits: 15 common hits (either between two or all three cell lines) and 13 selective hits for the MUG Chor, 8 selective hits for U-CH2 and 1 selective hit for U-CH1. These hits were included in the IC_{50} profiling (Figure 4.6 & Table 4.3).

The global hit rate was 16% for inhibitory hits (184/1153) and 3.7% for potential interferers/activators of cell growth (43/1153). Hits were either common or selective for chordoma cell lines. Identified compounds were profiled in a 10-point IC_{50} format in the three chordoma cell lines and a control cell line, Normal Adult Human Dermal Fibroblasts (NAHDF).

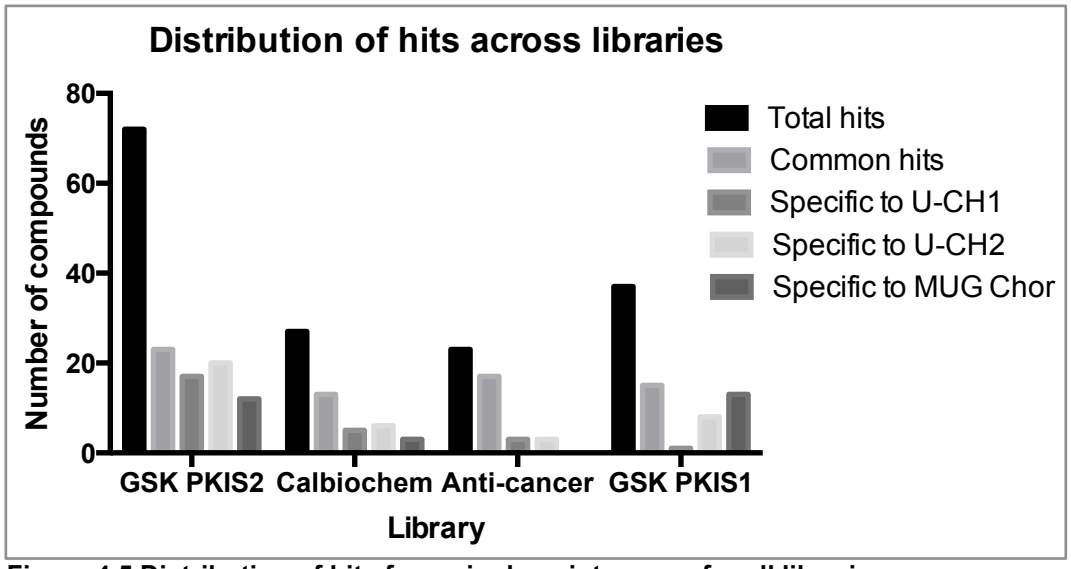

Figure 4.5 Distribution of hits from single point screen for all libraries
Hit distribution across libraries of interest according to cell lines (common or selective) with a total of 159 hits from all libraries, 68 hits were common to two or more cell lines, 27 hits were specific to U-CH2, 26 hits were specific to U-CH1, 28 hits specific to MUG Chor. The data for the epigenetic screen were not included in this figure, accounting for the discrepancy in the total number of hits.

4.5.3.1 Summary of single point screen for GSK PKIS1 library

The GSK PKIS1 library was analysed in more detail as the compound's target class has previously been published(739), whereas the compound targets for the GSK PKIS2 were revealed following the IC_{50} profiling.

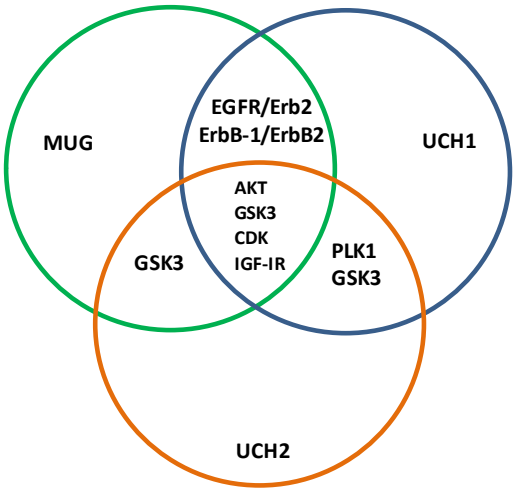

Figure 4.6 Compound targets with hits shared across cell lines
Graphical representation of target class from GSK PKIS1 by a Venn diagram showed overlap of target class common to two or all three cell lines.

Table 4.3 Selective hits for individual chordoma cell lines GSK PKIS1 library

MUG Chor

CRT ID	GSK Cpd ID	MUG Mean SP % Inhibition	Pathway
CRT0363776	GW683768X	46	CDK
CRT0363482	GW583373A	39	ErbB-1/ErbB2
CRT0363293	SB-725317	45	GSK-3
CRT0363705	SB-675259-M	52	GSK-3
CRT0363496	GSK2220400A	52	IGF-1R
CRT0363724	GSK1173862A	54	IGF-1R
CRT0363757	GSK2213727A	38	IGF-1R
CRT0363761	GSK2110236A	63	IGF-1R
CRT0363762	GSK2163632A	51	IGF-1R
CRT0363271	SB-737198	36	MSK-1
CRT0363573	GW440139A	37	RET
CRT0363377	GW410563A	35	VEGFR
CRT0363378	GW612286X	37	VEGFR

UCH2

CRT ID	GSK Cpd ID	UCH2 Mean SP % Inhibition	Pathway
CRT0363419	GSK614526A	35	AKT
CRT0363273	SB-750140	40	MSK-1
CRT0103145	SB-220025-R	33	p38 kinase
CRT0363345	GSK317314A	57	polo-like kinase 1
CRT0363347	GSK326090A	38	polo-like kinase 1
CRT0363348	GSK571989A	72	polo-like kinase 1
CRT0363350	GSK978744A	50	polo-like kinase 1
CRT0363390	GSK269962B	34	Rho-Kinase

UCH1

CRT ID	GSK Cpd ID	UCH1 Mean SP % Inhibition	Pathway
CRT0363358	GW461104A	29	ErbB-1/ErbB2

4.5.3.2 Summary of single point screen of anti-cancer library

To identify compounds already in clinical use, that could potentially be tested in combination with targeted therapy. To achieve this compounds from the anti-cancer library were selected based on the literature review of drugs tested in preclinical and clinical settings. Compounds reported to have demonstrated efficacy and chemotherapeutics currently used as standard of care in treatment for sarcoma were included. The compounds had various different mechanisms of action (Figure 4.7). For a full list of compounds included please see appendix.

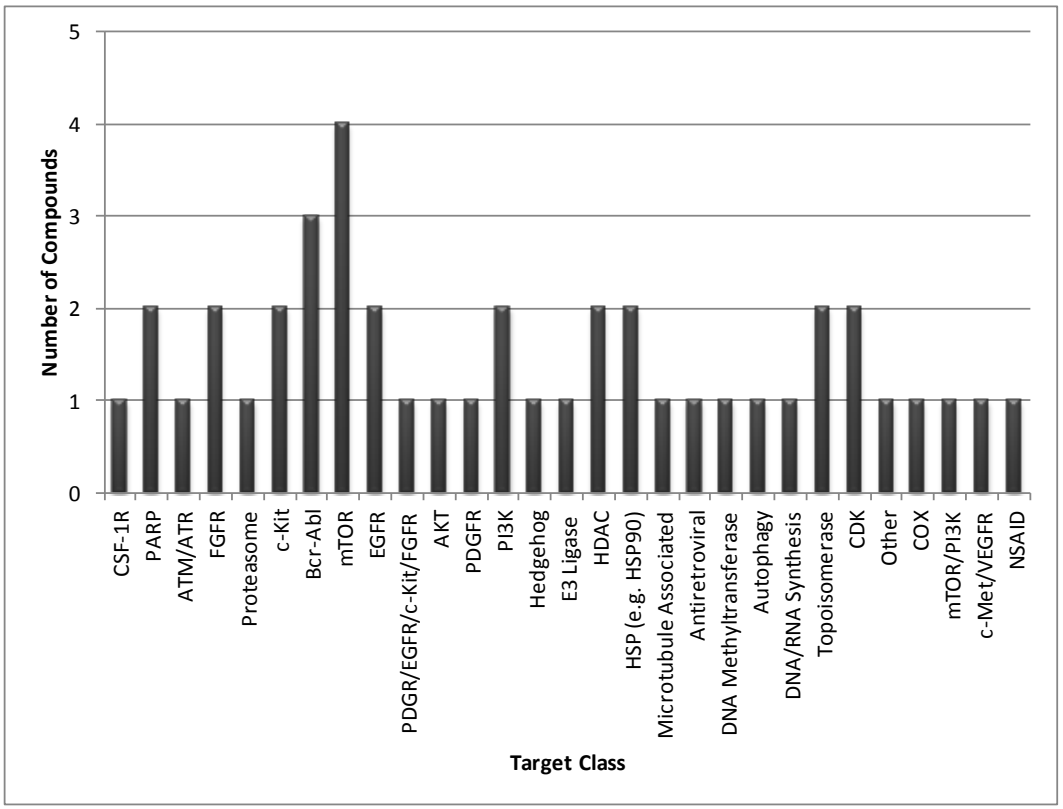

Figure 4.7 Mechanism of action (targets) of compounds, Anti-cancer library

Compounds from the Anti-cancer library were selected for the IC_{50} profiling according to the percentage inhibition determined by the single point screening. Compounds identified as hits are listed below in Table 4.4. Multiple compounds demonstrated an overlap whilst some showed selectivity between cell lines as demonstrated in the Venn diagram below (Figure 4.8). No compound showed selectivity for the MUG Chor cell line.

Table 4.4 Anti-cancer library compounds for IC_{50} screening

ID/Compound name	Target class	U-CH2 Mean % inhibition	U-CH1 Mean % inhibition	MUG Chor Mean % inhibition
Deforolimus (Ridaforolimus)	mTOR	53.1		
Everolimus	mTOR	55.63		
PHA-793887	CDK	55.23		
ABT-869 (Linifanib)	CSF-1R		57.15	
Decitabine	DNA Methyltransferase		58.4	
Lapatinib	EGFR		64.1	
Ellence	Toposiomerase	65.17		45.3
GDC-0559 (Vismodegib)	Hedgehog	67.3		46.93
OSI-930	c-Kit	84.5		67.37
BEZ235 (Dactolisib)	ATM/ATR	61.37	77.6	
Adriamycin (Doxorubicin)	DNA Synthesis	67.23	93.56	
Flavopiridol	CDK	71.67	75.7	
GSK1059615	mTOR/PI3K	52.8	48.35	
Docetaxel	Microtubule associated	48.7	63.8	58.7
AP24534 (Ponatinib)	Bcr-Abl	58.83	82.67	55.8
AZD2281 (Olaparib)	PARP	71.47	76.27	80.2
AZD8055	mTOR	59.13	76.33	82.45
Bortezomib	Proetasome inhibitor	97.5	96.23	49.5
SB939 (Pracinostat)	HDAC	85.57	64.37	80.25
GDC-0941	PI3K	55.8	64	59.3
Carboplatin	DNA Synthesis	100	100	87.15
17-DMAG (Alvespimycin)	HSP90	74.67	86.4	63
Belinostat	DHAC		83.43	80.35

Compound hit selection threshold: MUG Chor: 46% mean inhibition, U-CH1: 50% mean inhibition and for U-CH2: 53% mean inhibition was used as selection criteria for compounds to be included in the IC_{50} profiling.

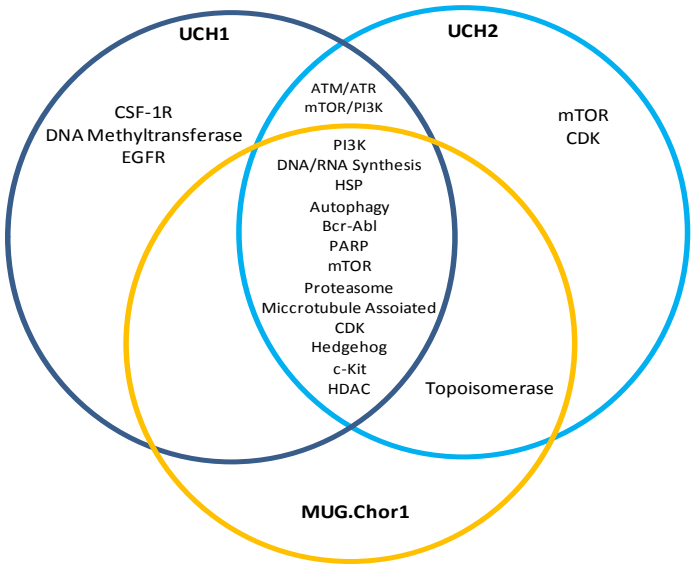

Figure 4.8 Venn diagram of anti-cancer compounds selectivity/commonality
Overview of mechanism of action or targets of compounds selected from the single point screen.

4.5.4 IC_{50} profiling for confirmation of compound hits

Confirmation of hits was assessed by comparing the data from the single point screen with equivalent doses tested in the IC_{50} profiling to assess reproducibility of the data. Confirmation rates were satisfactory.

4.5.4.1 Hit confirmation rate for GSK PKIS1 library

Hit confirmation rate for GSK PKIS1 library was conducted separately, as the single point data from this screen was in a different format. The hit confirmation rate for MUG Chor was 72%, U-CH1 was 89% and U-CH2 was 81% (Figure 4.9).

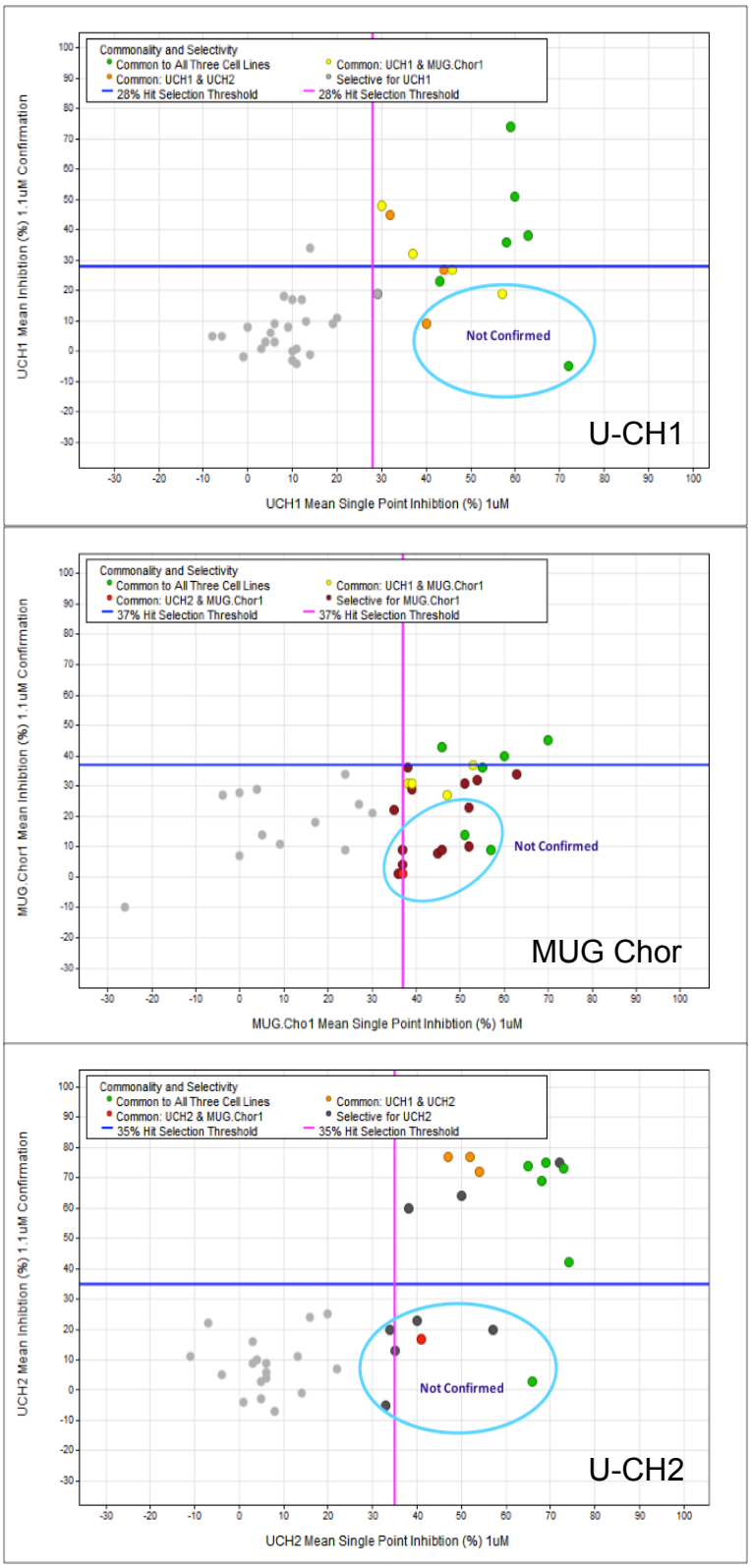

Figure 4.9 Confirmation of hits from single point screen GSK PKIS1 library
Illustration of confirmed hits in each cell line: right upper quadrant. Mean percentage inhibition for compounds at 1.1μM in 10-point IC_{50} assay *vs.* mean percentage inhibition for compounds at 1μM from the single point screen.

4.5.4.2 Hit confirmation for Calbiochem, GSK PKIS2 and anti-cancer libraries

The global hit confirmation rate (independent of the GSK PKIS1 library) for MUG Chor was 81%, U-CH1 72% and U-CH2 79%. There were no potential activators/interferers identified (i.e. no dose response curves inverted below -20% inhibition).

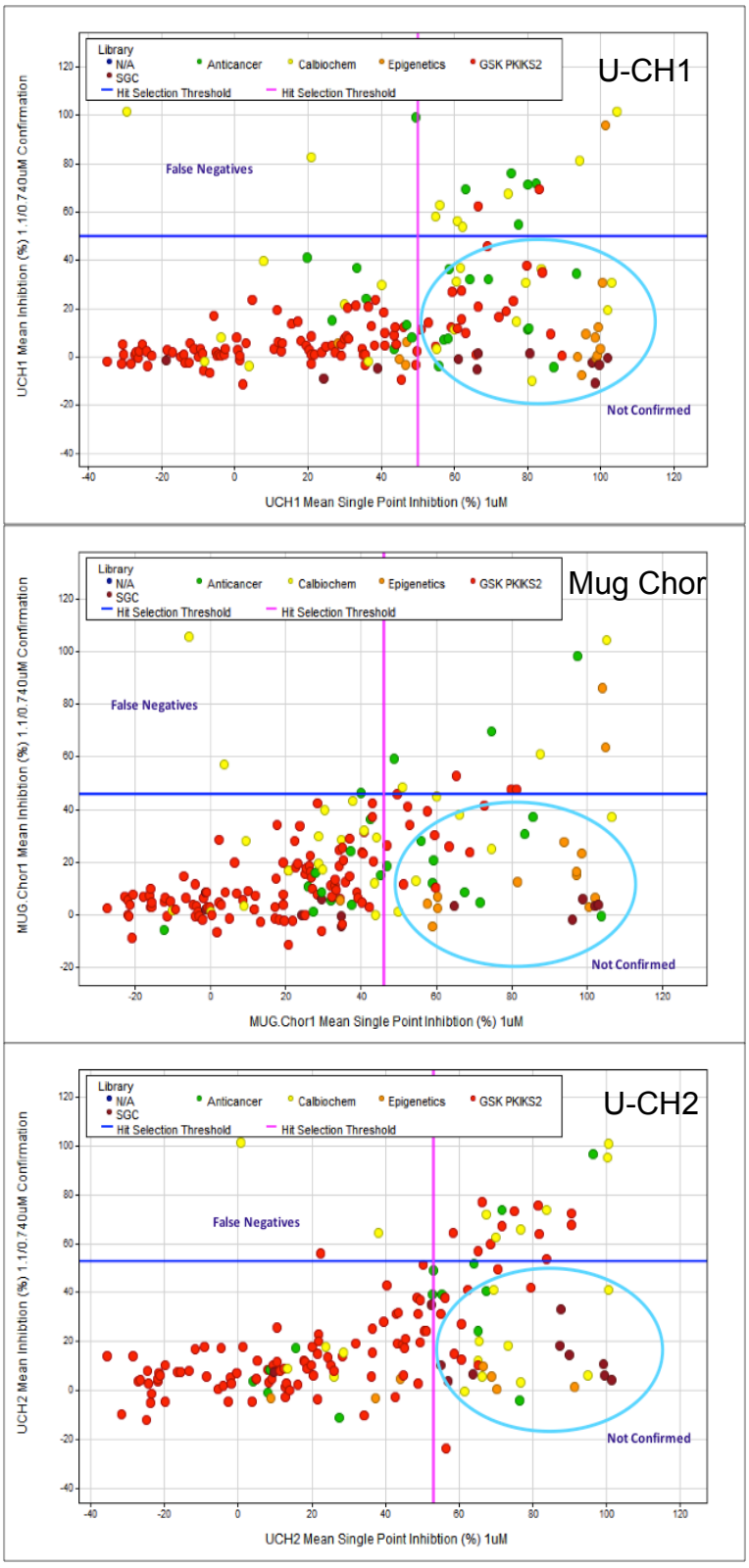

Figure 4.10 Confirmation of hits from the single point across 3 libraries
Hits identified in the single point screen were confirmed as hits in the IC_{50} profiling: right upper quadrant. A different colour represents each library. For each cell line the percentage inhibition at 1.1 to 0.740μM in the 10-point IC_{50} assay *vs.* percentage inhibition at 1μM in the single point screen.

4.5.4.3 Selectivity of compounds

The data from the IC_{50} screen generated dose response curves, which demonstrated the differential phenotypic effect allowing for comparison of effect between cell lines, as demonstrated in Figures 4.12 & 4.13 below (dose response curves for all compounds can be found in the appendix).

In order to identify compounds of target families potentially relevant to the disease, hits were triaged according to compounds eliciting selective cell death (toxicity) in chordoma cell lines compared to the 'normal' adult human dermal fibroblasts (NAHDF) control cell line. This was achieved by assessing the differential phenotypic effect.

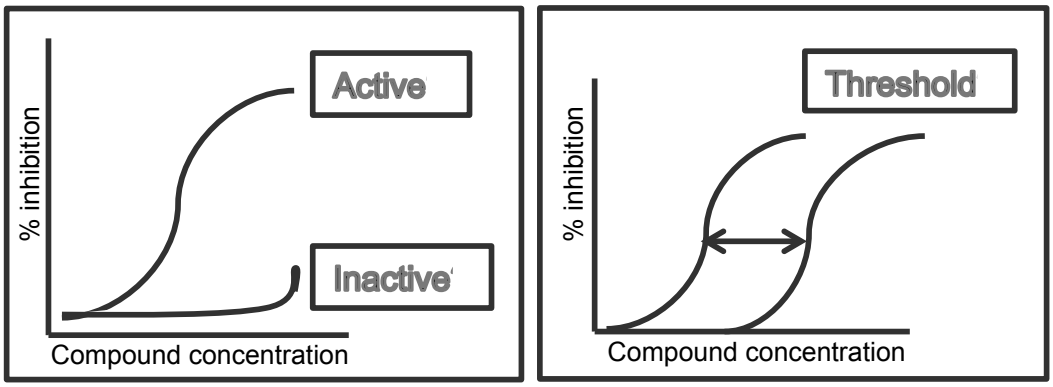

Figure 4.11 Profiling by IC50
IC_{50} profiling enabled us to validate a dose response curve for the compounds, identifying active and inactive compounds as depicted on the left. By using a counter screen it was possible to define if the compound had no effect in the 'normal' cell line (fibroblasts) or that there was a differential dose-response between the 'normal' and the chordoma cell lines as depicted on the right.

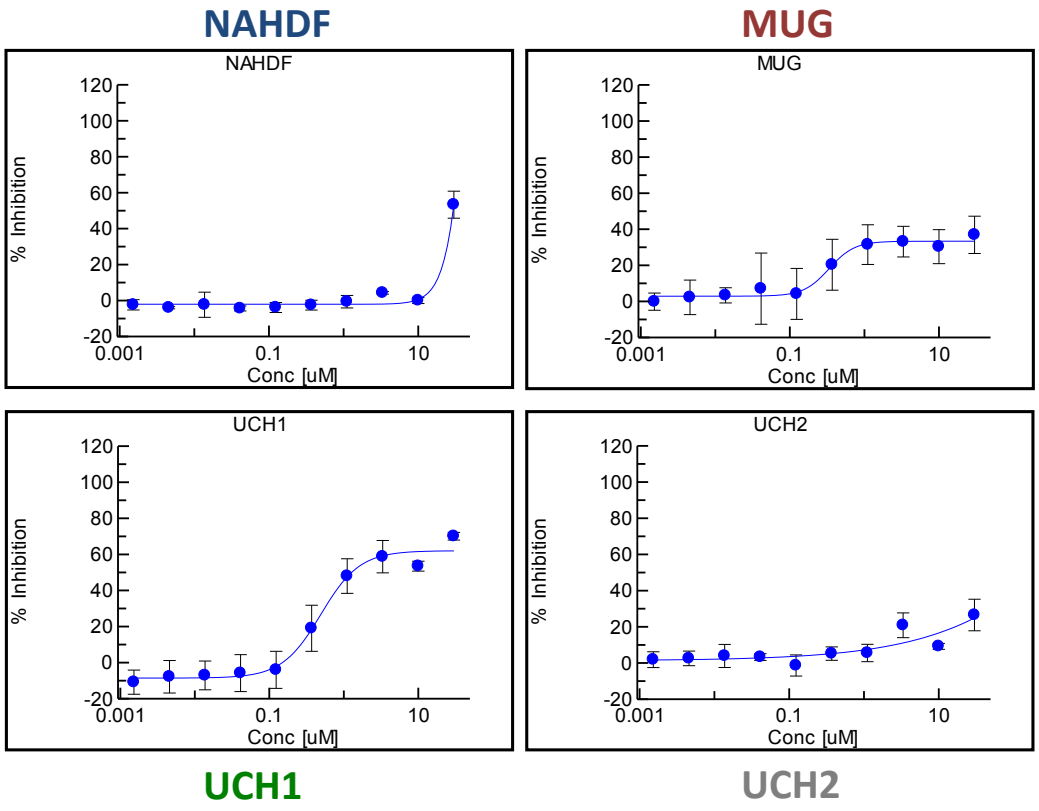

Figure 4.12 Differential phenotypic effects observed in different cell lines
Depiction of dose-response curve demonstrating the different phenotypic effect, observed in different cell lines, following compound treatment with an ErbB1/ErbB2 inhibitor. A differential phenotypic effect was observed between U-CH1 and NAHDF cell lines, a moderate effect was noted in the MUG Chor cell line (plateau around 35% Inhibition), and no effect in the U-CH2 cell line.

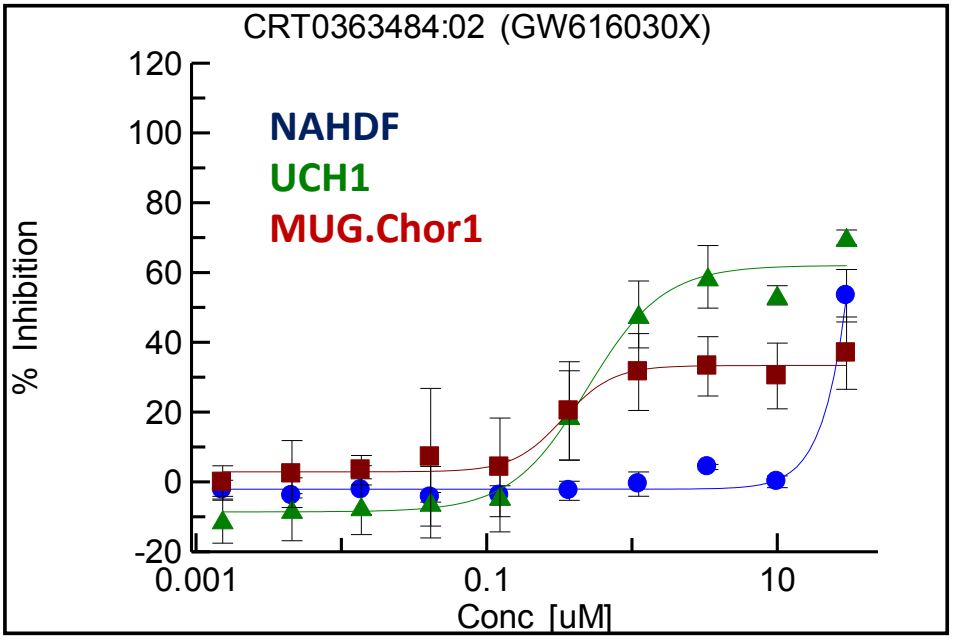

Figure 4.13 Differential phenotypic effect with ErbB1/ErbB2 targeting compound
Depiction of overlay of dose response curves from (U-CH1, MUG Chor and NAHDF), demonstrating the differential phenotypic effect. The graph is suggestive of a cytostatic effect in the U-CH1 cell line in doses > 1μM with maximum percentage inhibition reaching 60%.

4.5.5 EC_{50}

In order to compare efficacy of a compound that demonstrated heterogeneous effect between cell lines, EC_{50} values were used as a measure of potency on molecular targets. Values were determined from graphical plots of percentage inhibition *vs.* log [μM]. IC_{50} and EC_{50} are both used as a measure of potency, however, when using IC_{50}, a classic sigmoidal graphical profile would be expected to span between 0 to 100% inhibition. Therefore, if reporting $IC_{50,}$ this is only informative if data includes the maximum percentage inhibition when efficacy varies across cell lines. EC_{50} is defined as the *effective* concentration, which elicits a half-maximal response (e.g. half way between the baseline and maximum response).

To identify compounds that exerted differential effects in the three chordoma cell lines compared to the NAHDF cell line, the potency (pEC_{50} defined as the negative logarithm of EC_{50}) was calculated and plotted for each compound in each cell line (Figure 4.14 for all libraries screened at CRT, and figure 4.15 for GSK PKIS1 library). The mean pEC_{50} of each compound in chordoma cell lines *vs*. the NAHDF cell line was correlated using a threshold of <5μM for each chordoma cell line and >10μM for the NAHDF cell line. Off-target cytotoxicity was identified when there was no differential phenotypic effect between the chordoma cell lines and NAHDF.

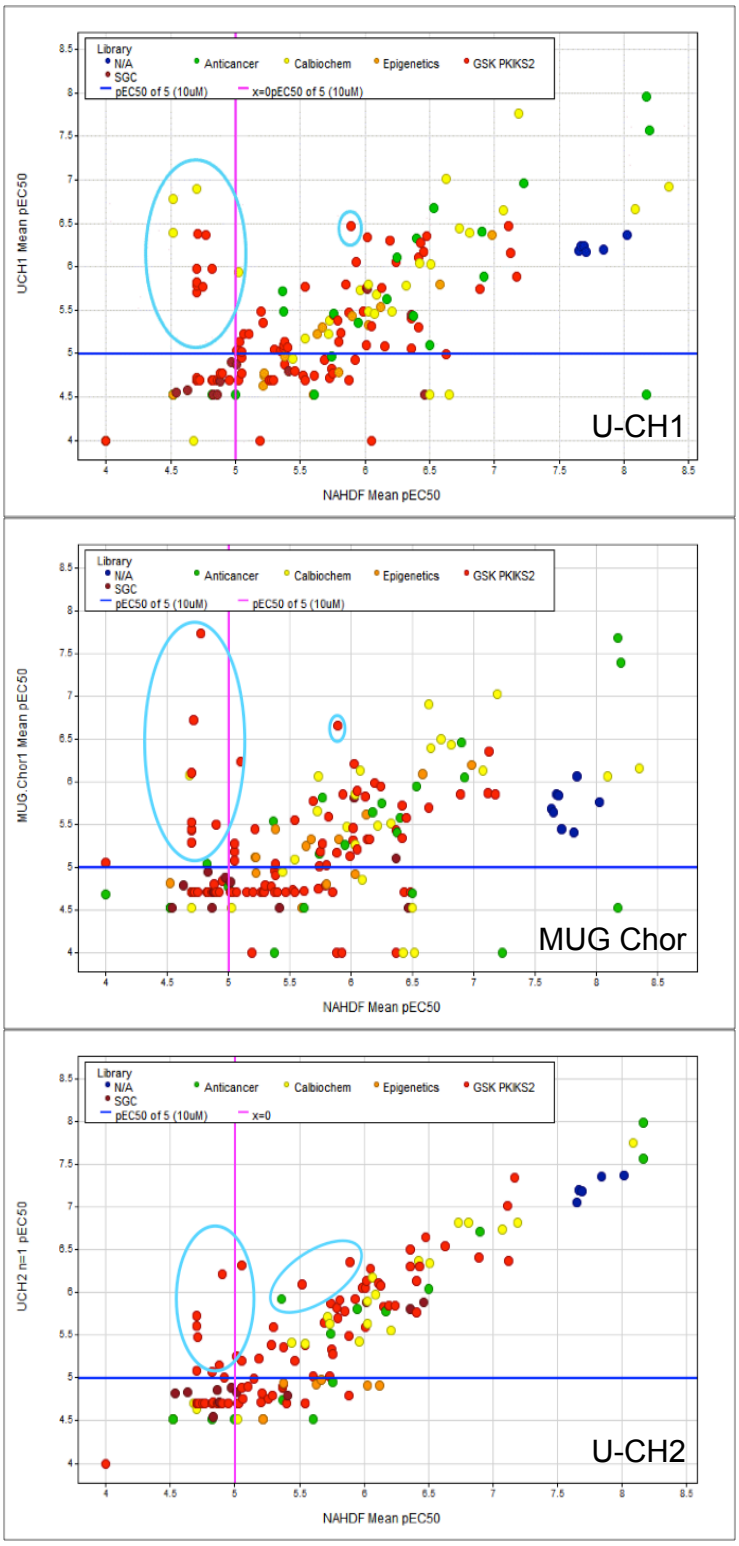

Figure 4.14 Selectivity of compounds all libraries excluding GSK PKIS1
Selectivity versus off-target cytotoxicity. U-CH1 cell line mean pEC_{50} *vs.* mean NAHDF pEC_{50} in 147 selected active and 43 potentially interfering or pathway activating compounds. 13 compounds for U-CH1, 11 compounds for MUG Chor and 8 compounds for U-CH2 of interest. Left upper quadrant: compounds of interest; right upper quadrant compounds with similar differential phenotypic effect in chordoma and control cell line, some included (circled) due to high percentage inhibition. Left and right lower quadrant: doses above set dose range for chordoma cell line. pEC_{50} was defined as the negative logarithm of the EC_{50}. The pEC_{50} scale equals: 6 = 1µM, 9 = 1nM.

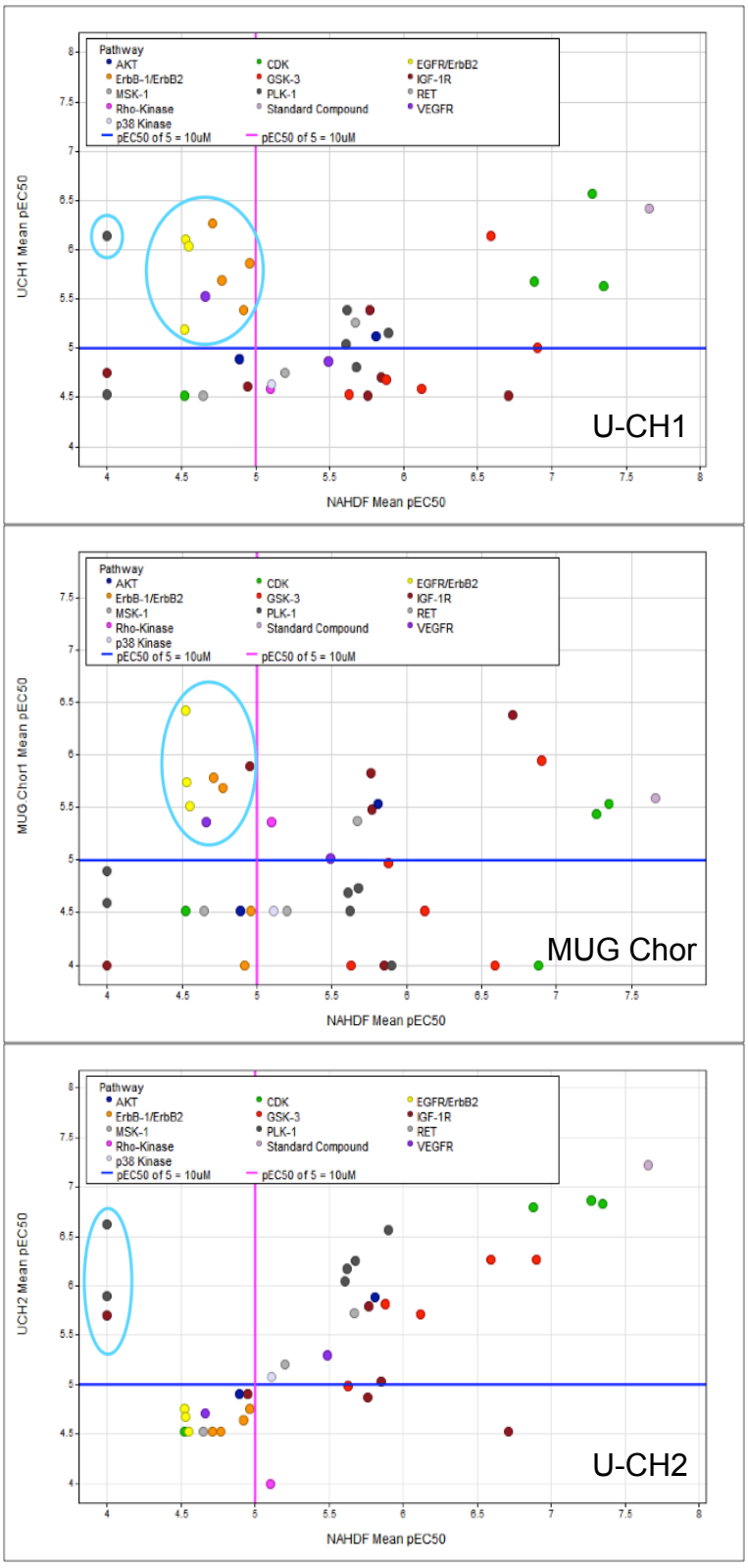

Figure 4.15 Selectivity of compounds GSK PKIS1 library
For each chordoma cell line mean pEC_{50} *vs.* mean NAHDF pEC_{50} for the 37 selected active compounds from the GSK PKIS1 library. 10 compounds for U-CH1 and 7 compounds for MUG Chor were of interest. There was a lack of selective cytotoxicity for U-CH2 cells. 3 compounds identified as selective for U-CH2 have a 'liability', as they are potentially biphasic in the control cell line. Left upper quadrant: compounds of interest; right upper quadrant compounds with similar differential phenotypic effect (in chordoma and NAHDF cell line); left and right lower quadrant: doses above set dose range for chordoma cell line.

4.5.6 Summary of compounds of interest across all libraries

4.5.6.1 EGFR inhibitors selective for chordoma

Differential phenotypic effect analysis yielded 28 of 184 compounds displaying chordoma selective cell death on 3 chordoma cell lines. The measure of the differential phenotypic effect was referred to as selectivity, i.e. the fold difference between NAHDF mean EC_{50} and the chordoma cell line mean EC_{50}. Higher selectivity accounts for an increased differential effect. Compounds showed either a common differential phenotypic effect (selectivity for more than one chordoma cell line, though sometimes to varying degrees), or a specific differential phenotypic effect for one cell line. Selectivity values varied between compounds/cell lines therefore no triaging was conducted at this point.

GSK released the target classes for the hits from the PKIS2 library. 14 compounds from this library had demonstrated differential phenotypic effect of which 10 compounds (71%) were EGFR/ErbB family inhibitors. Five of these only targeted the *EGFR/ErbB* family, whilst three were classified as dual inhibitors as they also targeted *BRAF* and two targeted *ErbB, BRAF* and *Src*. In addition, one activin receptor-like kinase 5 (ALK5) inhibitor and two multi-kinase inhibitors co-targeting rho-associated, coiled-coil-containing protein kinase 1 (*ROCK1*), protein kinases A (*PKA*) and B (*AKT*), *p70S6 kinase*, *Aurora A kinase* and *BRAF*, were identified. For one compound the target(s) were unknown. CRT0423639:01 in the GSK PKIS2 library was revealed to be Erlotinib, a FDA-approved EGFR inhibitor. The targets from the additional libraries included 12 EGFR/ErbB family inhibitors, one phosphatidylinositol-3-kinase (PI3K) inhibitor and one VEGFR/FGFR inhibitor (CRT0363377:02), which was a commercial VEGFR2 inhibitor, Pazopanib HCl.

The differential phenotypic screen had identified 27 compounds with identified targets of which 22 (81%) targeted the *EGFR/ErbB* family receptors.

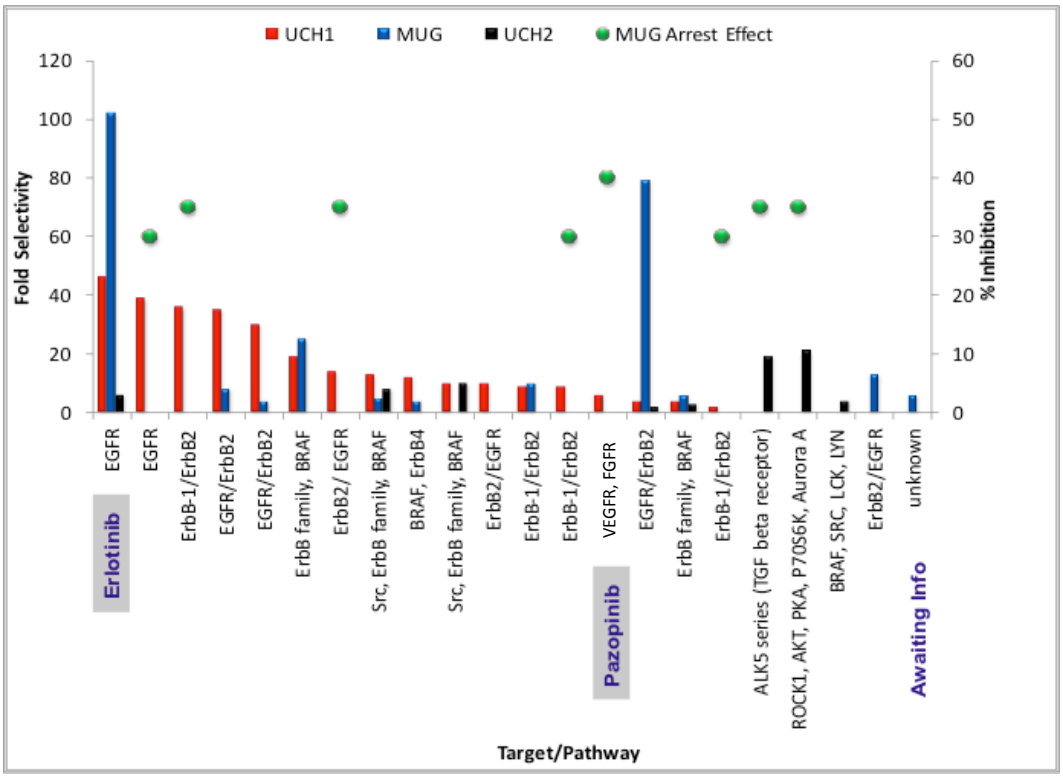

Figure 4.16 Compound selectivity: GSK PIKS1 and PIKS2 libraries
Data compiled from the two GSK libraries showed a trend for selectivity for targeting the EGFR pathway. U-CH1 showed a differential phenotypic effect as indicated by 'fold selectivity' for more compounds compared to the other chordoma cell lines, although with a low percentage inhibition.

The U-CH1 cell line was found to be sensitive to a larger number of EGFR/Erb inhibitors, although with low percentage inhibition, while moderate sensitivity to this compound class was observed in the MUG Chor cell line. The MUG Chor cell line had a liability in maximum response e.g. had <1μM potency but a maximum response (inhibition) less than 100% (50-75%). U-CH2 cells were sensitive to the ALK5 inhibitor, multi-kinase inhibitors and EGFR/Erb family dual inhibitors, which also targeted BRAF.

Table 4.5 Compounds with a differential phenotypic effect

Compound ID	GSK ID/Compound Name	Library	Pathway	UCH1	UCH2	MUG.Chor	Effect
CRT0047607:05	AG1478	Calbiochem	EGFR	Biphasic (Potency not Quantified)		Arrest (~40%) between 0.122-30uM	Kill UCH1, Moderate Arrest MUG.Chor
CRT0103071:02	Compound 56	Calbiochem	EGFR	153			Kill UCH1
CRT0103079:02	EGFR/ErbB2/ErbB4 Inhibitor	Calbiochem	EGFR/ErbB-2/ErbB-4	8		Arrest (~30%) between 1.1-30uM	Kill UCH1, Moderate Arrest MUG.Chor
CRT0103123:02	PD 174780	Calbiochem	EGFR	176		Arrest (~35%) between 0.366-30uM	Kill UCH1, Moderate Arrest MUG.Chor
CRT0103124:02	PD 174265	Calbiochem	EGFR	73		Arrest (~30%) between 3.3-30uM	Kill in UCH1, Moderate Arrest MUG.Chor
CRT0159097:02	GDC-0941	Anticancer	Class 1A PI3K Inhibitor		4		Kill in UCH2
CRT0363358:02	GW461104A	PKIS1	ErbB-1/ErbB2	9		10	Kill UCH1 & MUG.Chor
CRT0363377:02	GW410563A	PKIS1	VEGFR2, FGFR	6		Arrest (~40%) between 3.3-30uM	Kill in UCH1, Moderate Arrest MUG.Chor
CRT0363431:01	GW282449A	PKIS1	EGFR/ErbB2	35		8	Kill UCH1, Arrest MUG.Chor
CRT0363431:02	GW282449A	PKIS1	EGFR/ErbB2	30		4	Kill UCH1, Arrest MUG.Chor
CRT0363479:02	GW576609A	PKIS1	ErbB-1/ErbB2	2		Arrest (~30%) between 1.1-10uM	Potential Kill in UCH1, Moderate Arrest MUG.Chor
CRT0363482:02	GW583373A	PKIS1	ErbB-1/ErbB2	9		Arrest (~30%) between 1.1-30uM	Kill in UCH1, Moderate Arrest MUG.Chor
CRT0363484:02	GW616030X	PKIS1	ErbB-1/ErbB2	36		Arrest (~35%) between 1.1-30uM	Kill in UCH1, Moderate Arrest MUG.Chor
CRT0363568:02	GW680191X	PKIS1	EGFR/ErbB2	4	2	79	Kill UCH2, Arrest MUG.Chor, Potential Kill in UCH1
CRT0423387:01	GI230329A	PKIS2	EGFR	39		Arrest (~30%) between 0.082-20uM	Kill UCH1, Moderate Arrest MUG.Chor
CRT0423403:01	GSK1307810A	PKIS2	ROCK1, AKT, PKA, P70S6K, Aurora A		21	Arrest (~35%) between 2.2-20uM	Kill UCH2, Moderate Arrest MUG.Chor
CRT0423493:01	GSK1660437A	PKIS2	BRAF, SRC, LCK, LYN		4		Kill UCH2
CRT0423504:01	GSK198271A	PKIS2	ErbB family, BRAF	4	3	6	Kill UCH1, Moderate Kill Effect in UCH2 & MUG.Chor
CRT0423580:01	GSK299495A	PKIS2	Src, ErbB family, BRAF	13	8	5	Kill UCH1, Moderate Kill Effect in UCH2 & MUG.Chor
CRT0423587:01	GSK326180A	PKIS2	ErbB family, BRAF	19		25	Kill UCH1, Moderate Kill Effect in MUG.Chor
CRT0423593:01	GSK357952A	PKIS2	Src, ErbB family, BRAF	10	10		Moderate Kill Effect in UCH2 & UCH1
CRT0423594:01	GSK361061A	PKIS2	BRAF, ErbB4	12		4	Moderate Kill Effect in UCH1 & MUG.Chor
CRT0423639:01	GW459135A	Erlotinib (PKIS2)	EGFR	46	6	102	Kill UCH1, Moderate Kill MUG.Chor & UCH2
CRT0423669:01	GW569716A	PKIS2	ErbB2/EGFR			13	Moderate Kill MUG.Chor
CRT0423674:01	GW582764A	PKIS2	ErbB2/EGFR	10			Moderate Kill UCH1
CRT0423676:01	GW583340C	PKIS2	ErbB2/ EGFR	14		Arrest (~35%) between 0.740-20uM	Kill UCH1, Moderate Arrest MUG.Chor
CRT0423770:01	GW876731X	PKIS2	ALK5 series (TGF beta receptor)		19	Arrest (~35%) between 0.246-20uM	Kill UCH2, Moderate Arrest MUG.Chor
CRT0423890:01	SKF-97184	PKIS2	Unknown			6	Moderate Kill MUG.Chor

28 compounds elicited a differential phenotypic effect. Threshold of <5uM in chordoma cell line, >10uM in NAHDF cell line applied in conjunction with visual inspection of graphical curve overlays.

4.5.7 Selectivity of anti-cancer library

From the CRT Anti-cancer Library, 43 compounds were screened in the single-point profiling, which identified 23 compounds based on 2x SD hit selection threshold from each cell line. These compounds were profiled in a 10-point IC_{50} format for hit confirmation. Only one of the compounds for the anti-cancer library showed differential phenotypic effect between NAHDF and U-CH2, this was a PI3K kinase inhibitor: GDC-0941 (Figure 4.17).

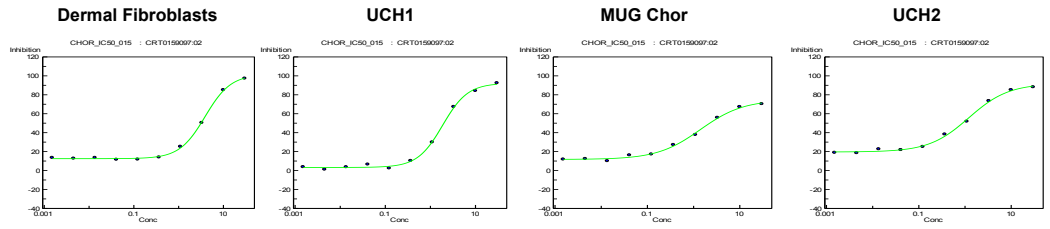

Compound ID	Batch Ref.	NAHDF Geomean [uM]	NAHDF Mean Max % Inhibition	UCH1 Geomean [uM]	UCH1 Mean Max % Inhibition	MUG.Chor1 Geomean [uM]	MUG.Chor1 Mean Max % Inhibition	UCH2 n=1 EC50 [uM]	UCH2 n=1 Max % Inhibition
CRT0159097	02	4.38	92.09	1.89	91.58	2.90	65.39	1.21	88.16

Figure 4.17 GDC-0941 compound with a differential phenotypic effect in U-CH2
From the anti-cancer library, only one compound showed differential phenotypic effect. The compound targets the PI3K kinase pathway.

There were several classes of inhibitors with different potency rankings in each chordoma cell line, with no, limited or similar differential phenotypic effect in normal dermal fibroblast cells, which may still play a role in the treatment of chordoma. Bortezomib, a proteasome inhibitor was the most potent compound in all three chordoma cell lines (10-20nM), but was also equipotent in normal dermal fibroblasts (Figure 4.18). Several clinically approved drugs tested in this screen were observed to be efficacious in the chordoma cell lines, all of which showed toxicity in 'normal' cells (Table 4.6).

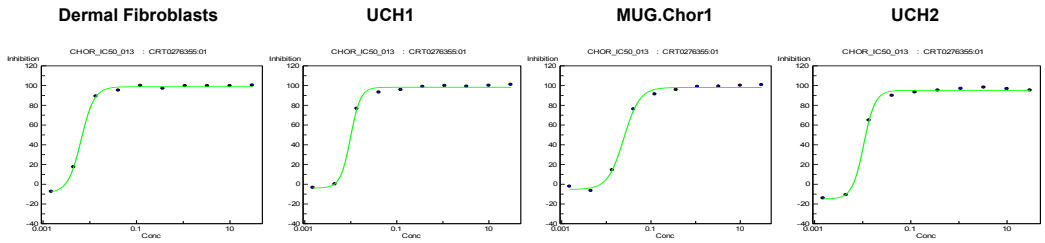

Compound ID	Batch Ref.	NAHDF Geomean [uM]	NAHDF Mean Max % Inhibition	UCH1 Geomean [uM]	UCH1 Mean Max % Inhibition	MUG.Chor1 Geomean [uM]	MUG.Chor1 Mean Max % Inhibition	UCH2 n=1 EC50 [uM]	UCH2 n=1 Max % Inhibition
CRT0276355	01	0.01	100.13	0.01	100.53	0.02	100.59	0.01	98.15

Figure 4.18 Phenotypic effect of Bortezomib
Bortezomib, a proteasome inhibitor, was found to be highly potent in all cell lines. Maximum percentage inhibition was 100% at doses ranging from 10-20nM.

Additional standard of care drugs, not initially included in the screening, were added based on the identified targets of interest. These drugs included: Foretinib (MET/VEGFR2), Erlotinib (EGFR), Gefitinib (EGFR), Tivozanib (VEGFR), Cediranib (VEGFR), and Regorafenib (VEGFR) kinase inhibitors, which were included in the follow-on screen. Imatinib (Bcl-Abl, PDGFR, c-Kit) was also included as patients have been treated with this drug and it is considered potentially effective in chordoma treatment. No effect was observed in any of the chordoma cell lines following treatment with Imatinib (Table 4.6).

Table 4.6 Potency of compounds determined by IC_{50} profiling of anti cancer library

Compound ID	Supplier ID/Compound Name	NAHDF Geomean [uM]	NAHDF Mean Max % Inhibition	UCH1 Geomean [uM]	UCH1 Mean Max % Inhibition	MUG.Chor1 Geomean [uM]	MUG.Chor1 Mean Max % Inhibition	UCH2 Geomean [uM]	UCH2 Mean Max % Inhibition
CRT0276355	Bortezomib	0.01	100.00	0.01	100.53	0.02	99.74	0.01	98.15
CRT0276378	Docetaxel (Taxotere)	0.01	74.69	0.03	48.06	0.06	30.55	0.02	43.73
CRT0276190	17-DMAG	0.08	100.87	0.15	97.88	0.14	101.72	0.17	98.88
CRT0276344	AZD8055	0.37	82.32	0.21	77.77	0.88	53.74	0.32	70.13
CRT0276385	Erlotinib Hydrochloride	29.72	39.90	0.26	80.38	30.00	31.79	6.52	47.75
CRT0276390	Flavopiridol(Alvocidib)	0.78	71.12	0.37	65.29	0.45	48.43	0.19	71.78
CRT0159098	BEZ235(NVP-BEZ235)	0.80	91.98	0.89	79.65	2.37	43.03	1.38	73.43
CRT0276427	SB939	1.16	100.23	0.90	100.64	1.85	98.55	2.09	65.14
CRT0276325	Adriamycin	0.20	78.59	1.37	70.91	0.89	46.44	0.30	59.32
CRT0276395	GDC-0449(Vismodegib)	0.67	90.23	2.37	46.32	2.31	50.96	1.67	85.62
CRT0159097	GDC-0941	3.99	84.76	2.68	92.95	3.57	70.81	3.63	79.05
CRT0276404	Lapatinib Ditosylate	5.94	100.53	3.35	96.92	8.40	89.26	20.67	69.74
CRT0276347	Belinostat(PXD101)	1.73	99.43	3.78	97.06	1.64	91.21	11.15	73.53
CRT0276444	XL880(GSK1363089)	3.05	97.00	3.80	104.22	1.53	100.71	2.77	83.27
CRT0276331	AP24534	0.60	101.33	4.20	103.02	3.98	105.48	1.40	97.79
CRT0276398	GSK1059615	1.13	97.46	4.51	85.88	5.51	68.58	1.57	93.95
CRT0162212	Carboplatin	30.00	3.88	5.16	26.72	30.00	19.08	30.00	19.90
CRT0276422	PHA-793887	0.31	90.66	8.17	63.91	20.57	61.91	0.90	71.52
CRT0276452	Ellence	1.82	99.52	10.89	89.66	7.14	93.98	3.02	93.52
CRT0276337	AV-951(Tivozanib)	30.00	28.66	11.21	81.15	7.13	41.85	14.21	80.53
CRT0276346	BAY 73-4506(Regorafenib)	15.41	42.08	28.13	48.60	17.98	79.17	15.01	45.90
CRT0276194	ABT-869(Linifanib)	19.02	45.25	30.00	16.57	13.78	39.05	30.00	20.10
CRT0162533	Cisplatin (In Water)	6.72	86.50	30.00	5.00	30.00	30.50	30.00	8.50
CRT0276341	AZD2281(Olaparib)	10.01	49.49	30.00	32.47	17.00	39.65	30.00	22.02
CRT0276362	Cediranib(AZD2171)	2.65	35.94	30.00	42.51	30.00	13.58	15.34	44.88
CRT0276374	Decitabine	2.44	48.69	30.00	20.17	30.00	-0.20	30.00	23.90
CRT0276375	Deforolimus(MK-8669)	0.01	45.00	30.00	31.97	30.00	3.20	0.03	49.14
CRT0276400	Imatinib Mesylate	30.00	-5.44	30.00	32.07	30.00	12.61	30.00	39.11
CRT0276415	OSI-930	29.93	44.35	30.00	0.03	30.00	4.01	18.06	60.00
CRT0276417	Pazopanib Hydrochloride	7.23	42.04	30.00	32.37	30.00	13.02	30.00	38.74
CRT0276387	Everolimus(RAD001)	100.00	99.15	100.00	57.80	18.22	60.29	100.00	68.52

Compound concentration and percentage inhibition for each compound in each cell line. The most intense red colour indicates the lowest effective compound concentration, whereas the lightest blue colour indicated the highest percentage inhibition. (Geomean: Geometric mean: average ratios of change)

4.6 Mechanism of cell death

The mechanism of cell death was assessed for all 27 hits confirmed from the IC_{50} profiling, as well as the additional compounds listed above. Chemotherapy kills cells primarily by inducing apoptosis(740). On target effect was assessed by mechanism of cell death by confirmation of apoptosis as the identified by induction of caspase 3/7. The assay was combined with assessment of cell viability of compound treated cells compared to controls, reported as percentage inhibition. An example of the read out for this assay has been demonstrated in chordoma cells treated with Bortezomib (Figure 4.19-4.21).

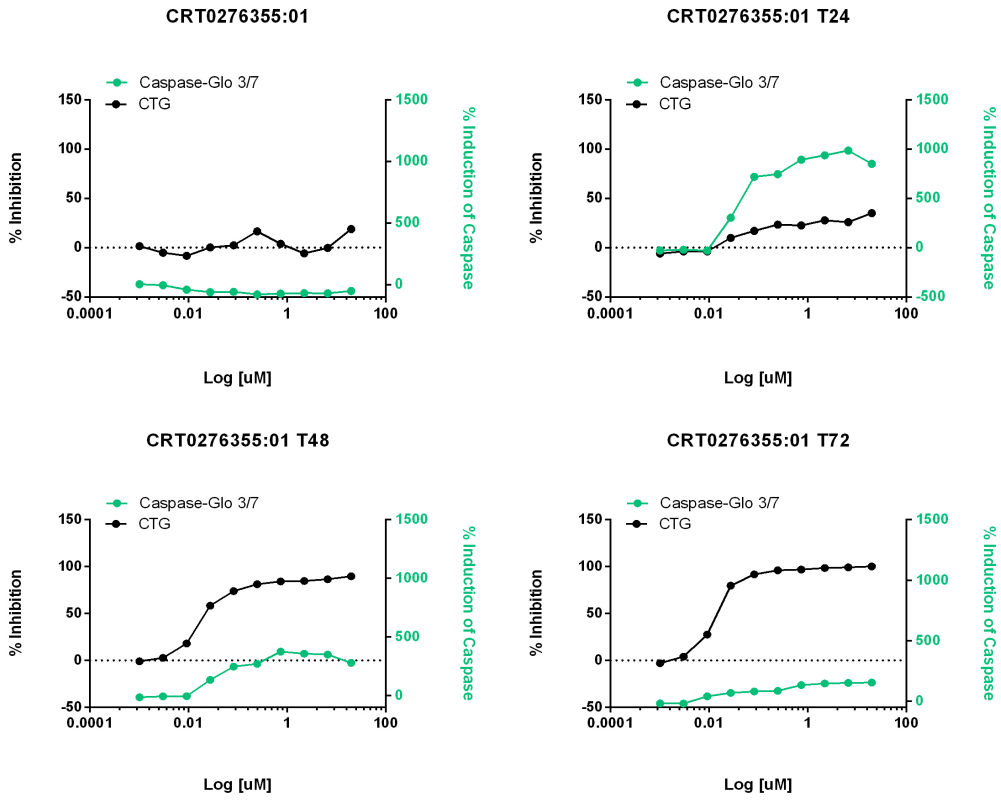

Figure 4.19 Mechanism of cell death MUG Chor
Mechanism of cell death by induction of apoptosis related to percentage inhibition. MUG Chor cell line treated with Bortezomib (CRT0276355). The caspase Glo (CG) 3/7 assay was used for detection of induction of apoptosis and Cell Titre Glow (CTG) assay, a cell viability assay, was used to determine the number of viable cells. The percentage induction of caspase (green) and percentage inhibition of compound treated cells compared to controls (black) is shown at 0 hour (top left), 24 hours (top right), 48 hours (bottom left) & 72 hours (bottom right). Each assay was performed on separate plates (for each time point).

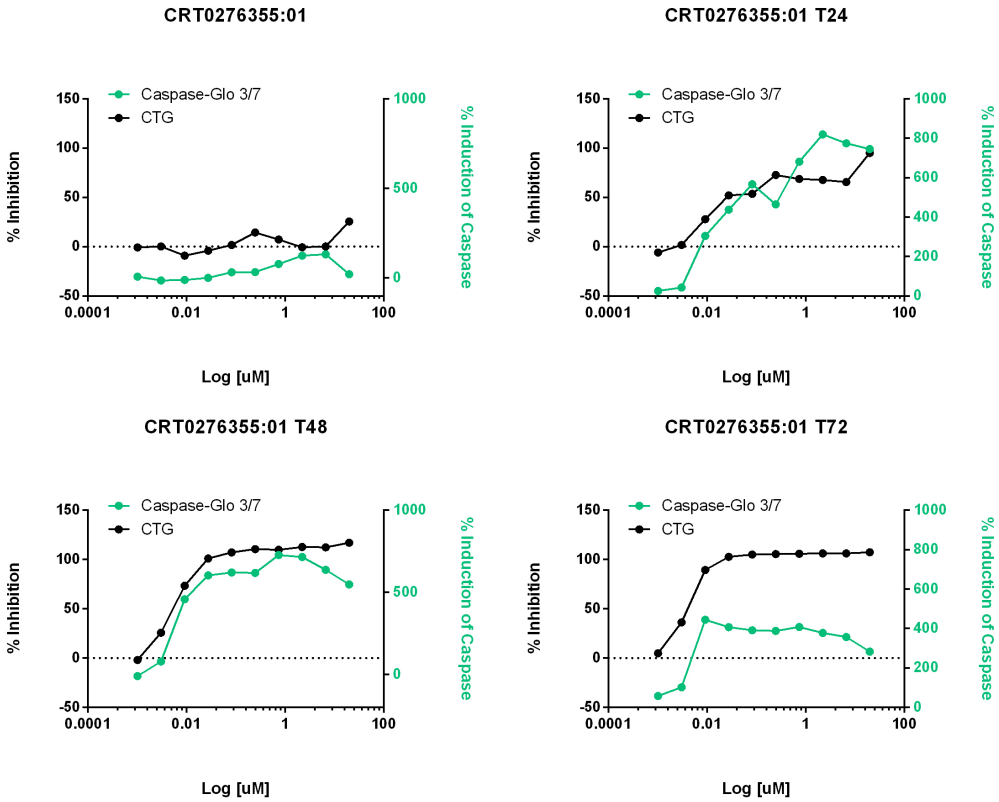

Figure 4.20 Mechanism of cell death U-CH1
Mechanism of cell death by induction of apoptosis related to percentage inhibition. U-CH1 cell line was treated with Bortezomib (CRT0276355) and assessed both for percentage inhibition (black), and percentage induction of caspase (green) at 0 (top left), 24 hours (top right), 48 hours (bottom left) & 72 hours (bottom right).

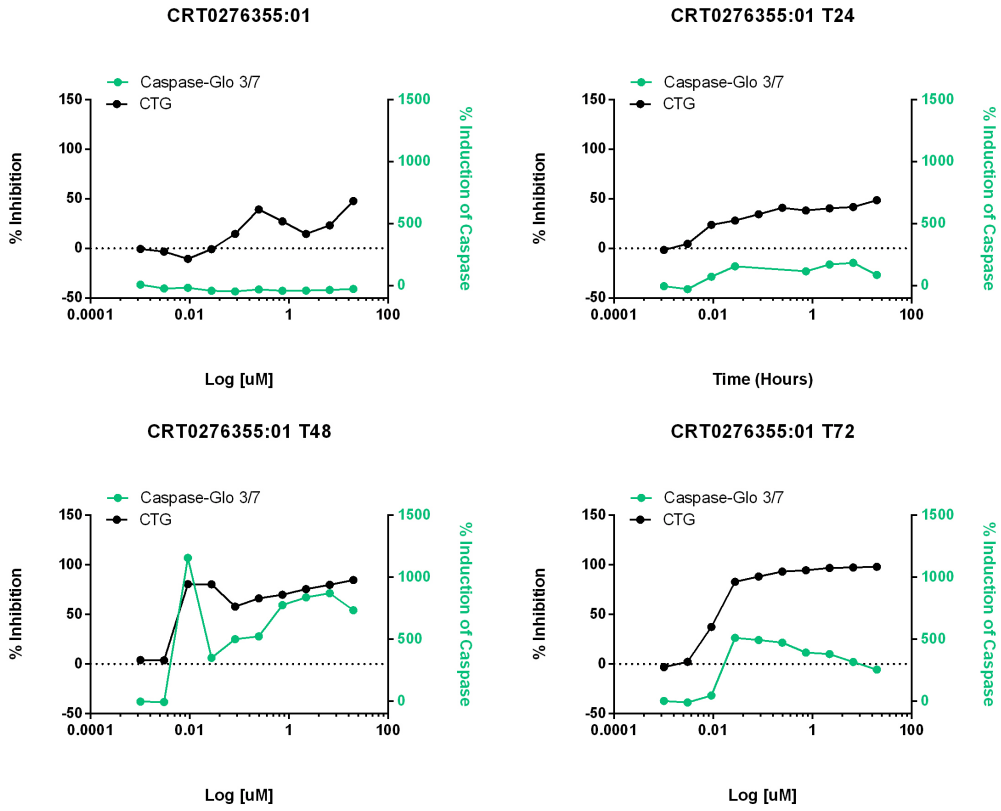

Figure 4.21 Mechanism of cell death U-CH2
Mechanism of cell death by induction of apoptosis related to percentage inhibition U-CH2 cell line was treated with Bortezomib (CRT0276355) and assessed for both percentage inhibition (black), and percentage induction of caspase (green) at 0 (top left), 24 hours (top right), 48 hours (bottom left) & 72 hours (bottom right).

4.6.1 Validation of compounds of interest

In view of the high number of EGFR/ErbB inhibitors selected during the screening process of U-CH1 and MUG Chor cell lines, this was the primary target identified to validate. Five commercially available EGFR/ErbB family inhibitors, either FDA-approved or in clinical trials were purchased (referred to as the targeted therapy or TT set). Afatinib and Canertinib had an irreversible mode of action (MOA). The other three EGFR inhibitors Erlotinib, Gefitinib and Sapitinib were reversible.

Hits identified in the IC_{50} profiling (Table 4.5) were re-tested using a second batch of compounds and profiled alongside the additional 5 EGFR inhibitors in a 10-point IC_{50} format in the WST-1 assay for NAHDF, U-CH1, U-CH2 and MUG Chor cell lines. This was done to ensure that each compound was tested at least twice. Irreversible compounds in the targeted therapy set appeared potentially biphasic in some cell lines, assessed by differential phenotypic effect, and therefore fold selectivity and potency were not calculated (Table 4.7). EGFR inhibitors showed variability of effect between different compounds. U-CH1 proved most sensitive to EGFR inhibitors at low doses and with high maximum percentage inhibition. MUG Chor confirmed response but with liability in maximum percentage inhibition whilst U-CH2 demonstrated little or no effect. The fold selectivity indicating differential phenotypic effect between the individual chordoma cell lines and NAHDF demonstrated good selectivity between U-CH1 and MUG Chor compared to NAHDF, whilst U-CH2 confirmed selectivity with an EGFR inhibitor also targeting *BRAF* and *ALK5* (TGF-β receptor) (Table 4.7). The differential phenotypic effect observed between supposedly identical targets raised the potential to identify specific chemotypes within the compound group of EGFR inhibitors.

Table 4.7 Confirmation of selected hits and target therapy compounds

Compound ID	GSK ID/ Commercial name	Library	Pathway	NAHDF EC50 Geomean [uM]	NAHDF Mean M%I	UCH1 EC50 Geomean [uM]	UCH1 Mean M%I	UCH2 EC50 Geomean [uM]	UCH2 Mean M%I	MUG.Chor1 EC50 Geomean [uM]	MUG.Chor1 Mean M%I	UCH1 Fold Selectivity	UCH2 Fold Selectivity	MUG.Chor1 Fold Selectivity
CRT0047607	AG 1478	Calbiochem	EGFR	20.74	10	Small Span.Potency not Quantified	76	18.82	52	0.08	64	Selectivity not Calculated	1	248
CRT0103071	Compound 56	Calbiochem	EGFR	22.79	77	0.57	86	20.00	27	0.01	62	40	1	2349
CRT0103079	EGFR/ERBB2/ERBB4 Inhibitor	Calbiochem	EGFR/ERBB2/ERBB4	12.91	96	0.18	79	16.69	38	0.02	64	72	1	548
CRT0103123	PD174780	Calbiochem	EGFR	30.00	29	0.21	80	19.66	35	0.10	55	143	2	296
CRT0103124	PD174265	Calbiochem	EGFR	30.00	11	0.38	75	13.25	43	0.15	70	78	2	201
CRT0159097	GDC-0941	Anticancer	Class 1A PI3K Inhibitor	3.99	85	2.68	93	3.63	79	3.57	71	1	1	1
CRT0276366	Canertinib	Targeted Therapy	EGFR/ErbB2	5.19	100	0.13	81	9.30	60	Potentially Biphasic. Potency not Quantified	95	41	1	Selectivity not Calculated
CRT0276385	Erlotiniib	Targeted Therapy	EGFR	14.57	48	0.35	86	15.50	40	0.22	74	42	1	66
CRT0276396	Gefitinib	Targeted Therapy	EGFR	11.18	87	0.22	76	9.84	79	0.36	68	50	1	31
CRT0363358	GW461104A	GSK PKIS1	ErbB-1/ErbB2	17.08	85	2.02	80	30.00	32	2.06	58	8	1	8
CRT0363377	GW410563A	GSK PKIS1	VEGFR	22.03	68	1.91	80	19.39	67	4.41	47	12	1	5
CRT0363431	GW282449A	GSK PKIS1	EGFR/ErbB2	29.30	55	0.80	65	20.88	34	1.80	45	37	1	16
CRT0363431	GW282449A	GSK PKIS1	EGFR/ErbB2	28.12	70	0.93	66	30.00	33	6.54	49	30	1	4
CRT0363479	GW576609A	GSK PKIS1	ErbB-1/ErbB2	12.10	85	4.06	77	23.04	38	100.00	49	3	1	0
CRT0363482	GW583373A	GSK PKIS1	ErbB-1/ErbB2	10.96	62	1.39	71	17.93	44	30.00	32	8	1	0
CRT0363484	GW616030X	GSK PKIS1	ErbB-1/ErbB2	19.40	53	0.54	69	30.00	27	1.62	39	36	1	12
CRT0363568	GW680191X	GSK PKIS1	EGFR/ErbB2	30.00	41	1.26	86	17.83	61	0.37	45	24	2	81
CRT0423387	GI230329A	GSK PKIS2	EGFR	16.87	96	Potentially Biphasic. Potency not Quantified	94	20.00	40	0.19	41	Selectivity not Calculated	1	90
CRT0423403	GSK1307810A	GSK PKIS2	ROCK1, AKT, PKA, P70S6K, Aurora A	13.65	100	16.44	61	1.85	64	5.68	30	1	7	2
CRT0423493	GSK1660437A	GSK PKIS2	BRAF, SRC, LCK, LYN	3.02	78	15.41	45	1.00	58	18.44	56	0	3	0
CRT0423504	GSK198271A	GSK PKIS2	ErbB family, BRAF	3.70	48	0.34	78	3.09	43	0.22	50	11	1	17
CRT0423580	GSK299495A	GSK PKIS2	Src, ErbB family, BRAF	20.00	38	1.49	79	3.90	49	6.54	38	13	5	3
CRT0423587	GSK326180A	GSK PKIS2	ErbB family, BRAF	20.00	35	0.89	74	0.43	44	2.96	48	22	46	7
CRT0423593	GSK357952A	GSK PKIS2	Src, ErbB family, BRAF	20.00	17	1.99	61	6.19	40	20.00	31	10	3	1
CRT0423594	GSK361061A	GSK PKIS2	BRAF, ErbB4	22.13	17	1.51	56	22.89	28	11.26	33	15	1	2
CRT0423639	GW459135A	GSK PKIS2	EGFR	19.34	60	0.42	69	3.33	46	0.19	58	46	6	101
CRT0423669	GW569716A	GSK PKIS2	ErbB2/EGFR	8.77	99	4.74	81	13.48	71	0.59	46	2	1	15
CRT0423674	GW582764A	GSK PKIS2	ErbB2/EGFR	21.10	78	1.72	54	22.89	20	22.13	25	12	1	1
CRT0423676	GW583340C	GSK PKIS2	ErbB2/ EGFR	15.13	55	1.06	66	13.08	40	20.00	34	14	1	1
CRT0423770	GW876731X	GSK PKIS2	ALK5 series (TGF beta receptor)	8.88	83	10.92	94	0.58	74	12.76	39	1	15	1
CRT0423890	SKF-97184	GSK PKIS2	Unknown	20.00	9	19.17	55	20.00	24	6.37	42	1	1	3
CRT0509501	Afatinib	Targeted Therapy	EGFR/ErbB2	5.88	100	Potentially Biphasic. Potency not quantified	89	5.14	100	Potentially Biphasic. Potency not quantified	100	Selectivity not Calculated	1	Selectivity not Calculated
CRT0509503	Sapitinib (AZD 8931)	Targeted Therapy	EGFR/ErbB2	20.00	39	0.05	82	8.98	47	0.24	68	417	2	83

Repeat screen of selected hits and TT compounds. Geomean EC_{50}, maximum percentage inhibition and differential phenotypic effect selectivity data of 28 compounds from libraries tested (hits) and 5 commercial compounds (TT) for NAHDF, U-CH1, U-CH2 and MUG Chor cell lines (Geomean: Geometric mean: average ratios of change). Fold selectivity used to determine the differential phenotypic effect between NADPH and chordoma cell lines. Darkest red: lowest concentration, darkest green: highest percentage inhibition, darkest blue; highest fold selectivity.

4.7 Chemotype and Substituent Trend Analysis (GSK)

GSK carried out a chemotype analysis of the 22 EGFR/ErbB hits from the differential phenotypic effect triaging and the 5 EGFR/ErbB commercial compounds in the targeted therapy library. Two chemotypes were identified: Quinazoline and Pyrimidine(741). Further analysis by substituent trend (R groups around the core) showed two subtypes of Quinazoline compounds those with large substituents on position 4 and those with small substituents at position 4.

The potency observed in the different chordoma cell lines treated with various EGFR inhibitors were correlated with the chemotypes. This produced a shortlist of compounds to undergo further screening. This list included 22 compounds consisting of 2 Pyrimidines, 7 Quinazoline 'large R group' compounds and 13 Quinazoline 'small R group' compounds including known EGFR inhibitors: Erlotinib, Gefitinib, Sapitinib, and Afatinib. Lapatinib was added to the shortlist based on its Quinazoline 'large R groups' as a comparison to hits of the same chemotype. Lapatinib was also of interest as it had been used in a clinical trial where it demonstrated minimal activity(179) (Table 4.8).

Table 4.8 EGFR inhibitor according to chemotypes

Compound ID	GSK ID /Commercial Name	Library	Pathway	Chemotype	NAHDF EC50 Geomean [uM]	NAHDF Mean M%I	UCH1 EC50 Geomean [uM]	UCH1 Mean M%I	UCH2 EC50 Geomean [uM]	UCH2 Mean M%I	MUG.Chor1 EC50 Geomean [uM]	MUG.Chor1 Mean M%I
CRT0423504	GSK198271A	GSK PKIS2	ErbB family, BRAF	Pyramidine	3.70	48	0.34	78	3.09	43	0.22	50
CRT0423587	GSK326180A	GSK PKIS2	ErbB family, BRAF	Pyramidine	20.00	35	0.89	74	0.43	44	2.96	48
CRT0276404	Lapatinib Ditosylate	Anticancer	EGFR	Quinazoline large	5.94	101	3.35	97	11.13	90	8.40	89
CRT0363431	GW282449A	GSK PKIS1	EGFR/ErbB2	Quinazoline large	29.30	55	0.80	65	20.88	34	1.80	45
CRT0363482	GW583373A	GSK PKIS1	ErbB-1/ErbB2	Quinazoline large	10.96	62	1.39	71	17.93	44	30.00	32
CRT0363484	GW616030X	GSK PKIS1	ErbB-1/ErbB2	Quinazoline large	19.40	53	0.54	69	30.00	27	1.62	39
CRT0423669	GW569716A	GSK PKIS2	ErbB2/EGFR	Quinazoline large	8.77	99	4.74	81	13.48	71	0.59	46
CRT0423674	GW582764A	GSK PKIS2	ErbB2/EGFR	Quinazoline large	21.10	78	1.72	54	22.89	20	22.13	25
CRT0423676	GW583340C	GSK PKIS2	ErbB2/ EGFR	Quinazoline large	15.13	55	1.06	66	13.08	40	20.00	34
CRT0103071	Compound 56	Calbiochem	EGFR	Quinazoline small	22.79	77	0.57	86	20.00	27	0.01	62
CRT0103079	EGFR/ERBB2/ERBB4 Inhibitor	Calbiochem	EGFR/ERBB2/ERBB4	Quinazoline small	12.91	96	0.18	79	16.69	38	0.02	64
CRT0103123	PD174780	Calbiochem	EGFR	Quinazoline small	30.00	29	0.21	80	19.66	35	0.10	55
CRT0103124	PD174265	Calbiochem	EGFR	Quinazoline small	30.00	11	0.38	75	13.25	43	0.15	70
CRT0276366	Canertinib	Targeted Therapy	EGFR/ErbB2	Quinazoline small	5.19	100	0.13	81	9.30	60	Potentially Biphasic. Potency not Quantified	95
CRT0276385	Erlotiniib	Targeted Therapy	EGFR	Quinazoline small	14.57	48	0.35	86	15.50	40	0.22	74
CRT0276396	Gefitinib	Targeted Therapy	EGFR	Quinazoline small	11.18	87	0.22	76	9.84	79	0.36	68
CRT0363358	GW461104A	GSK PKIS1	ErbB-1/ErbB2	Quinazoline small	17.08	85	2.02	80	30.00	32	2.06	58
CRT0363568	GW680191X	GSK PKIS1	EGFR/ErbB2	Quinazoline small	30.00	41	1.26	86	17.83	61	0.37	45
CRT0423387	GI230329A	GSK PKIS2	EGFR	Quinazoline small	16.87	96	Potentially Biphasic. Potency not Quantified	94	20.00	40	0.19	41
CRT0423639	GW459135A (Erlotinib)	GSK PKIS2	EGFR	Quinazoline small	19.34	60	0.42	69	3.33	46	0.19	58
CRT0509503	Sapitinib (AZD 8931)	Targeted Therapy	EGFR/ErbB2	Quinazoline small	20.00	39	0.05	82	8.98	47	0.24	68
CRT0509501	Afatinib	Targeted Therapy	EGFR/ErbB2	Quinazoline small	5.88	100	Potentially Biphasic. Potency not Quantified	89	5.14	101	Potentially Biphasic. Potency not Quantified	101

Analysis of potency according to chemotype. Geomean EC_{50} and mean maximum percentage inhibition of shortlist of 22 compounds from table 4.7 based on chemotype and potency in sensitive chordoma cell lines. Orange to Red = nM to µM for potency. Light blue to Dark blue = High to low maximum percentage inhibition.

The trend in terms of cell line sensitivity (potency), ranked: U-CH1 > MUG Chor > U-CH2 with a maximum response liability in MUG Chor with compounds demonstrating 50-75% inhibition. In terms of trend with regard to chemotype/substituent trend, it appeared, albeit with a small number of compounds, that Quinazoline 'large' compounds exerted activity in U-CH1 but were less potent in the MUG Chor cell line. Quinazoline 'small' compounds exerted activity in the U-CH1 and MUG Chor cell lines but neither subset was routinely active in the U-CH2 cell line. The two Pyrimidine compounds (GSK198271A and GSK326180A) were generally pan-inhibitors across three chordoma cell lines with a potency range of 217nM to 3uM.

At this stage of the screening cascade several EGFR/ErbB inhibitors were identified from independent pharmacologically active libraries. These hits were used to benchmark commercially available compounds to help understand the chemistry. The favourable chemotype, determined from chemotype/substituent analysis by GSK, was the Quinazoline with small R groups at position 4. Sapitinib (AZD 8931) was identified as the 'lead' candidate for further screening, based on its compound profile. Sapitinib, a dual EGFR/HER2 inhibitor(742), demonstrated phenotypic potencies of 50nM, 242nM and 9μM in U-CH1, MUG Chor and U-CH2 respectively, with reversible mode of action, and differential phenotypic effect fold selectivity of 417 in the most sensitive cell line (U-CH1) (Table 4.7 & Figure 4.22).

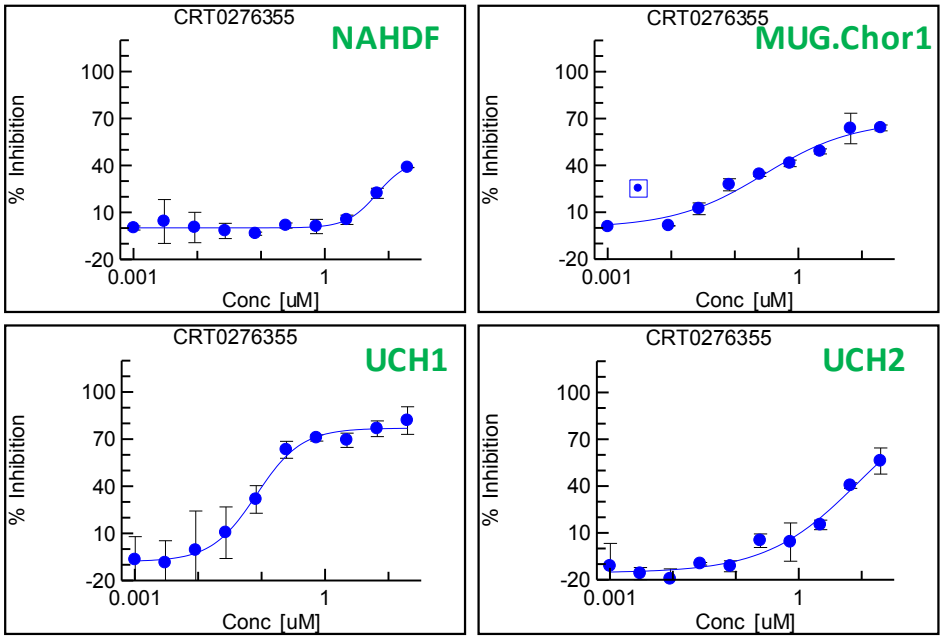

Figure 4.22 Differential phenotypic effect with Sapitinib (AZD 8931)
Graphical plot demonstrating percentage inhibition in a 10-point dosing (IC_{50}), using the WST-1 assay in NAHDF, MUG Chor, U-CH1 and U-CH2 cell lines. Data representative of at least n=2. Phenotypic Geomean EC_{50}: NAHDF >20μM, MUG Chor 0.24μM, U-CH1 0.05μM, U-CH2 6.88μM (Table 4.7).

4.7.1 EGFR inhibitors in chordoma

A general trend was observed with EGFR/ErbB inhibitors inducing caspase-3/7 activity between 6 to 24 hours post compound treatment, followed by a decrease in cell viability from 24 hours in the U-CH1 cell line. Minimal induction of caspase-3/7 activity (<30% induction) was observed in U-CH2 and MUG Chor cells. This observation was reflected in the phenotypic assay with U-CH1 being the most sensitive cell line (Appendix).

Sapitinib displayed high induction of caspase-3/7 activity in the U-CH1 cell line between 6 and 48 hours followed by decrease in cell viability observed from 24 hours onwards. MUG Chor showed high induction of caspase-3/7 activity and >40% growth inhibition at 72 hours. The U-CH2 cell line showed ~50% induction of caspase-3/7 activity between 24 and 72 hours at the three top concentrations of the dose-response (20μM, 6.6μM and 2.2μM) but <40% growth inhibition was observed (Figure 4.23).

Erlotinib was used as a bench mark compound for comparison to Sapitinib as Erlotinib has previously been used in the treatment of patients with chordoma.

Erlotinib induced caspase-3/7 activity in the U-CH1 cells between 24 to 72 hours and a decrease in cell viability from 48 hours. Minimal caspase-3/7 induction was observed in U-CH2 and MUG Chor cell lines at all time points (Figure 4.24).

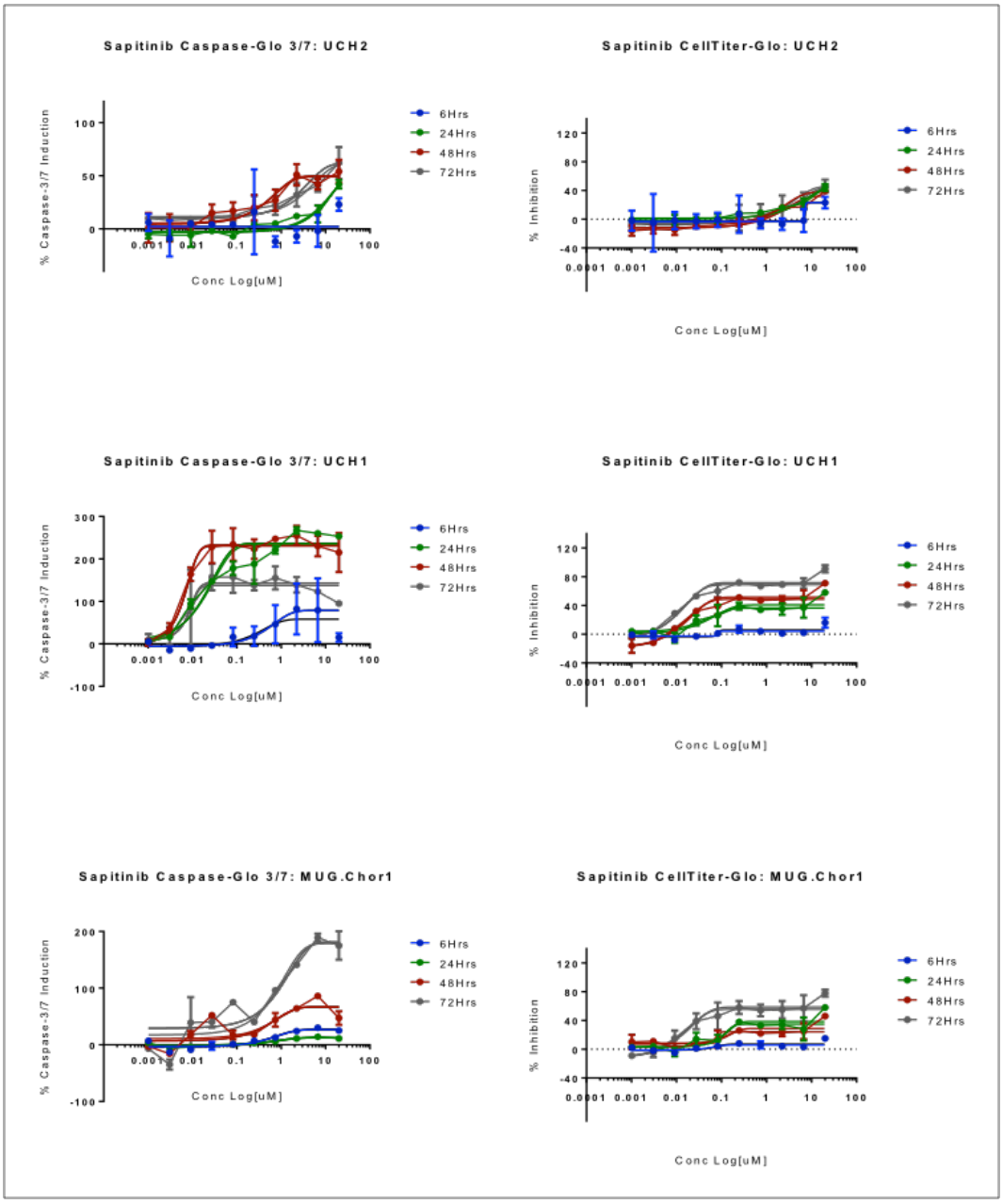

Figure 4.23 Caspase-Glo 3/7 and CellTitre-Glo assay for Sapitinib treated cells
Graphical plots of Sapitinib in the Caspase-Glo 3/7 (left) and CellTiter-Glo (right) assay. Data are representative for each cell line at 6, 24, 48 and 72 hours. Increase in percentage caspase induction correlates with increase in percentage inhibition (n=3).

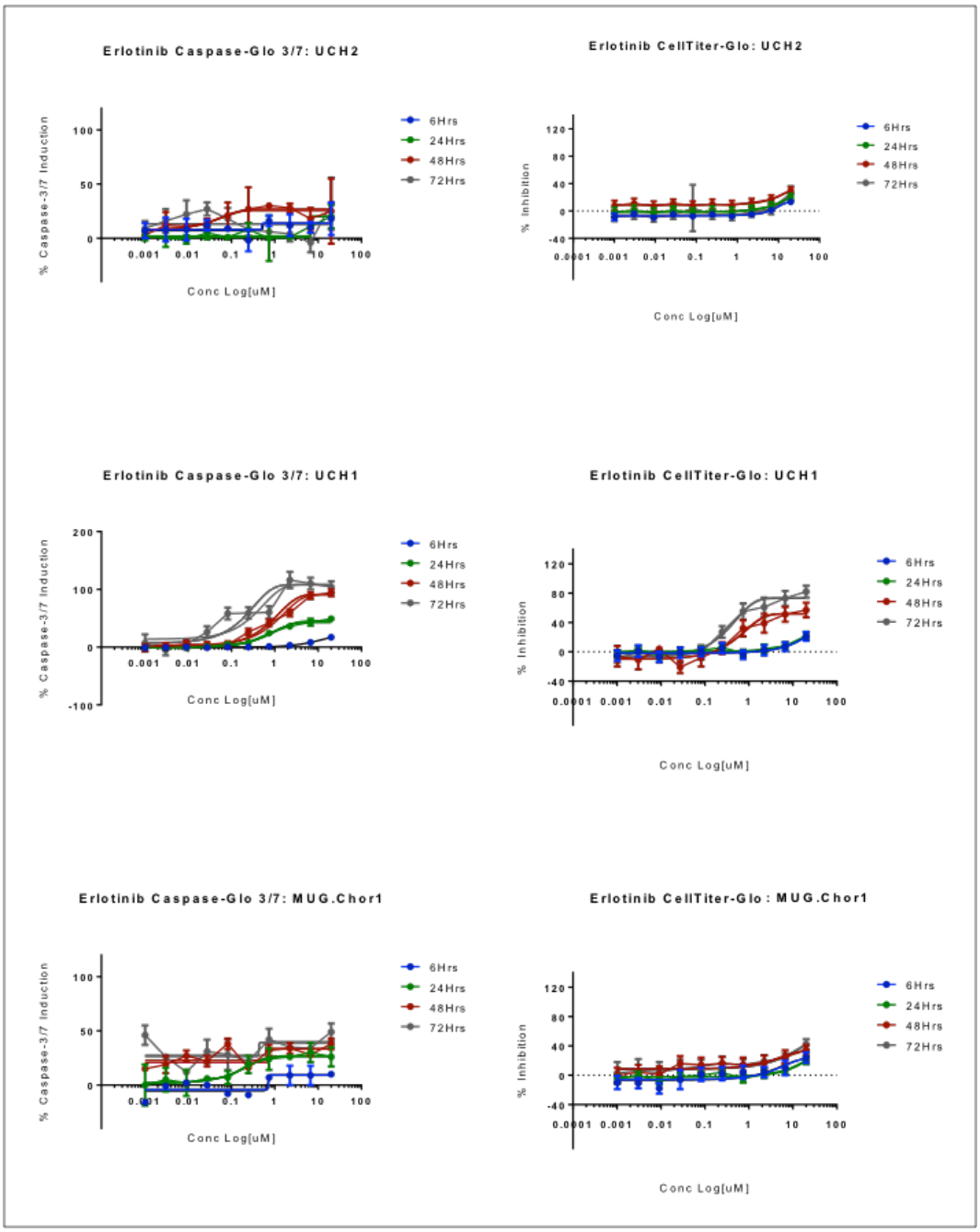

Figure 4.24 Caspase-Glo 3/7 and CellTitre-Glo assay for Erlotinib treated cells
Graphical plots of Erlotinib in the Caspase-Glo 3/7 (left) and CellTiter-Glo (right) assay. Data are representative for each cell line at 6, 24, 48 and 72 hours. Increase in percentage caspase induction correlates with increase in percentage inhibition.

4.8 Discussion

In this study we used three fully characterised chordoma cell lines authenticated with STR DNA profiling. The objective of this project was to identify compounds that elicit a kill or growth arrest on chordoma cell lines. Nearly 1200 compounds were screened by single point screening, and compounds that elicited kill or growth arrest were taken forward for IC_{50} screening. The single point screen is a fairly crude screening process and compounds of interest may have been missed. An alternative approach would have been to perform an IC_{50} screen of all the compounds but reducing it from a 10-point screen to a 4- or 6-point screen. To avoid potential exclusion of effective compounds the selection criteria was based on 2x SD rather than 1.5x SD to increase the number of compounds entered into the IC_{50} screen.

Of the 1153 compounds screened, 1046 were small molecule kinase inhibitors. 27 compounds of interest were identified of which 22 (81%) targeted the EGFR/ErbB family. Five commercially available EGFR inhibitors were used to benchmark our results and help understand the chemistry.

EGFR was the first growth factor to be linked with tumorigenesis(743-745). Amplification and mutations were first identified and associated with the altered expression of EGFR in brain tumours(746,747), but have subsequently been identified in other cancers(729,735,736). Response to EGFR inhibitors has been shown to be associated with specific mutations(730,734). *EGFR* is expressed by the majority of chordomas(166,186) yet no *EGFR* mutation or mutations within the signalling pathway have been identified to account for the increased activation. A proportion of chordomas exhibit polysomy 7 which can explain the overexpression of *EGFR* in those tumours(735). 70-80% of cells used in this study, from all three chordoma cell lines, have been observed to have polysomy 7 by FISH analysis. No *EGFR* amplification was detected (personal correspondence by Professor A. Flanagan, data provided by Hongtao Ye, Royal National Orthopaedic Hospital). In addition no *EGFR* mutation was identified in the cell lines. The absence of *EGFR* mutations in chordoma is shared with other cancers which despite this are known to respond to anti-EGFR therapy to a varying degree(748). These include pancreatic cancer(749), colorectal cancer(750) and head and neck squamous cell carcinoma(751,752). As with these tumours, the majority of chordomas express the activated form of

EGFR(164,165,180). The chordoma cell lines used in this study all express the activated form of the receptor (Appendix).

Variation of efficacy was demonstrated between different EGFR inhibitors. Chemotype analysis identified the favourable chemotype to be Quinazoline derivatives with a small substituent group in the 4th position of the quinazoline ring. The compounds in this group included Erlotinib, Gefitinib and Sapitinib, as well as two irreversible compounds: Afatinib and Canertinib. Sapitinib, a dual EGFR/HER2 inhibitor(742), was identified as the 'lead' compound based on its profile. It is currently in clinical trials for breast cancer and NSCLC(753,754) but has never been studied in chordoma. Erlotinib and Gefitinib have previously been found to inhibit chordoma proliferation of U-CH1 *in vitro* and *in vivo* in a PDX(178,185). There are also reports of beneficial activity of Erlotinib in patients with chordoma: one patient achieved stabilisation of disease following single drug therapy(206), as did three patients treated with Erlotinib and Bevacizumab(176). Lapatinib, a Quinazoline large chemotype, was recently used in a phase II trial in patients with advanced chordoma where it showed minimal activity(179). Lapatinib has also been tested in PDX models where it demonstrated incomplete and heterogeneous switching off of *EGFR* and its signalling(177). No clinical studies in chordoma patients have included post-treatment biopsies to assess the tumour response and potential resistance mechanism. Lapatinib in the study reported here demonstrated high mean percentage inhibition in all cell lines but at relative high dose concentrations (3-11μM) and showed no differential phenotypic effect between the chordoma cell lines and the normal fibroblasts. The irreversible EGFR inhibitors demonstrated a biphasic response suggesting non-specific cytotoxicity(755).

Variation in the sensitivity to EGFR inhibitors was demonstrated between the three cell lines, with U-CH1 and MUG Chor being the most sensitive cell lines, with little response in the U-CH2 cell line. This suggests an inherent resistance to EGFR inhibition in the U-CH2 cell line. There is support for resistance from other sources. Various mechanisms of resistance to EGFR inhibitors have been described(729). In NSCLC the emergence of a specific mutation conferring resistance to Gefitinib is well recognised(734). Other mechanisms of resistance to EGFR inhibitors include *KRAS, BRAF and PI3K* mutations(756,757) which in their absence, does not account for the variation in response to EGFR inhibitors in the chordoma cell lines. *PTEN* has been found to be a modulator of drug

sensitivity with loss of *PTEN* expression leading to resistance to EGFR inhibitors(735,750). *PTEN* loss in chordoma has been reported in 25-80% of chordomas, as a consequence of chromosomal abnormality(128,129,197,661). Sensitivity to EGFR inhibitors in the cell lines did not correlate with PTEN expression(134,197,661) (WB data in appendix). Loss of *PTEN* expression in chordoma and other cancers has been associated with increased levels of mTOR expression, increased invasiveness and a decrease in EFS(129,735,758,759).

Rapamycin, an mTOR inhibitor, has been reported to reduce tumour growth in one patient with chordoma. This tumour had a *KRAS* mutation(193), a mutation which has not been reported in other studies in chordoma(130,180). Four mTOR inhibitors were included in the study reported here. None of these compounds showed differential phenotypic effect, yet some of the compounds have been approved for cancer therapy, having demonstrated an accepted toxicity prolife(760-763). Deforolimus which targets the FKBP12-rapamycin binding domain(764) demonstrated 50% maximum inhibition at low doses (nM) in the U-CH2 cell line. Though similar effect was noted in the NAHDF cell line, it is potentially interesting as two phase I mTOR inhibitors with dual inhibition of PI3K (AZD8055 and GSK1059615) both demonstrated high percentage inhibition at low doses (nM) in all cell lines. In addition the only compound from the anti-cancer library with differential phenotypic effect between the NAHDF and the U-CH2 cell lines was a PI3K inhibitor. This compound has been reported in multiple pre-clinical settings(765) and has recently been tested in a phase I clinical trial(766). Few compounds demonstrated an effect on the U-CH2 cell line.

In this compound screen several clinically approved drugs demonstrated activity in chordoma cell lines, but also exerted toxicity in ‘normal’ cells. As these drugs are already approved for clinical use, with a known toxicity profile, further testing to assess response in PDX models, potentially in combination with targeted therapy, could identify treatment options for chordoma. From this study compounds to highlight as potentially interesting include HDAC inhibitors and compounds targeting HSP90. In concordance with the results from Xia et al(185) no effect was observed in any of the chordoma cell lines following treatment with Imatinib.

Bortezomib a proteasome inhibitor demonstrated potency in all three chordoma cell lines at <20nM doses. This correlates with the findings of a recent high-

throughput screen in U-CH1 and U-CH2(185). Bortezomib has been used in a chordoma PDX. Treatment resulted in significantly reduced tumour growth and has the potential to be an important component in chordoma drug therapy(767).

Bortezomib has FDA approval for treatment of multiple myeloma(768) and is being tested in multiple early phase trials for solid tumours(769-773). It is a selective inhibitor of the ubiquitin-proteasome pathway, which is essential for the degradation of most regulatory intracellular proteins(774). Preclinical studies have shown that treatment with proteasome inhibitors results in decreased proliferation, induction of apoptosis, and sensitisation of tumour cells to conventional chemotherapeutic agents and irradiation. The effects were conferred to stabilisation of *p21, p27, Bax, TP53* and inhibition of nuclear factor-κB *(NF-κB)* activation(775). Gene expression in the chordoma PDX tumours treated with Bortezomib showed down regulation of *NF-κB* target genes *Bcl-2, IL-6, IL-8 and CD44* compared with untreated mice. Interestingly two other target genes, *Bcl-x* and *AKT,* were upregulated in the drug-treated chordoma xenograft tumours compared with controls(767). Activation of *AKT* leads to phosphorylation of *PI3K* with subsequent inactivation of *TSC1/TSC2* complex and phosphorylation of *mTOR*(40). Expression of *AKT* in chordoma has been found to be inversely correlated to outcome(166,758). These associations demonstrate a potential mechanism for the beneficial effects of bortezomib in chordoma as well as highlights possible mechanisms for the tumour to circumvent the effect of treatment.

In hepatocellular carcinoma and in head and neck squamous cellular carcinoma preclinical studies with Bortezomib found that induced up-regulation of phosphorylated *AKT (pAKT)* protected cells from Bortezomib induced apoptosis(776-778). Subsequent preclinical studies have combined Bortezomib with a PI3K pathway inhibitor for synergistic effect, and have found enhanced Bortezomib induced apoptosis(779-781). It would be of interest to investigate this combination in the chordoma PDX and in early clinical trials.

The complete selectivity profile of compounds is rarely known, making it difficult to be confident that a cellular effect is due to inhibition of a single kinase. The more compounds that share a common target and demonstrate similar phenotypic effect, the more likely it is that the effect of the compound is due to target specificity(682). More than 1000 TKIs were included in the screen

reported here. EGFR inhibitors represented 81% of the compounds identified as hits. Additional EGFR inhibitors were included and experiments were repeated with different batches of reagents confirming the target effect. Subsequent experiments have been undertaken by S. Scheipl and M. Barnard. This further work has confirmed dose response and 'on-target' effect, including effect on the downstream signalling pathways following treatment with EGFR inhibitors. Additional cell lines have become available for a focussed screen of EGFR inhibitors, which may improve the understanding of the heterogeneous response between cell lines and possible mechanisms of resistance.

A comprehensive study including well-characterised patient samples is required to address issues of resistance. Specifically a clinical trial examining patient samples before and after EGFR inhibitor treatment is likely to be informative.

5 XENOGRAFT MODEL FOR ONCOLOGY DRUG DEVELOPMENT

5.1 Background

Over the past 10 years molecular targets have been identified in chordoma with the potential for therapeutic drug development(40,163,164,180,210). However, the decision on when targeted treatment is to be given and how a compound is selected is often flawed. For instance, therapeutic agents are often selected for treatment of recurrent disease on the basis that the primary lesion harbours the targetable molecule without confirmation that the target is present in the recurrent disease(177,616). Another example includes the use of targeted therapies being used in the absence of an evidence basis(171,179).

Progress in oncological drug development has been difficult due to a lack of preclinical models able to reliably predict clinical activity(589). Immortalised human cancer cell lines are valuable for understanding the pathophysiology of disease and can be successfully used to predict the clinical effect of cancer therapies(782-785). Chordoma cell lines have proven difficult to establish and until very recently there was no cell line generated from a clival chordoma. Currently seven characterised chordoma cell lines are available through the Chordoma foundation (www.chordoma.org). The availability of multiple cell lines provides a better representation of the inter-tumour heterogeneity(786).

Recently a zebrafish model of chordoma was discovered following stable expression of *HRASV12* in notochord cells during development. Extensive intra-notochordal tumour development was found with 100% penetrance ultimately leading to larval death. The HRASV12-expressing zebrafish tumours had histological, immunohistochemical and structural features similar to human chordoma. Mutations of *RAS* family members are not common in patients with chordoma(787). Activation of *HRAS* can mimic an increase in downstream signaling pathways driven by cell surface receptors, such as *EGFR* which has been implicated in the pathogenesis of chordoma(181,182,184,206). Zebrafish lend themselves to high throughput drug screening(788,789), however the chordoma zebrafish model has some limitations due to an inability to test upstream inhibitors of HRAS such as EGFR. Rapamycin was tested in this chordoma zebrafish model demonstrating a delay in onset of tumour phenotype and longer survival(787).

A recent study using integrated functional genomics identified several target genes of brachyury(127), suggesting that the mechanism of chordoma formation involves multiple signaling pathways directly or indirectly controlled by the transcription factor.

Limited *in vitro* models and a lack of *in vivo* models has hindered the translation of these observations into novel therapies(767).

There has been a rapidly growing interest in the establishment of patient-derived mouse xenografts (PDX). PDX models have been found to closely recapitulate primary tumour biology and clinical outcome(590,592,602,767). Numerous studies have demonstrated that PDX models sustain genotypical and phenotypical features over subsequent generations(589,790,791). They may serve as important models to investigate mechanisms of resistance to targeted therapies and for preclinical testing of novel treatment strategies(589,592,792). The PDX model has been described as the Avatar model, which has been used for guiding personalised therapy(592,793). Hidalgo et al. generated PDX models for 14 patients with refractory solid or early-stage, poor prognosis tumours of different types and treated them with 63 drugs in order to guide the choice of chemotherapy(592). Eleven patients were treated with 17 treatment regimens based on their corresponding PDX tumours and 15 of these regimens resulted in durable partial remission. PDX models have been found to retain all primary tumour mutations and display mutation enrichment patterns resembling the metastases. The identification of emerging mutations in the PDX models improves the understanding of tumour progression and treatment resistance(794). The ability of tumours to engraft has been found to be a poor prognostic marker(794-796), but may represent a useful tool for identifying treatment options for the patients.

Only recently has the development of mouse models for chordoma been undertaken as a means to advance understanding of chordoma biology(89,91,609,767). The different chordoma models have been reviewed previously.

5.2 Aim

To establish two novel chordoma mouse models. The first PDX chordoma model to establish the method, monitor engraftment and review the phenotypic and genotypic features in comparison to the parent tumour. This model has been shared with Gary Gallia in Harvard for *in vivo* drug screen and frozen tumour sections were sent via the Chordoma Foundation to the START lab (South Texas Accelerated Research Therapeutics) to start a PDX-model from frozen tissue from the xenograft. The second model, a cell line xenograft (CLX), was generated for *in vivo* imaging of the tumour for the purpose of testing the viral vector delivering RNAi as described in chapter 3.

5.3 Objective

1. To establish a chordoma PDX model and assess molecular and phenotypic features and determine genetic stability.
2. To generated at CLX with tumours expressing luciferase and assess molecular and phenotypic features in the CLX tumour.
3. To generate CLX models for gene therapy study.

I performed the experiments involving the patient-derived xenograft with support from Dr M. Eskandapour PhD, Dr N. Presneau PhD, and Dr S. Scheipl MD.

5.4 Results

5.4.1 Establishment of a primary chordoma xenograft

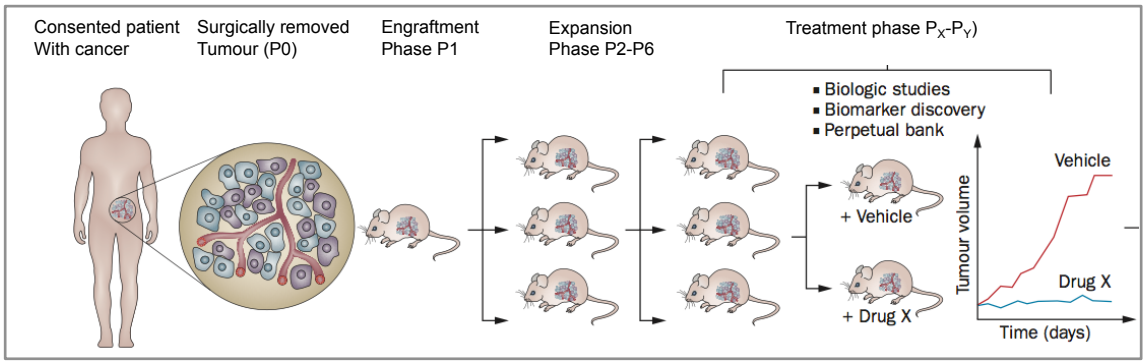

Figure 5.1 Overview of procedure for establishing PDX
Adapted from Tentler et al. (589).

The patient from whom the xenograft was generated presented at the age of 47 with a primary coccygeal conventional chordoma with poorly differentiated areas. Initial treatment consisted of surgical resection and Proton beam radiation therapy. The tumour recurred locally five years after initial presentation and re-excision was attempted. INI1 expression was maintained. Fluorescence in situ hybridisation (FISH) revealed that brachyury was disomic. EGFR showed a low level of polysomy (Figure 5.2).

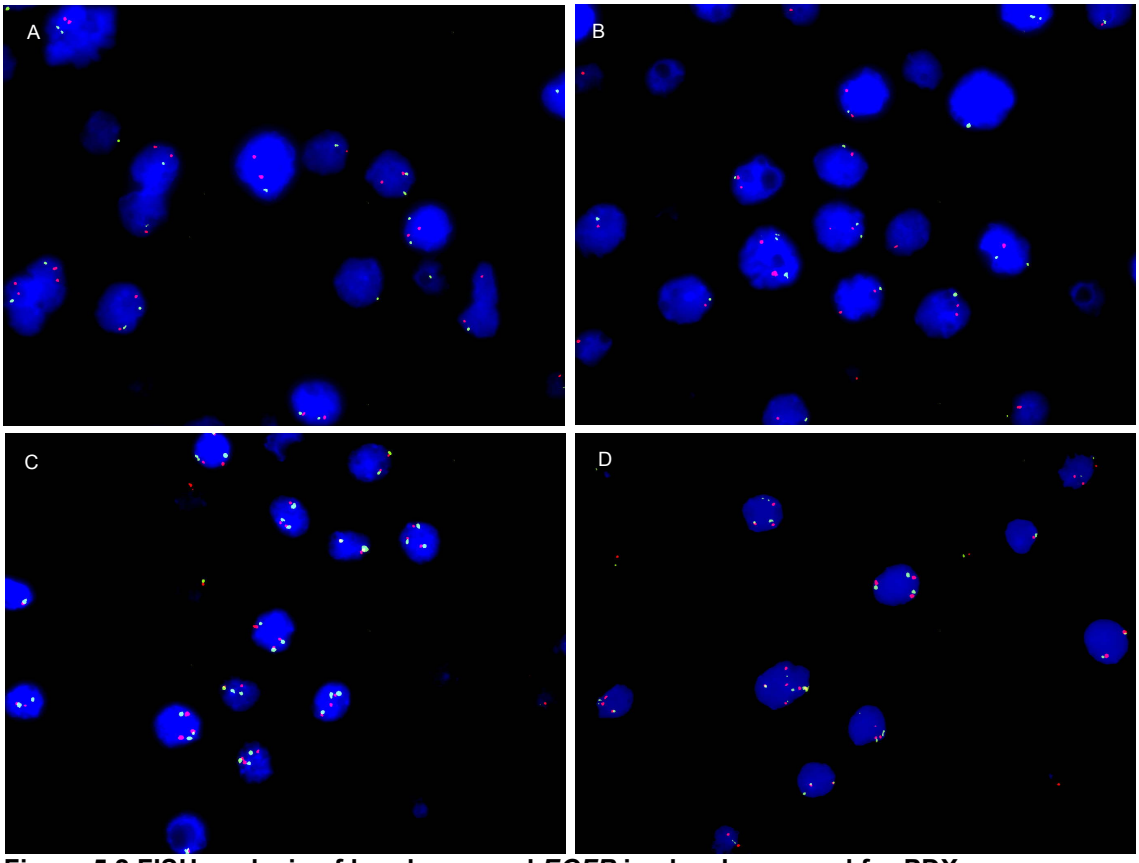

Figure 5.2 FISH analysis of brachyury and *EGFR* in chordoma used for PDX
Brachyury (A&B) and EGFR (C&D) red signal probe. Green signals represent chromosome enumeration probe (CEP) to correct for chromosomal region. Disomy of brachyury with 2 signals for brachyury and 2 signals for CEP6. EGFR demonstrating low level of polysomy compared to CEP7 (> 2 copies/cell in ≤ 40% of cells). Images kindly provided by Roberto Tirabosco, Pathologist Royal National Orthopaedic Hospital.

The tumour was implanted into two BalbC/nude mice. The first PDX tumours grew from about 8 weeks and were serially transplanted over the course of 14 months. The xenograft lineage was passaged 5 times. On each occasion the tumour was passaged into new mice and tumour was snap frozen for histology and DNA extraction. A small piece was put into formalin for immunohistochemistry and when available tumour was frozen in re-engraftment medium. Tissue from the primary tumour and the xenograft passage 1, 4 and 6 confirmed concordance of histology (Figure 5.3) and brachyury expression was maintained in the xenograft (Figure 5.4).

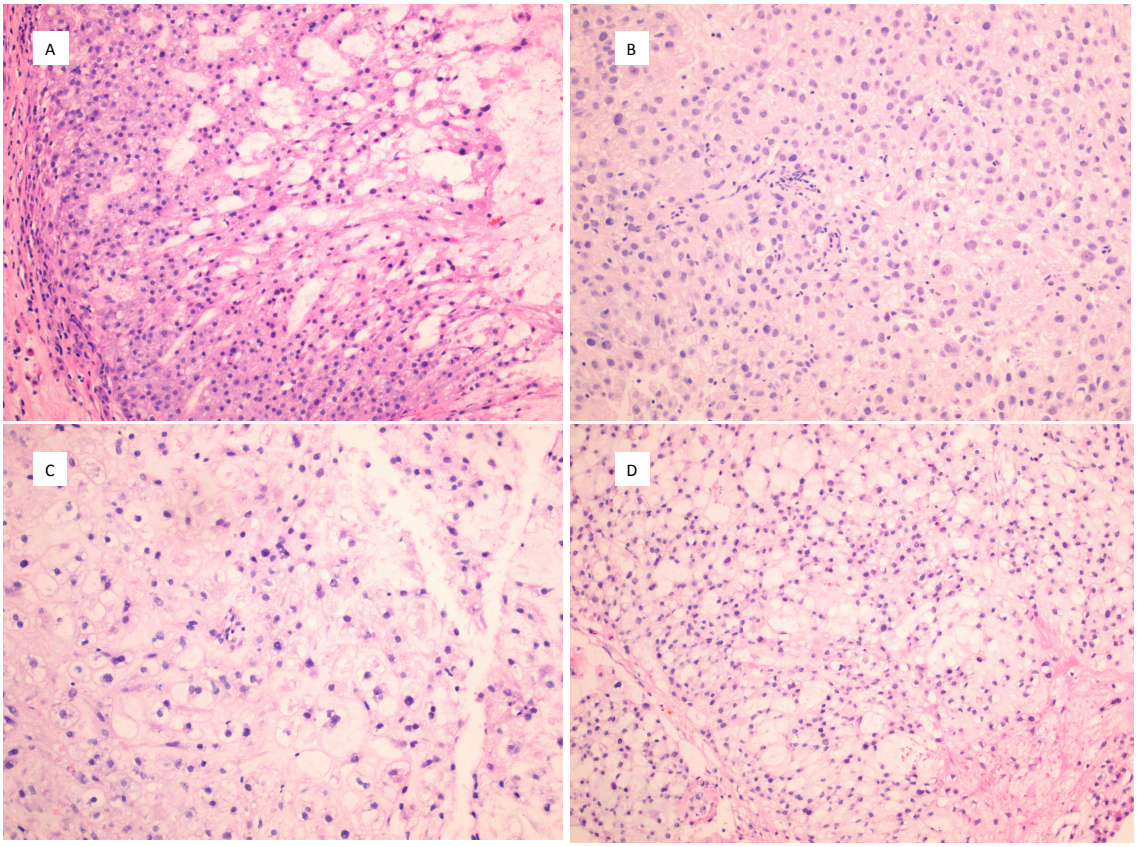

Figure 5.3 Morphology primary tumour and patient derived xenograft
Photo-microscopy H&E-stained tumour which was used to generate a PDX-derived xenograft (A) and xenograft (B) P1, (C) P4, (D) P6.

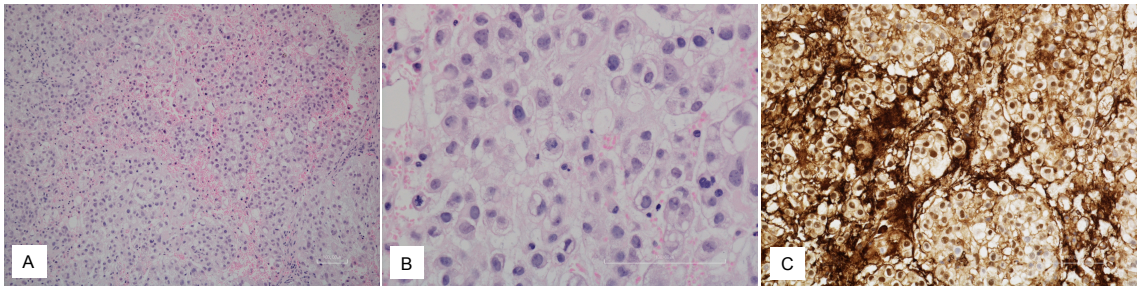

Figure 5.4 Xenograft tumour from PDX
PDX P6. Photo-microscopy H&E-stained tumour (A) 10x and (B) 40x (C) brachyury immunoreactivity.

5.4.2 Genomic analysis of resected tumour and PDX tumour

5.4.2.1 *TP53* and *PI3K* mutation in the patient tumour

The recurrent tumour used for the PDX underwent whole genome sequencing at the Wellcome Trust Sanger Institute Hinxton, Cambridge and was found to have a *TP53* and a *PI3K* mutation (Table 5.1).

Table 5.1 Sequencing data from patient tumour used for PDX

Gene	Freq gene	Paired or unpaired	Assay	CDS	Protein	Effect	Cosmic	Visual
TP53	17	paired	Genome	c.814G>A	p.V272M	missense	32	somatic
TP53	17	paired	Genome	c.814G>A	p.V272M	missense	32	somatic
HLA-C	66	paired	Genome	c.419C>A	p.S140Y	missense	0	.
ROS1	20	paired	Genome	c.3530C>T	p.T1177M	missense	1	.
BRAF	17	paired	Genome	c.31G>T	p.G11C	missense	0	.
NCOR1	14	paired	Genome	c.1375T>G	p.F459V	missense	0	.
PDE4DIP	3	paired	Genome	c.180G>A	p.W60*	nonsense	0	.
PIK3R1	3	paired	Genome	c.812_816delTGCTT	p.M271fs*9	frameshift	0	somatic
DNAJC10	1	paired	Genome	c.820C>T	p.Q274*	nonsense	0	.
C5orf39	1	paired	Genome	c.308C>A	p.P103H	missense	0	.
ENSG00000205857	1	paired	Genome	c.55G>A	p.A19T	missense	0	.
FBLN2	1	paired	Genome	c.872C>T	p.A291V	missense	0	.
INTS1	1	paired	Genome	c.5317G>T	p.D1773Y	missense	0	.
MYT1	1	paired	Genome	c.938T>A	p.F313Y	missense	0	.
PHRF1	1	paired	Genome	c.3084C>A	p.S1028R	missense	0	.

Whole genome sequencing data from tumour compared with constitutional DNA. The *TP53* mutation is listed in the COSMIC database. This tumour also had a PIK3 mutation but not at a common site (COSMIC). Information within the table: The frequency or percentage of cells identified with the mutation , the effect of the mutation (missense) and when visualised and compared to constitutional DNA identified if the mutation was determined as a somatic mutation. CDS: Coding DNA sequence with identified location of mutation within exons coding for protein.

5.4.3 *TP53* mutation in the PDX

The PDX tumour DNA from P6 was screened using a large panel for common cancer mutations identified in the COSMIC *(Catalogue Of Somatic Mutations In Cancer http://cancer.sanger.ac.uk/)* database, performed by the UCL Advanced Diagnostic laboratory. The identical *TP53* mutation: p.Val272Met, c.814G>A COSM10891 was detected at 100% variant frequency i.e. 100% of the cells carried the mutation. In the original tumour the *TP53* mutation was identified in 17% of the cells, suggesting that a clonal expansion of the cells containing the *TP53* mutation occurred in the xenograft. No other mutations were detected in the xenograft tumour DNA using the panel for common cancer mutations.

5.4.4 Xenograft for *in vivo* imaging

5.4.4.1 Luciferase expressing U-CH1 cell line

The U-CH1 cell line was engineered to stably express the firefly luciferase gene to enable *in vivo* imaging of cell line engraftment in BalbC/nude mice. This was done for the purpose of assessing the response to viral vector delivered gene therapy using an AAV vector carrying RNAi targeting brachyury.

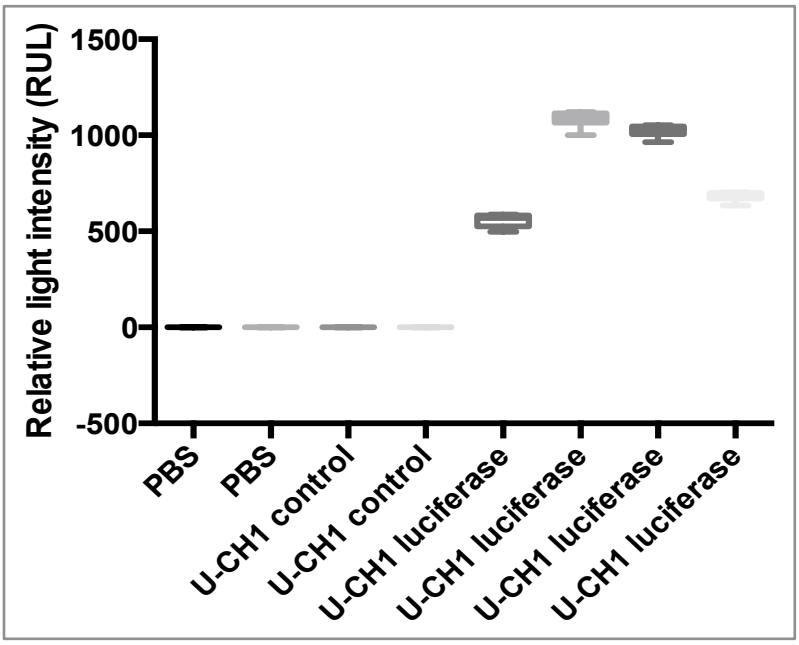

Figure 5.5 Luciferase expression in U-CH1
Luminescence was measured using a luminometer. Relative light intensity was compared between the engineered U-CH1_luciferase cell line and the un-transduced U-CH1 cell line as well as PBS. 4 different passages of U-CH1_luciferase cells were measured. Each sample was measured in triplicate. The results are expressed as the mean+/- SD.

5.4.4.2 Engraftment of CLX

The generated cell line was injected into the flank of BalbC/nude mice. Successful engraftment of the U-CH1 cell line has been achieved previously and confirmed in this study(89). CLX engrafted over 8-10 weeks. Luminescence and tumour growth was assessed at regular intervals (Figure 5.6).

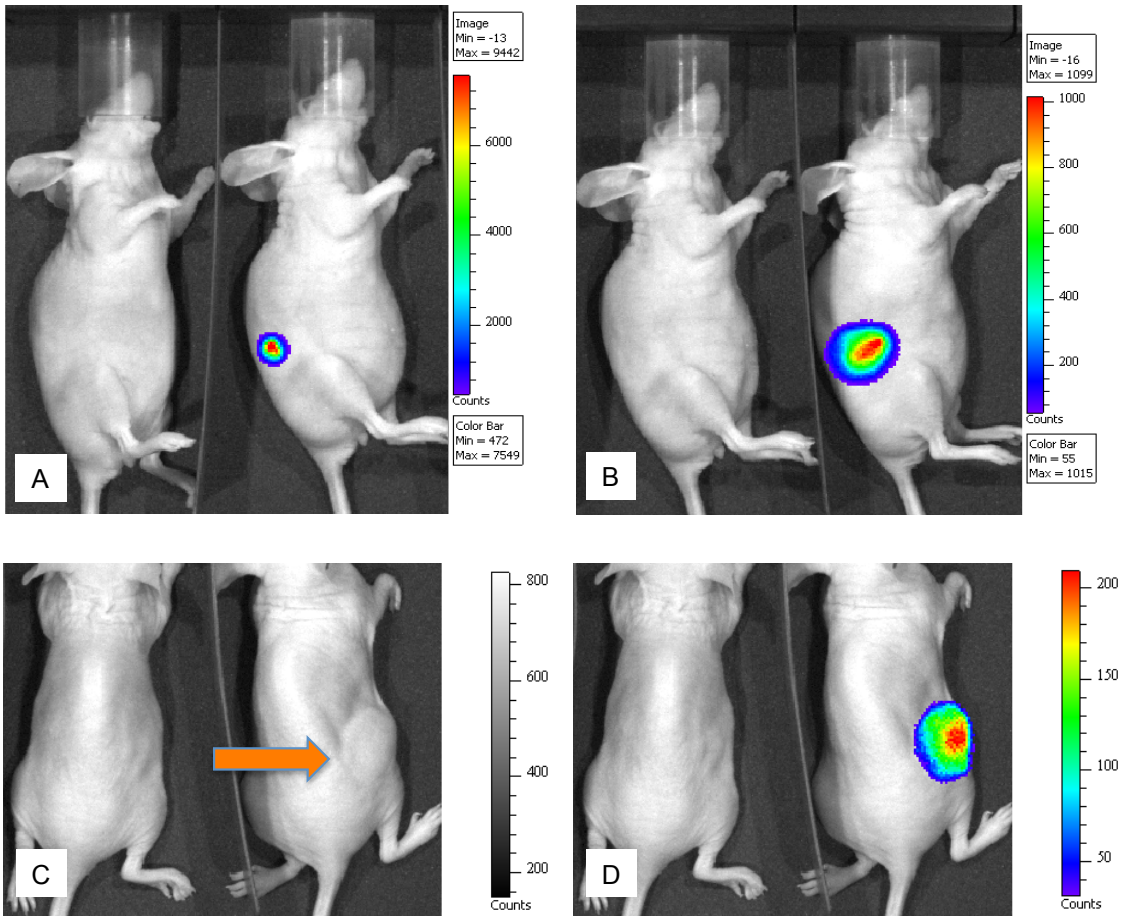

Figure 5.6 Image of xenograft with luciferase-expressing tumour
Image of two BalbC/nude mice both injected with U-CH1_luciferase expressing cells, only one mouse developed a tumour as identified by the arrow (C). (A) and (B) images of the mice at different time-points indication tumour growth and increase in luciferase expression (images acquired 3 weeks apart). Image (C) is a white light photographic image used for overlaying the bioluminescence signal as demonstrated in (D) taken 4 weeks after (A). D-luciferin was injected into both mice at all time-points.

5.4.4.3 CLX morphology and histology resembles chordoma

Figure 5.7 Chordoma CLX
BalbC/nude mouse xenograft generated from the U-CH1_luciferase cell line (left). Image on the left is the subcut exophytic nodule (generated from $1x10^7$ cells). The middle image shows a well-circumscribed nodule surrounded by a thin fibrous membrane loosely attached to the sub-dermal layer. In 10 xenografts a single feeder arterial/venous blood supply was observed. Tumour from an animal injected grossly resembled chordoma with grey-white complexion and lobulated appearance (image on right).

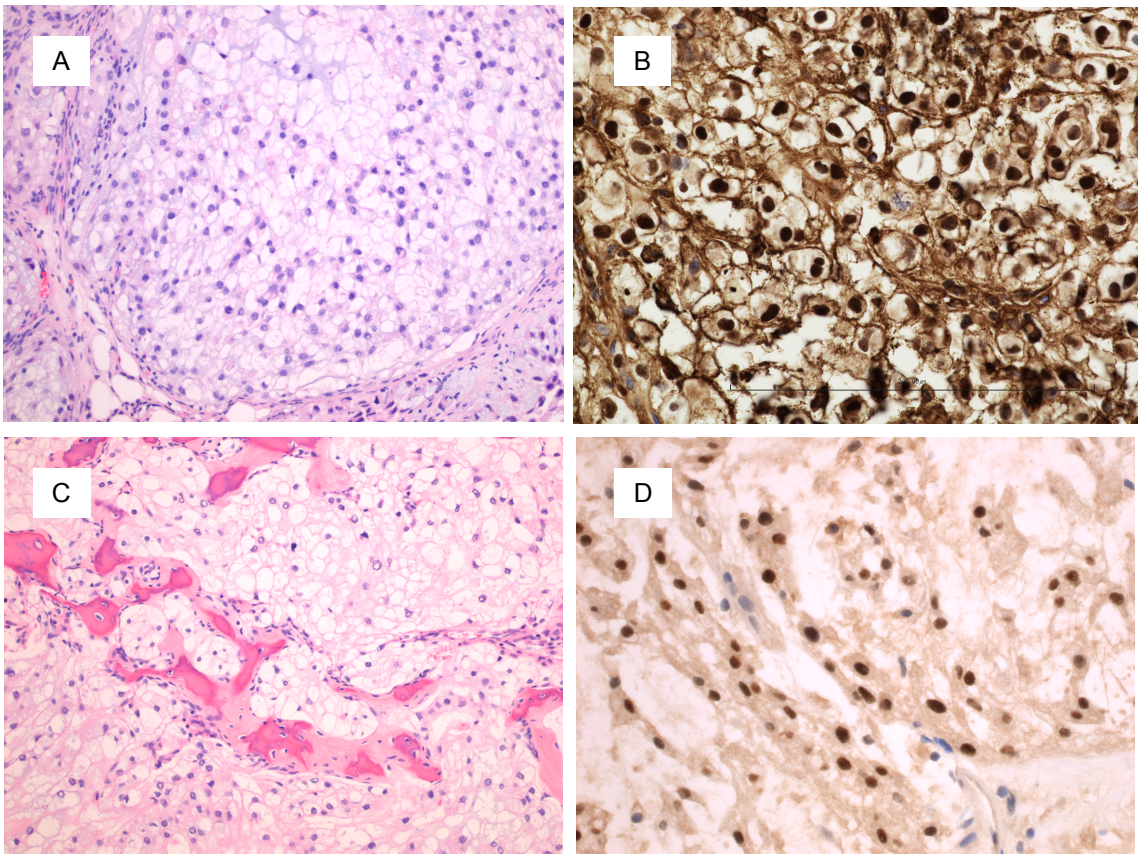

Figure 5.8 Morphology and immunoreactivity CLX and human chordoma
(A) CLX U-CH1_luciferase tumour, haematoxylin and eosin stain (H&E) demonstrating 'classic' lobulated appearance; with a myxoid matrix, embedded cords and tumour cells with eosinophilic cytoplasm as well as vacuolated tumour cells, known as physalipherous cells (x10). (B) CLX immunoreactive for brachyury. (C) Human chordoma specimen typical chordoma physalipherous cells embedded in abundant eosinophilic extracellular matrix; (D) Human chordoma; brachyury antibody highlights the nucleus. IHC was kindly done by the members of the histopathology lab at the Royal National Orthopaedic Hospital, under supervision of Professor A. Flanagan.

5.5 Discussion

The aim of this study was achieved. Two different preclinical xenograft models were constructed to allow for future investigation of tumourigenesis and development and evaluation of therapeutics.

The luciferase-expressing CLX model offers an opportunity for *in vivo* functional (metabolic) imaging. This provides an advantage over using RECIST criteria for assessing tumour response. The lessons from chordoma patients treated with Imatinib showed that the RECIST criteria for assessing tumour response were inadequate(722). In this patient group a limited alteration in tumour size was identified following treatment, however there was a change in tumour density and vascularity identified by positron emission tomography (PET) imaging, using fluorine-18-fluorodeoxyglucose (^{18}F-FDG). PET was found to be highly sensitive for detecting early response to treatment with Imatinib in chordoma patients(722). The uptake of ^{18}F-FDG by tissue is a marker for the tissue uptake of glucose, which correlates with tissue metabolism(797). The use of luciferase in our xenograft model offers a similar correlation with cell viability. The photon flux that is measured as bioluminescence is proportional to live cells expressing luciferase and can therefore be used for monitoring tumour growth and cell death. Luciferase expression was more sensitive than caliper measurement of the tumour size and therefore gave a better assessment of cell number/cell death, in concordance with reported data(798,799). The model described here was used for evaluation of the therapeutic effect of gene therapy using an AAV vector for delivery of RNAi described in Chapter 3 and can be used for screening of drug efficacy.

The PDX model was developed as part of an international collaboration to establish new models for drug screening. It is increasingly clear that models representing cancer heterogeneity are required for pre-clinical drug development, as well as the development of biomarkers for assessment of response to therapy. These models offer the opportunity to support this research. Genetic, phenotypic and tumour microenvironment heterogeneity is likely to have implications for the ability to recapitulate accurate cancer biology in cell line-, CLX and PDX models. Using cell lines to generate tumour models has its limitations. The cells can undergo clonal selection *in vitro* leading to high homogeneity of established cell lines. This results in tumours that do not always exhibit the histological characteristics observed in the clinical specimens(568,592,786). The cell line used for the CXL described here was

characterised by STR to confirm authenticity against the initial U-CH1 cell line (as discussed in Chapter 3). In addition immunoreactivity and histology were retained in the CXL, resembling the features of chordoma. Yet, it is accepted that cell lines derived and cultured from a single biopsy may not represent the overall phenotype of the original tumour(591,786). This was demonstrated by Barranco et al. who generated 4 melanoma cell lines from a single melanoma nodule and observed differential effect to therapy between the different cell lines(800). Others have demonstrated differential morphology, growth rate, tumourigenicity and therapeutic sensitivity between clones generated from the same tumour(801,802). In circumstances where tumour features are not preserved it is difficult to interpret outcomes to therapeutic intervention.

PDX models have been shown to have stable gene expression and similar histopathology to the tumour of origin(609,790,791). As PDX models are generated from small human tumour fragments obtained from surgically resected tumours or metastatic biopsy specimens, they potentially have similar limitation in their representation of the original tumour(593,614,786). This was reported in colorectal cancer where multiple samples from the same tumour were engrafted in PDX models which demonstrated differential response to therapy(795). However multiple studies have reported the utility of PDX models to predict treatment response(589,592,793,803) supporting their use for evaluating treatment response in preclinical studies.

A particular advantage of the PDX model is the ability to combine sequencing data with biological data to help understand the significance of the mutations identified and their relevance as a target for therapies(793). For example, in the chordoma used for the PDX model reported here, a PI3K mutation was detected. It would be possible to confirm the presence of the mutation, and if detected, use the PDX model to assess response to treatment with a PI3K inhibitor(766,804). In a recent systematic review and meta-analysis of activation of the PI3K/AKT/mTOR pathway in solid tumours and the impact on patient survival, activation of the pathway was confirmed to be associated with a significantly worse outcome(805). Garralda et al.(793) described a PDX model where the sequencing data from the primary tumour had identified a PI3K mutation, however the PDX model did not respond to treatment with a PI3K inhibitor. The PDX model enabled a more complete analysis demonstrating that the PI3K pathway was not activated despite the presence of the mutation(793).

Creating PDX models for individual tumours has been found to provide prognostic information. Tumours which are able to engraft, often are the more aggressive and have greater metastatic potential(590,796). It has been reported that the signature of the PDX tumours is often genetically closer to the metastatic lesions than the primary tumour, suggesting that selection occurs within the initial passaging of the xenografts(590,794-796). The transformation into a more aggressive tumour was described in a chordoma PDX where a tumour characterised as a classical chordoma was used for engraftment, but transformed into a dedifferentiated chordoma in the PDX model. The transformed characterisation was in concordance with the recurrent tumour observed on relapse in the patient(767). This has the potential to provide useful information for appropriate therapeutic intervention in the clinical setting. The PDX model presented here transformed after implantation. The tumour demonstrated clonal selection of TP53 mutated cells. Sequencing of the PDX tumour identified the *TP53* mutation with 100% penetrance. The sequencing data from the primary tumour was not available for *TP53* mutation review, but in the recurrent tumour the allele frequency was 17%. This finding emphasises the importance of this mutation for tumour development, and represents a potential target for therapy(253,806-809). This effect has been observed in other tumours with respect to *TP53* mutations. In medulloblastoma it was identified that *MYC* gene amplification and *TP53* mutations commonly emerges at relapse suggesting a clonal expansion and a aggressive tumour(602). *TP53* expression has been reported to be associated with aggressive growth and significantly shorter recurrence-free survival in skull base chordomas, though this has been reported only in one study where the detection was based on an immunohistochemistry assay(810). TP53 copy number loss has also been reported in chordoma identified CGH (microarray-based comparative genomic hybridization) (125). In a recent study using targeted sequencing of 9 chordoma a *TP53* mutation was identified in 8 (89%) of the tumours. The specific mutation is a known germline mutation thought to be benign(811).

The xenograft models presented here have identified some of the inherent challenges associated with these techniques. They include immense resources in expense and time, compounded by the fact that primary chordomas are very slow to establish and as seen with similar models, a proportion of tumours do not engraft(177,589,609). Other limitations of the mouse model include the need for using immunocompromised mice for tumour engraftment and propagation and therefore have limited use for screening of immune-mediating compounds, such as vaccines and immune-modulators. Another critical aspect is the substitution of human stromal cell

compartment with murine stromal cells. Multiple studies have demonstrated that after 3-5 passages, when the model is ready for drug testing, the stromal cells are of murine origin(589,592). These changes may impact on cancer biology, altering paracrine regulation and physical properties. This is an important consideration when using therapeutics targeting the microenvironment(587,812).

It is becoming increasingly clear that novel preclinical models that closely recapitulate the heterogeneity of human tumours are needed for biological studies. For many cancers it is becoming increasingly common practice to analyse a set of 50 to 100 relevant cancer genes for hundreds of mutations. From this approach, numerous potential targets have emerged for individual patients that may potentially be linked to clinical response. In addition to bioinformatics and in silico prediction data from cancer cell line data, personalised PDX models may be useful in this setting, as they facilitate testing of candidate regimens in the patient's own tumour(582,592,813).

With the addition of our PDX to the wider chordoma research community there is an opportunity for validation of drugs that enter clinical trials for chordoma patients and provide a model for investigating chordoma cell biology. Interestingly the PDX model reported here, provided information regarding the possible driver mutation *(TP53)* for this particular tumour. This may be of therapeutic significance further supporting the role of PDX models in guiding individualised therapy.

6 BIOMARKERS IN CHORDOMA

6.1 Tumour Biomarkers

6.1.1 Circulating tumour DNA

The ever-increasing availability of sequencing data allows identification of tumour-specific genetic alterations in individual patients. These alterations include point mutations, amplifications and rearrangements. Recent technical advances have allowed these alterations to be detected in plasma(617,618,644). This can now be exploited in clinical practice for risk stratification, monitoring of disease and guiding therapy(618,634,639,652,814-816).

6.1.2 Burden of disease and minimal residual disease

The concept of monitoring for minimal residual disease by detection of persistent or recurrent mutations in childhood leukaemia and its utility to risk stratify, prognosticate, and guide treatment decisions is well established(817,818), as is monitoring for the BCR-ABL1 fusion gene in specific forms of leukaemia. Digital PCR leukaemia(819-821) was first described by Sykes et al. in 1992(822) as a method for quantifying the total number of DNA target molecules initially present in a sample, rather than PCR amplified products. This was done in an attempt to track and measure the absolute lowest number of leukaemic cells with the aim of monitoring residual disease, allowing patients with detectable recurrent disease to be treated at the earliest opportunity(823).

Many somatic cancer genes have been identified in solid tumours. Since the launch of the Catalogue Of Somatic Mutations In Cancer (COSMIC) in 2004, 136 cancer genes and more than 12000 cancer genomes have been fully curated. Currently 572 genetic mutations have been causally implicated in cancer and are listed on the Cancer Genome Consensus website (cancer.sanger.ac.uk)(824,825). Inter-tumour heterogeneity and lack of recurrent mutations have delayed the opportunity to apply the concept of monitoring for minimal residual disease in patients with solid tumours. The availability of sequencing data from individual tumours combined with technical advances has improved detection of ctDNA in plasma. This has led to the concept of ‘liquid biopsy’ with ctDNA providing the same genetic information as a tissue biopsy(623). There are clear advantages to monitoring ctDNA as a marker of tumour dynamics over conventional protein biomarkers and imaging studies; the short half-life of ctDNA allows for evaluation of treatment response and recurrence which are more sensitive than protein markers(637) and early detection of tumour specific mutation after surgery can detect recurrence predating imaging studies(618,634,636,815).

Several studies have shown that ctDNA can be a surrogate for tumour burden in patients with advanced disease. Rapid increase in ctDNA levels indicates disease progression and decline in levels correspond with response to treatment(618,634,637,826-828). Levels of ctDNA may predict treatment response early during the course of therapy, which may allow for real-time modification of the treatment regimen, avoiding prolonged exposure to toxic treatment with little or no effect(623).

In tumours where no single recurrent mutation has been identified, as in chordoma, whole tumour genome or exome sequencing is required to identify specific mutations. To date the majority of evidence of ctDNA monitoring in solid tumours is from patients with advanced disease or high-grade tumours rather than low grade or slow growing tumours(634-636).

6.1.3 Protein serum markers

Efforts have been made to discover novel cancer biomarkers but few have made it into clinical practice(829,830). Serum-based protein markers are currently used for detection and monitoring for a few specific cancers(831-833).

6.1.3.1 Aldo-keto reductase 1B10 (AKR1B10) as a serum marker

AKR1B10 is a human member of the aldo–keto reductase (AKR) superfamily, a group of proteins implicated in intracellular detoxification. *AKR1B10* was originally identified as an aldose reductase like protein mainly expressed in the human colon, the large and small intestines, the adrenal glands and at low levels in the liver. It catalyses the NAD(P)H-dependent oxidoreduction of various carbonyl compounds(834,835). More recently *AKR1B10* has been implicated in tumorigenesis and identified as a potential biomarker(836).

AKR1B10 reduces retinal to retinol, thus limiting retinoic acid formation, an important signalling molecule directing cell differentiation, thereby controlling the retinoid signalling pathway stimulating carcinogenesis(837). Under physiological conditions, highly reactive aldehyde and ketone groups lead to cell death by carbonyl-induced apoptosis. *AKR1B10* plays a role in the detoxification of cytotoxic carbonyl compounds and promotes cell survival by controlling carbonyl metabolism(838). Furthermore, *AKR1B10* can reduce the carbonyl groups and participate in the metabolism of some anticancer drugs, thereby decreasing effectiveness and has been linked with drug resistance in cancer derived cell lines(836,839-841).

6.1.3.2 *AKR1B10* and tumorigenic formation

AKR1B10 in cancer was initially described in hepatocellular carcinoma (HCC)(842) and found to be a prognostic biomarker. High levels of expression indicate less aggressive tumour behaviour(843) and low levels correlate with advanced disease(844). More recently *AKR1B10* was found to be up-regulated in pre-neoplastic conditions such as chronic hepatitis and cirrhosis(845,846) suggesting a role in the pathogenesis of HCC. *AKR1B10* has also been found to be implicated in tumour carcinogenesis in breast cancer(847), bladder cancer(848), smoking induced lung cancer(849,850), endometrial cancer(851) and pancreatic cancer(852).

AKR1B10 has been described as a potential protein biomarker in patients with breast cancer. Overexpression was found to be associated with increased tumour size, lymph node metastasis and inversely with patient survival. Expression in the primary tumour correlated with metastatic deposits in lymph nodes and protein levels were found to be significantly elevated in serum from patients with breast cancer supporting its use as a potential serum marker(853).

6.1.3.3 AKR1B10 and it role in chordoma

The AKR1B10 gene locus (7q33) has been identified as a putative chordoma susceptibility region by genome-wide linkage studies in familial chordoma(19). No mutations or loss of heterozygosity have been identified for the gene, but chromosomal gain of the region has been described(125,135). *AKR1B10* is differentially expressed in chordoma compared to other bone and soft tissue tumours(33). It has been found to be expressed in all benign and malignant notochordal tumours but not in embryonic notochord or notochordal rests(197,854). AKR1B10 has also been linked with brachyury. Brachyury was found to indirectly regulate *AKR1B10* expression in the U-CH1 chordoma cell line(127). Despite this potential association no previous work has investigated AKR1B10 as a biomarker in chordoma. *AKR1B10* expression levels may be prognostic if correlated with clinical outcome, and could potentially be a plasma marker for monitoring disease.

6.2 Aim

The aim of this work was to establish proof of concept for detecting ctDNA in plasma from chordoma patients, and to establish if AKR1B10 could be detected and used as a protein serum biomarker for disease monitoring.

6.3 Objectives

1. To select mutations, identified by Sanger Sequencing, in a group of chordoma patients for which TaqMan assays could be developed and to establish proof of concept for mutation detection in ctDNA from chordoma patients.
2. To compare dPCR to Ion Torrent sequencing for detection and quantification of mutations in chordoma.
3. To establish if AKR1B10 protein represents a potential tumour marker in patients with chordoma.

The work in this chapter on circulating DNA was done with support from Tim Forshew PhD and Alice Gutteridge from Tim Forshew's lab at UCL, London.

6.4 Results

6.4.1 Mutations detected in chordoma

Whole genome (n=9) and exome (n=23) sequencing of chordoma from 32 chordoma patients was performed at the Wellcome Trust Sanger Institute. Only 12 of these tumours had mutations detected in known cancer genes; *CDKN2A* (n=6), *PTEN* (n=1), *PIK3CA* (n=2), *SOX5/6* (n=3), *TP53* (n=1), *PTPRD* (n=1), *ARID1A* (n=1), *MIFT* (n=1), *SMAD4* (n=1), *PBRM1* (n=1), *SETD2* (n=1). Some tumours had 2 mutations (n=4) whilst 2 tumours had a total of 3 mutations in known cancer genes. Of these 12 tumours 4 were identified for this project, each with one or two mutations of interest.

Mutations were selected based on the ability to design a TaqMan probe by which they could be detected and for whom plasma samples were available. For 2 of 4 patients pre-op plasma samples were available, one patient had surgery 8 years earlier but had recurrent progressive disease at the time of plasma sampling and was included as a pre-op sample in view of progressive and measurable disease. No sequential samples were available for this patient. For one mutation, which was selected for the study, it was subsequently discovered that only a post-op plasma sample was available. The patient sample was included in the analysis.

Patient demographics were collected (Table 6.1). The follow-up time was between 3-12 years (mean 6 years). Three patients are alive and in clinical remission, one patient (patient 4) had died of metastatic disease. This patient was known to have recurrent disease with small volume metastases at the time of the tumour biopsy, and collection of plasma.

Table 6.1 Patient demographic, treatment and mutations detected in tumour

Patient ID	Sex	Age	Tumour	Histology	Disease status	Treatment	Mutation
1 (3814)	F	74	Sacral	Conventional	Stable	Surgery & Radiotherapy	*PIK3CA*
2 (7187)	F	65	Sacral	Conventional	Stable	Surgery & Radiotherapy	*PIK3CA* *SETD2*
3 (4927)	M	56	Sacral	Conventional	Stable	Surgery	*GENE X*
4 (7186)	M	67	Metastatic lesions (multiple) small volume	Conventional	Progressive	Surgery & proton beam therapy + TKI	*GENE X*

Mutation sequences are listed in Table 6.2. Please note the name of one mutation has been changed to *GENE X* as publication for this data is pending. The primer sequences are listed in Material and Methods Chapter 2. Selection and optimisation of the primers included target amplification visualised by electrophoresis and target sequencing confirming specificity of primers (data not shown). The assay probes were tested using tumour DNA from formalin-fixed paraffin-embedded (FFPE) samples. Optimisation of assays included testing primers across a temperature gradient, dilution of DNA samples in order to dilute potential inhibitors remaining in the sample after DNA extraction, and performing restriction digest to overcome cross-linking caused by formalin from FFPE samples. Data for this can be found in the appendix. Only the temperature optimisation of primers was relevant for evaluating ctDNA in the plasma samples.

Table 6.2 Mutations (annotated sequences)

PIK3CA (1) Wild-type (WT)	CCDS43171.1 / r.1790g>a / c.1633G>A / p.E545K / **missense** chr3:178935992-178936191 5'pad=100 3'pad=100 TTACAGAGTAACAGACTAGCTAGAGACAATGAATTAAGGGAAAATG ACAAAGAACAGCTCAAAGCAATTTCTACACGAGATCCTCTCTCTGA AATCACT**G**AGCAGGAGAAAGATTTTCTATGGAGTCACAGGTAAGT GCTAAAATGGAGATTCTCTGTTTCTTTTTCTTTATTACAGAAAAAAT AACTGAATTTGGCTGA
PIK3CA (1) Mutant (MT) ID: 3814	TTACAGAGTAACAGACTAGCTAGAGACAATGAATTAAGGGAAAATG ACAAAGAACAGCTCAAAGCAATTTCTACACGAGATCCTCTCTCTGA AATCACT**A**AGCAGGAGAAAGATTTTCTATGGAGTCACAGGTAAGT GCTAAAATGGAGATTCTCTGTTTCTTTTTCTTTATTACAGAAAAAAT AACTGAATTTGGCTGA
PIK3CA (2) WT	CCDS43171.1 / r.3286g>u / c.3129G>T / p.M1043I Sub **missense** chr3:178951975-178952174 GCCAGAACTACAATCTTTTGATGACATTGCATACATTCGAAAGACC CTAGCCTTAGATAAAACTGAGCAAGAGGCTTTGGAGTATTTCATGA AACAAAT**G**AATGATGCACATCATGGTGGCTGGACAACAAAAATGG ATTGGATCTTCCACACAATTAAACAGCATGCATTGAACTGAAAAGA TAACTGAGAAAATGAAA
PIK3CA (2) MT ID: 7187	GCCAGAACTACAATCTTTTGATGACATTGCATACATTCGAAAGACC CTAGCCTTAGATAAAACTGAGCAAGAGGCTTTGGAGTATTTCATGA AACAAAT**T**AATGATGCACATCATGGTGGCTGGACAACAAAAATGGA TTGGATCTTCCACACAATTAAACAGCATGCATTGAACTGAAAAGAT AACTGAGAAAATGAAA
SETD WT	CCDS2749.2 / r.6799delC / c.6756delC p.S2253fs*56 **Del** **frameshift** chr3:47098418-47098617 ACTGCTGCTGTACACTGACAGACTGTTGGTTTGAATCCCAAACACT ATAATTCTGTCCCTGAACTGGGCCGGGGGCCGGCACTGGCAAGA CAGCAACG**C**TGGAGTCTTGGTGTACTACACCATCACTCTGGGCCA CATACTGGGAACTGGAAACTTCCACAGGAGCTGCCACATGTGGCA CCACTGGTACTGGTGGAGGG
SETD	ACTGCTGCTGTACACTGACAGACTGTTGGTTTGAATCCCAAACACT

MT ID: 7187	ATAATTCTGTCCCTGAACTGGGCCGGGGGCCGGCACTGGCAAGA CAGCAACG_TGGAGTCTTGGTGTACTACACCATCACTCTGGGCCA CATACTGGGAACTGGAAACTTCCACAGGAGCTGCCACATGTGGCA CCACTGGTACTGGTGGAGGG
GENE X (1) WT	CCDS31062.1 r.9069_9073delGUUAU c.8894_8898delGTTAT p.C2965fs*6 **Del frameshift** chr1:2358[redacted]-2358[redacted] GACCATAGTTCTCTGCTATATTTATATGTTGAGTCAAGAAGCCACT ATTACCT[redacted]ATCCCTAAGGAGATACTTATTTGGAA TAGTTA**AATAAC**ATCTCTGTAAACGTCTCCTCTCTCGATTTGGCCC TTCTGTTG[redacted]CATGAGGTTGGATAGTAGATGGGGTC ATACCATACTGCTCTG
GENE X (1) MT ID 4927	GACCATAGTTCTCTGCTATATTTATATGTTGAGTCAAGAAGCCACT ATTACC[redacted]ATCCCTAAGGAGATACTTATTTGGAA TAGTTA**A**ATCTCTGTAAACGTCTCCTCTCTCGATTTGGCCCTTCTG TTGGATC[redacted]GTTGGATAGTAGATGGGGTCATACC ATACTGCTCTG
GENE X (2) WT	CCDS31062.1 / r.2960_2961insggcu / c.2785_2786insGGCT p.Y929fs*3 **Ins frameshift** chr1:2359[redacted]-23596[redacted] TCTGCTGCTTGGTGCATATGTTCAGGAGAAGGCAAGACAAGGCTC TCGAGAGA[redacted]TATGACTTAAAGGCTCGCTGGCT GTGCTGTCA**T**AGCCAGAAGTATCTTCTGAGTCATTGGCCGACTCC CTGTCAG[redacted]TTACGCATAAAAAAGCCACACAGA GGAATAGGTTTATTGTGTT
GENE X (2) MT ID: 7186	TCTGCTGCTTGGTGCATATGTTCAGGAGAAGGCAAGACAAGGCTC TCGAGAGAT[redacted]TATGACTTAAAGGCTCGCTGGCT GTGCTGTCA**TAGCC**AGCCAGAAGTATCTTCTGAGTCATTGGCCGA CTCCCTGTC[redacted]TACTTACGCATAAAAAAGCCACA CAGAGGAATAGGTTTATTGTGTT

Mutations (MT): (blue)/ Wild-type (WT) black, specific mutation highlighted (red/black) identifying the change. CCDS-number is the identifier in the NCBI Consensus Coding Sequence Database.

Two patients had known hotspot mutations in the *PIK3CA* gene. Alterations was found in *GENE X* in two chordomas, which has not been linked with any other cancer, but was confirmed to be somatic through evaluation of germline DNA from the same patients. CtDNA was assessed by droplet digital Polymerase Chain Reaction (dPCR), described in Materials and Methods.

6.4.2 Capture of mutation by digital PCR is as sensitive as Ion torrent

Each assay was individually designed to enable patient-specific mutation detection. The advantage of using dPCR includes a quick turn around time as each assay can run with a few samples at no extra cost. Two of the mutations identified were within the *PIK3CA* gene. This gene is known to have well characterised cancer hotspot mutations, identifiable using a cancer-gene panel. To evaluate the methodology it was of interest to establish if the sensitivity of dPCR was comparable to Ion Torrent

sequencing, which is currently the gold standard for detection and quantification of mutations, using specific cancer-gene panels for known cancer gene mutations. The Ion Torrent is a more expensive technique, and there is a delay in data output, as the assay requires a higher number of samples per run to be cost efficient.

The allele frequency was tested using tumour DNA from the two patients with *PIK3CA* mutations. The sensitivity correlated well between dPCR and the Ion Torrent *(the Ion Torrent analysis was run by Carlos De Andrea, PhD Scientist in UCL Advanced Diagnostic).*

Table 6.3 Sensitivity of detection rate with Digital PCR and Ion Torrent

Patient ID	Detection by ddPCR	Detection by Ion Torrent
1 (3814)	22.7%	25.07%
2 (7187)	19.4%	21.34%

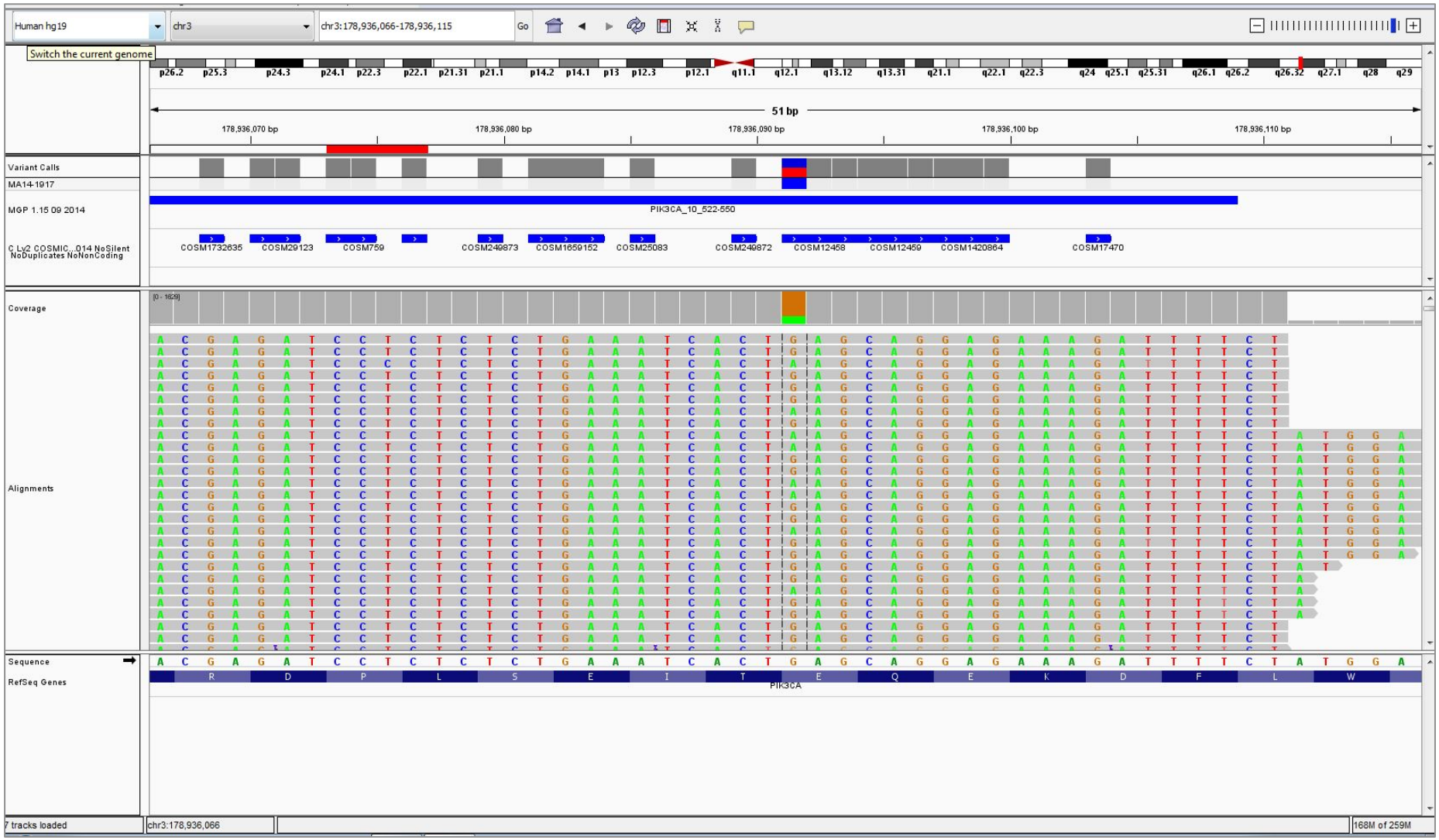

Figure 6.1 Ion Torrent detection of *PIK3CA* mutation

Screen shot showing the *PIK3CA* mutation: p.Glu545Lys (c.1633G>A, allele frequency: 25.07%). A: green, G: brown; mutation. *PIK3CA* p.E545K hotspot mutation has been reported nearly 2000 times in COSMIC database.

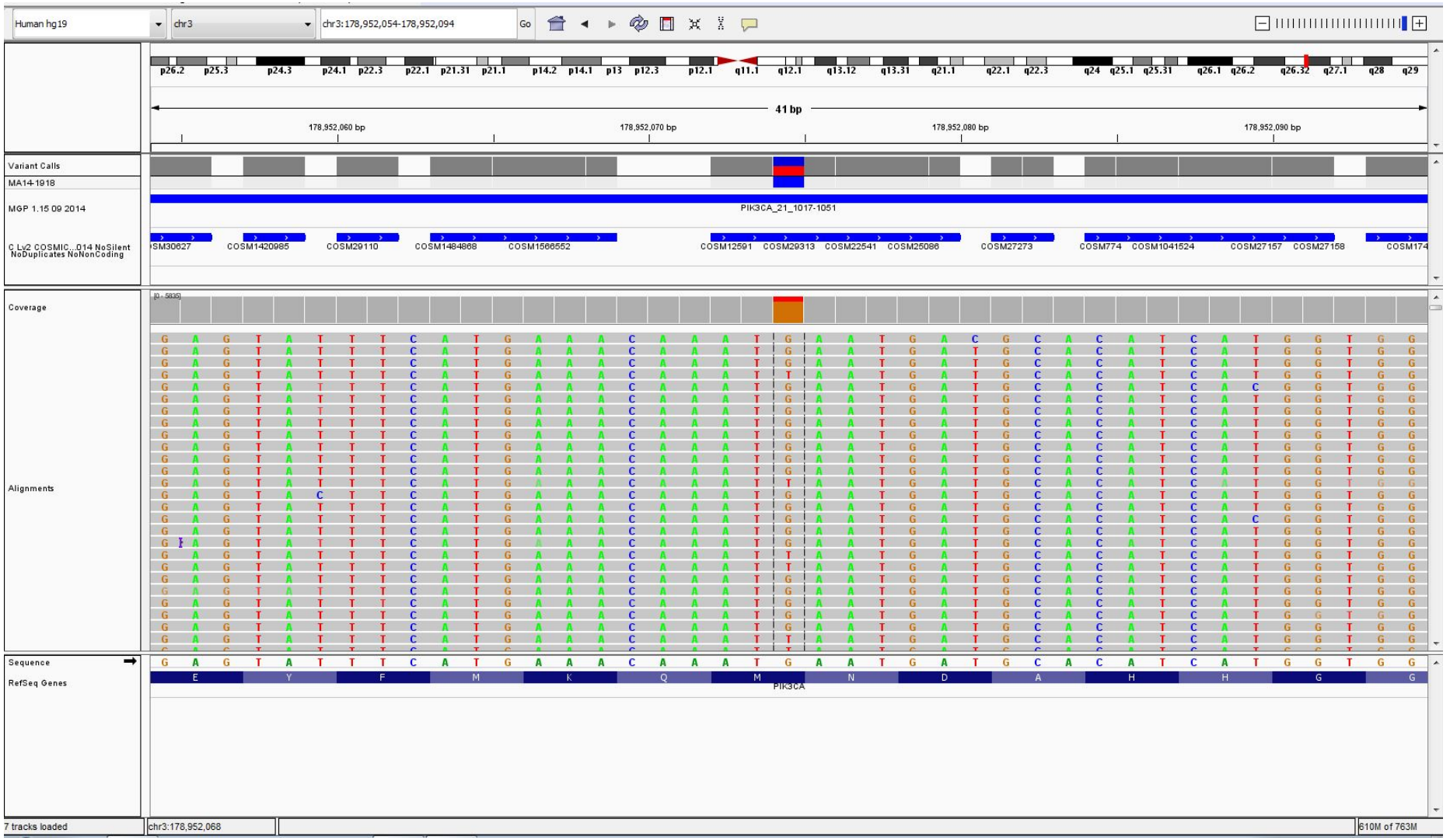

Figure 6.2 Ion Torrent detection of *PIK3CA* mutation
Screen shot showing the *PIK3CA* mutation: p.Met1043Ile (c.3129G>T, allele frequency: 21.34%). G: brown, T: red; mutation. *PIK3CA* p.M1043I hotspot mutation has been reported about 60 times in COSMIC database.

6.4.3 Detection of tumour-specific ctDNA in plasma

Detection of tumour-specific mutations in plasma was done by dPCR. Low levels of copy numbers were detected for three of four patients. The development of the probe for one of the *GENE X* mutations failed, as no differentiation was possible between the mutation and the wild-type sequence in the tumour sample. The plasma sample was therefore not analysed.

Below is the dPCR data from the multiplexed experiments viewed in a 2-D plot. The detection of mutation (channel 2 / y-axis) is plotted against the wild-type sequence (channel 1 / x-axis). The data represents detection of the mutation/wild-type in the tumour demonstrating the presence of the targets and the ability of the assay to detect the target sequences. Notably the frequency of mutation detection in the plasma is much lower than in the tumour DNA (Table 6.4).

Figure 6.3 Result of dPCR for *PIK3CA*(1) mutation in tumour and plasma
Data from a duplex experiment in which two targets are PCR amplified and viewed in a 2-D plot: channel 1 fluorescence (FAM/mutant)(y-axis) is plotted against channel 2 fluorescence (VIC/wild-type)(x-axis) for each droplet. Analysis by QX200 droplet reader; the blue dots indicates droplets with the amplified mutant sequence, the green dots represents droplets containing the wild-type sequence, the orange droplets contains both wild-type and mutant molecules, and the grey dots are droplets that did not contain the amplified target sequence. (A) Assay for the FFPE tumour sample. (B) Plasma: one mutant molecule was detected; this was noted in 2 of 4 runs. The blue and green droplet identification is manual. Non-template control (NTC)(i.e. water) was negative.

Figure 6.4 Result of dPCR for *PIK3CA*(2) mutation in tumour and plasma
Analysis by QX200 droplet reader; the blue dots indicates droplets with the amplified mutant sequence, the green dots represents droplets containing the wild-type sequence, the orange droplets contains both wild-type and mutant molecules, and the grey dots are droplets that did not contain the amplified target sequence. (A) FFPE tumour sample, (B) plasma: 1 mutant molecule was detected.

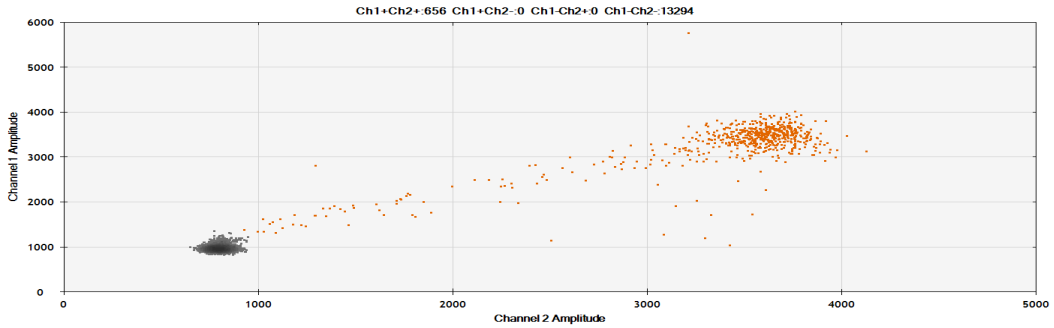

Figure 6.5 Result of dPCR for *SETD2* mutation in tumour sample
Analysis by QX200 droplet reader; *SETD2* insertion mutation run at 60°C; the assay did not work as the SETD2-probe was non-specific for mutant/wild-type tested in FFPE tumour sample. The orange droplets contain both the wild-type and mutant DNA indicating the probes inability to discriminate between the two sequences. Grey droplets are either empty or does not contain the amplified target sequence.

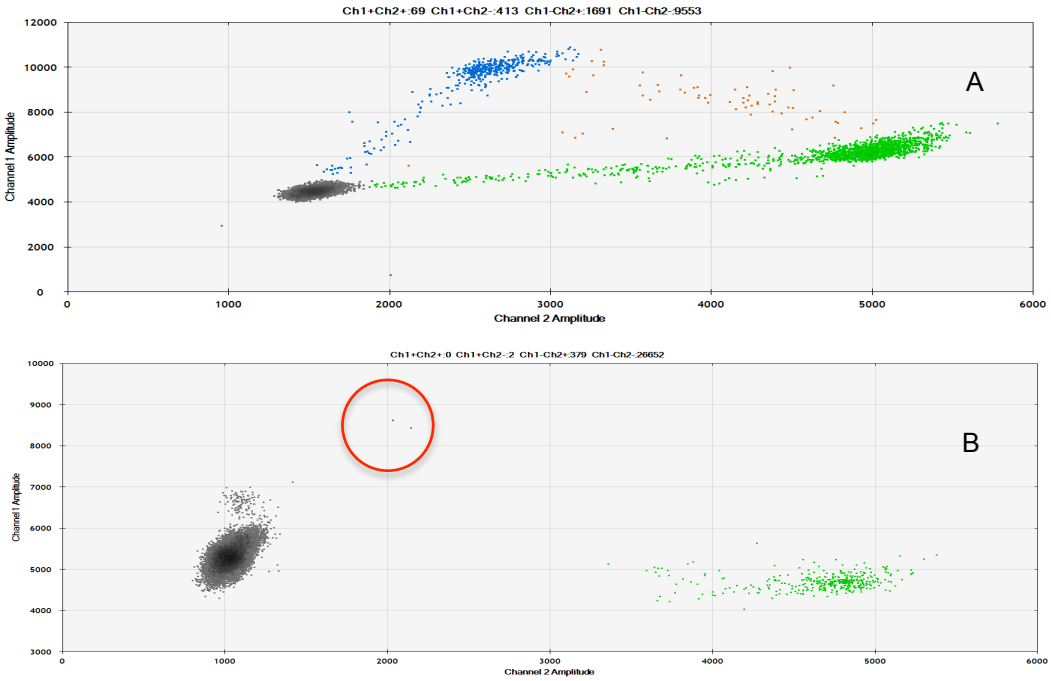

Figure 6.6 Results of dPCR for *GENE X*(2) mutation in tumour and plasma
Droplet Digital PCR data from a duplex experiment in which two targets are PCR amplified viewed in a 2-D plot in which channel 1 fluorescence (FAM/mutant) is plotted against channel 2 fluorescence (VIC/wild-type) for each droplet. Analysis by QX200 droplet reader; *GENE X*(2) insertion frame-shift mutation. (A) Tumour sample assay, (B) plasma: two mutant molecules were detected in plasma (demonstrated within the red circle), in total 4 molecules were detected in approximately 1,8mL of plasma (2 molecules/run).

Table 6.4 Results of ctDNA in plasma from 3 chordoma patients

Patient ID	Surgery status	Mutation	# FAM-positive droplets	Mutant copies/mL plasma	Total copies/mL plasma	% Mutant	Equivalent plasma volume (µL)	Mean mutant copies/mL plasma
1 (3814)	POST	PIK3CA	0	0.0	1243	0.0%	1122	0.6
			1	1.3	1172	0.1%	1046	
			0	0.0	925	0.0%	1072	
			1	1.2	1200	0.1%	1086	
2 (7187)	PRE 1	PIK3CA	0	0.0	1004	0.0%	835	0.3
			1	1.5	857	0.2%	949	
			0	0.0	1141	0.0%	786	
			0	0.0	747	0.0%	850	
			0	0.0	624	0.0%	740	
			0	0.0	489	0.0%	962	
4 (7186)	Recurrent	GENE X	2	4.5	1220	0.4%	794	4.1
			2	3.7	1143	0.3%	703	

Summary table of the results, patient ID, timing of samples taken in relation to surgery (pre-/post op, or at recurrence), mutation identified by exome sequencing, positive droplets (total/run), mutant copies/mL and total copies of droplets (wIld-type and mutant), percentage of mutant copies compared to wild-type, plasma volume tested, and mutant copy number/mL of plasma total from all runs.

For patient 1 (ID 3814) the plasma sample used was taken 5 years after surgical resection and radiotherapy. The sample tested positive at low levels for tumour-specific mutant *PIK3CA*. The patient has no clinical evidence of recurrent disease 3 years after the sample was taken. No pre-op or additional samples were available for this patient.

For patient 2 (ID 7187) a pre-op sample was tested, this patient had both a *PIK3CA* and a *SETD2* mutation. This patient had low levels of mutant DNA detected using the PIK3CA probe. The Taqman probe for the *SETD2* mutation did not work, as the SETD2 probe was non-specific for mutant/wild-type. The patient had been treated with surgery and radiotherapy. A recent MRI reported stable disease, serial post-op samples were not tested for the mutation, as levels were low prior to surgery and the patient continue to be in clinical remission.

For patient 3 (ID 4927), no results are available, as various attempts to generate a probe for the *GENE X* deletion failed.

Patient 4 (ID 7168) had recurrent metastatic disease at the time the sample was taken. The tumour harboured a *GENE X* mutation. The initial surgical resection for the patient's primary disease had been done 8 years earlier. Since then the patient has suffered multiple recurrences, undergone further surgery, and received proton beam therapy. Various targeted therapies including: Sirolimus, Imatinib, and Dasatinib had been trialled. This patient had the highest level of mutant copies detected compared to the other patient samples tested, though still accounting for a low level of mutant copies.

6.4.3.1 Sensitivity and specificity

Pooled plasma controls (blood collected from 12 healthy controls, from whom the plasma was mixed to generate identical aliquots) and high quality genomic DNA (Bioline) was tested to assess for false positive droplets. No false positive (mutant droplets) were observed in the pooled plasma or the genomic DNA. The false positive rate for the PIK3CA(1) assay was determined to be lower than 1 in 18945 wild-type copies of DNA equivalent to < 0.005% combining all runs with this assay. The false positive rate for the PIK3CA(2) assay was less than 0.003% and the false positive rate for the GENE X assay was determined to be lower than 1 in 12,536 wild-type copies of good-quality human genomic DNA (equivalent to 0.008%), and lower than 1 in 29,930 for heat-denatured DNA (equivalent to 0.003%). Combining the runs for the GENE X

assay the false positive rate was determined to be less than 1 in 42,466 wild-type copies equivalent to less than 0.002%. None of the non-template controls (NTC) run with each assay had positive droplets ensuring no cross contamination across wells.

Table 6.5 Control for false positive droplets

Assay	Sum of mutant	Sum of wild-type	Sum of WT and MT	Sum of Total copies	Equivalent mutant %
PIK3CA_1 (total)	**0**	**16850**	**5**	**18945**	**0.005%**
Denatured DNA	**0**	**3683**	**1**	**3971**	0.025%
Pooled plasma control	0	257	1	265	
BioLine gDNA	0	3426	0	3706	
non-denatured DNA (total)	**0**	**13167**	**4**	**14974**	0.007%
Pooled plasma control	0	168	0	172	
BioLine gDNA	0	12999	4	14802	
PIK3CA_2 (total)	**0**	**32514**	**5**	**39323**	**0.003%**
Denatured DNA	**0**	**19741**	**4**	**28644**	0.003%
BioLine gDNA	0	19741	4	28644	
non-denatured DNA	**0**	**12773**	**1**	**10679**	0.009%
BioLine gDNA	0	12773	1	10679	
LYST_2 (total)	**0**	**32611**	**0**	**42466**	**0.002%**
Denatured DNA	**0**	**23076**	**0**	**29930**	0.003%
Pooled plasma control	0	56	0	57	
BioLine gDNA	0	23020	0	29873	
non-denatured DNA	**0**	**9535**	**0**	**12536**	0.008%
Pooled plasma control	0	55	0	56	
BioLine gDNA	0	9480	0	3056	

This table shows that no 'mutant only' (blue) droplets were detected in our controls (false positive). Pooled plasma was tested from healthy controls as well as purchased genomic DNA (gDNA) both were tested as denatured DNA, and non-denatured DNA. The wild-type detection rate in green column (WT) and the sum of total copies include all droplets (orange column). False positive rate was calculates as <1 per total number of droplets for each individual run of gDNA and pooled plasma DNA. The total false positive detection rate was calculated as <1 per total number of droplet for each assay. The difference here is between positive droplets (coloured columns) and copies screened ('sum of total copies'). The Poisson distribution is applied to the droplet counts to get the copies screened, in order to account for multiple copies of DNA co-occurring in a single droplet – the orange droplets have at least 1 mutant and 1 wild-type sequence. The more concentrated the sample, the more likely that a mutant/wild-type droplet also has more than one copy inside it. The false positive detection rate for the PIK3CA(1) assay was <0.005%, for the PIK3CA(2) the false detection rate was < 0.03% and for the GENE X assay was determined to be lower than 0.002%.

6.4.3.2 Extraction efficiency of DNA from plasma

The extraction efficiency of DNA from plasma was assessed by adding an exogenous (frog/XenT) DNA spike into the plasma sample prior to DNA extraction in order to establish the efficiency and to rule out that the low mutation detection rate was not due to poor DNA extraction(685). The extraction efficiency of DNA was consistent with a mean of 75% of DNA recovered from the samples.

Table 6.6 Extraction efficiency for each assay

Mutation	Patient ID	# FAM-positive droplets*	Mutant copies/mL plasma	Total copies/mL plasma	XenT efficiency
PIK3CA(1)	3814	0	0	1243	**79%**
	3814	1	1	1172	**85%**
	3814	0	0	925	**71%**
	3814	1	1	1200	**81%**
GENE X(2)	7186	2	5	1220	**72%**
	7186	2	4	1143	**73%**
PIK3CA(2)	7187	0	0	1004	**79%**
	7187	1	2	857	**81%**
	7187	0	0	1141	**85%**
	7187	0	0	747	**67%**
	7187	0	0	624	**70%**
	7187	0	0	489	**59%**
				Mean:	**0.7515107**
				SD:	**8%**

Percentage of XenT recovered. Relative detection of the XenT was compared to a endogenous control RPP30.

6.5 AKR1B10 in chordoma

AKR1B10 protein has been reported to be measurable at low levels in plasma from healthy controls(853). To establish if AKR1B10 was detectable at elevated levels in plasma from patient with chordoma, plasma samples taken prior to surgery were used. Four patients with large sacrococcygeal chordomas for whom plasma samples were available had been identified for the study. None of the patients had metastatic disease. Enzyme-linked immunosorbent assay (ELISA) was used for detection of AKR1B10 in plasma samples as described in Materials and Methods.

Table 6.7 Demographic of Patients in study for AKR1B10 detection in plasma

Sample ID	Sex	Age at diagnosis	Tumour location	Tumour size (mm)	Histology type	Outcome	Metastatic disease Y/N
31403	M	67	Sacrum	155 x 70 x 130	Conventional	Deceased	N
20603	F	67	Sacrum	170 x 110 x 140	Conventional	Recurrence	N
29192	M	60	Sacrum	280 x 150	Conventional	Stable	N
6583	M	63	Sacrum	210 x 110 x 30	Conventional	Recurrence	N

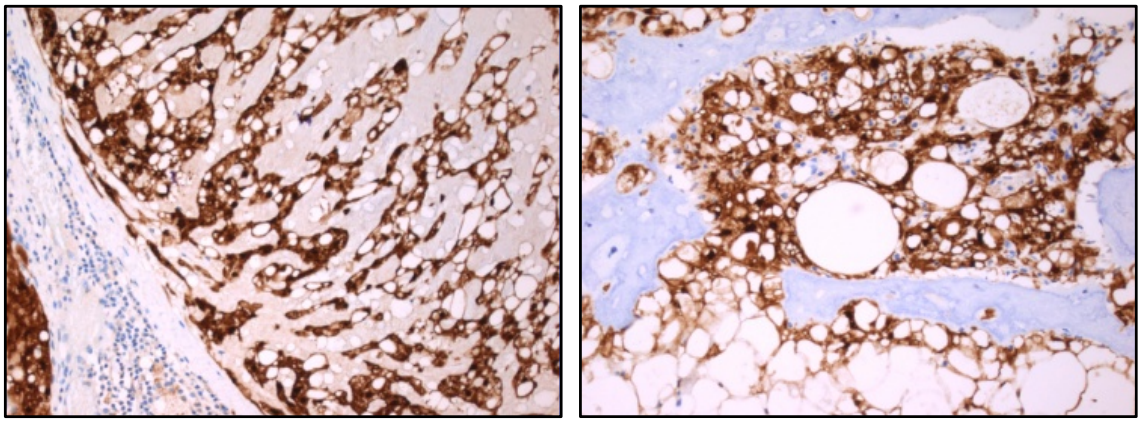

Figure 6.7 AKR1B10 protein expression in chordoma
Light photomicrograph of a representative case of a chordoma showing immunoreactivity for AKR1B10 (images provided by Professor A. Flanagan).

Three chordoma cell lines were tested for *AKR1B10* gene expression by RT qPCR. Variation in expression levels was observed between cell lines. The expression levels of *AKR1B10* correlate with the relative gene expression level of brachyury.

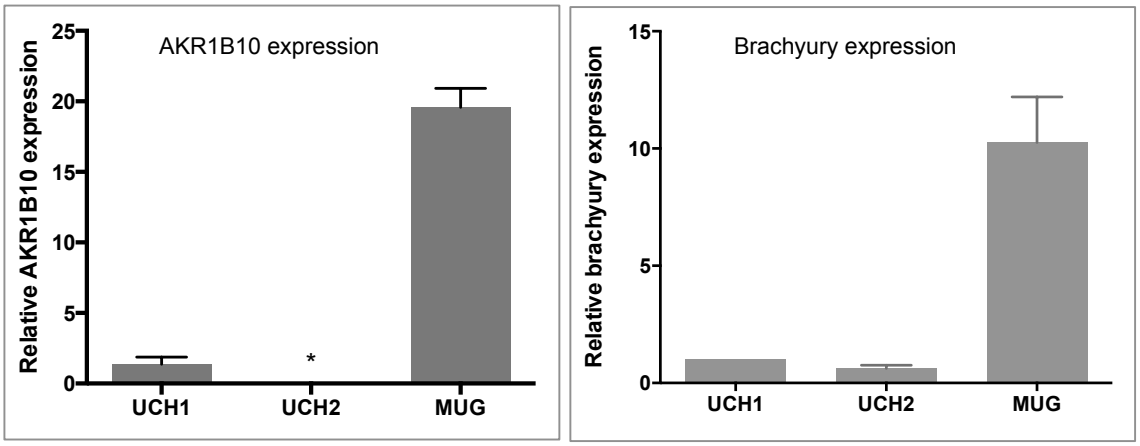

Figure 6.8 *AKR1B10* gene expression (mRNA) in chordoma cell lines
RT qPCR data for relative expression levels of *AKR1B10* and brachyury across three chordoma cell lines: U-CH1, U-CH2 and MUG Chor (*UCH2 *AKR1B10* expression 0.0003). Expression of *AKR1B10* and brachyury was corrected to the endogenous *PGK* expression as a reference gene, and normalised to U-CH1 expression levels. Error bars demonstrate SD.

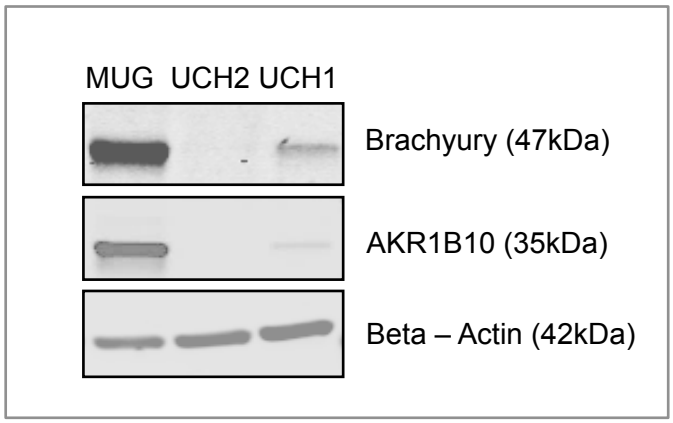

Figure 6.9 AKR1B10 expression (protein) in chordoma cell lines
Western blot demonstrating brachyury and AKR1B10 expression with Beta-actin used as a loading control.

6.5.1 AKR1B10 not detectable in plasma from chordoma patients

AKR1B10 protein was not detected in plasma from the chordoma patients despite all of their tumours demonstrating immunoreactivity for this protein (data not shown), and having large tumours in situ at the time of the sampling. The levels detected were below the detection level for the negative control. Lysate from the MUG Chor cell line used as a positive control, had levels above 1.25ng/mL.

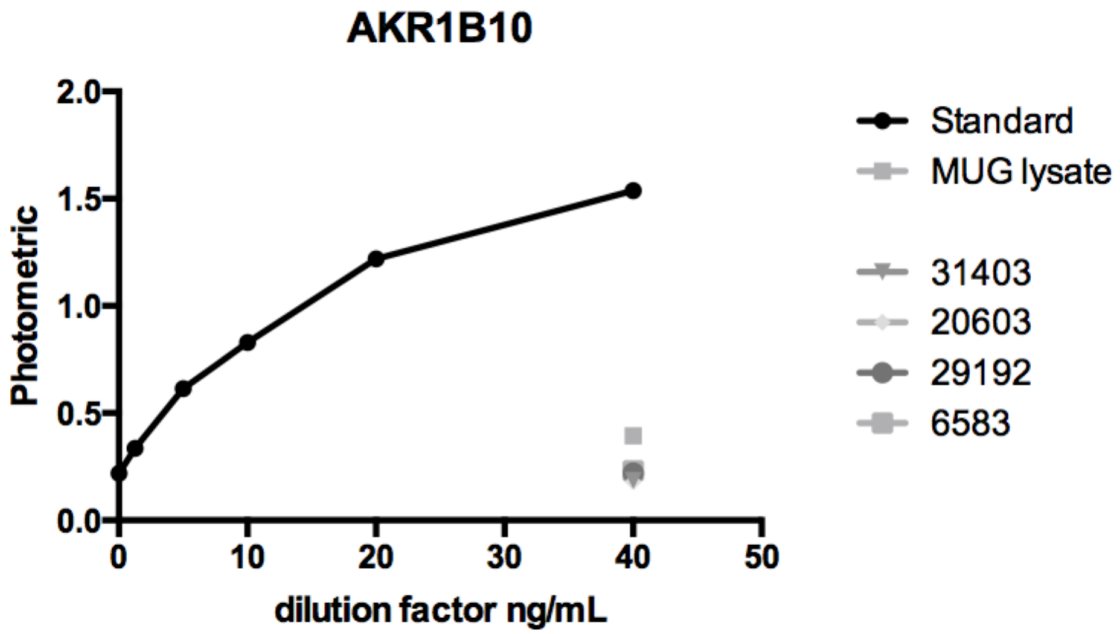

Figure 6.10 AKR1B10 protein not detectable in plasma from chordoma patients
ELISA assay of AKR1B10 level in patients samples (31403, 20603, 29192, 6583) were at the level of the negative control. Photometric readout was done measuring absorbance at 450nm with the correction wavelength set at 540nm, using a 96-well plate reader Anthos 2001 spectrophotometer. The samples and the positive control were plotted with the un-diluted sample (the stock solution of 40ng/mL). Data represent 2 separate experiments run with duplicate samples. The standard: serial dilution of recombinant AKR1B10 (0-40ng/mL).

6.6 Discussion

Genomic analysis had identified tumour specific mutations in chordoma. The work presented here establish proof of concept that tumour-specific ctDNA is detectable in plasma from chordoma patients, though at very low levels. The assays worked well for the tumour DNA samples, providing confidence in the generated probes and their ability to detect the mutations. The amplitude for the *PIK3CA*(1) mutation detected in patient 1 was low suggesting a need for caution regarding calling this a true mutant droplet. A low amplitude or fluorescence could be a technical issue or might indicate damaged DNA or late amplification due to inhibitors, neither of which is commonly seen in plasma(685). The clinical scenario suggest that this result may represent a false positive as this patient had surgery 5 years prior to the sample collection, which was done 3 years ago. In this time frame the patient has remained in clinical remission. For the other mutations detected (*PIK3CA* and *GENE X*) the amplitude was satisfactory, and those samples were collected whilst the patients had measurable disease. With very low copy numbers it can be assumed that this value directly correlates to the number of mutant molecules, and the reason for low detection may reflect low mutant allele frequency(855,856). Experiences so far suggest that false positive are unlikely as benign lesions and non-neoplastic conditions do not give rise to ctDNA mutations(617,857,858).

6.6.1 Sensitivity and specificity of ctDNA

Digital PCR has been shown to be highly sensitive and specific(641), Milbury et al. (859) detected 1 mutant molecule in 180.000 wild-type molecules and one mutant molecule in over four million WT molecules when screening 70 million copies of DNA, with the limit of detection (LoD) being restricted by the amount of amplifiable DNA analysed. Mutation detection assays using dPCR can have false-positive molecules detected which might arise from the fluorescence detection (“system”) noise, and molecular biology (“assay”) noise(859). It is known that PCR polymerase error can occur at approximately $1x10^{-5}$ with a propensity to base substitute A-T to G-C(860). The false positive detection rate in the same study by Milbury et al. (859) was 1 in 14 million. Other studies have reported detection of mutant molecules at levels down to 1-2 molecules/mL accepting these as positive samples as their negative control assays did not show any mutant molecules(635,651). In a study of 52 breast cancer patients the sensitivity of dPCR assay allowed for the detection of a mutant allele fraction of 0.1% or more(634) which is similar to the detection in the 3 of 4 chordomas. Importantly no false positives were detected in the controls used for the study reported

here. The mutant template was not detected in all samples (false negative), this can be explained by low copy number due to the low turnover of cells characterising a slow growing tumour such as chordoma. This may also explain why the levels of wild-type molecules generated from plasma from patients with chordoma were not elevated as often observed in cancer patients, particularly in advanced disease. Diehl at al. describe levels in healthy controls ranging from 1150-8280 DNA fragments/mL whilst for patients with colorectal cancer the levels ranged from 1350-230,000 DNA fragments/mL(617,635,861). In the samples used there the highest levels of wild-type DNA was about 1200 copies (fragments)/mL.

The ability to isolate ctDNA is dependent on adherence to stringent standards of procedures for sample collection and storage as well as the methodology for extraction of DNA from plasma. This has in particular been demonstrated in the use of cfDNA in prenatal diagnostics(862-865). It is well described that the level of cfDNA increases with time following the venepuncture as lysis of white cell leads to release of genomic DNA. This may result in decreased sensitivity of detection of ctDNA(864,866). For the study presented here peripheral blood was collected into EDTA collecting tubes and was stored on ice until it was subjected to centrifugation for separation of plasma, within one hour. Isolation of plasma was done in accordance with published protocols(618). It has been reported that the absolute quantity of fetal DNA remained stable for up to 24 hours when the sample was left unprocessed at room temperature(865,867). And a different study did not detect differences in quantities of cfDNA after samples had been thawed and refrozen(868). The low level of detection of ctDNA reported here is therefore not likely to be due to potential divergence from the standard of procedure. Extraction of DNA from plasma is critical in ensuring clinical sensitivity for measuring small quantities of ctDNA(685). The kit used for this study has been reported to have the highest extraction efficiency when compared with other similar kits(685). The efficiency for all the assays were analysed demonstrating a 70-85% recovery. One aspect however, which may have compromised the detection of ctDNA in this study, is the dPCR analysis on the 200QX BioRad analyser. After completion of the analysis reported here, and following servicing of the machine it was discovered that there had been an issue with dead-space. Analysis had therefore been performed on approximately 10000 droplets rather then the expected 20,000 droplets/sample, potentially underestimating the level of ctDNA.

Bettegowda et al.(635) found the concentration of ctDNA in plasma correlated with the stage of disease. Yet, they were able to detect the presence of ctDNA in 50% of patients across 14 tumour types with early stage (localised) disease. Most chordomas are localised and recur locally(56). The patient with evidence of systemic disease with widespread metastases included in the study presented here had the highest level of ctDNA. Interestingly in the study by Bettegowda et al. they found that mucinous histology was associated with low detection of ctDNA. Chordomas are mucinous tumours, and the fact that they are slow growing with limited necrosis formation account for factors recognised to influence the level of ctDNA(623), and further explain the low levels detected in plasma from the patients with chordoma presented here.

To increase the specificity for tumours with low levels of ctDNA to ensure confidence in the detection of tumour recurrence without imaging studies to support this. Screening for more than one tumour-specific mutation or for tumour-specific rearrangements could be considered. Most solid tumours have up to a dozen rearrangements or translocations, with the majority being passengers rather than driver mutations(869). In chordoma numerical and structural rearrangement have been described(125,134,135), and rearrangements due to chromothripsis have been reported to be observed more frequently in chordoma than many other cancers(131), emphasising using this method for detection of ctDNA. One of the tumours used for the study reported here had two mutations identified. Unfortunately due to technical difficulties it was not possible to detect the 2nd mutation. In order to increase the sensitivity of detection of ctDNA in chordoma, an increase in sample size may be required. This, strategy, is currently being evaluated.

In cancer patients the proportion of ctDNA has been demonstrated to relate to burden of disease. Regular sampling can demonstrate the dynamic of the disease(634,653,815). For our patients only a single time-point was assessed, in order to establish proof of concept of detection of ctDNA in a slow growing tumour. Preferably the utility of the test would be to identify mutations or rearrangement in the primary chordoma and to monitor for these gene alterations following surgery, with serial sampling to monitor for disease recurrence. It has been suggested that a tumour containing approximately 50 million malignant cells is sufficient for the detection of ctDNA, however a tumour of that size will not be definable by imaging(126,636,855).

For chordoma patients, and indeed other bone tumours where surgical resection is the main therapy, excision may be technically easier and potentially associated with less morbidity if recurrence is detected early. It is perceivable that ctDNA can be used to guide timing of imaging and surgical resection.

For cancer with mutations that represents druggable targets, and mutations leading to treatment resistance, ctDNA has true clinical application. This has been shown for colorectal cancer(870,871) and NSCLC(638,872), where patients treated with EGFR inhibitors demonstrated initial clinical response, but subsequently developed resistance by the emergence of specific *EGFR* mutations. Circulation tumour DNA offers and excellent opportunity to monitor for the emergence of resistant clones to guide therapy(637,657,873). Though EGFR has not been found to be mutated in chordoma as previously discussed, the work presented in this thesis demonstrated evidence of EGFR's involvement in chordoma. Future trials may identify genomic alterations, which can be used as a biomarker, to help guide therapy in chordoma.

6.6.2 AKR1B10

The work in this chapter has shown that AKR1B10 protein was not detectable in plasma samples from chordoma patients. Though only a few samples were included, they came from patients with large tumours, immunoreactive for AKR1B10, suggesting that AKR1B10 may not have a utility as a serum protein biomarker in patients with chordoma. This data is in contrast to the published data for patients with breast cancer. In the study by Ma et al.(853) breast cancer patients had AKR1B10 levels of 15.18 +/- 9.08ng/mL with the highest level measuring 58.4ng/mL. The levels correlated to outcome. The controls had levels of 3.34 +/- 2.27ng/mL, in the serum measured by ELISA. The standard containing recombinant AKR1B10 used in the experiments reported here worked well, and the level for the MUG Chor lysate was detectable though at low levels. It is possible that the processing or storage of the plasma samples rendered the sample suboptimal. However, these were biobanked according to standard operating procedures and were all stored within 4 hours of being taken from patients. The samples included were collected at different time points so even if a delay had occurred in processing one of the samples, for none of the samples to work suggests that the levels in chordoma patients are too low to measure. The role of AKR1B10 in chordoma patients is still to be determined.

7 CONCLUSIONS AND FUTURE WORK

Treatment options are currently limited for patients with chordoma and in particular for patients with recurrent disease. The work presented here provides insight into different modalities of treatment for chordoma.

In the absence of recurrent targetable genetic alterations in chordoma a phenotypic screening approach was undertaken to identify the mechanism/s by which this disease is driven, and targets which could potentially be translated into clinic practice. Targeted therapy for chordoma has to date been chosen based on immunoreactivity and activated molecular pathways in chordoma. Only one large *in vitro* compound screen has previously been reported in chordoma cell lines. In the work presented here from the high-throughput compound screen which included 1152 compounds, 28 compounds were identified to have a selective cell kill effect on the chordoma cell lines. 81% of these compounds were found to be EGFR/ErbB family inhibitors. Analysis of substituent patterns suggested that EGFR-inhibitors with small aniline substituents in the 4th position of the quinazoline ring were more effective than inhibitors with large substituents in that position. Chemotype analysis thereby identified the compounds Sapitinib and Erlotinib as the EGFR inhibitors most likely to succeed in a clinical trial for chordoma. Not all of the cell lines demonstrated equal sensitivity to EGFR inhibitors and further work is required to uncover the different mechanisms for treatment resistance. Next generation sequencing failed to detect mutations covering the hotspots in 22 tumour-related genes which included *EGFR, ERBB2* and *ERBB4* and their downstream effectors *(KRAS, BRAF, PIK3CA, AKT1, PTEN, NRAS, MAPK)*. Thus, no obvious genetic explanations for sensitivity and/or resistance in the cell line screened. Work is currently being completed screening an additional four cell lines with the identified compounds. In addition experiments have been undertaken to establish the on-target effect of the compounds by Western Blot and ELISA analysis. Future work is to include testing the most efficacious compounds in the CLX and PDX models to test if the compounds reduce tumour growth in vivo. Sapitinib has recently showed promising result significantly reducing tumour growth in 2 xenograft models (U-CH1 xenograft and a patient-derived xenograft SF8894(874)) tested at South Texas Accelerated Research Therapeutics (START) (Personal communication Professor Flanagan). The xenograft models may help understand the pathways involved in tumour growth and treatment response. Ultimately, whether some patients with chordoma benefit from the TKIs identified is likely only to be resolved in a clinical trial. Any such study should involve in depth biological studies of the tumour samples pre-

and post-treatment, with the aim of explaining the mechanism by which some chordomas are primarily resistant or develop secondary resistance to EGFR inhibitors.

It is unlikely that a single treatment compound will cure chordoma. Screening of combination of compounds is being planned to identify compounds with synergistic effect aiming to optimise treatment.

As an alternative approach to treatment, representing untested teritory, I developed an AAV vector for silencing brachyury in a xenograft model. *In vitro* work demonstrated that knockdown of brachyury in chordoma cell lines induced growth arrest and apoptosis. The work presented here demonstrated chordoma cell lines to be permissive to AAV5 and the *in vitro* work demonstrated growth arrest in the U-CH1 and MUG Chor cell lines following transduction with the generated AAV vector. This work also highlighted the difficulties involved in using RNAi technology. The *in vivo* work demonstrated a beneficial effect on the tumour causing growh arrest or reduction in size. Luciferase expression was reduced in the tumour suggesting loss of viable cells. Though the sample size is too small to assess the statistical significance of this particular vector model the study shows a signal of anti-tumour effect and therefore the potential supporting further developmen as a bigger study would be needed to establish efficacy. Whilst undertaking the work for this study RNAi techonology has made great advances with the introduction of gene editing using CRISPR/Cas9 for targeted genome editing. This technology is promising and may have the potential to target brachyury leading to sustained silencing in chordoma. Multiple options for vector optimisations are available and include considerations such as a different choice of vector for delivery and options for engineering the vector to elicit an immune-stimulatory response. The use of nano-technology enables repeat dosing in contrast to the viral vector which is a one-off therapeutic option, and nano-technology should therefore be considered as a model for delivery. Multiple improvements to the experiments should be done, including optimisation of the xenograft model.

1. The viral vector delivering the gene-silencing construct could be engineered to express a different bioluminescent or immunofluorescent marker to identify the transduced cells. This would offer an opportunity to assess if persistent brachyury expression was due to failure of transduction, or failure of the vector (cells overcoming the gene silencing).

2. The U-CH1 cells could also be engineered to stably express brachyury from a viral vector (cDNA) upstream from a flourescent or luminescent marker which would not be expressed if the brachyury gene upstream was silenced.
3. An alternative to this would be to engineer the U-CH1 cell to stably express GFP or a different colour luciferase and then engineer the vector to deliver a GFP or luciferase silencing shRNA as well as the brachyury silencing expression cassette to confirm the presence and efficacy of the viral vector in the situation where brachyury silencing was not maintained.

The lack of brachyury silencing, observed four weeks after the vector injection, may reflect the chordoma cells ability to overcome the silencing as discussed in chapter 3. To establish this the xenograft experiment could include sacrificing some of the mice at earlier timepoints to assess the immunoreactivity of brachyury (kinetic study).

An alternative to sacrificing the xenograft or modifying the tumour cells (the U-CH1 cell line) would be to monitor response to therapy by quantifying ctDNA in the plasma from the xenograft(875,876), this would enable serial monitoring and reduce the number of mice needed for the experiments. As the DNA from the tumour is human origin it would not rely on tumour specific mutations. The method could be applied both to the gene therapy experiments and drug screening in the xenograft model.

Targeting brachyury holds promise for potentially overcoming treatment resistance to other therapeutics. The transformation of epithelial cancers by the process of EMT has demonstrated increase resistance to therapy. Brachyury has been implicated in EMT and reversal of the process has been observed after silencing of brachyury(106). Though EMT is not fully understood it raised the possibility that targeting brachyury in chordoma may render the tumours sensitive to chemotherapy. This will need to be assessed in future studies, preliminary data could be obtained using a xenograft model. A current vaccine study targeting brachyury is combining the vaccine with radiotherapy, it will be interesting if this approach demonstrates better local control(298).

This work has also reported on the experience of the development of two xenograft models. The PDX model identified *TP53* mutation as a driver of tumourigenicity demonstrated by the clonal expansion of *TP53* mutated cells in the xenograft. This finding, together with similar reports of PDX models being representative of tumour

progression, supports the use of these models for drug screening and biological studies to understand the significance of identified mutations. The Avatar model may help assess the patient's risk of recurrence and identify drivers as well as potential actionable targets to guide compounds treatment in the PDX providing the biological rationale for targeting certain mutations(793). The concept of the Avatar model has the potential to revolutionise drug development and optimise personalised medicine. The model presented here has been shared with collaborators for further development. To set up a lab generating Avatar models a significant commitment on time and funding is required, however due to the slow growth of many chordomas the personal model may truly benefit the patient as there is time to establish the model, screen for mutations and treat the mice in real time. Compounds can be selected based on preclinical studies or according to individual targetable mutations.

Assays developed for detection of ctDNA in chordoma was also established. Detection of ctDNA in low-grade tumours has been reported to be less successful and optimisation will be required for this method to be a useful and consistent tool for detection of recurrence and evaluation of response to treatment. Further evaluation is currently being undertaken to determine if a larger sample size will increase the level of detection. Another method for optimising specificity in cancers with low levels of ctDNA would be to identify more than one mutation for each tumour, including gene rearrangements or amplified genes, this would add confidence and validity when levels are low. With the increased availability of sequencing data for the majority of tumours, ctDNA is likely to become as important in solid tumours as it currently is in leukaemia for disease stratification and detection of minimal residual disease. Mutation panels are under development for various cancer groups to be used for detection of tumour specific mutations by sequencing. Sequencing of additional chordoma samples may identify mutations, which frequently occur in chordoma enabling a panel to be developed. With further technological advances detection threshold for ctDNA is likely to further improve and become an integrated part of standard of care for many cancers.

8 REFERENCES

1. Whelan J, McTiernan A, Cooper N, Wong YK, Francis M, Vernon S, et al. Incidence and survival of malignant bone sarcomas in England 1979-2007. Int J Cancer. 2012 Aug 15;131(4):E508–17.

2. Mindell ER. Chordoma. J Bone Joint Surg Am. 1981 Mar;63(3):501–5.

3. Chugh R, Tawbi H, Lucas DR, Biermann JS, Schuetze SM, Baker LH. Chordoma: the nonsarcoma primary bone tumor. Oncologist. 2007 Nov;12(11):1344–50.

4. Ishida T, Dorfman HD. Chondroid chordoma versus low-grade chondrosarcoma of the base of the skull: can immunohistochemistry resolve the controversy? J Neurooncol. 1994;18(3):199–206.

5. Cheng EY, Ozerdemoglu RA, Transfeldt EE, Thompson RC. Lumbosacral chordoma. Prognostic factors and treatment. Spine. 1999 Aug 15;24(16):1639–45.

6. McMaster ML, Goldstein AM, Bromley CM, Ishibe N, Parry DM. Chordoma: incidence and survival patterns in the United States, 1973-1995. Cancer Causes Control. 2001 Jan;12(1):1–11.

7. Smoll NR, Gautschi OP, Radovanovic I, Schaller K, Weber DC. Incidence and relative survival of chordomas: the standardized mortality ratio and the impact of chordomas on a population. Cancer. 2013 Jun 1;119(11):2029–37.

8. Chambers KJ, Lin DT, Meier J, Remenschneider A, Herr M, Gray ST. Incidence and survival patterns of cranial chordoma in the United States. Laryngoscope. 2013 Oct 1.

9. Jones PS, Aghi MK, Muzikansky A, Shih HA, Barker FG, Curry WT. Outcomes and patterns of care in adult skull base chordomas from the Surveillance, Epidemiology, and End Results (SEER) database. J Clin Neurosci. 2014 Sep;21(9):1490–6.

10. Lauer SR, Edgar MA, Gardner JM, Sebastian A, Weiss SW. Soft tissue chordomas: a clinicopathologic analysis of 11 cases. Am J Surg Pathol. 2013 May;37(5):719–26.

11. Kikuchi Y, Yamaguchi T, Kishi H, Azuhata K, Kimizuka G, Hiroshima K, et al. Pulmonary tumor with notochordal differentiation: report of 2 cases suggestive of benign notochordal cell tumor of extraosseous origin. Am J Surg Pathol. 2011 Aug;35(8):1158–64.

12. Park SY, Kim SR, Choe YH, Lee KY, Park SJ, Lee HB, et al. Extra-Axial Chordoma Presenting as a Lung Mass. Respiration. 2009;77(2):219–23.

13. Tirabosco R, Mangham DC, Rosenberg AE, Vujovic S, Bousdras K, Pizzolitto S, et al. Brachyury expression in extra-axial skeletal and soft tissue chordomas: a marker that distinguishes chordoma from mixed tumor/myoepithelioma/parachordoma in soft tissue. Am J Surg Pathol. 2008 Apr;32(4):572–80.

14. O'donnell P, Tirabosco R, Vujovic S, Bartlett W, Briggs TWR, Henderson S, et al. Diagnosing an extra-axial chordoma of the proximal tibia with the help of brachyury, a molecule required for notochordal differentiation. Skeletal Radiol. 2007 Jan;36(1):59–65.

15. Lantos JE, Agaram NP, Healey JH, Hwang S. Recurrent skeletal extra-axial chordoma confirmed with brachyury: Imaging features and review of the literature. Skeletal Radiol. 2013 Oct;42(10):1451–9.

16. Difrancesco LM, Castillo CAD, Temple WJ. Extra-axial chordoma. Arch Pathol Lab Med. 2006 Dec;130(12):1871–4.

17. Heffelfinger MJ, Dahlin DC, MacCarty CS, Beabout JW. Chordomas and cartilaginous tumors at the skull base. Cancer. 1973 Aug;32(2):410–20.

18. Lee J, Bhatia NN, Hoang BH, Ziogas A, Zell JA. Analysis of Prognostic Factors for Patients with Chordoma with Use of the California Cancer Registry. J Bone Joint Surg Am. The Journal of Bone and Joint Surgery; 2012 Feb 15;94(4):356–63.

19. Kelley MJ, Korczak JF, Sheridan E, Yang X, Goldstein AM, Parry DM. Familial chordoma, a tumor of notochordal remnants, is linked to chromosome 7q33. Am J Hum Genet. 2001 Aug;69(2):454–60.

20. Hoch BL, Nielsen GP, Liebsch NJ, Rosenberg AE. Base of skull chordomas in children and adolescents: a clinicopathologic study of 73 cases. Am J Surg Pathol. 2006 Jul;30(7):811–8.

21. Virchow R. Untersuchungen über die Entwickelung des Schädelgrundes im gesunden und krankhaften zustand: und über den einfluss derselben auf Schädelform, …. 1857.

22. Owen CI, Hershey LN, Gurdjian ES. Chordoma Dorsalis of the Cervical Spine. The American Journal of Cancer. 1932 Jul 1;16(4):830–40.

23. Ribbert H. Ecchordosis physaliphora sphenooccipitalis. Zbl alg Path path Anat. 1894.

24. Salisbury JR. The pathology of the human notochord. J Pathol. 1993 Dec;171(4):253–5.

25. Salisbury JR, Deverell MH, Cookson MJ, Whimster WF. Three-dimensional reconstruction of human embryonic notochords: clue to the pathogenesis of chordoma. J Pathol. 1993 Sep;171(1):59–62.

26. Choi K-S, Cohn MJ, Harfe BD. Identification of nucleus pulposus precursor cells and notochordal remnants in the mouse: Implications for disk degeneration and chordoma formation. Dev Dyn. 2008 Dec;237(12):3953–8.

27. Yamaguchi T, Yamato M, Saotome K. First histologically confirmed case of a classic chordoma arising in a precursor benign notochordal lesion: differential diagnosis of benign and malignant notochordal lesions. Skeletal Radiol. 2002 Jul;31(7):413–8.

28. Yamaguchi T, Suzuki S, Ishiiwa H, Ueda Y. Intraosseous benign notochordal cell tumours: overlooked precursors of classic chordomas? Histopathology. 2004 Jun;44(6):597–602.

29. Deshpande V, Nielsen GP, Rosenthal DI, Rosenberg AE. Intraosseous benign notochord cell tumors (BNCT): further evidence supporting a relationship to chordoma. Am J Surg Pathol. 2007 Oct;31(10):1573–7.

30. Kyriakos M, Totty WG, Lenke LG. Giant vertebral notochordal rest: a lesion distinct from chordoma: discussion of an evolving concept. Am J Surg Pathol. 2003 Mar;27(3):396–406.

31. Vujovic S, Henderson S, Presneau N, Odell E, Jacques TS, Tirabosco R, et al. Brachyury, a crucial regulator of notochordal development, is a novel biomarker for chordomas. J Pathol. 2006;209(2):157–65.

32. Shen J, Shi Q, Lu J, Wang D-L, Zou T-M, Yang H-L, et al. Histological study of chordoma origin from fetal notochordal cell rests. Spine. 2013 Dec 1;38(25):2165–70.

33. Henderson SR, Guiliano D, Presneau N, McLean S, Frow R, Vujovic S, et al. A molecular map of mesenchymal tumors. Genome Biol. 2005;6(9):R76.

34. Stepanek J, Cataldo SA, Ebersold MJ, Lindor NM, Jenkins RB, Unni K, et al. Familial chordoma with probable autosomal dominant inheritance. Am J Med Genet. 1998 Jan 23;75(3):335–6.

35. Dalprà L, Malgara R, Miozzo M, Riva P, Volonte M, Larizza L, et al. First cytogenetic study of a recurrent familial chordoma of the clivus. Int J Cancer. 1999 Mar 31;81(1):24–30.

36. Yang XR, Ng D, Alcorta DA, Liebsch NJ, Sheridan E, Li S, et al. T (brachyury) gene duplication confers major susceptibility to familial chordoma. Nat Genet. 2009 Oct 4;41(11):1176–8.

37. Dutton RV, Singleton EB. Tuberous sclerosis: a case report with aortic aneurysm and unusual rib changes. Pediatr Radiol. 1975 Jun 13;3(3):184–6.

38. Schroeder BA, Wells RG, Starshak RJ, Sty JR. Clivus chordoma in a child with tuberous sclerosis: CT and MR demonstration. J Comput Assist Tomogr. 1987 Jan;11(1):195–6.

39. McMaster ML, Goldstein AM, Parry DM. Clinical features distinguish childhood chordoma associated with tuberous sclerosis complex (TSC) from chordoma in the general paediatric population. J Med Genet. 2011 Jul;48(7):444–9.

40. Presneau N, Shalaby A, Idowu B, Gikas P, Cannon SR, Gout I, et al. Potential therapeutic targets for chordoma: PI3K/AKT/TSC1/TSC2/mTOR pathway. Br J Cancer. Nature Publishing Group; 2009 May 5;100(9):1406–14.

41. Fletcher CDM. WHO Classification of Tumours of Soft Tissue and Bone. World Health Organization; 2013. 1 p.

42. Almefty K, Pravdenkova S, Colli BO, Al-Mefty O, Gokden M. Chordoma and chondrosarcoma: similar, but quite different, skull base tumors. Cancer. 2007 Dec 1;110(11):2457–67.

43. Saito A, Hasegawa T, Shimoda T, Toda G, Hirohashi S, Tajima G, et al. Dedifferentiated chordoma: a case report. Jpn J Clin Oncol. 1998 Dec;28(12):766–71.

44. Hanna SA, Tirabosco R, Amin A, Pollock RC, Skinner JA, Cannon SR, et al. Dedifferentiated chordoma: a report of four cases arising 'de novo'. J Bone Joint Surg Br. 2008 May;90(5):652–6.

45. Meis JM, Raymond AK, Evans HL, Charles RE, Giraldo AA. “Dedifferentiated” chordoma. A clinicopathologic and immunohistochemical study of three cases. Am J Surg Pathol. 1987 Jul;11(7):516–25.

46. Jambhekar NA, Rekhi B, Thorat K, Dikshit R, Agrawal M, Puri A. Revisiting chordoma with brachyury, a “new age” marker: analysis of a validation study on 51 cases. Arch Pathol Lab Med. 2010 Aug;134(8):1181–7.

47. Walcott BP, Nahed BV, Mohyeldin A, Coumans J-V, Kahle KT, Ferreira MJ. Chordoma: current concepts, management, and future directions. Lancet Oncol. 2012 Feb;13(2):e69–76.

48. Disler DG, Miklic D. Imaging findings in tumors of the sacrum. AJR Am J Roentgenol. 1999 Dec;173(6):1699–706.

49. Chambers PW, Schwinn CP. Chordoma. A clinicopathologic study of metastasis. Am J Clin Pathol. 1979 Nov;72(5):765–76.

50. Fagundes MA, Hug EB, Liebsch NJ, Daly W, Efird J, Munzenrider JE. Radiation therapy for chordomas of the base of skull and cervical spine: patterns of failure and outcome after relapse. Int J Radiat Oncol Biol Phys. 1995 Oct 15;33(3):579–84.

51. Bjornsson J, Wold LE, Ebersold MJ, Laws ER. Chordoma of the mobile spine. A clinicopathologic analysis of 40 patients. Cancer. 1993 Feb 1;71(3):735–40.

52. Kishimoto R, Omatsu T, Hasegawa A, Imai R, Kandatsu S, Kamada T. Imaging characteristics of metastatic chordoma. Jpn J Radiol. 2012 Jul;30(6):509–16.

53. Sopta J, Tulic G, Mijucic V, Mamontov P, Mandic N. Solitary lymph node metastasis without local recurrence of primary chordoma. Eur Spine J. 2009 Jul;18 Suppl 2:191–5.

54. Ruiz HA, Goldberg LH, Humphreys TR, Blacklock JB. Cutaneous metastasis of chordoma. Dermatol Surg. 2000 Mar;26(3):259–62.

55. Boriani S, Chevalley F, Weinstein JN, Biagini R, Campanacci L, De Iure F,

et al. Chordoma of the spine above the sacrum. Treatment and outcome in 21 cases. Spine. 1996 Jul 1;21(13):1569–77.

56. Stacchiotti S, Sommer J, Chordoma Global Consensus Group. Building a global consensus approach to chordoma: a position paper from the medical and patient community. Lancet Oncol. 2015 Feb;16(2):e71–83.

57. York JE, Kaczaraj A, Abi-Said D, Fuller GN, Skibber JM, Janjan NA, et al. Sacral chordoma: 40-year experience at a major cancer center. Neurosurgery. 1999 Jan;44(1):74–9–discussion79–80.

58. Azzarelli A, Quagliuolo V, Cerasoli S, Zucali R, Bignami P, Mazzaferro V, et al. Chordoma: natural history and treatment results in 33 cases. J Surg Oncol. 1988 Mar;37(3):185–91.

59. Boriani S, Bandiera S, Biagini R, Bacchini P, Boriani L, Cappuccio M, et al. Chordoma of the mobile spine: fifty years of experience. Spine. 2006 Feb 15;31(4):493–503.

60. Bergh P. Prognostic Factors in Chordoma of the Sacrum and Mobile Spine. Cancer. 2000 May 1;88(9):2122–34.

61. Sundaresan N, Huvos AG, Krol G, Lane JM, Brennan M. Surgical treatment of spinal chordomas. Arch Surg. 1987 Dec;122(12):1479–82.

62. Wold LEL, Laws ERE. Cranial chordomas in children and young adults. Journal of Neurosurgery. 1983 Dec 1;59(6):1043–7.

63. Borba LA, Al-Mefty O, Mrak RE, Suen J. Cranial chordomas in children and adolescents. Journal of Neurosurgery. 1996 Apr;84(4):584–91.

64. Coffin CM, Swanson PE, Wick MR, Dehner LP. Chordoma in childhood and adolescence. A clinicopathologic analysis of 12 cases. Arch Pathol Lab Med. 1993 Sep;117(9):927–33.

65. Kaneko Y, Sato Y, Iwaki T, Shin RW, Tateishi J, Fukui M. Chordoma in early childhood: a clinicopathological study. Neurosurgery. 1991 Sep;29(3):442–6.

66. Matsumoto J, Towbin RB, Ball WS. Cranial chordomas in infancy and childhood. A report of two cases and review of the literature. Pediatr Radiol. 1989;20(1-2):28–32.

67. Sibley RK, Day DL, Dehner LP, Trueworthy RC. Metastasizing chordoma in early childhood: a pathological and immunohistochemical study with review of the literature. Pediatr Pathol. 1987;7(3):287–301.

68. Mobley BC, McKenney JK, Bangs CD, Callahan K, Yeom KW, Schneppenheim R, et al. Loss of SMARCB1/INI1 expression in poorly differentiated chordomas. Acta Neuropathol. 2010 Dec;120(6):745–53.

69. Yin H, Dorris KMO, Wagner LM, Collins MH, Towbin A, Nagarajan R. INI1 and mib-1 expression in childhood chordomas. ASCO Meeting Abstracts. 2011 May 20;29(15_suppl):9556.

70. Yadav R, Sharma MC, Malgulwar PB, Pathak P, Sigamani E, Suri V, et al. Prognostic value of MIB-1, p53, epidermal growth factor receptor, and INI1 in childhood chordomas. Neuro-oncology. 2013 Dec 17.

71. Tirabosco R, Jacques T, Berisha F, Flanagan AM. Assessment of integrase interactor 1 (INI-1) expression in primary tumours of bone. Histopathology. 2012 Jun 17;:–.

72. Jian BJ, Bloch OG, Yang I, Han SJ, Aranda D, Parsa AT. A comprehensive analysis of intracranial chordoma and survival: a systematic review. Br J Neurosurg. 2011 Aug;25(4):446–53.

73. Uhl M, Mattke M, Welzel T, Roeder F, Oelmann J, Habl G, et al. Highly effective treatment of skull base chordoma with carbon ion irradiation using a raster scan technique in 155 patients: First long-term results. Cancer. 2014 Nov 1;120(21):3410–7.

74. Holliday EB, Frank SJ. Proton radiation therapy for head and neck cancer: a review of the clinical experience to date. Int J Radiat Oncol Biol Phys. 2014 Jun 1;89(2):292–302.

75. Edwards YH, Putt W, Lekoape KM, Stott D, Fox M, Hopkinson DA, et al. The human homolog T of the mouse T(Brachyury) gene; gene structure, cDNA sequence, and assignment to chromosome 6q27. Genome Research. 1996 Mar;6(3):226–33.

76. Mariman E, Edwards YH. Genetic mapping of the human homologue (T) of mouse T (Brachyury) and. Human Molecular Genetics. 1996.

77. Stemple DL. Structure and function of the notochord: an essential organ for chordate development. Development. 2005 Jun;132(11):2503–12.

78. Stemple DL. The notochord. Curr Biol. 2004 Oct 26;14(20):R873–4.

79. Herrmann BG, Labeit S, Poustka A, King TR, Lehrach H. Cloning of the T gene required in mesoderm formation in the mouse. Nature. 1990 Feb 15;343(6259):617–22.

80. Wilkinson DG, Bhatt S, Herrmann BG. Expression pattern of the mouse T gene and its role in mesoderm formation. Nature. 1990 Feb 15;343(6259):657–9.

81. Chesley P. Development of the short-tailed mutant in the house mouse. J Exp Zool. 1935 May;70(3):429–59.

82. Postma AV, Alders M, Sylva M, Bilardo CM, Pajkrt E, van Rijn RR, et al. Mutations in the T (brachyury) gene cause a novel syndrome consisting of sacral agenesis, abnormal ossification of the vertebral bodies and a persistent notochordal canal. J Med Genet. 2013 Nov 19.

83. Ghebranious N, Blank RD, Raggio CL, Staubli J, McPherson E, Ivacic L, et al. A missense T (Brachyury) mutation contributes to vertebral malformations. J Bone Miner Res. 2008 Oct;23(10):1576–83.

84. Jensen LE, Barbaux S, Hoess K, Fraterman S, Whitehead AS, Mitchell LE. The human T locus and spina bifida risk. Hum Genet. 2004 Nov;115(6):475–82.

85. Zhang L, Guo S, Schwab JH, Nielsen GP, Choy E, Ye S, et al. Tissue microarray immunohistochemical detection of brachyury is not a prognostic indicator in chordoma. PLoS ONE. 2013;8(9):e75851.

86. Nibu Y, José-Edwards DS, Di Gregorio A. From notochord formation to hereditary chordoma: the many roles of Brachyury. BioMed Research International. 2013;2013:826435.

87. Kelley MJ, Shi J, Ballew B, Hyland PL, Li W-Q, Rotunno M, et al. Characterization of T gene sequence variants and germline duplications in familial and sporadic chordoma. Hum Genet. 2014 Oct;133(10):1289–97.

88. Yang C, Schwab JH, Schoenfeld AJ, Hornicek FJ, Wood KB, Nielsen GP, et al. A novel target for treatment of chordoma: signal transducers and activators of transcription 3. Molecular Cancer Therapeutics. 2009 Sep;8(9):2597–605.

89. Presneau N, Shalaby A, Ye H, Pillay N, Halai D, Idowu B, et al. Role of the transcription factor T (brachyury) in the pathogenesis of sporadic chordoma: a genetic and functional-based study. J Pathol. 2010 Nov 24;223(3):327–35.

90. Pillay N, Plagnol V, Tarpey PS, Lobo SB, Presneau N, Szuhai K, et al. A common single-nucleotide variant in T is strongly associated with chordoma. Nat Genet. 2012 Nov;44(11):1185–7.

91. Hsu W, Mohyeldin A, Shah SR, ap Rhys CM, Johnson LF, Sedora-Roman NI, et al. Generation of chordoma cell line JHC7 and the identification of Brachyury as a novel molecular target. Journal of Neurosurgery. 2011 Oct;115(4):760–9.

92. Thiery JP. [Epithelial-mesenchymal transitions in cancer onset and progression]. Bull Acad Natl Med. 2009 Dec 1;193(9):1969–9.

93. Fernando RI, Litzinger M, Trono P, Hamilton DH, Schlom J, Palena C. The T-box transcription factor Brachyury promotes epithelial-mesenchymal transition in human tumor cells. J Clin Invest [Internet]. 2010 Feb 1;120(2):533–44. Available from: http://www.pubmedcentral.nih.gov/articlerender.fcgi?artid=2810072

94. Thiery JP, Acloque H, Huang RYJ, Nieto MA. Epithelial-mesenchymal transitions in development and disease. Cell. 2009 Nov 25;139(5):871–90.

95. Roselli M, Fernando RI, Guadagni F, Spila A, Alessandroni J, Palmirotta R, et al. Brachyury, a driver of the epithelial-mesenchymal transition, is overexpressed in human lung tumors: an opportunity for novel interventions against lung cancer. Clin Cancer Res. 2012 Jul 15;18(14):3868–79.

96. Larocca C, Cohen JR, Fernando RI, Huang B, Hamilton DH, Palena C. An

autocrine loop between TGF-β1 and the transcription factor brachyury controls the transition of human carcinoma cells into a mesenchymal phenotype. Molecular Cancer Therapeutics. 2013 Sep;12(9):1805–15.

97. Sarkar D, Shields B, Davies ML, Müller J, Wakeman JA. BRACHYURY confers cancer stem cell characteristics on colorectal cancer cells. Int J Cancer. 2011 May 28;130(2):328–37.

98. Shimoda M, Sugiura T, Imajyo I, Ishii K, Chigita S, Seki K, et al. The T-box transcription factor Brachyury regulates epithelial-mesenchymal transition in association with cancer stem-like cells in adenoid cystic carcinoma cells. BMC Cancer. 2012;12(1):377.

99. Imajyo I, Sugiura T, Kobayashi Y, Shimoda M, Ishii K, Akimoto N, et al. T-box transcription factor Brachyury expression is correlated with epithelial-mesenchymal transition and lymph node metastasis in oral squamous cell carcinoma. Int J Oncol. 2012 Dec;41(6):1985–95.

100. Haro A, Yano T, Kohno M, Yoshida T, Koga T, Okamoto T, et al. Expression of Brachyury Gene Is a Significant Prognostic Factor for Primary Lung Carcinoma. Ann Surg Oncol. 2013 Mar 1.

101. Du R, Wu S, Lv X, Fang H, Wu S, Kang J. Overexpression of brachyury contributes to tumor metastasis by inducing epithelial-mesenchymal transition in hepatocellular carcinoma. J Exp Clin Cancer Res. 2014 Dec 14;33(1):105.

102. Xu K, Liu B, Liu Y. Impact of Brachyury on epithelial-mesenchymal transitions and chemosensitivity in non-small cell lung cancer. Mol Med Rep. 2015 Feb 13.

103. Palena C, Polev DE, Tsang KY, Fernando RI, Litzinger M, Krukovskaya LL, et al. The Human T-Box Mesodermal Transcription Factor Brachyury Is a Candidate Target for T-Cell-Mediated Cancer Immunotherapy. Clinical Cancer Research. 2007 Apr 15;13(8):2471–8.

104. Palena C, Roselli M, Litzinger MT, Ferroni P, Costarelli L, Spila A, et al. Overexpression of the EMT driver brachyury in breast carcinomas: association with poor prognosis. J Natl Cancer Inst. 2014 May;106(5).

105. Pinto F, Pértega-Gomes N, Pereira MS, Vizcaíno JR, Monteiro P, Henrique RM, et al. T-box Transcription Factor Brachyury Is Associated with Prostate Cancer Progression and Aggressiveness. Clin Cancer Res. 2014 Jul 9.

106. Palena C, Fernando RI, Litzinger MT, Hamilton DH, Huang B, Schlom J. Strategies to target molecules that control the acquisition of a mesenchymal-like phenotype by carcinoma cells. Experimental Biology and Medicine. 2011 May 6;236(5):537–45.

107. Hamilton DH, Litzinger MT, Fernando RI, Huang B, Palena C. Cancer vaccines targeting the epithelial-mesenchymal transition: tissue distribution of brachyury and other drivers of the mesenchymal-like phenotype of carcinomas. Semin Oncol. 2012 Jun;39(3):358–66.

108. Hamilton DH, Fernando RI, Schlom J, Palena C. Aberrant expression of the embryonic transcription factor brachyury in human tumors detected with a novel rabbit monoclonal antibody. Oncotarget. 2014 Dec 26.

109. Kobayashi Y, Sugiura T, Imajyo I, Shimoda M, Ishii K, Akimoto N, et al. Knockdown of the T-box transcription factor Brachyury increases sensitivity of adenoid cystic carcinoma cells to chemotherapy and radiation in vitro: implications for a new therapeutic principle. Int J Oncol. 2014 Apr;44(4):1107–17.

110. Thiery JP. Epithelial-mesenchymal transitions in tumour progression. Nat Rev Cancer. 2002 Jun;2(6):442–54.

111. Onder TT, Gupta PB, Mani SA, Yang J, Lander ES, Weinberg RA. Loss of E-cadherin promotes metastasis via multiple downstream transcriptional pathways. Cancer Research. 2008 May 15;68(10):3645–54.

112. Guarino M. Epithelial-mesenchymal transition and tumour invasion. Int J Biochem Cell Biol. 2007;39(12):2153–60.

113. Naka T, Kuester D, Boltze C, Scheil-Bertram S, Samii A, Herold C, et al. Expression of hepatocyte growth factor and c-MET in skull base chordoma. Cancer. 2008 Jan 1;112(1):104–10.

114. Froehlich EV, Scheipl S, Lazáry A, Varga PP, Schmid C, Stammberger H, et al. Expression of ezrin, MMP-9, and COX-2 in 50 chordoma specimens: a clinical and immunohistochemical analysis. Spine. 2012 Jun 1;37(13):E757–67.

115. Horiguchi H, Sano T, Qian ZR, Hirokawa M, Kagawa N, Yamaguchi T, et al. Expression of cell adhesion molecules in chordomas: an immunohistochemical study of 16 cases. Acta Neuropathol. 2004 Feb;107(2):91–6.

116. Sloane JP, Ormerod MG. Distribution of epithelial membrane antigen in normal and neoplastic tissues and it value in diagnostic tumor pathology. Cancer. 1981 Apr 1;47(7):1786–95.

117. Cho H-Y, Lee M, Takei H, Dancer J, Ro JY, Zhai QJ. Immunohistochemical comparison of chordoma with chondrosarcoma, myxopapillary ependymoma, and chordoid meningioma. Appl Immunohistochem Mol Morphol. 2009 Mar;17(2):131–8.

118. Laskin WB, Miettinen M. Epithelial-type and neural-type cadherin expression in malignant noncarcinomatous neoplasms with epithelioid features that involve the soft tissues. Arch Pathol Lab Med. 2002 Mar 31;126(4):425–31.

119. Hu Y, Mintz A, Shah SR, Quiñones-Hinojosa A, Hsu W. The FGFR/MEK/ERK/brachyury pathway is critical for chordoma cell growth and survival. Carcinogenesis. 2014 Jan 20.

120. Peinado H, Olmeda D, Cano A. Snail, Zeb and bHLH factors in tumour progression: an alliance against the epithelial phenotype? Nat Rev Cancer.

2007 Jun;7(6):415–28.

121. Wu S-Y, McClay DR. The Snail repressor is required for PMC ingression in the sea urchin embryo. Development. 2007 Mar;134(6):1061–70.

122. Barrallo-Gimeno A, Nieto MA. The Snail genes as inducers of cell movement and survival: implications in development and cancer. Development. 2005.

123. Ciruna B, Rossant J. FGF signaling regulates mesoderm cell fate specification and morphogenetic movement at the primitive streak. Dev Cell. 2001 Jul;1(1):37–49.

124. Rinner B, Weinhaeusel A, Lohberger B, Froehlich EV, Pulverer W, Fischer C, et al. Chordoma characterization of significant changes of the DNA methylation pattern. PLoS ONE. 2013;8(3):e56609.

125. Hallor KH, Staaf J, Jönsson G, Heidenblad M, Vult von Steyern F, Bauer HCF, et al. Frequent deletion of the CDKN2A locus in chordoma: analysis of chromosomal imbalances using array comparative genomic hybridisation. Br J Cancer. 2008 Jan 29;98(2):434–42.

126. Diaz RJ, Guduk M, Romagnuolo R, Smith CA, Northcott P, Shih D, et al. High-resolution whole-genome analysis of skull base chordomas implicates FHIT loss in chordoma pathogenesis. Neoplasia. 2012 Sep;14(9):788–98.

127. Nelson AC, Pillay N, Henderson S, Presneau N, Tirabosco R, Halai D, et al. An integrated functional genomics approach identifies the regulatory network directed by brachyury (T) in chordoma. J Pathol. 2012 Nov;228(3):274–85.

128. Le LP, Nielsen GP, Rosenberg AE, Thomas D, Batten JM, Deshpande V, et al. Recurrent chromosomal copy number alterations in sporadic chordomas. PLoS ONE. 2011;6(5):e18846.

129. Choy E, MacConaill LE, Cote GM, Le LP, Shen JK, Nielsen GP, et al. Genotyping cancer-associated genes in chordoma identifies mutations in oncogenes and areas of chromosomal loss involving CDKN2A, PTEN, and SMARCB1. PLoS ONE. 2014;9(7):e101283.

130. Shalaby AA, Presneau N, Idowu BD, Thompson L, Briggs TR, Tirabosco R, et al. Analysis of the fibroblastic growth factor receptor-RAS/RAF/MEK/ERK-ETS2/brachyury signalling pathway in chordomas. Nature Publishing Group; 2009 May 1;22(8):996–1005.

131. Stephens PJ, Mcbride DJ, Lin M-L, Varela I, Pleasance ED, Simpson JT, et al. Complex landscapes of somatic rearrangement in human breast cancer genomes. Nature. 2009 Dec 24;462(7276):1005–10.

132. Forment JV, Kaidi A, Jackson SP. Chromothripsis and cancer: causes and consequences of chromosome shattering. Nat Rev Cancer. 2012 Oct;12(10):663–70.

133. Stephens PJ, Greenman CD, Fu B, Yang F, Bignell GR, Mudie LJ, et al. Massive genomic rearrangement acquired in a single catastrophic event during cancer development. Cell. 2011 Jan 7;144(1):27–40.

134. Scheil S, Brüderlein S, Liehr T, Starke H, Herms J, Schulte M, et al. Genome-wide analysis of sixteen chordomas by comparative genomic hybridization and cytogenetics of the first human chordoma cell line, U-CH1. Genes Chromosom Cancer. 2001 Nov;32(3):203–11.

135. Scheil-Bertram S, Kappler R, Baer von A, Hartwig E, Sarkar M, Serra M, et al. Molecular profiling of chordoma. Int J Oncol. 2014 Jan 21.

136. Meng T, Yin H, Li B, Li Z, Xu W, Zhou W, et al. Clinical features and prognostic factors of patients with chordoma in the spine: a retrospective analysis of 153 patients in a single center. Neuro-oncology. 2014 Dec 8;0(2014):3311–31.

137. Sen C, Triana AI, Berglind N, Godbold J, Shrivastava RK. Clival chordomas: clinical management, results, and complications in 71 patients. Journal of Neurosurgery. 2010 Nov;113(5):1059–71.

138. Wu Z, Zhang J, Zhang L, Jia G, Tang J, Wang L, et al. Prognostic factors for long-term outcome of patients with surgical resection of skull base chordomas-106 cases review in one institution. Neurosurg Rev. 2010 Oct;33(4):451–6.

139. Di Maio S, Kong E, Yip S, Rostomily R. Converging paths to progress for skull base chordoma: Review of current therapy and future molecular targets. Surg Neurol Int. 2013;4:72.

140. Ahmed R, Sheybani A, Menezes AH, Buatti JM, Hitchon PW. Disease outcomes for skull base and spinal chordomas: a single center experience. Clin Neurol Neurosurg. 2015 Mar;130:67–73.

141. Moran D, Zadnik PL, Taylor T, Groves ML, Yurter A, Wolinsky J-P, et al. Maintenance of bowel, bladder, and motor functions after sacrectomy. Spine J. 2015 Feb 1;15(2):222–9.

142. Dubory A, Missenard G, Lambert B, Court C. “En bloc” resection of sacral chordomas by combined anterior and posterior surgical approach: a monocentric retrospective review about 29 cases. Eur Spine J. 2014 Sep;23(9):1940–8.

143. Bugoci DM, Girvigian MR, Chen JCT, Miller MM, Rahimian J. Photon-based fractionated stereotactic radiotherapy for postoperative treatment of skull base chordomas. Am J Clin Oncol. 2013 Aug;36(4):404–10.

144. Amichetti M, Cianchetti M, Amelio D, Enrici RM, Minniti G. Proton therapy in chordoma of the base of the skull: a systematic review. Neurosurg Rev. 2009 Oct;32(4):403–16.

145. DeLaney TF, Liebsch NJ, Pedlow FX, Adams J, Dean S, Yeap BY, et al. Phase II study of high-dose photon/proton radiotherapy in the management of spine sarcomas. Int J Radiat Oncol Biol Phys. 2009 Jul

1;74(3):732–9.

146. Holliday EB, Mitra HS, Somerson JS, Rhines LD, Mahajan A, Brown PD, et al. Post-operative Proton Therapy for Chordomas and Chondrosarcomas of the Spine: Adjuvant vs. Salvage Radiation Therapy. Spine. 2015 Jan 23.

147. DeLaney TF, Liebsch NJ, Pedlow FX, Adams J, Weyman EA, Yeap BY, et al. Long-term results of Phase II study of high dose photon/proton radiotherapy in the management of spine chordomas, chondrosarcomas, and other sarcomas. J Surg Oncol. 2014 Aug;110(2):115–22.

148. Hug EB, Loredo LN, Slater JD, DeVries A, Grove RI, Schaefer RA, et al. Proton radiation therapy for chordomas and chondrosarcomas of the skull base. Journal of Neurosurgery. 1999 Sep;91(3):432–9.

149. Combs SE, Ellerbrock M, Haberer T, Habermehl D, Hoess A, Jäkel O, et al. Heidelberg Ion Therapy Center (HIT): Initial clinical experience in the first 80 patients. Acta Oncol. 2010 Oct;49(7):1132–40.

150. Imai R, Kamada T, Tsuji H, Sugawara S, Serizawa I, Tsujii H, et al. Effect of carbon ion radiotherapy for sacral chordoma: results of Phase I-II and Phase II clinical trials. Int J Radiat Oncol Biol Phys. 2010 Aug 1;77(5):1470–6.

151. Nishida Y, Kamada T, Imai R, Tsukushi S, Yamada Y, Sugiura H, et al. Clinical outcome of sacral chordoma with carbon ion radiotherapy compared with surgery. Int J Radiat Oncol Biol Phys. 2011 Jan 1;79(1):110–6.

152. Dhall G, Traverso M, Finlay JL, Shane L, Gonzalez-Gomez I, Jubran R. The role of chemotherapy in pediatric clival chordomas. J Neurooncol. 2011 Jul;103(3):657–62.

153. Cummings BJ, Hodson DI, Bush RS. Chordoma: the results of megavoltage radiation therapy. Int J Radiat Oncol Biol Phys. 1983 May;9(5):633–42.

154. Razis DV, Tsatsaronis A, Kyriazides I, Triantafyllou D. Chordoma of the cervical spine treated with vincristine sulfate. J Med. 1974;5(5):274–7.

155. Sundaresan N, Galicich JH, Chu FC, Huvos AG. Spinal chordomas. Journal of Neurosurgery. 1979 Mar;50(3):312–9.

156. Chugh R, Dunn R, Zalupski MM, Biermann JS, Sondak VK, Mace JR, et al. Phase II study of 9-nitro-camptothecin in patients with advanced chordoma or soft tissue sarcoma. J Clin Oncol. 2005 May 20;23(15):3597–604.

157. VR A. Camptothecins in Cancer Therapy. Adams VR, Burke TG, editors. Totowa, NJ: Humana Press; 2005.

158. Scimeca PG, James-Herry AG, Black KS, Kahn E, Weinblatt ME. Chemotherapeutic treatment of malignant chordoma in children. J Pediatr

Hematol Oncol. 1996 May;18(2):237–40.

159. Ashwood N, Hoskin PJ, Saunders MI. Metastatic chordoma: pattern of spread and response to chemotherapy. Clin Oncol (R Coll Radiol). 1994;6(5):341–2.

160. Flemming G, Samuels BL. Dedifferentiated Chrodoma. 1993 Aug 1;:1–5.

161. Druker BJ, Sawyers CL, Kantarjian H, Resta DJ, Reese SF, Ford JM, et al. Activity of a specific inhibitor of the BCR-ABL tyrosine kinase in the blast crisis of chronic myeloid leukemia and acute lymphoblastic leukemia with the Philadelphia chromosome. N Engl J Med. 2001 Apr 5;344(14):1038–42.

162. Buchdunger E, Cioffi CL, Law N, Stover D, Ohno-Jones S, Druker BJ, et al. Abl protein-tyrosine kinase inhibitor STI571 inhibits in vitro signal transduction mediated by c-kit and platelet-derived growth factor receptors. J Pharmacol Exp Ther. 2000 Oct;295(1):139–45.

163. Tamborini E, Miselli F, Negri T, Lagonigro MS, Staurengo S, Dagrada GP, et al. Molecular and biochemical analyses of platelet-derived growth factor receptor (PDGFR) B, PDGFRA, and KIT receptors in chordomas. Clin Cancer Res. 2006 Dec 1;12(23):6920–8.

164. Tamborini E, Virdis E, Negri T, Orsenigo M, Brich S, Conca E, et al. Analysis of receptor tyrosine kinases (RTKs) and downstream pathways in chordomas. Neuro-oncology. 2010 Aug;12(8):776–89.

165. Fasig JH, Dupont WD, LaFleur BJ, Olson SJ, Cates JMM. Immunohistochemical analysis of receptor tyrosine kinase signal transduction activity in chordoma. Neuropathol Appl Neurobiol. 2008 Feb;34(1):95–104.

166. de Castro Msc CV, Guimaraes G, Aguiar S, Lopes A, Baiocchi G, da Cunha IW, et al. Tyrosine kinase receptor expression in chordomas: phosphorylated AKT correlates inversely with outcome. Hum Pathol. 2013 Sep;44(9):1747–55.

167. Casali PG, Stacchiotti S, Messina A, Tamborini E, Martini C, Ripamonti C, et al. Imatinib mesylate in 18 advanced chordoma patients. ASCO Meeting Abstracts. 2005 Jun 1;23(16_suppl):9012.

168. Casali PG, Stacchiotti S, Sangalli C, Olmi P, Gronchi A. Chordoma. Curr Opin Oncol. 2007 Jul;19(4):367–70.

169. Stacchiotti S, Marrari A, Tamborini E, Palassini E, Virdis E, Messina A, et al. Response to imatinib plus sirolimus in advanced chordoma. Ann Oncol. 2009 Oct 27;20(11):1886–94.

170. Therasse P, Arbuck SG, Eisenhauer EA, Wanders J, Kaplan RS, Rubinstein L, et al. New Guidelines to Evaluate the Response to Treatment in Solid Tumors. JNCI Journal of the National Cancer Institute. 2000 Feb 2;92(3):205–16.

171. Stacchiotti S, Longhi A, Ferraresi V, Grignani G, Comandone A, Stupp R, et al. Phase II study of imatinib in advanced chordoma. J Clin Oncol. 2012 Mar 20;30(9):914–20.

172. Hindi N, Casali PG, Morosi C, Messina A, Palassini E, Pilotti S, et al. Imatinib in advanced chordoma: A retrospective case series analysis. Eur J Cancer. 2015 Aug 14.

173. Hof H, Welzel T, Debus J. Effectiveness of cetuximab/gefitinib in the therapy of a sacral chordoma. Onkologie. 2006 Dec;29(12):572–4.

174. George S, Merriam P, Maki RG, Van den Abbeele AD, Yap JT, Akhurst T, et al. Multicenter phase II trial of sunitinib in the treatment of nongastrointestinal stromal tumor sarcomas. J Clin Oncol. 2009 Jul 1;27(19):3154–60.

175. Lindén O, Stenberg L, Kjellén E. Regression of cervical spinal cord compression in a patient with chordoma following treatment with cetuximab and gefitinib. Acta Oncol. 2009;48(1):158–9.

176. Asklund T, Sandström M, Shahidi S, Riklund K, Henriksson R. Durable stabilization of three chordoma cases by bevacizumab and erlotinib. Acta Oncol. 2014 Jan 23.

177. Bozzi F, Manenti G, Conca E, Stacchiotti S, Messina A, Dagrada G, et al. Development of transplantable human chordoma xenograft for preclinical assessment of novel therapeutic strategies. Neuro- …. 2014.

178. Siu I-M, Ruzevick J, Zhao Q, Connis N, Jiao Y, Bettegowda C, et al. Erlotinib inhibits growth of a patient-derived chordoma xenograft. PLoS ONE. 2013;8(11):e78895.

179. Stacchiotti S, Tamborini E, Vullo Lo S, Bozzi F, Messina A, Morosi C, et al. Phase II study on lapatinib in advanced EGFR-positive chordoma. Ann Oncol. 2013 Apr 4.

180. Shalaby A, Presneau N, Ye H, Halai D, Berisha F, Idowu B, et al. The role of epidermal growth factor receptor in chordoma pathogenesis: a potential therapeutic target. J Pathol. 2011 Feb;223(3):336–46.

181. Weinberger PM, Yu Z, Kowalski D, Joe J, Manger P, Psyrri A, et al. Differential expression of epidermal growth factor receptor, c-Met, and HER2/neu in chordoma compared with 17 other malignancies. Arch Otolaryngol Head Neck Surg. 2005 Aug;131(8):707–11.

182. Dewaele B, Maggiani F, Floris G, Ampe M, Vanspauwen V, Wozniak A, et al. Frequent activation of EGFR in advanced chordomas. Clin Sarcoma Res. BioMed Central Ltd; 2011 Jul 25;1(1):4.

183. Walter BA, Begnami M, Valera VA, Santi M, Rushing EJ, Quezado M. Gain of chromosome 7 by chromogenic in situ hybridization (CISH) in chordomas is correlated to c-MET expression. J Neurooncol. 2011 Jan;101(2):199–206.

184. Ptaszyński K, Szumera-Ciećkiewicz A, Owczarek J, Mrozkowiak A, Pekul M, Barańska J, et al. Epidermal growth factor receptor (EGFR) status in chordoma. Pol J Pathol. 2009;60(2):81–7.

185. Xia M, Huang R, Sakamuru S, Alcorta D, Cho M-H, Lee D-H, et al. Identification of repurposed small molecule drugs for chordoma therapy. Cancer Biol Ther. 2013 Jul;14(7):638–47.

186. Akhavan-Sigari R, Abili M, Gaab MR, Rohde V, Zafar N, Emami P, et al. Immunohistochemical expression of receptor tyrosine kinase PDGFR-α, c-Met, and EGFR in skull base chordoma. Neurosurg Rev. 2014 Oct 17.

187. Akhavan-Sigari R, Gaab MR, Rohde V, Abili M, Ostertag H. Prognostic significance of immunohistochemical expression of VEGFR2 and iNOS in spinal chordoma. Eur Spine J. 2014 Nov;23(11):2416–22.

188. Organ SL, Tsao MS. An overview of the c-MET signaling pathway. Therapeutic Advances in Medical Oncology. 2011 Nov 1;3(1 Suppl):S7–S19.

189. Yuan TL, Cantley LC. PI3K pathway alterations in cancer: variations on a theme. Oncogene. Nature Publishing Group; 2008 Sep 15;27(41):5497–510.

190. De Luca A, Maiello MR, D'Alessio A, Pergameno M, Normanno N. The RAS/RAF/MEK/ERK and the PI3K/AKT signalling pathways: role in cancer pathogenesis and implications for therapeutic approaches. Expert Opin Ther Targets. 2012 Apr;16 Suppl 2:S17–27.

191. Sebolt-Leopold JS, Herrera R. Targeting the mitogen-activated protein kinase cascade to treat cancer. Nat Rev Cancer. Nature Publishing Group; 2004 Dec;4(12):937–47.

192. Schwab J, Antonescu C, Boland P, Healey J, Rosenberg A, Nielsen P, et al. Combination of PI3K/mTOR inhibition demonstrates efficacy in human chordoma. Anticancer Res. 2009 Jun;29(6):1867–71.

193. Ricci-Vitiani L, Runci D, D'Alessandris QG, Cenci T, Martini M, Bianchi F, et al. Chemotherapy of skull base chordoma tailored on responsiveness of patient-derived tumor cells to rapamycin. Neoplasia. 2013 Jul;15(7):773–82.

194. Akhavan-Sigari R, Gaab MR, Rohde V, Brandis A, Tezval H, Abili M, et al. Expression of vascular endothelial growth factor receptor 2 (VEGFR-2), inducible nitric oxide synthase (iNOS), and Ki-M1P in skull base chordoma: a series of 145 tumors. Neurosurg Rev. 2013 Sep 3.

195. Chen K-W, Yang H-L, Lu J, Wang G-L, Ji Y-M, Wu G-Z, et al. Expression of vascular endothelial growth factor and matrix metalloproteinase-9 in sacral chordoma. J Neurooncol. 2010 Jun 15;101(3):357–63.

196. Asklund T, Danfors T, Henriksson R. PET response and tumor stabilization under erlotinib and bevacizumab treatment of an intracranial lesion non-invasively diagnosed as likely chordoma. Clin Neuropathol. 2011

Sep;30(5):242–6.

197. Brüderlein S, Sommer JB, Meltzer PS, Li S, Osada T, Ng D, et al. Molecular characterization of putative chordoma cell lines. Sarcoma. 2010;2010:630129.

198. Scheipl S, Lohberger B, Rinner B, Froehlich EV, Beham A, Quehenberger F, et al. Histone deacetylase inhibitors as potential therapeutic approaches for chordoma: An immunohistochemical and functional analysis. J Orthop Res. 2013 Jul 24.

199. Liu X, Nielsen GP, Rosenberg AE, Waterman PR, Yang W, Choy E, et al. Establishment and characterization of a novel chordoma cell line: CH22. J Orthop Res. 2012 Apr 13;30(10):1666–73.

200. Bayrak OF, Aydemir E, Gulluoglu S, Sahin F, Sevli S, Yalvac ME, et al. The effects of chemotherapeutic agents on differentiated chordoma cells. J Neurosurg Spine. American Association of Neurological Surgeons; 2011 Dec;15(6):620–4.

201. Yang C, Hornicek FJ, Wood KB, Schwab JH, Choy E, Mankin H, et al. Blockage of Stat3 with CDDO-Me inhibits tumor cell growth in chordoma. Spine. 2010 Aug 15;35(18):1668–75.

202. Yang C, Hornicek FJ, Wood KB, Schwab JH, Choy E, Iafrate J, et al. Characterization and analysis of human chordoma cell lines. Spine. 2010 Jun 1;35(13):1257–64.

203. Han S, Polizzano C, Nielsen GP, Hornicek FJ, Rosenberg AE, Ramesh V. Aberrant hyperactivation of akt and Mammalian target of rapamycin complex 1 signaling in sporadic chordomas. Clin Cancer Res. 2009 Mar 15;15(6):1940–6.

204. Adenis A, Ray-Coquard I, Italiano A, Chauzit E, Bui-Nguyen B, Blay J-Y, et al. A dose-escalating phase I of imatinib mesylate with fixed dose of metronomic cyclophosphamide in targeted solid tumours. Br J Cancer. 2013 Nov 12;109(10):2574–8.

205. Al-Adra D, Bennett A, Gill R, Lees G. Pediatric metastatic sacrococcygeal chordoma treated with surgery. Eur J Pediatr Surg. 2011 May;21(3):196–8.

206. Launay SG, Chetaille B, Medina F, Perrot D, Nazarian S, Guiramand J, et al. Efficacy of epidermal growth factor receptor targeting in advanced chordoma: case report and literature review. BMC Cancer. BioMed Central Ltd; 2011 Oct 4;11(1):423.

207. Ferraresi V, Nuzzo C, Zoccali C, Marandino F, Vidiri A, Salducca N, et al. Chordoma: clinical characteristics, management and prognosis of a case series of 25 patients. BMC Cancer. 2010;10:22.

208. Geoerger B, Morland B, Ndiaye A, Doz F, Kalifa G, Geoffray A, et al. Target-driven exploratory study of imatinib mesylate in children with solid malignancies by the Innovative Therapies for Children with Cancer (ITCC) European Consortium. Eur J Cancer. 2009 Sep;45(13):2342–51.

209. Singhal N, Kotasek D, Parnis FX. Response to erlotinib in a patient with treatment refractory chordoma. Anticancer Drugs. 2009 Nov;20(10):953–5.

210. Casali PG, Messina A, Stacchiotti S, Tamborini E, Crippa F, Gronchi A, et al. Imatinib mesylate in chordoma. Cancer. 2004 Oct 18;101(9):2086–97.

211. Kay MA. State-of-the-art gene-based therapies: the road ahead. Nat Rev Genet. Nature Publishing Group; 2011 Apr 6;12(5):316–28.

212. Klug B, Celis P, Carr M, Reinhardt J. Regulatory structures for gene therapy medicinal products in the European Union. Meth Enzymol. 2012;507:337–54.

213. Sia RH, Dawson MH. In Vitro Transformation Of Pneumococcal Types : Ii. The Nature Of The Factor Responsible For The Transformation Of Pneumococcal Types. J Exp Med. 1931 Oct 31;54(5):701–10.

214. Dawson MH, Sia RH. In Vitro Transformation Of Pneumococcal Types : I. A Technique For Inducing Transformation Of Pneumococcal Types In Vitro. J Exp Med. 1931 Oct 31;54(5):681–99.

215. Lynch RG. Pneumococcal Transformation: Genes are Made of DNA. Journal of Experimental Medicine. 1944.

216. Zinder ND, Lederberg J. GENETIC EXCHANGE IN SALMONELLA. J Bacteriol. 1952.

217. Lederberg J. A view of genetics. Les Prix Nobel en. 1958.

218. Rogers S, Pfuderer P. Use of viruses as carriers of added genetic information. Nature. 1968 Aug 17;219(5155):749–51.

219. Rogers S, Lowenthal A, Terheggen HG, Columbo JP. Induction of arginase activity with the Shope papilloma virus in tissue culture cells from an argininemic patient. J Exp Med. 1973 Apr 1;137(4):1091–6.

220. Terheggen HG, Lowenthal A, Lavinha F, Colombo JP, Rogers S. Unsuccessful trial of gene replacement in arginase deficiency. Z Kinderheilkd. 1975;119(1):1–3.

221. Wirth T, Parker N, Ylä-Herttuala S. History of gene therapy. Gene. 2013 Apr 23.

222. Jackson DA, Symons RH, Berg P. Biochemical method for inserting new genetic information into DNA of Simian Virus 40: circular SV40 DNA molecules containing lambda phage genes and the galactose operon of Escherichia coli. Proc Natl Acad Sci USA. 1972 Oct;69(10):2904–9.

223. Lobban PE, Kaiser AD. Enzymatic end-to-end joining of DNA molecules. J Mol Biol. 1973.

224. Cohen SN, Chang AC, Boyer HW, Helling RB. Construction of biologically functional bacterial plasmids in vitro. Proc Natl Acad Sci USA. 1973 Nov;70(11):3240–4.

225. Blaese RM, Culver KW, Miller AD, Carter CS, Fleisher T, Clerici M, et al. T lymphocyte-directed gene therapy for ADA- SCID: initial trial results after 4 years. Science. 1995 Oct 20;270(5235):475–80.

226. Stolberg SG. The biotech death of Jesse Gelsinger. The New York times magazine. 1999 Nov 28;:136–140–149–150.

227. Cavazzana-Calvo M, Hacein-Bey S, de Saint Basile G, Gross F, Yvon E, Nusbaum P, et al. Gene therapy of human severe combined immunodeficiency (SCID)-X1 disease. Science. 2000 Apr 28;288(5466):669–72.

228. Hacein-Bey-Abina S, Kalle von C, Schmidt M, Le Deist F, Wulffraat N, McIntyre E, et al. A serious adverse event after successful gene therapy for X-linked severe combined immunodeficiency. N Engl J Med. 2003 Jan 16;348(3):255–6.

229. Kohn DB. Update on gene therapy for immunodeficiencies. Clin Immunol. 2010 May;135(2):247–54.

230. Hacein-Bey-Abina S, Pai S-Y, Gaspar HB, Armant M, Berry CC, Blanche S, et al. A modified γ-retrovirus vector for X-linked severe combined immunodeficiency. N Engl J Med. 2014 Oct 9;371(15):1407–17.

231. High KH, Nathwani A, Spencer T, Lillicrap D. Current status of haemophilia gene therapy. Haemophilia. 2014 May;20 Suppl 4:43–9.

232. Sauer AV, Di Lorenzo B, Carriglio N, Aiuti A. Progress in gene therapy for primary immunodeficiencies using lentiviral vectors. Curr Opin Allergy Clin Immunol. 2014 Dec;14(6):527–34.

233. Knight S, Zhang F, Mueller-Kuller U, Bokhoven M, Gupta A, Broughton T, et al. Safer, silencing-resistant lentiviral vectors: optimization of the ubiquitous chromatin-opening element through elimination of aberrant splicing. J Virol. 2012 Sep;86(17):9088–95.

234. Schambach A, Zychlinski D, Ehrnstroem B, Baum C. Biosafety features of lentiviral vectors. Human Gene Therapy. 2013 Feb;24(2):132–42.

235. Nathwani AC, Tuddenham EGD, Rangarajan S, Rosales C, McIntosh J, Linch DC, et al. Adenovirus-Associated Virus Vector–Mediated Gene Transfer in Hemophilia B. N Engl J Med. 2011 Dec 22;365(25):2357–65.

236. Hareendran S, Balakrishnan B, Sen D, Kumar S, Srivastava A, Jayandharan GR. Adeno-associated virus (AAV) vectors in gene therapy: immune challenges and strategies to circumvent them. Rev Med Virol. 2013 Nov;23(6):399–413.

237. Mittermeyer G, Christine CW, Rosenbluth KH, Baker SL, Starr P, Larson P, et al. Long-term evaluation of a phase 1 study of AADC gene therapy for Parkinson's disease. Human Gene Therapy. 2012 Apr;23(4):377–81.

238. Loring HS, Flotte TR. Current status of gene therapy for α-1 antitrypsin deficiency. Expert Opin Biol Ther. 2015 Mar;15(3):329–36.

239. Stroes ES, Nierman MC, Meulenberg JJ, Franssen R, Twisk J, Henny CP, et al. Intramuscular administration of AAV1-lipoprotein lipase S447X lowers triglycerides in lipoprotein lipase-deficient patients. Arterioscler Thromb Vasc Biol. 2008 Dec;28(12):2303–4.

240. Nierman MC, Rip J, Twisk J, Meulenberg JJM, Kastelein JJP, Stroes ESG, et al. Gene therapy for genetic lipoprotein lipase deficiency: from promise to practice. Neth J Med. 2005 Jan;63(1):14–9.

241. Flemming A. Regulatory watch: Pioneering gene therapy on brink of approval. Nat Rev Drug Discov. Nature Publishing Group; 2012 Aug 31;11(9):664–4.

242. Gruber K. Europe gives gene therapy the green light. The Lancet. Elsevier; 2012 Nov 17;380(9855):e10.

243. Ylä-Herttuala S. Endgame: glybera finally recommended for approval as the first gene therapy drug in the European union. Molecular Therapy. 2012 Oct;20(10):1831–2.

244. Gancberg D, Kessler C, Hoeveler A, Draghia-Akli R. European Union Support of Gene Therapy Research: A Success Story. Molecular Therapy. Nature Publishing Group; 2012 Dec;20(12):2191–3.

245. Zhu X, McTiernan CF, Rajagopalan N, Shah H, Fischer D, Toyoda Y, et al. Immunosuppression decreases inflammation and increases AAV6-hSERCA2a-mediated SERCA2a expression. Human Gene Therapy. 2012 Jul;23(7):722–32.

246. Zouein FA, Booz GW. AAV-mediated gene therapy for heart failure: enhancing contractility and calcium handling. F1000Prime Rep. 2013;5:27.

247. Giacca M, Zacchigna S. Virus-mediated gene delivery for human gene therapy. J Control Release. 2012 Jul 20;161(2):377–88.

248. Brenner MK, Gottschalk S, Leen AM, Vera JF. Is cancer gene therapy an empty suit? Lancet Oncol. 2013 Oct;14(11):e447–56.

249. Ginn SL, Alexander IE, Edelstein ML, Abedi MR, Wixon J. Gene therapy clinical trials worldwide to 2012 - an update. J Gene Med. 2013 Feb;15(2):65–77.

250. Jazwa A, Florczyk U, Jozkowicz A, Dulak J. Gene therapy on demand: Site specific regulation of gene therapy. Gene. 2013 Apr 6.

251. Luo J, Luo Y, Sun J, Zhou Y, Zhang Y, Yang X. Adeno-associated virus-mediated cancer gene therapy: current status. Cancer Letters. 2015 Jan 28;356(2 Pt B):347–56.

252. Amer MH. Gene therapy for cancer: present status and future perspective. 2014 Sep 10;2(1):1–19.

253. Hong B, Pieter J van den Heuvel A, V Prabhu V, Zhang S, S El-Deiry W. Targeting Tumor Suppressor p53 for Cancer Therapy: Strategies,

Challenges and Opportunities. Current drug …. Bentham Science Publishers; 2014.

254. Roth JA, Swisher SG, Meyn RE. p53 tumor suppressor gene therapy for cancer. Oncology (Williston Park, NY). 1999 Oct;13(10 Suppl 5):148–54.

255. Clayman GL, el-Naggar AK, Lippman SM, Henderson YC, Frederick M, Merritt JA, et al. Adenovirus-mediated p53 gene transfer in patients with advanced recurrent head and neck squamous cell carcinoma. J Clin Oncol. 1998 Jun;16(6):2221–32.

256. Hanahan D, Weinberg RA. Hallmarks of Cancer: The Next Generation. Cell. Elsevier Inc; 2011 Mar 4;144(5):646–74.

257. Muller PAJ, Vousden KH. Mutant p53 in cancer: new functions and therapeutic opportunities. Cancer Cell. 2014 Mar 17;25(3):304–17.

258. Leroy B, Anderson M, Soussi T. TP53 mutations in human cancer: database reassessment and prospects for the next decade. Hum Mutat. 2014 Jun;35(6):672–88.

259. Zhao H, Wang D-D, Xu Y-X, Zhu C-Q. [Localization and expression pattern of MDM2 in axon initial segments of neuron in rodent brain]. Sheng Li Xue Bao. 2014 Apr 25;66(2):107–17.

260. Cheok CF, Verma CS, Baselga J, Lane DP. Translating p53 into the clinic. Nat Rev Clin Oncol. 2011 Jan;8(1):25–37.

261. Pearson S, Jia H, Kandachi K. China approves first gene therapy. Nature Biotechnology. 2004 Jan;:3–4.

262. Peng Z. Current status of gendicine in China: recombinant human Ad-p53 agent for treatment of cancers. Human Gene Therapy. 2005 Sep;16(9):1016–27.

263. Yang Z-X, Wang D, Wang G, Zhang Q-H, Liu J-M, Peng P, et al. Clinical study of recombinant adenovirus-p53 combined with fractionated stereotactic radiotherapy for hepatocellular carcinoma. J Cancer Res Clin Oncol. 2010 Apr;136(4):625–30.

264. Voon Y-L, Ahmad M, Wong P-F, Husaini R, Ng WT-W, Leong C-O, et al. Nutlin-3 sensitizes nasopharyngeal carcinoma cells to cisplatin-induced cytotoxicity. Oncol Rep. 2015 Oct;34(4):1692–700.

265. Zeimet AG, Marth C. Why did p53 gene therapy fail in ovarian cancer? Lancet Oncology. 2003 Jul;4(7):415–22.

266. Shi J, Zheng D. An update on gene therapy in China. Curr Opin Mol Ther. 2009 Oct;11(5):547–53.

267. Speetjens FM, Kuppen PJK, Welters MJP, Essahsah F, Voet van den Brink AMEG, Lantrua MGK, et al. Induction of p53-specific immunity by a p53 synthetic long peptide vaccine in patients treated for metastatic colorectal cancer. Clin Cancer Res. 2009 Feb 1;15(3):1086–95.

268. Chiappori AA, Soliman H, Janssen WE, Antonia SJ, Gabrilovich DI. INGN-225: a dendritic cell-based p53 vaccine (Ad.p53-DC) in small cell lung cancer: observed association between immune response and enhanced chemotherapy effect. Expert Opin Biol Ther. 2010 Jun;10(6):983–91.

269. Zhao Y, Aguilar A, Bernard D, Wang S. Small-Molecule Inhibitors of the MDM2-p53 Protein-Protein Interaction (MDM2 Inhibitors) in Clinical Trials for Cancer Treatment. J Med Chem. 2015 Feb 12;58(3):1038–52.

270. Russell SJ, Peng K-W, Bell JC. Oncolytic virotherapy. Nat Biotech. 2012 Jul;30(7):658–70.

271. Kelly E, Russell SJ. History of oncolytic viruses: genesis to genetic engineering. Mol Ther. 2007 Apr;15(4):651–9.

272. Kaufman HL, Bines SD. OPTIM trial: a Phase III trial of an oncolytic herpes virus encoding GM-CSF for unresectable stage III or IV melanoma. Future Oncology. Future Medicine Ltd London, UK; 2010 Jun;6(6):941–9.

273. Meerani S, Yao Y. Oncolytic viruses in cancer therapy. Eur J Sci Res. 2010.

274. Varghese S, Rabkin SD. Oncolytic herpes simplex virus vectors for cancer virotherapy. Cancer Gene Therapy. 2002 Dec;9(12):967–78.

275. Rogulski KR, Wing MS, Paielli DL, Gilbert JD, Kim JH, Freytag SO. Double suicide gene therapy augments the antitumor activity of a replication-competent lytic adenovirus through enhanced cytotoxicity and radiosensitization. Human Gene Therapy. 2000 Jan 1;11(1):67–76.

276. Gabel M, Kim JH, Kolozsvary A, Khil M, FREYTAG S. Selective in vivo radiosensitization by 5-fluorocytosine of human colorectal carcinoma cells transduced with the E. coli cytosine deaminase (CD) gene. Int J Radiat Oncol Biol Phys. 1998 Jul 1;41(4):883–7.

277. Kim JH, Kolozsvary A, Rogulski K, Khil MS, Brown SL, Freytag SO. Selective radiosensitization of 9L glioma in the brain transduced with double suicide fusion gene. Cancer J Sci Am. 1998 Nov;4(6):364–9.

278. Freytag SO, Movsas B, Aref I, Stricker H, Peabody J, Pegg J, et al. Phase I Trial of Replication-competent Adenovirus-mediated Suicide Gene Therapy Combined with IMRT for Prostate Cancer. Molecular Therapy. 2007 Mar 20;15(5):1016–23.

279. Moolten FL. Tumor chemosensitivity conferred by inserted herpes thymidine kinase genes: paradigm for a prospective cancer control strategy. Cancer Research. 1986 Oct;46(10):5276–81.

280. Moolten FL, Wells JM. Curability of tumors bearing herpes thymidine kinase genes transferred by retroviral vectors. J Natl Cancer Inst. 1990 Feb 21;82(4):297–300.

281. Nyati MK, Symon Z, Kievit E, Dornfeld KJ, Rynkiewicz SD, Ross BD, et al. The potential of 5-fluorocytosine/cytosine deaminase enzyme prodrug

gene therapy in an intrahepatic colon cancer model. Gene Ther. 2002 Jul;9(13):844–9.

282. Yamada S, Kuroda T, Fuchs BC, He X, Supko JG, Schmitt A, et al. Oncolytic herpes simplex virus expressing yeast cytosine deaminase: relationship between viral replication, transgene expression, prodrug bioactivation. Cancer Gene Therapy. 2012 Mar;19(3):160–70.

283. Freytag SO, Stricker H, Lu M, Elshaikh M, Aref I, Pradhan D, et al. Prospective randomized phase 2 trial of intensity modulated radiation therapy with or without oncolytic adenovirus-mediated cytotoxic gene therapy in intermediate-risk prostate cancer. Int J Radiat Oncol Biol Phys. 2014 Jun 1;89(2):268–76.

284. Senzer NN, Kaufman HL, Amatruda T, Nemunaitis M, Reid T, Daniels G, et al. Phase II clinical trial of a granulocyte-macrophage colony-stimulating factor-encoding, second-generation oncolytic herpesvirus in patients with unresectable metastatic melanoma. J Clin Oncol. 2009 Dec 1;27(34):5763–71.

285. Sheridan C. Amgen announces oncolytic virus shrinks tumors : Nature Biotechnology : Nature Publishing Group. Nat Biotech. 2013.

286. Andtbacka RHI, Kaufman HL, Collichio F, Amatruda T, Senzer N, Chesney J, et al. Talimogene Laherparepvec Improves Durable Response Rate in Patients With Advanced Melanoma. J Clin Oncol. 2015 May 26.

287. Rosenberg SA, Yang JC, Restifo NP. Cancer immunotherapy: moving beyond current vaccines. Nat Med. 2004 Sep;10(9):909–15.

288. Palucka K, Banchereau J. Cancer immunotherapy via dendritic cells. Nat Rev Cancer. Nature Publishing Group; 2012 Mar 22;12(4):265–77.

289. Goldman B, DeFrancesco L. The cancer vaccine roller coaster. Nat Biotech. 2009 Feb;27(2):129–39.

290. Zhou P, Shaffer DR, Alvarez Arias DA, Nakazaki Y, Pos W, Torres AJ, et al. In vivo discovery of immunotherapy targets in the tumour microenvironment. Nature. 2014 Feb 6;506(7486):52–7.

291. Cheever MA, Allison JP, Ferris AS, Finn OJ, Hastings BM, Hecht TT, et al. The prioritization of cancer antigens: a national cancer institute pilot project for the acceleration of translational research. Clin Cancer Res. 2009 Sep 1;15(17):5323–37.

292. Ridgway D. The first 1000 dendritic cell vaccinees. Cancer Invest. 2003;21(6):873–86.

293. Nencioni A, Grünebach F, Schmidt SM, Müller MR, Boy D, Patrone F, et al. The use of dendritic cells in cancer immunotherapy. Critical Reviews in Oncology/Hematology. 2008 Mar;65(3):191–9.

294. Palena C, Fernando RI, Hamilton DH. An immunotherapeutic intervention against tumor progression: Targeting a driver of the epithelial-to-

mesenchymal transition. Oncoimmunology. 2014 Jan 1;3(1):e27220.

295. Hamilton DH, Litzinger MT, Jales A, Huang B, Fernando RI, Hodge JW, et al. Immunological targeting of tumor cells undergoing an epithelial-mesenchymal transition via a recombinant brachyury-yeast vaccine. Oncotarget. 2013 Oct;4(10):1777–90.

296. Tucker JA, Jochems C, Boyerinas B, Fallon J, Greiner JW, Palena C, et al. Identification and characterization of a cytotoxic T-lymphocyte agonist epitope of brachyury, a transcription factor involved in epithelial to mesenchymal transition and metastasis. Cancer Immunol Immunother. 2014 Dec;63(12):1307–17.

297. Donahue RN, Grenga I, Lepone L, Gulley JL, Heery CR, Madan RA, et al. Identification of tumor associated immune responses against brachyury, a transcription factor and driver of EMT, in chordoma patients receiving a yeast-brachyury vaccine (gi-6301). J Immunother Cancer. BioMed Central; 2014;2(Suppl 3):P148.

298. Heery CR, Singh BH, Rauckhorst M, Marte JL, Donahue RN, Grenga I, et al. Phase I trial of a yeast-based therapeutic cancer vaccine (GI-6301) targeting the transcription factor brachyury. Cancer Immunol Res. 2015 Jun 30.

299. Small EJ, Schellhammer PF, Higano CS, Redfern CH, Nemunaitis JJ, Valone FH, et al. Placebo-controlled phase III trial of immunologic therapy with sipuleucel-T (APC8015) in patients with metastatic, asymptomatic hormone refractory prostate cancer. J Clin Oncol. 2006 Jul 1;24(19):3089–94.

300. Kantoff PW, Higano CS, Shore ND, Berger ER, Small EJ, Penson DF, et al. Sipuleucel-T immunotherapy for castration-resistant prostate cancer. N Engl J Med. 2010 Jul 29;363(5):411–22.

301. Higano CS, Small EJ, Schellhammer P, Yasothan U, Gubernick S, Kirkpatrick P, et al. Sipuleucel-T. Nature reviews Drug discovery. 2010 Jul;:513–4.

302. Sonpavde G, Di Lorenzo G, Higano CS, Kantoff PW, Madan R, Shore ND. The role of sipuleucel-T in therapy for castration-resistant prostate cancer: a critical analysis of the literature. Eur Urol. 2012 Apr;61(4):639–47.

303. Di Lorenzo G, Ferro M, Buonerba C. Sipuleucel-T (Provenge®) for castration-resistant prostate cancer. BJU Int. 2012 Jul;110(2 Pt 2):E99–104.

304. Hodi FS, O'Day SJ, McDermott DF, Weber RW, Sosman JA, Haanen JB, et al. Improved Survival with Ipilimumab in Patients with Metastatic Melanoma. N Engl J Med. 2010 Aug 19;363(8):711–23.

305. Restifo NP, Dudley ME, Rosenberg SA. Adoptive immunotherapy for cancer: harnessing the T cell response. Nat Rev Immunol. 2012 Apr;12(4):269–81.

306. Maus MV, Grupp SA, Porter DL, June CH. Antibody-modified T cells: CARs take the front seat for hematologic malignancies. Blood. 2014 Apr 24;123(17):2625–35.

307. Kakarla S, Gottschalk S. CAR T cells for solid tumors: armed and ready to go? Cancer J. 2014 Mar;20(2):151–5.

308. Sioud M. RNA interference: mechanisms, technical challenges, and therapeutic opportunities. Methods Mol Biol. 2015;1218:1–15.

309. Alvarado V, Scholthof HB. Plant responses against invasive nucleic acids: RNA silencing and its suppression by plant viral pathogens. Semin Cell Dev Biol. 2009 Dec;20(9):1032–40.

310. Jeang K-T. RNAi in the regulation of mammalian viral infections. BMC Biol. 2012;10:58.

311. Russo A, Potenza N. Antiviral effects of human microRNAs and conservation of their target sites. FEBS Lett. 2011 Aug 19;585(16):2551–5.

312. Waterhouse PM, Wang MB, Lough T. Gene silencing as an adaptive defence against viruses. Nature. 2001 Jun 14;411(6839):834–42.

313. Pasquinelli AE, Ruvkun G. Control of developmental timing by micrornas and their targets. Annu Rev Cell Dev Biol. 2002;18:495–513.

314. Bartel DP. MicroRNAs: genomics, biogenesis, mechanism, and function. Cell. 2004 Jan 23;116(2):281–97.

315. Wienholds E, Plasterk R. MicroRNA function in animal development. FEBS Lett. 2005.

316. Cheng Y, Zhang C. MicroRNA-21 in Cardiovascular Disease. J of Cardiovasc Trans Res. Springer US; 2010 May 1;3(3):251–5.

317. Christensen M, Schratt GM. microRNA involvement in developmental and functional aspects of the nervous system and in neurological diseases. Neuroscience Letters. 2009 Dec;466(2):55–62.

318. Pencheva N, Tavazoie SF. Control of metastatic progression by microRNA regulatory networks. Nat Cell Biol. Nature Publishing Group; 2013 Jun 3;15(6):546–54.

319. Fuchs U, Damm-Welk C, Borkhardt A. Silencing of disease-related genes by small interfering RNAs. Curr Mol Med. 2004 Aug;4(5):507–17.

320. Jorgensen R. Altered gene expression in plants due to trans interactions between homologous genes. Trends Biotechnol. 1990 Dec;8(12):340–4.

321. Napoli C, Lemieux C, Jorgensen R. Introduction of a Chimeric Chalcone Synthase Gene into Petunia Results in Reversible Co-Suppression of Homologous Genes in trans. Plant Cell. 1990 Apr;2(4):279–89.

322. Fire A, Xu S, Montgomery MK, Kostas SA, Driver SE, Mello CC. Potent

and specific genetic interference by double-stranded RNA in Caenorhabditis elegans. Nature. 1998 Feb 19;391(6669):806–11.

323. Montgomery MK, Fire A. Double-stranded RNA as a mediator in sequence-specific genetic silencing and co-suppression. Trends Genet. 1998 Jul;14(7):255–8.

324. Tuschl T, Zamore PD, Lehmann R, Bartel DP, Sharp PA. Targeted mRNA degradation by double-stranded RNA in vitro. Genes & Development. 1999 Dec 15;13(24):3191–7.

325. Elbashir SM, Harborth J, Lendeckel W, Yalcin A, Weber K, Tuschl T. Duplexes of 21-nucleotide RNAs mediate RNA interference in cultured mammalian cells. Nature. 2001 May 24;411(6836):494–8.

326. Montgomery MK, Xu S, Fire A. RNA as a target of double-stranded RNA-mediated genetic interference in Caenorhabditis elegans. Proc Natl Acad Sci USA. 1998 Dec 22;95(26):15502–7.

327. Hannon GJ. RNA interference. Nature. 2002 Jul 11;418(6894):244–51.

328. Zamore PD, Tuschl T, Sharp PA, Bartel DP. RNAi: double-stranded RNA directs the ATP-dependent cleavage of mRNA at 21 to 23 nucleotide intervals. Cell. 2000 Mar 31;101(1):25–33.

329. Wang Z, Rao DD, Senzer N, Nemunaitis J. RNA Interference and Cancer Therapy. Pharm Res. 2011 Oct 19;28(12):2983–95.

330. Wu SY, Lopez-Berestein G, Calin GA, Sood AK. RNAi therapies: drugging the undruggable. Science Translational Medicine. 2014 Jun 11;6(240):240ps7.

331. Deng JH, Deng P, Lin S-L, Ying S-Y. Targeting bcr-abl Transcripts with siRNAs in an Imatinib-Resistant Chronic Myeloid Leukemia Patient: Challenges and Future Directions. Methods Mol Biol. 2015;1218:321–40.

332. Hutvágner G, Zamore PD. A microRNA in a multiple-turnover RNAi enzyme complex. Science. 2002 Sep 20;297(5589):2056–60.

333. Brummelkamp TR, Bernards R, Agami R. A system for stable expression of short interfering RNAs in mammalian cells. Science. 2002 Apr 19;296(5567):550–3.

334. Brummelkamp TR, Bernards R, Agami R. Stable suppression of tumorigenicity by virus-mediated RNA interference. Cancer Cell. 2002 Sep;2(3):243–7.

335. Meister G, Tuschl T. Mechanisms of gene silencing by double-stranded RNA. Nature. 2004 Sep 16;431(7006):343–9.

336. Zhang H, Kolb FA, Brondani V, Billy E, Filipowicz W. Human Dicer preferentially cleaves dsRNAs at their termini without a requirement for ATP. EMBO J. 2002 Nov 1;21(21):5875–85.

337. Park J-E, Heo I, Tian Y, Simanshu DK, Chang H, Jee D, et al. Dicer recognizes the 5′ end of RNA for efficient and accurate processing. Nature. Nature Publishing Group; 2011 Jul 13;475(7355):201–5.

338. Matranga C, Tomari Y, Shin C, Bartel DP, Zamore PD. Passenger-strand cleavage facilitates assembly of siRNA into Ago2-containing RNAi enzyme complexes. Cell. 2005 Nov 18;123(4):607–20.

339. Meister G, Landthaler M, Patkaniowska A, Dorsett Y. Human Argonaute2 Mediates RNA Cleavage Targeted by miRNAs and siRNAs. Mol Cell. 2004.

340. Moore CB, Guthrie EH, Huang MT-H, Taxman DJ. Short hairpin RNA (shRNA): design, delivery, and assessment of gene knockdown. Methods Mol Biol. 2010;629:141–58.

341. Rao DD, Vorhies JS, Senzer N, Nemunaitis J. siRNA vs. shRNA: similarities and differences. Adv Drug Deliv Rev. 2009 Jul 25;61(9):746–59.

342. Castanotto D, Rossi JJ. The promises and pitfalls of RNA-interference-based therapeutics : Abstract : Nature. Nature. 2009.

343. Paddison PJ, Caudy AA, Bernstein E, Hannon GJ, Conklin DS. Short hairpin RNAs (shRNAs) induce sequence-specific silencing in mammalian cells. Genes & Development. 2002 Apr 15;16(8):948–58.

344. Lee Y, Jeon K, Lee J-T, Kim S, Kim VN. MicroRNA maturation: stepwise processing and subcellular localization. EMBO J. 2002 Sep 2;21(17):4663–70.

345. Lee Y, Ahn C, Han J, Choi H, Kim J, Yim J, et al. The nuclear RNase III Drosha initiates microRNA processing. Nat Cell Biol. Nature Publishing Group; 2003 Sep 25;425(6956):415–9.

346. Cullen BR. Transcription and processing of human microRNA precursors. Mol Cell. 2004 Dec 22;16(6):861–5.

347. Yi R, Qin Y, Macara IG, Cullen BR. Exportin-5 mediates the nuclear export of pre-microRNAs and short hairpin RNAs. Genes & Development. 2003 Dec 15;17(24):3011–6.

348. Lee YS, Nakahara K, Pham JW, Kim K, He Z, Sontheimer EJ, et al. Distinct roles for Drosophila Dicer-1 and Dicer-2 in the siRNA/miRNA silencing pathways. Cell. 2004 Apr 2;117(1):69–81.

349. Rand TA, Petersen S, Du F, Wang X. Argonaute2 Cleaves the Anti-Guide Strand of siRNA during RISC Activation. Cell. 2005 Nov;123(4):621–9.

350. Preall JB, Sontheimer EJ. RNAi: RISC gets loaded. Cell. 2005 Nov 18;123(4):543–5.

351. Perwitasari O, Bakre A, Tompkins SM, Tripp RA. siRNA Genome Screening Approaches to Therapeutic Drug Repositioning.

Pharmaceuticals (Basel). 2013;6(2):124–60.

352. Flowers GP, Timberlake AT, McLean KC, Monaghan JR, Crews CM. Highly efficient targeted mutagenesis in axolotl using Cas9 RNA-guided nuclease. Development. 2014 May;141(10):2165–71.

353. Doudna JA, Charpentier E. The new frontier of genome engineering with CRISPR-Cas9. Science. 2014.

354. Koo T, Lee J, Kim J-S. Measuring and Reducing Off-Target Activities of Programmable Nucleases Including CRISPR-Cas9. Mol Cells. 2015 Jun 30;38(6):475–81.

355. Hsu PD, Lander ES, Zhang F. Development and Applications of CRISPR-Cas9 for Genome Engineering. Cell. 2014.

356. Ran FA, Hsu PD, Wright J, Agarwala V, Scott DA, Zhang F. Genome engineering using the CRISPR-Cas9 system. Nature Protocols. Nature Publishing Group; 2013 Oct 24;8(11):2281–308.

357. Whelan J. First clinical data on RNAi. Drug Discovery Today. 2005.

358. Kaiser PK, Symons RCA, Shah SM, Quinlan EJ, Tabandeh H, Do DV, et al. RNAi-based treatment for neovascular age-related macular degeneration by Sirna-027. Am J Ophthalmol. 2010 Jul;150(1):33–39.e2.

359. Davidson BL, McCray PB. Current prospects for RNA interference-based therapies. Nat Rev Genet. 2011 May;12(5):329–40.

360. Weinstein IB. Cancer. Addiction to oncogenes--the Achilles heal of cancer. Science. 2002 Jul 5;297(5578):63–4.

361. Berns K, Hijmans EM, Mullenders J, Brummelkamp TR, Velds A, Heimerikx M, et al. A large-scale RNAi screen in human cells identifies new components of the p53 pathway. Nature. 2004 Mar 25;428(6981):431–7.

362. Lord CJ, Martin SA, Ashworth A. RNA interference screening demystified. J Clin Pathol. 2009 Mar;62(3):195–200.

363. Murugaesu N, Iravani M, van Weverwijk A, Ivetic A, Johnson DA, Antonopoulos A, et al. An In Vivo Functional Screen Identifies ST6GalNAc2 Sialyltransferase as a Breast Cancer Metastasis Suppressor. Cancer Discovery. 2014 Feb 11.

364. Silva JM, Li MZ, Chang K, Ge W, Golding MC, Rickles RJ, et al. Second-generation shRNA libraries covering the mouse and human genomes. Nat Genet. 2005 Nov;37(11):1281–8.

365. Brummelkamp TR, Fabius AWM, Mullenders J, Madiredjo M, Velds A, Kerkhoven RM, et al. An shRNA barcode screen provides insight into cancer cell vulnerability to MDM2 inhibitors. Nat Chem Biol. 2006 Apr;2(4):202–6.

366. Bernards R, Brummelkamp TR, Beijersbergen RL. shRNA libraries and their use in cancer genetics - Nature Methods. Nat Methods. 2006.

367. Iorns E, Lord CJ, Grigoriadis A, McDonald S, Fenwick K, Mackay A, et al. Integrated functional, gene expression and genomic analysis for the identification of cancer targets. PLoS ONE. 2009;4(4):e5120.

368. Iorns E, Ward TM, Dean S, Jegg A, Thomas D, Murugaesu N, et al. Whole genome in vivo RNAi screening identifies the leukemia inhibitory factor receptor as a novel breast tumor suppressor. Breast Cancer Res Treat. 2012 Aug;135(1):79–91.

369. Phalon C, Rao DD, Nemunaitis J. Potential use of RNA interference in cancer therapy. Expert Rev Mol Med. 2010;12:e26.

370. Yang W-Q, Zhang Y. RNAi-mediated gene silencing in cancer therapy. Expert Opin Biol Ther. 2012 Nov;12(11):1495–504.

371. Lam AQ, Freedman BS, Morizane R, Lerou PH, Valerius MT, Bonventre JV. Rapid and Efficient Differentiation of Human Pluripotent Stem Cells into Intermediate Mesoderm That Forms Tubules Expressing Kidney Proximal Tubular Markers. J Am Soc Nephrol. 2013 Dec 19.

372. Li C, Feng Y, Coukos G, Zhang L. Therapeutic MicroRNA Strategies in Human Cancer. AAPS J. 2009 Oct 29;11(4):747–57.

373. Burnett JC, Rossi JJ, Tiemann K. Current progress of siRNA/shRNA therapeutics in clinical trials. Biotechnol J. 2011 Sep;6(9):1130–46.

374. Gandhi NS, Tekade RK, Chougule MB. Nanocarrier mediated delivery of siRNA/miRNA in combination with chemotherapeutic agents for cancer therapy: Current progress and advances. J Control Release. 2014 Sep 7;194C:238–56.

375. Zhou Y, Zhang C, Liang W. Development of RNAi technology for targeted therapy - A track of siRNA based agents to RNAi therapeutics. J Control Release. 2014 May 6.

376. Davis ME, Zuckerman JE, Choi CHJ, Seligson D, Tolcher A, Alabi CA, et al. Evidence of RNAi in humans from systemically administered siRNA via targeted nanoparticles. Nature. 2010 Apr 15;464(7291):1067–70.

377. Tabernero J, Shapiro GI, LoRusso PM, Cervantes A, Schwartz GK, Weiss GJ, et al. First-in-humans trial of an RNA interference therapeutic targeting VEGF and KSP in cancer patients with liver involvement. Cancer Discovery. 2013 Apr;3(4):406–17.

378. Ramanathan. Abstract LB-289: A phase I dose escalation study of TKM-080301, a RNAi therapeutic directed against PLK1, in patients with advanced solid tumors. Cancer Research. 2013;73(8 Supplement):LB–LB–289.

379. Rolle K, Nowak S, Wyszko E, Nowak M, Zukiel R, Piestrzeniewicz R, et al. Promising human brain tumors therapy with interference RNA intervention

(iRNAi). Cancer Biol Ther. 2010 Mar 1;9(5):396–406.

380. Zukiel R, Nowak S, Wyszko E, Rolle K, Gawrońska I, Barciszewska MZ, et al. Suppression of human brain tumor with interference RNA specific for tenascin-C. Cancer Biol Ther. 2006 Aug;5(8):1002–7.

381. Wyszko E, Rolle K, Nowak S, Zukiel R, Nowak M, Piestrzeniewicz R, et al. A multivariate analysis of patients with brain tumors treated with ATN-RNA. Acta Pol Pharm. 2008 Nov;65(6):677–84.

382. Nguyen QD, Schachar RA, Nduaka CI, Sperling M, Basile AS, Klamerus KJ, et al. Phase 1 dose-escalation study of a siRNA targeting the RTP801 gene in age-related macular degeneration patients. Eye (Lond). 2012 May 25;26(8):1099–105.

383. Khvalevsky EZ, Gabai R, Rachmut IH, Horwitz E, Brunschwig Z, Orbach A, et al. Mutant KRAS is a druggable target for pancreatic cancer. Proceedings of the …. 2013.

384. Landen CN, Chavez-Reyes A, Bucana C, Schmandt R, Deavers MT, Lopez-Berestein G, et al. Therapeutic EphA2 gene targeting in vivo using neutral liposomal small interfering RNA delivery. Cancer Research. 2005 Aug 1;65(15):6910–8.

385. Dannull J, Haley NR, Archer G, Nair S, Boczkowski D, Harper M, et al. Melanoma immunotherapy using mature DCs expressing the constitutive proteasome. J Clin Invest. 2013 Jul 1;123(7):3135–45.

386. Strumberg D, Schultheis B, Traugott U, Vank C, Santel A, Keil O, et al. Phase I clinical development of Atu027, a siRNA formulation targeting PKN3 in patients with advanced solid tumors. Int J Clin Pharmacol Ther. 2012 Jan;50(1):76–8.

387. Hansen BJ, Westergaard M, Frieden M, Hansen HF, Kjaerulff LS, Thrue CA, et al. SPC2996--A Bcl-2 RNA antagonist being studied in chronic lymphocytic leukemia. ASCO Meeting Abstracts. 2006 Jun 20;24(18_suppl):6610.

388. Senzer N, Barve M, Kuhn J, Melnyk A, Beitsch P, Lazar M, et al. Phase I trial of “bi-shRNAi(furin)/GMCSF DNA/autologous tumor cell” vaccine (FANG) in advanced cancer. Molecular Therapy. 2012 Mar;20(3):679–86.

389. Alexis F, Pridgen E, Molnar LK, Farokhzad OC. Factors affecting the clearance and biodistribution of polymeric nanoparticles. Mol Pharm. 2008 Jul;5(4):505–15.

390. Kanasty R, Dorkin JR, Vegas A, Anderson D. Delivery materials for siRNA therapeutics. Nat Mater. 2013 Nov;12(11):967–77.

391. Judge AD, Sood V, Shaw JR, Fang D, McClintock K, MacLachlan I. Sequence-dependent stimulation of the mammalian innate immune response by synthetic siRNA. Nat Biotech. 2005 Apr;23(4):457–62.

392. Sioud M, Furset G, Cekaite L. Suppression of immunostimulatory siRNA-

driven innate immune activation by 2'-modified RNAs. Biochemical and Biophysical Research Communications. 2007 Sep 14;361(1):122–6.

393. Sioud M. Overcoming the challenges of siRNA activation of innate immunity: design better therapeutic siRNAs. Methods Mol Biol. 2015;1218:301–19.

394. Hornung V, Guenthner-Biller M, Bourquin C, Ablasser A, Schlee M, Uematsu S, et al. Sequence-specific potent induction of IFN-alpha by short interfering RNA in plasmacytoid dendritic cells through TLR7. Nat Med. 2005 Mar;11(3):263–70.

395. Cekaite L, Furset G, Hovig E, Sioud M. Gene expression analysis in blood cells in response to unmodified and 2'-modified siRNAs reveals TLR-dependent and independent effects. J Mol Biol. 2007 Jan 5;365(1):90–108.

396. Lambeth LS, Smith CA. Short Hairpin RNA-Mediated Gene Silencing - Springer. siRNA Design. 2013.

397. Lambeth LS, Smith CA. Short hairpin RNA-mediated gene silencing. Methods Mol Biol. 2013;942:205–32.

398. Guzman-Villanueva D, El-Sherbiny IM, Herrera-Ruiz D, Vlassov AV, Smyth HDC. Formulation approaches to short interfering RNA and MicroRNA: challenges and implications. J Pharm Sci. 2012 Nov;101(11):4046–66.

399. Rao MK, Wilkinson MF. Tissue-specific and cell type-specific RNA interference in vivo. Nature Protocols. 2006;1(3):1494–501.

400. Zhu Z, Zheng T, Lee CG, Homer RJ, Elias JA. Tetracycline-controlled transcriptional regulation systems: advances and application in transgenic animal modeling. Semin Cell Dev Biol. 2002 Apr;13(2):121–8.

401. Czauderna F, Santel A, Hinz M, Fechtner M, Durieux B, Fisch G, et al. Inducible shRNA expression for application in a prostate cancer mouse model. Nucleic Acids Research. 2003 Nov 1;31(21):e127.

402. Zhou H-S, Liu D-P, Liang C-C. Challenges and strategies: the immune responses in gene therapy. Med Res Rev. 2004 Nov;24(6):748–61.

403. Mingozzi F, Hasbrouck NC, Basner-Tschakarjan E, Edmonson SA, Hui DJ, Sabatino DE, et al. Modulation of tolerance to the transgene product in a nonhuman primate model of AAV-mediated gene transfer to liver. Blood. 2007 Oct 1;110(7):2334–41.

404. Mingozzi F, High KA. Immune responses to AAV in clinical trials. Curr Gene Ther. 2007 Oct;7(5):316–24.

405. Jackson AL, Bartz SR, Schelter J, Kobayashi SV, Burchard J, Mao M, et al. Expression profiling reveals off-target gene regulation by RNAi. Nat Biotech. 2003 Jun;21(6):635–7.

406. Clark PR, Pober JS, Kluger MS. Knockdown of TNFR1 by the sense

strand of an ICAM-1 siRNA: dissection of an off-target effect. Nucleic Acids Research. 2008 Mar;36(4):1081–97.

407. Jackson AL, Linsley PS. Recognizing and avoiding siRNA off-target effects for target identification and therapeutic application. Nat Rev Drug Discov. 2010 Jan;9(1):57–67.

408. Ui-Tei K, Naito Y, Takahashi F, Haraguchi T, Ohki-Hamazaki H, Juni A, et al. Guidelines for the selection of highly effective siRNA sequences for mammalian and chick RNA interference. Nucleic Acids Research. 2004. pp. 936–48.

409. Taxman DJ, Livingstone LR, Zhang J, Conti BJ, Iocca HA, Williams KL, et al. Criteria for effective design, construction, and gene knockdown by shRNA vectors. BMC Biotechnology. 2006;6:7.

410. Reynolds A, Leake D, Boese Q, Scaringe S, Marshall WS, Khvorova A. Rational siRNA design for RNA interference. Nat Biotech. 2004 Mar;22(3):326–30.

411. Gu S, Jin L, Zhang Y, Huang Y, Zhang F, Valdmanis PN, et al. The loop position of shRNAs and pre-miRNAs is critical for the accuracy of dicer processing in vivo. Cell. 2012 Nov 9;151(4):900–11.

412. Grimm D, Streetz KL, Jopling CL, Storm TA, Pandey K, Davis CR, et al. Fatality in mice due to oversaturation of cellular microRNA/short hairpin RNA pathways. Nature. Nature Publishing Group; 2006 May 25;441(7092):537–41.

413. Suhy DA, Kao S-C, Mao T, Whiteley L, Denise H, Souberbielle B, et al. Safe, Long-term Hepatic Expression of Anti-HCV shRNA in a Nonhuman Primate Model. Molecular Therapy. 2012 Jun 26;20(9):1737–49.

414. McBride JL, Boudreau RL, Harper SQ, Staber PD, Monteys AM, Martins I, et al. Artificial miRNAs mitigate shRNA-mediated toxicity in the brain: implications for the therapeutic development of RNAi. Proceedings of the National Academy of Sciences. 2008 Apr 15;105(15):5868–73.

415. Ehlert EM, Eggers R, Niclou SP, Verhaagen J. Cellular toxicity following application of adeno-associated viral vector-mediated RNA interference in the nervous system. BMC Neurosci. 2010;11:20.

416. Martin JN, Wolken N, Brown T, Dauer WT, Ehrlich ME, Gonzalez-Alegre P. Lethal toxicity caused by expression of shRNA in the mouse striatum: implications for therapeutic design. Gene Ther. 2011 Jul;18(7):666–73.

417. Boudreau RL, Martins I, Davidson BL. Artificial MicroRNAs as siRNA Shuttles: Improved Safety as Compared to shRNAs In vitro and In vivo. Molecular Therapy. Nature Publishing Group; 2008 Nov 11;17(1):169–75.

418. Giering JC, Grimm D, Storm TA, Kay MA. Expression of shRNA from a tissue-specific pol II promoter is an effective and safe RNAi therapeutic. Molecular Therapy. 2008 Sep;16(9):1630–6.

419. Yuan X, Naguib S, Wu Z. Recent advances of siRNA delivery by nanoparticles. Expert Opin Drug Deliv. 2011 Apr;8(4):521–36.

420. Cho K, Wang X, Nie S, Chen ZG, Shin DM. Therapeutic nanoparticles for drug delivery in cancer. Clin Cancer Res. 2008 Mar 1;14(5):1310–6.

421. Lee J-M, Yoon T-J, Cho Y-S. Recent developments in nanoparticle-based siRNA delivery for cancer therapy. BioMed Research International. 2013;2013:782041.

422. Majidi S, Zeinali Sehrig F, Samiei M, Milani M, Abbasi E, Dadashzadeh K, et al. Magnetic nanoparticles: Applications in gene delivery and gene therapy. Artif Cells Nanomed Biotechnol. 2015 Mar 2;:1–8.

423. Koenig O, Walker T, Perle N, Zech A, Neumann B, Schlensak C, et al. New aspects of gene-silencing for the treatment of cardiovascular diseases. Pharmaceuticals (Basel). 2013;6(7):881–914.

424. Landesman-Milo D, Ramishetti S, Peer D. Nanomedicine as an emerging platform for metastatic lung cancer therapy. Cancer Metastasis Rev. 2015 May 7.

425. Whitehead KA, Langer R, Anderson DG. Knocking down barriers: advances in siRNA delivery. Nat Rev Drug Discov. 2009 Feb;8(2):129–38.

426. Judge AD, Robbins M, Tavakoli I, Levi J, Hu L, Fronda A, et al. Confirming the RNAi-mediated mechanism of action of siRNA-based cancer therapeutics in mice. J Clin Invest. 2009 Mar;119(3):661–73.

427. Li L, Wang R, Wilcox D, Zhao X, Song J, Lin X, et al. Tumor vasculature is a key determinant for the efficiency of nanoparticle-mediated siRNA delivery. Gene Ther. 2012 Jul;19(7):775–80.

428. Ribas A, Kalinoski L, Heidel JD, Peterkin J, Seligson DB, Zuckerman JE, et al. Systemic delivery of siRNA via targeted nanoparticles in patients with cancer: Results from a first-in-class phase I clinical trial. ASCO Meeting Abstracts. 2010 May 20;28(15_suppl):3022.

429. Guo W, Chen W, Yu W, Huang W, Deng W. Small interfering RNA-based molecular therapy of cancers. Chin J Cancer. 2013 Jan 18.

430. Coelho T, Adams D, Silva A, Lozeron P, Hawkins PN, Mant T, et al. Safety and efficacy of RNAi therapy for transthyretin amyloidosis. N Engl J Med. 2013 Aug 29;369(9):819–29.

431. Bouard D, Alazard-Dany D, Cosset F-L. Viral vectors: from virology to transgene expression. Br J Pharmacol. 2009 May;157(2):153–65.

432. Thomas CE, Ehrhardt A, Kay MA. Progress and problems with the use of viral vectors for gene therapy. Nat Rev Genet. 2003 May;4(5):346–58.

433. Weber C, Neacsu I, Krautz B, Schlegel P, Sauer S, Raake P, et al. Therapeutic safety of high myocardial expression levels of the molecular inotrope S100A1 in a preclinical heart failure model. Gene Ther. 2014

Feb;21(2):131–8.

434. Gong Y, Mu D, Prabhakar S, Moser A, Musolino P, Ren J, et al. Adenoassociated Virus Serotype 9-Mediated Gene Therapy for X-Linked Adrenoleukodystrophy. Molecular Therapy. 2015 Jan 16.

435. Nathwani AC, Rosales C, McIntosh J, Rastegarlari G, Nathwani D, Raj D, et al. Long-term safety and efficacy following systemic administration of a self-complementary AAV vector encoding human FIX pseudotyped with serotype 5 and 8 capsid proteins. Molecular Therapy. 2011 May;19(5):876–85.

436. Mingozzi F, High KA. Immune responses to AAV vectors: overcoming barriers to successful gene therapy. Blood. 2013 Apr 17.

437. Mingozzi F, High KA. Therapeutic in vivo gene transfer for genetic disease using AAV: progress and challenges. Nat Rev Genet. 2011 May;12(5):341–55.

438. Calcedo R, Vandenberghe LH, Gao G, Lin J, Wilson JM. Worldwide epidemiology of neutralizing antibodies to adeno-associated viruses. J Infect Dis. 2009 Feb 1;199(3):381–90.

439. Samulski RJ, Muzyczka N. AAV-Mediated Gene Therapy for Research and Therapeutic Purposes. Annual Review of Virology. 2014 Nov 3;1(1):427–51.

440. Stilwell JL, Samulski RJ. Adeno-associated virus vectors for therapeutic gene transfer. Biotech. 2003 Jan;34(1):148–50–152–154passim.

441. Nathwani AC, Reiss UM, Tuddenham EGD, Rosales C, Chowdary P, McIntosh J, et al. Long-term safety and efficacy of factor IX gene therapy in hemophilia B. N Engl J Med. 2014 Nov 20;371(21):1994–2004.

442. Dismuke DJ, Tenenbaum L, Samulski RJ. Biosafety of recombinant adeno-associated virus vectors. Curr Gene Ther. 2013 Dec;13(6):434–52.

443. Atchison Rw, Casto Bc, Hammon Wm. Adenovirus-Associated Defective Virus Particles. Science. 1965 Aug 13;149(3685):754–6.

444. Berns KI, Giraud C. Biology of adeno-associated virus. Curr Top Microbiol Immunol. 1996;218:1–23.

445. Buller RM, Janik JE, Sebring ED, Rose JA. Herpes simplex virus types 1 and 2 completely help adenovirus-associated virus replication. J Virol. 1981 Oct;40(1):241–7.

446. Carter BJ, Koczot FJ, Garrison J, Rose JA, Dolin R. Separate helper functions provided by adenovirus for adenovirus-associated virus multiplication. Nature New Biol. 1973 Jul 18;244(133):71–3.

447. Dong JY, Fan PD, Frizzell RA. Quantitative analysis of the packaging capacity of recombinant adeno-associated virus. Human Gene Therapy. 1996 Nov 10;7(17):2101–12.

448. Hoggan MD, Thomas GF. Continuous carriage of adenovirus-associated virus genome in cell culture in the absence of helper adenovirus. In Proceedings of the Fourth Lepetit Colloquium. 1972.

449. R M Kotin RMLKIB. Characterization of a preferred site on human chromosome 19q for integration of adeno-associated virus DNA by non-homologous recombination. EMBO J. Nature Publishing Group; 1992 Dec 1;11(13):5071.

450. R J Samulski. Targeted integration of adeno-associated virus (AAV) into human chromosome 19. EMBO J. Nature Publishing Group; 1991 Dec 1;10(12):3941.

451. Duan D, Sharma P, Yang J, Yue Y, Dudus L, ZHANG Y, et al. Circular intermediates of recombinant adeno-associated virus have defined structural characteristics responsible for long-term episomal persistence in muscle tissue. J Virol. 1998 Nov;72(11):8568–77.

452. Koczot FJ, Carter BJ, Garon CF, Rose JA. Self-complementarity of terminal sequences within plus or minus strands of adenovirus-associated virus DNA. Proc Natl Acad Sci USA. 1973 Jan;70(1):215–9.

453. Ni TH, McDonald WF, Zolotukhin I, Melendy T, Waga S, Stillman B, et al. Cellular proteins required for adeno-associated virus DNA replication in the absence of adenovirus coinfection. J Virol. 1998 Apr;72(4):2777–87.

454. Im DS, Muzyczka N. The AAV origin binding protein Rep68 is an ATP-dependent site-specific endonuclease with DNA helicase activity. Cell. 1990 May 4;61(3):447–57.

455. Im DS, Muzyczka N. Partial purification of adeno-associated virus Rep78, Rep52, and Rep40 and their biochemical characterization. J Virol. 1992 Feb;66(2):1119–28.

456. King JA, Dubielzig R, Grimm D, Kleinschmidt JA. DNA helicase-mediated packaging of adeno-associated virus type 2 genomes into preformed capsids. EMBO J. 2001 Jun 15;20(12):3282–91.

457. Weitzman MD, Linden RM. Adeno-associated virus biology. Methods Mol Biol. 2011;807:1–23.

458. Grieger JC, Snowdy S, Samulski RJ. Separate basic region motifs within the adeno-associated virus capsid proteins are essential for infectivity and assembly. J Virol. 2006 Jun;80(11):5199–210.

459. Wu Z, Asokan A, Samulski RJ. Adeno-associated virus serotypes: vector toolkit for human gene therapy. Mol Ther. 2006 Sep;14(3):316–27.

460. Bleker S, Sonntag F, Kleinschmidt JA. Mutational analysis of narrow pores at the fivefold symmetry axes of adeno-associated virus type 2 capsids reveals a dual role in genome packaging and activation of phospholipase A2 activity. J Virol. 2005 Feb;79(4):2528–40.

461. Girod A, Wobus CE, Zádori Z, Ried M, Leike K, Tijssen P, et al. The VP1

capsid protein of adeno-associated virus type 2 is carrying a phospholipase A2 domain required for virus infectivity. J Gen Virol. 2002 May;83(Pt 5):973–8.

462. Sonntag F, Schmidt K, Kleinschmidt JA. A viral assembly factor promotes AAV2 capsid formation in the nucleolus. 2010 Jun 1;107(22):10220–5.

463. Sonntag F, Kother K, Schmidt K, Weghofer M, Raupp C, Nieto K, et al. The Assembly-Activating Protein Promotes Capsid Assembly of Different Adeno-Associated Virus Serotypes. J Virol. 2011 Nov 3;85(23):12686–97.

464. Naumer M, Sonntag F, Schmidt K, Nieto K, Panke C, Davey NE, et al. Properties of the adeno-associated virus assembly-activating protein. J Virol. 2012 Dec;86(23):13038–48.

465. Gonçalves MA. Adeno-associated virus: from defective virus to effective vector. Virol J. 2005;2(1):43.

466. Lusby E, Bohenzky R, Berns KI. Inverted terminal repetition in adeno-associated virus DNA: independence of the orientation at either end of the genome. J Virol. 1981 Mar;37(3):1083–6.

467. Zhou X, Muzyczka N. In vitro packaging of adeno-associated virus DNA. J Virol. 1998 Apr;72(4):3241–7.

468. Muzyczka N. Use of adeno-associated virus as a general transduction vector for mammalian cells. Curr Top Microbiol Immunol. 1992;158:97–129.

469. Samulski RJ, Chang LS, Shenk T. A recombinant plasmid from which an infectious adeno-associated virus genome can be excised in vitro and its use to study viral replication. J Virol. 1987 Oct;61(10):3096–101.

470. Berns KI, Adler S. Separation of two types of adeno-associated virus particles containing complementary polynucleotide chains. J Virol. 1972 Feb;9(2):394–6.

471. McCarty DM, Monahan PE, Samulski RJ. Self-complementary recombinant adeno-associated virus (scAAV) vectors promote efficient transduction independently of DNA synthesis. Gene Ther. 2001 Aug;8(16):1248–54.

472. Nakai H, Storm TA, Kay MA. Recruitment of single-stranded recombinant adeno-associated virus vector genomes and intermolecular recombination are responsible for stable transduction of liver in vivo. J Virol. 2000 Oct;74(20):9451–63.

473. McCarty DM. Self-complementary AAV vectors; advances and applications. Molecular Therapy. 2008 Oct;16(10):1648–56.

474. Nathwani AC, Gray JT, Ng CYC, Zhou J, Spence Y, Waddington SN, et al. Self-complementary adeno-associated virus vectors containing a novel liver-specific human factor IX expression cassette enable highly efficient transduction of murine and nonhuman primate liver. Blood. 2006 Apr

1;107(7):2653–61.

475. McCarty DM, Fu H, Monahan PE, Toulson CE, Naik P, Samulski RJ. Adeno-associated virus terminal repeat (TR) mutant generates self-complementary vectors to overcome the rate-limiting step to transduction in vivo. Gene Ther. 2003 Dec;10(26):2112–8.

476. Rabinowitz JE, Rolling F, Li C, Conrath H, Xiao W, Xiao X, et al. Cross-packaging of a single adeno-associated virus (AAV) type 2 vector genome into multiple AAV serotypes enables transduction with broad specificity. J Virol. 2002 Jan;76(2):791–801.

477. Hoggan MD, Blacklow NR, Rowe WP. Studies of small DNA viruses found in various adenovirus preparations: physical, biological, and immunological characteristics. Proc Natl Acad Sci USA. 1966 Jun;55(6):1467–74.

478. Hauck B, Xiao W. Characterization of tissue tropism determinants of adeno-associated virus type 1. J Virol. 2003 Feb;77(4):2768–74.

479. Gurda BL, Dimattia MA, Miller EB, Bennett A, McKenna R, Weichert WS, et al. Capsid Antibodies to Different Adeno-Associated Virus Serotypes Bind Common Regions. J Virol. 2013 Jun 12.

480. Boutin S, Monteilhet V, Veron P, Leborgne C, Benveniste O, Montus MF, et al. Prevalence of Serum IgG and Neutralizing Factors Against Adeno-Associated Virus (AAV) Types 1, 2, 5, 6, 8, and 9 in the Healthy Population: Implications for Gene Therapy Using AAV Vectors. Human Gene Therapy. Mary Ann Liebert, Inc. 140 Huguenot Street, 3rd Floor New Rochelle, NY 10801 USA; 2010 Jun;21(6):704–12.

481. Märsch S, Huber A, Hallek M, Büning H, Perabo L. A novel directed evolution method to enhance cell-type specificity of adeno-associated virus vectors. Comb Chem High Throughput Screen. 2010 Nov;13(9):807–12.

482. Asokan A, Schaffer DV, Samulski RJ. The AAV vector toolkit: poised at the clinical crossroads. Molecular Therapy. 2012 Apr;20(4):699–708.

483. Weinberg MS, Nicolson S, Bhatt AP, McLendon M, Li C, Samulski RJ. Recombinant adeno-associated virus utilizes cell-specific infectious entry mechanisms. J Virol. 2014 Nov;88(21):12472–84.

484. Hacker UT, Wingenfeld L, Kofler DM, Schuhmann NK, Lutz S, Herold T, et al. Adeno-associated virus serotypes 1 to 5 mediated tumor cell directed gene transfer and improvement of transduction efficiency. J Gene Med. 2005 Nov;7(11):1429–38.

485. Asokan A, Schaffer DV, Samulski RJ. Molecular Therapy - The AAV Vector Toolkit: Poised at the Clinical Crossroads. Molecular Therapy. 2012.

486. Wu Z, Asokan A, Grieger JC, Govindasamy L, Agbandje-McKenna M, Samulski RJ. Single amino acid changes can influence titer, heparin binding, and tissue tropism in different adeno-associated virus serotypes. J Virol. 2006 Nov;80(22):11393–7.

487. Summerford C, Samulski RJ. Membrane-associated heparan sulfate proteoglycan is a receptor for adeno-associated virus type 2 virions. J Virol. 1998 Feb;72(2):1438–45.

488. Akache B, Grimm D, Pandey K, Yant SR, Xu H, Kay MA. The 37/67-kilodalton laminin receptor is a receptor for adeno-associated virus serotypes 8, 2, 3, and 9. J Virol. 2006 Oct;80(19):9831–6.

489. Xie Q, Lerch TF, Meyer NL, Chapman MS. Structure-function analysis of receptor-binding in adeno-associated virus serotype 6 (AAV-6). Virology. 2011 Nov 10;420(1):10–9.

490. Di Pasquale G, Davidson BL, Stein CS, Martins I, Scudiero D, Monks A, et al. Identification of PDGFR as a receptor for AAV-5 transduction. Nat Med. 2003 Oct;9(10):1306–12.

491. Walters RW, Yi SM, Keshavjee S, Brown KE, Welsh MJ, Chiorini JA, et al. Binding of adeno-associated virus type 5 to 2,3-linked sialic acid is required for gene transfer. J Biol Chem. 2001 Jun 8;276(23):20610–6.

492. Wu Z, Miller E, Agbandje-McKenna M, Samulski RJ. Alpha2,3 and alpha2,6 N-linked sialic acids facilitate efficient binding and transduction by adeno-associated virus types 1 and 6. J Virol. 2006 Sep;80(18):9093–103.

493. Shen S, Bryant KD, Brown SM, Randell SH, Asokan A. Terminal N-linked galactose is the primary receptor for adeno-associated virus 9. J Biol Chem. 2011 Apr 15;286(15):13532–40.

494. Bartlett JS, Wilcher R, Samulski RJ. Infectious entry pathway of adeno-associated virus and adeno-associated virus vectors. J Virol. 2000 Mar;74(6):2777–85.

495. Nakai H, Yant SR, Storm TA, Fuess S, Meuse L, Kay MA. Extrachromosomal recombinant adeno-associated virus vector genomes are primarily responsible for stable liver transduction in vivo. J Virol. 2001 Aug;75(15):6969–76.

496. Clark KR, Sferra TJ, Lo W, Qu G, Chen R, Johnson PR. Gene transfer into the CNS using recombinant adeno-associated virus: analysis of vector DNA forms resulting in sustained expression. J Drug Target. 1999 Dec;7(4):269–83.

497. Schnepp BC, Jensen RL, Clark KR, Johnson PR. Infectious molecular clones of adeno-associated virus isolated directly from human tissues. J Virol. 2009 Feb;83(3):1456–64.

498. Song S, Laipis PJ, Berns KI, Flotte TR. Effect of DNA-dependent protein kinase on the molecular fate of the rAAV2 genome in skeletal muscle. Proc Natl Acad Sci USA. 2001 Mar 27;98(7):4084–8.

499. Flotte TR, Afione SA, Zeitlin PL. Adeno-associated virus vector gene expression occurs in nondividing cells in the absence of vector DNA integration. Am J Respir Cell Mol Biol. 1994 Nov;11(5):517–21.

500. Penaud-Budloo M, Le Guiner C, Nowrouzi A, Toromanoff A, Chérel Y, Chenuaud P, et al. Adeno-associated virus vector genomes persist as episomal chromatin in primate muscle. J Virol. 2008 Aug;82(16):7875–85.

501. Vincent-Lacaze N, Snyder RO, Gluzman R, Bohl D, Lagarde C, Danos O. Structure of Adeno-Associated Virus Vector DNA following Transduction of the Skeletal Muscle. Journal of Virology1999.

502. Flotte TR, Afione SA, Conrad C, McGrath SA, Solow R, Oka H, et al. Stable in vivo expression of the cystic fibrosis transmembrane conductance regulator with an adeno-associated virus vector. Proc Natl Acad Sci USA. 1993 Nov 15;90(22):10613–7.

503. Kaplitt MG, Leone P, Samulski RJ, Xiao X, Pfaff DW, O'Malley KL, et al. Long-term gene expression and phenotypic correction using adeno-associated virus vectors in the mammalian brain. Nat Genet. 1994 Oct;8(2):148–54.

504. Lalwani AK, Walsh BJ, Carvalho GJ, Muzyczka N, Mhatre AN. Expression of adeno-associated virus integrated transgene within the mammalian vestibular organs. Am J Otol. 1998 May;19(3):390–5.

505. Hauswirth WW, Lewin AS, Zolotukhin S, Muzyczka N. Production and purification of recombinant adeno-associated virus. Meth Enzymol. 2000;316:743–61.

506. Maguire AM, High KA, Auricchio A, Wright JF, Pierce EA, Testa F, et al. Age-dependent effects of RPE65 gene therapy for Leber's congenital amaurosis: a phase 1 dose-escalation trial. Lancet. 2009 Nov 7;374(9701):1597–605.

507. Flotte TR. Adeno-associated virus-mediated gene transfer for lung diseases. Human Gene Therapy. 2005 Jun;16(6):643–8.

508. McCarty DM, Young SM, Samulski RJ. Integration of adeno-associated virus (AAV) and recombinant AAV vectors. Annu Rev Genet. 2004;38:819–45.

509. Gernoux G, Guilbaud M, Dubreil L, Larcher T, Babarit C, Ledevin M, et al. Early interaction of adeno-associated virus serotype 8 vector with the host immune system following intramuscular delivery results in weak but detectable lymphocyte and dendritic cell transduction. Human Gene Therapy. 2015 Jan;26(1):1–13.

510. Geoffrey L Rogers ATMGVAGRJASRWH. Innate Immune Responses to AAV Vectors. Front Microbiol. Frontiers Media SA; 2011;2.

511. Chirmule N, Propert K, Magosin S, Qian Y, Qian R, Wilson J. Immune responses to adenovirus and adeno-associated virus in humans. Gene Ther. 1999 Sep;6(9):1574–83.

512. He Y, Weinberg MS, Hirsch M, Johnson MC, Tisch R, Samulski RJ, et al. Kinetics of Adeno-Associated Virus Serotype 2 (AAV2) and AAV8 Capsid Antigen Presentation In Vivo Are Identical. Human Gene Therapy. 2013

May;24(5):545–53.

513. Hernandez YJ, Wang J, Kearns WG, Loiler S, Poirier A, Flotte TR. Latent adeno-associated virus infection elicits humoral but not cell-mediated immune responses in a nonhuman primate model. 1999.

514. Li CC, He YY, Nicolson SS, Hirsch MM, Weinberg MSM, Zhang PP, et al. Adeno-associated virus capsid antigen presentation is dependent on endosomal escape. J Clin Invest. 2013 Mar 1;123(3):1390–401.

515. Manno CS, Pierce GF, Arruda VR, Glader B, Ragni M, Rasko JJ, et al. Successful transduction of liver in hemophilia by AAV-Factor IX and limitations imposed by the host immune response. Nat Med. 2006 Mar;12(3):342–7.

516. Herzog RW, Hagstrom JN, Kung SH, Tai SJ, Wilson JM, Fisher KJ, et al. Stable gene transfer and expression of human blood coagulation factor IX after intramuscular injection of recombinant adeno-associated virus. Proc Natl Acad Sci USA. 1997 May 27;94(11):5804–9.

517. High KA, Herzog RW, Yang EY, Couto LB, Hagstrom JN, Elwell D, et al. Long-term correction of canine hemophilia B by gene transfer of blood coagulation factor IX mediated by adeno-associated viral vector. Nat Med. Nature Publishing Group; 1999 Jan 1;5(1):56–63.

518. Hagstrom JN, Couto LB, Scallan C, Burton M, McCleland ML, Fields PA, et al. Improved muscle-derived expression of human coagulation factor IX from a skeletal actin/CMV hybrid enhancer/promoter. Blood. American Society of Hematology; 2000 Apr 15;95(8):2536–42.

519. Kay MA, Manno CS, Ragni MV, Larson PJ, Couto LB, McClelland A, et al. Evidence for gene transfer and expression of factor IX in haemophilia B patients treated with an AAV vector. Nat Genet. 2000 Mar;24(3):257–61.

520. Manno CS, Chew AJ, Hutchison S, Larson PJ, Herzog RW, Arruda VR, et al. AAV-mediated factor IX gene transfer to skeletal muscle in patients with severe hemophilia B. Blood. 2003 Apr 15;101(8):2963–72.

521. Mingozzi F, High KA. Immune responses to AAV in clinical trials. Curr Gene Ther. 2011 Aug;11(4):321–30.

522. Kotterman MA, Yin L, Strazzeri JM, Flannery JG, Merigan WH, Schaffer DV. Antibody neutralization poses a barrier to intravitreal adeno-associated viral vector gene delivery to non-human primates. Gene Ther. 2015 Feb;22(2):116–26.

523. Scott LJ. Alipogene tiparvovec: a review of its use in adults with familial lipoprotein lipase deficiency. Drugs. 2015 Feb;75(2):175–82.

524. Zaiss AK, Muruve DA. Immunity to adeno-associated virus vectors in animals and humans: a continued challenge. Gene Ther. 2008 Jun;15(11):808–16.

525. Gao G-P, Alvira MR, Wang L, Calcedo R, Johnston J, Wilson JM. Novel

adeno-associated viruses from rhesus monkeys as vectors for human gene therapy. Proc Natl Acad Sci USA. 2002 Sep 3;99(18):11854–9.

526. Grimm D, Lee JS, Wang L, Desai T, Akache B, Storm TA, et al. In Vitro and In Vivo Gene Therapy Vector Evolution via Multispecies Interbreeding and Retargeting of Adeno-Associated Viruses. J Virol. 2008 May 22;82(12):5887–911.

527. Asokan A, Conway JC, Phillips JL, Li C, Hegge J, Sinnott R, et al. Reengineering a receptor footprint of adeno-associated virus enables selective and systemic gene transfer to muscle. Nat Biotech. 2009 Dec 27;28(1):79–82.

528. Arruda VR, Xiao W. It's all about the clothing: capsid domination in the adeno-associated viral vector world - ARRUDA - 2006 - Journal of Thrombosis and Haemostasis - Wiley Online Library. Journal of Thrombosis and Haemostasis. 2007.

529. Tseng Y-S, Gurda BL, Chipman P, McKenna R, Afione S, Chiorini JA, et al. Adeno-associated virus serotype 1 (AAV1)- and AAV5-antibody complex structures reveal evolutionary commonalities in parvovirus antigenic reactivity. J Virol. 2015 Feb;89(3):1794–808.

530. Gurda BL, Raupp C, Popa-Wagner R, Naumer M, Olson NH, Ng R, et al. Mapping a neutralizing epitope onto the capsid of adeno-associated virus serotype 8. J Virol. 2012 Aug;86(15):7739–51.

531. Li C, Narkbunnam N, Samulski RJ, Asokan A, Hu G, Jacobson LJ, et al. Neutralizing antibodies against adeno-associated virus examined prospectively in pediatric patients with hemophilia. Gene Ther. 2012 Mar;19(3):288–94.

532. Erles K, Sebökovà P, Schlehofer JR. Update on the prevalence of serum antibodies (IgG and IgM) to adeno-associated virus (AAV). J Med Virol. 1999 Nov;59(3):406–11.

533. Chiorini JA, Kim F, Yang L, Kotin RM. Cloning and characterization of adeno-associated virus type 5. J Virol. 1999 Feb;73(2):1309–19.

534. Kotin RM, Menninger JC, Ward DC, Berns KI. Mapping and direct visualization of a region-specific viral DNA integration site on chromosome 19q13-qter. Genomics. 1991.

535. Nakai H, Montini E, Fuess S, Storm TA, Grompe M, Kay MA. AAV serotype 2 vectors preferentially integrate into active genes in mice. Nat Genet. 2003 Jul;34(3):297–302.

536. Deyle DR, Russell DW. Adeno-associated virus vector integration. Curr Opin Mol Ther. 2009 Aug;11(4):442–7.

537. Inagaki K, Piao C, Kotchey NM, Wu X, Nakai H. Frequency and spectrum of genomic integration of recombinant adeno-associated virus serotype 8 vector in neonatal mouse liver. J Virol. 2008 Oct;82(19):9513–24.

538. Miller DG, Wang P-R, Petek LM, Hirata RK, Sands MS, Russell DW. Gene targeting in vivo by adeno-associated virus vectors. Nat Biotech. 2006 Aug;24(8):1022–6.

539. Nakai H, Iwaki Y, Kay MA, Couto LB. Isolation of recombinant adeno-associated virus vector-cellular DNA junctions from mouse liver. J Virol. 1999 Jul;73(7):5438–47.

540. Nakai H, Wu X, Fuess S, Storm TA, Munroe D, Montini E, et al. Large-scale molecular characterization of adeno-associated virus vector integration in mouse liver. J Virol. 2005 Mar;79(6):3606–14.

541. Rosas LE, Grieves JL, Zaraspe K, La Perle KM, Fu H, McCarty DM. Patterns of scAAV vector insertion associated with oncogenic events in a mouse model for genotoxicity. Molecular Therapy. 2012 Nov;20(11):2098–110.

542. Chandler RJ, LaFave MC, Varshney GK, Trivedi NS, Carrillo-Carrasco N, Senac JS, et al. Vector design influences hepatic genotoxicity after adeno-associated virus gene therapy. J Clin Invest. 2015 Feb;125(2):870–80.

543. Donsante A, Vogler C, Muzyczka N, Crawford JM, Barker J, Flotte T, et al. Observed incidence of tumorigenesis in long-term rodent studies of rAAV vectors. Gene Ther. 2001 Sep;8(17):1343–6.

544. Donsante A, Miller DG, Li Y, Vogler C, Brunt EM, Russell DW, et al. AAV vector integration sites in mouse hepatocellular carcinoma. Science. 2007 Jul 27;317(5837):477.

545. Bell P, Moscioni AD, McCarter RJ, Wu D, Gao G, Hoang A, et al. Analysis of tumors arising in male B6C3F1 mice with and without AAV vector delivery to liver. Mol Ther. 2006 Jul;14(1):34–44.

546. Wu K, Li S, Bodhinathan K, Meyers C, Chen W, Campbell-Thompson M, et al. Enhanced expression of Pctk1, Tcf12 and Ccnd1 in hippocampus of rats: Impact on cognitive function, synaptic plasticity and pathology. Neurobiol Learn Mem. 2012 Jan;97(1):69–80.

547. Bell P, Wang L, Lebherz C, Flieder DB, Bove MS, Wu D, et al. No evidence for tumorigenesis of AAV vectors in a large-scale study in mice. Mol Ther. 2005 Aug;12(2):299–306.

548. Li H, Malani N, Hamilton SR, Schlachterman A, Bussadori G, Edmonson SE, et al. Assessing the potential for AAV vector genotoxicity in a murine model. Blood. 2011 Mar 24;117(12):3311–9.

549. Barretina J, Caponigro G, Stransky N, Venkatesan K, Margolin AA, Kim S, et al. The Cancer Cell Line Encyclopedia enables predictive modelling of anticancer drug sensitivity. Nature. Nature Publishing Group; 2012 Mar 29;483(7391):603–7.

550. Mahadevan M, Liu Y, You C, Luo R, You H, Mehta JL, et al. Generation of robust cytotoxic T lymphocytes against prostate specific antigen by transduction of dendritic cells using protein and recombinant adeno-

associated virus. Cancer Immunol Immunother. 2007 Oct;56(10):1615–24.

551. Chiu T-L, Peng C-W, Wang M-J. Enhanced anti-glioblastoma activity of microglia by AAV2-mediated IL-12 through TRAIL and phagocytosis in vitro. Oncol Rep. 2011 May;25(5):1373–80.

552. Yiang G-T, Harn H-J, Yu Y-L, Hu S-C, Hung Y-T, Hsieh C-J, et al. Immunotherapy: rAAV2 expressing interleukin-15 inhibits HeLa cell tumor growth in mice. J Biomed Sci. 2009;16:47.

553. Yiang G-T, Chou P-L, Tsai H-F, Chen L-A, Chang W-J, Yu Y-L, et al. Immunotherapy for SV40 T/t antigen-induced breast cancer by recombinant adeno-associated virus serotype 2 carrying interleukin-15 in mice. Int J Mol Med. 2012 May;29(5):809–14.

554. Han T, Abdel-Motal UM, Chang DK, Sui J, Muvaffak A. PLOS ONE: Human Anti-CCR4 Minibody Gene Transfer for the Treatment of Cutaneous T-Cell Lymphoma. PLoS ONE. 2012.

555. Meijer DH, Maguire CA, LeRoy SG, Sena-Esteves M. Controlling brain tumor growth by intraventricular administration of an AAV vector encoding IFN-beta. Cancer Gene Therapy. 2009 Aug;16(8):664–71.

556. Liu X, Lu J, He ML, Li Z, Zhang B, Zhou LH, et al. Antitumor Effects of Interferon-Alpha on Cell Growth and Metastasis in Human Nasopharyngeal Carcinoma. Current cancer drug …. Bentham Science Publishers; 2012.

557. Nieto K, Kern A, Leuchs B, Gissmann L, Müller M, Kleinschmidt JA. Combined prophylactic and therapeutic intranasal vaccination against human papillomavirus type-16 using different adeno-associated virus serotype vectors. Antivir Ther (Lond). 2009;14(8):1125–37.

558. Li R, Hu H, Ma H, Chen L, Zhou B, Liu Y, et al. The anti-tumor effect and increased tregs infiltration mediated by rAAV-SLC vector. Mol Biol Rep. 2013 Oct;40(10):5615–23.

559. Di L, Zhu Y, Jia J, Yu J, Song G, Zhang J, et al. Clinical safety of induced CTL infusion through recombinant adeno-associated virus-transfected dendritic cell vaccination in Chinese cancer patients - Springer. Clinical and …. 2012.

560. Le DT, Wang-Gillam A, Picozzi V, Greten TF, Crocenzi T, Springett G, et al. Safety and Survival With GVAX Pancreas Prime and Listeria Monocytogenes-Expressing Mesothelin (CRS-207) Boost Vaccines for Metastatic Pancreatic Cancer. J Clin Oncol. 2015 Jan 12.

561. De Remigis A, de Gruijl TD, Uram JN, Tzou S-C, Iwama S, Talor MV, et al. Development of thyroglobulin antibodies after GVAX immunotherapy is associated with prolonged survival. Int J Cancer. 2015 Jan 1;136(1):127–37.

562. Soares KC, Rucki AA, Wu AA, Olino K, Xiao Q, Chai Y, et al. PD-1/PD-L1 blockade together with vaccine therapy facilitates effector T-cell infiltration

into pancreatic tumors. J Immunother. 2015 Jan;38(1):1–11.

563. Agarwal N, Di Lorenzo G, Sonpavde G, Bellmunt J. New agents for prostate cancer. Ann Oncol. 2014 Sep;25(9):1700–9.

564. Duraiswamy J, Freeman GJ, Coukos G. Therapeutic PD-1 pathway blockade augments with other modalities of immunotherapy T-cell function to prevent immune decline in ovarian cancer. Cancer Research. 2013 Dec 1;73(23):6900–12.

565. Nemunaitis J. Vaccines in cancer: GVAX, a GM-CSF gene vaccine. Expert Rev Vaccines. 2005 Jun;4(3):259–74.

566. Haycock JW. 3D cell culture: a review of current approaches and techniques. Methods Mol Biol. 2011;695:1–15.

567. Dawson CW, Port RJ, Young LS. The role of the EBV-encoded latent membrane proteins LMP1 and LMP2 in the pathogenesis of nasopharyngeal carcinoma (NPC). Semin Cancer Biol. 2012 Apr;22(2):144–53.

568. Choi SYC, Lin D, Gout PW, Collins CC, Xu Y, Wang Y. Lessons from patient-derived xenografts for better in vitro modeling of human cancer. Adv Drug Deliv Rev. 2014 Dec 15;79-80:222–37.

569. Kola I, Landis J. Can the pharmaceutical industry reduce attrition rates? Nat Rev Drug Discov. 2004 Aug;3(8):711–5.

570. Reichert JM, Wenger JB. Development trends for new cancer therapeutics and vaccines. Drug Discovery Today. 2008 Jan;13(1-2):30–7.

571. Thakur Das M, Pryer NK, Singh M. Mouse tumour models to guide drug development and identify resistance mechanisms. J Pathol. 2013 Dec 10;232(2):103–11.

572. Masters JR. HeLa cells 50 years on: the good, the bad and the ugly. Nat Rev Cancer. 2002 Apr;2(4):315–9.

573. Gey GO, Coffman WD. Gey: Tissue culture studies of the proliferative... - Google Scholar. Cancer. 1952.

574. Weinstein JN. Drug discovery: Cell lines battle cancer. Nature. 2012 Mar 29;483(7391):544–5.

575. Masters JRW. Access : Human cancer cell lines: fact and fantasy : Nature Reviews Molecular Cell Biology. Nat Rev Mol Cell Biol. 2000 Dec 1;1(3):233–6.

576. Garnett MJ, Edelman EJ, Heidorn SJ, Greenman CD, Dastur A, Lau KW, et al. Systematic identification of genomic markers of drug sensitivity in cancer cells. Nature. 2012 Mar 29;483(7391):570–5.

577. Drews J. Drug discovery: a historical perspective. Science. 2000 Mar 17;287(5460):1960–4.

578. Davies H, Bignell GR, Cox C, Stephens P, Edkins S, Clegg S, et al. Mutations of the BRAF gene in human cancer. Nature. 2002 Jun 27;417(6892):949–54.

579. Flaherty KT, Puzanov I, Kim KB, Ribas A, McArthur GA, Sosman JA, et al. Inhibition of Mutated, Activated BRAF in Metastatic Melanoma. N Engl J Med. 2010 Aug 26;363(9):809–19.

580. Bollag G, Hirth P, Tsai J, Zhang J, Ibrahim PN, Cho H, et al. Clinical efficacy of a RAF inhibitor needs broad target blockade in BRAF-mutant melanoma. Nature. 2010 Sep 30;467(7315):596–9.

581. Chapman PB, Hauschild A, Robert C, Haanen JB, Ascierto P, Larkin J, et al. Improved Survival with Vemurafenib in Melanoma with BRAF V600E Mutation. N Engl J Med. 2011 Jun 30;364(26):2507–16.

582. Barretina J, Caponigro G, Stransky N, Venkatesan K, Margolin AA, Kim S, et al. The Cancer Cell Line Encyclopedia enables predictive modelling of anticancer drug sensitivity. Nature. 2012 Mar 29;483(7391):603–7.

583. Jaeger S, Duran-Frigola M, Aloy P. Drug sensitivity in cancer cell lines is not tissue-specific. Mol Cancer. 2015 Dec;14(1):312.

584. Ravi M, V P, Sr K, E A, Paul SFD. 3D Cell Culture Systems - Advantages and Applications. J Cell Physiol. 2014 Jun 9.

585. Loessner D, Stok KS, Lutolf MP, Hutmacher DW, Clements JA, Rizzi SC. Bioengineered 3D platform to explore cell-ECM interactions and drug resistance of epithelial ovarian cancer cells. Biomaterials. 2010 Nov;31(32):8494–506.

586. Richmond A, Su Y. Mouse xenograft models vs GEM models for human cancer therapeutics. Dis Model Mech. 2008 Sep;1(2-3):78–82.

587. De Wever O, Mareel M. Role of tissue stroma in cancer cell invasion. J Pathol. 2003 Jul;200(4):429–47.

588. Morton CL, Houghton PJ. Establishment of human tumor xenografts in immunodeficient mice. Nature Protocols. 2007 Feb;2(2):247–50.

589. Tentler JJ, Tan AC, Weekes CD, Jimeno A, Leong S, Pitts TM, et al. Patient-derived tumour xenografts as models for oncology drug development. Nat Rev Clin Oncol. 2012 Jun;9(6):338–50.

590. Whittle JR, Lewis MT, Lindeman GJ, Visvader JE. Patient-derived xenograft models of breast cancer and their predictive power. Breast Cancer Res. 2015 Dec;17(1):523.

591. Gillet J-P, Calcagno AM, Varma S, Marino M, Green LJ, Vora MI, et al. Redefining the relevance of established cancer cell lines to the study of mechanisms of clinical anti-cancer drug resistance. Proceedings of the National Academy of Sciences. 2011 Nov 15;108(46):18708–13.

592. Hidalgo M, Amant F, Biankin AV, Budinska E, Byrne AT, Caldas C, et al.

Patient-Derived Xenograft Models: An Emerging Platform for Translational Cancer Research. Cancer Discovery. 2014 Sep 1;4(9):998–1013.

593. Burrell RA, Swanton C. The evolution of the unstable cancer genome. Curr Opin Genet Dev. 2014 Feb;24:61–7.

594. Sipos F, Constantinovits M, Műzes G. Intratumoral functional heterogeneity and chemotherapy. World J Gastroenterol. 2014 Mar 14;20(10):2429–32.

595. Turner NC, Reis-Filho JS. Genetic heterogeneity and cancer drug resistance. Lancet Oncol. 2012 Apr;13(4):e178–85.

596. Klco JM, Spencer DH, Miller CA, Griffith M, Lamprecht TL, O'Laughlin M, et al. Functional heterogeneity of genetically defined subclones in acute myeloid leukemia. Cancer Cell. 2014 Mar 17;25(3):379–92.

597. Zembutsu H, Ohnishi Y, Tsunoda T, Furukawa Y, Katagiri T, Ueyama Y, et al. Genome-wide cDNA Microarray Screening to Correlate Gene Expression Profiles with Sensitivity of 85 Human Cancer Xenografts to Anticancer Drugs. Cancer Research. 2002.

598. Spreafico A, Tentler JJ, Pitts TM, Tan AC, Gregory MA, Arcaroli JJ, et al. Rational combination of a MEK inhibitor, selumetinib, and the Wnt/calcium pathway modulator, cyclosporin A, in preclinical models of colorectal cancer. Clin Cancer Res. 2013 Aug 1;19(15):4149–62.

599. Micel LN, Tentler JJ, Tan AC, Selby HM, Brunkow KL, Robertson KM, et al. Antitumor activity of the MEK inhibitor TAK-733 against melanoma cell lines and patient-derived tumor explants. Molecular Cancer Therapeutics. 2015 Feb;14(2):317–25.

600. Aparicio S, Hidalgo M, Kung AL. Examining the utility of patient-derived xenograft mouse models. Nat Rev Cancer. 2015 Apr 24;15(5):311–6.

601. Chesler L, Weiss WA. Genetically engineered murine models--contribution to our understanding of the genetics, molecular pathology and therapeutic targeting of neuroblastoma. Semin Cancer Biol. 2011 Oct;21(4):245–55.

602. Hill RM, Kuijper S, Lindsey JC, Petrie K, Schwalbe EC, Barker K, et al. Combined MYC and P53 Defects Emerge at Medulloblastoma Relapse and Define Rapidly Progressive, Therapeutically Targetable Disease. Cancer Cell. 2014 Dec 18.

603. Clark AK, Taubenberger AV, Taylor RA, Niranjan B, Chea ZY, Zotenko E, et al. A bioengineered microenvironment to quantitatively measure the tumorigenic properties of cancer-associated fibroblasts in human prostate cancer. Biomaterials. 2013 Jul;34(20):4777–85.

604. Stratton MR. Exploring the genomes of cancer cells: progress and promise. Science. 2011 Mar 25;331(6024):1553–8.

605. Greaves M. Darwinian medicine: a case for cancer. Nat Rev Cancer. 2007 Mar;7(3):213–21.

606. Grimmer MR, Weiss WA. Childhood tumors of the nervous system as disorders of normal development. Curr Opin Pediatr. 2006 Dec;18(6):634–8.

607. Mack SC, Witt H, Piro RM, Gu L, Zuyderduyn S, Stütz AM, et al. Epigenomic alterations define lethal CIMP-positive ependymomas of infancy. Nature. 2014 Feb 27;506(7489):445–50.

608. Karikari IO, Gilchrist CL, Jing L, Alcorta DA, Chen J, Richardson WJ, et al. Molecular characterization of chordoma xenografts generated from a novel primary chordoma cell source and two chordoma cell lines. J Neurosurg Spine. 2014 Jun 6;:1–8.

609. Siu I-M, Salmasi V, Orr BA, Zhao Q, Binder ZA, Tran C, et al. Establishment and characterization of a primary human chordoma xenograft model. Journal of Neurosurgery. 2012 Apr;116(4):801–9.

610. Bozzi F, Manenti G, Conca E, Stacchiotti S, Messina A, Dagrada G, et al. Development of transplantable human chordoma xenograft for preclinical assessment of novel therapeutic strategies. Neuro-oncology. 2013 Dec 16.

611. Haagensen EJ, Thomas HD, Wilson I, Harnor SJ, Payne SL, Rennison T, et al. The enhanced in vivo activity of the combination of a MEK and a PI3K inhibitor correlates with [18F]-FLT PET in human colorectal cancer xenograft tumour-bearing mice. PLoS ONE. 2013;8(12):e81763.

612. Bex A, Fournier L, Lassau N, Mulders P, Nathan P, Oyen WJG, et al. Assessing the response to targeted therapies in renal cell carcinoma: technical insights and practical considerations. Eur Urol. 2014 Apr;65(4):766–77.

613. O'Connor J, Jackson A, Asselin MC, Buckley DL. Quantitative imaging biomarkers in the clinical development of targeted therapeutics: current and future perspectives. Lancet Oncol. 2008.

614. Gerlinger M, Rowan AJ, Horswell S, Larkin J, Endesfelder D, Gronroos E, et al. Intratumor heterogeneity and branched evolution revealed by multiregion sequencing. N Engl J Med. 2012 Mar 8;366(10):883–92.

615. Campbell PJ, Yachida S, Mudie LJ, Stephens PJ, Pleasance ED, Stebbings LA, et al. The patterns and dynamics of genomic instability in metastatic pancreatic cancer. Nature. 2010 Oct 28;467(7319):1109–13.

616. Bedard PL, Hansen AR, Ratain MJ, Siu LL. Tumour heterogeneity in the clinic. Nature. 2013 Sep 19;501(7467):355–64.

617. Diehl F, Dressman D, Vogelstein B. Detection and quantification of mutations in the plasma of patients with colorectal tumors. PNAS. 2005 Oct 31;102(45):163686–116373.

618. Diehl F, Schmidt K, Choti MA, Romans K, Goodman S, Li M, et al. Circulating mutant DNA to assess tumor dynamics. Nat Med. 2007 Jul 31;14(9):985–90.

619. Lo YM, Corbetta N, Chamberlain PF, Rai V, Sargent IL, Redman CW, et al. Presence of fetal DNA in maternal plasma and serum. The Lancet. 1997 Aug 16;350(9076):485–7.

620. Lo YMD, Chiu RWK. Genomic analysis of fetal nucleic acids in maternal blood. Annu Rev Genomics Hum Genet. 2012;13:285–306.

621. Lo KK, Boustred C, Chitty LS, Plagnol V. RAPIDR: an analysis package for non-invasive prenatal testing of aneuploidy. Bioinformatics. 2014 Oct 15;30(20):2965–7.

622. Beulen L, Grutters JPC, Faas BH, Feenstra I, van Vugt JMG, Bekker MN. The consequences of implementing non-invasive prenatal testing in Dutch national health care: a cost-effectiveness analysis. Eur J Obstet Gynecol Reprod Biol. 2014 Nov;182:53–61.

623. Diaz LA, Bardelli A. Liquid biopsies: genotyping circulating tumor DNA. J Clin Oncol. 2014 Feb 20;32(6):579–86.

624. Choi J-J, Reich CF, Pisetsky DS. The role of macrophages in the in vitro generation of extracellular DNA from apoptotic and necrotic cells. Immunology. 2005 May;115(1):55–62.

625. Fleischhacker M, Schmidt B. Circulating nucleic acids (CNAs) and cancer--a survey. Biochim Biophys Acta. 2007 Jan;1775(1):181–232.

626. Delgado PO, Alves BCA, Gehrke F de S, Kuniyoshi RK, Wroclavski ML, Del Giglio A, et al. Characterization of cell-free circulating DNA in plasma in patients with prostate cancer. Tumor Biol. 2013 Apr;34(2):983–6.

627. Hashad D, Sorour A, Ghazal A, Talaat I. Free circulating tumor DNA as a diagnostic marker for breast cancer. J Clin Lab Anal. 2012 Nov;26(6):467–72.

628. No JH, Kim K, Park KH, Kim Y-B. Cell-free DNA level as a prognostic biomarker for epithelial ovarian cancer. Anticancer Res. 2012 Aug;32(8):3467–71.

629. Park J-L, Kim HJ, Choi BY, Lee H-C, Jang H-R, Song KS, et al. Quantitative analysis of cell-free DNA in the plasma of gastric cancer patients. Oncol Lett. 2012 Apr 1;3(4):921–6.

630. Schwarzenbach H, Alix-Panabières C, Müller I, Letang N, Vendrell J-P, Rebillard X, et al. Cell-free tumor DNA in blood plasma as a marker for circulating tumor cells in prostate cancer. Clin Cancer Res. 2009 Feb 1;15(3):1032–8.

631. Schwarzenbach H, Hoon DSB, Pantel K. Cell-free nucleic acids as biomarkers in cancer patients. Nat Rev Cancer. 2011 Jun;11(6):426–37.

632. Jahr S, Hentze H, Englisch S, Hardt D, Fackelmayer FO, Hesch RD, et al. DNA fragments in the blood plasma of cancer patients: quantitations and evidence for their origin from apoptotic and necrotic cells. Cancer Research. 2001 Feb 15;61(4):1659–65.

633. Yoon K-A, Park S, Lee SH, Kim JH, Lee JS. Comparison of circulating plasma DNA levels between lung cancer patients and healthy controls. J Mol Diagn. 2009 May;11(3):182–5.

634. Dawson S-J, Tsui DWY, Murtaza M, Biggs H, Rueda OM, Chin S-F, et al. Analysis of circulating tumor DNA to monitor metastatic breast cancer. N Engl J Med. 2013 Mar 28;368(13):1199–209.

635. Bettegowda C, Sausen M, Leary RJ, Kinde I, Wang Y, Agrawal N, et al. Detection of circulating tumor DNA in early- and late-stage human malignancies. Science Translational Medicine. 2014 Feb 19;6(224):224ra24.

636. Roschewski M, Dunleavy K, Pittaluga S, Moorhead M, Pepin F, Kong K, et al. Circulating tumour DNA and CT monitoring in patients with untreated diffuse large B-cell lymphoma: a correlative biomarker study. Lancet Oncol. 2015 Apr 1.

637. Forshew T, Murtaza M, Parkinson C, Gale D, Tsui DWY, Kaper F, et al. Noninvasive identification and monitoring of cancer mutations by targeted deep sequencing of plasma DNA. Science Translational Medicine. 2012 May 30;4(136):136ra68.

638. Newman AM, Bratman SV, To J, Wynne JF, Eclov NCW, Modlin LA, et al. An ultrasensitive method for quantitating circulating tumor DNA with broad patient coverage. Nat Med. 2014 Apr 6.

639. Murtaza M, Dawson S-J, Tsui DWY, Gale D, Forshew T, Piskorz AM, et al. Non-invasive analysis of acquired resistance to cancer therapy by sequencing of plasma DNA. Nature. 2013 Apr 7.

640. Vogelstein B, Kinzler KW. Digital PCR. Proc Natl Acad Sci USA. 1999 Aug 3;96(16):9236–41.

641. Bidard F-C, Weigelt B, Reis-Filho JS. Going with the flow: from circulating tumor cells to DNA. Science Translational Medicine. 2013 Oct 16;5(207):207ps14.

642. Hindson BJ, Ness KD, Masquelier DA, Belgrader P, Heredia NJ, Makarewicz AJ, et al. High-throughput droplet digital PCR system for absolute quantitation of DNA copy number. Anal Chem. 2011 Nov 15;83(22):8604–10.

643. Bratman SV, Newman AM, Alizadeh AA, Diehn M. Potential clinical utility of ultrasensitive circulating tumor DNA detection with CAPP-Seq. Expert Review of Molecular Diagnostics. 2015 Mar 16;:1–5.

644. Higgins MJ, Jelovac D, Barnathan E, Blair B, Slater S, Powers P, et al. Detection of tumor PIK3CA status in metastatic breast cancer using peripheral blood. Clin Cancer Res. 2012 Jun 15;18(12):3462–9.

645. Richardson AL, Iglehart JD. BEAMing up personalized medicine: mutation detection in blood. Clin Cancer Res. 2012 Jun 15;18(12):3209–11.

646. Rosell R, Molina MA, Serrano MJ. EGFR mutations in circulating tumour DNA. Lancet Oncol. 2012 Oct;13(10):971–3.

647. Schneck H, Blassl C, Meier-Stiegen F, Neves RP, Janni W, Fehm T, et al. Analysing the mutational status of PIK3CA in circulating tumor cells from metastatic breast cancer patients. Mol Oncol. 2013 Oct;7(5):976–86.

648. Maheswaran S, Sequist LV, Nagrath S, Ulkus L, Brannigan B, Collura CV, et al. Detection of mutations in EGFR in circulating lung-cancer cells. N Engl J Med. 2008 Jul 24;359(4):366–77.

649. Racila E, Euhus D, Weiss AJ, Rao C, McConnell J, Terstappen LW, et al. Detection and characterization of carcinoma cells in the blood. Proc Natl Acad Sci USA. 1998 Apr 14;95(8):4589–94.

650. Yu M, Bardia A, Wittner BS, Stott SL, Smas ME, Ting DT, et al. Circulating breast tumor cells exhibit dynamic changes in epithelial and mesenchymal composition. Science. 2013 Feb 1;339(6119):580–4.

651. Bidard F-C, Madic J, Mariani P, Piperno-Neumann S, Rampanou A, Servois V, et al. Detection rate and prognostic value of circulating tumor cells and circulating tumor DNA in metastatic uveal melanoma. Int J Cancer. 2014 Mar 1;134(5):1207–13.

652. Olsson E, Winter C, George A, Chen Y, Howlin J, Tang M-HE, et al. Serial monitoring of circulating tumor DNA in patients with primary breast cancer for detection of occult metastatic disease. EMBO Mol Med. 2015 May 18.

653. Madic J, Kiialainen A, Bidard F-C, Birzele F, Ramey G, Leroy Q, et al. Circulating tumor DNA and circulating tumor cells in metastatic triple negative breast cancer patients. Int J Cancer. 2015 May 1;136(9):2158–65.

654. Yoo C, Ryu M-H, Na YS, Ryoo B-Y, Park SR, Kang Y-K. Analysis of serum protein biomarkers, circulating tumor DNA, and dovitinib activity in patients with tyrosine kinase inhibitor-refractory gastrointestinal stromal tumors. Ann Oncol. 2014 Nov;25(11):2272–7.

655. Misale S, Yaeger R, Hobor S, Scala E, Janakiraman M, Liska D, et al. Emergence of KRAS mutations and acquired resistance to anti-EGFR therapy in colorectal cancer. Nature. 2012 Jun 28;486(7404):532–6.

656. Qiu M, Wang J, Xu Y, Ding X, Li M, Jiang F, et al. Circulating tumor DNA is effective for the detection of EGFR mutation in non-small cell lung cancer: a meta-analysis. Cancer Epidemiol Biomarkers Prev. 2015 Jan;24(1):206–12.

657. Misale S, Arena S, Lamba S, Siravegna G, Lallo A, Hobor S, et al. Blockade of EGFR and MEK Intercepts Heterogeneous Mechanisms of Acquired Resistance to Anti-EGFR Therapies in Colorectal Cancer. Science Translational Medicine. 2014 Feb 19;6(224):224ra26.

658. Diaz LA, Williams RT, Wu J, Kinde I, Hecht JR, Berlin J, et al. The molecular evolution of acquired resistance to targeted EGFR blockade in

colorectal cancers. Nature. 2012 Jun 28;486(7404):537–40.

659. Gevensleben H, Garcia-Murillas I, Graeser MK, Schiavon G, Osin P, Parton M, et al. Noninvasive Detection of HER2 Amplification with Plasma DNA Digital PCR. Clinical Cancer Research. 2013 Jun 13;19(12):3276–84.

660. Bidard F-C, Pierga J-Y, Soria J-C, Thiery JP. Translating metastasis-related biomarkers to the clinic--progress and pitfalls. Nat Rev Clin Oncol. 2013 Mar;10(3):169–79.

661. Rinner B, Froehlich EV, Buerger K, Knausz H, Lohberger B, Scheipl S, et al. Establishment and detailed functional and molecular genetic characterisation of a novel sacral chordoma cell line, MUG-Chor1. Int J Oncol. 2012 Feb;40(2):443–51.

662. Sanger F, Nicklen S, Coulson AR. DNA sequencing with chain-terminating inhibitors. Proc Natl Acad Sci USA. 1977 Dec;74(12):5463–7.

663. Graham FL, Smiley J, Russell WC, Nairn R. Characteristics of a human cell line transformed by DNA from human adenovirus type 5. J Gen Virol. 1977 Jul;36(1):59–74.

664. Campeau E, Ruhl VE, Rodier F, Smith CL, Rahmberg BL, Fuss JO, et al. A versatile viral system for expression and depletion of proteins in mammalian cells. PLoS ONE. 2009;4(8):e6529.

665. Osaka E, Yang X, Shen JK, Yang P, Feng Y, Mankin HJ, et al. MicroRNA-1 (miR-1) inhibits chordoma cell migration and invasion by targeting slug. J Orthop Res. 2014 Aug;32(8):1075–82.

666. Zhang Y, Schiff D, Park D, Abounader R. MicroRNA-608 and microRNA-34a regulate chordoma malignancy by targeting EGFR, Bcl-xL and MET. PLoS ONE. 2014;9(3):e91546.

667. Euhus DM, Hudd C, LaRegina MC, Johnson FE. Tumor measurement in the nude mouse. J Surg Oncol. 1986 Apr;31(4):229–34.

668. Sato A, Klaunberg B, Tolwani R. In vivo bioluminescence imaging. Comp Med. 2004 Dec;54(6):631–4.

669. Greer LF, Szalay AA. Imaging of light emission from the expression of luciferases in living cells and organisms: a review. Luminescence. 2002 Jan;17(1):43–74.

670. Inoue Y, Kiryu S, Watanabe M, Tojo A, Ohtomo K. Timing of imaging after d-luciferin injection affects the longitudinal assessment of tumor growth using in vivo bioluminescence imaging. Int J Biomed Imaging. 2010;2010:471408.

671. Paroo Z, Bollinger RA, Braasch DA, Richer E, Corey DR, Antich PP, et al. Validating bioluminescence imaging as a high-throughput, quantitative modality for assessing tumor burden. Mol Imaging. 2004 Apr;3(2):117–24.

672. Baba S, Cho SY, Ye Z, Cheng L, Engles JM, Wahl RL. How reproducible

is bioluminescent imaging of tumor cell growth? Single time point versus the dynamic measurement approach. Mol Imaging. 2007 Sep;6(5):315–22.

673. Inoue Y, Kiryu S, Izawa K, Watanabe M, Tojo A, Ohtomo K. Comparison of subcutaneous and intraperitoneal injection of D-luciferin for in vivo bioluminescence imaging. Eur J Nucl Med Mol Imaging. 2009 May;36(5):771–9.

674. Boden D, Pusch O, Silbermann R, Lee F, Tucker L, Ramratnam B. Enhanced gene silencing of HIV-1 specific siRNA using microRNA designed hairpins. Nucleic Acids Research. 2004;32(3):1154–8.

675. Sambrook J, Russell DW. Molecular cloning. 2001.

676. Landy A. Dynamic, structural, and regulatory aspects of lambda site-specific recombination. Annu Rev Biochem. 1989;58:913–49.

677. Hartley JL, Temple GF, Brasch MA. DNA cloning using in vitro site-specific recombination. Genome Research. 2000 Nov;10(11):1788–95.

678. Liang X, Peng L, Baek C-H, Katzen F. Single step BP/LR combined Gateway reactions. Biotech. 2013 Nov;55(5):265–8.

679. Chang K, Marran K, Valentine A, Hannon GJ. Creating an miR30-based shRNA vector. Cold Spring Harbor Protocols. 2013 Jul;2013(7):631–5.

680. Vandenberghe LH, Xiao R, Lock M, Lin J, Korn M, Wilson JM. Efficient Serotype-Dependent Release of Functional Vector into the Culture Medium During Adeno-Associated Virus Manufacturing. Human Gene Therapy. Mary Ann Liebert, Inc. 140 Huguenot Street, 3rd Floor New Rochelle, NY 10801 USA; 2010 Oct;21(10):1251–7.

681. Zhang J, Chung T, Oldenburg K. A Simple Statistical Parameter for Use in Evaluation and Validation of High Throughput Screening Assays. J Biomol Screen. 1999;4(2):67–73.

682. Bamborough P, Drewry D, Harper G, Smith GK, Schneider K. Assessment of chemical coverage of kinome space and its implications for kinase drug discovery. J Med Chem. 2008 Dec 25;51(24):7898–914.

683. Houghton BC, Booth C, Thrasher AJ. Lentivirus technologies for modulation of the immune system. Curr Opin Pharmacol. 2015 Sep 9;24:119–27.

684. Messaoudi El S, Rolet F, Mouliere F, Thierry AR. Circulating cell free DNA: Preanalytical considerations. Clin Chim Acta. 2013 Sep 23;424:222–30.

685. Devonshire AS, Whale AS, Gutteridge A, Jones G, Cowen S, Foy CA, et al. Towards standardisation of cell-free DNA measurement in plasma: controls for extraction efficiency, fragment size bias and quantification. Anal Bioanal Chem. 2014 May 24.

686. Verdine GL, Walensky LD. The challenge of drugging undruggable targets in cancer: lessons learned from targeting BCL-2 family members. Clin

Cancer Res. 2007 Dec 15;13(24):7264–70.

687. Zhang X, Yuan X, Zhu W, Qian H, Xu W. SALL4: an emerging cancer biomarker and target. Cancer Letters. 2015 Feb 1;357(1):55–62.

688. Malhotra M, Toulouse A, Godinho BMDC, Mc Carthy DJ, Cryan JF, O'Driscoll CM. RNAi therapeutics for brain cancer: current advancements in RNAi delivery strategies. Mol Biosyst. 2015 Sep 15;11(10):2635–57.

689. Paddison PJ, Hannon GJ. RNA interference: the new somatic cell genetics? Cancer Cell. 2002 Jul;2(1):17–23.

690. Hemann MT, Fridman JS, Zilfou JT, Hernando E, Paddison PJ, Cordon-Cardo C, et al. An epi-allelic series of p53 hypomorphs created by stable RNAi produces distinct tumor phenotypes in vivo. Nat Genet. 2003 Mar;33(3):396–400.

691. McCaffrey AP, Nakai H, Pandey K, Huang Z, Salazar FH, Xu H, et al. Inhibition of hepatitis B virus in mice by RNA interference. Nat Biotech. 2003 Jun;21(6):639–44.

692. Carmell MA, Zhang L, Conklin DS, Hannon GJ, Rosenquist TA. Germline transmission of RNAi in mice. Nat Struct Biol. 2003 Feb;10(2):91–2.

693. Zincarelli C, Soltys S, Rengo G, Rabinowitz JE. Analysis of AAV serotypes 1-9 mediated gene expression and tropism in mice after systemic injection. Molecular Therapy. 2008 Jun;16(6):1073–80.

694. Lebbink RJ, Lowe M, Chan T, Khine H, Wang X, McManus MT. Polymerase II promoter strength determines efficacy of microRNA adapted shRNAs. PLoS ONE. 2011;6(10):e26213.

695. Elbashir SM, Martinez J, Patkaniowska A, Lendeckel W, Tuschl T. Functional anatomy of siRNAs for mediating efficient RNAi in Drosophila melanogaster embryo lysate. EMBO J. 2001 Dec 3;20(23):6877–88.

696. Miller VM, Xia H, Marrs GL, Gouvion CM, Lee G, Davidson BL, et al. Allele-specific silencing of dominant disease genes. Proc Natl Acad Sci USA. 2003 Jun 10;100(12):7195–200.

697. Semizarov D, Frost L, Sarthy A, Kroeger P, Halbert DN, Fesik SW. Specificity of short interfering RNA determined through gene expression signatures. Proc Natl Acad Sci USA. 2003 May 27;100(11):6347–52.

698. Lin X, Ruan X, Anderson MG, McDowell JA, Kroeger PE, Fesik SW, et al. siRNA-mediated off-target gene silencing triggered by a 7 nt complementation. Nucleic Acids Research. 2005;33(14):4527–35.

699. Boudreau RL, Monteys AM, Davidson BL. Minimizing variables among hairpin-based RNAi vectors reveals the potency of shRNAs. RNA. 2008 Sep;14(9):1834–44.

700. Oohashi T, Zhou XH, Feng K, Richter B, Mörgelin M, Perez MT, et al. Mouse ten-m/Odz is a new family of dimeric type II transmembrane

proteins expressed in many tissues. J Cell Biol. 1999 May 3;145(3):563–77.

701. Levine A, Bashan-Ahrend A, Budai-Hadrian O, Gartenberg D, Menasherow S, Wides R. Odd Oz: a novel Drosophila pair rule gene. Cell. 1994 May 20;77(4):587–98.

702. Mieda M, Kikuchi Y, Hirate Y, Aoki M, Okamoto H. Compartmentalized expression of zebrafish ten-m3 and ten-m4, homologues of the Drosophila ten(m)/odd Oz gene, in the central nervous system. Mech Dev. 1999 Sep;87(1-2):223–7.

703. Rubin BP, Tucker RP, Brown-Luedi M, Martin D, Chiquet-Ehrismann R. Teneurin 2 is expressed by the neurons of the thalamofugal visual system in situ and promotes homophilic cell-cell adhesion in vitro. Development. 2002 Oct;129(20):4697–705.

704. Trzebiatowska A, Topf U, Sauder U, Drabikowski K, Chiquet-Ehrismann R. Caenorhabditis elegans teneurin, ten-1, is required for gonadal and pharyngeal basement membrane integrity and acts redundantly with integrin ina-1 and dystroglycan dgn-1. Mol Biol Cell. 2008 Sep;19(9):3898–908.

705. Mosca TJ, Hong W, Dani VS, Favaloro V, Luo L. Trans-synaptic Teneurin signalling in neuromuscular synapse organization and target choice. Nature. 2012 Apr 12;484(7393):237–41.

706. Pan X, Yue Y, Zhang K, Hakim C, Kodippili K, McDonald T, et al. AAV-8 is more efficient than AAV-9 in transducing neonatal dog heart. Hum Gene Ther Methods. 2015 Mar 12.

707. Hoffman RM. The multiple uses of fluorescent proteins to visualize cancer in vivo. Nat Rev Cancer. 2005 Oct;5(10):796–806.

708. Gu W, Payne E, Sun S, Burgess M, McMillan NAJ. Inhibition of cervical cancer cell growth in vitro and in vivo with dual shRNAs. Cancer Gene Therapy. 2011 Mar;18(3):219–27.

709. Gu W, Putral L, McMillan N. siRNA and shRNA as anticancer agents in a cervical cancer model. Methods Mol Biol. 2008;442:159–72.

710. Fish RJ, Kruithof EKO. Short-term cytotoxic effects and long-term instability of RNAi delivered using lentiviral vectors. BMC Mol Biol. 2004 Aug 3;5:9.

711. Tang S, Tao M, McCoy JP, Zheng ZM. Short-term induction and long-term suppression of HPV16 oncogene silencing by RNA interference in cervical cancer cells. Oncogene. 2006 Mar 30;25(14):2094–104.

712. Zheng Z-M, Tang S, Tao M. Development of resistance to RNAi in mammalian cells. Ann N Y Acad Sci. 2005 Nov;1058:105–18.

713. Brake ter O, Konstantinova P, Ceylan M, Berkhout B. Silencing of HIV-1 with RNA interference: a multiple shRNA approach. Mol Ther. 2006

Dec;14(6):883–92.

714. Bobbin ML, Burnett JC, Rossi JJ. RNA interference approaches for treatment of HIV-1 infection. Genome Med. 2015;7(1):50.

715. Rao DD, Senzer N, Wang Z, Kumar P, Jay CM, Nemunaitis J. Bifunctional short hairpin RNA (bi-shRNA): design and pathway to clinical application. Methods Mol Biol. 2013;942:259–78.

716. Rao DD, Maples PB, Senzer N, Kumar P, Wang Z, Pappen BO, et al. Enhanced target gene knockdown by a bifunctional shRNA: a novel approach of RNA interference. Cancer Gene Therapy. 2010 Nov;17(11):780–91.

717. Nathwani AC, Nienhuis AW, Davidoff AM. Our journey to successful gene therapy for hemophilia B. Human Gene Therapy. 2014 Nov;25(11):923–6.

718. Fields PA, Kowalczyk DW, Arruda VR, Armstrong E, McCleland ML, Hagstrom JN, et al. Role of vector in activation of T cell subsets in immune responses against the secreted transgene product factor IX. Mol Ther. 2000 Mar;1(3):225–35.

719. Roitt IM, Cooke A. Idiotypic interactions in autoimmunity: an editorial overview. J Autoimmun. 1988 Feb;1(1):3–6.

720. Mond JJ, Scher I, Cossman J, Kessler S, Mongini PK, Hansen C, et al. Role of the thymus in directing the development of a subset of B lymphocytes. J Exp Med. 1982 Mar 1;155(3):924–36.

721. Wortis HH, Burkly L, Hughes D, Roschelle S, Waneck G. Lack of mature B cells in nude mice with X-linked immune deficiency. J Exp Med. 1982 Mar 1;155(3):903–13.

722. Stacchiotti S, Casali PG. Systemic therapy options for unresectable and metastatic chordomas. Curr Oncol Rep. 2011 Aug;13(4):323–30.

723. Muro K, Das S, Raizer JJ. Chordomas of the craniospinal axis: multimodality surgical, radiation and medical management strategies. Expert Rev Neurother. 2007 Oct;7(10):1295–312.

724. Arteaga CL. Overview of epidermal growth factor receptor biology and its role as a therapeutic target in human neoplasia. Semin Oncol. 2002 Oct;29(5 Suppl 14):3–9.

725. Slamon DJ, Leyland-Jones B, Shak S, Fuchs H, Paton V, Bajamonde A, et al. Use of chemotherapy plus a monoclonal antibody against HER2 for metastatic breast cancer that overexpresses HER2. N Engl J Med. 2001 Mar 15;344(11):783–92.

726. Heinrich MC, Corless CL, Demetri GD, Blanke CD, Mehren von M, Joensuu H, et al. Kinase mutations and imatinib response in patients with metastatic gastrointestinal stromal tumor. J Clin Oncol. 2003 Dec 1;21(23):4342–9.

727. Moore MJ, Goldstein D, Hamm J, Figer A, Hecht JR, Gallinger S, et al. Erlotinib plus gemcitabine compared with gemcitabine alone in patients with advanced pancreatic cancer: a phase III trial of the National Cancer Institute of Canada Clinical Trials Group. J Clin Oncol. 2007 May 20;25(15):1960–6.

728. Kobayashi M, Tojo A. The BRAF-V600E mutation in circulating cell-free DNA is a promising biomarker of high-risk adult Langerhans cell histiocytosis. Blood. 2014 Oct 16;124(16):2610–1.

729. Stewart EL, Tan SZ, Liu G, Tsao M-S. Known and putative mechanisms of resistance to EGFR targeted therapies in NSCLC patients with EGFR mutations-a review. Transl Lung Cancer Res. 2015 Feb;4(1):67–81.

730. Lynch TJ, Bell DW, Sordella R, Gurubhagavatula S, Okimoto RA, Brannigan BW, et al. Activating mutations in the epidermal growth factor receptor underlying responsiveness of non-small-cell lung cancer to gefitinib. N Engl J Med. 2004 May 20;350(21):2129–39.

731. Remon J, Morán T, Reguart N, Majem M, Carcereny E, Lianes P. Beyond EGFR TKI in EGFR-mutant Non-Small Cell Lung Cancer patients: Main challenges still to be overcome. Cancer Treat Rev. 2014 Jul;40(6):723–9.

732. Wagle N, Emery C, Berger MF, Davis MJ, Sawyer A, Pochanard P, et al. Dissecting therapeutic resistance to RAF inhibition in melanoma by tumor genomic profiling. Journal of Clinical Oncology. 2011 Aug 1;29(22):3085–96.

733. Nazarian R, Shi H, Wang Q, Kong X, Koya RC, Lee H, et al. Melanomas acquire resistance to B-RAF(V600E) inhibition by RTK or N-RAS upregulation. Nature. 2010 Dec 16;468(7326):973–7.

734. Kobayashi S, Boggon TJ, Dayaram T, Jänne PA, Kocher O, Meyerson M, et al. EGFR mutation and resistance of non-small-cell lung cancer to gefitinib. N Engl J Med. 2005 Feb 24;352(8):786–92.

735. Yarden Y, Pines G. The ERBB network: at last, cancer therapy meets systems biology. Nat Rev Cancer. Nature Publishing Group; 2012 Jul 12;12(8):553–63.

736. Tebbutt N, Pedersen MW, Johns TG. Targeting the ERBB family in cancer: couples therapy. Nat Rev Cancer. Nature Publishing Group; 2013 Aug 16;13(9):663–73.

737. Drewry DH, Willson TM, Zuercher WJ. Seeding collaborations to advance kinase science with the GSK Published Kinase Inhibitor Set (PKIS). Curr Top Med Chem. 2014;14(3):340–2.

738. Young L, Sung J, Stacey G, Masters JR. Detection of Mycoplasma in cell cultures. Nature Protocols. Nature Publishing Group; 2010 Apr 22;5(5):929–34.

739. Dranchak P, MacArthur R, Guha R, Zuercher WJ, Drewry DH, Auld DS, et al. Profile of the GSK published protein kinase inhibitor set across ATP-

dependent and-independent luciferases: implications for reporter-gene assays. PLoS ONE. 2013;8(3):e57888.

740. Igney FH, Krammer PH. Death and anti-death: tumour resistance to apoptosis. Nat Rev Cancer. 2002 Apr;2(4):277–88.

741. Zhou W, Ercan D, Chen L, Yun C-H, Li D, Capelletti M, et al. Novel mutant-selective EGFR kinase inhibitors against EGFR T790M. Nature. 2009 Dec 24;462(7276):1070–4.

742. Hickinson DM, Klinowska T, Speake G, Vincent J, Trigwell C, Anderton J, et al. AZD8931, an equipotent, reversible inhibitor of signaling by epidermal growth factor receptor, ERBB2 (HER2), and ERBB3: a unique agent for simultaneous ERBB receptor blockade in cancer. Clin Cancer Res. 2010 Feb 15;16(4):1159–69.

743. Downward J, Yarden Y, Mayes E, Scrace G, Totty N, Stockwell P, et al. Close similarity of epidermal growth factor receptor and v-erb-B oncogene protein sequences. Nature. 1984 Feb;307(5951):521–7.

744. Hendler FJ, Ozanne BW. Human squamous cell lung cancers express increased epidermal growth factor receptors. J Clin Invest. 1984 Aug;74(2):647–51.

745. Libermann TA, Razon N, Bartal AD, Yarden Y, Schlessinger J, Soreq H. Expression of epidermal growth factor receptors in human brain tumors. Cancer Research. 1984 Feb;44(2):753–60.

746. Libermann TA, Nusbaum HR, Razon N, Kris R, Lax I, Soreq H, et al. Amplification, enhanced expression and possible rearrangement of EGF receptor gene in primary human brain tumours of glial origin. Nature. 1985 Jan;313(5998):144–7.

747. Sugawa N, Ekstrand AJ, James CD, Collins VP. Identical splicing of aberrant epidermal growth factor receptor transcripts from amplified rearranged genes in human glioblastomas. Proceedings of the National Academy of Sciences. 1990 Nov 1;87(21):8602–6.

748. Chong CR, Jänne PA. The quest to overcome resistance to EGFR-targeted therapies in cancer. Nat Med. 2013 Nov;19(11):1389–400.

749. Ardito CM, Grüner BM, Takeuchi KK, Lubeseder-Martellato C, Teichmann N, Mazur PK, et al. EGF receptor is required for KRAS-induced pancreatic tumorigenesis. Cancer Cell. 2012 Sep 11;22(3):304–17.

750. Frattini M, Saletti P, Romagnani E, Martin V, Molinari F, Ghisletta M, et al. PTEN loss of expression predicts cetuximab efficacy in metastatic colorectal cancer patients. Br J Cancer. 2007 Oct 22;97(8):1139–45.

751. Vermorken JB, Mesia R, Rivera F, Remenar E, Kawecki A, Rottey S, et al. Platinum-based chemotherapy plus cetuximab in head and neck cancer. N Engl J Med. 2008 Sep 11;359(11):1116–27.

752. Bonner JA, Harari PM, Giralt J, Azarnia N, Shin DM, Cohen RB, et al.

Radiotherapy plus cetuximab for squamous-cell carcinoma of the head and neck. N Engl J Med. 2006 Feb 9;354(6):567–78.

753. Singleton KR, Kim J, Hinz TK, Marek LA, Casás-Selves M, Hatheway C, et al. A receptor tyrosine kinase network composed of fibroblast growth factor receptors, epidermal growth factor receptor, v-erb-b2 erythroblastic leukemia viral oncogene homolog 2, and hepatocyte growth factor receptor drives growth and survival of head and neck squamous carcinoma cell lines. Mol Pharmacol. 2013 Apr;83(4):882–93.

754. Morrison G, Fu X, Shea M, Nanda S, Giuliano M, Wang T, et al. Therapeutic potential of the dual EGFR/HER2 inhibitor AZD8931 in circumventing endocrine resistance. Breast Cancer Res Treat. 2014 Apr;144(2):263–72.

755. O'Brien PJ, Irwin W, Diaz D, Howard-Cofield E, Krejsa CM, Slaughter MR, et al. High concordance of drug-induced human hepatotoxicity with in vitro cytotoxicity measured in a novel cell-based model using high content screening. Arch Toxicol. 2006 Sep;80(9):580–604.

756. Di Fiore F, Blanchard F, Charbonnier F, Le Pessot F, Lamy A, Galais MP, et al. Clinical relevance of KRAS mutation detection in metastatic colorectal cancer treated by Cetuximab plus chemotherapy. Br J Cancer. 2007 Apr 23;96(8):1166–9.

757. Benvenuti S, Sartore-Bianchi A, Di Nicolantonio F, Zanon C, Moroni M, Veronese S, et al. Oncogenic activation of the RAS/RAF signaling pathway impairs the response of metastatic colorectal cancers to anti-epidermal growth factor receptor antibody therapies. Cancer Research. 2007 Mar 15;67(6):2643–8.

758. Chen K, Mo J, Zhou M, Wang G, Wu G, Chen H, et al. Expression of PTEN and mTOR in sacral chordoma and association with poor prognosis. Med Oncol. Springer US; 2014 Feb 18;31(4):886–5.

759. Lee D-H, Zhang Y, Kassam AB, Park M-J, Gardner P, Prevedello D, et al. Combined PDGFR and HDAC Inhibition Overcomes PTEN Disruption in Chordoma. PLoS ONE. 2015;10(8):e0134426.

760. Capozzi M, Caterina I, De Divitiis C, Arx von C, Maiolino P, Tatangelo F, et al. Everolimus and pancreatic neuroendocrine tumors (PNETs): Activity, resistance and how to overcome it. Int J Surg. 2015 Sep;21 Suppl 1:S89–94.

761. Timpe LC, Li D, Yen T-Y, Wong J, Yen R, Macher BA, et al. Mining the Breast Cancer Proteome for Predictors of Drug Sensitivity. J Proteomics Bioinform. 2015;8(9):204–11.

762. Dabney R, Devine R, Sein N, George B. New agents in renal cell carcinoma. Target Oncol. 2014 Sep;9(3):183–93.

763. Hasskarl J. Everolimus. Recent Results Cancer Res. 2014;201:373–92.

764. Shimobayashi M, Hall MN. Making new contacts: the mTOR network in

metabolism and signalling crosstalk. Nat Rev Mol Cell Biol. 2014 Mar;15(3):155–62.

765. Ehrhardt MJ, Karst J, Donohoue PA, Maheshwari M, McClain KL, Bingen K, et al. Recognition and treatment of concurrent active and neurodegenerative langerhans cell histiocytosis: a case report. J Pediatr Hematol Oncol. 2015 Jan;37(1):e37–40.

766. Sarker D, Ang JE, Baird R, Kristeleit R, Shah K, Moreno V, et al. First-in-human phase I study of pictilisib (GDC-0941), a potent pan-class I phosphatidylinositol-3-kinase (PI3K) inhibitor, in patients with advanced solid tumors. Clin Cancer Res. 2015 Jan 1;21(1):77–86.

767. Trucco MM, Awad O, Wilky BA, Goldstein SD, Huang R, Walker RL, et al. A Novel Chordoma Xenograft Allows In Vivo Drug Testing and Reveals the Importance of NF-κB Signaling in Chordoma Biology. PLoS ONE. 2013;8(11):e79950.

768. Moreau P, Richardson PG, Cavo M, Orlowski RZ, San Miguel J-F, Palumbo A, et al. Proteasome inhibitors in multiple myeloma: 10 years later. Blood. 2012 Aug 2;120(5):947–59.

769. Denlinger CS, Meropol NJ, Li T, Lewis NL, Engstrom PF, Weiner LM, et al. A Phase II Trial of the Proteasome Inhibitor Bortezomib in Patients With Advanced Biliary Tract Cancers. Clin Colorectal Cancer. 2014 Jun;13(2):81–6.

770. Zavrski I, Kleeberg L, Kaiser M, Fleissner C, Heider U, Sterz J, et al. Proteasome as an emerging therapeutic target in cancer. Curr Pharm Des. 2007;13(5):471–85.

771. Muscal JA, Thompson PA, Horton TM, Ingle AM, Ahern CH, McGovern RM, et al. A phase I trial of vorinostat and bortezomib in children with refractory or recurrent solid tumors: A Children's Oncology Group phase I consortium study (ADVL0916). Pediatr Blood Cancer. 2012 Aug 9;60(3):390–5.

772. Deming DA, Ninan J, Bailey HH, Kolesar JM, Eickhoff J, Reid JM, et al. A Phase I study of intermittently dosed vorinostat in combination with bortezomib in patients with advanced solid tumors. Invest New Drugs. 2014 Apr;32(2):323–9.

773. Evens AM, Smith MR, Lossos IS, Helenowski I, Millenson M, Winter JN, et al. Frontline bortezomib and rituximab for the treatment of newly diagnosed high tumour burden indolent non-hodgkin lymphoma: a multicentre phase II study. Br J Haematol. 2014 Apr 25.

774. Adams J, Palombella VJ, Sausville EA, Johnson J, Destree A, Lazarus DD, et al. Proteasome inhibitors: a novel class of potent and effective antitumor agents. Cancer Research. 1999 Jun 1;59(11):2615–22.

775. Zavrski I, Jakob C, Kaiser M, Fleissner C, Heider U, Sezer O. Molecular and clinical aspects of proteasome inhibition in the treatment of cancer. Recent Results Cancer Res. 2007;176:165–76.

776. Chen K-F, Yeh P-Y, Yeh K-H, Lu Y-S, Huang S-Y, Cheng A-L. Down-regulation of phospho-Akt is a major molecular determinant of bortezomib-induced apoptosis in hepatocellular carcinoma cells. Cancer Research. 2008 Aug 15;68(16):6698–707.

777. Chen K-F, Liu C-Y, Lin Y-C, Yu H-C, Liu T-H, Hou D-R, et al. CIP2A mediates effects of bortezomib on phospho-Akt and apoptosis in hepatocellular carcinoma cells. Oncogene. 2010 Nov 25;29(47):6257–66.

778. Lin Y-C, Chen K-C, Chen C-C, Cheng A-L, Chen K-F. CIP2A-mediated Akt activation plays a role in bortezomib-induced apoptosis in head and neck squamous cell carcinoma cells. Oral Oncol. 2012 Jul;48(7):585–93.

779. Lin L, Gaut D, Hu K, Yan H, Yin D, Koeffler HP. Dual targeting of glioblastoma multiforme with a proteasome inhibitor (Velcade) and a phosphatidylinositol 3-kinase inhibitor (ZSTK474). Int J Oncol. 2014 Feb;44(2):557–62.

780. Demel H-R, Feuerecker B, Piontek G, Seidl C, Blechert B, Pickhard A, et al. Effects of topoisomerase inhibitors that induce DNA damage response on glucose metabolism and PI3K/Akt/mTOR signaling in multiple myeloma cells. Am J Cancer Res. 2015;5(5):1649–64.

781. Kim A, Park S, Lee J-E, Jang W-S, Lee S-J, Kang HJ, et al. The dual PI3K and mTOR inhibitor NVP-BEZ235 exhibits anti-proliferative activity and overcomes bortezomib resistance in mantle cell lymphoma cells. Leuk Res. 2012 Jul;36(7):912–20.

782. Voskoglou-Nomikos T, Pater JL, Seymour L. Clinical predictive value of the in vitro cell line, human xenograft, and mouse allograft preclinical cancer models. Clin Cancer Res. 2003 Sep 15;9(11):4227–39.

783. Johnson JI, Decker S, Zaharevitz D, Rubinstein LV, Venditti JM, Schepartz S, et al. Relationships between drug activity in NCI preclinical in vitro and in vivo models and early clinical trials. Br J Cancer. 2001 May 18;84(10):1424–31.

784. Benson JD, Chen Y-NP, Cornell-Kennon SA, Dorsch M, Kim S, Leszczyniecka M, et al. Validating cancer drug targets. Nature. 2006 May 25;441(7092):451–6.

785. Zheng W, Thorne N, McKew JC. Phenotypic screens as a renewed approach for drug discovery. Drug Discovery Today. 2013 Nov;18(21-22):1067–73.

786. Crockford A, Jamal-Hanjani M, Hicks J, Swanton C. Implications of intratumour heterogeneity for treatment stratification. J Pathol. 2013 Dec 10;232(2):264–73.

787. Burger A. A zebrafish model of chordoma initiated by notochord-driven expression of HRAS12 [Internet]. 2013 [cited 2015 Jul 19]. Available from: http://dmm.biologists.org.libproxy.ucl.ac.uk/content/7/7/907.full.pdf+html

788. Peterson RT, Link BA, Dowling JE, Schreiber SL. Small molecule

developmental screens reveal the logic and timing of vertebrate development. Proc Natl Acad Sci USA. 2000 Nov 21;97(24):12965–9.

789. Rennekamp AJ, Peterson RT. 15 years of zebrafish chemical screening. Curr Opin Chem Biol. 2015 Feb;24:58–70.

790. Kopetz S, Lemos R, Powis G. The promise of patient-derived xenografts: the best laid plans of mice and men. Clin Cancer Res. 2012 Oct 1;18(19):5160–2.

791. Decaudin D. Primary human tumor xenografted models ("tumorgrafts") for good management of patients with cancer. Anticancer Drugs. 2011 Oct;22(9):827–41.

792. Stewart EL, Mascaux C, Pham N-A, Sakashita S, Sykes J, Kim L, et al. Clinical Utility of Patient-Derived Xenografts to Determine Biomarkers of Prognosis and Map Resistance Pathways in EGFR-Mutant Lung Adenocarcinoma. Journal of Clinical Oncology. 2015 Aug 1;33(22):2472–80.

793. Garralda E, Paz K, Lopez-Casas PP, Jones S, Katz A, Kann LM, et al. Integrated Next-Generation Sequencing and Avatar Mouse Models for Personalized Cancer Treatment. Clinical Cancer Research. 2014 Apr 30;20(9):2476–84.

794. Ding L, Ellis MJ, Li S, Larson DE, Chen K, Wallis JW, et al. Genome remodelling in a basal-like breast cancer metastasis and xenograft. Nature. 2010 Apr 15;464(7291):999–1005.

795. Julien S, Merino-Trigo A, Lacroix L, Pocard M, Goéré D, Mariani P, et al. Characterization of a large panel of patient-derived tumor xenografts representing the clinical heterogeneity of human colorectal cancer. Clin Cancer Res. 2012 Oct 1;18(19):5314–28.

796. Garrido-Laguna I, Uson M, Rajeshkumar NV, Tan AC, de Oliveira E, Karikari C, et al. Tumor engraftment in nude mice and enrichment in stroma- related gene pathways predict poor survival and resistance to gemcitabine in patients with pancreatic cancer. Clin Cancer Res. 2011 Sep 1;17(17):5793–800.

797. Almuhaideb A, Papathanasiou N, Bomanji J. 18F-FDG PET/CT imaging in oncology. Ann Saudi Med. 2011 Jan;31(1):3–13.

798. Maguire CA, Bovenberg MS, Crommentuijn MH, Niers JM, Kerami M, Teng J, et al. Triple bioluminescence imaging for in vivo monitoring of cellular processes. Mol Ther Nucleic Acids. 2013;2:e99.

799. Kim J-B, Urban K, Cochran E, Lee S, Ang A, Rice B, et al. Non-invasive detection of a small number of bioluminescent cancer cells in vivo. PLoS ONE. 2010;5(2):e9364.

800. Barranco SC, Ho DH, Drewinko B, Romsdahl MM, Humphrey RM. Differential sensitivites of human melanoma cells grown in vitro to arabinosylcytosine. Cancer Research. 1972 Dec;32(12):2733–6.

801. Heppner GH, Dexter DL, DeNucci T, Miller FR, Calabresi P. Heterogeneity in drug sensitivity among tumor cell subpopulations of a single mammary tumor. Cancer Research. 1978 Nov;38(11 Pt 1):3758–63.

802. Wang J, Li L, Zhang K, Yu Y, Li B, Li J, et al. Characterization of two novel cell lines with distinct heterogeneity derived from a single human bile duct carcinoma. PLoS ONE. 2013;8(1):e54377.

803. Villarroel MC, Rajeshkumar NV, Garrido-Laguna I, De Jesus-Acosta A, Jones S, Maitra A, et al. Personalizing cancer treatment in the age of global genomic analyses: PALB2 gene mutations and the response to DNA damaging agents in pancreatic cancer. Molecular Cancer Therapeutics. 2011 Jan;10(1):3–8.

804. Spoerke JM, O'Brien C, Huw L, Koeppen H, Fridlyand J, Brachmann RK, et al. Phosphoinositide 3-kinase (PI3K) pathway alterations are associated with histologic subtypes and are predictive of sensitivity to PI3K inhibitors in lung cancer preclinical models. Clin Cancer Res. 2012 Dec 15;18(24):6771–83.

805. Ocana A, Vera-Badillo F, Al-Mubarak M, Templeton AJ, Corrales-Sanchez V, Diez-Gonzalez L, et al. Activation of the PI3K/mTOR/AKT pathway and survival in solid tumors: systematic review and meta-analysis. PLoS ONE. 2014;9(4):e95219.

806. Desilet N, Campbell TN, Choy FYM. p53-based anti-cancer therapies: An empty promise? Curr Issues Mol Biol. 2010;12(3):143–6.

807. Razzak M. Targeted therapies: One step closer to drugging p53. Nat Rev Clin Oncol. 2013 Mar 19;10(5):246–6.

808. Warso MA, Richards JM, Mehta D, Christov K, Schaeffer C, Rae Bressler L, et al. A first-in-class, first-in-human, phase I trial of p28, a non-HDM2-mediated peptide inhibitor of p53 ubiquitination in patients with advanced solid tumours. Br J Cancer. 2013 Mar 19;108(5):1061–70.

809. Deben C, Wouters A, Op de Beeck K, van Den Bossche J, Jacobs J, Zwaenepoel K, et al. The MDM2-inhibitor Nutlin-3 synergizes with cisplatin to induce p53 dependent tumor cell apoptosis in non-small cell lung cancer. Oncotarget. 2015 Jun 10.

810. Pallini R, Maira G, Pierconti F, Falchetti ML, Alvino E, Cimino-Reale G, et al. Chordoma of the skull base: predictors of tumor recurrence. Journal of Neurosurgery. 2003 Apr;98(4):812–22.

811. Fischer C, Scheipl S, Zopf A, Niklas N, Deutsch A, Jorgensen M, et al. Mutation Analysis of Nine Chordoma Specimens by Targeted Next-Generation Cancer Panel Sequencing. Journal of Cancer. 2015;6(10):984–9.

812. Junttila MR, de Sauvage FJ. Influence of tumour micro-environment heterogeneity on therapeutic response. Nature. 2013 Sep 19;501(7467):346–54.

813. Abaan OD, Polley EC, Davis SR, Zhu YJ, Bilke S, Walker RL, et al. The exomes of the NCI-60 panel: a genomic resource for cancer biology and systems pharmacology. Cancer Research. 2013 Jul 15;73(14):4372–82.

814. Leary RJ, Kinde I, Diehl F, Schmidt K, Clouser C, Duncan C, et al. Development of Personalized Tumor Biomarkers Using Massively Parallel Sequencing. Science Translational Medicine 2010 Feb 24;2(20):20ra14–4.

815. Mcbride DJ, Orpana AK, Sotiriou C, Joensuu H, Stephens PJ, Mudie LJ, et al. Use of cancer-specific genomic rearrangements to quantify disease burden in plasma from patients with solid tumors. Genes Chromosom Cancer. 2010 Nov;49(11):1062–9.

816. Leary RJ, Sausen M, Kinde I, Papadopoulos N, Carpten JD, Craig D, et al. Detection of chromosomal alterations in the circulation of cancer patients with whole-genome sequencing. Science Translational Medicine. 2012 Nov 28;4(162):162ra154.

817. Vora A, Goulden N, Wade R, Mitchell C, Hancock J. Treatment reduction for children and young adults with low-risk acute lymphoblastic leukaemia defined by minimal residual disease (UKALL 2003): a randomised controlled trial. Lancet Oncol. 2013.

818. Moorman AV, Robinson H, Schwab C, Richards SM, Hancock J, Mitchell CD, et al. Risk-Directed Treatment Intensification Significantly Reduces the Risk of Relapse Among Children and Adolescents With Acute Lymphoblastic Leukemia and Intrachromosomal Amplification of Chromosome 21: A Comparison of the MRC ALL97/99 and UKALL2003 Trials. J Clin Oncol. 2013 Sep 17;31(27):3389–96.

819. Radich JP, Gooley T, Bryant E, Chauncey T, Clift R, Beppu L, et al. The significance of bcr-abl molecular detection in chronic myeloid leukemia patients “late,” 18 months or more after transplantation. Blood. 2001 Sep 15;98(6):1701–7.

820. Mahon F-X, Etienne G. Deep molecular response in chronic myeloid leukemia: the new goal of therapy? Clin Cancer Res. 2014 Jan 15;20(2):310–22.

821. Egan DN, Beppu L, Radich JP. Patients with Philadelphia-positive leukemia with BCR-ABL kinase mutations before allogeneic transplantation predominantly relapse with the same mutation. Biol Blood Marrow Transplant. 2015 Jan;21(1):184–9.

822. Sykes PJ, Neoh SH, Brisco MJ, Hughes E, Condon J, Morley AA. Quantitation of targets for PCR by use of limiting dilution. Biotech. 1992 Sep;13(3):444–9.

823. Wan JH, Sykes PJ, Orell SR, Morley AA. Rapid method for detecting monoclonality in B cell lymphoma in lymph node aspirates using the polymerase chain reaction. J Clin Pathol. 1992 May;45(5):420–3.

824. Forbes SA, Bindal N, Bamford S, Cole C, Kok CY, Beare D, et al. COSMIC: mining complete cancer genomes in the Catalogue of Somatic

Mutations in Cancer. Nucleic acids …. 2010.

825. Forbes SA, Beare D, Gunasekaran P, Leung K, Bindal N, Boutselakis H, et al. COSMIC: exploring the world's knowledge of somatic mutations in human cancer. Nucleic Acids Research. 2015 Jan;43(Database issue):D805–11.

826. Shinozaki M, O'Day SJ, Kitago M, Amersi F, Kuo C, Kim J, et al. Utility of circulating B-RAF DNA mutation in serum for monitoring melanoma patients receiving biochemotherapy. Clin Cancer Res. 2007 Apr 1;13(7):2068–74.

827. Olsson L, Paulsson K, Bovée JVMG, Nord KH. Clonal Evolution through Loss of Chromosomes and Subsequent Polyploidization in Chondrosarcoma. Katoh M, editor. PLoS ONE. 2011 Sep 20;6(9):e24977.

828. Dorner AJ, Badola S, Niu H. Characterization of circulating tumor DNA for genetic assessment of solid tumors. Clin Pharmacol Ther. 2015 Apr 7.

829. Ludwig JA, Weinstein JN. Biomarkers in cancer staging, prognosis and treatment selection. Nat Rev Cancer. 2005 Nov;5(11):845–56.

830. Füzéry AK, Levin J, Chan MM, Chan DW. Translation of proteomic biomarkers into FDA approved cancer diagnostics: issues and challenges. Clin Proteomics. 2013;10(1):13.

831. Martinez SJ, Moreno CC, Vinson EN, Dodd LG, Brigman BE. Angiomatoid fibrous histiocytoma: novel MR imaging findings. Skeletal Radiol. 2016 Feb 27.

832. Mäbert K, Cojoc M, Peitzsch C, Kurth I, Souchelnytskyi S, Dubrovska A. Cancer biomarker discovery: current status and future perspectives. Int J Radiat Biol. 2014 Aug;90(8):659–77.

833. Henry NL, Hayes DF. Cancer biomarkers. Mol Oncol. 2012 Apr;6(2):140–6.

834. Cao D, Fan ST, Chung SS. Identification and characterization of a novel human aldose reductase-like gene. J Biol Chem. 1998 May 8;273(19):11429–35.

835. Gallego O, Ruiz FX, Ardèvol A, Domínguez M, Alvarez R, de Lera AR, et al. Structural basis for the high all-trans-retinaldehyde reductase activity of the tumor marker AKR1B10. Proceedings of the National Academy of Sciences. 2007 Dec 26;104(52):20764–9.

836. Kumar R, Son M, Bavi R, Lee Y, Park C, Arulalapperumal V, et al. Novel chemical scaffolds of the tumor marker AKR1B10 inhibitors discovered by 3D QSAR pharmacophore modeling. Acta Pharmacol Sin. 2015 Jun 8.

837. Ruiz FX, Gallego O, Ardèvol A, Moro A, Domínguez M, Alvarez S, et al. Aldo-keto reductases from the AKR1B subfamily: retinoid specificity and control of cellular retinoic acid levels. Chem Biol Interact. 2009 Mar 16;178(1-3):171–7.

838. Balendiran GK, Martin H-J, El-Hawari Y, Maser E. Cancer biomarker AKR1B10 and carbonyl metabolism. Chem Biol Interact. 2009 Mar 16;178(1-3):134–7.

839. Matsunaga T. Aldo–keto reductase 1B10 and its role in proliferation capacity of drug-resistant cancers. 2012 Jan 27;:1–11.

840. Morikawa Y, Kezuka C, Endo S, Ikari A, Soda M, Yamamura K, et al. Acquisition of doxorubicin resistance facilitates migrating and invasive potentials of gastric cancer MKN45 cells through up-regulating aldo-keto reductase 1B10. Chem Biol Interact. 2015 Mar 25;230:30–9.

841. Zhong L, Shen H, Huang C, Jing H, Cao D. AKR1B10 induces cell resistance to daunorubicin and idarubicin by reducing C13 ketonic group. Toxicol Appl Pharmacol. 2011 Aug 15;255(1):40–7.

842. Scuric Z, Stain SC, Anderson WF, Hwang JJ. New member of aldose reductase family proteins overexpressed in human hepatocellular carcinoma. Hepatology. 1998 Apr;27(4):943–50.

843. Schmitz KJ, Sotiropoulos GC, Baba HA, Schmid KW, Müller D, Paul A, et al. AKR1B10 expression is associated with less aggressive hepatocellular carcinoma: a clinicopathological study of 168 cases. Liver Int. 2011 Jul;31(6):810–6.

844. Heringlake S, Hofdmann M, Fiebeler A, Manns MP, Schmiegel W, Tannapfel A. Identification and expression analysis of the aldo-ketoreductase1-B10 gene in primary malignant liver tumours. J Hepatol. 2010 Feb;52(2):220–7.

845. Semmo N, Weber T, Idle JR, Beyoğlu D. Metabolomics reveals that aldose reductase activity due to AKR1B10 is upregulated in hepatitis C virus infection. J Viral Hepat. 2015 Jul;22(7):617–24.

846. Tsuzura H, Genda T, Sato S, Murata A, Kanemitsu Y, Narita Y, et al. Expression of aldo-keto reductase family 1 member b10 in the early stages of human hepatocarcinogenesis. Int J Mol Sci. 2014;15(4):6556–68.

847. Ma J, Yan R, Zu X, Cheng J-M, Rao K, Liao D-F, et al. Aldo-keto reductase family 1 B10 affects fatty acid synthesis by regulating the stability of acetyl-CoA carboxylase-alpha in breast cancer cells. J Biol Chem. 2008 Feb 8;283(6):3418–23.

848. Hashimoto Y, Imanishi K, Tokui N, Okamoto T, Okamoto A, Hatakeyama S, et al. Carboplatin-gemcitabine combination chemotherapy upregulates AKR1B10 expression in bladder cancer. Int J Clin Oncol. 2013 Feb;18(1):177–82.

849. Wang R, Wang G, Ricard MJ, Ferris B, Strulovici-Barel Y, Salit J, et al. Smoking-induced upregulation of AKR1B10 expression in the airway epithelium of healthy individuals. Chest. 2010 Dec;138(6):1402–10.

850. Fukumoto S-I, Yamauchi N, Moriguchi H, Hippo Y, Watanabe A, Shibahara J, et al. Overexpression of the aldo-keto reductase family

protein AKR1B10 is highly correlated with smokers' non-small cell lung carcinomas. Clin Cancer Res. 2005 Mar 1;11(5):1776–85.

851. Hevir N, Sinkovec J, Lanišnik Rižner T. Decreased levels of AKR1B1 and AKR1B10 in cancerous endometrium compared to adjacent non-cancerous tissue. Chem Biol Interact. 2013 Feb 25;202(1-3):226–33.

852. Zhang W, Li H, Yang Y, Liao J, Yang G-Y. Knockdown or inhibition of aldo-keto reductase 1B10 inhibits pancreatic carcinoma growth via modulating Kras-E-cadherin pathway. Cancer Letters. 2014 Dec 28;355(2):273–80.

853. Ma J, Luo D-X, Huang C, Shen Y, Bu Y, Markwell S, et al. AKR1B10 overexpression in breast cancer: association with tumor size, lymph node metastasis and patient survival and its potential as a novel serum marker. Int J Cancer. 2012 Sep 15;131(6):E862–71.

854. Tirabosco R. Aldoketoreductasis 1 B10 (AKR1B10) Expression in Tissues and Tumours Showing Notochordal Differentiation. A Role as a Neoplastic Biomarker and a Potential Therapeutic Target.

855. Sausen M, Phallen J, Adleff V, Jones S, Leary RJ, Barrett MT, et al. Clinical implications of genomic alterations in the tumour and circulation of pancreatic cancer patients. Nat Commun. 2015;6:7686.

856. Patel KM, Tsui DWY. The translational potential of circulating tumour DNA in oncology. Clin Biochem. 2015 Apr 15.

857. Gormally E, Vineis P, Matullo G, Veglia F, Caboux E, Le Roux E, et al. TP53 and KRAS2 mutations in plasma DNA of healthy subjects and subsequent cancer occurrence: a prospective study. Cancer Research. 2006 Jul 1;66(13):6871–6.

858. Chan KCA, Hung ECW, Woo JKS, Chan PKS, Leung S-F, Lai FPT, et al. Early detection of nasopharyngeal carcinoma by plasma Epstein-Barr virus DNA analysis in a surveillance program. Cancer. 2013 May 15;119(10):1838–44.

859. Milbury CA, Zhong Q, Lin J, Williams M, Olson J. Determining lower limits of detection of digital PCR assays for cancer-related gene mutations. Biomolecular Detection …. 2014.

860. McInerney P, Adams P, Hadi MZ. Error Rate Comparison during Polymerase Chain Reaction by DNA Polymerase. Mol Biol Int. 2014;2014:287430.

861. Leon SA, Shapiro B, Sklaroff DM, Yaros MJ. Free DNA in the serum of cancer patients and the effect of therapy. Cancer Research. 1977 Mar;37(3):646–50.

862. Barrett AN, Zimmermann BG, Wang D, Holloway A, Chitty LS. Implementing Prenatal Diagnosis Based on Cell-Free Fetal DNA: Accurate Identification of Factors Affecting Fetal DNA Yield. Novelli G, editor. PLoS ONE. 2011 Oct 4;6(10):e25202.

863. Wong D, Moturi S, Angkachatchai V, Mueller R, DeSantis G, van den Boom D, et al. Optimizing blood collection, transport and storage conditions for cell free DNA increases access to prenatal testing. Clin Biochem. 2013 Aug;46(12):1099–104.

864. Lee TH, Montalvo L, Chrebtow V, Busch MP. Quantitation of genomic DNA in plasma and serum samples: higher concentrations of genomic DNA found in serum than in plasma. Transfusion. 2001 Feb;41(2):276–82.

865. Angert RM, LeShane ES, Lo YMD, Chan LYS, Delli-Bovi LC, Bianchi DW. Fetal cell-free plasma DNA concentrations in maternal blood are stable 24 hours after collection: analysis of first- and third-trimester samples. Clin Chem. 2003 Jan;49(1):195–8.

866. Toro PV, Erlanger B, Beaver JA, Cochran RL, VanDenBerg DA, Yakim E, et al. Comparison of cell stabilizing blood collection tubes for circulating plasma tumor DNA. Clin Biochem. 2015 Oct;48(15):993–8.

867. Barrett AN, Zimmermann BG, Wang D, Holloway A, Chitty LS. Implementing prenatal diagnosis based on cell-free fetal DNA: accurate identification of factors affecting fetal DNA yield. PLoS ONE. 2011;6(10):e25202.

868. Fleischhacker M, Schmidt B, Weickmann S, Fersching DMI, Leszinski GS, Siegele B, et al. Methods for isolation of cell-free plasma DNA strongly affect DNA yield. Clin Chim Acta. 2011 Nov 20;412(23-24):2085–8.

869. Vogelstein B, Papadopoulos N, Velculescu VE, Zhou S, Diaz LA, Kinzler KW. Cancer genome landscapes. Science. 2013 Mar 29;339(6127):1546–58.

870. Reinert T, Schøler LV, Thomsen R, Tobiasen H, Vang S, Nordentoft I, et al. Analysis of circulating tumour DNA to monitor disease burden following colorectal cancer surgery. Gut. 2015 Feb 4.

871. Kidess E, Heirich K, Wiggin M, Vysotskaia V, Visser BC, Marziali A, et al. Mutation profiling of tumor DNA from plasma and tumor tissue of colorectal cancer patients with a novel, high-sensitivity multiplexed mutation detection platform. Oncotarget. 2015 Feb 10;6(4):2549–61.

872. Kimura H, Kasahara K, Kawaishi M, Kunitoh H, Tamura T, Holloway B, et al. Detection of epidermal growth factor receptor mutations in serum as a predictor of the response to gefitinib in patients with non-small-cell lung cancer. Clin Cancer Res. 2006 Jul 1;12(13):3915–21.

873. Gazdar AF. Activating and resistance mutations of EGFR in non-small-cell lung cancer: role in clinical response to EGFR tyrosine kinase inhibitors. Oncogene. 2009 Aug;28 Suppl 1:S24–31.

874. Davies JM, Robinson AE, Cowdrey C, Mummaneni PV, Ducker GS, Shokat KM, et al. Generation of a patient-derived chordoma xenograft and characterization of the phosphoproteome in a recurrent chordoma. Journal of Neurosurgery. 2013 Nov 29.

875. Gorges TM, Schiller J, Schmitz A, Schuetzmann D, Schatz C, Zollner TM, et al. Cancer therapy monitoring in xenografts by quantitative analysis of circulating tumor DNA. Biomarkers. 2012 Sep;17(6):498–506.

876. Dokmanovic M, Wu WJ. Monitoring Trastuzumab Resistance and Cardiotoxicity: A Tale of Personalized Medicine. Adv Clin Chem. 2015;70:95–130.

9 APPENDIX

9.1 Supplement data

Table 9.1 Luciferase raw data expression data from Living image software

Image Number	ROI	Image Layer	Total Flux (p/s)	Avg Radiance (p/s/cm2/sr)	Stdev Radiance	Min Radiance	Max Radiance	Mouse #	Treatment	Time point
CR20140821113107	ROI 1	Overlay	6.63E+08	2.89E+07	2.05E+07	2.27E+06	7.02E+07	Mouse 1	KD	day 0
CR20140821113107	ROI 2	Overlay	4.05E+08	2.91E+07	1.96E+07	2.24E+06	6.86E+07	Mouse 2	GFP	day 0
CR20140821113107	ROI 3	Overlay	2.36E+09	7.53E+07	7.39E+07	3.03E+06	2.06E+08	Mouse 6	KD	day 0
CR20140828154620	ROI 1	Overlay	1.87E+08	6.54E+06	6.70E+06	2.64E+05	2.81E+07	Mouse 1	KD	day 7
CR20140828154620	ROI 2	Overlay	1.70E+07	6.66E+05	4.99E+05	3.07E+04	1.68E+06	Mouse 2	GFP	day 7
CR20140828154620	ROI 3	Overlay	1.28E+08	5.88E+06	5.22E+06	3.72E+05	1.87E+07	Mouse 6	KD	day 7
CR20140904144739	ROI 1	Overlay	9.62E+07	7.12E+06	3.51E+06	1.21E+06	1.70E+07	Mouse 1	KD	day 14
CR20140904144739	ROI 2	Overlay	8.85E+08	3.02E+07	2.61E+07	1.24E+06	9.79E+07	Mouse 2	GFP	day 14
CR20140904144739	ROI 3	Overlay	3.80E+08	1.88E+07	1.49E+07	1.23E+06	5.07E+07	Mouse 6	KD	day 14
CR20140910141854	ROI 1	Overlay	4.33E+07	2.11E+06	1.29E+06	1.67E+05	6.04E+06	Mouse 1	KD	day 21
CR20140910141854	ROI 2	Overlay	9.40E+08	2.70E+07	2.35E+07	1.32E+06	8.32E+07	Mouse 2	GFP	day 21
CR20140910141854	ROI 3	Overlay	6.31E+08	2.43E+07	2.24E+07	1.34E+06	7.48E+07	Mouse 6	KD	day 21
CR20140828160617	ROI 1	Overlay	3.79E+07	2.04E+06	2.15E+06	1.13E+05	7.65E+06	Mouse 4	PBS	day 7
CR20140904143425	ROI 1	Overlay	5.11E+08	1.95E+07	1.99E+07	8.22E+05	7.74E+07	Mouse 4	PBS	day 14
CR20140904143425	ROI 2	Overlay	2.22E+08	1.47E+07	1.18E+07	1.11E+06	3.94E+07	Mouse 5	PBS	day 14
CR20140910142927	ROI 1	Overlay	5.43E+08	2.03E+07	2.03E+07	7.35E+05	7.63E+07	Mouse 4	PBS	day 21
CR20140910142927	ROI 2	Overlay	2.87E+08	1.44E+07	1.33E+07	4.37E+05	4.45E+07	Mouse 5	PBS	day 21

Crude data from living image software, CR number is the label for the individual images (identifiable at the top of the pictures in the figures above), Region of interest (ROI) is assigned in grouped images identifying each mouse – further identified by mouse id number and treatment given. The luciferase expression is measured by photons, max/min/average and with standard deviation. The different time points have been added far right column.

9.2 Drug screening appendix

9.2.1 Cancer hot spot mutation screen

	1	2	3	4	5	6
A	BRAF	IDH1 132	FGFR1_K656	FGFR4_V510	SF3B1_E622	GNAS1_Q227
B	KRAS G12	IDH2 140	FGFR2_S252	FGFR3_R428	SF3B1_G742	GNAS1_K233
C	EGFR L858R / L861	IDH2 172	FGFR2_N549	FGFR3_A391	JAK2_v617	NRAS_1 (Q61)
D	EGFR G719X	H3F3B_K37	FGRF2_660	FGFR3_G370-2	JAK2_N542_E5	NRAS_2 (12-13)
E	EGFR Exon 19 del	H3F3A_K37	FGFR3_T435	NOTCH1_L1574	JAK2_R683	NRAS_K117
F	EGFR Exon 20 ins	H3F3A_K27	FGFR3_K650	NOTCH1_L1600	GNAS1_K876	NRAS_A146
G	EGFR T790M	FGFR1_T141	FGFR3_G697	NOTCH1_L1678	GNAS1_R844	CTNNB1_34-45 (b catenin 1)
H	KRAS K61	FGFR1_N546	FGFR3_K717	NOTCH1_R1598	GNAS1_R201	CTNNB1_15_22 (b catenin 2)

	1	2	3	4	5	6
A	BRAF	EGFR T790M	KIT-9	GNAS1_K876	H3F3A_K37	P53-6
B	KRAS 12	IDH1 132	KIT-10	NRAS_G12	PTEN-7 PDGFRA-5	P53-7
C	EGFR L858R / L861	KIT-3	NRAS-1	CTNNB1_34-45 (b catenin 1)	H3F3A_K27	P53-8
D	EGFR G719X	KIT-4	NRAS-2	PTEN-1 PDGFRA-4	P53-1	P53-9
E	EGFR Exon 19 del	KIT-5	GNAS1_R201	NRAS_K117	P53-2	P53-10
F	EGFR Exon 20 ins	KIT-6	GNAS1_Q227	NRAS_A146	P53-3	P53-11
G	KRAS K61	IDH2 140	GNAS1_K233	CTNNB1_15_22 (b catenin 2)	P53-4	P53-12
H	PDGFRA 1	IDH2 172	GNAS1_R844	H3F3B_K37	P53-5	P53-13

Primer map for Fluidigm hot spot mutation

9.2.2 Optimisation of WST-1 assay

Comparison of WST-1 with “gold standard” method Cell titre Glo (CTG) assay

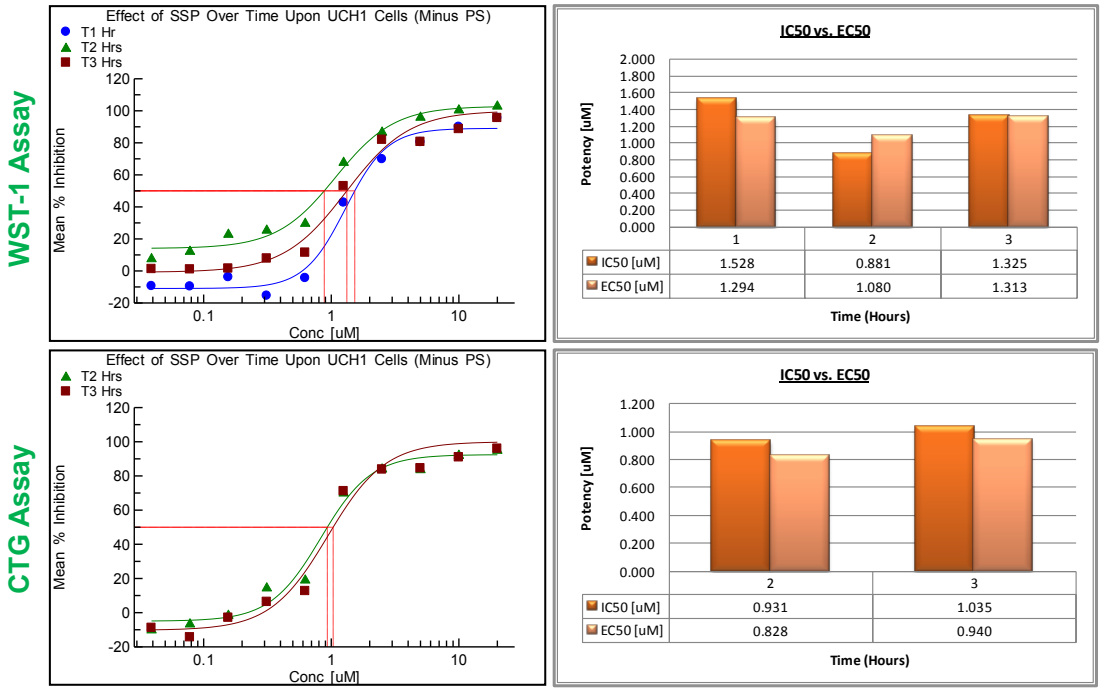

Figure 9.1 Optimisation of WST1
WST-1 assay was compared with Cell titre glow (CTG) as this is the gold standard for assessing viability in compound treated cells. As the initial screen on the GSK PKIS1 library was done using WST-1 the comparability and stability between the two assays was assessed. Similar graphical plots for WST-1 and CTG assays at a 3-hour end point read. Potency measured using WST-1 Assay shows slight variability over time. The data supports the recommendation to read plates @ 3 hours. IC_{50} of SSP at 3 hours is ~ 1.3µM.

9.2.3 DMSO tolerance - optimisation

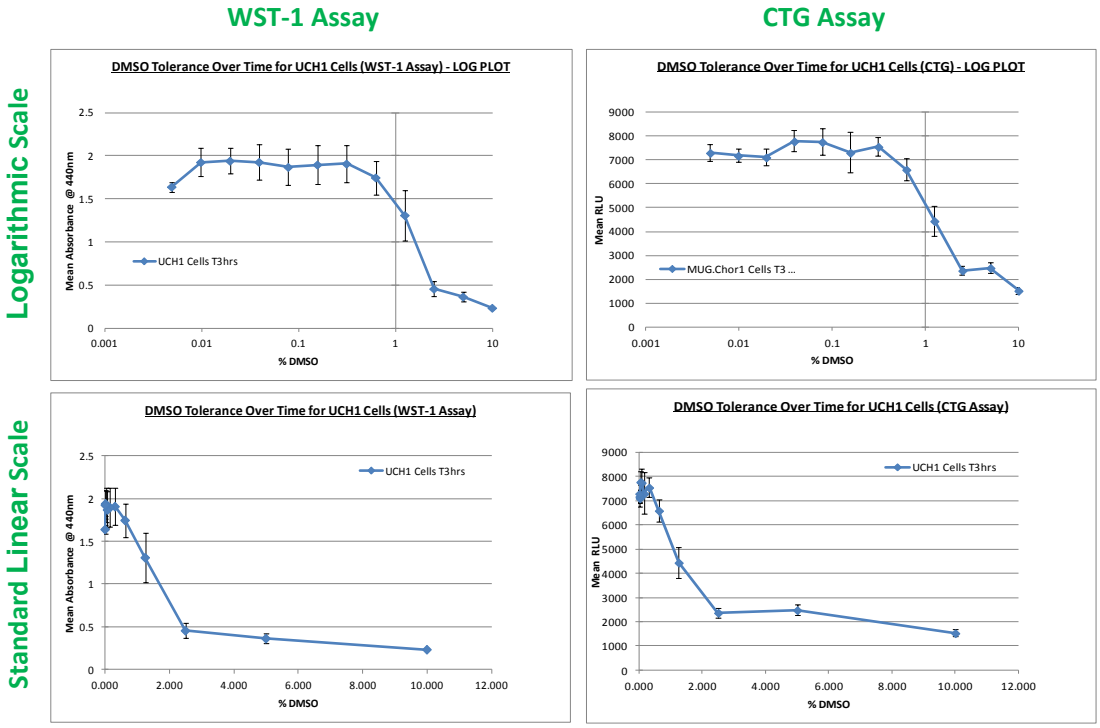

Figure 9.2 Optimisation of DMSO tolerance in U-CH1 cells
Example of the DMSO tolerance for U-CH1 cells. No data has been corrected for background. DMSO titration range from 0% (medium) to 10%. WST-1 data indicates cells can tolerate up to 0.625% DMSO, any increase in concentration causes a decrease in signal. Cell titre glow (CTG) data shows toleration up to 0.315% DMSO only, an increase in concentration leads to loss of signal (e.g. Cell death). This data was generated at 3 hours incubations with the WST-1 reagent. UCH1 Cells are fairly sensitive to DMSO compared to other cell types (e.g. Up to 1% DMSO). DMSO tolerance of U-CH1 cells in line with the MUG Chor and U-CH2 cell lines and therefore 0.315% will be used for all.

9.2.4 Anti-cancer library compounds

SelleckChem ID/Name	SelleckChem Target Class	Information
ABT-869(Linifanib)	CSF-1R	Potent ATP-competitive VEGFR/PDGFR Inhibitor for KDR, CSF-1R, Flt-1/3 and PDGFRβ. Mostly Effective in Mutant Kinase-Dependent Cancer Cells (i.e. FLT3). Phase 3.
ABT-888 (Veliparib)	PARP	PARP1/2
BEZ235(NVP-BEZ235) (Dactolisib)	ATM/ATR	Dual ATP-competitive Inhibitor PI3K and mTOR
BIBF1120 (Nintedanib)	FGFR	Triple Angiokinase Inhibitor for VEGFR1/2/3, FGFR1/2/3 and PDGFRα/β
Bortezomib	Proteasome	20S proteasome Inhibitor
CHIR-258(Dovitinib)	c-Kit	Multitargeted RTK inhibitor, mostly for class III (FLT3/c-Kit), Class IV (FGFR1/3) and class V (VEGFR1-4) RTKs. Less potent to InsR, EGFR, c-Met, EphA2, Tie2, IGF-1R and HER2. Phase 4.
Dasatinib	Bcr-Abl	Multi-targeted Inhibitor Abl, Src and c-Kit
Deforolimus(MK-8669) (Ridaforolimus)	mTOR	Selective mTOR Inhibitor. Not classified as a prodrug, mTOR inhibition and FKBP12 binding is similar to rapamycin.
Imatinib Mesylate	Bcr-Abl	Multi-target Inhibitor of v-Abl, c-Kit and PDGFR
Lapatinib Ditosylate	EGFR	(GW572016, GW2016) Potent EGFR and ErbB2 Inhibitor
Pazopanib Hydrochloride	PDGR/EGFR/c-Kit/FGFR	(GW786034) Multi-target Inhibitor of VEGFR1, VEGFR2, VEGFR3, PDGFR, FGFR, c-Kit and c-Fms.

SelleckChem ID/Name	SelleckChem Target Class	Information
Perifosine	AKT	Akt Inhibitor. Targets Pleckstrin Homology Domain of Akt. Phase 2.
Sorafenib Tosylate	PDGFR	Multikinase Inhibitor of Raf-1, B-Raf and VEGFR-2.
Temsirolimus	mTOR	mTOR Inhibitor
AZD2281(Olaparib)	PARP	Selective Inhibitor of PARP1/2. Less Effective Against tankyrase-1. Phase 1/2.
GDC-0941	PI3K	Potent Inhibitor of PI3Kα/δ, with Modest Selectivity Against p110β (11-fold) and p110γ (25-fold).
GDC-0449(Vismodegib)	Hedgehog	Hedgehog Inhibitor and P-gp
Brivanib(BMS-540215)	FGFR	ATP-competitive Inhibitor Against VEGFR2. Moderate potency against VEGFR-1 and FGFR-1, but >240-fold against PDGFR-β. Phase 3.
Belinostat(PXD101)	HDAC	HDAC Inhibitor with Activity Demonstrated in Ciisplatin-Resistant Tumors. Phase 1/2.
XL147	PI3K	Selective and Reversible Class I PI3K inhibitor for PI3Kα/δ/γ. Less potent to PI3Kβ. Phase 1/2.
Everolimus(RAD001)	mTOR	mTOR Inhibitor of FKBP12
YM155 (Sepantronium Bromide)	E3 Ligase	Potent Survivin Suppressant by Inhibiting Survivin Promoter Activity. Does not Significantly Inhibit SV40 Promoter Activity, but is Observed to Slightly Inhibit the Interaction of Survivin with XIAP. Phase 1/2.

SelleckChem ID/Name	SelleckChem Target Class	Information
17-AAG (Tanespimycin)	HSP (e.g. HSP90)	HSP90 Inhibitor
17-DMAG(Alvespimycin)	HSP (e.g. HSP90)	HSP90 Inhibitor
Docetaxel (Taxotere)	Microtubule Associated	Inhibitor of Depolymerisation of Microtubules by Binding to Stabilized Microtubules.
Ritonavir	Antiretroviral	Antiretroviral Drug which Inhibits a particular Liver Enzyme that normally Metabolizes Protease Inhibitors, Cytochrome P450-3A4 (CYP3A4).
CUDC-101	EGFR	Potent Multi-targeted Inhibitor Against HDAC, EGFR and HER2 and inhibits class I/II HDACs, but not class III, Sir-type HDACs. Phase 1.
Decitabine	DNA Methyltransferase	Potent Inhibitor of DNA Methylation
Adriamycin (Doxorubicin)	Autophagy	Antibiotic Agent that Inhibits DNA Topoisomerase II and Induces DNA Damage and Apoptosis.
Carboplatin	DNA/RNA Synthesis	DNA Synthesis Inhibitor by Binding to DNA and Interfering with the Cell's Repair Mechanism.
OSI-930	c-Kit	Inhibitor of Kit, KDR and CSF-1R. Also Potent to Flt-1, c-Raf and Lck and low activity against PDGFRα/β, Flt-3 and Abl. Phase 1.
Ellence	Topoisomerase	Semisynthetic L-arabino Derivative of Doxorubicin, is an Antineoplastic Agent by Inhibiting Topoisomerase.
Etoposide(Etopophos)	Topoisomerase	Semisynthetic Derivative of Podophyllotoxin, which Inhibits DNA Synthesis via Topoisomerase II Inhibition Activity.

SelleckChem ID/Name	SelleckChem Target Class	Information
Flavopiridol(Alvocidib)	CDK	Competes with ATP to Inhibit CDKs including CDK1, CDK2, CDK4 and CDK6. 7.5-fold more selective for CDK1, 2, 4, 6 versus CDK7. Flavopiridol is initially found to inhibit EGFR and PKA. Phase 1/2.
Leucovorin Calcium	Other	Reduced Folic Acid
Celecoxib	COX	Selective COX-2 Inhibitor
GSK1059615	mTOR/PI3K	Dual Inhibitor of PI3Kα/β/δ/γ (Reversible) and mTOR. Phase 1
MGCD-265	c-Met/VEGFR	Multi-target and ATP-competitive Inhibitor of c-Met and VEGFR1/2/3. Also Inhibits Ron and Tie2. Phase 1/2.
PHA-793887	CDK	Inhibitor of CDK2, CDK5 and CDK7. It is greater than 6-fold more selective for CDK2, 5, and 7 than CDK1, 4, and 9. Phase 1.
AP24534 (Ponatinib)	Bcr-Abl	Potent Multi-target Inhibitor of Abl, PDGFRα, VEGFR2, FGFR1 and Src.
AZD8055	mTOR	ATP-competitive mTOR inhibitor with excellent selectivity (1,000-fold) against PI3K isoforms and ATM/DNA-PK. Phase 1.
SB939 (Pracinostat)	HDAC	Pan-HDAC Inhibitor with exception for HDAC6. It has no activity against the class III isoenzyme SIRT I. Phase 2.
Ibuprofen	NSAID	NSAID

9.2.5 Protein expression in chordoma cell lines

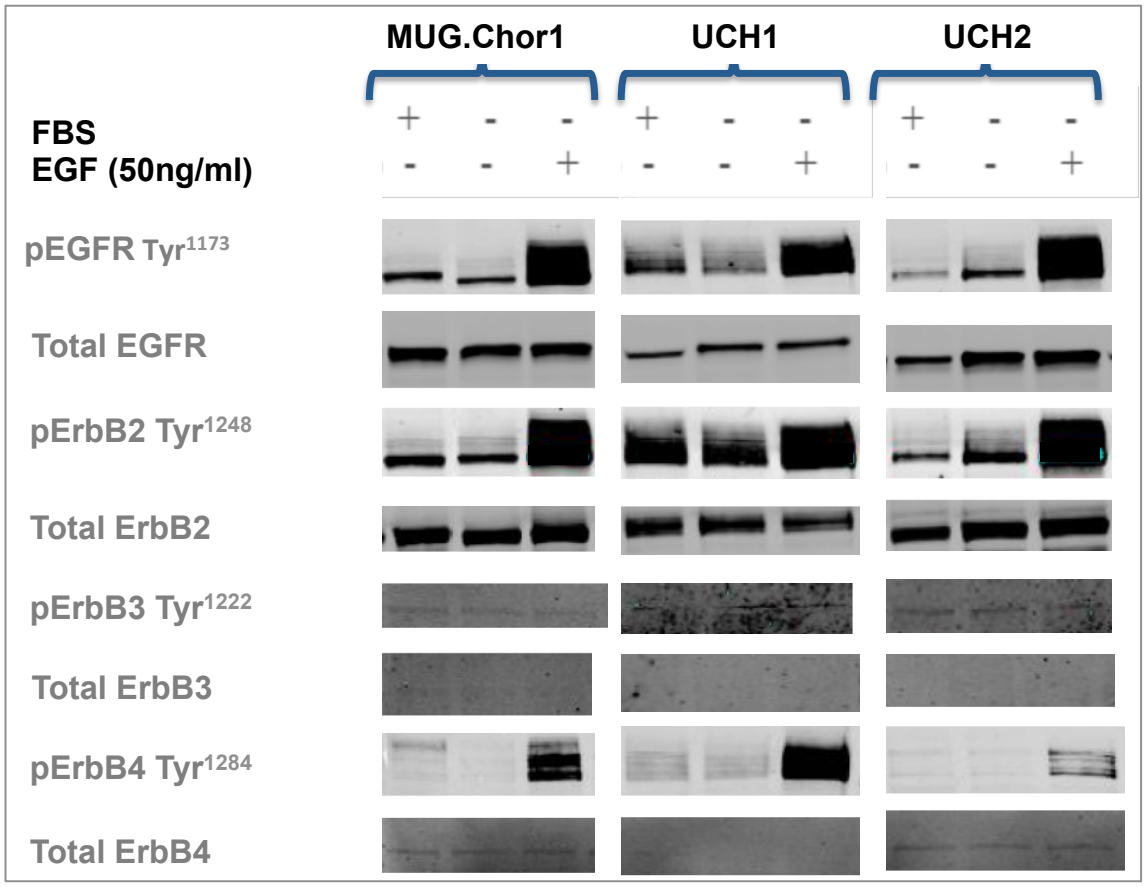

Protein expression in chordoma cell lines +/- EGF spiking indicates hetero-dimerisation of EGFR:ErbB2 / EGFR:ErbB4 and a homodimer of EGFR:EGFR across all lines to varying degrees. Kindly provided by Dr Susanne Scheipl.

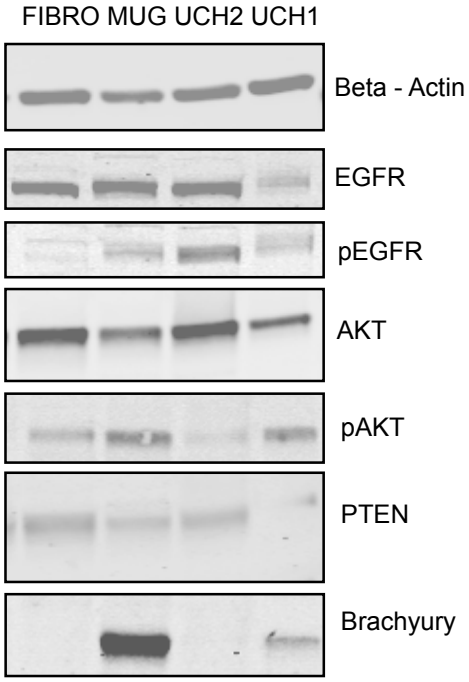

9.3 Dose response and DPE IC_{50} profiling

Compound ID	GSK ID/Compound Name	Library	Pathway	UCH1 Caspase-Glo 3/7	UCH1 CellTiter-Glo	UCH2 Caspase-Glo 3/7	UCH2 CellTiter-Glo	MUG.Chor1 Caspase-Glo 3/7	MUG.Chor1 CellTiter-Glo
CRT0047607:05	AG1478	Calbiochem	EGFR	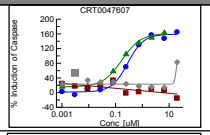	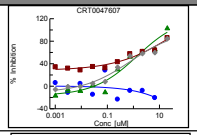	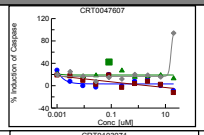	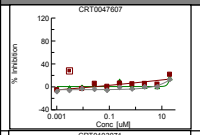	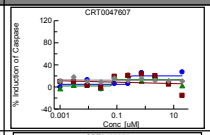	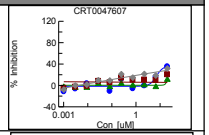
CRT0103071:02	Compound 56	Calbiochem	EGFR	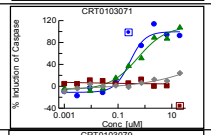	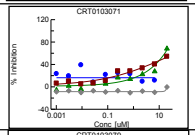	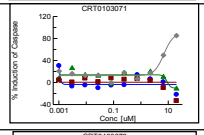	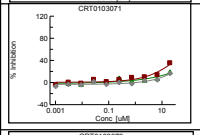	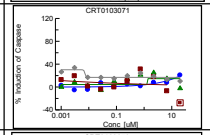	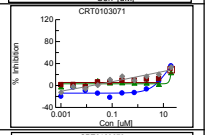
CRT0103079:02	EGFR/ErbB2/ErbB4 Inhibitor	Calbiochem	EGFR/ErbB-2/ErbB-4	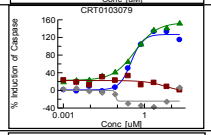	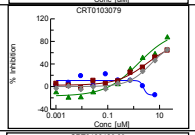	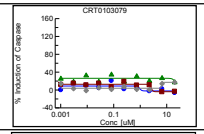	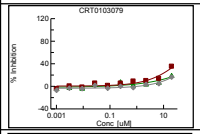	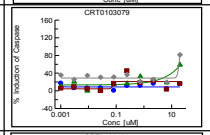	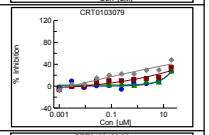
CRT0103123:02	PD 174780	Calbiochem	EGFR	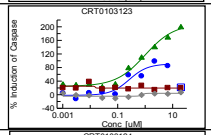	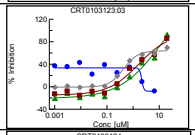	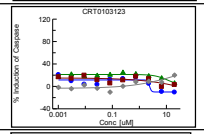	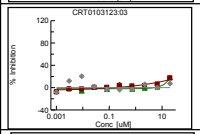	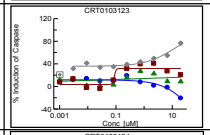	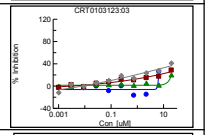
CRT0103124:02	PD 174265	Calbiochem	EGFR	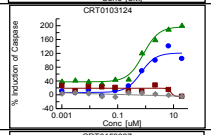	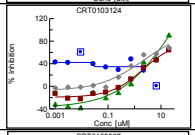	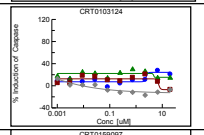	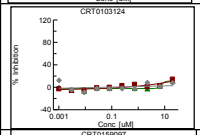	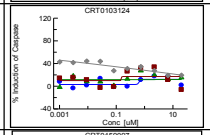	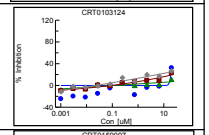
CRT0159097:02	GDC-0941	Anticancer	Class 1A PI3K Inhibitor	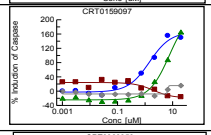	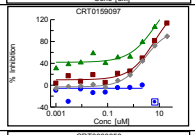	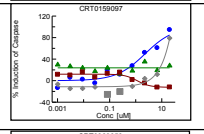	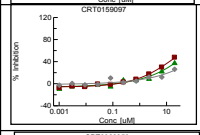	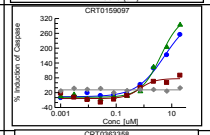	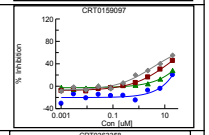
CRT0363358:02	GW461104A	PKIS1	ErbB-1/ErbB2	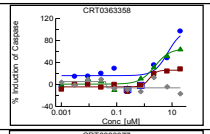	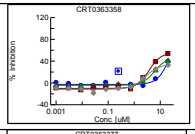	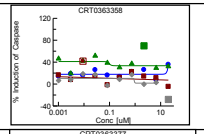	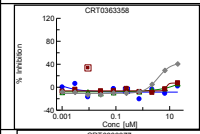	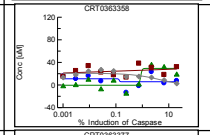	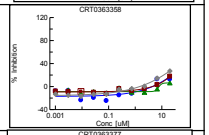
CRT0363377:02	GW410563A	PKIS1	VEGFR2, EFGR	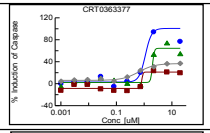	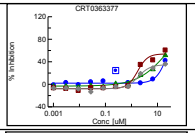	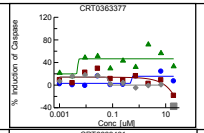	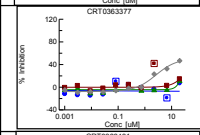	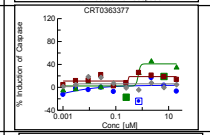	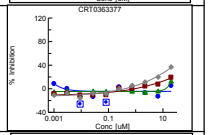
CRT0363431:01	GW282449A	PKIS1	EGFR/ErbB2	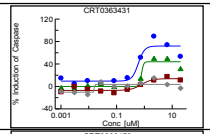	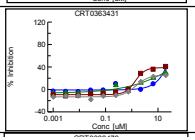	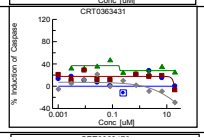	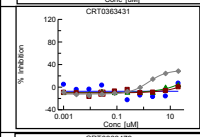	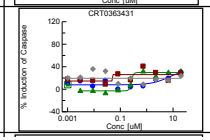	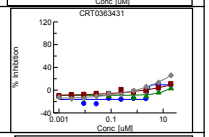

CRT0363484:02	GW616030X	PKIS1	ErbB-1/ErbB2	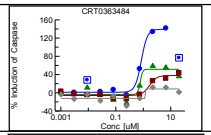	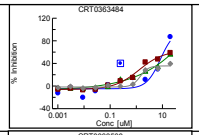	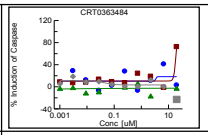	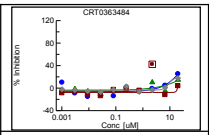	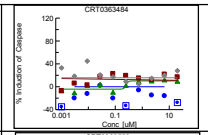	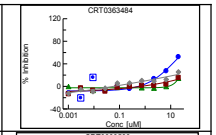
CRT0363568:02	GW680191X	PKIS1	EGFR/ErbB2	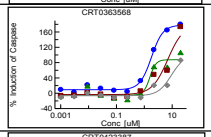	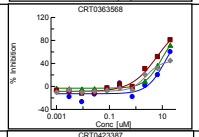	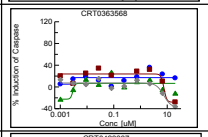	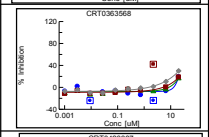	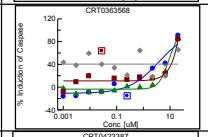	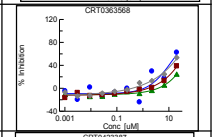
CRT0423387:01	GI230329A	PKIS2	EGFR	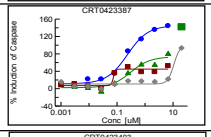	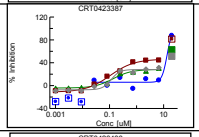	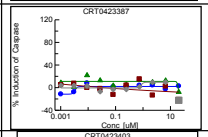	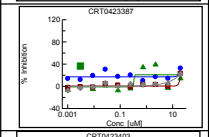	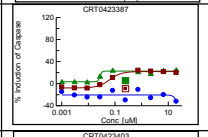	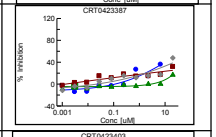
CRT0423403:01	GSK1307810A	PKIS2	ROCK1, AKT, PKA, P70S6K, Aurora A	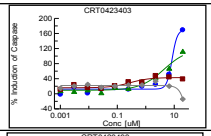	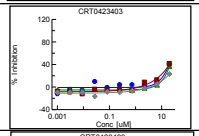	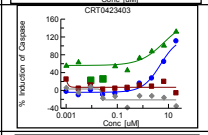	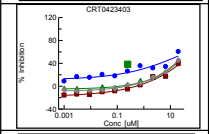	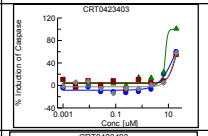	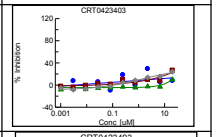
CRT0423493:01	GSK1660437A	PKIS2	BRAF, SRC, LCK, LYN	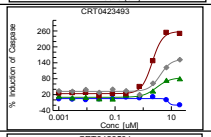	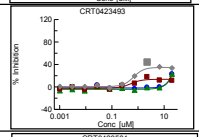	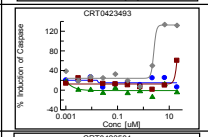	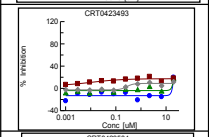	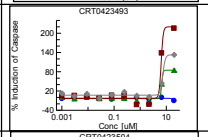	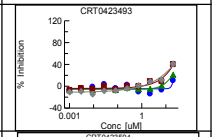
CRT0423504:01	GSK198271A	PKIS2	ErbB family, BRAF	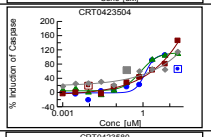	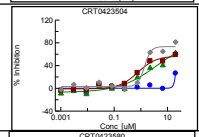	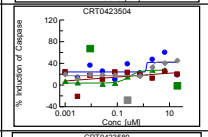	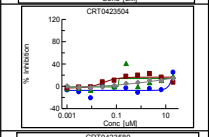	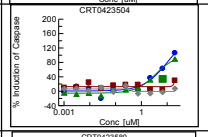	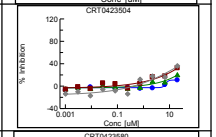
CRT0423580:01	GSK299495A	PKIS2	Src, ErbB family, BRAF	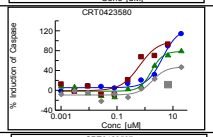	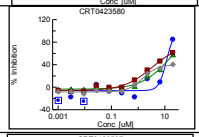	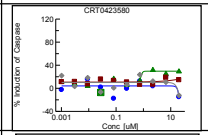	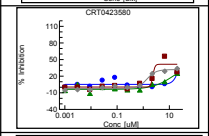	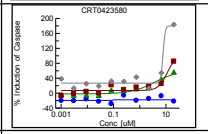	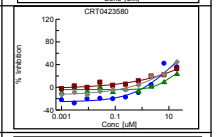
CRT0423587:01	GSK326180A	PKIS2	ErbB family, BRAF	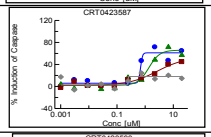	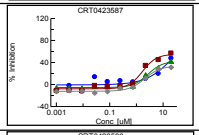	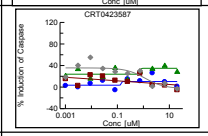	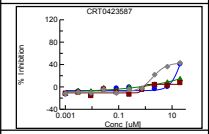	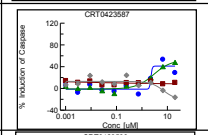	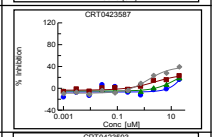
CRT0423593:01	GSK357952A	PKIS2	Src, ErbB family, BRAF	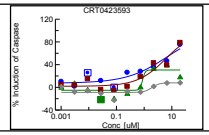	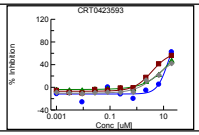	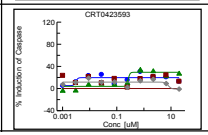	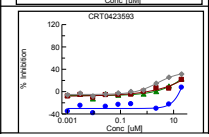	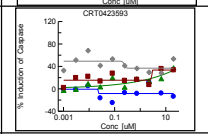	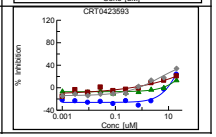

CRT0423594:01	GSK361061A	PKIS2	BRAF, ErbB4	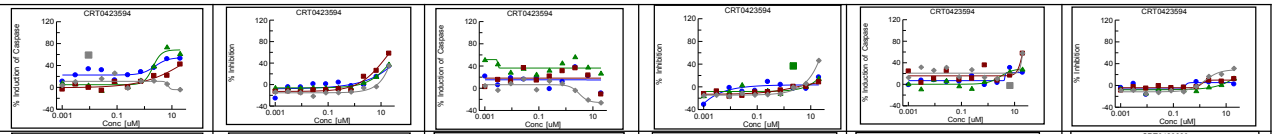
CRT0423639:01	GW459135A	Erlotinib (PKIS2)	EGFR	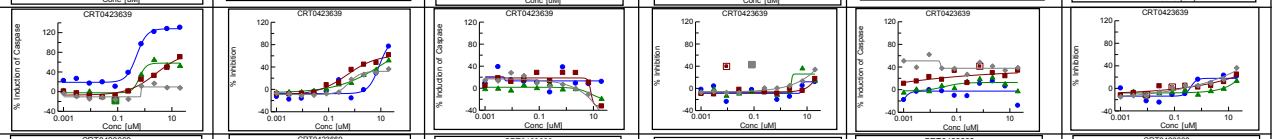
CRT0423669:01	GW569716A	PKIS2	ErbB2/EGFR	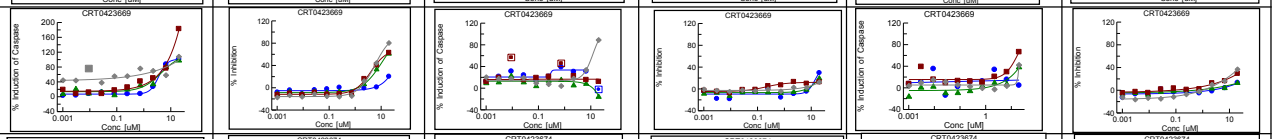
CRT0423674:01	GW582764A	PKIS2	ErbB2/EGFR	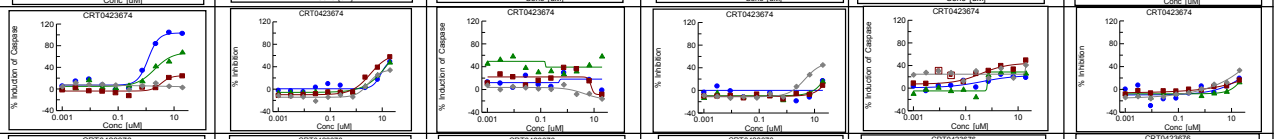
CRT0423676:01	GW583340C	PKIS2	ErbB2/ EGFR	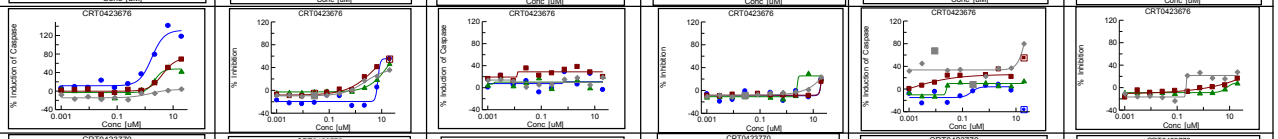
CRT0423770:01	GW876731X	PKIS2	ALK5 series (TGF beta receptor)	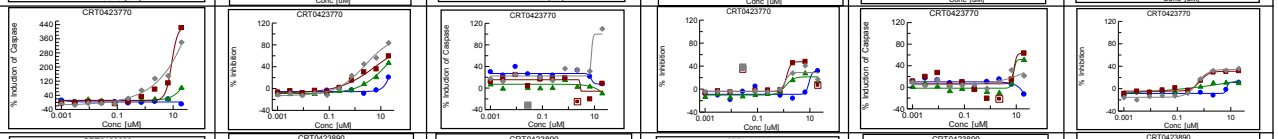
CRT0423890:01	SKF-97184	PKIS2	Unknown	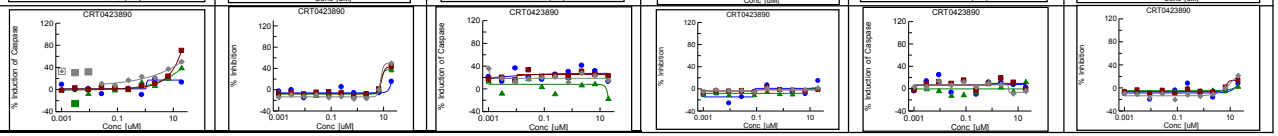

Figure 9.3 Differential phenotypic effect, induction of apoptosis and cell death
Caspase-Glo-3/7 and CellTiter-Glo output as curves for U-CH1, U-CH2 and MUG Chor cell lines at 6 hours (Blue), 24 hours (Green), 48 hour (Brown) and 72 hours (Grey) demonstrating differential phenotypic effect following treatment with 22 EGFR inhibitors. Induction of apoptosis and percentage inhibition (cell death)

9.4 Optimisation of methods for ctDNA

9.4.1 Extraction efficiency of DNA from plasma

Mutation	# FAM-positive droplets*	Mutant copies/mL plasma	Total copies/mL plasma	XenT efficiency	Expt of XenT	Pooled plasma ID
PIK3CA(1)	0	0	1243	79%	48	B
	1	1	1172	85%	48	B
	0	0	925	71%	48	B
	1	1	1200	81%	48	B
LYST(2)	2	5	1220	72%	48	B
	2	4	1143	73%	48	B
PIK3CA(2)	0	0	1004	79%	48	B
	1	2	857	81%	48	B
	0	0	1141	85%	31	A
	0	0	747	67%	31	A
	0	0	624	70%	48	B
	0	0	489	59%	48	B
				Mean:	75%	
				SD:	8%	

Pooled plasma results

Pooled plasma ID	XenT efficiency	Expt of XenT	Copies RPP30/mL	Expt of RPP30
A	64%	31	1391	31
B	81%	48	1357	48
		Mean:	1498	
		SD:	195	

Figure 9.4 Extraction efficiency of DNA from plasma
Extraction efficiency was assessed by spiking frog DNA (XenT) approximately 20,000 molecules into the plasma prior to extraction to assess recovery. The percentage of XenT recovered was compared to a reference dPCR result of spike diluted in 50µL water (to emulate the final concentration of the spike in plasma at the end of extraction). Results are within one standard deviation of the mean, n=23.

9.4.2 Overcoming DNA crosslinking on PPFE samples

9.4.2.1 DNA Enzyme digest and/or dilution of DNA

Exp020 (2 µL neat, 60'C)

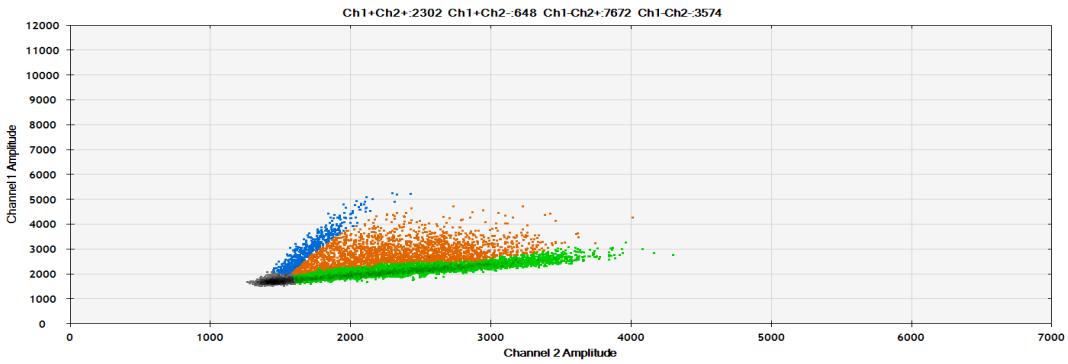

Exp024 (2 µL diluted 1 in 18, 57'C)

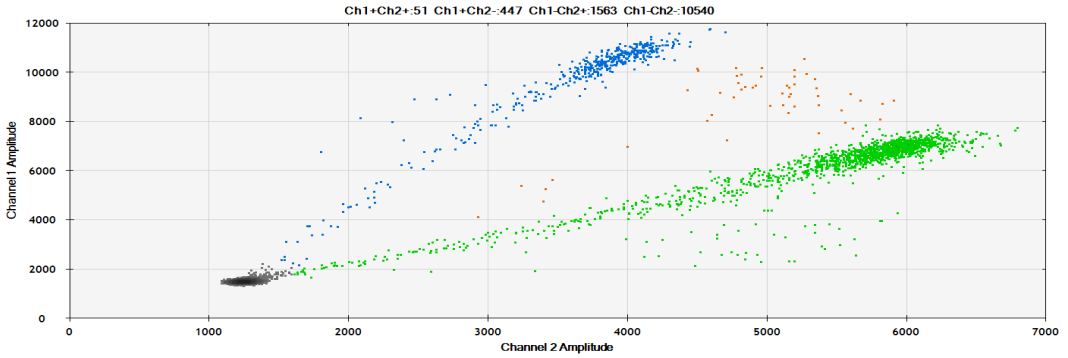

Exp024 (2 µL diluted 1 in 9, 59'C, HindIII digest)

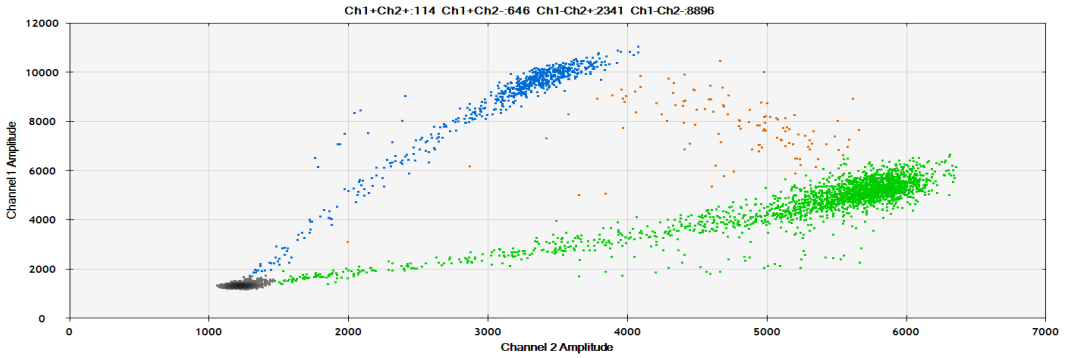

Figure 9.5 *PIK3CA*(1) assay optimisation for tumour DNA
Image on the top shows neat tumour DNA assay for *PIK3CA*(1), it is not possible to separate the different molecules making the result unreliable. For optimisation we diluted DNA and used restriction digest to overcome cross-linking caused by formalin from FFPE samples, and dilution to dilute inhibitors in the sample. Tumour DNA was diluted (1:18) (middle image), and bottom image: dilution 1:9 and the DNA had undergone restriction digest using HindIII restriction enzyme. With the optimisation we achieved to establish the optimal temperature, the dilution factor, and that restriction digest was not required if the sample was diluted (data below).

Exp020 (2 µL neat, 60'C)

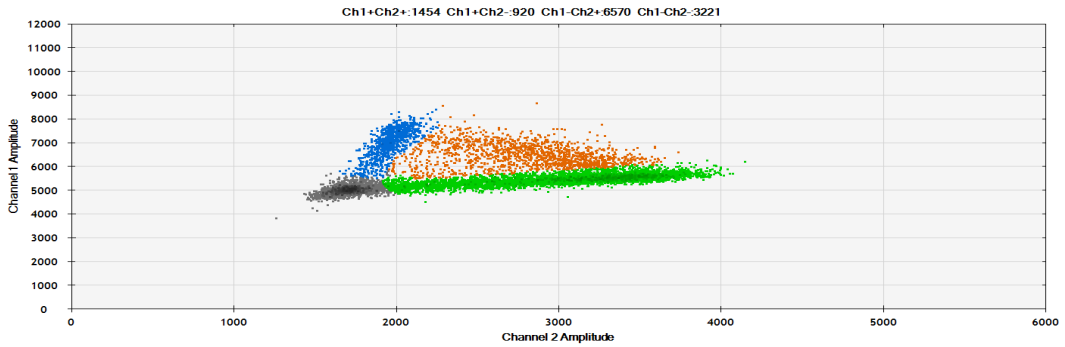

Exp024 (2 µL diluted 1 in 15, 57'C)

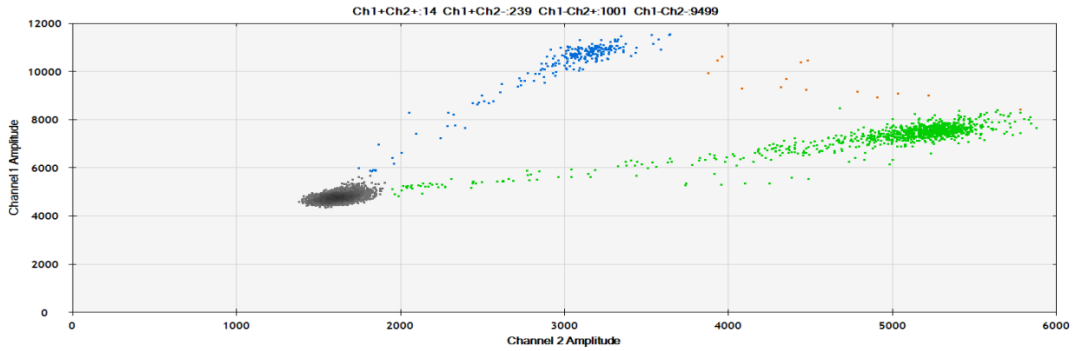

Exp024 (2 µL diluted 1 in 8, 59'C, HindIII digest)

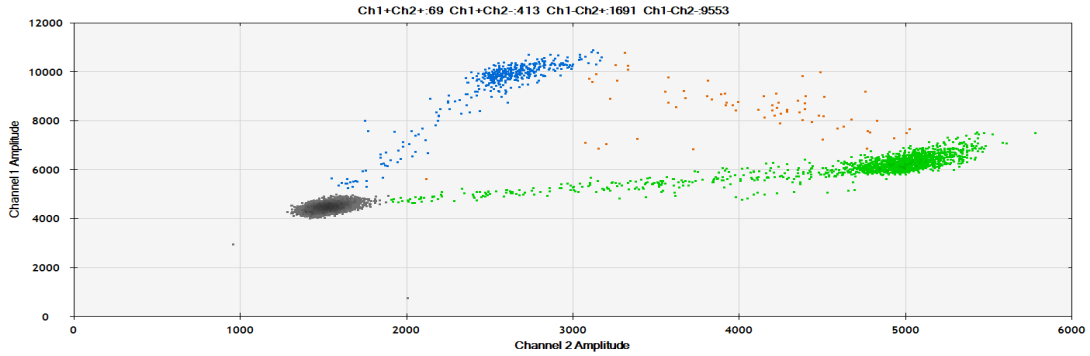

Figure 9.6 *PIK3CA*(2) assay optimisation for tumour DNA
Image on the top shows neat tumour DNA assay for *PIK3CA*(2), it is not possible to separate the different molecules making the result unreliable. For optimisation we diluted DNA and used restriction digest to overcome cross-linking caused by formalin from FFPE samples, and dilution to dilute inhibitors in the sample. Tumour DNA was diluted (1:18) (middle image), and bottom image: dilution 1:9 and the DNA had undergone restriction digest using HindIII restriction enzyme. With the optimisation we achieved to establish the optimal temperature, the dilution factor, and that restriction digest was not required if the sample was diluted.

9.4.3 Optimisation of PCR and primers

9.4.3.1 PCR run with temperature gradient for optimisation of primers

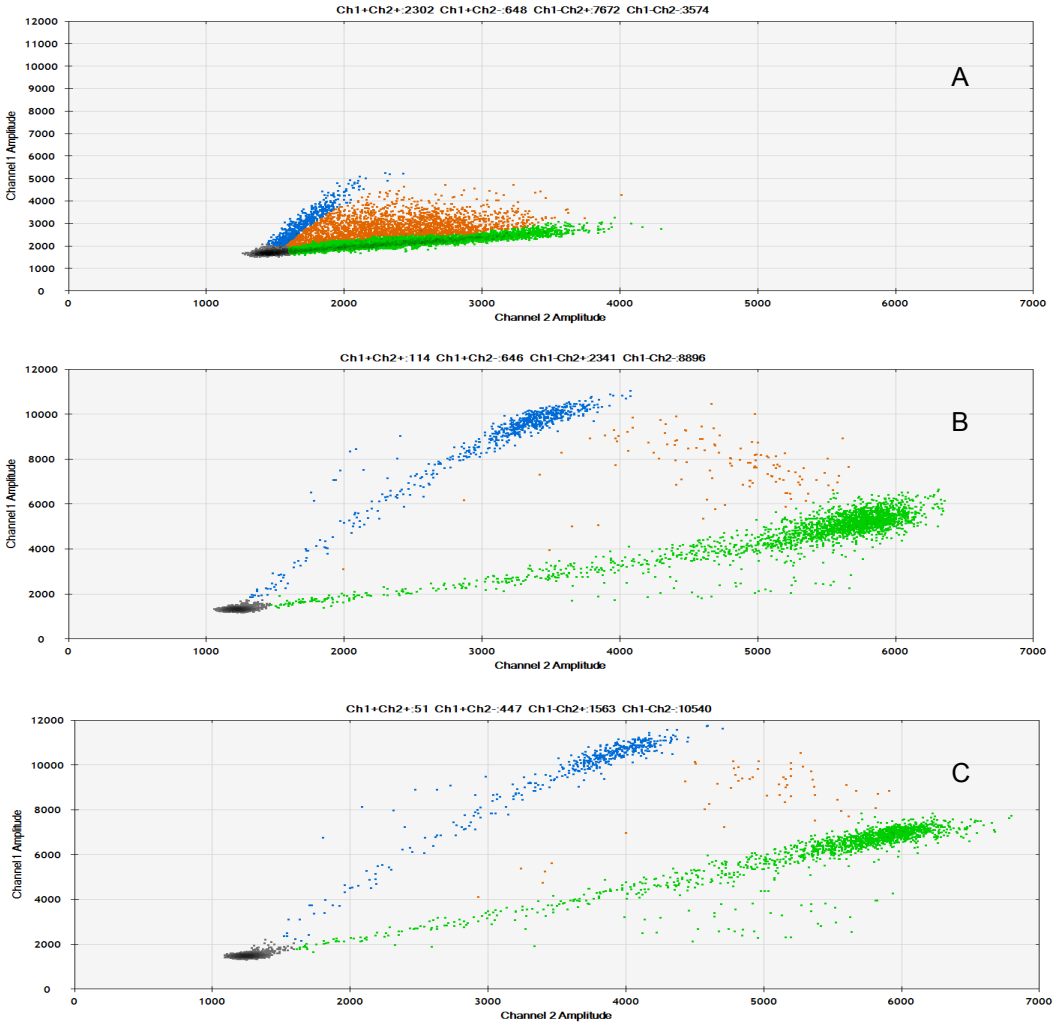

Figure 9.7 Optimisation of PCR *PIK3CA*(1)
PCR run with temperature gradient for primer optimisation. Imaging generated from QX200 droplet reader (analysis), optimising primer for *PIK3CA*(1) mutation on tumour DNA. A: 60°C, B: 59°C, C: 57°C. The optimal temperature: 59°C. FFPE tumour sample.

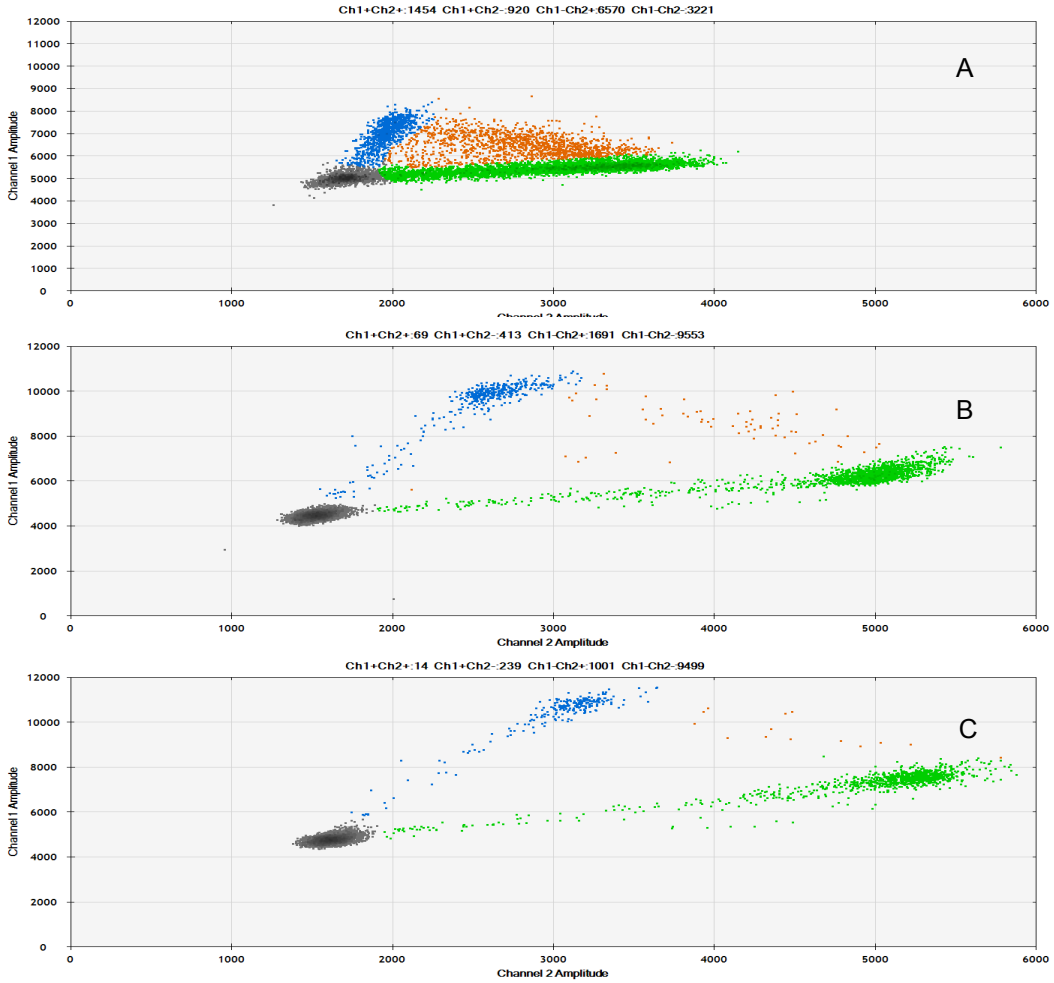

Figure 9.8 Optimisation of PCR *PIK3CA*(2)
Analysis from QX200 droplet reader. Optimisation of the temperature for the primer for *PIK3CA*(2) mutation on tumour DNA. A: 60°C, B: 59°C; C: 57°C. The optimal temperature: 57-59°C, FFPE tumour sample.

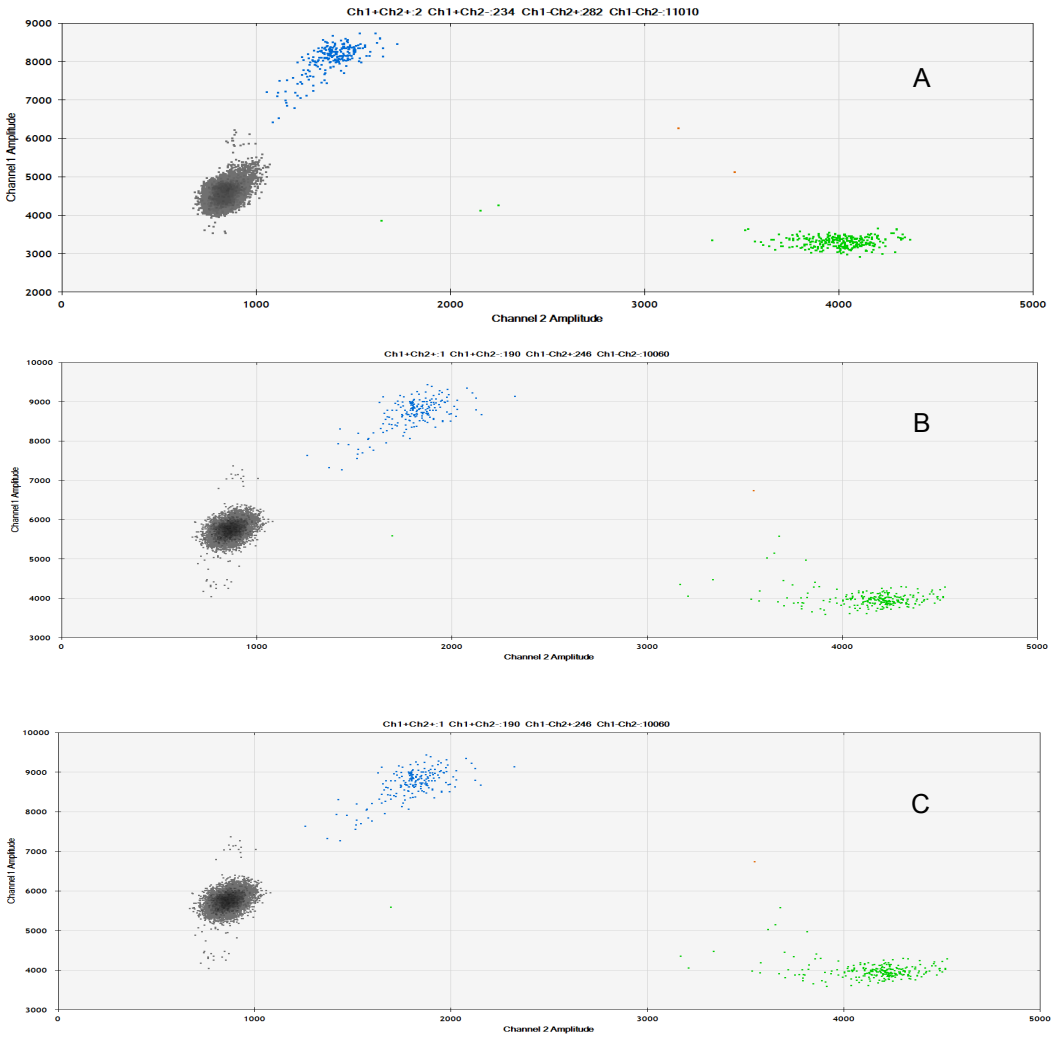

Figure 9.9 Optimisation of PCR *GENE X*(2)
Optimisation of the temperature for the primer for GENE X2 mutation on tumour DNA. Analysis by QX200 droplet reader; *GENE X*(2) insertion frame shift mutation run at (A) 60°C; (B) 57°C; (C) 55°C the assay worked best at 60°C, FFPE tumour sample.

9.4.4 Failed primers and probe

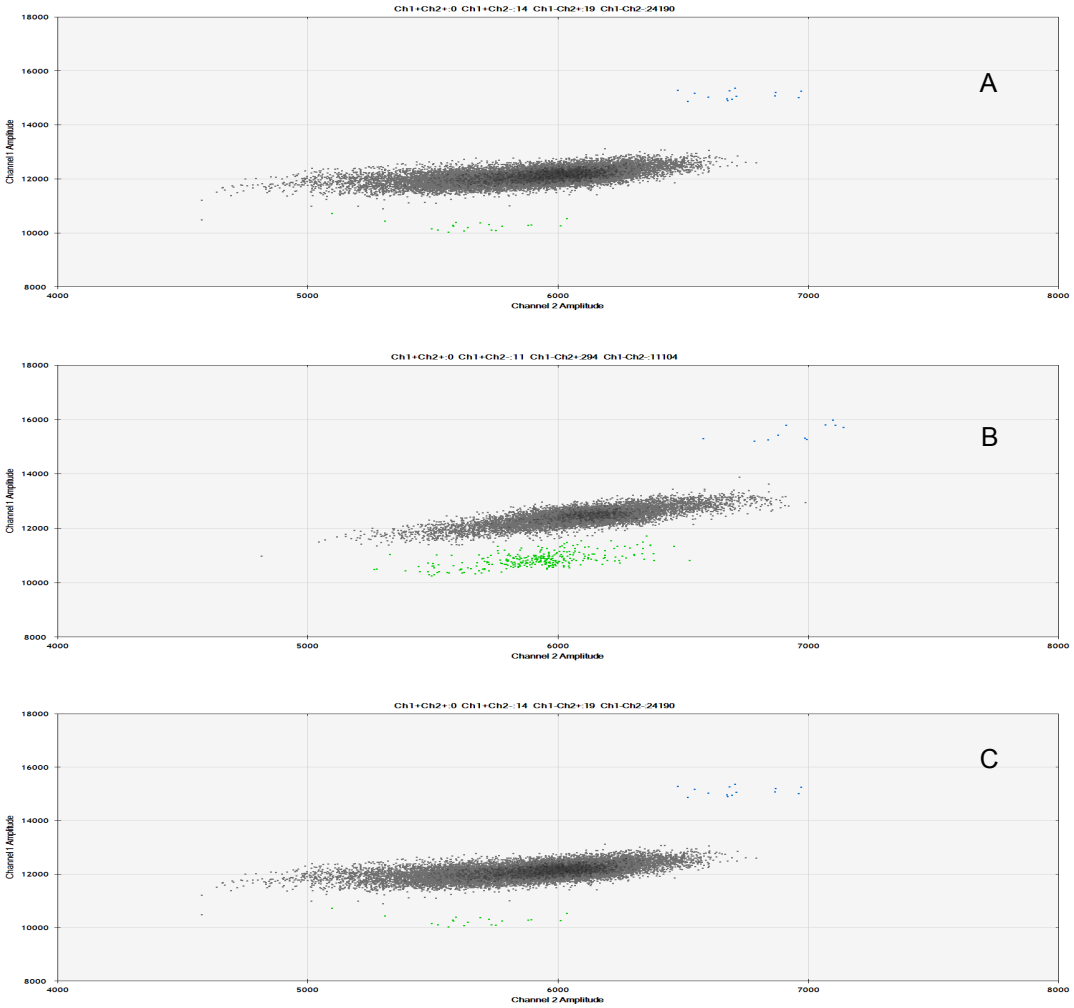

Figure 9.10 Results of ddPCR for *GENE X*(1) mutation in tumour sample
Analysis by QX200 droplet reader; *GENE X*(1) deletion frame shift mutation run at a temperature gradient; assay did not work at any temperature (A: 61-63°C B: 59°C, C: 57°C). The GENE X(1) probe was not specific for mutant/wild-type, and we were unable to design primers and probe for this mutation.